A novel bioactive nano-composite: synthesis and characterisation with potential use as dental restorative material

Khan, Abdul Samad

A Novel Bioactive Nano-Composite:
Synthesis and Characterisation with Potential Use as Dental Restorative Material

Abdul Samad Khan

A thesis submitted to the University of London for the degree of Doctor of Philosophy

June 2009

School of Engineering and Materials Science
Queen Mary University of London

DEDICATIONS

The one, *Almighty*, who created this world and has knowledge of every thing-

"Behold! In the creation of heavens and the earth, and the alternation of night and day, there are indeed Signs for men of understanding." [Aale Imran 3:190]

Prophet Mohammad (*peace be upon him*)-

My Parents
Dr. and Mrs. Mohammad Shamshad Ali Khan

My Wife
Dr. Maria Khan

and

My late grandfather- whose *unseen presence* always guides me in every step of life-

Declaration

Except for the help listed in the Acknowledgements, the contents of this thesis are entirely my own work. This work has not previously been submitted, in part or in full, for a degree or diploma of this or any other university or examining board.

…….. **June 2009**

Abdul Samad Khan

5A Pier Road

North Woolwich

London E16 2JJ

United Kingdom

Abstract

It is desirable for a dental restorative material to have bioactive and bonding properties. This study focuses on the synthesis of a covalently-linked polyurethane/nano-hydroxyapatite (PU/nHA) composite and evaluates its chemical, physical, thermal and biochemical characteristics.

nHA powder was produced from the sol-gel and novel composite material was chemically prepared by utilising solvent polymerisation. The resulting composites were analysed by chemical, thermal, and mechanical characterisations and electrospun to form fibre mats. The composites were hydrolytically degraded in deionised water and phosphate buffer solution (PBS) and were analysed. Bioactive behaviour was determined in modified-simulated body fluid. The bioadhesion with dentine was analysed in distilled water and artificial saliva. Cell growth and proliferation was measured and number of adhering bacteria was determined and serial dilution followed by plating for colony forming units per disc.

Spectral analyses showed the grafted isocyanate and ether peaks on nHA indicating that urethane linkage was established. Covalent-linkage between nHA and PU were found in this novel composite with no silane agent. The physical and thermal properties were enhanced by nHA. These composites had high resistance toward hydrolysis and little degradation was observed. Bioadhesion and bioactivity analysis showed the composite adhered firmly on the tooth surface (dentine) and bond strength was similar to existing obturating material. Higher nHA content composite showed a thicker layer of adhesion. Cells were proliferated although at a lower rate of growth compared to PU, whereas, there was reduction in bacteria adhering to the grafted composite compared to PU. With its low bacterial adhesion and biocompatibility it may provide a promising solution to reduce infections. The electrospun nano-fibres were successfully developed and revealed no loose nHA particles. Hence, this novel composite has the potential to be used as a bioactive dental restorative material.

Acknowledgments

I would like to express my special gratitude to my supervisor Dr. I.U. Rehman for his invaluable supervision, guidance, patience and understanding. I am also indebted to Dr. F.S.L. Wong for his interest, enthusiasm and his faith towards this project and especially for the constant motivation he provided.

I would like to acknowledge Prof Michael Braden, Dr. Mangala Patel and Dr. Sandra Parker (Biomaterials in relation to Dentistry) for their guidance and support. I am thankful to Prof. M. J. Edirisinghe and Dr. Z Ahmad for their support and guidance during my project work on Electrospinning at University College London. The advices and support during the developmental process were invaluable; to Dr. I.J. McKay and Dr. R. Whiley for collaborative projects on cell culturing and microbiology respectively at Institute of Cell and Molecular Science, Barts and the London School of Medicine and Dentistry

I am grateful to Dr. Monisha Phillips for her expert advices and valuable technical guidance; to Dr. Zofia Luklinska and Mr. Mick Willis for helping out with the SEM and TEM; to Dr Rory Wilson for XRD characterisations; to Dr. Greg Coumbarides (School of Biological and Chemical Sciences) for his input in NMR characterisations; Mr. Bill Godwin and Mr. Vince Ford deserve credit for their excellent job in preparing the moulds. Thanks are due to Ms. Victoria Wells, Mr. Jonathan Hill and Mr. Edward.

I am thankful to School of Engineering and Materials Science for giving me support and financial help; to Armourers and Brasiers and IOM3 for conference travel grants; to Leche Trust and Hammond Trust for international student support grants.

Other fellows and friends that I would like to thank are Mr. Saroash, Mr. Talal who made my time memorable and enjoyable; to Mr. Anil, Miss. Raheleh and all those that I have had the opportunity to share an office with; to Dr. Nima, Dr. Depeen and Dr. Aqif for their valuable advices.

I will always praise Dr. Maria (my wife) for her moral support and wishes throughout this time, without which I would never have got this far. I will always be

very grateful for unconditional love, generous support and encouragement from my grandmother - without her *prayers* I would not be where I am today; from parents Mr. & Mrs. Shamshad, for whom I did this effort; from Dr. Shahla (sister), Mr. Omar (brother) and their families. Thank you for all the support - GOD BLESS YOU ALL, *Amin.*

Table of Contents

List of Figures

Chapter 2

Chapter 3

Chapter 4

Chapter 5

Appendix 1

Appendix 2

Appendix 3

Appendix 4

Appendix 5

Appendix 6

Appendix 7

List of Tables

Chapter 2

Chapter 3

Chapter 4

Chapter 5

List of Abbreviations

%	Percentage
$(NH_4)_2HPO_4$	Ammonium hydrogen phosphate
µm	Micrometer
Å	Angstrom
ACP	Amorphous calcium phosphate
ASPA	Aluminosilicate polyacrylate
BD	*1.4*-Butanediol
BET	Brunauer-Emmett-Teller
Bis-GMA	Bisphenol glycol methacrylic acid
C=C	Benzene group
C=O	Carbonyl group
Ca	Calcium
$Ca(NO_3)_2.4H_2O$	Calcium nitrate tetrahydrate
$Ca(OH)_2$	Calcium hydroxide
$Ca_{10}(PO_4)_6(OH)_2$	Hydroxyapatite
$Ca_4(PO_4)_2O$	Tetracalcium phosphate
$Ca_8H_2(PO_4)_6.5H_2O$	Octacalcium phosphate.pentahydrate
$CaCl_2$	Calcium chloride
$CaCO_3$	Calcium Carbonate
$CaHPO_4$	Calcium hydrogen phosphate
cal	Calorie
CaO	Calcium oxide
$CaSO_4$	Calcium Sulphate
CH_2	Methyl
CH_3I	Iodomethane
CH_3OH	Methanol
Cl	Chlorine
ClCOOR	Chloroformates
cm	Centimetre
cm^2	Centimetre square
CO_2	Carbon dioxide

CO_3^{2-}	Carbonate
C—O—C	Ether group
COOH	Carboxyl group
DMF	*N, N*'-Dimethylformamide
DSC	Differential Scanning Calorimetry
DW	Deionised water
e.g.	For example
EDS	Energy Dispersion Spectroscopy
eq.	Equation
F	Fluorine
FDA	Food & Drug Administration
FTIR	Fourier Transform Infrared
g or gm	Gram
GIC	Glass Ionomer Cement
GP	Gutta Percha
GPa	Gigapascal
H_{12}MDI	4,4'- dicyclohexyl methane diisocyanate
H_2O	Water
H_2PO_4	Dihydrogen Phosphate
H_3PO_4	Phosphoric Acid
HA	Hydroxyapatite
HCl	Hydrochloric acid
HCN	Hydrogen Cyanide
HCO_3	Bicarbonate
HDI	*1,6*-hexamethylene diisocyanate
HEMA	Hydroxy ethylmethacrylate
HEPES	2-(4-(2-hydroxyethyl)-1-piperazinyl) ethanesulfonic acid
HPO_4	Hydrogen Phosphate
hr	hour
i.e.	That is
ICMS	Institute of Cell and Molecular Science
IPDI	1,6—hexamthylene diisocyanate, isophorone diisocyanate
IR	Infrared
J	Joule

KCl	Potassium Chloride
KV	Kilovolt
m	Meter
MDI	*4, 4'*- Methylenediphenyldiisocyanate
mg	Milligram
Mg	Magnesium
$MgSO_4$	Magnesium Sulphate
min	Minute
mm	Millimetre
mol	Mole
MPa	Mega Pascal
m-SBF	Modified-simulated body fluid
MTA	Mineral Trioxide Aggregates
M_w	Molecular Weight
Na	Sodium
NH_4OH	Ammonium hydroxide
NCO	Isocyanate
NDI	1,5-naphthalene diisocyanate
NH	Amide
NH_2	Amine group
NH_4HF_2	Ammonium hydrogen difluoride
NH_4NO_3	Ammonium Nitrate
NH_4OH	Ammonium hydroxide
nHA	Nano-Hydroxyapatite
nm	Nanometer
NMR	Nuclear magnetic resonance
No.	Number
ºC	Degree Celsius
OH	Hydroxyl
P	Phosphorous
PAS	Photoacoustic spectroscopy
Pb	Lead
PBA	Poly (butylenes adipate)
PBS	Poly (butylenes succinate)

PBS	Phosphate buffer saline
PDMS	Polydimethylsiloxane
PEO	Polyethylene oxide
PES	Poly (ethylene succinate)
PGA	Poly (glycolic acid)
PHMO	Poly (hexamethylene oxide)
PLA	Poly (lactic acid)
PO_4^{3-}	Phosphate
PPDI	*p*-Phenylene diisocyanate
PTMO	Polytetramethylene oxide
PU	Polyurethane
s	Second
S. sanguinis	Streptococcus sanguinis
SD	Standard deviation
SEM	Scanning electron microscopy
sq	Square
TDI	Toluenediisocyanate
TEGMA/TEGDMA	Triethylene glycol dimethacrylate
TEM	Transmission electron microscopy
T_g	Glass transition temperature
TGA	Thermogravimetric Analysis
THF	Tetrahydrofuran
TMDI	2.4.4-trimethyl-1.6-hexamethylene diisocyanate
UDMA	Urethane dimethacrylate
VHN	Vicker hardness
VO_4	Orthovanadate
vol	Volume
wt	Weight
XRD	X-ray diffraction
Zn	Zinc
α	Alpha
β	Beta
θ	Theta

Chapter 1 Introduction

1.1- Research Motive

It is desirable for a restorative dental material to have bioactive and bonding properties at the interface between the material and tissue to prevent micro-leakage and ingress of bacteria. Current dental restorative composites, which consist mainly of polymer matrix, filler particles, and coupling agent, do not exhibit these properties. The presence of discrete zones at the interface between these three components could cause water absorption and the osmotic effect would result in swelling and residual pressure on tooth structure. Silane coupling agent contact with the fillers could also cause a decrease in the polymerisation of resin-based composite. Urethane derivatives in restorative composites have been studied with 2,2-bis-[4-(2-hydroxy-3-methacryloxypropoxy)phenyl]propane) (Bis-GMA), these derivatives have much lower viscosities and water uptake than Bis-GMA and exhibit higher conversion of vinyl group without increasing (and perhaps decreasing) polymerisation shrinkage. Urethane based polymers, along with other materials such as acrylic resins or silicone, are often used in dentistry for the tissue bearing surface of an extra-oral prosthesis. Nano-hydroxyapatite have tendency to show osteoconductivity, high surface area to volume ratio, superior chemical homogeneity and micro structural uniformity. Hence, it would be advantageous to combine these two materials to form a new dental material that would possess the above desirable properties. The requirement of a specific material differs according to the nature of application and there are different techniques in modifying and fabricating different compositions to achieve exact requirements for clinical use (Rehman, 1996). Polymeric based biomaterials have been used in medical and surgical applications for a number of years and it has been clear that there are different ways in which materials and tissue can interact (Williams, 2008).

1.2- Structure of Tooth

Tooth is the hardest and chemically most stable tissue in the body. In humans, the function of teeth is the comminution of food by a process referred to as mastication.

Structure of tooth consists of enamel, dentine, pulp, cementum and periodontal ligament, where the main bulk of tooth comprises of dentine. Dentine can be regarded as a natural composite consisting of apatite crystallites and an organic matrix (Katz, 1971). The inorganic component consists mainly of hydroxyapatite. About 56% of the mineral phase is within the collagen, which makes dentine slightly harder than bone and softer than enamel (Ten Cate, 1998). The apatite filler phase contributes most of the strength, while the collagen matrix provides elasticity and stress distribution (Mammone and Hudson, 1993). Like bone and enamel, dentine contains Calcium (Ca)-deficient hydroxyapatite with more than trace amounts of carbonate (Linde, 1984). Mechanical properties of tooth vary relating to test location and local chemistry i.e. degree of mineralisation. In addition to having variations in the degree of mineral content, hydroxyapatite is known to be an elastically anisotropic material and mechanical testing has indicated that differences in values may be due to the variations in prism orientation (Cuy *et al.,* 2002). The mechanical properties of restorative materials should match as closely as possible to those of tooth structure (Angker *et al.,* 2003).

1.3- Restorative Materials

Damage and infection in the teeth have been restored or replaced with a variety of materials including endodontic obturations, glass ionomer cements, and resin-based composites. The main advancement in direct type restorative materials occurred in the 1960s and 1970s with the synthesis of new polymeric systems and the introduction of inorganic fillers. The hybrid restoratives contain components of conventional chemically cured glass ionomers and light cured resins i.e. Bis-GMA and triethylene glycol dimethacrylate (TEGDMA) (Croll and Killian, 1992; Gladys *et al.,* 1997). The advantages of composite include minimal intervention, mechano-chemical bonding with tooth and their application in anterior as well as posterior restoration (Bonilla *et al.,* 2001: Kahler *et al.,* 2005). However, existing polymer based restorative materials have certain limitations such as secondary caries, restoration fracture, marginal defects, water absorption, polymerisation shrinkage, and high viscosity (Watanabe *et al.,* 2008; Sakaguchi *et al.,* 2005). To overcome these issues urethane derivative resins have been used successfully in

dentistry and are available for light activated composite formulated specifically for fabrication (Wakasa *et al.,* 1997; Whitworth *et al.,* 1999). The most common is urethane dimethacrylate (UDMA), which can be synthesised by using trimethlhexamethylenediisocyanate (TMDI) (Moszner *et al.,* 2008). Hence, polyurethane structure blocks, i.e. polyols, isocyanates, chain extenders and other modifying ingredients have enabled designing of materials for different applications (Atai *et al.,* 2007).

1.4- Polyurethane

Polyurethanes are a versatile class of polymers and are one of the most interesting classes of synthetic elastomers, having unique properties. They are used in a broad range of applications, due to their better physical properties and biocompatibility (Bouchemal *et al.,* 2004). Polyurethane is a family of heterogeneous polymers that contain the urethane linkage, similar to carbonate group in organic chemistry, within the polymer chains. They consist of three main components i.e. soft segments (polyols), hard segments (isocyanate) and chain extenders, which can affect properties of the final material. A great deal of attention has been given to the synthesis, morphology, chemical, and mechanical properties of this family of materials (Kuan *et al.,* 2005). Synthesis of polyurethane can be achieved by various methods such as solvent based polymerisation (Hong *et al.,* 2002), melt polymerisation (Kultys, 2001) and supercritical fluid techniques (Fu *et al.,* 1997). Depending on the field of application, ester and ether types of polyols have generally been incorporated as soft segment, whereas aliphatic or cycloaliphatic diisocyanate has been incorporated as hard segments extended by diol or diamine (Kim *et al.,* 2005). Polyether type polyols possess good physical strength, abrasion resistance, water resistance, fatigue life, and biocompatible character (Liu *et al.,* 1997). Research on polyurethane and its potential application in dentistry has been studied as facial prosthesis and is based on its inherent environmental stability, high tear resistance, and low modulus without the use of plasticisers, and good ultimate strength and elongation. This material can accept intrinsic colouring and is amenable to maxillofacial processing techniques (Tang *et al.,* 1975; Goldberg *et al.,* 1978; Labella *et al.,* 1994). Polyether based impression materials have been used in

restorative dentistry to record intra-oral structures for fabrication of definitive restorations (Ritter *et al.,* 2000). From the material's science dimension, a single material type is not able to provide the necessary mechanical and chemical properties required for biomedical applications. From a biological viewpoint, combination of polymer and ceramic material to fabricate a bioactive composite scaffold is a natural strategy (Chen and Boccanccini, 2006).

1.5- Hydroxyapatite

Nano-hydroxyapatite (nHA) has been proved to be an osteoconductive material (Hench *et al.,* 1998) that also binds chemically to enamel and dentine. A significant characteristic of these bioactive materials is their ability to bond with living tissue through the formation of a hydroxyapatite interfacial layer (Wu and Chang, 2006). The use of hydroxyapatite (HA) in restorative dentistry offers several advantages, including, intrinsic radio-opaque response, enhanced polishability and improved wear performance and the biocompatibility due to its bioactive nature (Domingo *et al.,* 2001). The reduction in hydroxyapatite particle size maximise surface area to volume ratio allowing a high percentage of atoms to be present at the surface. Therefore, the properties of nano-modified hydroxyapatite are regulated by their intrinsic properties i.e. surface energy and morphology rather than their bulk properties.

1.6- Polymer Composites

Hence, in recent years, considerable attention has been focused towards the development of polymer composites to fulfil properties required for biomedical applications. The significance of using a composite material is due to the fact that the amount and type of reinforcing material and, the mechanical and biological properties can be tailored for each specific application. It has been reported that various polymers such as poly-lactic acid, poly-glycolic acid, poly-ε-caprolactone, polyethylene, polyetheretherketone, and polyurethane were used with hydroxyapatite (HA) as composite materials (Liu *et al.,* 1998; Choi *et al.,* 2004). The interface adhesion of HA particles and polymer matrix plays a very important role among the

major factors affecting properties of composites (Liu *et al.,* 1996; Hong *et al.,* 2005). Surface modification: surface adsorption and grafting of HA by polymers will provide an effective way to manipulate the surface properties of HA. When nano-particles and polymers form a composite, provided that homogenous dispersion of nano-particles is achieved at microscopic level, the mechanical properties are expected to improve and/or new unexpected features might appear (Liu *et al.,* 1996). Dental restorative composites consist of continuous polymeric matrix reinforced with a dispersed phase or filler. Commonly used filler particles are barium or zinc glasses, quartz, zirconia, silica or alumina. These are silanated inorganic fillers in restorative composites, whereas, an acceptable substitute with similar chemical and physico-mechanical characteristics should be considered. The mineral phase of human bone and teeth is mainly hydroxyapatite; therefore, dental resins reinforced with dispersed hydroxyapatite crystals seem to be a favourable restorative material for human tooth tissue.

1.7- Project Overview

Nano-hydroxyapatite (nHA) was synthesised by a sol-gel technique and were characterised with Fourier Transform Infrared (FTIR) spectroscopy, Raman spectroscopy, X-ray diffraction (XRD) and the nano-size and high surface area were confirmed with Transmission electron microscopy (TEM), Scanning electron microscopy (SEM) and Brunauer Emmett Teller (BET) respectively. Polyurethane and polyurethane/nano-hydroxyapatite (PU/nHA) composites were synthesised by *in-situ* solvent polymerisation. Primarily supercritical fluid technique was used during the early stage of this study, but it did not provide the required results. Various methods (physical and chemical) and different ratios of the components were used and finally the best possible combination of ratios was applied, which will be explained in Chapter 3. Initially polyether was tried with different molecular weights, finally polyether soft segment (Poly (tetramethylene glycol 1400 g mol^{-1}), *4, 4'*- Methylene Diphenyl Diisocyanate (MDI) hard segment and *1.4*-Butanediol (BD) chain extender was used with nano-hydroxyapatite. The resulting material was characterised by using structural [FTIR, Raman spectroscopy, ^{13}C Nuclear Magnetic Resonance (^{13}C NMR)], physical (XRD), and thermal (Thermo Gravimetric Analysis; TGA, Differential Scanning Calorimetric; DSC) techniques.

Chemical analysis showed that there were structural changes and covalent linkage established between nHA and polymer. The physical and thermal analysis further confirmed that with the chemically linked PU/nHA, the properties of composite improved.

Polyethers are hydrolytically stable but due to the presence of hygroscopic materials, hydrolytic stability of the composite was analysed. The biostable polymers must have certain performance criteria including long-term stability and biocompatibility. The specific properties of bioactive polymers result from distribution of the bioactive components with specific chemical groups on the polymeric surfaces. Depending on the chemical nature of the functional groups and their relative proportions in the final product, these bioactive polymers are able to bind with living tissues, which will range from non-specific to highly specific. The biostability of the experimental composite was analysed and characterised by using chemical and physical analysis. *In-vitro* bioactivity was analysed with modified simulated body fluid and adhesion was evaluated with human extracted molar teeth mainly with dentine. These studies were conducted with pre-determined time interval.

The biocompatibility is the ability of the material that is intentionally placed within the body for transient diagnostic or therapeutic purpose to be able to perform its intended function. The main purpose is that the material should not induce uncontrolled activation of cellular and protein cascades. The factors which can affect the degree of biocompatibility are: the type of material, genetic inheritance of the patient, site of application, and the contact duration (Pavithra and Doble, 2008). The biocompatibility test was performed by cell-culturing and bacterial adhesion analysis. Electrospinning was used to synthesise fibres from both physically and chemically mixed composites and were analytically compared with surface characteristics of the fibres.

1.8- Outline of Thesis

This thesis provides comprehensive review of the literature, which includes the structure of tooth, development of restorative materials, polyurethane, and nano-hydroxyapatite (**Chapter 2**). It also outlines the investigated materials, experimental

techniques and brief description of these methods (**Chapter 3**). Obtained results (**Chapter 4**) and the relevant discussion (**Chapter 5**) are explained. At the end (**Chapter 6**) it concludes the findings of the project and finally presents the future work followed by a list of references and appendices.

Chapter 2 Literature Review

2.1- Structure of Tooth

Teeth are the hardest and chemically most stable tissue in the body. The anatomical crown of the tooth is covered with enamel. Enamel is thickest over the region of the crown, used for biting, and tapers towards the neck (cervical region) of the tooth. Where enamel finishes, it is usually continuous with a layer of cementum, which covers the root area. The cementum is hard tissue, which attaches tooth to the surrounding alveolar bone by means of collagen fibres. The dentine is situated between the pulp and enamel and is interlinked with dentino-enamel junction. The pulp is a highly vascular connective tissue, which provides nutrition as well as sensory nerves to the cell forming the dentine (Antonio, 2003; Yu and Abbott, 2007). Figure 2.1 shows the structure of tooth.

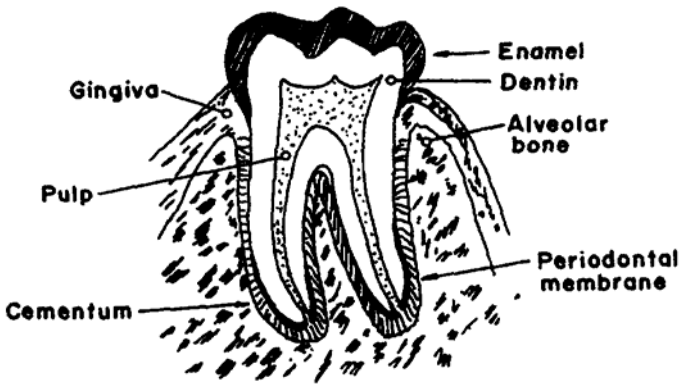

Figure 2.1 Structure of Tooth (Ten Cate, 1998)

2.1.1- Enamel

Human teeth are composed mainly of dentine capped on the working surface by a thin hard layer of enamel. Enamel contains 97% by weight (92% by vol.) of inorganic material, 1% organic material and 2% water. The inorganic material is a calcium deficient apatite containing 2-5% by weight carbonate and inclusion of numerous other trace elements. The mineral crystals are of the order of 25 nm thick, 40-120 nm wide

and 160-1000 nm long. The hydroxyapatite crystals in enamel form well-defined rod or prism like structures about 4 μm in diameter (Suchanek *et al.,* 1998).

2.1.2- Dentine

In restorative dentistry, dentine microstructure and properties are the principal determinants of nearly all procedures (Zaslansky *et al.,* 2006). Dentine can be regarded as a natural composite, much like bone, consisting of a microscopic filler phase made up of apatite crystallites and an organic matrix made up primarily of collagen (Sano *et al.,* 1994). Table 2.1 shows the composition of dentine by weight and by volume. The organic phase is type I collagen with inclusion of glycoproteins, proteoglycans and phosphoproteins (lipids and noncollagenous matrix protein) and a small amount of type III and V collagens (Ten Cate, 1998).

Table 2.1 Composition of dentine by weight and volume (Ten Cate, 1998)

Composition	**By weight (%)**	**By volume (%)**
Inorganic material	70	45
Organic material	20	33
Water	10	22

The inorganic component consists mainly of hydroxyapatite. About 56% of the mineral phase is within the collagen, which makes dentine slightly harder than bone and softer than enamel (Ten Cate, 1998). The size of the apatite crystals is much smaller (approximately 5 x 30 x 100 nm) than the apatite found in enamel, and contains 4-5% carbonate as compared with hydroxyapatite. The major components are distributed into distinctive morphological features to form a complex and vital hydrated composite in which the morphology varies with location and undergoes alterations with stimuli (age and diseases) (Marshall *et al.,* 1997).

The other components of tooth structure are pulp, which is a soft tissue containing thin collagenous fibres, nerve cells, blood vessels etc. The cementum surrounds the root. The

thickness of layer varies from 20-50 μm at the cervix to 150-200 μm at the apex. Approximately half of cementum is composed of organic and half is inorganic and water. The periodontal membrane is made of collagenous fibres and glycoproteins (protein-polysaccharide complex) (Suchanek *et al,,* 1998; Ten Cate, 1998).

2.1.3- Dental Caries and Restoration

Dental caries is a multi-factorial disease involving interaction among the diet, saliva, the plaque micro-flora and a susceptible tooth surface (Marsh, 1995). Caries results initially from an imbalance between demineralisation and remineralisation of the tooth structure (Thylstrup *et al.,* 1994). Cavities in the teeth have been restored or replaced since ancient time to the eight century with a variety of materials including stone chips, ivory, human teeth, turpentine resin, cork, gums, and metal foils. More recently amalgams, unfilled synthetic resins, cement, metal modified cements, resin-based composites, and ceramics have been used for tooth restorations (Anusavice, 2003). Aesthetic dental composites were introduced in the mid-1960s for the restoration of anterior teeth and inert fillers were incorporated with resin matrix. Since then resin composites have been the material of choice for anterior restorations. In the 1980s, the first application of resin composites on load bearing posterior teeth, were introduced, where better mechanical properties are required (Bowen and Marjenhoff, 1992). This section will describe the literature review of development of dental restorative materials, mainly the endodontic obturating materials, and aesthetic dental materials such as glass ionomer cements and resin based composites.

2.2- Development of Restorative Materials

2.2.1- Introduction

Dental materials science for restorative dentistry is derived from material science. Material science is classified into four categories i.e., metals, ceramics, polymers and composites. Each of these materials has characteristic microstructures and resulting

properties (Roberson *et al.,* 2002). A large number of materials have been used in dentistry for a wide spectrum of applications (Moszner and Klapdohr, 2004). Restorative dental materials include synthetic components, acid base cements, amalgam, resin-based composites, noble and base metals, ceramics and denture polymers (Craig and Power, 2002; Anusavice, 2003).

The ideal restorative material should be biocompatible, bond permanently to tooth structure or bone, match the natural appearance of tooth structure and other visible tissues, and be capable of initiating tissue repair or regeneration of missing or damaged tissues (Anusavice, 2003).

2.2.2- Obturating Materials

Endodontics (root canal treatment) is defined as the combination of mechanical instrumentation of root canal system, its chemical debridement and filling with an inert material and design to maintain the health of all, or part of the pulp (Ng *et al.,* 2007). The two major steps in root canal system are: the preparation of root canal and the obturation of canals.

2.2.2.1- Ideal Requirements of Obturating Material

The requirements of the ideal root canal filling materials (Ingle, 2002; Stock, 2004; Gutmann, 2006):

1. should be easily introduced into a root canal, where the shape of canal varies
2. should seal the canal laterally as well as apically
3. should not shrink after being inserted
4. should be impervious to moisture
5. should be bacteriostatic or at least not encourage bacterial growth
6. should be radiopaque
7. should not stain tooth structure
8. should not irritate periradicular tissue or should be biocompatible

9. should be sterile and quickly sterilised immediately before insertion
10. should be removed easily from the root canal if necessary
11. should have long shelf life
12. should be cost effective (cheap)

2.2.2.2- Materials Used for Obturation

There are certain materials which have been using for obturation and can be grouped as; plastics (gutta percha) (Kulild *et al.,* 2007), solids (silver cones) (Schilder, 2006), resins (Gesi *et al.,* 2005), pastes and cements (mineral trioxide aggregate) (Roberts *et al.,* 2008).

Gutta Percha (GP) is by far the most universally used solid-core root canal filling material and may be classified as a plastic. It is a *trans*-1,4-polyisoprene and has an approximately 60% crystalline form. Chemically pure gutta percha exist in two distinctly different crystalline forms (alpha and beta) that can be converted to each other. The forms differ only in molecular repeat distance and single carbon-bond configuration (Maniglia-Ferreira *et al.,* 2005). The third form of GP is amorphous (molten). The composition of GP is: Gutta Percha 19-22 %, Zinc Oxide (stiffness) 59-75 %, Metal sulphate (radiopacity) 1.1-17 %, Waxes/resins (hardening properties) 1-4 %, Colouring agent (visual) < 1 (Friedman *et al.,* 1977; Gurgel-Filho *et al.,* 2003). However it varies according to manufacturers.

The advantages of GP are compressibility or compatibility, radiopacity, becomes plastic when warmed, has known solvent: chloroform and xylene. However, the disadvantages are; dependent on sealer for bonding with tooth structure i.e. no dentinal adhesion, lack of sufficient rigidity, and shrinks during cooling or solvent evaporation, exhibit degree of tissue irritation due to high content of zinc oxide, which is known to be an irritant (Qualtrough, 2005; Manogue, 2005; Hsieh *et al.,* 2008).

A new polymer-based obturating material, Resilon has been developed, by combining methacrylate-based resin sealers with polyester; it has been claimed that a monoblock-bonding concept could be achieved. This material showed less microbial leakage,

reduced periapical inflammation, and higher bond strength compared to gutta percha. However, some undesirable properties include low push-out bond strength and low cohesive strength and could not achieve a complete hermetic apical seal (Sly *et al.,* 2007; Hsieb *et al.,* 2008).

The complete obturation of the root canal system has been proposed as goals for successful endodontic treatment. The standard method of obturation of the root canal treatment uses a core material in combination with a root canal sealer. It has been documented that the complete sealing of the root canal system with currently available materials and obturation technique is not a predictable procedure (Saleh *et al.,* 2002). Microleakage from an apical or coronal direction is a clinical problem and a possible source of failure. It has been stated that approximately 60% of endodontic failures are due to inadequate obturations of the root canal systems. These failures have been linked with the penetration of substances from the apical tissue into the canal (Saleh *et al.,* 2002; Brosco *et al.,* 2003). Studies have been conducted on different techniques of obturation, warm vertical compaction (Schilder, 1967), the continuous wave of condensation technique (Buchanan, 1996), the multiphase gutta percha obturation technique (McSpadden, 1993). Apart from using different techniques of obturation when the obturated root canal system is exposed to the oral environment, ingress of micro-organisms occurs (Davalou *et al.,* 1999).

2.2.3- Development of Aesthetic Restorative Materials

In 1963 the idea of polyelectrolyte cement was developed which involved the reaction of a metal oxide with reactive water-soluble polymers. Based on this concept the first zinc polyacrylate cement was produced by using zinc oxide and poly acrylic acid, which was capable of chemically bonding to the tooth structure, due to the use of polyacrylic acid. The latter has the ability to complex calcium ions and form hydrogen bonds with collagen (Beech, 1972).

2.2.3.1- Glass Ionomer Cements (GIC)

Wilson and Kent made a major development by taking polyacrylic acid and mixing it with an ion leachable glass (Wilson and Kent, 1972). The resultant product was given the name aluminosilicate polyacrylate (ASPA) or glass-ionomer, which was a hybrid of the dental silicate cement and the carboxylate cement. Ever since its introduction, Glass Ionomer Cements (GIC) has received a mixed response from the world of clinical dentistry. On one hand it is acknowledged for its ion exchange adhesion and continuing fluoride release (Wilson, 1989; Smith, 1998), but on the other it is subjected to criticism due to its lack of physical strength and translucency (Crisp *et al.* 1976; Mount and Makinson 1982; Mount and Hume, 1998; Mount, 1998). The matrix of glass ionomer cements not only release fluoride but also have the ability to absorb fluoride from a high concentration aqueous medium (Forsten, 1998).

Various modifications have come up which have better characteristics. These modifications are, use of acrylic/maleic acid as the poly acid component (Nicholson, 1998), use of dried polymer powders blended with the glass and activated by the addition of water (Prosser *et al.,* 1984), development of cermet containing cements in which the filler consists of calcium fluoroaluminosilicate glass fused to silver (McLean and Gasser, 1985), metal reinforced cements (Williams *et al.,* 1992), and resin-modified cements (Wilson, 1990).

2.2.3.2- Development of Resin-Based Composites (RBC)

Polymer resin-based composites have become one of the most significant advanced materials used in the area of engineering, biomedical and broad-spectrum dental applications (Babu *et al.,* 2005). After the rejection of silicate-based composites, acrylic resins were used because of their tooth-like appearance, insolubility in the oral fluid, ease of manipulation and low cost. The current trend towards “minimally invasive dentistry” and in response to the growing patient demand for aesthetics, resin composites is the material of choice for restoration of anterior teeth (Yoshida *et al.,* 2002). Traditionally, the dental composites used for direct aesthetic restorations consist

of mainly polymer matrix and dispersed reinforcing inorganic filler particles (FDA, 1998).

Adhesive dentistry has evolved remarkably, greatly due to development, in the late 1950s, of methacrylate monomer, Bis-GMA and an organic silane-coupling agent (Braga *et al.,* 2005). This resin enables the formation of bonds between filler particles and resin matrix (Braga and Feracane, 2004). Composite materials are well suited for repair of damaged tooth and decayed structures because in addition to an aesthetic appearance, they can easily be accepted for a wide variety of direct placement application and be bonded chemically to the tooth (Stansbury *et al.,* 2005). The other advantage of using composites is that the need to remove only the infected irreversibly deteriorated tissue, not the additional tissue (Park and Robertson, 1998).

However, dimethacrylate are commonly used in dental composite but due to their brittle nature, they are susceptible to fracture and wear during mastication in the oral environment (Kerby *et al.,* 2003). Microscopic and nano-filler particles are easily mixed with dental resins to a high proportion due to their high surface area and are widely used in dentistry (Arcis *et al.,* 2002; Moszner and Klapdohr, 2004).

2.2.3.2.1- Composition

Dental composites mainly consist of an organic matrix loaded with a finely dispersed glass or silica filler that is bonded to the matrix polymer through a silane coupling agent (Yashida *et al.,* 2002). The matrix/filler interaction can be induced by the impregnation of filler particles on surface of resin with a bifunctional coupling agent (Palin *et al.,* 2003; Arcis *et al.,* 2002).

Resin Matrix

Resins contain a modified methacrylate or acrylate and are a blend of aromatic and aliphatic dimethacrylate monomer, the oligomers; Bis-GMA and UDMA, together with triethylene glycol dimethacrylate (TEGMA), added to control the viscosity. Bis-GMA is

a major monomer in the resin, it is a viscous, bulky bifunctional monomer and has a high reactivity, high molecular weight, and undergoes low polymerisation shrinkage. To overcome its high viscosity some low molecular weight diluents monomer such as TEGMA must be added. It has been reported that an increase of TEGMA/ Bis-GMA ratio in a resin composite will lead to a more favourable viscous flow property (Feilzer and Dauvillier, 2003).

Filler Particles

The material properties of filler particles in a resin matrix depend on type of filler particles, concentration, size of particles and their distribution. Commonly used fillers are quartz, fused silica, and glasses like alumino-silicate, boro-silicate and barium oxide. Some composites contain large (macro-fillers, 20-30 μm) spherical, irregularly shaped, micro-fine (0.04-0.3 μm) and fine (0.4-3 μm) particles and the blend of fine and mirofine (hybrid) particles (McCabe and Walls, 1998; Anusavice, 2003).

The filler geometry and shapes are likely to present distinct surface area, which affects the amount of resin matrix in the interfacial region between particles (Turssi *et al.,* 2005). It is established that nano-particles can improve general properties such as adhesion, aesthetics, and elastic moduli of the resin based composites (Silikas *et al.,* 2007).

Coupling Agents

The significance of a coupling agent is to form bonds between organic flexible oligomers and inorganic fillers and allow the transfer of stress from their matrix to higher modulus filler particles (Halvorson *et al.,* 2003). Titanates and Zirconates can be used as coupling agents but the most common coupling agents are organosilanes such as γ-methacryloxypropyl trimethoxysilane (Anusavice, 2003). It improves the distribution and stress transmission from flexible resin matrix to the stiffer and stronger inorganic filler particles (Calais and Soderholm, 1998).

Activator-Initiator System

Generally in dental materials, polymerisation is initiated by free radicals and these free radicals can be generated either by chemical activation or by external energy activation (heat, light, or microwave). Chemical activation can be initiated by an organic amine (catalyst) reacting with an organic peroxide to produce free radicals, which attack the carbon double bond causing polymerisation. Light activation is accomplished with visible blue light system with a peak wavelength of 460-470 nm. It produces an excited state of the photosensitiser (camphorquinone) which reacts with amine to form free radicals that initiate polymerisation. Amines, such as ethyl p-dimethylaminobenzoate (DMBA) or *N, N*- dimethylaminoethyl methacrylate (DMAEMA) are used as accelerators and form initiating radicals via proton and electron transferring (Moszner and Klapdohr, 2004).

2.2.3.2.2- Properties

Mechanical Strength

The mechanical properties depend upon the filler content, the type of filler, the size of filler particles, the efficiency of filler-resin coupling process and the degree of porosity in polymerized materials. It also depends on the reinforcement effect of polymer by fillers (Alberola *et al.,* 1999; Adabo *et al.,* 2003).

Physical Properties

Polymerisation Shrinkage

Dental composite polymerisation shrinkage ranges between 2 to 6 % by volume (Labella *et al.,* 1999). Factors which contribute to their shrinkage reduction are: larger monomer and comonomer molecules and additional filler. Bis-GMA has lower polymerisation shrinkage than methyl methacrylate and TEGMA. The more the Bis-GMA is replaced by TEGMA, the higher the composite shrinkage (Feilzer and Dauvillier, 2003). Shrinkage also causes stress on the tooth substance. These strains can severely affect the

interfacial bond between composite and the tooth (McCabe and Walls, 1998; Craig and Power, 2002). One of the problems associated with composite material is its marginal leakage due to shrinkage during curing. This leads to formation of a gap and the consequent problems of marginal staining and secondary caries. This problem can be improved by the application of a dentine bonding system which increases adhesion between the material and tooth structure (Kohler *et al.,* 2000).

Water Sorption

The major disadvantage of current resin based composites is the sequence of dimensional changes during and following placement and constantly interacting with surrounding environment. The principal interaction occurs with water which diffuses into the matrix (Martin and Jedynakiewicz, 1998). The absorption of water by composite resin is dependent on the matrix resin, filler and the properties of interface between the matrix and the filler. Mechanical properties such as strength are affected by water sorption into the resin (Asaoka and Hiranno, 2003).

2.2.3.2.3- Limitations of Bis-GMA

The main disadvantages of Bis-GMA resin are its significant water absorption, high viscosity and incomplete polymerisation, which means some monomer still exists in the material after polymerisation. It is suggested that the glycidyl methacrylate reacts with bisphenol A and a tertiary amine used to catalyse the addition of phenolic hydroxyl group to the epoxide groups. After poorly purified reaction some unreacted monomer i.e. both glycidyl methacrylate and bisphenol A remains there and causes allergic effects (Soderholm and Mariotti, 1999). Bis-GMA based resins shows final double bond conversion of only 55-75%. The incomplete conversion of dimethacrylate system is due to complex diffusion controlled reaction mechanism. With the progression of reaction, both the termination and propagation reactions become diffusion limited. During the polymerisation of methacrylate-based monomer, unreacted monomer molecules are incorporated into the polymer chains as units containing pendant C=C double bond.

With the increase in reactivity of pendant C=C bonds, cyclisation (intramolecular crosslinking) and formation of high density region or mirogels occurs. Further reaction occurs by chemical bonding of the microgels leading to agglomeration and increase in heterogeneity of the polymer system. These factors lead to decrease in cross-link density and promote the water absorption and possible hydrolytic degradative reactions (Elliott *et al.,* 2001; Sideridou *et al.,* 2003). There are certain disadvantages associated with incomplete polymerisation. The release of unreacted monomer may stimulate bacterial growth around the restoration and promote allergic reaction. The unreacted monomers act as plasticiser, reducing the mechanical properties and increasing swelling (Hansel *et al.,* 1998).

2.2.3.2.4- Urethane Derivative Resins

Over the period of time, some new components have been introduced in dental composite materials. Urethane derivatives (UDMA) have been studied with Bis-GMA (Labella *et al.,* 1994) and they form weak hydrogen bonding but have a high cohesive energy density. This resin is comparable in size with Bis-GMA but differs in its chemical structural features which affect critical properties such as viscosity, diffusity, polymerisation shrinkage, water uptake, physiochemical and mechanical properties. These derivatives have much lower viscosities and water uptake than Bis-GMA and exhibit higher conversion of vinyl group without increasing (and perhaps decreasing) polymerisation shrinkage of dental resin systems. Due to urethane group UDMA is known to form weaker hydrogen bonds with water molecules than the hydroxyl groups of BisGMA and TEGDMA molecules reducing the hydrophilic nature of the constituent monomer units (Palin *et al.,* 2005).

It has been investigated that UDMA has shown better tensile properties, faster and more complete conversion, and its lower viscosity allows its use without low viscosity diluents (Gohring *et al.,* 2005). Palin *et al.,* (2003) reported that on curing, decreased volumetric shrinkage of resin composites can be achieved if the composite system does not contain dimethacrylate monomers. Research on polyurethane and its potential application in dentistry has been studied as facial prosthesis and is based on its inherent

environmental stability, high tear resistance, and low modulus without the use of plasticiser, and good ultimate strength and elongation. This material can accept intrinsic colouring and are amenable to maxillofacial processing techniques (Tang *et al.,* 1975; Goldberg *et al.,* 1978; Labella *et al.,* 1994). Polyether based impression material have been used in restorative dentistry to record intra-oral structure for fabrication of definitive restorations (Donovan and Chee, 2004).

2.3- Polyurethane

Polymeric materials have been used in medical and surgical applications, often in situations, where they are in direct contact with living tissues (Rehman, 1996). Polyurethane forms a versatile class of polymers and is one of the most interesting classes of synthetic elastomers that have unique properties, which are used in a broad range of applications due to their better physical properties and biocompatibility (Bouchemal *et al.,* 2004). It is established that polyurethane has functions to improve cell growth and proliferation, and controllable degradation kinetics. This material has been used as a biomaterial for hard and soft tissues due to its tailor made mechanical properties (Bonzani *et al.,* 2007). It comprises a class of materials which can vary from rubbery to glassy thermoplastics and from being a linear polymer to being a thermoset (Ho *et al.,* 1999; Hsieh *et al.,* 1999). Traditionally, polyurethane elastomers have been regarded as materials with relatively high cost and needing special technical expertise to successfully manufacture products (Hepburn, 1992).

2.3.1- History of Polyurethane

Polyurethane is a group of polymeric material first produced and investigated by Dr. Otto Bayer in 1937 (Frisch, 1981). It is a polymer in which the repeating unit contains a urethane moiety. In the mid-1950s, rigid foamed polyurethanes were implanted for bone replacement and as bone adhesives; soft foams for heart valves, suturing rings, vascular grafts and catheter cuffs (Brenda, 1992). The medical community and polymer research groups have produced polyurethanes with a wide

range of properties and have shown that there are different techniques to modifying and fabricating different compositions to achieve exact requirements (Rehman, 1996). A great deal of attention has been given to the synthesis, morphology, chemical, and mechanical properties of this family of materials (Kuan *et al.,* 2005).

2.3.2- Structure of Polyurethane

The properties of polymeric materials depend on the molecular characteristics and morphology at both the micro- and macroscales. Molecular parameters such as the molecular weight (averages and distributions), molecular architecture (linear, branched, crosslinked, blocks or grafts and tacticity), copolymer composition and distribution (blocks and branches), and residual concentrations of low-molecular-weight materials are significantly influenced and can be controlled in the polymerisation process (Šebenik *et al.,* 2003). The group of polyurethane comprises all polymers that contain urethane, urea or other isocyanate-derived group, even if they are only a minor part of the total structure (Howard, 2002).

Currently the polyurethane industry is based on the use of intermediates which themselves are polymeric in nature such as polyester and polyether with terminal groups (usually –OH or –NCO), which are capable of further reaction and to increase molecular size by chain extension. These polyurethane elastomers are essentially copolymers such as polyester urethanes or polyether urethanes (Zia *et al.,* 2008).

Polyurethane elastomer can vary in properties over a very wide range of strength and stiffness by modification of the three basic building blocks: the polyol (B-B), diisocyanate (A) and chain extender (C) as shown in Figure 2.2. They can be explained as block copolymers in which one block of the polymer chain consists of a relatively long flexible ‘soft segment’ (B-B), derived from a hydroxyl-terminated aliphatic polyester, polyether or polyalkene, with a molecular weight between 500-5000. The second, stiff, highly polar block of the copolymer, commonly known as ‘hard-segment’ is formed by the reaction of diisocyanates (A), with low molecular weight diol of diamine chain extender (C).

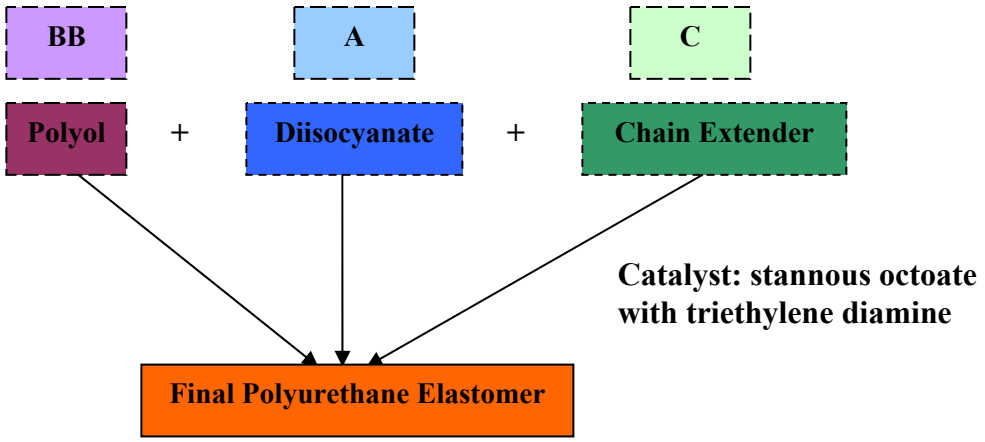

Figure 2.2 Process for polyurethane elastomer preparation

2.3.3- Synthesis of Polyurethane

The complex chemistry of polyurethane has provided various techniques for its synthesis. Generally polymers are synthesis by two main methods.

a) Addition polymerisation

b) Condensation polymerisation

In addition polymerisation, the double bond of the monomer molecule is broken down to initiate the reaction with formation of free radicals. Polyurethane polymerisation contains features of both addition and condensation polymerisation (Rehman, 1996; Lamba *et al,* 1998).

2.3.3.1- One Step Process

One-step process is the simplest and quickest process. A di- functional or multi-functional isocyanate and diol are mixed together and allowed to react. An elastomeric

material is formed with a slightly cross-linked structure and basically a random distribution of monomer units along the chain (Lamba, 1998).

2.3.3.2- Two-Step Process

A two-step process provides better control over the chemistry of the reaction, the structure, physical properties, reactivity and processability, therefore it is the preferred method. In the first step a pre-polymer is formed from di-isocynate and di-hydroxy compound. Usually the prepolymer has low molecular weight and can be stabilised with 0.01 to 0.1% acid chlorides. In the second step the prepolymer reacts with a diol or diamine chain extender to produce a multi-block co-polymer. Thus, if the reagents are di- or polyfunctional, polymer formation can take place. It should be noted that in most reactions the particular advantage is the lack of by-products requiring removal (Rehman, 1996; Lamba, 1998).

If the reactants are bi-functional then the result would be linear products but higher functionality results in the formation of branched chain or crosslinked materials. Additional reaction of the isocyanate with the urea, urethane and amide groups produced by the initial polymerisation is also possible (Hepburn, 1992). To achieve a soft, flexible and pliable film, it is important to have a linear polymer. Some other reactions can occur during the synthesis of polyurethane. The major side reactions are trimerisation, dimerisation, carbodiimide, biuret and allophanate formation (Hepburn, 1992). These side reactions change the initial stoichiometry of the extension and thereby limit the final molecular weight and yield branched or even crosslinked polymers (Dusek, 1987). Li et al. (1998) has reported the synthesis of polyurethane with different ratios of polyols, isocyanates and chain extender and found variation in the values of mechanical properties by using the change in the ratio of chain extender. Figure 2.3 shows the schematic structure of polyurethane formation with urethane and urea linkage.

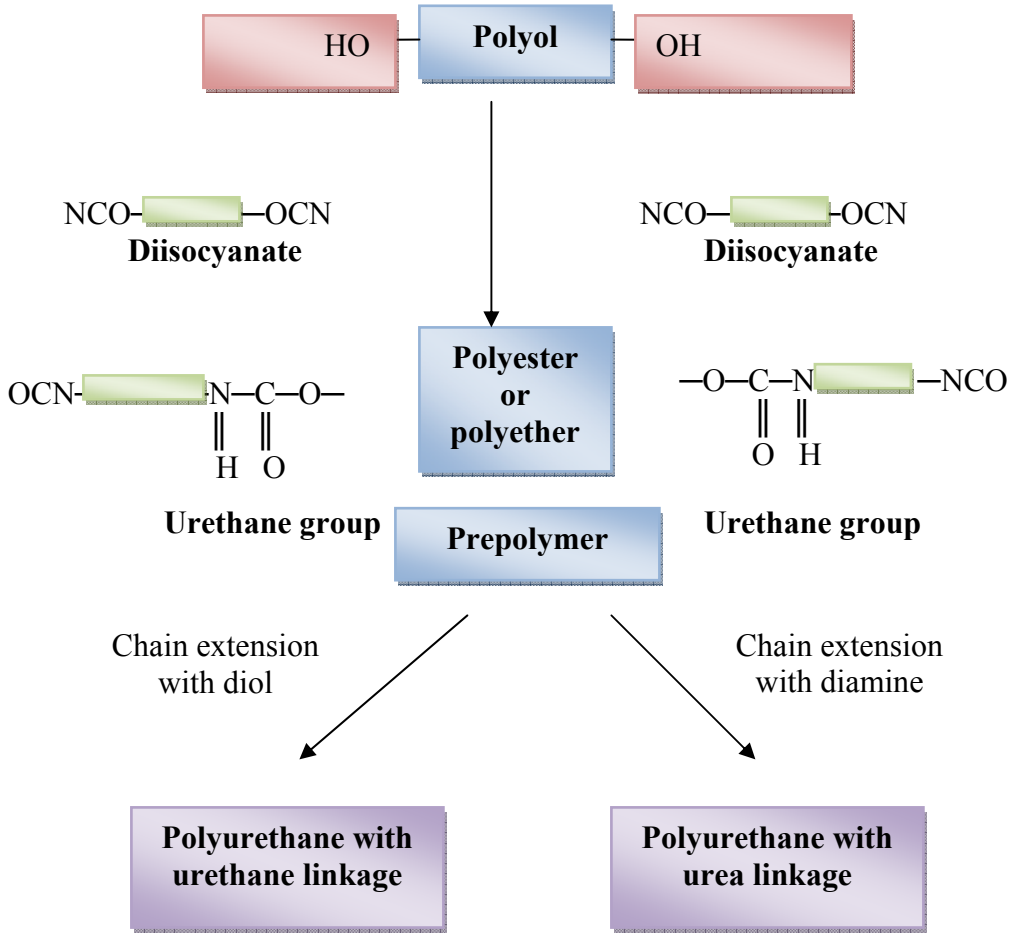

Figure 2.3 Schematic diagram of polyurethane formation with urethane and urea linkage

2.3.4- Types of Polyurethane

The main type of polyurethane is segmented polyurethane (phase separated, thermoplastic).

2.3.4.1- Segmented Polyurethane

The segmented polyurethane elastomers can vary their properties over a wide range of strength and stiffness by modification of their three basic building blocks. This concept of molecular tailoring introduces units giving the required mechanical and physical

properties. It has been widely used due to their good biocompatibility and biomechanical and desirable physical properties (Mathur *et al.,* 1997; Christenson *et al.,* 2005). The combination of high biocompatibility and the wide variety of physical and chemical properties that can be achieved make this polymer very interesting for the biomedical field (Heijkants *et al.,* 2005). The properties of segmented polyurethane depend on the structure of hard and soft segment, length and concentration, as well as the interaction of both phases. Hard segment consists of glassy or crystalline domain and soft segment domain consists of continuous amorphous structure. Due to the incompatibility of these two domains, these materials are generally of a two-phase morphology. The domain between hard and soft segment is due to hydrogen bonding between the oxygen of the soft segment and N—H group of urethane (Wang, 2005).

The hard segment domains provide rigidity and mechanical strength, whereas, soft segment domains impart elastomeric properties i.e. extensibility and resilience. Hard and soft segment structure, molecular weight, crosslinking and poly-dispersity in either phase influence micro-phase separation in these copolymers. Phase separation is primarily responsible for their good mechanical properties. Even many physical properties of these elastomers are due to this micro-phase separation (Rutnakornpituk and Ngamdee, 2006)**.** Therefore, it has been studied that quantitative and qualitative evaluation of degree of phase separation and certain factors such as molecular weight, chemical structure and functionality of components and hydrogen bond between segments affect the phase-separation of the polymer (Jung *et al.,* 2000; Adhikari *et al.,* 1999; Rosthauser *et al.,* 1997). It has been experimented that the length of soft segment heavily influences their crystallinity and the phase separation in the soft domain. The phase separation was enhanced with an increase in soft segment length (Wang, 2005).

2.3.4.1.1- Hard Segments: Isocyanates

The rigid segments are usually formed by the reaction of diisocyanate with a glycol or diamine. They are low molecular weight polyurethanes and their properties determine the inter-chain interactions in the elastomers to a large extent. The effects of increasing

hard segment at constant soft segment molecular weight are; higher crystallinity, higher crystalline melting point due to the thick lamella possible with harder soft segment, increase in glass transition temperature, and increase in hardness and tensile strength (Hepburn, 1992; Adhikari *et al.,* 1999; Jung *et al.,* 2000).

Commonly used diisocyanates are:

1-Aromatic Diisocyanate

- Diphenylmethane-4-4'-diisocyanate (MDI) } Most Common
- Toluenediisocyanate (TDI) }
- *p*-Phenylene diisocyanate (PPDI)
- 1,5-naphthalene diisocyanate (NDI)
- 4,4',4'-triphenyl methane triisocyanate (TMDI) → triisocyanate

2-Aliphatic Diisocyanates

- 1,6-hexamethylene diisocyanate (HDI)
- 1,6—hexamethylene diisocyanate, isophorone diisocyanate (IPDI)
- 4,4'- dicyclohexyl methane diisocyanate (H_{12}MDI)
- 1,4-cyclohexane diisocyanate

Aromatic Diisocyanates

MDI and TDI have bulky or hindered structures; to some extent their stereo configurations thus limit linearity in the polymer chain, which is an essential feature of strength, and elasticity in all rubber like materials. Polyether based elastomers show higher values of hardness, modulus, tensile strength and tear strength with an increase in the ratio of MDI, but the elongation at break decreases (Hepburn, 1992). MDI based polyurethane is typically chain extended with 1,4-butandiol to form polyurethane elastomers containing almost exclusively urethane linkages. TDI based polyurethanes are usually chain extended with aromatic diamines to form polyurethanes that contain both urethane and urea linkages. MDI prepolymers are not normally extended with diamines due to their higher reactivity compared to TDI-based ones

(Adhikari *et al.,* 1999). Aliphatic diisocyanates are less reactive than aromatic diisocyanates. The relative reactivity of the various diisocyanates is given below: (Rehman, 1996).

MDI:	NDI:	CHD:	IPID:	HDI:	H_{12}MDI
1.00:	0.37:	0.28:	0.15:	0.14:	0.13

Currently polyurethane elastomers based on MDI and TDI have property limitations, such as: (Hepburn, 1992).

- Rapid reduction in time dependent properties of set and creep, at elevated temperature, e.g. above 120˚C
- Relatively poor hydrolysis resistance at high temperature

Aliphatic Diisocyanates

To overcome these limitations, some new developments in the diisocyanate field have been introduced, such as aliphatic diisocyanate and also some more rigid, rod like structure such as that of paraphenylene diisocyanate (PPDI). Cyclic diisocyanate e.g. H_{12}MDI generally produce polyurethanes of higher strength and thermal stability to those of the straight chain aliphatic diisocyanate (HDI, IPDI, TMDI). Aliphatic isocyanates have also been seen to show increased phase separation behaviour over aromatic isocyanates. Glass transition of aliphatic isocyanates such as HDI, H_{12}MDI and IPDI are lower than that of aromatic isocyanates systems. This attributes to strong hydrogen bonding being obtained in the hard segment domain (Hepburn, 1992). H_{12}MDI, used as a building block for polyurethane elastomer requires light stability and resistance to hydrolysis. This group of diisocyanates is supplied as a mixture of three geometrical isomers (Adhikari *et al.,* 1999): trans, trans isomers, cis-trans isomers, cis, cis isomers. Usually IPDI is a mixture of 28% trans and 72% cis isomers, while H_{12}MDI commonly contains 65% cis-trans, 30% trans-trans and 5% cis-cis isomers. The limitation of cycloaliphatic diisocyanate is higher cost than those of their aromatic analogues by factor of 3-4 (Hepburn, 1992; Adhikari *et al.,* 1999). It is expected that the diacylisocyanate might be a good substitute for regularly used diisocyanates. Heijkants et al. (2005) suggested that these compounds have activated isocyanate groups due to

the neighbouring carbonyl group, which makes these compounds much more reactive towards hydroxyl groups and thus very suitable for chain extension without a catalyst. It is concerned that the resulting polymers hydrolyse relatively fast and are expected to release terephtalamide and/or terepthalic acid upon degradation, which is considered to be non-toxic.

2.3.4.1.2- Soft Segments: Polyols

Polyols used for the synthesis of polyurethanes are hydroxyl terminated and their characteristics such as molecular weight, molecular structure, and functionality control the properties of resulting polyurethanes (Rehman, 1996). The usage of macromolecules such as polymeric analogues of simple diols, leads to extremely tough, elastomeric materials with many applications. Polyesters and polyethers are the most common materials as these flexible segments, latterly; polycaprolactones have also been used with them (Brenda, 1992). For the synthesis of elastomers, polyols are available in the range of 600-2000 molecular weight. They are typically based on polytetramethylene glycol for polyether series or polyethylene glycol adipate for the polyester series. However, it was observed that when single linear polyols are used in elastomer production the resulting elastoplastic or rubber often hardens in storage due to *in-situ* crystallisation (the cold hardening phenomenon). To avoid this, it is common to add a small proportion, ca 5-10% of a branched polyols into linear polyols (e.g. polypropylene glycol adipate for the polyester series or polyoxypropylene glycol for the polyether series) to suppress the cold hardening (Hepburn, 1992):

Commonly used polyols are;

- Polyether such as poly (tetramethyleneoxide)
- Polysiloxane such as poly (dimethylsiloxane)
- Polyester such as poly (ε-caprolactone)
- Hydrocarbon based polyols such as polybutadiene

Polyether

Polyethers have been used as flexible blocks in the synthesis of polyurethane elastomers. Polyether diols are synthesised by the addition of alkylene oxides (ethylene oxide, propylene oxide) to diols, polyols or di- or polyamines, and by ring opening of tetradydrofuran. The polyether polyurethanes with relatively good physical properties are polytetramethylene oxide (PTMO) and hydrogenated polybutadiene and polyisobutylene based polyurethane (Rehman, 1996). They have weaker inter-chain interactive forces than polyesters, and subsequently give elastomers of decreased physical properties at low temperature. Linear polyethers produce higher strength but are expensive elastomers. However, It is reported that polyether type polyols possesses relatively better physical strength, abrasion resistance, water resistance, fatigue life, and biocompatible character (Liu *et al.,* 1997). Branched polyethers are cheaper but they produce weaker materials. These branched polyethers are generally polyoxypropylene glycols, the ether linkage is poly (ether-urethane) is resistant to hydrolysis and so these are used where hydrolytic stability is essentially required.

$HO - [(CH_2)_4 - O]_n - H$ (poly (tetramethylene-ether)glycol) → higher strength

$$HO - [CH(CH_3) - CH_2 - O]_n - H$$ (poly (oxypropylene)glycol) → lower strength

Polyether urethanes are hydrolytically stable yet are subject to oxidative degradation in various biomedical applications in the presence of metal ions (Tanzi *et al.,* 1997; Jayabalan *et al.,* 2000). The α-carbon of the polyether soft segment of the polyether polyurethane is highly susceptible to oxidation by oxygen radicals to form esters. In order to reduce the oxidation of the soft segment, antioxidant additives have been used. Another method to protect the polyether soft segment from oxidative cleavage is endcapping with PDMS; it creates a dimethlysiloxane-rich surface due to the high mobility of these endgroups, which imparts hydrophobic character to the polymer. Hydrophobic PDMS end groups protect the polyether soft segment from oxidative cleavage and provides in-*vivo* biostability by retarding hydrolysis (Mathur *et al.,* 1997).

Poly (dimethylsiloxane)

To enhance the biostability of the soft segment, modifications and substitutions have been made. The chemistry of soft segments has been substituting by using the polyether segment with a polybutadiene, polydimethylsiloxane (PDMS), polycarbonate and aliphatic hydrocarbon (Mathur *et al.,* 1997).

Polydimethylsiloxanes emerge as molecules with the potential to affect the surface properties of polymers to which they have been blended or copolymerised. This characteristic of low surface energy allows the siloxane segment to migrate to the top surface of the polymer interface and provide a very hydrophobic surface (Rehman, 1996). Siloxane polymers have unique properties of oxidative and hydrolytic stability, a wide service temperature range due to a low glass transition temperature (-123°C), low moisture permeability, and low surface energy. The interest in incorporating polyurethane with siloxane segment is to impart such properties to polyurethane, and to improve some inherent poor properties of siloxane polymers such as tear, abrasion and tensile strength. It has been identified that the problem associated with synthesising silxoane polyurethane is the incompatibility of the non polar siloxane segment with polar urethane hard segments, which resulted in polyurethane with poor mechanical properties; this was attributed to weak interfacial adhesion (Adhikhari *et al.,* 2000). Various studies (Adhikhari *et al.,* 2000; Vaidya and Chaudhury, 2002; Simmons *et al.,* 2004) demonstrated that when a small amount of second macrodiol (comacrodiol) such as poly (hexamethylene oxide) (PHMO) was incorporated as a part of soft segment along with PDMS, the compatibility of the siloxane soft and urethane hard segments could be significantly improved, which helps to strengthen the interfacial region. This enabled the synthesis of a new family of siloxane polyurethane elastomers with good mechanical properties, flexibility and biostability with relatively low hardness, tensile and flexural moduli.

Polyesters

Polyesters are prepared by polyesterification of dicarboxylic acids with diols. If a linear polymer segment is required then usually adipic acid, phtalic anhydride, sebacic acid,

oxalic acid, maleic acid or deimerised linelic acid are reacted with diols such as ethylene glycol, 1,2-propylene glycol, butylenes diol and hexylene diol. Polyesters derived from ε-caprolactone and hydroxyl-terminated aliphatic and cycloaliphatic polycarbonates have also been widely used in synthesis of polyurethane (Brenda, 1992).

It is mentioned that 90% of commercial polyurethanes are polyester based because they possess very high tensile strength, tear strength and abrasion resistance; they are low cost and can be easily fabricated (Oprea and Oprea, 2002).The main disadvantage of using polyester soft segment for the production of polyurethane is related to its hydrolytic stability. Experimental findings show that these polyurethanes should not be used for medical applications, due to their hydrolytic degradation when implanted in the body even for the short period of time (Tanzi *et al.,* 1997; Jayabalan *et al.,* 2000). However, this hydrolytic instability may be used to an advantage in the production of biodegradable materials. Generally, ester type polyols of high molecular weight crystallise at ambient condition. Polyester polyurethane loses the ability to crystallise for short segment length, due to steric hindrances. Branched polyols do not crystallise and their pendant bulky groups provide the thermal stability and steric hindrance for hydrolysis reaction of the ester group (Kim *et al.,* 2005).

Polycarbonate

Polycarbonate urethanes do not present ether linkages in their soft segment and currently appear to represent a new generation of more biostable elastomers. It is suggested that polyether urethanes and polycarbonate urethanes both shows better *in-vivo* and *in-vitro* chemical stability compared to polyester urethanes However, the mechanical properties of polycarbonate will be less affected as the macromolecular modifications were less pronounced in this polymer than in polyether (Tanzi *et al.,* 1997).

Thermal Behaviour of Polyols

The thermal behaviour of polyurethane elastomers is primarily described by the glass transition temperature (T_g) of the soft segment. This is not only influenced by the nature

of the soft blocks (usually polyethers have lower T_g than polyesters) but also by the degree of phase separation between hard and soft blocks. It was observed that the T_g of soft segments shifted to higher temperature as the molecular weight decreased. This is indicative of restriction of mobility upon the soft segment as phases become compatible at lower molecular weights (Tien and Wei, 2002).

Physical/Mechanical Properties of Polyols

The physical properties of polyurethanes are also considerably influenced by the molecular weight of the soft segment. With the increase in molecular weight (550-2000) hardness, tear strength and modulus decrease, while elongation at break increases. With an increase in molecular weight of soft segments at a fixed hard segment there is decrease in the tensile strength of the material. Ultimate tensile strength exhibits an optimum between a molecular weight of 830-1250 (Hepburn, 1992).

2.3.4.1.3- Chain Extenders

These monomeric additives in the synthesis of polyurethane may be difunctional substances such as diols or diamines, or polyfunctional, usually triols, quadrols, or polyamines. The formers are generally called chain extenders or curing agents, the latter are often called crosslinking or branching agents. The chain extension process has a significant influence on molecular weight growth of the polyurethane (Jhon *et al.,* 2001). The most important in this group are aliphatic and aromatic diols and diamines. Common chain extenders are;

1. Aliphatic diols; 1,2-ethane, 1,3-propane, 1,4-butane, 1,6-hexanediol
2. Aliphatic diamines; 1,2-ethane, 1,3-propane, 1,4-butane, 1,6-hexanediamines
3. Cyclic and Aromatic diamines

The selection of chain extender has an influence on the final properties of the resulting polymers. Aromatic extenders produce stiffer polyurethane compounds compared to aliphatic extenders. But if an aromatic diisocyanate is used with urethane and carbamate linkage then thermo-hydrolytic degradation of this linkage leads to cleavage forming

highly toxic aromatic dianilines (Jayabalan *et al.,* 2000). It is evidenced that the number of carbon atoms in the extender has a major influence on the structure of the hard segment and effect on properties like the degree of phase separation, melting point and strength of the final polymer. If the chain extender contains an even number of backbone carbon atoms, the hard segment can crystallise easier than when the number is odd (Rehman, 1996).

2.3.4.1.4- Others

Crosslinkers are low molecular weight compounds, containing active hydrogen and tend to increase the modulus and hardness of polyurethane. Certain additives such as catalysts, surfactants, fillers and plasticisers can be formulated into the polyurethane.

2.3.5- Properties of Polyurethane

Polyurethanes have a wide range of material properties attributed to the large variety of possible morphologies that may exist in the polymer (Chiou and Schoen, 2002). Polyurethanes based on polyether or polyester soft segments and a diisocyanate-based hard segment are known as tough materials and are usually used as an additive to enhance toughness of brittle materials as well as the thermal properties (Njuguna and Pielichowski, 2004).

2.3.5.1- Hydrogen Bond

Hydrogen bonding (H-bonding) plays an important role in determining the morphology and overall properties of polymers such as polyamides, polyurethanes, polyurethane-urea and other polymers, which have pendant functional groups capable of forming hydrogen bonding, such as polyvinyl alcohol, ploy (acrylic acid), polyhydroxyethers and their copolymers (Yilgor *et al.,* 2000). It has been accepted that properties of polyurethane are primarily due to the two-phase structure i.e. hard and soft segment, which is closely related to the relating H-bond. Polyurethane undergoes micro-phase separation resulting in hard segment domains, soft segment matrix and urethane bonded

inter-phase. Different polyurethane systems have different H-bond pattern due to incompatibility between hard segment and soft segment. The primary driving force for phase separation is the strong intermolecular interaction of the urethane units, which ultimately form intermolecular hydrogen bonding. The interconnected or isolated hard segments are distributed in the soft segment matrix, though the hard segment dissolve in the soft segment, which is evident from the hydrogen bonding of the urethane NH groups with the oxygen of the ether or ester linkages (Njuguna and Pielichowski, 2004; Ren *et al.,* 2003). The inter chain hydrogen bonding exerts strong influence on the rheological behaviour of polyurethanes (Pattanayak and Jana, 2005). The hard segment is derived from aggregation of urethane units through strong hydrogen bonding and is either glassy or semi-crystalline (Tien and Wei, 2002). It is speculated that for polyether based polyurethanes extended by diols have four types of H-bonding interaction patterns, since the urethane group (-NH—CO (O)-) provides one H-bond donor and three possible acceptors, and another acceptor of the ether oxygen from soft segment. The four types of H-bonding patterns are considered to be formed between the NH group and C=O group (type 1), urethane alkoxy oxygen (type 2), NH group to form (NH**….** NH) (type3) and ether C—O—C group (type 4). The first three types deal with the urethane-urethane linkage, while the last one concerns the interaction with urethane-soft segment (Ren *et al.,* 2003).

2.3.5.2- Physical Properties

The polyurethanes exhibit a broad range of physical properties, due to a variety in selecting the chemistries and molecular weight of the various components, and the ratios in which they are synthesised. The range of properties varies from very brittle and hard materials to soft, tacky and viscous materials (Lamba *et al.,* 1998). In polyurethanes, the unique elastomeric properties are observed due to microdomain formation: hard domain and soft domain. The hard domain provides both physical crosslink sites and filler like reinforcement to the soft-segment matrix. The physical properties of polyurethane depend on several factors such as the morphology, composition ratio of urethane and

polyols segments, the molecular weight of the individual segments, and segmental compatibility (Rosthauser *et al.,* 1997; Kim *et al.,* 1999).

2.3.5.3- Mechanical Properties

The mechanical properties are related to crosslinking density, the concentration of polar groups, the crystallinity, and other factors. It is indicated that mechanical properties exhibit profound changes in the region of glass transition temperature and is considered as the most important material characteristic of a polymer (Liaw, 1997). Variability in molecular masses of the hard and soft segment yields the possibility to tailor mechanical properties. The hard segment content significantly affects the physical as well as mechanical properties such as the hardness, Young's modulus, and tear strength. Polymers with low contents of hard segment have a high Young's modulus; however, the increase of hard segment concentration will enable hard segment to phase separate, which leads to increase in modulus (Heijkants *et al.,* 2005; Kim *et al.,* 1999). In addition, the performance of polyurethane elastomers at elevated temperature is dependent upon the structure of the rigid segments and their ability to remain coherent at high temperature. The tensile strength of polyurethane is dependent on temperature; therefore, the material shows diverse characteristics at different temperatures. Below the glass transition temperature of the soft segment, polyurethanes behave as a plastic; above the glass transition or melting temperature, they behave as an amorphous substance. Speckhard and Cooper (1986) reported the tensile properties of polyurethane elastomers and their results suggested that the lack of soft segment crystallinity under strain and a high degree of phase separation, limit the tensile properties with non-polar soft segment, which generally shows low tensile strength. It is also speculated that the storage moduli increased with the increasing hard segment contents. As the hard segment content increased, the glass transition temperature of soft segment increased which is due to decrease of phase separation with increasing hard segment content. The physical crosslinking is responsible for the elastic behaviour of polyurethane; it is due to the existence of hard domain through hydrogen bonding (Kim *et al.,* 1999). The mechanical properties of different types of polyurethanes are shown in Table 2.2 and Table 2.3.

Table 2.2 Properties of different polyurethanes (Kim *et al.*, 1999)

Polyurethane Diisocyanates/ polyols/chain Extender	**Hardness (A)**	**Tensile Strength (MPa)**	**Elongation at Break**	**Density (g cm^{-3})**	**Glass Transition (°C)**	**Water Absorption (%)**
HMDI/PTMG/ Bisphenol-AF	78	26	13.1	1.44	-65	1.60
MDI/PTMG/ Bisphenol-AF	56	35	15.8	1.41	-57	0.56
HMDI/PTMG/ Brominated Bisphenol-AF	26	16	3.1	1.65	-56	3.06

Table 2.3 Mechanical properties of different types of polyurethanes (Adhikari *et al.*, 2000)

Polyurethane(PU)	**Elongation at break (%)**	**UTS (MPa)**	**Young's Modulus (MPa)**	**Flexural Modulus (MPa)**	**Hardness (A)**
PU-PDMS	310	10.9	49	55	87
PU-PEO	471	10.4	23.6	25.9	74
PU-PTMO	342	22.7	27	36.5	83
PU-PHMO	370	22.1	22.5	38.9	85

Table 2.2 shows polyurethane with different types of soft segments (PDMS and Polyether series: PEO, PTMO, PHMO), the hard segment was MDI and 1,4-butanediol was used as chain extender with stannous octoate as a catalyst. The mechanical properties shown in Table 2.3 reveals that PDMS has comparatively low elongation at break and ultimate tensile strength and is a stiffer material due to a high Young's modulus and flexural modulus. The incorporation of PEO made the polyurethane more elastic and soft (low modulus and hardness), the tensile strength is poorer and almost identical to PDMS. Polyurethanes based on PTMO and PHMO show better tensile strength and flexural modulus.

2.3.5.4- Thermal Properties

The thermal properties of polyurethane depend largely on its overall composition, molecular weight, hydrogen bonding and processing history (Tien and Wei, 2002). The thermal stability of polyurethanes can be enhanced with the addition of low molar mass diols used as chain extenders (Liaw, 1997).

2.3.6- Degradation of Polyurethane

It is difficult to explain the definition of degradation; however, according to the American Society for Testing and Materials (ASTM), a plastic designed to undergo a significant change in chemical structure under specific environmental conditions resulting in a loss of some properties and its application in a period of time (ASTM, D20-96). It has been noticed that polyurethane can be efficiently degraded into non-toxic water soluble oligomers by a great number of micro-organisms such as bacteria, fungi and so on, and then water soluble oligomers can be reutilised finally into energy and products of carbon dioxide and water through several metabolic procedures of micro organisms (Cao *et al.,* 2002). Variations in the degradation pattern of polyurethanes were attributed to many properties such as topology, molecular orientation, crystallinity, crosslinking and chemical composition. Crystalline regions can be formed by regularity of polymers which allows the polymer chains to pack easily. It

was observed that polyurethane degradation proceeded in a selective manner, with the amorphous structure being degraded prior to the crystalline structures. Also, the polyurethanes with long repeating units and hydrolytic groups would be less likely to pack into the high crystalline structure as normal polyurethanes, and these polymers were more readily biodegraded (Howard, 2002).

The degradation of polyurethane involves two stages; the first stage is dominated by the degradation of the hard segment, and the second stage correlates with the dissociation of the soft segment (Tien and Wei, 2002). Degradability promoted researchers to modify and produce chemical or biodegradable polyurethanes. Aliphatic polyesters have been considered as the environmental friendly biodegradable polymers. Polycondensation of a dicarboxylic acid and diol as well as hydroxycarboxylic acid can produce high molecular weight aliphatic polyesters such as poly (ethylene succinate) (PES), poly (butylenes succinate) (PBS), poly (butylenes adipate) (PBA), poly (glycolic acid) (PGA), poly (lactic acid) (PLA) (Cao *et al.,* 2002). Polyester polyurethanes from polycaprolactone diols were derived in an effort to produce biodegradable polyurethanes for use in medical field. Different polyurethanes were made containing polyester subunits of various lengths, it was speculated that there was an increase in the biodegradability of the polyester polyurethanes with an increase in the chain length of the polyesters (Howard, 2002).

2.3.6.1- Hydrolytic Degradation of Polyurethane

Hydrolysis is considered as a chemical decomposition of a substance by water and is an important degradation mechanism in the biological environment. Hetero-chain polymers, particularly those containing nitrogen and/or oxygen atoms in the main chain, are susceptible to hydrolysis (Ratner *et al.,* 2004). Depending on structure, this might be favoured by either alkaline or acidic conditions and is faster at elevated temperatures.

Rehman (1996) has reported a detailed literature on hydrolytic degradation of polyurethane and suggested that polymers hydrolysed more in alkaline conditions; the physiological temperature of body is 37°C, which is sufficient to degrade a number of

polymers by hydrolysis. Initially there is a breakage of covalent bonds and the formation of active radicals due to absorption of energy from the external source. Upon increasing the temperature, thermal degradation occurs, the vibrational, rotational, or transitional energy exceeds the activation energy required to break a carbon/carbon bond, eventually, a mixture of chain fragments of varying sizes results. Hydrolytic degradation varies over a wide range and is dependent on chemical structure of the polyurethane. Hydrolytic degradation can be ranked in the following way:

Polyester > Polycaprolactone > Polyether

There are two possible ways of hydrolytic degradation:

- The attack of water on a carboxylic link in a polyesterurethane chain to produce two shorter chains. One of these has a hydroxyl end-group (-OH) and other a carboxyl group (-COOH), which is acidic.
- Hydrolysis of the urethane linkage producing two shorter chains: one ending in an amino group ($-NH_2$), the other in a hydroxyl group (-OH).

Hydrolysis leads to chain cleavage and consequently a reduction in average molecular weight. It was found that there was development of cracks (usually deep random crack) on the surface of elastomers due to reduction of molecular weight (Rehman, 1996).

2.3.6.2- Stability of Polyurethane

With the elucidation of additives to the chemical structure of polyurethanes, biodegradation can decrease. The degradation depends on the amount of hard segment within the polymer. With the increase in size of hard segment, a greater number of carbonyl groups are integrated into secondary hard segment structures through hydrogen bonding. It is also suggested that an increase in hard segment size does lead to restrictions in mobility of the polymer chain (Howard, 2002).

2.3.6.3- Thermal Decomposition of Polyurethane

Polyurethanes are chemically complex structures and contain a variety of thermal labile groups. Among the groups, biuret and allophanate are thermally weakest links.

Dissociation of both groups generally takes place above about 110°C and is completed by about 170°C. In the process of pyrolysis, both types of materials regenerate their precursors, isocyanate and urea, in case of allophanate, urethane, and isocyanate from biuret. Thermal stability can be classified in the following way:

Urethane < Urea < Isocyanurate < Polyether

The ether group is stated to be more stable than any of these, with possible exception of the isocyanurate group, which is claimed to be stable up to 270°C (Ravey and Pearce, 1997).

Dissociation of urethane group is one of the first reactions to happen when polyurethanes are heated above 200°C. It is observed that urethane of commercially available isocyanates, primary and secondary alcohol start to decompose at 150-200°C, and proceed at a measurable rate between 200-250°C. Random bond scission occurs at the urethane linkage up to 200°C, while unzipping of polyether chain occurs in the range of 250-320°C (Ravey and Pearce, 1997). The thermal degradation of polyurethane usually initiates from the urethane bonds of hard segment, followed by oxidation of the soft segment phase. If polyurethane is based on MDI (hard segment), 1,4-BD (chain extender) and PTMEG (soft segment), the decomposition starts from MDI-BD following oxidation at β-carbon next to the ether bond of PTMEG, which then breaks C—O bond and substantially unzips the molecular chain through several stages (Tien and Wei, 2002).

2.3.7- Biomedical/Dental Application of Polyurethane

The application of medical devices depend not only on the properties of the biomaterial or biomaterials used to fabricate the device, but also on numerous other factors such as manufacturing and processing history of the material and their specific applications. Polyurethane has been successfully used as a biomaterial due to its good mechanical properties and blood compatibility, specifically as a cardiovascular implant due to high flexural endurance (Trigwell, 2005). Table 2.4 shows the multiple applications of polyurethanes in the biomedical field.

Table 2.4 Biomedical applications of polyurethane (Trigwell, 2005)

- Blood bags, closures, fittings
- Blood oxygenating tubing
- Cardiac Assist pumps, bladder, tubing, coatings
- Catheters, Endotracheal tubes
- Heart Pacemaker and Valves
- Orthopaedic splints, bone adhesives
- Synthetic bile ducts
- Vascular grafts, suture materials.
- Others

2.3.7.1- Dental Application

Research on polyurethane and its potential application in dentistry has been studied. Its application as maxillofacial prosthesis is based on its inherent environmental stability, high tear resistance, and low modulus without the use of a plasticiser, good ultimate strength and elongation. This material can accept intrinsic colouring and is amenable to maxillofacial processing techniques (Goldberg *et al.,* 1978). It has been successfully used in the fabrication of facial prosthesis (Tang *et al.,* 1975).

Polyether based impression material have been used in prosthodontics to record intraoral structures for fabrication of definitive restorations. The hydrophilic nature of these materials facilitates the contact of unset material with intraoral tissue (Ritter and Swift, 2000). Urethane monomer was introduced in 1974 as a matrix resin and exhibits less viscosity as compared to Bis-GMA. These monomers/diluent monomers have been used in composite for direct filling material or as a veneering material with filler particles. Urethane based resins (UDMA) are available as light activated materials formulated specifically for fabrication (Wakasa *et al.,* 1997; Whitworth *et al.,* 1999).

2.3.8- Polyurethane Composites

Hybrid polymer–inorganic composites are promising for a variety of applications. These composites have been widely used as fillers to improve mechanical and thermal properties of polymers and polymer composites, to decrease shrinkage and internal stresses. Better understanding of inorganic particles and corresponding hybrid polymer–inorganic composite material applications occurred when researchers realised that reduction in dimensions of particles results in the appearance of a new phenomenon that does not exist in materials with larger grain sizes (Rozenberg and Tenne, 2008). Various inert inorganic particles/fibres such as carbon nanotubes (Meng *et al.,* 2005), silver particles (Guggenbichler *et al.,* 1999), and bioglass derived glass ceramics (Bretcanu *et al.,* 2008) have been used with polyurethane to improve its biocompatibility and mechanical properties. It has been reported that various polymers such as poly-lactic acid (Bleach *et al.,* 2002), poly-glycolic acid (Calandrelli *et al.,* 2000), poly-ε-caprolactone (Choi *et al.,* 2004), polyethylene (Wang and Bonefield, 2001), polyetheretherketone (Abu Bakar *et al.,* 2003), and polyurethane (Liu *et al.,* 1998; Chetty *et al.,* 2008) were used with HA as composite materials.

2.3.8.1- Chemical Linkages in Composites

Organic–inorganic hybrids have recently emerged as a new class of material. If the inorganic phase is nano-sized then homogeneous dispersion in the organic matrix can be achieved. Organic–inorganic hybrids were used to design and synthesise nano order organic–inorganic composite materials. The mechanical bond between the filler and polymer matrix is relatively weak, subsequently interfacial debonding will occur which will lead to cavitation around the reinforcing filler particles (Friedrich and Karsch, 1981). Chemical linkage has been used to improve the stability of interface. Silane coupling agents have been used in dentistry for chemical linkage; however silanes are not ideal for coupling with materials like hydroxyapatite (Deb et al., 1996). The interface adhesion of HA particles and polymer matrix plays a very important role among the major factors affecting properties of composites (Liu *et al.,* 1996; Hong *et al.,* 2005). When nano-particles (nHA) and polymers form a composite,

provided that homogenous dispersion of nano-particles is achieved at microscopic level, the mechanical properties are expected to improve and/or new unexpected features might appear (Liu *et al.,* 1997). The bioactive HA should be incorporated with organic polymers for potential applications because of its biocompatibility and bioactivity which can initiate the osteogenesis and its similar chemical composition, structure and mechanical properties to human bone/tooth (Ajayan and Tour, 2007; Zhao and Zhang, 2008).

Isocyanates are very reactive chemicals and are known for their role in producing polyurethanes. If isocyanates could be used as a coupling agent then it could lead to chemically linked polyurethane composite. Liu et al. (1996) and Dong et al. (2001) studied the reactivity of isocyanate (hexamethylene diisocyanate) with hydroxyapatite and calcium hydrogenphosphate ($CaHPO_4$, CHP) respectively. They observed that there was a covalent linkage between isocyanate and apatites and the urethane linkage between hexamethylene diisocyanate (HMDI) and CHP, showing that the hydroxyl (-OH) groups at the surface of nHA have reactivity towards organic functional groups (Liu *et al.,* 1998). The modification could be advantageous for chemical linkage of polymer composites. The homogeneous composites in which nano-hydroxyapatite align along the polyurethane are of interest due to their inherent properties.

2.4- Hydroxyapatite

2.4.1- Introduction

The restoration of tooth structure with durable, bondable and aesthetically acceptable material is the ultimate research goal (Xu, 2003). The chemical analysis of bone, enamel and dentine exhibit calcium and phosphate as principal components and that the inorganic phase of bone and teeth are basically calcium hydroxyapatite (LeGeros *et al.,* 1995). Various calcium phosphate containing compounds have been considered as possible starting reagents for calcium phosphate cements. These cements based on tetracalcium phosphate ($Ca_4(PO_4)_2O$), monocalcium phosphate monohydrate

($Ca(H_2PO_4)_2.H_2O$), β-tricalcium phosphate (β-Ca_3 $(PO_4)_2$) and α-tricalcium phosphate (α-$Ca_3(PO_4)_2$) and octacalcium phosphate ($Ca_8H_2(PO_4)_6.5H_2O$. Octacalcium phosphate has been considered as a precursor of biological apatite crystals. Its structure stacks apatitic layers alternatively with hydrated layers and that the transition of octacalcium to hydroxyapatite is thermodynamically favoured. There is evidence of presence of ocatacalcium phosphate in the central part of a dentine crystal and apatite in the outer most layers of the same crystal. The resulting biological apatitic crystal constitute of poorly crystalline hydroxyapatite with a low Ca/P ratio, i.e. Ca-deficient hydroxyapatite containing ions such as carbonate and fluoride (Suzuki *et al.,* 2006). Formation of chemical bond with hard tissue offers HA a greater advantage in clinical applications (Yan *et al.,* 2006; Liu *et al.,* 2001). Due to this property, these biomaterials have been used as implants in clinical bone repair and regeneration materials, coating materials in tissue engineering, drug delivery devices, and tumour treatment (Yan *et al.,* 2006). It may be suitable as filler for resin-based dental composites (Santos *et al.,* 2002) and has been used for furcation sealing, root surface desensitisation, and root apex sealing or root canal filling (Yoshimin and Maeda, 1995; Bilginer *et al,* 1997).

2.4.2- Biological Apatite

Apatite or apatite calcium phosphates are the principal inorganic constituents of bone and teeth. Human enamel apatite has larger a-axis dimensions than pure HA (0.944 nm compared to 0.942 nm). The composition, crystal size, morphology and stoichiometry of biological apatite are different from the pure HA. The Ca/P molar ratio is 1.67 for pure HA and for enamel and dentine it is 1.62 and 1.64 respectively. Generally, biological apatites are calcium deficient or non-stoichiometric. The other minors e.g. magnesium (Mg), carbonate (CO_3), sodium (Na), chloride (Cl), acid phosphate (HPO_4) etc and traces such as strontium (Sr), lead (Pb) elements are associated with these apatites. The biological apatites can be classified as:

- Carbonate apatite (CO_3)-AP
- Fluor-carbonate apatite (F, CO_3)-AP

They can be represented by the following chemical formula:

$$\mathbf{A_{10}(BO_4)_6X_2}$$

where,

- A_{10} is Ca, Na, Sr, Pb, Cd, Mg, and K
- BO_4 is $(PO_4, CO_3, VO_4, SiO_4, AsO_4, HPO_4)_6$
- X is $(OH, Cl, CO3F)_2$

where A represents traces of cations with concentrations less than 0.1wt%.

The minor elements, carbonates, magnesium and fluoride are responsible for stability or instability of biological apatites. Water has also been found in the apatite structure in several forms.

2.4.3- Hydroxyapatite

The term "apatite" applies to a broad category of structures comprised of different constituents. Hydroxyapatite is one such constituent, another being carbonate (hydroxyl) apatite, where carbonate ions substitute for some of the hydroxyl ions (A-type) or carbonate ions may be present on the phosphate sites (B-type) (Jillavenkatesa and Condrate Sr., 1998). Synthetic hydroxyapatite is a representative material for a bone substance because of its chemical similarities with the inorganic phase of bone and is capable of undergoing bonding osteogenesis and is chemically stable for long period of time *in-vivo* (Ruys *et al.,* 1995; Rhee, 2001). Calcium hydroxyapatite is a compound of a definite composition and definite crystallographic structure and shows the exact atomic position in the crystal (Liu *et al.,* 2001).

The structure of non-stoichiometric hydroxyapatite as shown in Figure 2.4 belongs to $P6_3/m$ with a = 9.421 and c = 6.884 Å, but the stoichiometric form is monoclinic with space group $P2_1/b$. This is characterised by ordering within OH^- ion columns to form a sequence $OH^- OH^- OH^- OH^-$ indicating that it has a six fold axis of symmetry parallel to c-axis, as well as a screw axis along the c-axis. The symbol /m indicate that there is a mirror plane perpendicular to the screw- and c-axis (Elliott, 1994; Morgan *et al.,* 2000).

The unit cell of hydroxyapatite is based around two types of calcium ion sites. Firstly there is "columnar calcium" or Ca_I. The second type of calcium site is the "hexagonal calcium" or Ca_{II}, which is arranged as equilateral triangles around the OH^- ions located on the c-axis. Three Ca_{II}^{2+} ions surround each OH^- ions, with each successive traingle along the c-axis (around each successive OH^-ion) being offset by a rotation of 60°. When the structure is viewed along the c-axis (along the line of the OH^- ions), the Ca_{II} ions appear in the shape of hexagons centered on the OH- ions. The Ca_{II} ions are located on planes parallel to the base planes, at c=1/4 or c=3/4. The phosphate tetrahedral is located on the same planes as the triangularly arranged Ca_{II} ions.

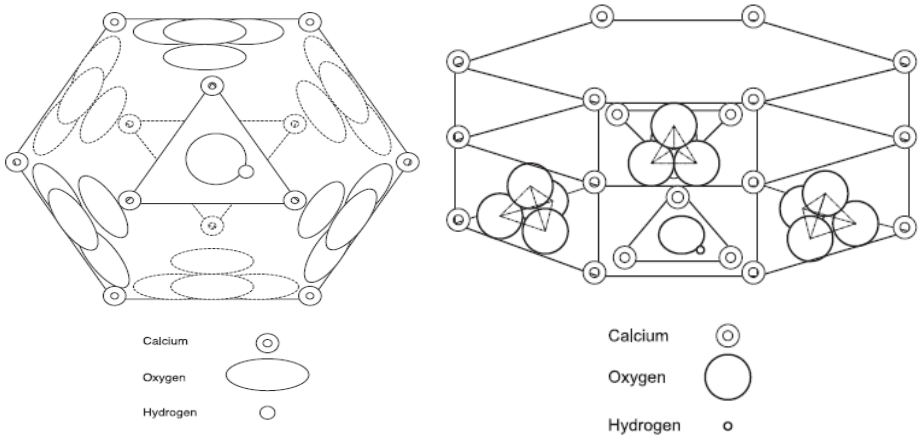

Figure 2.4 (a) overview of an apatite unit cell, lower level is indicated by dot lines, (b) a prospective view of an apatite unit cell (Sarig, 2004)

There are six phosphate ions per unit cell, two located fully within the cell, the remaining four being the eight ions located on the faces of the unit cell parallel to the c-axis, each of these ions being shared between two unit cells (Best, 1990). The network of phosphate groups provides the structural framework which gives the apatite its stability. The oxygen of phosphate groups is described as one O_I, one O_{II}, and two O_{III}. The fluoride and chloride substitute the OH^- groups in the apatite structure; the atomic arrangement for F^- apatite and Cl^- apatite is $Ca_{10}(PO_4)_6F_2$ and $Ca_{10}(PO_4)_6Cl_2$ respectively. The F and Cl atoms substituted for OH differ in the respective position of the OH for which they substitute. The apatite structure allows the substitutions of many

other ions resulting in a change in properties, such as lattice parameters, morphology, solubility, without changing the hexagonal symmetry (Vallet-Regi and Gonzalez-Calbet, 2004). However, Cl substitution causes the loss of hexagonal symmetry and exhibits monoclinic symmetry because of the alternating positions of the Cl atoms and an enlargement of the cell. The substitutions of F for OH cause a contraction and are usually associated with an increase in the crystallinity, reflecting increase in crystal size (and/or decrease in crystal strain) and gives greater stability to the structure (Hench and Wilson, 1999). The composition and crystallographic properties of HA are shown in Table 2.5. The chemical structure, chemical composition, and textural properties (pore structure, pore size, pore volume) of biomaterials may have complex influence on the development of the hydroxyapatite layer (Yan *et al.,* 2006).

Table 2.5 Composition and Crystallographic properties of general hydroxyapatite (Elliott, 1994)

Constituents	**Hydroxyapatite (wt%)**
Calcium, Ca^{2+}	39.6
Phosphorous, P	18.5
Ca/P ratio	1.67
Sodium, Na	tr
Potassium, K^{+}	tr
Magnesium, Mg^{2+}	tr
Inorganic	100

Among the wide range of calcium phosphate, or with potential formulation as shown in Table 2.6, it is important to note the close relation between the Ca/P ratios. The lower Ca/P ratio increases the solubility and acidity of mixture. If Ca/P <1 both solubility and acidity are significantly high, and both parameters decrease substantially for Ca/P ratios close to 1.67, which is the value of stoichiometric HA (Vallet-Regi and Gonzalez-Calbet, 2004). The apatite structure can be preserved with Ca/P ratios as low as 1.5. Therefore, HA with a lower than normal ratio (1.67) is characterised as calcium

deficient or non-stoichiometric. When molar ratio is lower than 1.67, HA partially decomposes to β-tricalcium phosphate at temperature higher than 1200°C (Fanovich *et al.,* 2001). The anisotropic behaviours of HA have been restricted to protein absorption, dissolution and crystal growth. It has been expected that anisotropic behaviours may have some involvements in a possible bonding mechanism between bone and HA implant initiating from dissolution and reprecipitation of HA through protein absorption and cell adhesion and differentiation, to either epitaxial or non-epitaxial boding of bone apatite to HA (Ito *et al.,* 1996).

Table 2.6 Chemical formula and ratio of different calcium phosphate groups (Vallet-Regi and Gonzalez-Calbet, 2004)

Name	Formula	Ca/P
Tetracalcium phosphate	$Ca_4O(PO_4)_2$	2.0
Hydroxyapatite	$Ca_{10}(PO_4)_6(OH)_2$	1.67
Tricalcium phosphate	$Ca_3(PO_4)_2$	1.50
Octacalcium phosphate	$Ca_8H_2(PO_4)_6.5H_2O$	1.33
Dicalcium phosphate dihydrate	$CaHPO_4.2H_2O$	1.0
Dicalcium phosphate	$Ca_2P_2O_7$	1.0
Monocalcium phosphate monohydrate	$Ca(H_2PO_4)_2.H_2O$	0.5
Calcium metaphosphate	$Ca(PO_3)_2$	0.5

2.4.3.1- Methods of Preparation

HA with different morphology, stoichiometry and level of crystallinity can be obtained by multiple preparation techniques (Shuk *et al.,* 2001) and it essentially affects the bioactivity, mechanical properties and dissolution behavior in biological environment. The interest is not only controlling the stoichiometry of synthetic HA but also controlling the crystal size and shape of agglomeration characteristics of the powder (Mostafa, 2005). Therefore, it is always important to develop HA synthesis methods with precise control of particle size, morphology, crystallinity degree and chemical composition (Guo and Xiao, 2005). It is possible to prepare dense and/or porous HA

with controlled microstructure and chemical composition (Suchanek and Yoshimura, 1998). Synthetic HA with desired properties can be prepared by:

- Wet-Chemical Method
    1. Sol-Gel
    2. Precipitation
    3. Hydrothermal
    4. Hydrolysis
- Dry Method
    1. Solid-State Reaction
- Mechano-Chemical Hydrothermal Method
- Emulsion Processing
- Spray Pyrolysis
- Microwave Irradiation
- Mechano-Chemical Method

2.4.3.1.1- Wet-Chemical Method

Wet-chemical methods allow the synthesis of materials with good crystallinity, physiological stability and with the morphological characteristics of the hard tissue but the physical, chemical and mechanical properties of the product mainly depend on the specific method used in synthesis (Tadic *et al.,* 2002). Donadel et al. (2005) reported the two wet-chemical methods using a precipitation process over other wet and dry methods which can result in calcium phosphate materials produced with a low cost technique using low temperature under pressure.

2.4.3.1.2- Sol-Gel Method

The sol-gel process, which has been a method for the synthesis of ceramic materials for more than one and a half centuries is gaining importance. “Sol” is a dispersion of colloidal particles and a “Gel” is an interconnected polymeric network formed by the assembly of the sol (Aurobind *et al.,* 2006). The earlier procedures to synthesise HA led to the formation of fragile materials with considerable shrinkage during drying. However, it has been suggested that the use of additives might help to overcome these problems. The drying process plays an important role in the fabrication of sol-gel materials because a substantial shrinkage happens when the liquid phase is removed (Balamurugan *et al.,* 2003).

The sol-gel method is a wet chemical process that needs no high pH value and no high sintering temperature. The high reactivity of the sol-gel powders allows a reduction of the processing temperature and of any degradation phenomenon during sintering (Feng *et al.,* 2005). The advantages of this method include high product purity, homogenous composition, and low synthesis temperature, the ability to generate nano-crystalline powders and particles, fusion of the apatite crystals, bulk amorphous monolithic solids and thin films and the microstructure of solids can be modified by changing chemistry and/or processing conditions (Lopatin *et al.,* 2001; Liu *et al.,* 2002; Bigi *et al.,* 2004; Kim and Kumta, 2004). This process has been used to produce a wide range of compositions (mostly oxides) including powders, fibres, organic/inorganic hybrids, coating, thin films, monoliths and porous membranes and has ability to produce porous oxides, which are potential bone-like HA-forming material (Viitala *et al.,* 2002). The mixing level of the solution usually produces a fine-grain microstructure containing a mixture of nano-to-submicron crystals (Liu *et al.,* 2002; Vijayalakshmi and Rajeswari, 2006). This method offers a molecular-level mixing of the precursors, which is capable of improving chemical homogeneity of the resulting powders to a significant level (Bose and Saha, 2003). The limitations in its application have been due to the shortcomings associated with hydrolysis of phosphates, and the higher cost of raw materials (Jillavenkatesa and Condrate Sr., 1998; Kim and Kumta, 2004).

Feng et al. (2005) reported a simple sol-gel method that does not require controlling pH values and long time for hydrolysis of phosphate. The first stage after making the sol is gelation, in which sufficient polymerisation has occurred to form crosslinking of molecules making up the skeletal structure. The next stage is ageing during which the resulting crosslinking structure of the molecules increases and then drying during which excess solvent is removed and the final stage is sintering, in which the porous structure is eliminated, the residual organics are removed, and the minerals are crystallised.

It has been reported that ethanol-based gels exhibit a weight loss, indicating the evaporation of ethanol and water, which is promoted by the destructuration effect of ethanol. The presence of ethanol in the reaction slightly effects the degree of crystallinity of HA, whereas, variation in the value of Ca/P ratio of sol can be used to control the crystallinity domain, and the thermal stability of gels (Bigi *et al.,* 2004). Kuriakose et al. (2004) reported the synthesis of pure, stoichiometric, nano crystalline HA with this technique and sintered at 1200°C and found stable HA.

Bose and Saha (2003) investigated the synthesis of HA using an aqueous solution of calcium nitrate, ammonium hydrogen phosphate, and sucrose. The advantage of addition of sucrose to the metal-ion solution made the solution viscous with no precipitation or segregation of ions from the homogenous solution. Han et al. (2004) adapted the citric acid sol-gel combustion method to synthesise nano-crystalline HA powder. Citric acid is a strong complex agent which can form stable complex compound with many metal ions.

2.4.3.1.3- Precipitation Method

It has been investigated that the conventional precipitation methods deal with the difficulty of synthesising well-defined and reproducible orthophosphates. The effect of various conditions on the stoichiometry and morphology of the powder enable to give good control on the final powder characteristics, which is promising to design calcium phosphate powders for different specific applications and/or requirements. It has been suggested that a surface area 10 m^2g^{-1} would probably be appropriate for the sintering

avoiding undesirable agglomerates that can be produced if powders with higher surface area were selected (Rodriguez-Lorenzo *et al.*, 2001).

Brown and Fulmer (1991) synthesised the low temperature formation of HA that involved aqueous phase acid-base reaction involving the consumption of particulate solid calcium phosphate. Fulmer et al. (1992) identified the problem that dissolution of $CaHPO_4$ had been rate limiting to the reaction, therefore, made modification of using $CaHPO_4.2H_2O$ instead of $CaHPO_4$. Normally apatite structure are characterised by the presence of channels along their hexagonal axes, and ions in these channels are less rigorously bound in comparison with those in the bulk, resulting in many specific structural, thermal, and chemical properties associated with precipitated HA that makes the material suitable for the bone implantation, ion exchangers, drug delivery systems and for chromatographic separation as catalysts (Sinha *et al.*, 2003).

Homogenous precipitation with a slow reaction rate is a relatively easy procedure for synthesising uniform hydroxyapatite particles (Zhang *et al.*, 2003). Sarig and Kahana (2002) obtained the nano-crystals of apatite by precipitation with microwave irradiation. The advantage is that the apatite aggregates in small sphrulites with open and loose structure and they remain dry, aggregated in loose clusters and forming a free flowing powder.

2.4.3.1.4- Hydrothermal Method

Hydrothermal method is known to synthesise apatite compounds with controlled morphology, which have prominent advantages over the other method for preparation of one dimensional nanostructure (Cao *et al.*, 2003). It can be controlled by experimental conditions that regulate nucleation, growth and aging processes (Liu *et al.*, 2003; Guo and Xiao, 2005). Several studies have reported the conversion of coral, calcite crystals and aragonite to HA with this method (Xu *et al.*, 2001; Jinawath *et al*, 2002; Yoshimura *et al.*, 2004). A study conducted by Kothapalli et al. (2005) investigated the synthesis of HA with hydrothermal method and the effect of reaction temperature and aging time on particle size. It was suggested that the morphology of HA crystals was

dependent on the reaction temperature and at a constant aging time, as the reaction temperature increased, the particle size and aspect ratio also increased. In a study (Teng *et al.,* 2006), gelatin was used in a high concentration as a medium to prevent the aggregation of HA crystals during solution synthesis. It was observed that a large number of nano-sized needles like crystals distributed randomly in gelatin matrix and with the increase in amount of HA these short crystal grow large sized HA with an average size of about 0.8 μm in length and 0.2 μm in width.

Continuous hydrothermal preparations have recently gained interest as a controllable and fast method for producing inorganic nano-materials (particles <500 nm) (Sue *et al.,* 2004: Hakuta *et al.,* 2005). Chaudhry et al. (2006) described the rapid, single step synthesis of crystalline nano-particle HA rods in a continuous hydrothermal flow system. The advantage of this process is that it does not use any organic templating agents and effectively reduces the time required for maturation of reagents from over 18 hours to a few seconds. Yan et al. (2001) used surfactants and the resultant product showed nano-sized rods. In an aqueous system, surfactants would ionise completely and result in tetrahedral cation structure.

2.4.3.1.5- Hydrolysis Method

The low temperature process such as hydrolysis of salts is important in the synthesis of HA. Shih et al. (2004) investigated the growth and morphology of nano-sized HA powder with various Ca/P ratios by a hydrolysis method.

2.4.3.1.6- Dry Method

Dry method such as mechanosynthesis, reactions can occur at low temperatures in a ball mill without any need for external heating. The ball mill may act as a chemical reactor in which a wide range of chemical reactions can be mechanically initiated (McCormick and Froes, 1998). This method has an advantage of the perturbation of surface-bonded species by pressure to enhance thermodynamic and kinetic reactions between solids. However, the energy transmitted to crystalline powders during milling results in a

dislocation cell structure that develops into random nanostructured grains with increasing milling time (Coreno *et al.,* 2005).

2.4.3.1.7- Mechano-Chemical-Hydrothermal Method

Shuk et al. (2001) investigated the mechanochemical-hydrothermal synthesis (also known as "wet" mechanochemical) of hydroxyapatite. This technique is located at the intersection of hydrothermal and mechanochemical processing. If the nonaqueous solution is used then the process would be defined as mechanochemical-solvothermal. The aqueous solution actively participates in synthesis reaction by dissolving one of the reactants.

2.4.3.1.8- Emulsion Processing

In recent years, modifications in the synthesis of nano-sized HA powder have been established with an emulsion method. It describes limited stability with milky appearance before the suspended droplets will agglomerate and the dispersed phase will separate. The stability of the dispersed system can be accentuated by additives such as surfactants (Norton *et al,* 2006). Microemulsion has been used for synthesis of nano-materials. Compositional changes, such as surfactant concentration and the molar ratio of water to surfactant, exert an influence (Wei *et al.,* 2005). Phillips et al. (2003) synthesised the small sized micro or nano-sized ceramic powder by "water in oil" emulsion method, which effectively reduces particle flocculation and to some extent limits particle growth. Wei et al. (2005) investigated the synthesis of HA and used Ca^{2+} ions incorporated into the micro-emulsions due to phase separation in presence of solution with high ions strength.

2.4.3.2- Properties of Hydroxyapatite

The properties of HA can be controlled by various parameters such as particle size and shape, particle distribution and agglomeration. Nano-crystalline HA powders show

greater surface area and provide improved sinterability and densification to reduce sintering temperature, which improves the fracture toughness. Nano-sized HA is expected to have better bioactivity than coarser crystals and it represents a unique and promising class of orthopedic/dental implant formulation with improved osseointegration (Han *et al.,* 2004).

2.4.3.2.1- Mechanical Properties

Dense HA shows superior mechanical properties, if the starting HA powder is stoichiometric i.e., the molar ratio of Ca/P is 1.67. If the ratio is more than 1.67, CaO forms during sintering, which decreases the strength and may cause de-cohesion of the material due to stresses arriving from formation of $Ca(OH)_2$, subsequently transforms into $CaCO_3$ that may also alter the rate of extent of biodegradation. It also forms slow crack growth and biodegradability of HA due to the formation of tricalcium phosphate (Suckhanek and Yoshimura, 1998).

It has been reported that the fracture toughness of pure, dense HA is in range of 0.8-1.2 $MPa.m^{-1}$, whereas, with the increase in porosity, it decreases linearly. From 10-30% porosity, the value decreases to almost 0.75-0.45 $MPa.m^{-1}$ (Orlovskii *et al.,* 2002). Bending strength, compressive strength and tensile strength of dense HA are in the ranges of 38-250 MPa, 120-150 MPa, and 38-300 MPa respectively (Aoki, 1991; Williams, 1994; Hench, 1995; Suchanek and Yoshimura, 1998) in comparison, the porous HA shows 2-11 MPa, 2-100 MPa and 3 MPa respectively (Hing *et al.,* 1999; Slosarczyk, 1999). It is expected that range of data is due to the statistical nature of strength distribution, influence of remaining micro-porosities, grain size and impurities.

HA behaves as a brittle material as Weibull modulus of dense material is in the range of n = 5-18, where as, Young's modulus of this material is in the range of 35-120 GPa, but it depends on measurement techniques. Young's modulus measured in bending is in between 44-88 GPa (Katz, 1980). The documented tensile modulus, compressive modulus and shear modulus of this material is 12.3 ± 0.8 GPa, 3.5 ± 0.8 GPa and 4.8 ± 0.3 GPa respectively (Charriere *et al.,* 2001).

Due to its low mechanical properties, this material has limitations to be used clinically. The main reason of its low mechanical properties is its porosity, which makes it easier for micro and macro cracks. Apparently the size of pores is 8-12 μm in diameter. Porosity can be controlled and it has been reported that if the porosity is zero, then the diameteral tensile strength could be 103 MPa (Ambard and Mueninghoff, 2006). The mechanical properties of HA can be improved by reinforcement methods. Studies have been conducted on these different reinforcement techniques including particles, whiskers, long fibres and nano-particles (deWith and Corbijn, 1989; Li *et al.,* 1990; Tian *et al.,* 1995; Suchanek *et al,* 1996). It has been reported that with the introduction of whiskers the density and hardness of composite decreases [6 MPa (non-reinforced hydroxyapatite) to 4 MPa], however, there was a significant increase in fracture toughness values and the range was 1.35-1.41 $MPa.m^{-1}$ (Suchanek *et al,* 1996).

2.4.3.2.2- Physical Properties

Hench (1998) reported the Vicker hardness (600HV) and density (3.16 $g.cm^{-3}$) of sintered HA. The particles have a tendency at rest to interlace opposing any movement. One of the reported viscosity value of HA suspension was 5210 Pa with a shear rate of 1000/s (Bouyer *et al.,* 2000).

The morphology of HA particles depend upon heat treatment. The temperature of synthesis effect on the nano-particle shape, at low temperature the crystals are in needle shape. Increasing the reaction temperature changes the crystal from needle shape to more regular shape close to circular (Bouyer *et al.,* 2000).

2.4.3.2.3- Biocompatibility and Bioactivity of Hydroxyapatite

Biocompatibility is defined as the ability of a material to perform with an appropriate host response in a specific application (William, 1999). The biocompatibility has profound ethical, social, technical and legal effects (Wataha, 2001; Watson, 2001). The concept of biomaterial's biocompatibility does not refer to total inertness, but rather the ability of a material to perform with an appropriate response in a specific application

(Anusavice, 2003). The interaction depends on the material, the host, the forces and conditions placed on the material. Biocompatibility is a dynamic process not a static one, any change may alter the condition that initially promoted an appropriate and desired biological response. It depends on interaction of material with its environment. It can be organised into four areas; safety of the patient, safety of dental staff, regular compliance issue, and legal liability (Watson, 2001).

During the last four decades, bioactive materials such as bioactive glasses, sintered HA, glass-ceramics, and composites have been synthesised and developed for medical applications. A significant characteristic of bioactive materials is their ability to bond with living tissue through the formation of a HA interfacial layer (Wu and Chang, 2006). It can be used in bulk form or as a coating and can be classified according to their porosity, form, and processing methods. These forms have good biocompatibility and are able to promote osteoconductivity and osseointegeration. HA coated implants have higher integration rate, faster bone attachment, and higher interfacial attachment strength to the bone (Ambard and Mueninghoff, 2006).

The disadvantage of HA includes its slow resorbability. The complications include the detachment of coating from implants and may cause the formation of fibrous tissue around the implant and peri-implant infection. HA is known not only as bioactive but also as an adsorbent material and can adsorb bacteria, causing an unfavourable tissue response, mainly if exposed to the oral environment.

Bioactivity can be classified into two types, which depend upon rate of tissue response to the implants. Rate of bonding depends mainly on the composition and microstructure of the bioactive materials. Class A bioactivity is the most rapid bone bonding and it also bonds to soft connective tissues. Table 2.7 compared the characteristics of Class A and Class B bioactive materials. Class A bioactive materials produce bone throughout the particle array, and it is known as osteoproduction. These materials also exhibit osteoconduction, which is defined as “The process of bond migration along a biocompatible surface”. Class B bioactive material such as synthetic hydroxyapatite shows only osteoconduction. Therefore, they lead to a very slow bond to bone, slow and

incomplete proliferation of bone throughout a particular array (Hench *et al.,* 1998). The bioactive ceramics not only have been useful in bone repairs and replacements, but also are inspiring new bioactive materials. The sintered HA has been also documented to integrate with bond tissue by forming bone-like apatite on its surface (Kim *et al.,* 2005).

Table 2.7 Comparison of bioactive materials (Hench *et al.,* 1998)

Class A	**Class B**
Osteoconductivity and osteoproductive	Only osteoconductive
Rapid bone bonding	Slow bone bonding
Enhanced bone proliferation	No enhancement of bone proliferation
Bonding to soft connective tissue	No bonding to soft connective tissue

The ability of bone integration of HA decreases as its sintered temperature increases. This suggests that the HA might reveal different kinetics of the bonelike apatite formation, and thereby different apatite forming abilities, by the sintered temperature. Specifically, the HA with different profiles of sintered temperature provide interesting model concerning the mechanism of bonelike apatite formation in both terms of process and kinetics (Niwa, 1983). The process of kinetics of apatite formation on HA could be affected by bulk factors such as density and surface area as well as surface factors such as composition and structure. On immersion in simulated body fluid (SBF), the HA could reveal negative surface charge by exposing hydroxyl and phosphate units in its crystal structure. The HA surfaces use this negative charge to interact specifically with the positive calcium ions in the fluid, consequently forming a Ca-rich ACP amorphous calcium phosphate (ACP). This formation of Ca-rich is assumed to take place in consecutive accumulation of the calcium ions, which makes Ca-rich ACP acquire and increase positive charge. The Ca-rich ACP on the HA therefore interacts specifically with the negative phosphate ions in the fluid to form a Ca-poor ACP. This type of Ca-poor ACP has been observed as a precursor, which eventually crystallises into bonelike apatite on various bioactive ceramics. The solubility of apatite is lower than any other calcium phosphate in water, and therefore thermodynamically the Ca-poor ACP could be stabilised by transforming into a crystal phase of apatite in SBF. Once formed in SBF

which is supersaturated with respect to apatite, the apatite grows spontaneously consuming the calcium and phosphate ions, incorporating minor ions such as sodium, magnesium and carbonate, and thereby developing bone mineral-like compositional and structural features (Kim *et al.,* 2005). Yamashita et al. (1996) showed that negative charged degree of HA surface could promote the apatite formation on its surface as well as cell adhesion and bone integration.

2.4.3.2.4- Particle Size and Shape

It is reported that the particle size is a key factor, which modifies significantly the properties and specifically affects the kinetics of chemical reaction and mechanical consolidation of the material. It is a useful parameter in order to adjust behaviour of the material to specific clinical applications. It can be expected that smaller the particle size higher the strength, because in small crystals there are more contact points, and the porosity is lower (Ginebra *et al.,* 2004). Reconstruction of bone and dental defects can be restored with the packing of porous and dense HA granules to achieve growth and repair of the defected area. For such conditions, the size and shape of particles is important. Particles with smaller diameter are fully resorbed and cannot act as a substrate for uptake of mesenchymal cells. Particles with irregular shape adjust poorly and create large voids. The sharp edges of the particles fracture easily.

The particle size and surface characteristics (micro and nanostructure) has recently been highlighted and the capability to process material with tailored structure at the micro and nano-scale level may provide the possibility to obtain responses from cells (Borum-Nicholas and Wilson, 2003). The nano-particles and nano-structured surfaces have a larger surface area for adhesion that increases the interaction between particles and the surrounding environment (Ginebra *et al.,* 2004). The interaction relates to surface structure and properties of the HA like surface charges, surface functional groups, acidity/basicity, porosity and hydrophobicity (Norton *et al,* 2006). It has been documented that biological molecules interact with the crystalline surface of HA by exposing their structure against the material surface to arrange their confirmation most

suitable for the adsorption; generally acid molecules are adsorbed onto the c-site and basic molecules adsorbed onto the P-site (Ducheyne and Qui, 1999; Yin *et al.*, 2002).

There are three types of P-OH groups on the surface in HA which are hydrophilic in nature and behave as adsorption sites for molecules such as H_2O, CH_3OH, CH_3I and CO_2.The pattern and structure of functional groups such as these participate in determining the mode of adsorption that takes place to the substrate surface. The number of the P-OH groups determines the surface properties, regulation of number of these surface groups will lead to surface modifications. These can change the material characteristics and properties such as the acidic and basic behaviour, affinity and reactivity to molecules and catalytic activity (El Shafei and Moussa, 2001). The advantage of micro or nano-sized material is the likeliness of producing novel composition. The biological activity and control of cellular behaviour, i.e., adhesion, proliferation, differentiation, migration depends on the dimensions of different domains (Norton *et al.*, 2006).

Nano-materials, both in scientific knowledge and in commercial application, are the most advanced at present (Murray *et al.*, 2003). The synthesis of nano sized HA crystals similar to the particle size found in human tissues will provide an enhancement in properties of the material, such as thermal and mechanical properties, in addition the formation and maintenance of healthy new bone. It has been established that nano-HA coated implant enhanced new bone formation as compared to micro-scale HA (Liu and Webster, 2007). From this background, it is important to understand the concept of nanotechnology.

2.5- Nanotechnology

Nanotechnology has revolutionised the field of science and technology. It is the production of functional materials and structures in the range of 0.1-100 nm -the nanoscale- by various physical and chemical methods and is also known as molecular nanotechnology or molecular engineering (Schulz, 2000). The interest in using

nano-materials stems from the idea that they can be used to manipulate the structure and properties of the materials (Mitra *et al.,* 2003).

Nanotechnology is of great interest in biomaterials engineering and the development of dental materials (Moszner and Klapdohr, 2004). Nano-particles have been found to be of much use for the controlled release of drugs and other bioactive compounds (Hrkach *et al.,* 1997). They should act as drug-delivery and drug-targeting systems, being small in size and are not recognised by the human body, migrate through cell membranes and are able to pass through blood-brain barriers (Logothetidis, 2006). The intrusion of a nano-material in the body triggers substrate effects at the nanoscale level at which structural components of biological systems are built, thus encouraging a strong affinity between molecules (Polizu *et al.,* 2006). Biomaterial scaffolds can be manipulated by nanotechnology and constructed into specific geometrical and topological structures and bring improved properties such as mechanical (stronger), physical (lighter and more porous), chemical reactivity (more active and corrosive), enhanced biocompatibility, contact guidance, reduce friction and therefore wear for joint applications and promoting tissue growth around the implant (Kricka and Fortina, 2002; Storm *et al.,* 2005). The development of three dimensional nano-fibrous scaffolds using a phase-separation technique from biodegradable synthetic polymers avoids the concern of pathogen transmission and immuno-rejection (Zhang and Ma, 2000). The nano-size electrospun fibres provide improved applications such as wound healing, cell attachment and proliferation of cells and fibroblasts (Kenaway *et al.,* 2003).

Nano-scope particles have more similarities to natural tooth as far as crystal size is concerned. Additionally, the high surface area of the nano-scopic particles would offer a good mechanical interlocking with the polymer matrix (Arcis *et al.,* 2002). This is true for purpose-designed nano-structures, which can be used to produce low shrinkage, high wear resistance and biocompatibility of the dental composite. The fundamental application is resistance of nano-particles filled materials to the loss of substance during propagation of micro-fracture through cyclic fatigue loading (Trussi et al., 2005). It is also interesting with regard to developing biocompatible or bioactive materials for dental implants and bioceramics (Hench, 1997).

Inorganic nano-particles are hard and dense and these characteristics make them interesting for improving a material's mechanical properties. The nano-particles are also characterised by a large surface area that increases the bond strength between resin and fillers. Due to large surface area, the particles show thixotropic thickening effect, low viscosity and improved handling properties. These nano-fillers can contribute to increase the modulus of elasticity and are useful as starting compounds for the synthesis of new dental ceramics composites. Furthermore, nano-fillers also show smooth surface effects and volume effects as well as high optical properties. In dental bonding agents, the nano-fillers increased adhesion to enamel and dentine and improved marginal integrity, increased abrasion resistance and surface hardness (Moszner and Klapdohr, 2004).

The high content loading of nano-particles into the organic matrix results in aggregation of the filler particles and porosity, which affects the mechanical properties of resulting material. During the preparation of composite material of polymer matrix filled nano-HA, the major problem is dispersion and strong interfacial combination between the nano-fillers and the matrix. It is known that covalent linkage of polymer chains to nano-fillers is one of the effective approaches to improve dispersability and combination of polymer matrix and nano-particles (Hong *et al.,* 2005). The large surface area of nano-HA results in high surface energy and more hydroxyl group on the surface. It is possible for nano-HA to crosslink with polymer more strongly by a reaction between the hydroxyl group and the functional groups (Zhao and Zhang, 2008).

To design a polyurethane/hydroxyapatite based scaffold various techniques have been used, to mimic natural extracellular matrices, many research groups have tried to fabricate nano-fibrous scaffolds by phase separation, self-assembly, solvent casting and electrospinning. The electrospinning method has been explored recently despite the simplicity of the process; it offers ultrafine polymer fibres, with high surface area (Ito *et al.,* 2005; Guan *et al.,* 2005).

2.6- Electrospinning

2.6.1- Introduction

Electrospinning is a novel process to develop nano-fibres that allows continuous production of fibres ranging from sub-micrometers to nano-meters (3 nm) for potential use as biomaterials. It is reported that this technique is not only applicable for healthcare, but also to a wide range of functions, from energy production to applications related to defence and security. Teo and Ramakrishna (2006) have used this method to collect fibres to fabricate porous tubes and thin films or fibre mats. The morphology of these fibres varies due to change in the processing parameters or polymeric solution.

2.6.2- Processing Technique

This technique has been developed by Formhals in 1934 (Formhals, 1934; Lee *et al.,* 2003). In this process, continuous filaments are drawn from a liquid polymer or melt through a spinneret by high electrostatic forces and later deposited on a conductive collector. The three main components for this technique are a high voltage power supply, a container for a polymer solution or melt with small opening to be used as a nozzle, and a conductive collecting device. An emitting electrode of power supply charges the polymer solution or melt by connecting the electrode to a conductive nozzle. Upon increasing the electrostatic field strength up to a critical value (up to 30 KV), a droplet acquires a cone like shape (Taylor cone). If electric field is above critical value, a charged polymer jet is ejected from apex of the cone and carried to the collector screen (distance of about 20 cm) by electrostatic force. It has been shown that capillary instability, resulting from surface tension, is typically prevented by the strong stabilising influence of viscoelastic stresses in electrospinning of the polymer solution. The Coulombic repulsion force is responsible for thinning of the charged jet during its flight to the collector. The charged jet elongates and, at the same time, dries out or solidifies to leave ultrafine fibre on the collector (Theron *et al.,* 2002; Theron *et al.,* 2004; Wutticharoenmonkol *et al.,* 2006). The enablement of an electrospinning system

depends on the physical properties and the phenomena at the nozzle outlet. The other factors which have an effect on the quality and morphology of fibres are controllable i.e. collecting distance on substrate, applied voltage and flow rate (Deitzel *et al.,* 2001).

Electro spraying is the technique to deposit particles on the surface. The basic principle of electrospraying is the generation of a spray of charged, micron-sized droplets. This is done by means of electrostatic atomisation. The sprayed droplets are directed towards a heated substrate as a result of applied potential difference (Leeuwenburgh *et al.,* 2004). The experimental section of this study will mainly focus on electrospinning of the polyurethane.

2.6.3- Effect of Factors

The electrospun polymers are either spun directly from the solution in which they were synthesised or dissolved in solvent before processing. The solvent plays an important role in the behaviour of polymer and the resultant fibres. Viscosity of solution affects the diameter of fibres (Wang *et al.,* 2006). Xin et al. (2006) reported that the applied voltage in addition with solvent have pivotal role in morphology of the fibres. Fridrikh et al. (2006) have mentioned how surface tension of the polymeric solution affects the processing and fibre formation. The effect of jetting mode was studied by Jaworek and Krupa (1999). The dynamics of the meniscus and the form of emitted fluid were assessed for different jet modes. Kidoaki et al. (2005) have described that using a mixture of solvents in the spinning process has an effect on the properties and structures of the spun fibres. The study was based on a solvent system comprised of tetrahydrofuran (THF) and *N,N'*-Dimethylformamide (DMF) and it is suggested that with the increase in ratio of DMF, bonding between the spun fibres increased. The speeds at which the fibres are spun also affect the mechanical properties of the material due to orientation of the fibres (Pedicini *et al.,* 2003).

The morphology of electrospun fibres depends on the following parameters including viscosity, conductivity and surface tension, controlled variables including hydrostatic pressure in the capillary, electric potential at the tip, and the distance between tip and the

collector, ambient parameters including temperature, humidity, and air velocity in the electrospinning chamber (Doshi and Reneker, 1995; Reneker and Chen, 1996; Lee *et al.,* 2003).

2.6.4- Application of the Electrospun Fibres

2.6.4.1- Biomedical Application

Due to high surface area to volume ratio of the electrospun fibres and high porosity on the sub-micrometer length scale of obtained non-woven mat, proposed applications for these materials are in areas such as nano-fibre-reinforced composites, nano-fibre as supports for enzymes and catalysts, and nano-fibrous membranes to be used in biomedical applications, including drug delivery, wound healing, and scaffolding for tissue engineering, cardiac grafts and guided bone regeneration. Electrospun fibre mats are suitable for use as scaffold because of their 3D structure with high porosity (Doshi and Reneker, 1995; Buchko *et al.,* 1999; Coombes *et al.,* 2004; Li *et al.,* 2005; Fujihara *et al.,* 2005; Wutticharoenmonkol *et al.,* 2006).

Many polymers such as poly (meta-phenylene isophthalamide), polyetherimide, poly ethylene oxide, polyethylene terephthalate, polyaniline, poly caprolactone, poly (L-lactic acid) have been successfully electrospun into nano-fibres (Reneker and Chun, 1996; Liu *et al.,* 2002; Theorn *et al.,* 2004; Shin *et al.,* 2004; Tan *et al.,* 2005). A few studies have been reported on a culture of chondrocytes and osteoblasts on poly caprolactone (Li *et al.,* 2005: Fujihara *et al.,* 2005); in addition, the incorporation of calcium carbonate or HA have also been reported (Coombes *et al.,* 2004; Fujihara *et al.,* 2005; Maeno *et al.,*2005; Wutticharoenmongkol *et al.,* 2006).

2.6.4.2- Dental Application

Dental polymers, Bis-GMA and TEGMA have been investigated with the reinforcing effect of electrospun Nylon 6 nano-fibres. It was found that the fibres have crystalline structure and are mechanically strong. The small diameter of nano-fibres also provide a

high ratio of surface area to volume, which could enhance the intermolecular hydrogen bonding between the filler of Nylon 6 nano-fibres and the matrix of resin polymers (Fong, 2004).

2.6.5- Electrohydrodynamic Methodologies

Electrospinning, electrospraying, co-axial jetting and electrohydrodynamic printing all stem form the same principles: the enablement of a cone with a jet, by means of passing an applied voltage to a flowing medium. Electrospraying and electrospinning result in the formation of relics and fibres respectively (Ahmad, 2007). Co-axial jetting has been used to prepare encapsulated materials as well as encapsulated fibres (Huang *et al.,* 2006). By using this technique there is a possibility of printing pattern polymeric materials and potential advantages over conventional techniques.

2.7- Characterisation of Polyurethane Based Composites

Interaction between the tissue and biomaterials depends on the physical and chemical characteristics of material and specifically on chemical composition and surface properties (Guo *et al.,* 2007). It is important to analyse materials *in-vivo* and *in-vitro* if they are to be used for any biomaterial purpose. Fabrication of crystalline nano-hydroxyapatite and to obtain nano-particles with agglomerated-free structure and uniform particle size is difficult. In case of polyurethane; toxic material such as isocyanates is one of the main components, so it is necessary to identify the concentration.

It is possible to follow a reaction and analyse the structural (chemical), thermal physical and biological properties of the material, by using the techniques such as Fourier Transform Infra red (FTIR), Raman spectroscopy, Nuclear Magnetic Resonance (NMR) for chemical, Thermo Gravimetric Analysis (TGA), Differential Scanning Calorimetry (DSC) for thermal, X-ray Diffraction (XRD) and Scanning Electron

Microscopy (SEM) with Energy Dispersive Spectroscopy (EDS) for physical and morphological and cell culturing and bacterial adhesion analysis for biological purposes. Infrared spectroscopy is used to identify certain bonds within a material. During the synthesis of polyurethane, some bonds will be broken (-N=C=O) and some new bonds will be formed (N—H, C=O). FTIR is the primary technique to detect the presence of these new bonds. Several studies have been conducted to analyse the polyurethane with FTIR and determine presence of bonds (Ren *et al.,* 2004; Mondal *et al.,* 2006), identify the surface modifications (Liu *et al.,* 2006; Stachelek *et al.,* 2006) and the degradation analysis (Zhi *et al.,* 2006; Pielichowski *et al.,* 2004). The presence of bonds can be detected by correlating vibrations of products with reactants. The quantitative nature of the bonds can be indicated by intensities of the peaks. The reaction kinetics of material can also be identified by using this technique (Burel *et al.*, 2005).

Segmented polyurethane has the characteristic of two phase structure. Raman is the technique to analyse how the two phases exist (Xia and Song, 2006). This method provides to assess distribution of the segments within structure.

Thermal characteristics of the material can be detected with TGA and DSC. The thermal decomposition and glass transition behaviour of polyurethane/composite can be analysed. Hence, it is important to utilise these techniques prior to use as biomaterial. This gives an indication of the purity of material which is being used.

Degradation of polyurethane and polyurethane based composites can be analysed by using FTIR and Raman spectroscopy. During the degradation process, some changes are expected in the chemical bonds. Umare and Chandure (2008) used FTIR, TGA and XRD techniques to analyse the degradative behaviour of polyurethane. The changes in the bonds can be detected by FTIR and Raman spectroscopy by correlating the shifting of peaks and the intensities of peaks can also give indications.

The design of composite materials offers the opportunity to combine polymers and bioactive inorganic phases, thus creating scaffolds with tailored bioactivity and improved physical and mechanical properties (Kazarian *et al.,* 2004). Spectroscopic imaging is the method of choice for monitoring and analysis of the *in vitro* bioactivity of

composites due to chemical specificity of this imaging approach. XRD can be employed to identify crystalline phases formed on the surface of bioactive composite. The formations of apatite phases on surfaces of the material can also be monitored by using a SEM coupled with EDS. SEM can evaluate the morphological aspect of bioactive composite applied on dentine and can also perform to take some information about interaction between the tooth structure and composite.

Bacterial adhesion and colonisation onto biomaterial surfaces are frequent reason for the failure of biomaterials. Bacterial adhesion is the critical event in pathogenesis of foreign body infection. However, adhesion to the surface depends on surface chemistry of bacterial cells and materials (Park *et al.,* 1998). The data shows that the polyurethane surface suppresses the bacterial adhesion and exhibits good resistance to encrustation (Park *et al.*, 2002).

Literature studies (Grad *et al.,* 2003; Wang *et al.,* 2008) show that biocompatibility of polyurethane based composites can be evaluated by using cell culturing. Biocompatibility is a surface phenomenon, represented by cell—cell, cell—polymer and polymer—protein interactions. The factors which affect the biocompatibility of polymers is; shape, size, surface chemistry and roughness, morphology and porosity, composition, sterility issues and rate of degradation (Pavithra and Doble, 2008). Lee et al. (1996) suggested that there are two crucial factors which should be considered when determining cell attachment and proliferation properties at the surface of polyurethane. The first factor is the surface morphology which may be regulated by dispersion of hard segment phase in the polymer and second, the hydrophilic property which is induced by high chain mobility.

2.8- Summary

It has been reported in literature that due to better intrinsic properties polyurethane based composites have the potential of being used as restorative composite and provide improved interfacial adhesion with surrounding tissues. Among several groups of polyurethanes, polyether based polyurethanes (Section 2.3.4.1.2) appear to be an

appropriate material considering their hydrolytic resistance (Section 2.3.6.1) and stability in body and good physical and mechanical properties. Synthetic hydroxyapatite (Section 2.4.3) is almost chemically similar to mineral components of human bone/teeth and is classed as bioactive component. They have the ability to integrate in bone structure and support bone growth. To improve the properties of polyether based polyurethane, they were subjected to series of modifications (Section 2.3.8). Polyurethane's versatile chemistry allows chemical modification on both pendant groups and backbone of the polymer chain, alternatively coupling with nano-apatites in polyurethanes matrix can improve their properties for biomedical and dental applications. For this purpose nano-hydroxyapatite containing polyurethane will be synthesised and subjected to several characterisation techniques to evaluate its properties for dental restorative materials.

2.9- Aim and Objectives

Polymer composites are not novel; the challenge is to have chemical linkage between the inorganic nano-particles to the organic polymer matrix to produce nano-composite. It is postulated that the inclusion of nano-hydroxyapatite in polyurethane will improve the physical, thermal and biological properties of the composite.

Hence, the main aim of this study was to develop a covalently linked novel bioactive restorative composite. The objectives of this project were;

(i) to develop a method to synthesise a nano-composite that has chemical linkage between polyurethane and nano-hydroxyapatite

(ii) to characterise and compare this novel composite with different concentrations of nano-hydroxyapatite in terms of their;
   a. chemical properties by FTIR, Raman and ^{13}C NMR Spectroscopies
   b. physical properties by SEM, TEM and XRD techniques
   c. thermal properties by TGA and DSC methods
   d. biological properties by cell culturing and bacterial adhesion techniques

(iii) to synthesise nano-composite fibres using electrospinning technique

Chapter 3 Materials and Methods

Section 1

3.1- Introduction

This chapter is divided into two main sections. Section 1 describes the materials and methods used in this study related to synthesis of nano-hydroxyapatite (nHA), polyurethane (PU) and polyurethane/nano-hydroxyapatite (PU/nHA) composites. Section 2 deals with the characterisations of synthesised polymer and composites.

Nano-hydroxyapatite particles were synthesised by sol-gel technique described in Section 2.4.3.1.2, Chapter 2. This method was combined with oven drying for ageing and heat-treated in furnace to achieve crystalline hydroxyapatite. The reactants used for the synthesis of nHA were calcium and phosphate precursors and the obtained ratio was 1.66. Ethanol and deionised water were used as in all reactions.

3.2- Materials for Nano-Hydroxyapatite

Following materials were used during the synthesis reactions of nano-hydroxyapatite. The description of these reactants is described in Table 3.1.

3.2.1- Calcium Precursor and Solvent

AnalaR grade calcium nitrate tetrahydrate [$Ca(NO_3)_2.4H_2O$] was used as supplied by VWR International (UK). Anhydrous grade ethanol (CH_3CH_2OH) from Sigma-Aldrich (UK) was used as solvent with calcium nitrate tetrahydrate.

3.2.2- Phosphate Precursor and Solvent

AnalaR grade ammonium hydrogen phosphate [$(NH_4)_2HPO_4$] was purchased from VWR International (UK) and was used as the phosphate precursor in the reactions

and deionised water (10 mega-ohms) from USF Elga Option 3 Water Purifier was used as solvent.

3.2.3- Ammonium Hydroxide

AnalaR grade ammonium hydroxide (NH_4OH) solution (specific gravity ≈ 0.88) was used for pH adjustment as supplied by VWR International (UK).

Table 3.1 Reactant details for nano-hydroxyapatite synthesis *Molecular Weight

Reactants	Grade	M_w*	Min.Assay, %	Supplier
$Ca(NO_3)_2.4H_2O$	AnalaR	236.15	99	VWR
$(NH_4)_2HPO_4$	AnalaR	132.06	99	VWR
CH_3CH_2OH	Anhydrous	46.07	99.5	Sigma-Aldrich
NH_4OH	AnalaR	17.03	35	VWR

3.3- Materials for Polyurethane

The chemical reactants and solvents used for synthesis of polyurethane and composites were all analytical grade (AnalaR). The details of materials used for polyurethane synthesis are listed in Table 3.2.

3.3.1- Purification of Chemicals

High level of purity of reactant chemicals and solvents is essential if high molecular weight polymer is to be obtained. Impurities act as a chain stopper, therefore resulting in low molecular weight polymers.

3.3.2- *4,4*-Methylenebis(phenyl) Diisocyanate (MDI)

AnalaR grade Diphenyl Methane Diisocyanate (MDI) was purchased from Sigma-Aldrich (UK) and was used as it was received. Before using, it was stored at 4°C and

prevented from moisture contamination. The chemical structure of MDI is given in Figure 3.1.

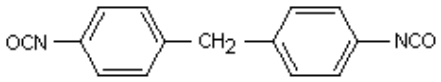

Figure 3.1 Chemical structure of MDI

3.3.3- *1,4*-Butane diol (BD)

AnalaR grade Butane diol (BD) was purchased from Sigma-Aldrich (UK) and was stored at 4°C to avoid moisture contamination. Before the experimental reaction it was dried in vacuum oven for 24 hours
at 80°C. Chemical structure of *1,4*-butane diol is given in Figure 3.2.

Figure 3.2 Chemical structure of *1,4*-Butane diol

3.3.4- Hydroxyl Terminated Polyethers

AnalaR grade hydroxyl terminated polyethers; polytetramethylene glycol (PTMG) from Sigma-Aldrich (UK) was used. PTMG was freeze dried (Virtis Advantage freeze dryer) at 1.3×10^{-4} bar by freezing to -40 °C on cold shelf and drying to 35°C in a 22 hour drying cycle, followed by storage in a vacuum desiccator at room temperature. The chemical structure is given in Figure 3.3.

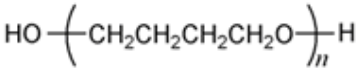

Figure 3.3 Chemical structure of PTMG

3.3.5- *N,N*- Dimethyl Formamide (DMF)

AnalaR grade *N,N*-Dimethyl formamide from Sigma-Aldrich (UK) was used as solvent. DMF was slightly decomposed at its normal boiling point to give small

amount of dimethylamine and carbon monoxide. It is likely that these impurities are present in commercial materials. Use of $CaSO_4$, $MgSO_4$, and silica gel or Linde type 4 Å-molecular sieves are preferred for their removal (Rehman, 1992). In this study, DMF was kept over Linde type 4 Å-molecular sieves for 72 hours prior to every reaction. The chemical structure is given in Figure 3.4.

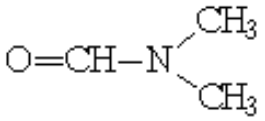

Figure 3.4 Chemical structure of DMF

3.3.6- Tetrahydrofuran

AnalaR grade tetrahydrofuran (THF) from Sigma-Aldrich (UK) was used to cast the resulting films. THF was kept over Linde type 4 Å-molecular sieves for 72 hours prior to every reaction. The chemical structure is given in Figue 3.5.

Figure 3.5 Chemical structure of THF

Table 3.2 Chemical reactant details for polyurethane synthesis *Molecular Weight

Reactants	Grade	M_w*	Supplier
Polytetramethylene Oxide	AnalaR	1400	Sigma-Aldrich
4,4-Methylenebis(phenyl) Diisocyanate	AnalaR	250.02	Sigma-Aldrich
1,4-Butane diol	AnalaR	90.12	Sigma-Aldrich
N,N-Dimethylformamide	AnalaR	73.09	Sigma-Aldrich

3.3.7- Calcium Chloride

GPR grade calcium chloride ($CaCl_2$) was purchased from BDH (UK) and was used as drying agent during reaction to absorb moisture.

3.3.8- Experimental Equipment

Glasswares used in all experiments were washed with neutral detergents, warm water and rinsed with deionised water followed by drying in oven at 130°C. In all reactions, stirring and heating were carried out using IKA Werke magnetic stirrer/heater. Polyethylene covered magnetic stirrer bars were used to allow the continuous stirring. The pH meter (Hanna Instruments HI 9024 pH probe) was calibrated with buffer solution at pH 4, 7, 10 and used to control the pH value during the nano-hydroxyapatite synthesis.

3.4- Sol-gel Method

Nano-hydroxyapatite were synthesised using sol-gel method (Section 2.4.3.1.2, Chapter 2) and this method was combined with oven drying (ageing) and heat treatment to produce nano-particles with high surface having enhanced crystallinity and potentially increased surface reactive hydroxyl (–OH) groups. The schematic flow chart of sol-gel technique is shown in Figure 3.6.

3.4.1- Synthesis of Nano-Hydroxyapatite

0.083 mol. (19.7 g) of calcium nitrate tetrahydrate [$Ca(NO_3)_2.4H_2O$] and 0.05 mol (6.6 g) of ammonium hydrogen phosphate [$(NH_4)_2HPO_4$] were measured before mixing and ratio of calcium and phosphate precursors was maintained at 1.66.

$Ca(NO_3)_2.4H_2O$ solution was prepared in 50 ml ethanol and solution stirred at 85°C for 15 min. While maintaining the $Ca(NO_3)_2.4H_2O$ solution at 85°C, $(NH_4)_2HPO_4$ was dissolved in 50 ml deionised water and the solution was added drop wise by using a glass-dropping funnel. NH_4OH was added into combined suspension to maintain the pH value using pH probe throughout the experiment. The pH of the mixture was maintained at 10.5. The stirring of combined suspension was continued for 4 hour as the gel formation occurred.

$$10Ca(NO_3)_2.4H_2O + 6(NH_4)_2HPO_4 + 8NH_4OH \longrightarrow Ca_{10}(PO_4)_6(OH)_2 + 20NH_4NO_3 + 6H_2O \quad \textbf{(eq. 3.1)}$$

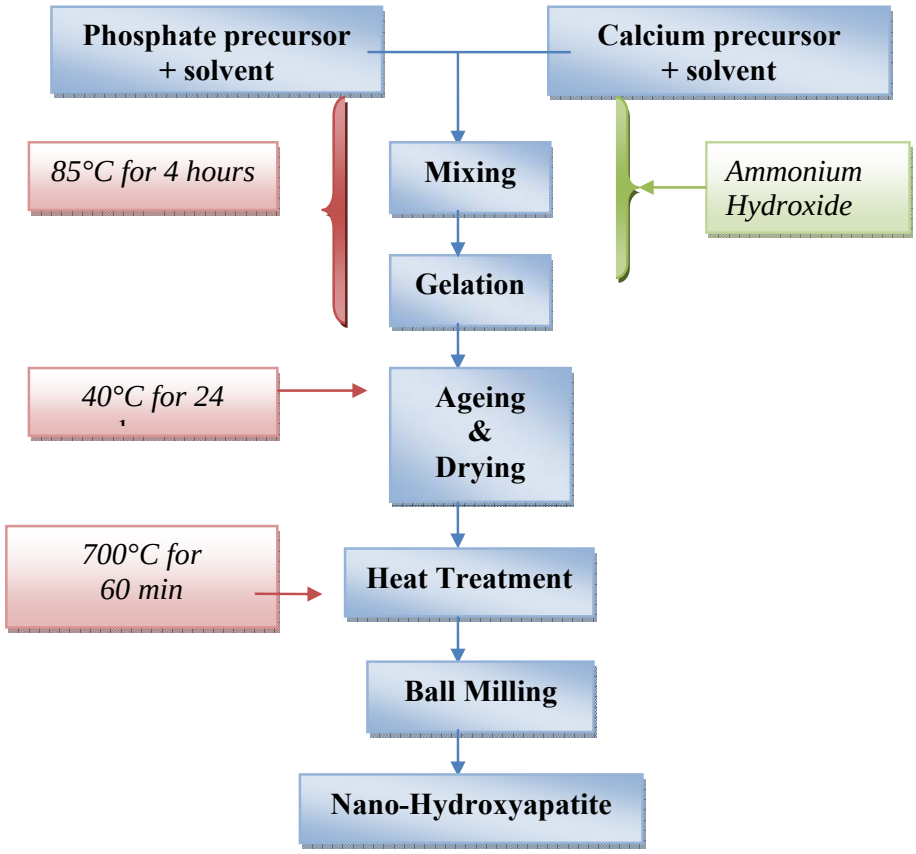

Figure 3.6 Schematic flow chart of Sol-Gel technique

.

3.4.1.1- Ageing and Heat Treatment

After synthesis, the nano-hydroxyapatite gel was filtered using a Buchner filter. The gel was not allowed to dry fully on the filter paper, but was taken off while still wet and placed in Petri Dish. The gel was spread by rolling the Petri dish, around the walls to increase the surface area being dried. The Petri dish was placed in oven for ageing at 40°C for 24 hours. After ageing the small particle size in its 'as prepared' state was heat treated in a furnace (Carbolite (Sheffield, UK) STF 16/75 1600°C tube furnace) in air at 700°C for 60 minutes at the rate of 10°C min^{-1} and then cooled down to 20°C at the rate of 10°Cmin^{-1}. The resulting heat treated nano-particles were ball milled for 12 hours to disintegrate the particles and produce fine powder.

3.5- Synthesis of Polyurethane

3.5.1- Introduction

Polyurethanes are step growth (condensation) polymers formed by the reaction of di or polyisocyanates with polyols. The chemistry involved in the synthesis of polyurethane centres around the reaction of the isocyanate group. Several reactions can occur involving the isocyanate groups such as adduct formation, oligomerisation, cyclo-addition and insertion reaction. Only oligomerisation and insertion reactions are important in the formation of polyurethanes (Rehman, 1992).

The principal primary reaction in the polymerisation of isocyanates is the insertion reaction. The reaction mechanism proceeds by a nucleophillic attack at the carbon atom in the isocyanate group. The product of this reaction comes in form of urethane linkage and the polymers containing urethane linkage are known as polyurethanes. Polyurethane elastomers typically exhibit a two-phase microstructure. This phase segregation results in the superior physical and mechanical properties. Factors affecting the degree of phase separation in polyurethanes include hydrogen bond formation between the urethane linkages and the carbonyl, segment length, segment polarity and crystallisability and composition (Rehman, 1992).

Polyurethanes were synthesised by polymerisation technique using PTMG, MDI, and BD employing DMF as a solvent.

3.5.2- Experimental Method

In the preliminary experiments PTMG with different molecular weights (M_w: 1000, 1400, 1500, 2000, and 2900) were used for synthesis. However, PTMG (M_w 1400) was selected after determination of results from initial characterisations. Various reactions were conducted with different mole ratio of PTMG, MDI and BD. In the preliminary experiments the ratio of PTMG: MDI: BD was 1:2:1, 1:3:0.5, 1:1:0.5, and 2:2:1 respectively. In this study, the stoichiometric amounts of the dried PTMG, MDI and BD were used. The mole ratio of PTMG: MDI: BD was 1:2.26:1.26 respectively and arrived at after a series of preliminary experiments.

All glass-wares were dried at 130°C prior to every experiment. The reaction was blanketed by a stream of dry oxygen-free nitrogen throughout the experimental reactions. The freeze dried PTMG (14.2 gm) was placed in three neck flask equipped with stirrer, condenser (guarded with calcium chloride drying tube), thermometer, and dropping funnel. DMF (10 ml) was added through the dropping funnel. Stirring and heating was carried out at 60°C until all the PTMG dissolved in DMF. The stirrer was rotated at 200 rpm through out the experiment.

Once the PTMG was completely dissolved in DMF then MDI (M_w, 250.2) solution [5.78 gm MDI (5% excess) and 25 ml DMF] was added drop wise in the flask with clean and dry dropping funnel. The flow of drops was maintained as 1 drop/sec. The temperature was continuously maintained at 60°C. After 35 minutes the addition of solution was completed and stirring was continued for further 40 minutes to give time for the monomers to react.

BD (M_w, 90.12) solution (0.95 gm BDO and 5 ml DMF) was added drop wise in the mixing solution with continuous stirring. Once the mixing of monomers were completed the stirring was maintained at 60°C for one hour.

After one hour the temperature was increased to 80°C. The material became slightly viscous at this stage, 25 ml DMF was added in the solution to allow it to stir for a further 30 minutes and then increased the temperature to 110°C for four hours to allow complete polymerisation. After four hours the solution became viscous and cloudy in appearance. The obtained solution was isolated in ice water. It was purified by further precipitation in ice-water/methanol. Once the sample was completely washed, the resulting sample was placed in vacuum pump for 48 hours and allowed it to dry completely over silica gel.

3.5.3- Film Casting

The resulting polymer sample was dissolved in THF to cast a film. The ratio of polyurethane sample and solvent was 1:10. The sample was dissolved for 45 minutes and the film was cast on dry Petri dishes.

3.6- Synthesis of Polyurethane/Nano-Hydroxyapatite Composite

3.6.1- Introduction

Several reactions were conducted to synthesise the composite based on PU and nHA.

3.6.2- Physical Synthesis

PU/nHA composite was physically synthesised by mixing the nano-hydroxyapatite and polyurethane. The method of nano-hydroxyapatite and polyurethane synthesis are described in section 3.4.1 and 3.5.2 respectively.

Prior to every reaction nano-hydroxyapatite was oven dried at 100°C for four hours to remove the surface moisture absorbed. Hydroxyapatite particles have tendency to absorb environmental moisture. Polyurethane was used as it was prepared and THF was used as solvent.

5 g of polyurethane was dissolved in 10% wt/wt of THF with continuous stirring at room temperature. Once the polyurethane was completely mixed in THF, nano-hydroxyapatite was added into the solution. The weight percentage of nHA was 5, 10, 15, and 20% wt/wt of polyurethane. The suspension was allowed to mix for overnight at room temperature. After mixing the films were cast on Petri dish from suspension and dried in inert atmosphere and then dried in vacuum pump for 48 hours.

3.6.3- Chemical Synthesis

Polymer composite was synthesised by chemical reaction using *in-situ* polymerisation technique. Various sequences of addition of monomers/particles were analysed and these chemical reactions were characterised. Finally, the sequence followed in this study is shown in schematic flow chart (Figure 3.7). Nano-hydroxyapatite and polyurethane were prepared in the laboratory as described in Sections 3.4.1 and 3.5.2 respectively. Prior to every reaction nano-hydroxyapatite

was oven dried at 100°C for four hours to remove the surface moisture. PTMG was freeze dried at 1.3×10^{-4} bar by freezing to -40 °C on cold shelf and drying to 35°C in a 22 hour drying cycle, followed by storage in a vacuum desiccator at room temperature. MDI was stored at 4ºC and sealed to prevent from moisture contamination. BD was vacuum dried at 80ºC for 24 hours. DMF was kept over 4 Å molecular sieves for 72 hour before every reaction.

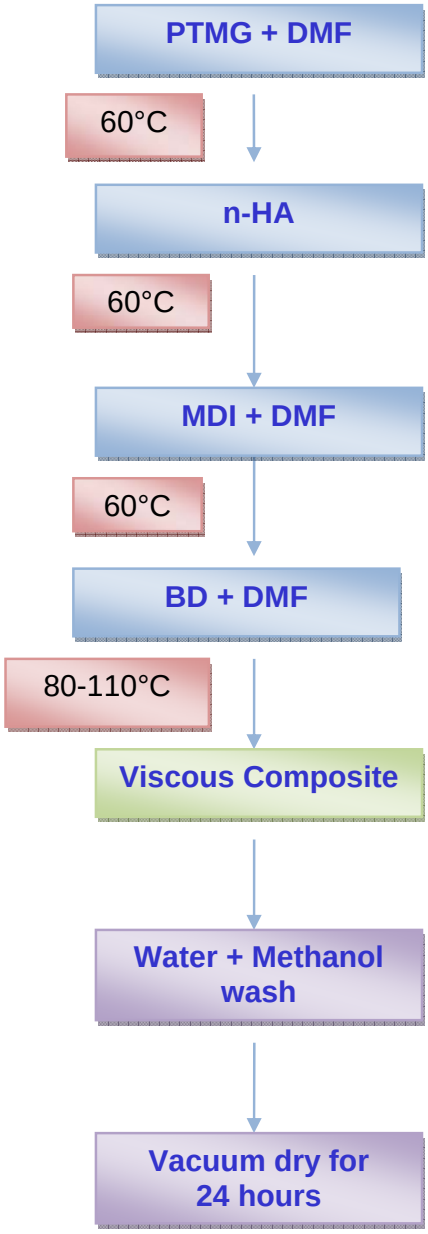

Figure 3.7 Schematic flow chart of chemical synthesis of PU/nHA composite

3.6.3.1- Experimental Method

Stoichiometric amounts of the dried PTMG, nHA, MDI and BD were used. The mole ratio of PTMG: MDI: BDO was 1:2.26:1.26 respectively. The concentration of nano-hydroxyapatite was 5, 10, 15, and 20% wt/wt relative to PTMG and denoted with PU/nHA5, PU/nHA10, PU/nHA15, and PU/nHA20 respectively.

Prior to every experiment all glass-wares were washed and dried at 130ºC. The reaction was blanketed by a stream of dry oxygen-free nitrogen throughout the reactions. The freeze dried PTMG (14.2 gm) was placed in three-neck flask equipped with stirrer, condenser (guarded with calcium chloride drying tube), thermometer, and dropping funnel. DMF (10 ml) was added through the dropping funnel. Stirring and heating was carried out at 60°C until all the PTMG dissolved in DMF. The stirrer was rotated at 200 rpm throughout the experiment.

Once the PTMG was completely dissolved in solvent nHA was added with specific concentrations (5, 10, 15, and 20 % wt/wt relative to PTMG) with 10 ml of DMF and stirred continuously at 60ºC for 45 minutes.

MDI solution [5.78 gm MDI (5% excess) and 25 ml DMF] was added drop wise in the flask with clean and dry dropping funnel. The flow of drops was maintained at 1 drop/sec. The temperature was maintained at 60°C. After 35 minutes the addition of solution was finished and stirring was continued for a further 60 minutes to give time for the monomers to react.

BD solution (0.95 gm BD and 5 ml DMF) was added drop wise in the mixing solution with continuous stirring. Once mixing was completed the stirring was maintained at 60°C for one hour.

After one hour the temperature was increased gradually to 80°C. The material became slightly viscous at this stage, 25 ml DMF was added in the solution to allow it to stir for further 30 minutes and then increased the temperature gradually to 110°C for four hours to allow complete polymerisation. The reaction was completed after the solution became viscous in appearance. The solution was filtered and washed three times with ice water and methanol to remove low molecular weight molecules, impurities and unreacted monomers. Once the sample was completely

washed, the resulting sample was placed in vacuum pump for 48 hours and allowed to dry completely over silica gel.

3.6.3.2- Film Casting

Thin films (0.05-0.1 mm thick) were prepared by casting from a 5% solution of the polymer. Films were cast on Petri dishes (90 mm in diameter) which had previously been cleaned and deactivated by washing in the detergent, rinsing in distilled water, then wiping with THF solvent to remove any contamination. The polymer solution was applied to the Petri dishes using glass micropipette. Each slide was flooded with 65 ml solution, so that the resulting films would have similar thickness of almost 0.5 mm. The Petri dishes were covered to avoid the environmental contamination and allowing the controlled evaporation of THF for 36 hours. The polymer films were removed from the slides by peeling or by floatation over distilled water. Films were dried under vacuum at room temperature over silica gel.

3.7- Synthesis of Electrospun Nano-fibres

Nano-fibres of PU and PU/nHA composites were synthesised using electrospinning method (Section 2.6, chapter 2). PU and PU/nHA10 composite were synthesised as described in Section 3.5.2 and 3.6.3 respectively.

3.7.1- Electrospinning Technique

The experimental setup for the electrospinning process is given in Figure 3.8. The conducting stainless steel nozzle had an internal diameter of 330 μm and was connected to the positive terminal of the high voltage supply (Glassman Europe Ltd), held together by epoxy resin. The polyurethane and composite materials were delivered to the nozzle by silicone tubing which was also attached to the perfusor (Harvard syringe pump, Harvard apparatus Ltd). A flow rate of 15 μl/min was deployed and the applied voltage was in the range of 7-9 kV. The fibers were collected 120 mm below the nozzle exit.

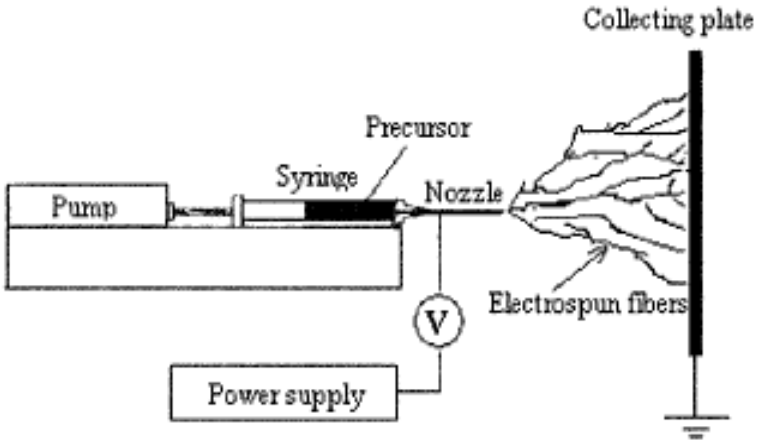

Figure 3.8 Schematic diagram of electrospinning technique (Adopted from Wu *et al.*, 2004)

Section 2

3.8- Characterisations

3.8.1- Introduction

Characterisation and analysis of a material constitute an important part within material science. The definition of the material characterisation is: *"characterisation describes those features of composition and structure (including defects) of a material that are significant for a particular preparation, study of properties, or use, and suffice for reproduction of a material"* (ASM International, 1996). This definition limits the characterisation methods and provides information about composition, structure, and defects and excludes those methods that give information mainly related to materials properties, such as thermal and mechanical properties In this study, different methods and techniques have been used to characterise the materials including:

1. Chemical
    - Fourier Transform Infrared Spectroscopy (FTIR)
    - Raman Spectroscopy
    - ^{13}C Nuclear Magnetic Resonance (^{13}C NMR)

2. Physical
    - X-ray Diffraction (XRD)
    - Scanning Electron Microscopy (SEM)
    - Transmission Electron Microscopy (TEM)
3. Thermal
    - Thermogravimetric Analysis (TGA)
    - Differential Scanning Calorimetric (DSC)
4. Biological
    - Biostability
    - Bioactivity
    - Bioadhesion
    - Biocompatibility
        i. Cell culturing
        ii. Bacterial Adhesion

3.8.2- Samples Preparation

3.8.2.1- Polyurethane and Polyurethane/Nano-Hydroxyapatite Composites

The samples of PU and PU/nHA were prepared by hot pressing technique using the Rondol technology machine (Rondol Technology Ltd, USA). Metal moulds were used with the dimensions of 90x15x2 mm^3 in length, width and thickness respectively. The schematic diagram of the metal mould is shown in Figure 3.9.

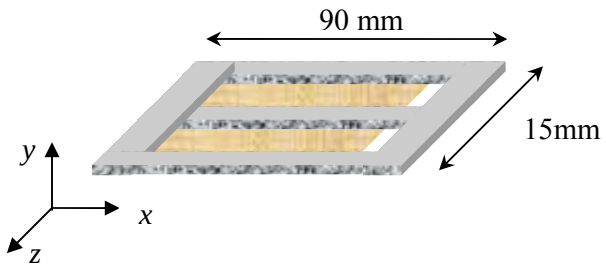

Figure 3.9 Schematic diagram of metal mould for hot pressing

The samples were cut into small pieces by sharp scalpel blade and placed in mould. The metal mould was sprayed with Teflon and covered with a Teflon sheet from

both sides. This was performed in order to avoid attachment of composite material with metal. The use of Teflon sheet results in good detachment of the sample as it acts as a separating media.

3.8.2.1.1- Hot Pressing Technique

The samples in moulds were placed in the hot pressing machine (Rondol technology). Hot pressing was conducted in step wise procedure. (i) Prior to placing the sample, the temperature was raised to 225^{o}C. Once the required temperature was achieved, samples were placed on hot plate and pressure was applied, (ii) One kilo Newton (KN) pressure was applied and held it for one minute, (iii) the pressure was raised to 35 KN and wait for one minute, (iv) the temperature was decreased to room temperature (average 23^{o}C) and the water supply was opened to cool it down. The sample was taken out from the machine to analyse it. The prepared samples were placed in a vacuum pump (Townson and Mercer Ltd, Altrincham England) at 50^{o}C and 25-30 Hg bar for drying. After 24 hours all the samples were taken out. Samples were cut with sharp scalpel blade into rectangular specimens.

3.8.3- Chemical Characterisations

Qualitative spectroscopy is one of the most powerful and versatile analytical technique (Coates, 2000). Spectroscopic methods play a fundamental role in the solution of many problems in organic and inorganic chemistry. Four spectroscopic techniques have been widely used:

1. Ultraviolet (UV) spectroscopy
2. Infrared (IR) spectroscopy
3. Nuclear magnetic resonance (NMR)
4. Mass spectrometry (MS)

Of the four spectroscopic techniques, three of them (UV, IR, and NMR) are considered as absorption spectroscopy, in which there is absorption of electromagnetic radiation by the sample under study over a range of wavelengths, whereas, MS is different to these in that it does not involve the absorption of

radiation. The infrared spectrum is produced as a result of the absorption of electromagnetic radiation at frequencies that correlates to the vibration of specific sets of chemical bonds within the molecule (Coates, 2000).

Standard text books (Banwell, 1994) and literature (Tsuda and Arends, 1997; Schmitt and Flemming, 1998; Gonon *et al.,* 2001; Chan and Kazarian, 2006) have explained in detail about the spectroscopy, types, and their mechanism of action.

3.8.3.1-Fourier Transform Infrared Spectroscopy (FTIR)

In this study, FTIR spectra of nHA powder, PU and PU/nHA composite samples, were obtained using a Nicolet 8700 FTIR spectrometer in conjunction with Photoacoustic Spectrum (PAS) cell (Figure 3.10). Spectra were obtained in the mid infrared region (4000-400 cm^{-1}) at 8 cm^{-1} resolution, averaging 256 cm^{-1} scans. The sample chamber of the PAS cell was purged with dry helium gas (pre-dried over a column of magnesium perchlorate). A background scan was obtained prior to each set of tests using carbon black specimens.

Figure 3.10 Photoacoustic Sampling for FTIR Spectroscopy

3.8.3.2- Raman Spectroscopy

In the broadest sense the Raman spectroscopy involves the scattering of light as a result of its interaction with matter. When monochromatic light from a laser strikes a

sample, almost all of the light is scattered elastically. This is known as Rayleigh scattering and certainly is the strongest component of the scattered radiation. A small fraction of the light is scattered inelastically: that is, there is an energy transfer between the incident light and the scattering molecules. This change in energy or frequency between the incident and scattered light corresponds to an excitation of the molecular system, most often in a vibrational mode (Katz *et al.,* 2003).

The Raman spectra were recorded by using Nicolet Almega XR dispersive Raman spectrometer (Figure 3.11). A background scan was obtained prior to each set of tests. The spectra were obtained in the range 4000-400 cm^{-1} over an average of 256 cm^{-1} scan times and 4 cm^{-1} resolution.

Figure 3.11 Raman Spectroscopy

3.8.3.3- ^{13}C Nuclear Magnetic Resonance (^{13}C NMR)

Nuclear Magnetic Resonance (NMR) was utilised to analyse the structural interaction. There are various ways to utilise NMR such as solid state NMR, ^{1}H NMR, ^{13}C NMR. NMR resonant frequencies for a particular substance are directly proportional to the applied magnetic field. All nuclei that contain odd number of protons or neutrons have an intrinsic magnetic moment and angular momentum. In this study ^{13}C NMR was utilised as the samples were dissolved in a solvent.

The samples used in this study were the PU and PU/nHA20. All the ^{13}C NMR spectra were recorded on Bruker 600 MHz NMR spectrometer using magnetic field frequency 100 MHz for ^{13}C nuclei. The solvent was THF for both samples (*courtesy of* Dr. Greg Coumbarides, School of Biological and Chemical Sciences, Queen Mary University of London).

3.8.4- Physical Characterisations

Physical properties of nano-hydroxyapatite and polyurethane are closely related to their morphology and phase separation. Surface properties have found to be one of the key parameters which affect biocompatibility. Surface properties regulate surface texture, surface energy, and composition which need to be analysed at micro- and nano-scale levels (Ratner *et al.* 1997). Combination of physical methods for investigating surface properties of nano-hydroxyapatite, polyurethane, and composites seems essential.

3.8.4.1- X-ray Diffraction Analysis (XRD)

X-ray diffraction is the interaction of physics of X-ray and the geometry of crystals. The two basics are a wave motion capable of interference (X-rays) and a set of periodically arranged scattered centres i.e., the atoms of a crystal (Cullity and Stock, 2001). It is one of the most frequent and important method in qualifying materials. Materials have been characterised not only by their chemical composition, but also by their crystal state and the quantity of crystalline components. The quantitative phase analysis is applied for the analysis of individual crystalline constituents in multicomponent mixtures. In these mixtures, the individual constituents show characteristic diffraction intensity independent of the presence of other components. The intensity is proportional with the amount of the components. Diffraction is due basically to the existence of certain phase relation between two or more waves. It is therefore, a scattering phenomenon and not one involving any type of interaction between X-rays and atoms. Atoms disperse incident X-rays in all directions and in some of these directions the scattered beams will be completely in phase and so reinforce each other to form diffracted beam and known as constructive interference.

In all other directions the scattered beams are out of phase and cancel each other and referred as destructive interference. However, the diffracted beam is strong compared to the sum of all the rays scattered in the same direction due to the reinforcement which occurs, but is weak compared to the incident beam as the atoms of a crystal scatter only a small fraction of the energy incident on them (Griger, 1987; Cullity and Stock, 2001).

The X-ray diffraction data were collected for the nHA powder and PU and PU/nHA composite samples using a Simens D 5000 diffractometer using Cu-Kα radiation (kα1 = 0.15406 nm). An attachment was used across the 2θ range. The samples were set at 1° and fixed, and the detector was scanned between 10 and 70°. A step size of 0.02° was used, with a step time of 2.5 seconds (*courtesy of* Dr. Rory Wilson, School of Engineering and Material Sciences, Queen Mary University of London). For nHA the identification of phases was achieved by comparing the diffraction pattern obtained to powder diffraction cards on the International Commission for Diffraction Data-Joint Committee on Powder Diffraction Standards (ICDD-JCPDS) database. Peak positions were obtained using the XRD evaluation software EVA™ (Bruker-AXS, Germany).

3.8.4.2- Transmission Electron Microscope (TEM)

The nHA particles were studied by using JEOL JEM 2010 High Resolution Transmission Electron Microscope (TEM) operating at 200 KeV. Samples were prepared by ultrasonically dispersing the powders in methanol prior to collection on carbon coated copper grids (Holey Carbon Film, 300 mesh Cu, Agar Scientific). Morphology and average particle size were estimated from the bright field images.

3.8.4.3- Scanning Electron Microscopy (SEM)

The scanning electron microscopy (SEM) has become an important tool for both applied and basic research applications. Its research extends from the science of physicists and the engineers to the biologists. It is a versatile instrument for the analysis of the micro-structural characteristics of the biological objects (Wischnitzer,

1980). These contributions of SEM resulted in high magnification with great depth of field and also produce images over a wide range of magnifications.

3.8.4.3.1- Sample Preparation

The morphology and size of nHA particles, PU, PU/nHA composites were characterised by SEM [JEOL 6300 JSM and FEI Inspect (Figure 3.12)] using EDS and field emission method. All samples were carbon coated with sputter coater, which used argon gas and electric field. Samples were analysed at 10 KV at various magnifications.

Figure 3.12 Scanning Electron Microscopy

3.8.4.4- Brunauer-Emmett-Teller (BET) Surface Area Analysis

The specific surface area of the powders was determined by the Brunauer-Emmett-Teller (BET) method using a Micromeritics Gemini II 2370 surface area analyser. The 5-point multipoint adsorption method was used. All powdered samples (0.2-0.5 g) were degassed with nitrogen using a Flow Prep 060 controller at 200°C for at least 3 hrs prior to analyses.

3.8.5- Thermal Analysis

The incompatibility between polar hard segment and less polar soft segment in polyurethane causes the heat of mixing to be positive and drives the two segments to

phase separate (Adhikari *et al.* 1999; Adhikari *et al.* 2000). Thermal analysis is important to investigate the heat decomposition and glass transition of polyurethane and composites.

3.8.5.1-Thermogravimetric Analysis (TGA)

Thermogravimetry is defined as a technique whereby the weight of a substance, in an environment heated or cooled at a controlled rate, is recorded as a function of time or temperature. Thermogravimetric Analysis (TGA) is an analytical technique used to determine the thermal stability and the fraction of volatile components by analysing the weight changes. This analysis relies on a high degree of precision in three measurements: weight, temperature and temperature change (Keattch and Dollimore, 1975; Wunderlich, 1990)

This technique is commonly employed to determine the characteristics of polymer materials, to analyse degradation temperatures, absorbed moisture content of the materials, the level of inorganic and organic components in materials, decomposition points and solvent residues. The measurement is normally carried out in air or in inert atmosphere such as Helium or Nitrogen. It is also measured in a lean oxygen atmosphere (1-5% O_2 in N_2 or He) to slow down oxidation.

TGA Q500 (TA Instruments 530) (Figure 3.13) with auto sampler was used to study the thermal decomposition of nHA, PU and PU/n–HA composite samples under non-isothermal conditions at a constant rate of 20°C.min^{-1} in inert nitrogen atmosphere from 20 to 800°C. For TGA analysis, films were cut into small pieces and approximately 20 mg of sample was taken for the measurements.

Figure 3.13 Thermogravimetric Analysis

3.8.5.2- Differential Scanning Calorimetry (DSC)

Differential Scanning Calorimetry (DSC) is a technique to measure the energy required to establish a nearly zero temperature difference between a substance and an inert reference material. DSC can be used to assess the thermal and structural properties of any material; it measures the heat flow (mW) as a function of temperature. This technique gives results about glass transition temperature (T_g), melting temperature (Tm) and polymerisation/ gelation temperature (Lourenco and Santos, 2005).

DSC (Perkin Elmer, USA) (Figure 3.14) was used in three sections of temperature range;

(i) -60 to 150°C, (ii) then quenched it back to -60°C with a cooling rate of 20°C.min^{-1}, (iii) again heat it up to 250°C with the heating rate of 5°C.min^{-1}. Nitrogen purge gas and aluminium crucibles of 40 µg were employed for all experiments.

Figure 3.14 Differential Scanning Calorimetry

The specimen was put in an aluminium crucible and closed by pressing aluminium cap, which was pierced by a needle on the top for degassing. The sample was heated once over the mentioned temperature range. The specimens were in film form and cut into small rectangular pieces. The average weight of each sample was approximately 3.6 ± 0.2 mg.

3.8.6- Biological Analysis

3.8.6.1- Biostability Analysis

The biostability of polymer is one of the essential parameter for their use as biomaterials. To ensure viability of these composite materials, their behaviour in wet environment has to be investigated, due to presence of intrinsic hygroscopic and hydrophilic nature of some of these materials such as nano-HA (Kumar and Kumar, 2006). The presence of ester and ether linkages in the backbone of polyurethanes inevitably results in some degree of hydrolysis; however, the rate of degradation is of prime importance and is dependent on the chemical structure of the polyurethane. There are certain factors which show impact on the biostability of polyurethane such as the hard segment/soft segment composition ratio. Materials that are in interaction with body fluid may involve dissolution or degradation of surface layers and may involve in leaching out of unbound or loosely bound components or an uptake of fluids into the structure of the material. The presence of discrete zones at the interface between the components could cause water absorption and the osmotic effect would result in swelling and residual pressure on the tissue and can damage the material and cause some undesirable effects such as softening of the resin matrix, resin degradation, and leakage of filler elements (Parker and Braden, 1989; Martin *et al.,* 2003; McCabe and Rusby, 2004).

3.8.6.1.1- Sample Preparation

Six samples from PU and PU/nHA (PU/nHA5, PU/nHA10, PU/nHA15, and PU/nHA20) composites were prepared by hot pressing technique (Section 3.8.2.1.1). Each of six samples was immersed in separate flat surface plastic bottles filled with 25 ml deionised water and phosphate buffer solution (pH 7.4) and placed in a 37°C incubator for 1, 7, 14, 21, 40, 90 days. After every 14 days the solutions were decanted off and replaced with fresh media. The samples were removed from the media after each period of immersion and then washed with distilled water and vacuum dried at 60°C for 24 hours to analyse. Before and after immersion the samples were characterised with contact angle measurement, weight loss

measurement, FTIR (3.8.3.1), Raman spectroscopy (3.8.3.2), XRD (3.8.4.1), and SEM (3.8.4.3) techniques.

3.8.6.1.2- Contact Angle Measurements

To evaluate the wetting properties of samples, advancing contact angle measurements of water were performed by a droplet expanding technique, using a CAM 200 Optical Contact Angle Meter (KSV Instruments Ltd. Finland) equipped with a video recorder that collected one image per second. Small holes were pressed through the film and water droplets (volume 5 µl) were enlarged at constant velocity from under the materials through the holes by using a syringe. Image analysis was performed with CAM 200 Software and contact angle calculation using curve fitting was based on the Young-Laplace equation, yielding contact angles on either side of the droplet and their mean value. Before contact angle measurements the films were cleaned and allowed to dry. Six samples of each film were prepared as described in Section 3.5.3.

3.8.6.1.3- Weight Loss Measurement

The weight of the samples was measured before and after solution ageing by using digital balance. The weight loss was measured in percentage over predetermined time intervals by using the formula:

$$\text{Weight loss (\%)} = \frac{100 \times (M_1 - M_2)}{M_1} \qquad \textbf{(eq. 3.2)}$$

where, M_1 and M_2 are the weight before and after immersion respectively.

3.8.6.2- Bioactivity Analysis

Bioactive materials can stimulate a specific response in the surrounding tissues by means of complex mechanism involving three main phases: ion leaching, partial dissolution of the ceramic surface and the precipitation of bonelike apatite layer on

the ceramic surface (Chatzistavrou *et al.,* 2006). For this the *in-vitro* apatite formation can be reproduced in simulated body fluid (SBF) with ion concentrations nearly equal to human blood plasma. The factors such as surface chemistry and topography of the substrate, and ionic concentrations and components of the SBF solution can influence on the growth rate of the apatite layer (Qu *et al.,* 2007). The *in-vitro* analysis was carried out in modified-simulated body fluid (m-SBF) at controlled temperature of 37°C.

3.8.6.2.1- Preparation of Modified Simulated Body Fluid

Modified simulated body fluid (m-SBF) was prepared, as described by Oyane et al. (2003), by dissolving reagent in deionised water as shown in Table 3.3, which is almost equal to those of human blood plasma, except HCO_3. All reagents were analytically graded and supplied by Sigma-Aldrich, UK. In m-SBF, the buffer agent, 2-(4-(2-hydroxyethyl)-1-piperazinyl) ethanesulfonic acid (HEPES) and the counter agent, aqueous 1.0 M NaOH were used.

In this experiment, all the apparatuses were washed with 1.0 M of HCl, neutral detergent, and ultra pure water. Initially, approximately 700 ml of deionised water were poured into a 1000 ml glass beaker, and this was stirred using a magnetic bar 37±0.5°C. After each preceding reagent had completely dissolved, the reagents were dissolved in the water in the sequence listed in Table 3.3.

The HEPES was previously dissolved in 100 ml of aqueous 0.2 M NaOH. The solution was adjusted to a pH of 7.4 by titring aqueous 1.0 M of NaOH into the dissolving solution. The solution was then cooled to room temperature (23°C), and the total volume adjusted to 1000 ml by adding deionised water. The resulting m-SBF was stored at cool place (4°C) for three days and 40 ml of the m-SBF was sealed in a 50 ml capacity polystyrene bottle fitted with a screw cap and kept at 37°C to examine the precipitates. All the m-SBF was clear and without showing any visible precipitation.

3.8.6.2.2- Sample Preparation

The films were prepared as described in Section 3.5.3. The resulting films were cut uniformly into 12 mm diameter by using diamond end cutter. Six samples of each material were used for this study. The samples were sterilised by soaking into 70% ethanol for predetermined time interval and dried before immersion. The sterilised samples were immersed in 15 ml m-SBF containing polystyrene tubes (Fischer Scientific, UK) covered with lids for 1, 7, 14, 21, and 40 days, which were maintained at 37°C.

The m-SBF was changed after 14 days to maintain a constant liquid composition. After different periods of immersion, the samples were removed from the solution, rinsed with distilled water, wiped and dried at 50°C overnight. The samples were characterised by using FTIR (3.8.3.1), Raman Spectroscopy (3.8.3.2), XRD (3.8.4.1) and SEM with EDS (3.8.4.3).

Table 3.3 Reagents used for preparation of modified simulated body fluid (Oyane *et al*., 2003)

Compounds	**Reagents**	**Amount**
Sodium Chloride	NaCl	5.403g
Sodium Bicarbonate	$NaHCO_3$	0.504g
Sodium Carbonate	Na_2CO_3	0.426g
Potassium Chloride	KCl	0.225g
Potassium Hydrogen Phosphate trihydrate	$K_2HPO_4.3H_2O$	0.230g
Magnesium Chloride hexahydrate	$MgCl_2.6H_2O$	0.311g
Sodium Hydroxide	0.2 M—NaOH	100 mL
	HEPES	17.892g
Calcium Chloride	$CaCl_2$	0.293g
Sodium Sulfate	Na_2SO_4	0.072g
Sodium Hydroxide	1.0 M—NaOH	15 mL

3.8.6.3- Bioadhesion Analysis

The interfacial linkage between PU and nHA is one of the major factors that determine the ultimate properties of the composite. The formation of apatite at the interface or bonding to already present apatite could create a much closer to natural state of restoration than the present composite systems (Mjor *et al.,* 2000; Engqvist *et al.,* 2004.

Different methods such as tensile strength, micro-tensile strength, and shear bond strength have been employed to analyse the bond strength of the materials with the tooth substrate (Drummond *et al.,* 1996; Mortazavi *et al.,* 2004). Push-out testing has been widely used to assess the mechanical strength developed at the material and the bone/tooth interface in both *in-vitro* and *in-vivo* tests. This method measures the interfacial shear strength that has been developed between a biomaterial and tissue (Thomson and Gregson, 1999).

Bioadhesion analysis was conducted on non-carious, extracted, human molar teeth (QMREC2006/26). The teeth were selected randomly and the criteria of selection were anonymous. The extracted teeth were stored in 70/30 water/ethanol to sterilise and keep the structure intact.

3.8.6.3.1- Sample Preparation

Extracted teeth were moulded in self-cured polymethylmeth acrylate (PMMA). Uniform occlusal cylindrical through dentine cavities of 4 mm diameter were prepared using diamond edged core drill (UKAM Industrial, CA USA) under the continuous flow of water to avoid the thermal damage of tooth structure. The cavities were filled with experiment materials i.e. glass ionomer cement (GC Fuji IX), the resin based composites, RBC (Filtek Supreme), PU and PU/nHA (10, 15, and 20% wt/wt) composites.

GC Fuji IX GP (GC International, Tokyo, Japan) radiopaque posterior glass ionomer capsules were used. The capsules were placed in a high speed amalgamator for 10 seconds and then packed in to the cavity with dough-like consistency material. The

cements were self-cured in 2.5-4.5 minutes. Excess cement from margin of the cavity was removed with sharp blade. After initial setting the samples were placed at 37°C and 100% relative humidity for 24 hours to achieve maturation. For Filtek Supreme (3M ESPE, UK), the cavities were etched with 36% orthophosphoric acid (Vococid, Voco Germany) for 20 seconds and then washed with water thoroughly to remove all the acid. After washing the cavities were dried and Scotchbond Multipurpose Adhesive (3M ESPE, UK) was applied on the inner surface of the cavities. The applied bond was cured by using blue visible light (DeTrey Dentsply, Germany; wavelength ≈ 472 nm) for 60 seconds. In the last step the cavities were filled in 2 mm increments of resin based composite and were light cured for 60 seconds. The distance of the light was maintained for each sample. The surface of the restorative composites was polished by using Soflex (3M ESPE, UK). The experiment materials, PU, PU/nHA (10, 15, and 20% wt/wt) were heated at 160°C and condensed in the cavity as shown in Figure 3.15, by using Teflon coated condenser. The filled teeth were immersed in deionised water and artificial saliva at 37±1°C and were analysed with pre-determined time interval of 7, 21, 40 and 90 days. After the materials were set inside the cavities the teeth were sectioned axially into2 mm thick disks using diamond blade under water flow. Five sections were obtained from each tooth

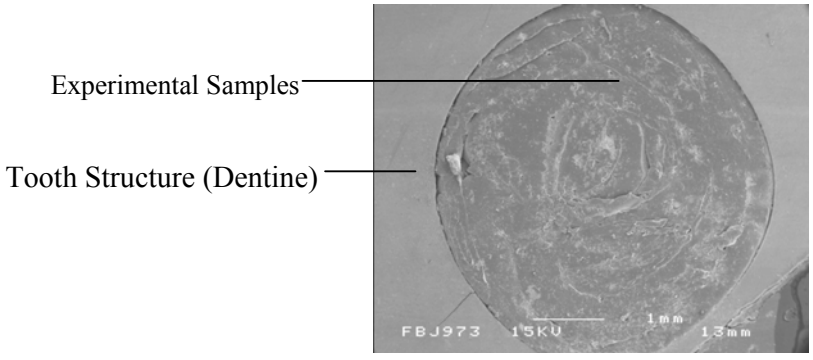

Figure 3.15 SEM image of experiment sample condense in tooth cavity

3.8.6.3.2- Artificial Saliva Preparation

Artificial saliva was prepared as it was described by Levallois et al. (1998). The reagents were analytically graded. All glass-wares were thoroughly cleaned with neutral detergent and washed with deionised water and dried completely at 130°C.

Initially, approximately 700 ml of deionised water were poured into a 1000 ml glass beaker, and this was stirred using a magnetic bar at 37±1°C. After each preceding reagent had completely dissolved, the reagents were dissolved in the water in the sequence listed in Table 3.4. The pH of the artificial saliva was 6.8. After mixing the artificial saliva was stored overnight at 37±1°C. The artificial saliva was clear and did not show any visible precipitation.

3.8.6.3.3- Push-out Test

The discs were dried prior to Push-out test for the shear bond strength. Push-out test was performed on Instron 6025 with the cross head speed of 1 mm min^{-1} and a load cell of 1 KN. It was maintained that Instron machine was calibrated before each test. The test was performed at 25±2°C and humidity was 55 ± 3%. A long stainless steel rod of 12 mm was used to push the samples from tooth. The metal rod was divided into two sections. The upper part of 9 mm length and 6 mm diameter was hollow to reduce the weight of the rod. The lower part was 3 mm in length and 4 mm in diameter. The schematic structure of push-out test method shows in Figure 3.16.

Table 3.4 Composition of artificial saliva (Levallois *et al.,* 1998)

Compound		**Source**	**Concentration (mg/l)**
Sodium chloride	NaCl	Sigma-Aldrich	125.64
Potassium chloride	KCl	Sigma-Aldrich	963.90
Potassium thiocyanate	KSCN	Aldrich	189.20
Potassium dihydrogen orthophosphate	KH_2PO_4	GPR	654.50
Urea	$CO(NH_2)_2$	Sigma	200.00
Calcium chloride dehydrate	$CaCl_2.2H_2O$	Aldrich	227.80
Sodium sulphate	$Na_2SO_4.10H_2O$	Aldrich	763.20
Sodium Hydrogen Carbonate	$NaHCO_3$	Sigma-Aldrich	630.80
Ammonium chloride	NH_4Cl	Sigma-Aldrich)	178.00

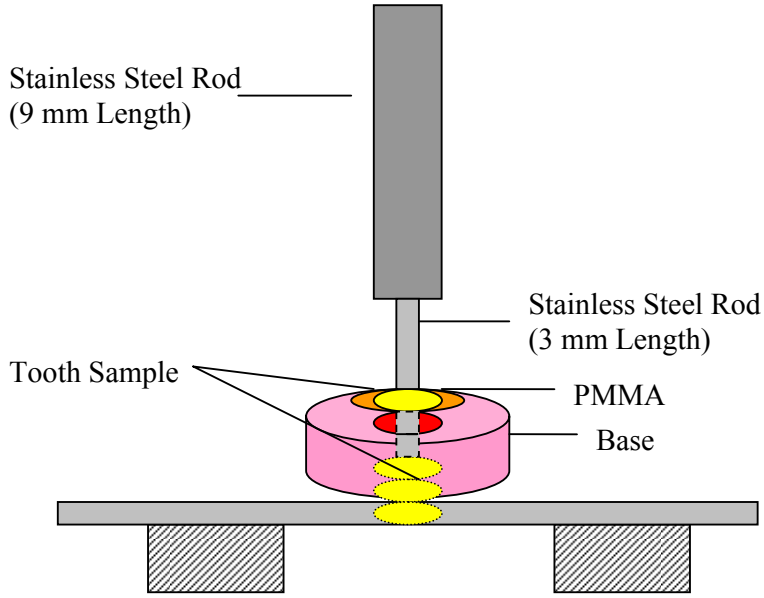

Figure 3.16 Schematic diagram of Push-out Test

3.8.6.3.4- Scanning Electron Microscopy (SEM)

After push-out test result, the resulting tooth discs were analysed. The morphology and surface analysis were characterised by Scanning Electron Microscopy, SEM (JEOL 6300 JSM and FEI Inspect) and EDS at an activation voltage of 10 kV. The samples were mounted and were sputter coated under vacuum with carbon.

3.8.6.4- Biocompatibility Analysis

3.8.6.4.1- Cell Culturing

3.8.6.4.1.1- Sample Preparation

PU and PU/nHA20 samples were used for cell culturing experiment. Six samples of each film were used for this experiment. Films were cast as it was mentioned in section 3.5.3.

3.8.6.4.1.2- Cells

Primary rat calvarial osteoblasts isolated by collagenase digestion isolated by explants culture were used in the experiments. The cells were cultured and maintained in Minimal Essential Medium (MEM) Alpha medium (Invitrogen, UK) which was supplemented with 10% of fetal calf serum (FCS) (Sigma Aldrich, UK), 0.3 µg/ml fungizone (Invitrogen) and 50 µg/ml penicillin- 50 µg/ml streptomycin (Invitrogen). The cells were grown in a humidified incubator at 37°C with 5% CO_2. The medium was replaced twice a week.

3.8.6.4.1.3- CellTiter 96® AQ_{ueous} Non-Radioactive Cell Proliferation Assay (MTS)

Cell proliferation on the films was assessed by an MTS assay. A solution of MTS (Promega UK Ltd) and phenazine methosulfate (PMS) (Sigma, UK) was used to determine the number of viable cells on the films.

3.8.6.4.1.4- Cell culture

To evaluate osteoblast proliferation on different films, cells were seeded on PU and PU/nHA20 composite films. Osteoblasts of 7-9th passage were used for the tests. 90% confluent cells were trypsinised and cell density was adjusted to 3×10^4 cells/ml. Sterile films were transferred into 24 well plates. The films were seeded with 3×10^4 cells × ml / well for 3, 5 and 7 days in triplicates. Wells with no films were used as controls. The films containing cells were placed in a humidified incubator at 37°C with 5% CO_2. Cell proliferation was analysed at day three.

3.8.6.4.1.5- MTS Assay Protocol

MTS changes colour on reacting with cells. The amount of colour change is directly proportional to the number of living cells. In order to measure cell proliferation, films were taken out from the medium at day 3, 5 and 7 and were placed in new 24 well plates. PMS and MTS solution were mixed at the concentration of 50 µl/ml and added to 200 µl/ ml medium. Then 500 µl of MTS/PMS solution containing medium was added to wells containing films.

The plates were incubated for three hours. After three hours, three samples of 100 µl each were taken out from each of the wells and transferred to 96 well plates. The colorimetric measurement was then performed using a spectrophotometer at 490 nm (FLUOstar Optima, BMG Labtech).

3.8.6.4.2- Bacterial Adhesion

Sample discs were incubated with standardised suspensions of *Streptococcus sanguinis* strain NCTC 7863 for 2hrs and washed in PBS. Six samples of 12 mm in diameter were prepared as described in Section 3.5.3.

Blood agar plate was prepared by using 40 g of blood agar (Oxoid Ltd, UK), dissolving in 1000 ml. 100 ml of Defibrinated Horse Blood (TCS Bioscience Ltd, UK) were dissolved in blood agar solution. Once dissolved, the solution was distributed in Petri dishes and dried at 37°C. The Petri dishes were sealed and placed at 4°C for overnight. Yeast (provided by Institute of Cell and Molecular Science, Queen Mary University of London) were spread on the prepared blood agar plates and placed in an anaerobic environment at 37°C and 10% CO_2 and allowed to make colonies.

The coated *Streptococcus sanguinis* (NCTC 7863 provided by ICMS, Queen Mary University of London) were spread on blood agar plates and placed in anaerobic environment at 37°C and 10% CO_2. The *Streptococcus sanguinis* were inoculated in broth solution and washed with 15 ml PBS and centrifuged for 10 min.

Sample films were sterilised with 70% alcohol and washed twice with PBS. Then 25 µl bacterial solutions were adhered on the surface of the experimental samples and placed in anaerobic environment at 37°C for 2 hours. After 2 hours, the number of adhering bacteria was determined by vortexing with glass beads (BDH, UK) and serial dilution followed by plating for colony forming units per disc.

Chapter 4 Results

4.1- Synthesis of Nano-Hydroxyapatite

Nano-hydroxyapatite was synthesised using sol-gel method (Section 3.4.1, Chapter 3). The resulting nano-particles were chalky white in appearance and after ball milling appeared as fine powder. After heat treatment the total yield was approximately 75%.

4.1.1- Fourier Transform Infrared Spectroscopy (FTIR)

FTIR spectra were obtained according to the procedure described in Section 3.8.3.1, Chapter 3. The FTIR spectrum for the nano-hydroxyapatite have peak positions that correlate well with studies reported previously by Chapman and Thirlwell (1964), Elliot et al. (1985), Rehman and Bonfield (1997), Gibson and Bonfield (2002), Koutsopoulos (2002), Krajewski et al. (2005). A representative of the spectra of as-prepared and heat treated nano-hydroxyapatite powder is shown in Figure 4.1 (a & b respectively) and the peak assignments of heat treated powder are tabulated in Table 4.1.

The FTIR spectra for the as-prepared nano-hydroxyapatite showed the hydroxyl (OH) stretch at 3571 cm^{-1} and the phosphate ν_3, phosphate ν_1, phosphate ν_4 and phosphate ν_2 vibrations at 1040, 946, 603-569 and 490-470 cm^{-1}, respectively. The carbonate ν_2 stretching vibration bands were presented at 873 cm^{-1} and the carbonate ν_3 stretching vibrations were observed between 1650-1410 cm^{-1} for heat treated ones whereas, for as-prepared, carbonate ν_3 (m) stretches were presented between 1730-1420 cm^{-1}, in addition the carbonate ν_3 (w) stretch was seen at 1250 cm^{-1}.

In addition to the expected peaks for nano-hydroxyapatite, weak bands were observed in the range 2140 & 2000 cm^{-1}. These peaks were believed to be due to cyanate (NCO^-) and cyanamide (NCN^{2-}) absorption bands (Dowker and Elliot, 1983).

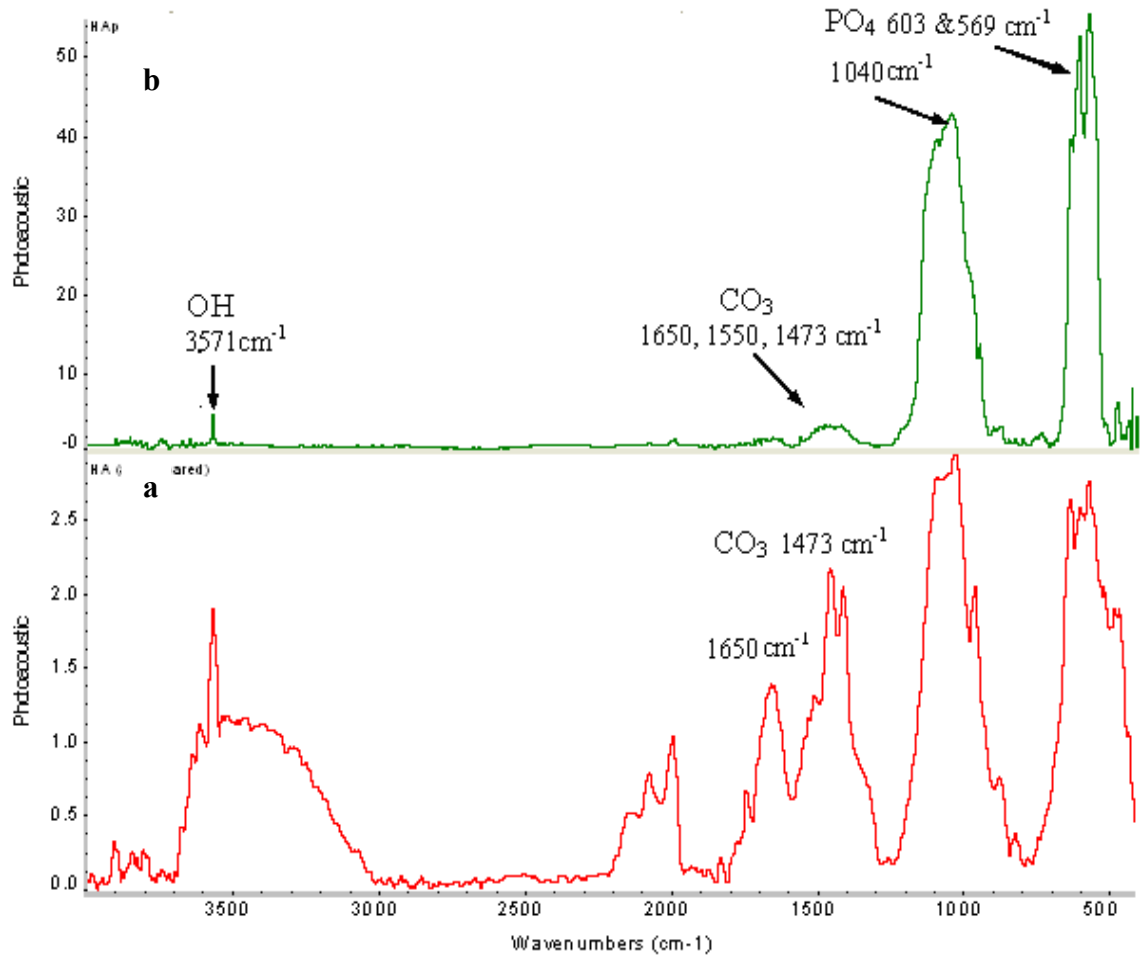

Figure 4.1 FTIR spectra of (a) as-prepared and (b) heat treated nano-hydroxyapatite showing OH (3571 cm^{-1}), CO_3 (1650-1473 cm^{-1}), stretching PO_4 (1040 cm^{-1}) and bending PO_4 (603 and 569 cm^{-1}) groups respectively

4.1.2- Raman Spectroscopy

Raman spectra were obtained according to the procedure described in Section 3.8.3.2, Chapter 3. A comparative representative of Raman spectra of as-prepared and heat treated nano-hydroxyapatite is given in Figure 4.2 (a & b respectively) and the characteristics peaks tabulated in Table 4.2. Raman spectroscopy provides the characteristics peaks of the nano-hydroxyapatite that corresponds to the previous studies reported by (Koutsopoulos, 2002; Pezzotti, 2005; Rapacz-Kmita *et al.,* 2005; Antonakos *et al.,* 2007).

Table 4.1 FTIR peaks assigned to heat treated nano-hydroxyapatite

Peaks (cm^{-1})	**Assignments**	**References**
3571	stretching mode (v_s) hydroxyl (OH)	Rehman and Bonfield (1997), Gibson *et al.,* 2000
1650	v_3 CO_3	Elliot *et al.,* 1985, Rehman and Bonfield, 1997
1550	CO_3 at A-site	Krajewski *et al.,* 2005
1473	v_3, stretching mode of CO_3	Elliot *et al.,* 1985, Rehman and Bonfield, 1997
1040	triply degenerated vibration v_3 of P—O	Chapman and Thirlwell, 1964
946	non-degenerated symmetric stretching mode v_1 of P—O	Arends *et al.,* 1987, Gibson and Bonfield, 2002
873	v_2 CO_3 at B-site	Krajewski *et al.,* 2005
631	liberation mode (v_L) OH	Koutsopoulos, 2002
603 569	triply degenerated bending mode v_4, of the O-P-O bond	Rehman and Bonfiled, 1997 Koutsopoulos, 2002

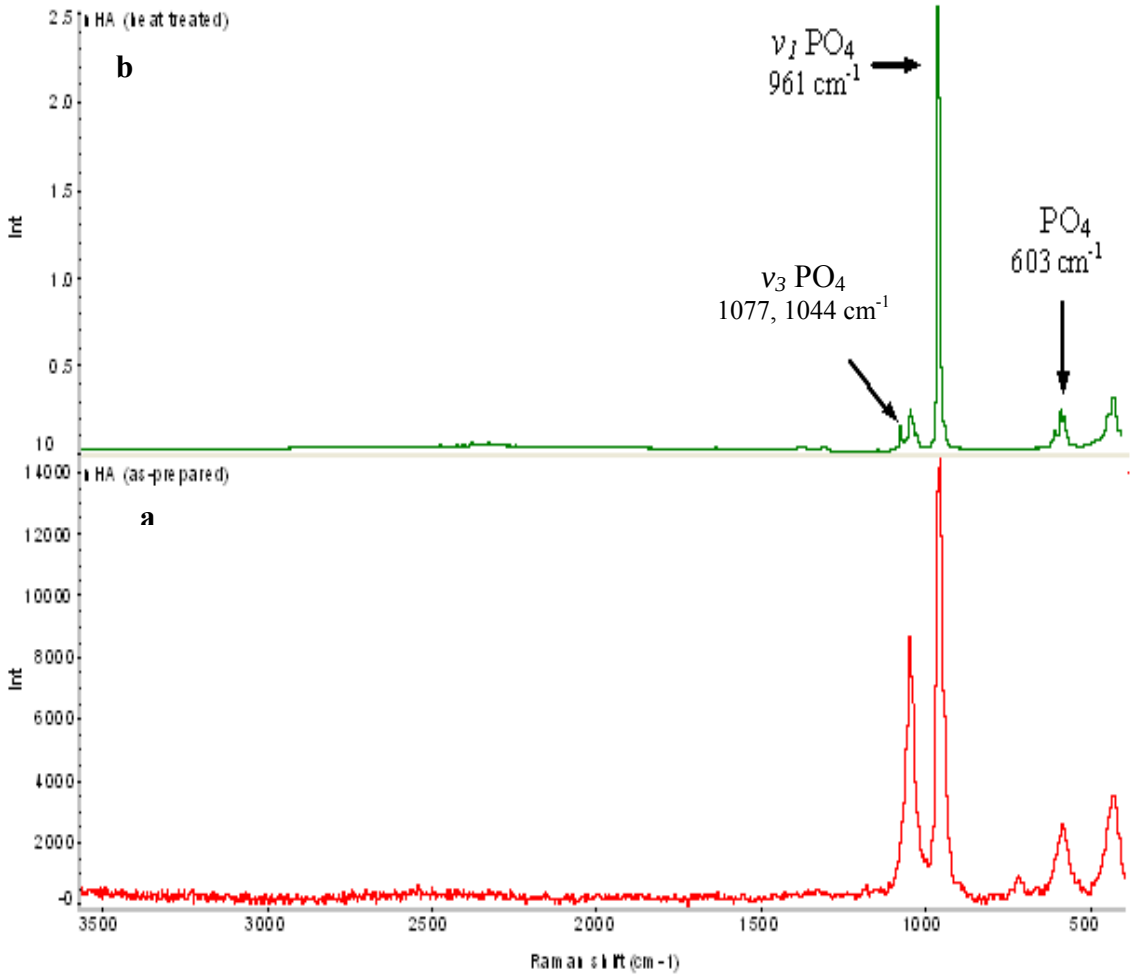

Figure 4.2 Raman spectroscopy of (a) as-prepared and (b) heat treated nano-hydroxyapatite showing v_3 PO_4 (1077, 1044 cm^{-1}), v_1 PO_4 (961 cm^{-1}), and v_4 PO_4 (603 cm^{-1})

Table 4.2 Raman spectroscopy peak of heat treated nano-hydroxyapatite

Peak (cm^{-1})	**Assignments**	**References**
	Phosphate	
1077	v_3	Koutsopoulos, 2002
1047	v_3	Antonakos *et al.*, 2007
961	v_1 stretching peak	Koutsopoulos, 2002
603, 586	v_4	Pezzotti, 2005
432	v_2	Rapacz-Kmita *et al.*, 2005

4.1.3- X-ray Diffraction (XRD)

XRD patterns were obtained according to the procedure described in Section 3.8.4.1, Chapter 3. During the confirmation process nano-hydroxyapatite was aged at 40°C for 24 hours and then heat treated at various temperatures i.e. 400, 700, and 900°C. The representatives of comparative patterns are given in Figure 4.3; whereas the general trend pattern of heat treated (700°C) nano-powder is given in Figure 4.4. The obtained patterns had a good match with the pattern for phase pure hydroxyapatite [JCPDS pattern 09-0432] and peak assignments were confirmed with Miller index of the corresponding reflections tabulated in Table 4.3. XRD pattern of 40°C aged as-prepared particles showed additional peaks at $2\theta \approx 17.9°$ and $2\theta \approx 22.4°$ attributed to NH_4NO_3. At 900°C, β-TCP appeared ($2\theta \approx 31.13°$) as impurity in nano-hydroxyapatite.

Table 4.3 XRD peaks of heat treated nano-hydroxyapatite in relation to Miller Index of the corresponding reflection

$2 \approx \theta$ (°)	**Miller Index of the corresponding reflections**
22.9	(111)
25.9	(002)
29.1	(210)
31.8	(211)
32.2	(112)
32.9	(300)
34.2	(202)
39.8	(310)

4.1.4- Morphology

Electron microscopy images i.e. TEM and SEM are obtained according to the procedure described in section 3.8.4.2 and 3.8.4.3, Chapter 3 respectively. TEM and SEM images of powder showed (Figure 4.5 a & b) a length of approximately 20-150 nm and width of approximately 15 nm. The morphological pattern of the nano-powder appeared spherical in shape; however few of them were needle-like in shape.

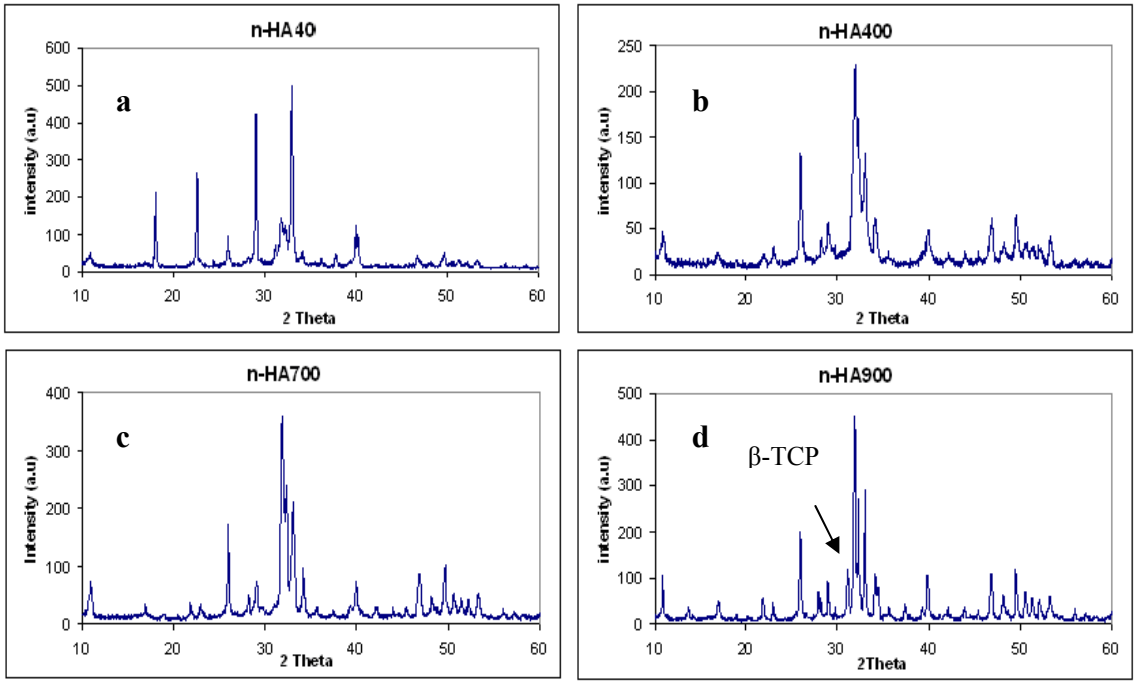

Figure 4.3 Comparative XRD pattern of hydroxyapatite aged at (a) 40°C and heat treated at (b) 400, (c) 700, and (d) 900°C

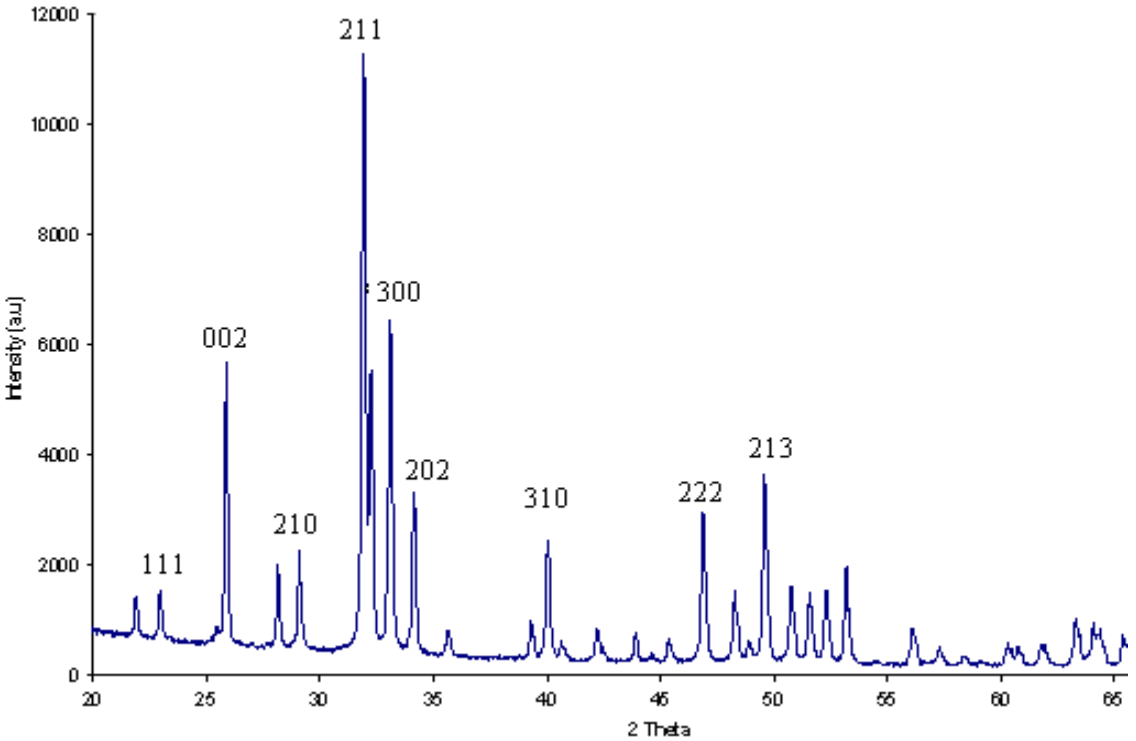

Figure 4.4 XRD pattern of nano-hydroxyapatite heat treated at 700°C

4.1.5- BET Analysis

BET analysis was performed according to the procedure described in Section 3.8.4.4, Chapter 3. Surface area was measured and the representative results before and after heat treatment at 700°C was 110 and 37 m^2/g respectively.

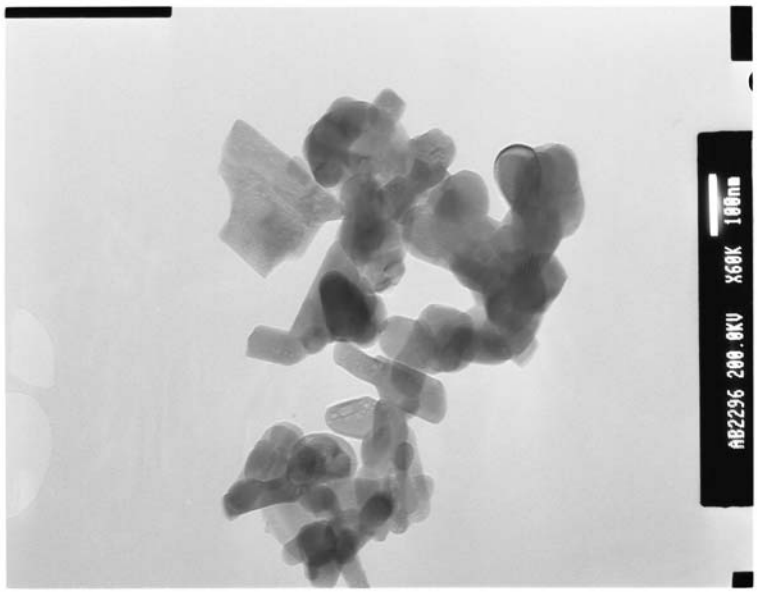

(a)

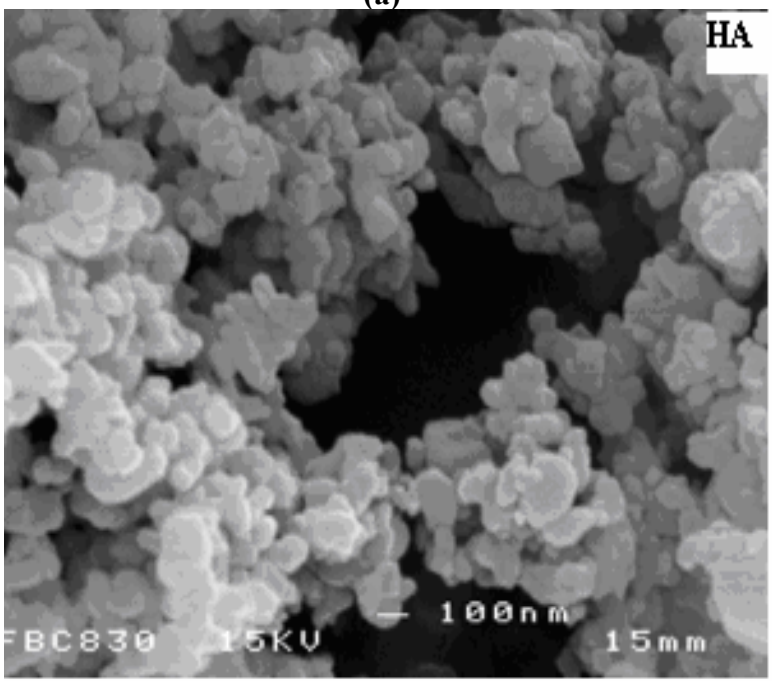

(b) x 40,000

Figure 4.5 (a) TEM and (b) SEM image of nano-hydroxyapatite

4.2- Synthesis of Polyurethane

The second step of this study was to synthesise polyurethane using *in-situ* polymerisation process. Polyurethanes were synthesised by addition polymerisation according to the procedure described in Section 3.5.2, Chapter 3. The resulting polymers were fully characterised prior to any further processing. Chemical structural properties were obtained by employing: FTIR (Section 3.8.3.1), Raman Spectroscopy (Section 3.8.3.2) and ^{13}C NMR spectroscopy (Section 3.8.3.3) techniques, physical properties were obtained by using XRD (Section 3.8.4.1), and thermal properties by TGA (Section 3.8.5.1) and DSC (Section 3.8.5.2) techniques.

4.2.1- Chemical Characterisations

4.2.1.1- Fourier Transform Infrared Spectroscopy (FTIR)

FTIR spectrum (Figure 4.6) presented the characteristic peaks of polyurethane and their attributions tabulated in Table 4.4. These all acquired FTIR spectrum peaks were in accordance with the previous studies by Lee and Hsu (1989), Lee et al. (1988), Hatchett et al. (2005), and Zhang et al. (2007).

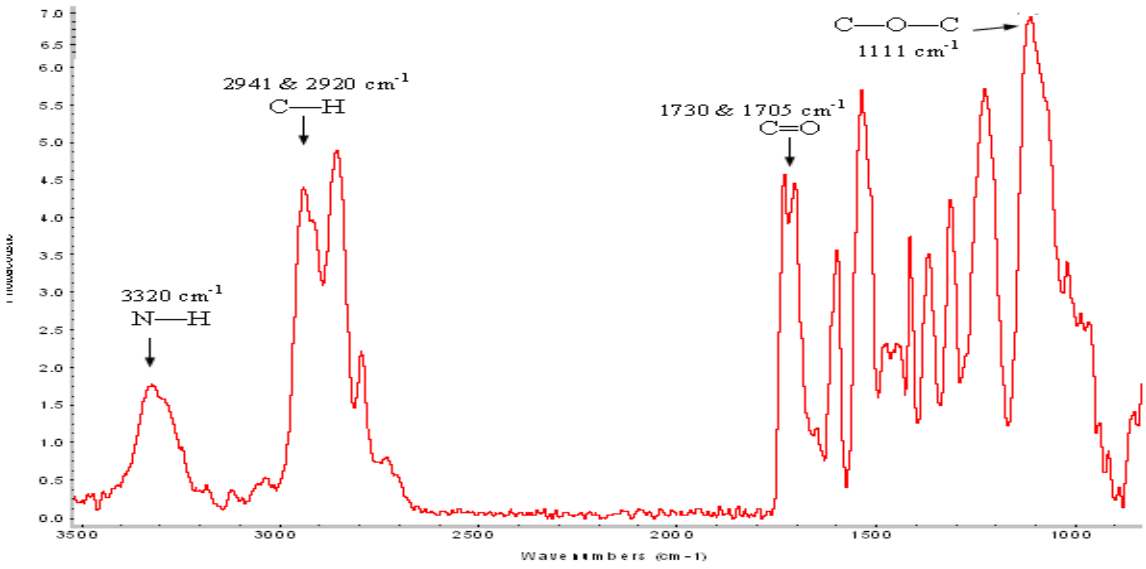

Figure 4.6 FTIR spectrum of polyurethane showing mainly N—H (3320 cm^{-1}), C—H (2941 & 2920 cm^{-1}), C=O (1730-1705 cm^{-1}) and C—O—C (1111 cm^{-1})

Table 4.4 FTIR spectroscopy peaks of polyurethane

Peaks (cm^{-1})	Assignments	References
3320	*v*(N—H)	Zhang *et al.,* 2007
3030	*v*(C—H) in benzene ring	Lee and Hsu, 1989
2941	Asymmetric stretching peak of CH_2	Lee *et al.,* 1988
2920	Symmetric stretching peak of CH_2	Lee and Hsu, 1989
1730	Free C=O stretching	Hatchett *et al.,* 2005
1705	Bonded C=O stretching	Zhang *et al.,* 2007
1599	*v*(C=C)	Lee and Hsu, 1989
1535	Amide II δ (N-H) + *v*(C==N)	Lee *et al.,* 1988
1481	CH_2	Zhang *et al.,* 2007
1413	*v*(C-C) in benzene ring	Hatchett *et al.,* 2005
1311	Amide III δ(N-H) + *v*(C==N)	Lee *et al.,* 1988
1222	δ(N-H) + *v*(C==N)	Lee *et al.,* 1988
1111	*v*(C—O—C)	Lee and Hsu, 1989
1017	β(C-H)	Lee and Hsu, 1989

4.2.1.2- Raman Spectroscopy

Raman spectrum of polyurethane is given in Figure 4.7 and the assigned peaks tabulated in Table 4.5. These all acquired Raman spectrum peaks were in accordance with the previous studies (Stephenson *et al.,* 1961; Ferry *et al.,* 1996; Parnell *et al.,* 2003; Cai and Singh, 2004).

4.2.1.3- ^{13}C Nuclear Magnetic Resonance (^{13}C NMR)

The ^{13}C NMR spectrum of polyurethane is given in Figure 4.8 and peak assignments can be seen in Table 4.6.

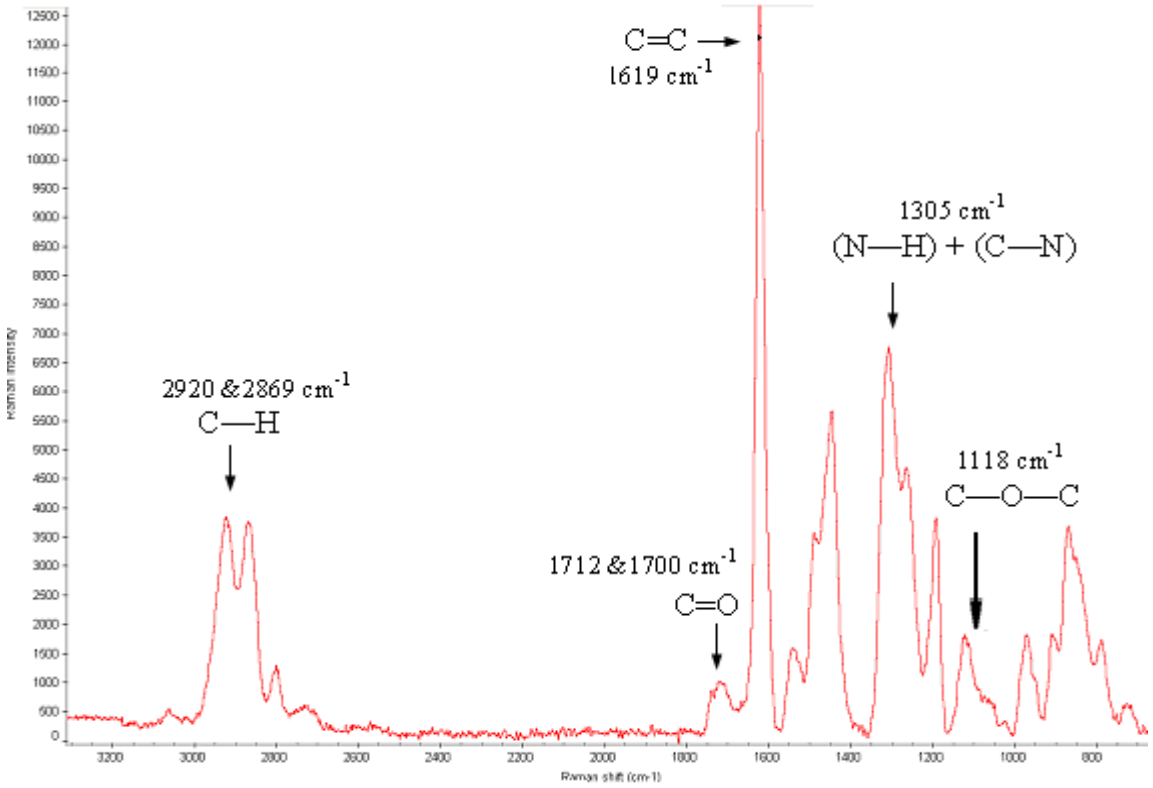

Figure 4.7 Raman Spectroscopy of polyurethane showing mainly C=O (1712-1700 cm^{-1}), (N—H) + (C—N) (1305 cm^{-1}) and C—O—C (1118 cm^{-1})

Table 4.5 Raman spectroscopy peaks of polyurethane

Peaks (cm^{-1})	**Assignments**	**References**
2920	Asymmetric stretching CH_2	Stephenson *et al.*, 1961
2869	Symmetric stretching CH_2	Ferry *et al.*, 1996
1712	Free C=O stretching	Parnell *et al.*, 2003
1700	Bonded C=O stretching	Cai and Singh, 2004
1619	Symmetric stretched vibration (C==C)	Cai and Singh, 2004
1528	*v*(aromatic, C==C), urethane amide II: *v*(C—N) + δ(N—H)	Stephenson *et al.*, 1961
1443	δ(CH_2)	Parnell *et al.*, 2003
1305	δ(CH), urethane III band	Parnell *et al.*, 2003
1118	(C—O—C) stretch	Cai and Singh, 2004
1080	C(O)—O—C	Parnell *et al.*, 2003

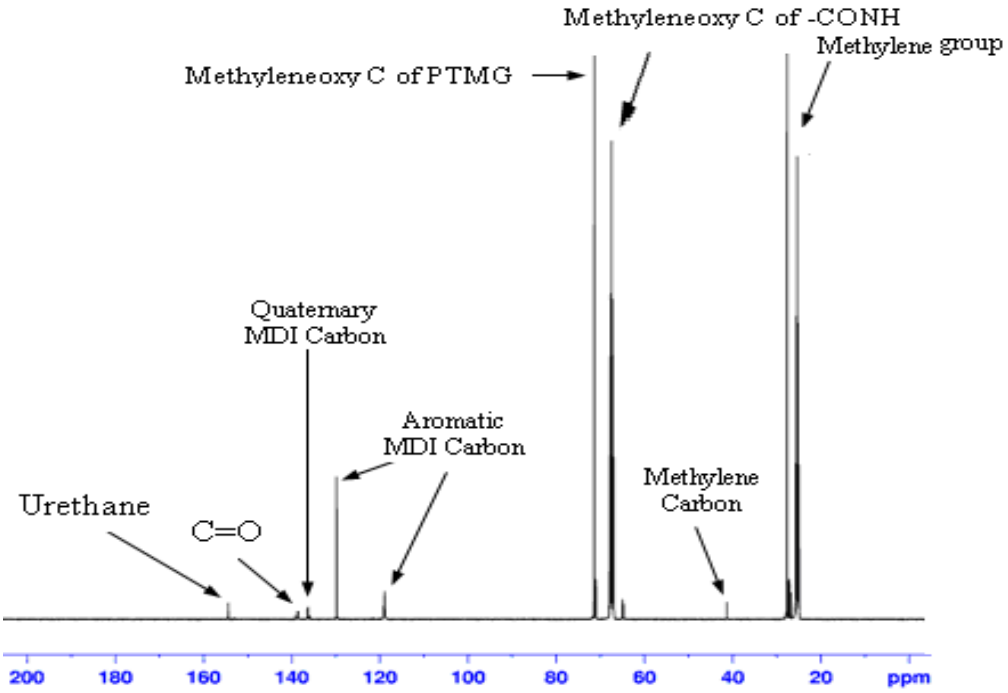

Figure 4.8 ^{13}C NMR spectrum of polyurethane at 100 MHz

Table 4.6 ^{13}C NMR peaks of polyurethane

Peaks (ppm)	**Assignments**	**References**
154.39	Quaternary carbon of urethane	Kaji *et al.*, 1992
153.12	Quaternary carbon of urethane	Kaji *et al.*, 1992
139.23	Quaternary carbon of C=O	Kaji *et al.*, 1992
138.62	Quaternary carbon of MDI	Kaji *et al.*, 1992
136	MDI ring carbon	Kaji *et al.*, 1992
129	Protonated aromatic MDI carbon and/or CH	Levy *et al.*, 1980 Kaji *et al.*, 1992
119.16	Protonated aromatic MDI carbon and/or $-CH_2$	Levy *et al.*, 1980 Kaji *et al.*, 1992
71.77	Methyleneoxy carbon of PTMG	Wang *et al.*, 2003
67.02	Methyleneoxy C of –CONH	Prasath *et al.*, 2004
41.23	Methylene Carbon	Wang *et al.*, 2003
28.09-25.27	Methylene group	Wang *et al.*, 2003

4.2.2- Physical Characterisations

4.2.2.1- X-ray Diffraction (XRD)

The XRD pattern of polyurethane is given in Figure 4.9 and tabulated in Table 4.7. The pattern showed the typical diffraction peak at 2θ ≈ 20° and the characteristic broad diffraction band in the range 15-29.6° was due to the presence of amorphous structure and the band was well correlated with the previous studies on polyurethane by Billmeyer Jr. (2000), Mondal and Hu, (2006a, b), and Chun et al. (2006).

Table 4.7 XRD pattern assignment of polyurethane

2θ (°)	Assignment	References
15-29.6	soft segment	Mondal and Hu, 2006a, b Chun *et al.*, 2006

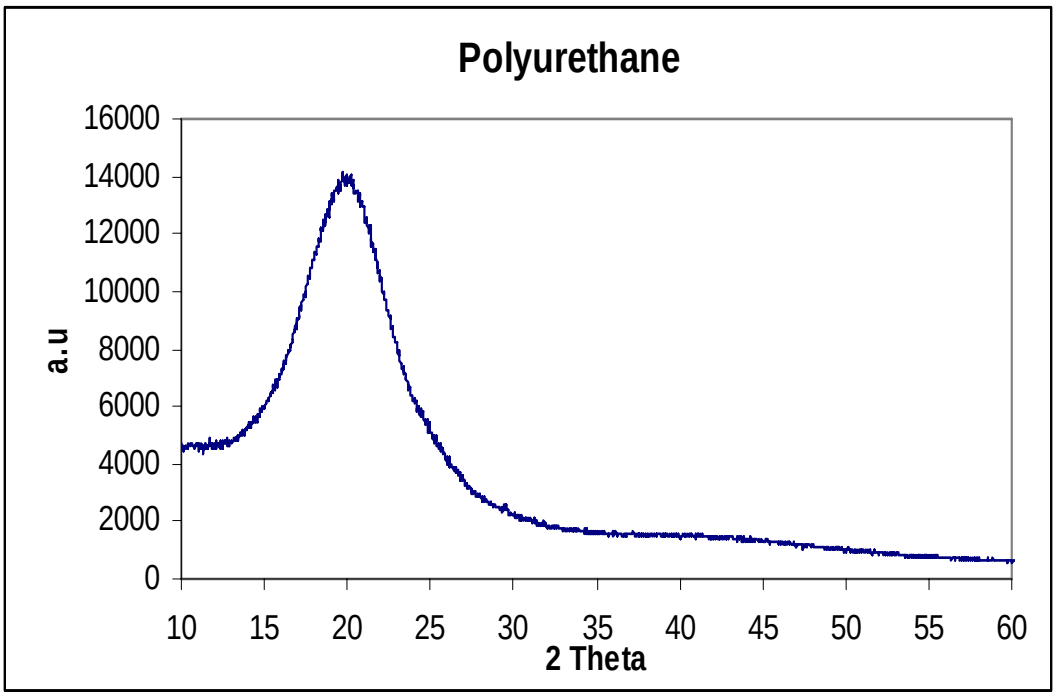

Figure 4.9 XRD pattern of polyurethane showing characteristic peak in between 2θ ~15-29.6°

4.2.3-Thermal Characterisations

4.2.3.1-Thermogravimetric Analysis (TGA)

The thermal stability of the polyurethane was investigated by TGA. The TGA profile in inert nitrogen under dynamic heating is given in Figure 4.13. The primary and secondary decomposition values of polyurethane tabulated in Table 4.8.

Table 4.8 The primary and secondary thermal decomposition of polyurethane

Thermal Decomposition	Temperature °C	References
First Stage:		
Initial Temperature (°C)	295	Desai *et al.*, 2000
Final Temperature (°C)	400	Herrera *et al.*, 2002
Second Stage:		
Initial Temperature (°C)	430	Kumar *et al.*, 2006
Final Temperature (°C)	680	James *et al*, 2006

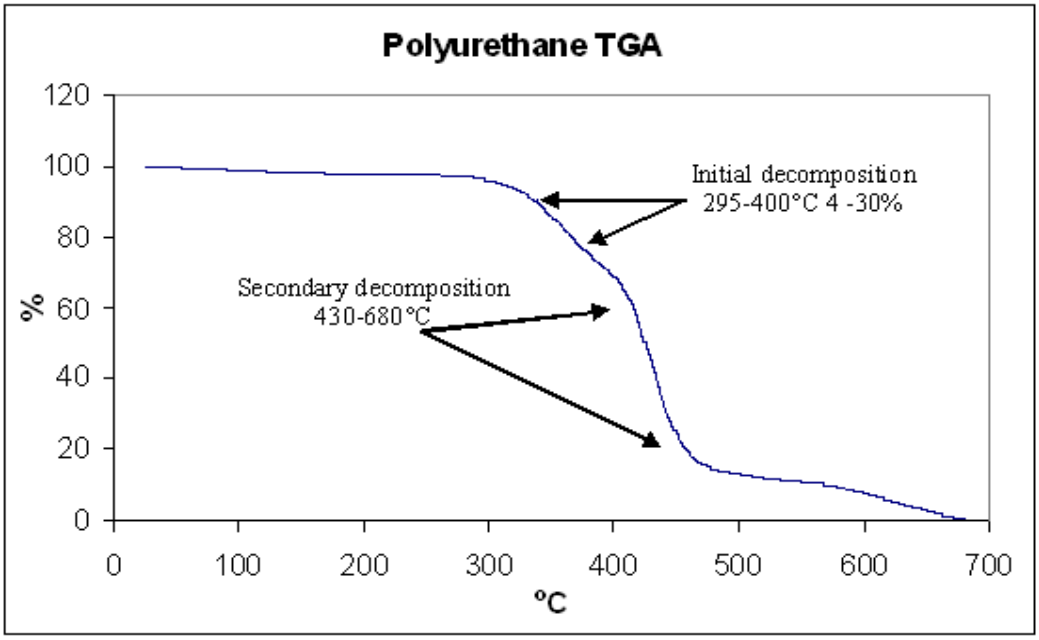

Figure 4.10 TGA profile of polyurethane showing initial and secondary thermal decompositions

4.2.3.2- Differential Scanning Calorimetry (DSC)

Differential Scanning Calorimetry (DSC) was carried out to measure the glass transition temperature (T_g) of polyurethane. The DSC thermogram pattern is given in Figure 4.11 and the T_g values are shown in Table 4.9.

Table 4.9 DSC glass transition values of polyurethane (van Bogart *et al.*, 1981; Song *et al.*, 1996)

Temperature (°C)	Assignments
- 45	T_g soft segment
78	Endotherm T_g short range hard segment
190	Endotherm T_g long range hard segment

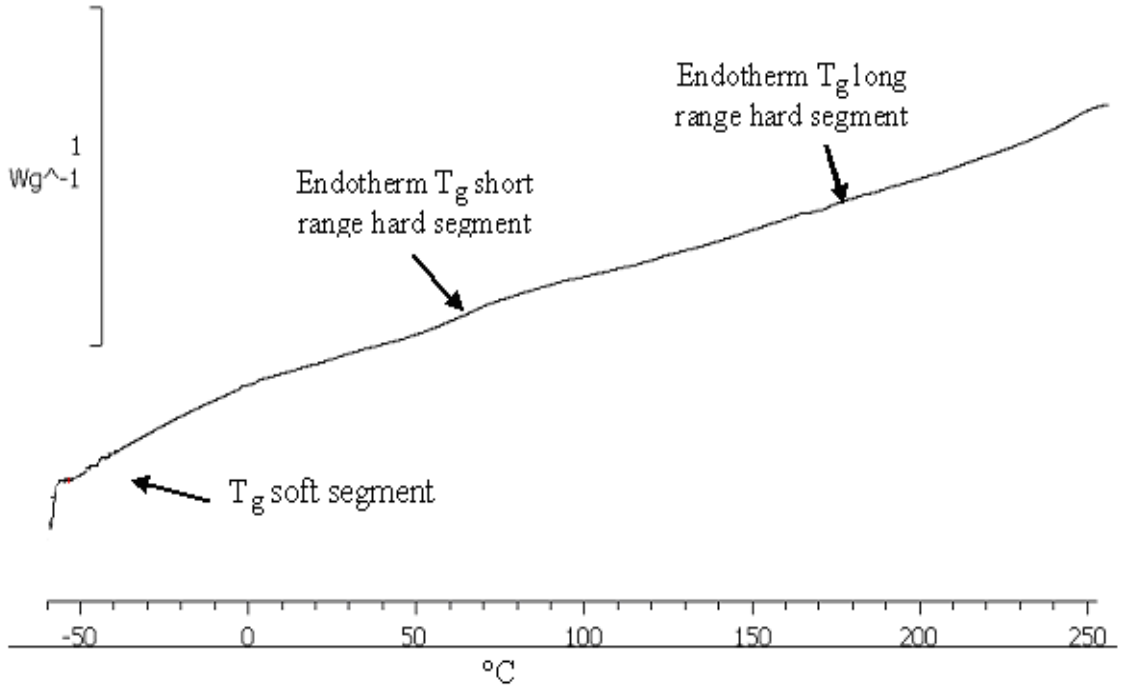

Figure 4.11 DSC thermogram of polyurethane showing endotherm T_g ~ 78 and 190°C

4.3- Synthesis of Polyurethane/Nano-Hydroxyapatite Composites

In recent years, the development of the restorative composites has focused on the use of organic–inorganic hybrid nano-composite materials. The organic–inorganic hybrid materials offer the advantage of bridging the property between polymers and ceramics. In particular, chemistry involves the use of different monomers and nHA as an inorganic component. This section will describe the result of the grafting of nano-apatite with MDI and then evaluation of difference between physical mixing and chemical mixing of nHA and PU. During the synthesis procedure the monomers were added by step-wise method to achieve the linear chain and complete polymerisation. The resulting composites were analysed initially using chemical [(FTIR, Raman Spectroscopy, and ^{13}C NMR) Section 3.8.3.1, 3.8.3.2, 3.8.3.3 respectively, Chapter 3], physical (XRD; Section 3.8.4.1, Chapter 3), and thermal [(TGA and DSC) Section 3.8.5.1, 3.8.5.2 respectively, Chapter 3] analysis. Later these properties were assessed using different concentrations of nHA. It was found that the step-wise chemical mixing of PU/nHA provided better results than physical mixing and with the increase in concentration of nHA, stronger covalent linkages and hydrogen bonding were observed which ultimately improved the chemical, physical and thermal properties of a novel composite. This section of the results will be explained on the basis of chemical, physical, and thermal characterisations.

4.3.1- Chemical Characterisations

4.3.1.1- Fourier Transform Infrared Spectroscopy (FTIR)

FTIR was conducted to evaluate the structural composition of experimental materials: (i) grafted MDI/nano-hydroxyapatite (MDI/nHA); (ii) physically mixed polyurethane/nano-hydroxyapatite composite; and (iii) chemically mixed polyurethane/nano-hydroxyapatite.

4.3.1.1.1- Grafted MDI/Nano-Hydroxyapatite

Once the nano-hydroxyapatite and polyurethane synthesis and processing were optimised, grafting to the surface was investigated. The materials studied include nano-hydroxyapatite and MDI. The comparative FTIR spectra of (a) nano-hydroxyapatite, (b) MDI and (c) MDI/nano-hydroxyapatite are presented in Figure 4.12 and the peaks tabulated in Table 4.10. The peaks of FTIR spectrum (Figure 4.12a) of nHA showed the characteristic peaks at 3571 cm^{-1} assigned to hydroxyl group and a peak at 1017 cm^{-1} was attributed to the phosphate group (Rehman and Bonfield, 1997). The FTIR spectrum (Figure 4.12b) of MDI presented a broad band of isocyanate group (NCO) in between 2400-2100 cm^{-1} (Hatchett *et al.,* 2005). The peak appearing at 1690 cm^{-1} was attributed to benzene (C=C) ring. The reacted MDI/nHA composite spectrum is given in Figure 4.12c. The characteristic peak of asymmetric N—H stretching was observed at 3330 cm^{-1} that showed the formation of urethane linkage. The phosphate (P—O) peak from nano-hydroxyapatite was observed at 1040 cm^{-1}. The other urethane peaks were observed at 1710, 1447, and 1236 cm^{-1}. It was observed that during the reaction the isocyanate band (2400-2100 cm^{-1}) completely disappeared.

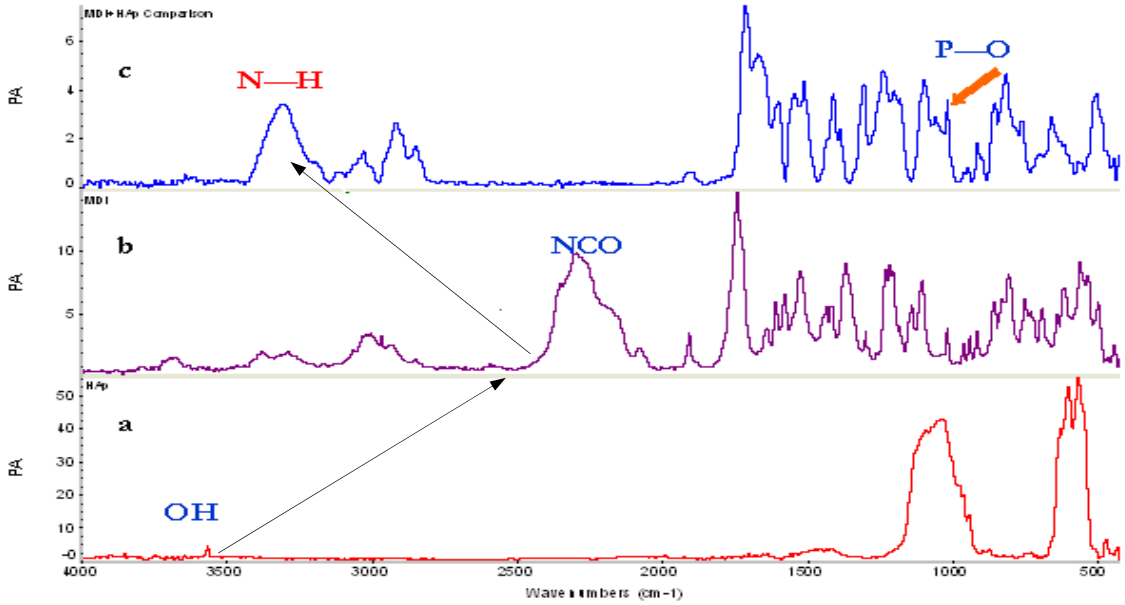

Figure 4.12 Comparative FTIR spectra of (a) nano-hydroxyapatite, (b) MDI and (c) grafted MDI/nano-hydroxyapatite showing Urethane linkage (N—H) formation (3330 cm^{-1})

Table 4.10 Comparative FTIR peaks of nHA, MDI and grafted MDI/nHA

Sample* and Peaks (cm^{-1})	Assignment	References
(a) nHA* 3571 1017	 OH group v_3 phosphate group	Rehman and Bonfield, 1997
(b) MDI* 2400-2100	 Isocyanate group	Hatchett *et al.,* 2005
(c) Grafted nHA/MDI* 3330	 N—H stretching (urethane linkage)	

4.3.1.1.2- Physically Mixed Polyurethane/Nano-hydroxyapatite Composites

The comparative spectra of nHA and physically mixed PU/nHA are shown in Figure 4.13 (a & b) respectively. The spectrum of physically mixed PU/nHA composite (Figure 4.13b) showed that the characteristic hydroxyl stretch that was still present at 3571 cm^{-1} after mixing suggested that grafting has not occurred via the physical mixing. The asymmetric and symmetric stretching peaks appeared at 2941 and 2855 cm^{-1} respectively. The carbonyl peaks were presented in the region 1729-1701 cm^{-1}. However, a broad intense band appeared in the range of 1100-900 cm^{-1} that showed the presence of nHA on the surface. The peaks assigned to nHA were seen at 1040 cm^{-1} for phosphate ν_3, 946 cm^{-1} for phosphate ν_1 and 603 & 569 cm^{-1} for phosphate ν_4 peaks in the physically mixed sample. These peaks were in quite similar pattern as in nHA as shown in Figure 4.13a.

4.3.1.1.3- Chemically Mixed Polyurethane/Nano-hydroxyapatite Composites

The general trend of FTIR spectrum of nHA treated polyurethane (PU) composite (PU/nHA20) is given in Figure 4.14. The shifting and emergence of new peaks were

observed in the spectrum after the *in-situ* polymerisation and comparative peaks of PU and PU/nHA20 tabulated in Table 4.11.

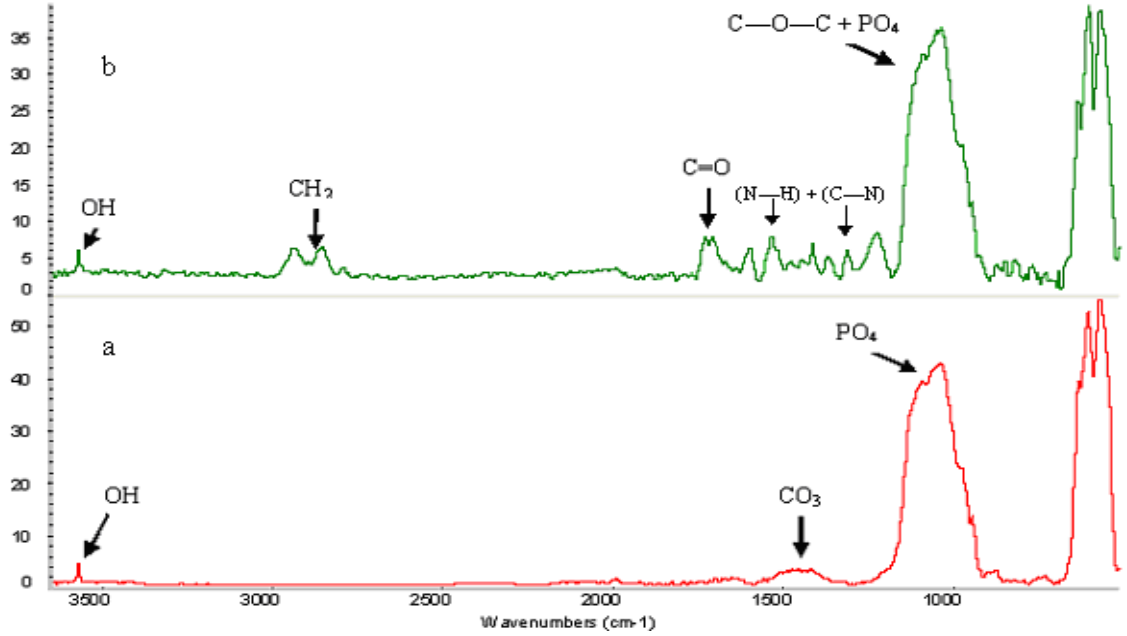

Figure 4.13 Comparative FTIR spectra of (a) nano-hydroxyapatite and (b) polyurethane/nano-hydroxyapatite (physically mixed) composite showing characteristic OH (3571 cm^{-1}) and PO_4 (1040 cm^{-1}) peaks in both spectra

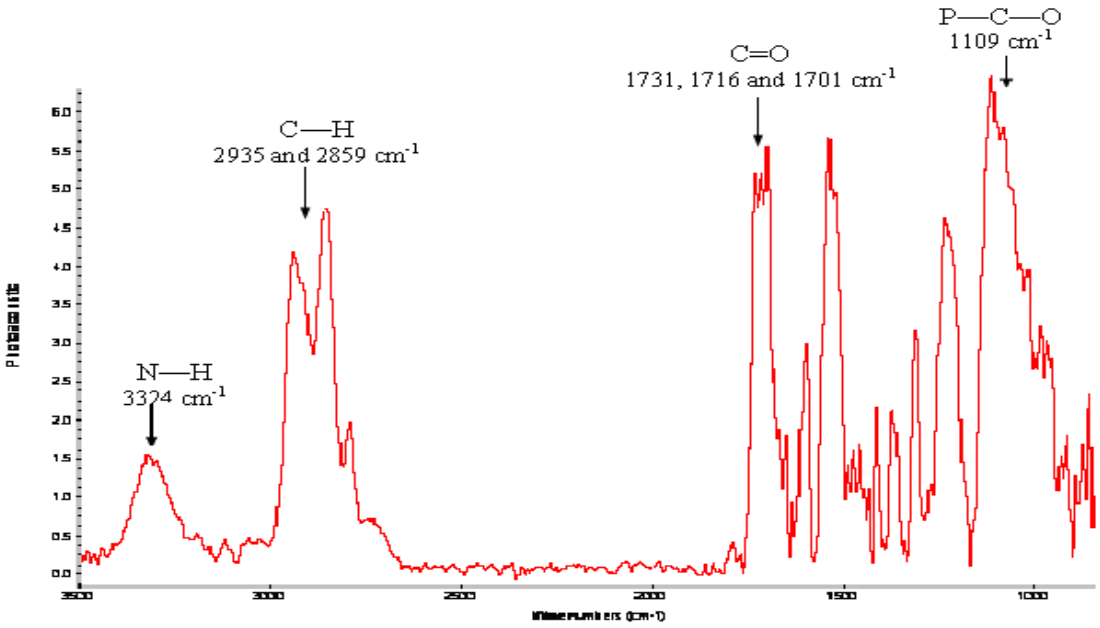

Figure 4.14 FTIR spectrum of PU/nHA20 composite showing N—H (3324 cm^{-1}), hydrogen bonded C=O (1716-1701 cm^{-1}) and P—C—O (1109 cm^{-1})

Table 4.11 Comparative FTIR peaks assignments of polyurethane (PU) and PU/nHA20 composite

Polyurethane (PU) (cm^{-1})	**PU/nHA20 Composite (cm^{-1})**	**Assignments**	**References**
3320	3324	*v*(N—H)	Zhang *et al.*, 2007
2941	2935	asymmetric stretching peak of CH_2	Lee and Hsu, 1989
2920	2859	symmetric stretching peak of CH_2	Lee *et al.*, 1988
1730	1731	free C=O stretching	Lee and Hsu, 1989
1705	1716 1701	bonded C=O stretching	Hatchett *et al.*, 2005
1599	1598	*v* (C=C)	Zhang *et al.*, 2007
1535	1539	amide II δ (N-H) + *v*(C==N)	Lee and Hsu, 1989
1111	--	C—O—C	Lee *et al.*, 1988
--	1100-950	P—O—C	

4.3.1.1.4- Comparison of Physically and Chemically Mixed Composites

The comparative spectra of (a) polyurethane (b) chemically mixed composites and (c) physically mixed composite are given in Figure 4.15. These spectra clearly showed the difference between the chemically mixed and physically mixed composites and the peaks tabulated in Table 4.12.

Table 4.12 Comparative FTIR peaks of PU, physically mixed PU/nHA, and chemically mixed PU/nHA assigned with groups and peak numbers (cm^{-1})

Assignments	**PU (cm^{-1})**	**Physically mixed PU/nHA (cm^{-1})**	**Chemically mixed PU/nHA (cm^{-1})**
OH (from nHA)	--	3571	--
N—H	3320	Not observed in spectrum due to low intensity	3324
C—H	2920	2922	2859
C=O	1730	1730	1731
Bonded C=O	1705	1706	1716 1701
C—O—C	1111	--	--
C—O—C (PU) + PO_4 (nHA)	--	1080	--
P—O—C	--	--	1100-950

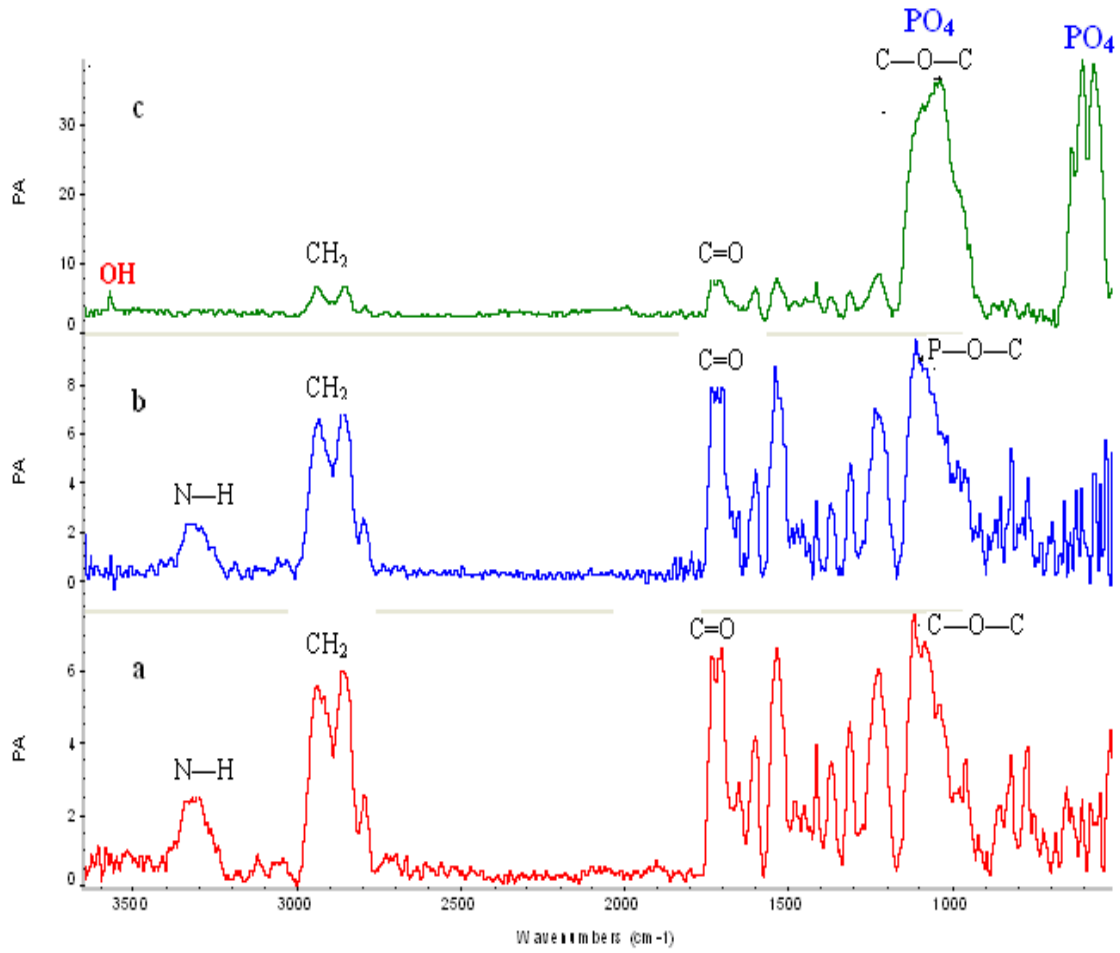

Figure 4.15 Comparative FTIR spectra of (a) polyurethane, (b) polyurethane/nano-hydroxyapatite (chemically mixed), and (c) polyurethane/nano-hydroxyapatite (physically mixed)

4.3.1.1.5- Comparative Spectra of Composites with Different Concentrations of Nano-hydroxyapatite

The comparative spectra of polyurethane/nano-hydroxyapatite composites with different concentration of nano-hydroxyapatite i.e. 5, 10, 15, and 20 % wt/wt are given in Figure 4.16.

The FTIR spectra showed the shifting of peaks with the increase in concentration of nHA. The urethane linkage appeared with the formation of N—H linkage in the region at 3400-3280 cm^{-1}. The peak values and the relevant intensities of the carbonyl (C=O)

region are tabulated in Table 4.13. The PU/nHA5 showed the free C=O at 1728 cm^{-1} and bonded C=O at 1706 cm^{-1}, whereas PU/nHA10 showed increase in the intensity of bonded C=O and peak shifted to 1713 cm^{-1}. However, PU/nHA15 showed higher intensity value of bonded C=O at 1701 cm^{-1} and a shoulder peak appeared at 1713 cm^{-1}. In PU/nHA20 spectrum the free C=O appeared at 1731 cm^{-1} and the bonded C=O peak appeared at 1701 and a new hydrogen bonded C=O peak presented at 1716 cm^{-1}. The absorption bands at 1520 and 1439 cm^{-1} were due to carbonyl (C=O) coupled with N—H and N—C—N stretching vibration respectively. The combination of N—H deformation and C—N stretching vibration was appeared at 1598 cm^{-1} and 1233 cm^{-1} was the absorption band of combined C—N and C—O stretching vibration. The peak of ether/phosphate (P—O—C) was observed at the position around 1100-950 cm^{-1} and it was noted that with the increase in concentration of nHA the shoulder peaks emergence in this region.

Table 4.13 Free and Bonded Carbonyl peaks and intensities of PU/nHA composites

Composite	**Free Carbonyl (cm^{-1})**	**Intensity**	**Bonded Carbonyl (cm^{-1})**	**Intensity**
PU/nHA5	1728	5.76	1706	5.86
PU/nHA10	1730	6.1	1713	6.5
PU/nHA15	1731	6.1	1701 1713 (shoulder)	6.9
PU/nHA20	1731	8.1	1716 1701	8.0 8.5

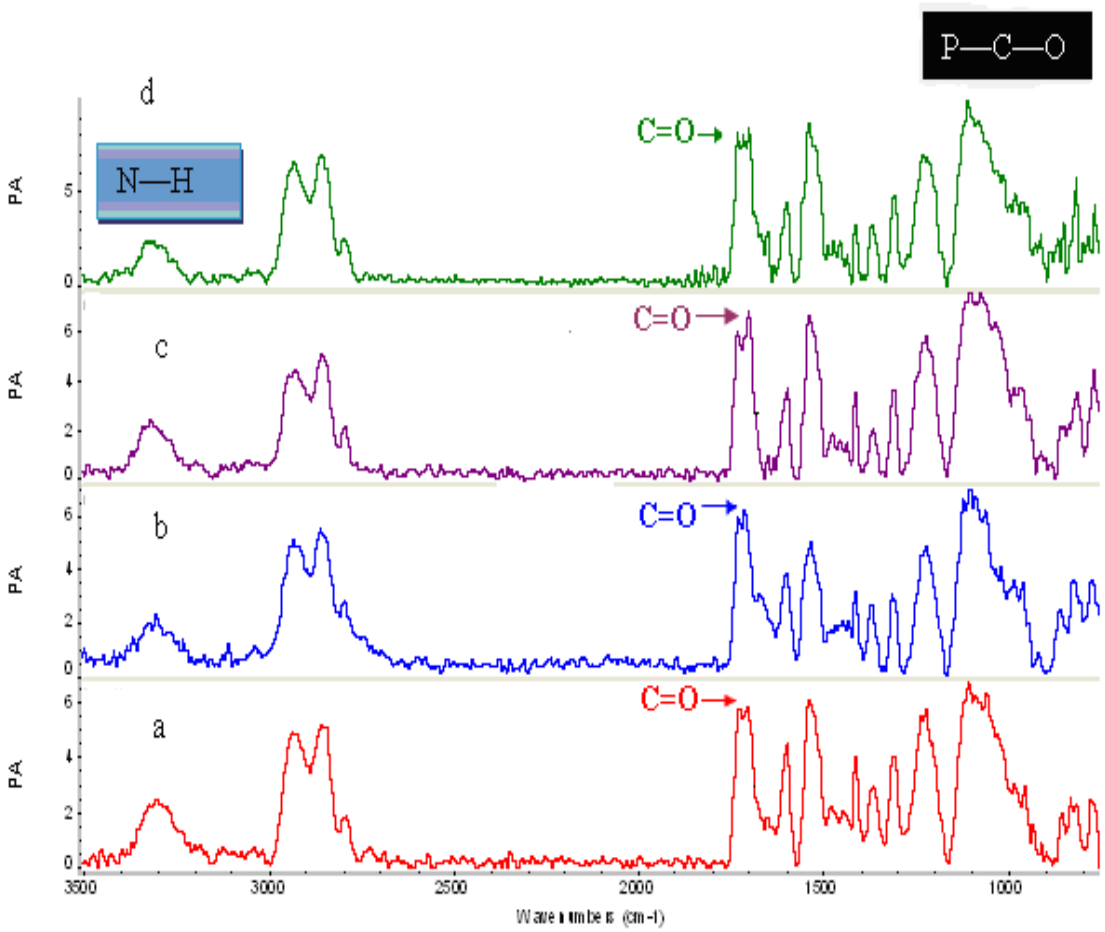

Figure 4.16 Comparative FTIR spectra of (a) PU/nHA5, (b) PU/nHA10, (c) PU/nHA15, and (d) PU/nHA20

4.3.1.2- Raman Spectroscopy

4.3.1.2.1- Physically Mixed Polyurethane/Nano-hydroxyapatite Composites

Raman spectrum of physically mixed PU/nHA composites is given in Figure 4.17. The characteristic peaks of asymmetric and symmetric stretch C—H appeared at 2924 and 2878 cm^{-1} respectively. The free and hydrogen bonded carbonyl region appeared in between 1730-1713 cm^{-1}. The intense peak at 1626 cm^{-1} was attributed to benzene (C=C). The ether region (C—O—C) appeared at 1130 cm^{-1}; however, the sharp intense peak of v_1 phosphate appeared with slight shift at 974 cm^{-1} suggesting that there was no linkage between nano-hydroxyapatite and polyurethane.

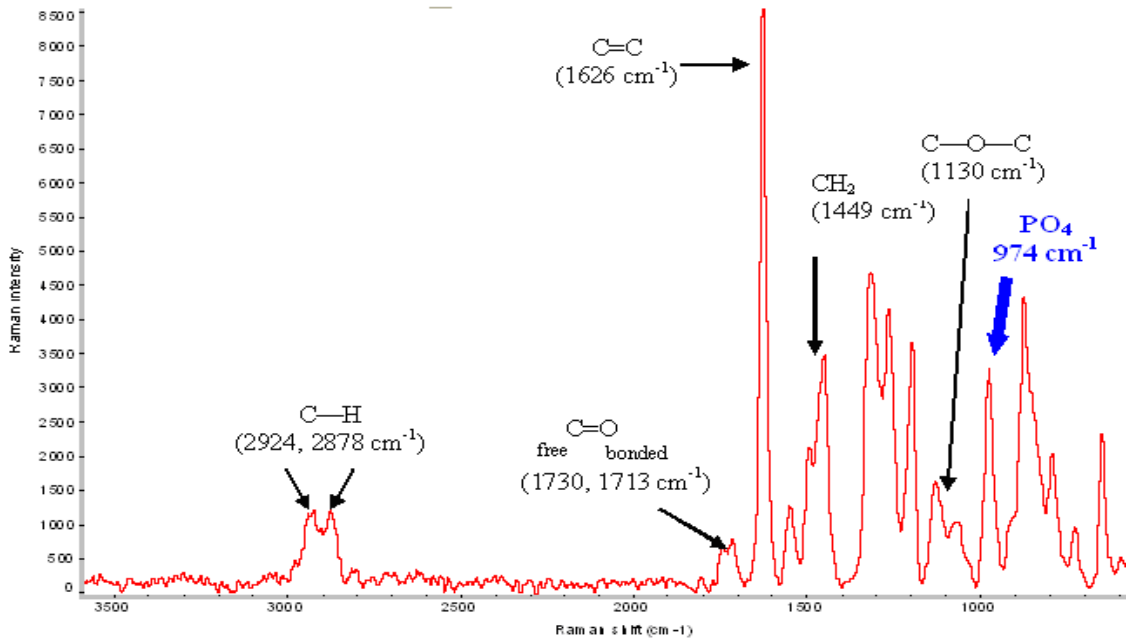

Figure 4.17 Raman spectrum of physically mixed PU/nHA composite showing intense PO_4 peak at 974 cm^{-1}

4.3.1.2.2- Chemically Mixed Polyurethane/Nano-hydroxyapatite Composites

Raman spectrum peaks of chemically mixed polyurethane/nano-hydroxyapatite composite (PU/nHA20) is given in Figure 4.18. The peak values in comparison with polyurethane tabulated in Table 4.14.

4.3.1.2.3- Comparison of Physically and Chemically Mixed Composites

The comparative spectra of polyurethane, chemically mixed and physically mixed composites are given in Figure 4.19 (a, b & c) respectively. The most obvious differences between the physically and chemically mixed spectra were the presence of phosphate stretch (974 cm^{-1}) peak in physically mixed spectrum. The chemically mixed spectrum showed the presence of shoulders and shifting of peaks in 1100-900 cm^{-1} region. This suggested an interaction between the phosphate group of nano-hydroxyapatite and polyurethane.

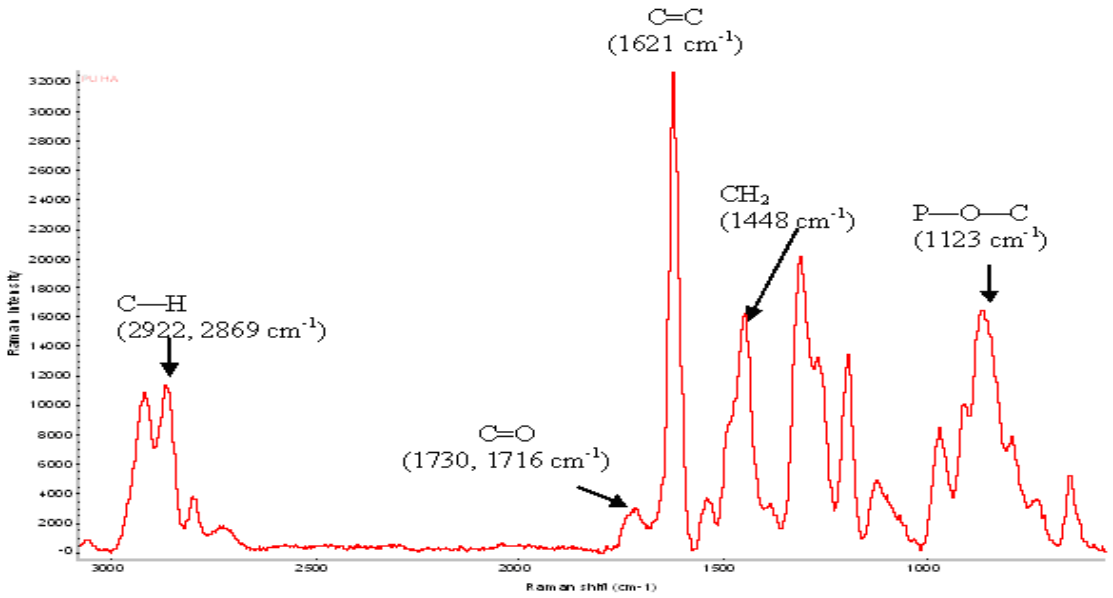

Figure 4.18 General trend of chemically mixed Raman Spectroscopy of PU/nHA composite showing bonded C=O (1716 cm^{-1}) and P—C—O (1123 cm^{-1})

Table 4.14 Comparative Raman spectroscopy peaks assignment of PU and PU/nHA composite

PU (cm^{-1})	**PU/nHA (cm^{-1})**	**Assignments**	**References**
2920	2922	asymmetric stretching CH_2	Stephenson *et al.*, 1961
1712	1730	free C=O	Ferry *et al.*, 1996
1700	1716	bonded C=O	Parnell *et al.*, 2003
1619	1621	symmetric stretched vibration (C==C)	Cai and Singh, 2004
1528	1541	*v*(aromatic, C==C), urethane amide II: *v*(C—N) + δ(N—H)	Cai and Singh, 2004
1443	1448	δ(CH_2)	Stephenson *et al.*, 1961
1305	1309	δ(CH), urethane III band	Parnell *et al.*, 2003
1118	--	(C—O—C) stretch	Parnell *et al.*, 2003
--	1123	P—O—C	

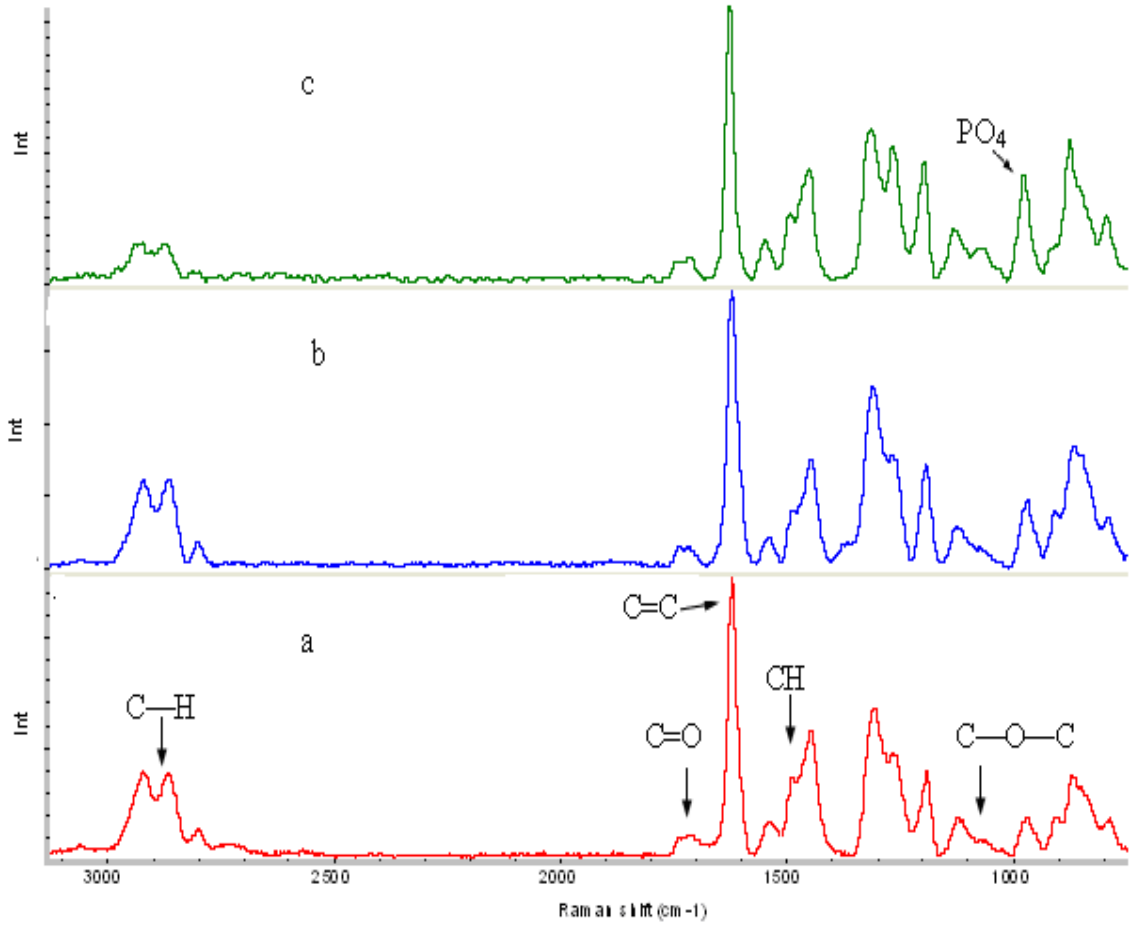

Figure 4.19 Comparative Raman spectra of (a) polyurethane, (b) chemically mixed, and (c) physically mixed PU/nHA composites

4.3.1.2.4- Comparative Spectra of Composites with Different Concentrations of Nano-hydroxyapatite

The comparative spectra of PU/nHA with different concentrations of nano-particles i.e. 5, 10, 15 and 20 % wt/wt are given in Figure 4.20. It was observed that with the increase in concentration of nHA the shifting of peaks occurred. The bonded C=O peak (1713 cm^{-1}) showed emergence of peak with the increase in concentration of nHA. The shoulders and shifting of peaks (1200-1000 cm^{-1}) were observed in ether/phosphate group range.

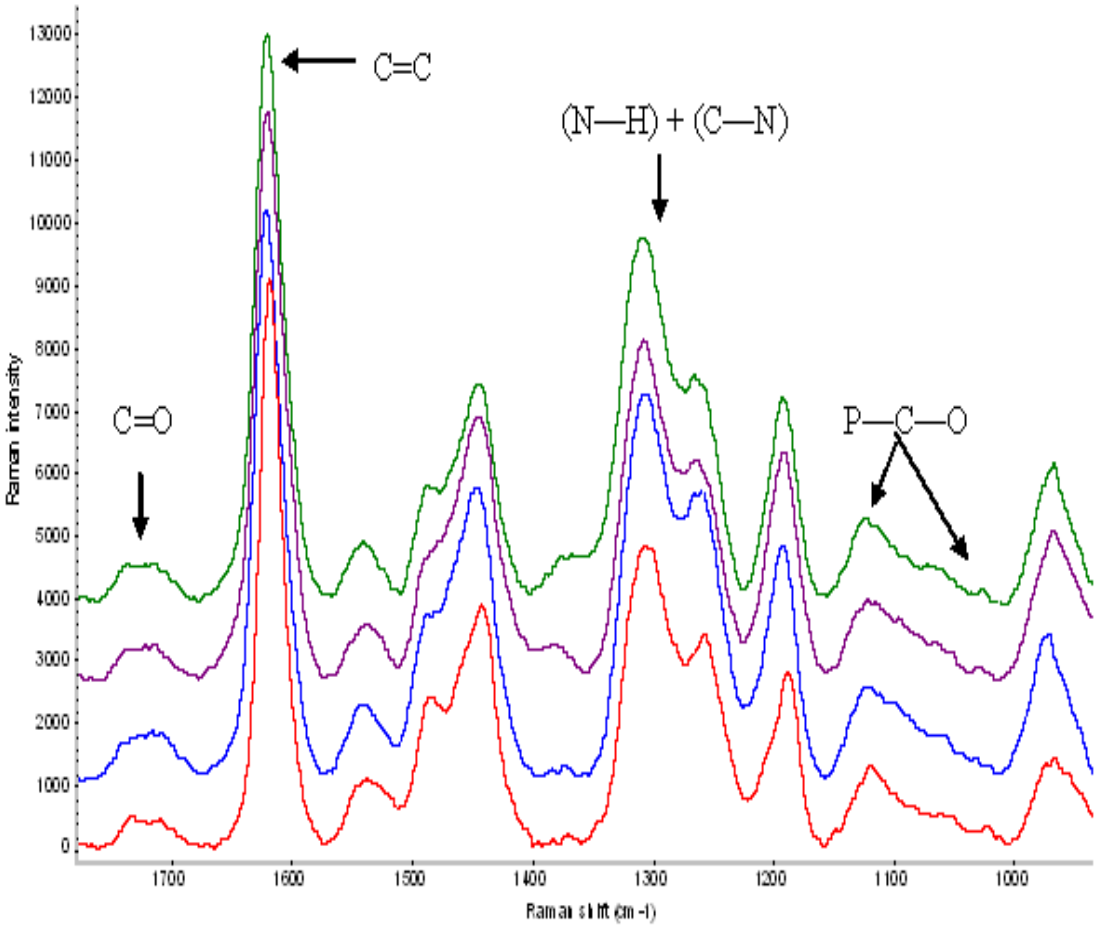

Figure 4.20 Comparative Raman Spectroscopy of polyurethane/nano-hydroxyapatite composites i.e. PU/nHA5 (red), PU/nHA10 (blue), PU/nHA15 (violet), and PU/nHA20 (green)

4.3.1.3- ^{13}C Nuclear Magnetic Resonance (^{13}C NMR)

The comparative ^{13}C NMR pattern of polyurethane (PU) and polyurethane/nano-hydroxyapatite (PU/nHA20) are given in Figure 4.21 and peaks tabulated in Table 4.15. The shifting and emergence of peaks observed at 65.15-62.3 ppm and 41.50 ppm which were expected due to reaction of carbon and isocyanate to form hydrogen bonded C=O and urethane linkage respectively. The peak at 30.38 ppm associated with soft-segment carbons adjacent to a urethane linkage.

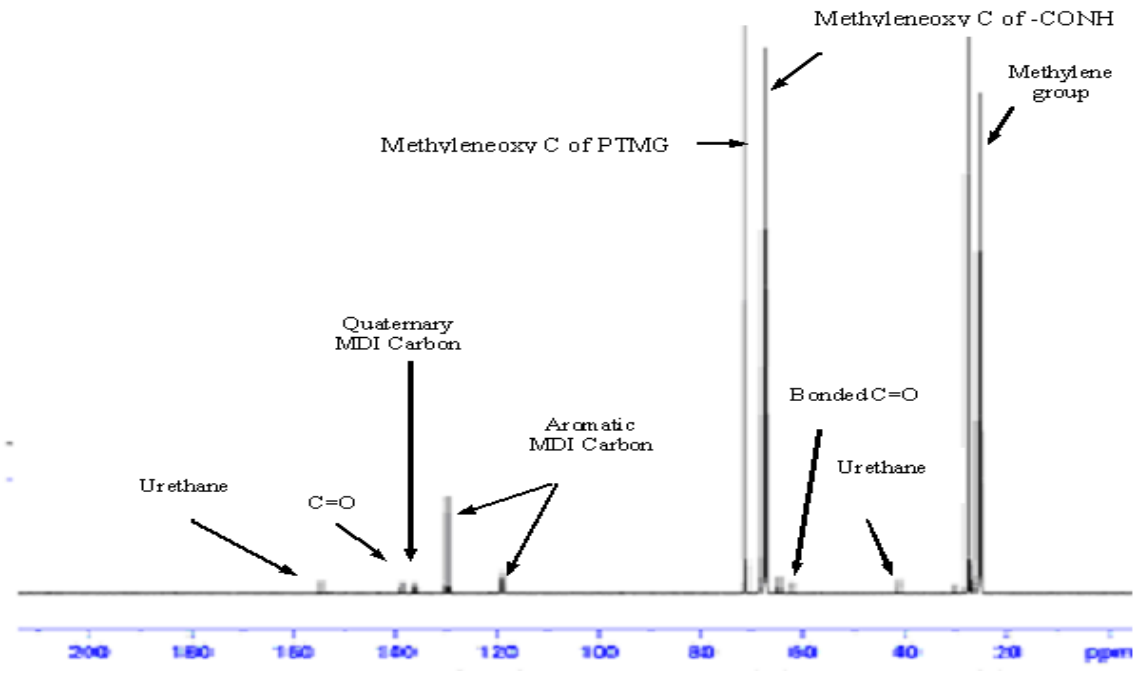

Figure 4.21 ^{13}C NMR spectrum of polyurethane/nano-hydroxyapatite composite

Table 4.15 ^{13}C NMR peaks of PU/nHA composite

Peaks (ppm)	**Assignments**	**References**
154.39	Quaternary carbon of urethane	Kaji *et al.*, 1992
153.12	Quaternary carbon of urethane	Kaji *et al.*, 1992
139.23	Quaternary carbon of C=O	Kaji *et al.*, 1992
138.62	Quaternary carbon of MDI	Kaji *et al.*, 1992
136	MDI ring carbon	Kaji *et al.*, 1992
129	Protonated aromatic MDI carbon and/or CH	Levy *et al.*, 1980 Kaji *et al.*, 1992
119.16	Protonated aromatic MDI carbon and/or –CH_2	Levy *et al.*, 1980 Kaji *et al.*, 1992
71.77	Methyleneoxy carbon of PTMG	Wang *et al.*, 2003
67.02	Methyleneoxy C of –CONH	Prasath *et al.*, 2004
65.15-62.3	bonded C=O	Prasath *et al.*, 2004
41.50	Urethane	Prasath *et al.*, 2004
41.23	Methylene Carbon	Wang *et al.*, 2003
28.09-25.27	Methylene group	Wang *et al.*, 2003

4.3.2- Physical Characterisations

4.3.2.1- X-ray Diffraction of Polyurethane/Nano-hydroxyapatite Composites

The XRD patterns of PU/nHA composites are given in Figure 4.22 to 4.25 (PU/nHA5, PU/nHA10, PU/nHA15, and PU/nHA20) respectively. The assigned peak at 22.97° (111) of nHA was expected to overlap by the high intense broad band of PU. However, the other nHA peaks i.e. 25.87° (002), 31.78° (211), 32.18° (112), 33.92° (300), 39.24° (310), and 46.7° (222) were observed with slight shift in the XRD pattern of PU/nHA composites. The comparative shifted peaks of current study with the original peaks of nano-hydroxyapatite are tabulated in Table 4.16 with reference to Miller Index of the corresponding reflection. The comparative XRD patterns of nHA, chemically mixed and physically mixed polyurethane/nano-hydroxyapatite are presented in Figure 4.26. The comparative XRD pattern of nHA and physically mixed composite confirmed the presence of nHA particles on the surface of polyurethane and were clearly visible. In comparison, the XRD pattern of chemically mixed samples confirmed the presence of nHA but not on the surface and the broad band of polyurethane (15-26°) emerged as the main peak of the pattern.

Table 4.16 Shifting of nHA peaks after interaction with PU

2θ (°) nHA (used in current study)	**Miller Index of the Corresponding Reflection**	**2θ (°) PU/nHA Composite**
25.87	(002)	26.10
31.78	(211)	32.05
32.18	(112)	32.49
33.92	(300)	33.22
39.24	(212)	39.60
39.84	(310)	40.1
46.7	(222)	47.02

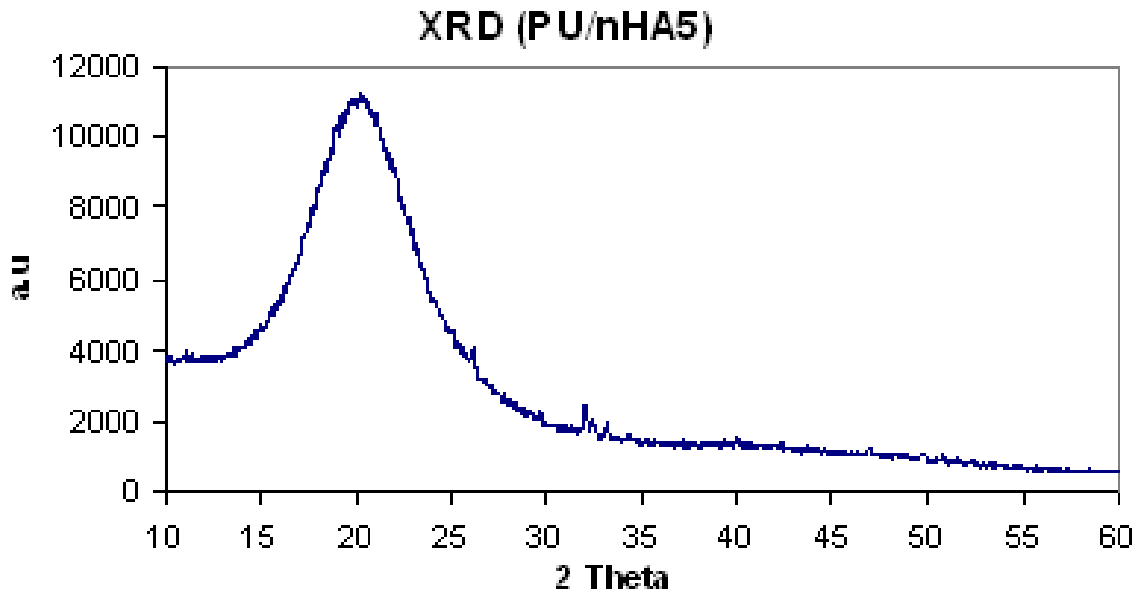

Figure 4.22 XRD pattern of chemically mixed PU/nHA5 showing characteristic peak of polyurethane (15-29°) and hydroxyapatite (32.05° and 32.49°)

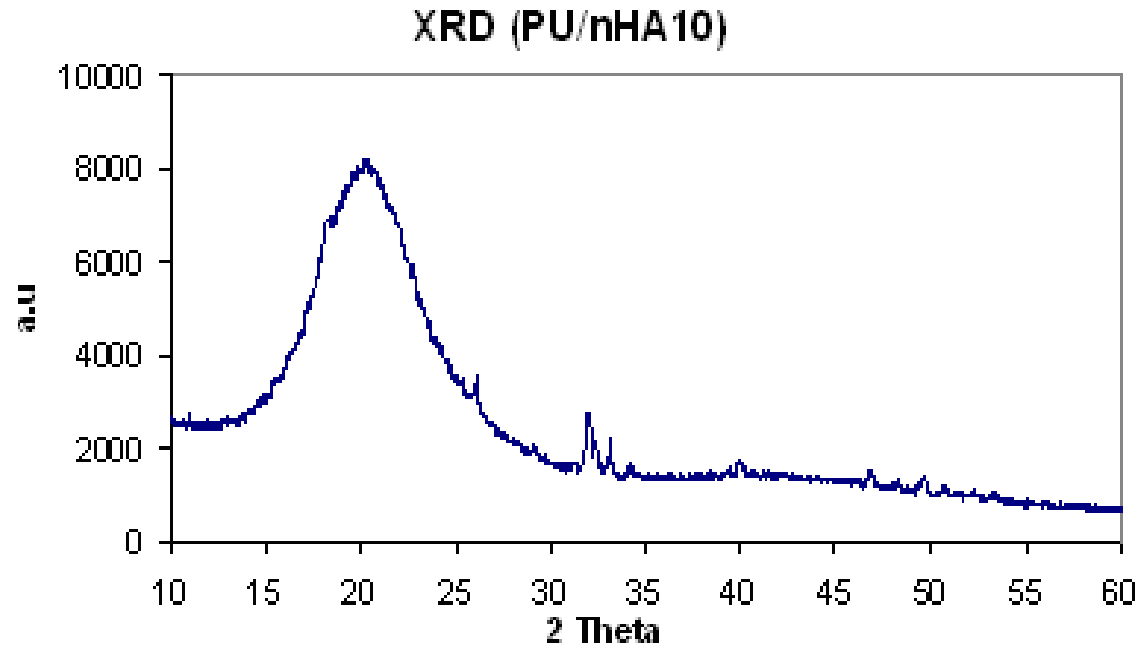

Figure 4.23 XRD pattern of chemically mixed PU/nHA10 showing characteristic peak of polyurethane (15-29°) and hydroxyapatite (32.05°, 32.49° and 33.22°)

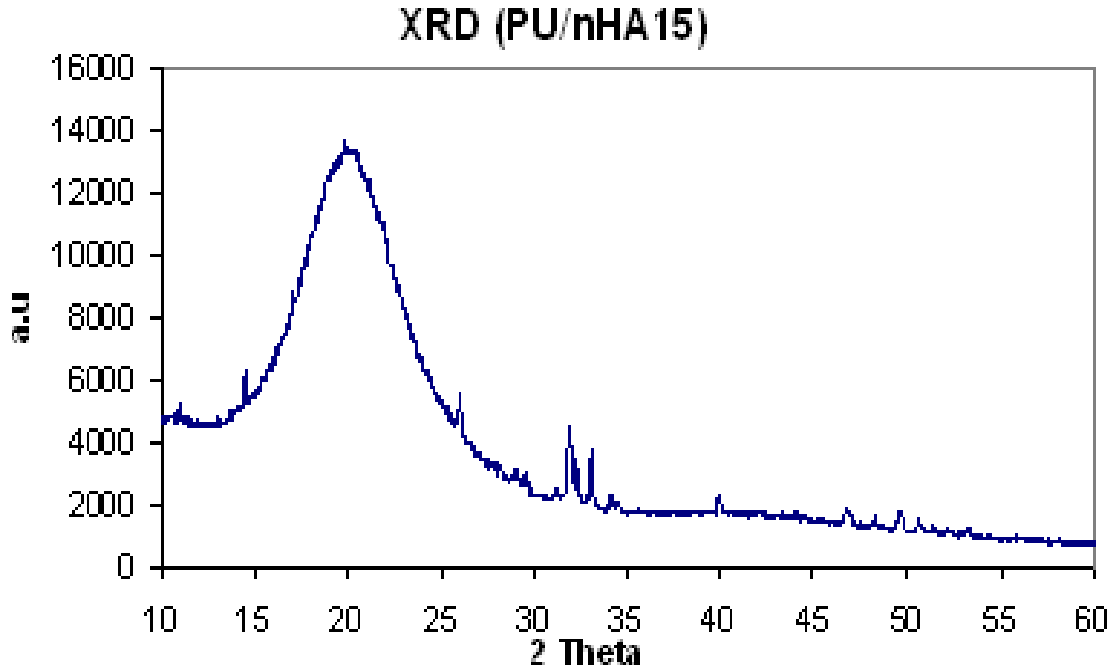

Figure 4.24 XRD pattern of chemically mixed PU/nHA15 showing characteristic peak of polyurethane (15-29°) and hydroxyapatite (26.10°, 32.05°, 32.49° and 33.22°)

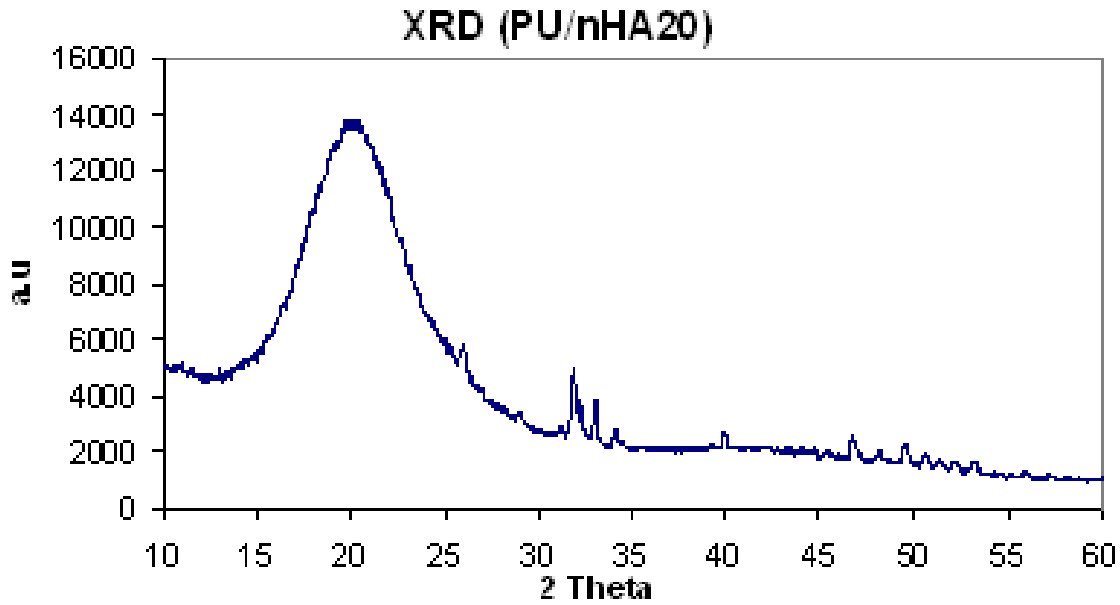

Figure 4.25 XRD pattern of chemically mixed PU/nHA20 showing characteristic peak of polyurethane (15-29°) and hydroxyapatite (26.10°, 32.05°, 32.49° and 33.22°)

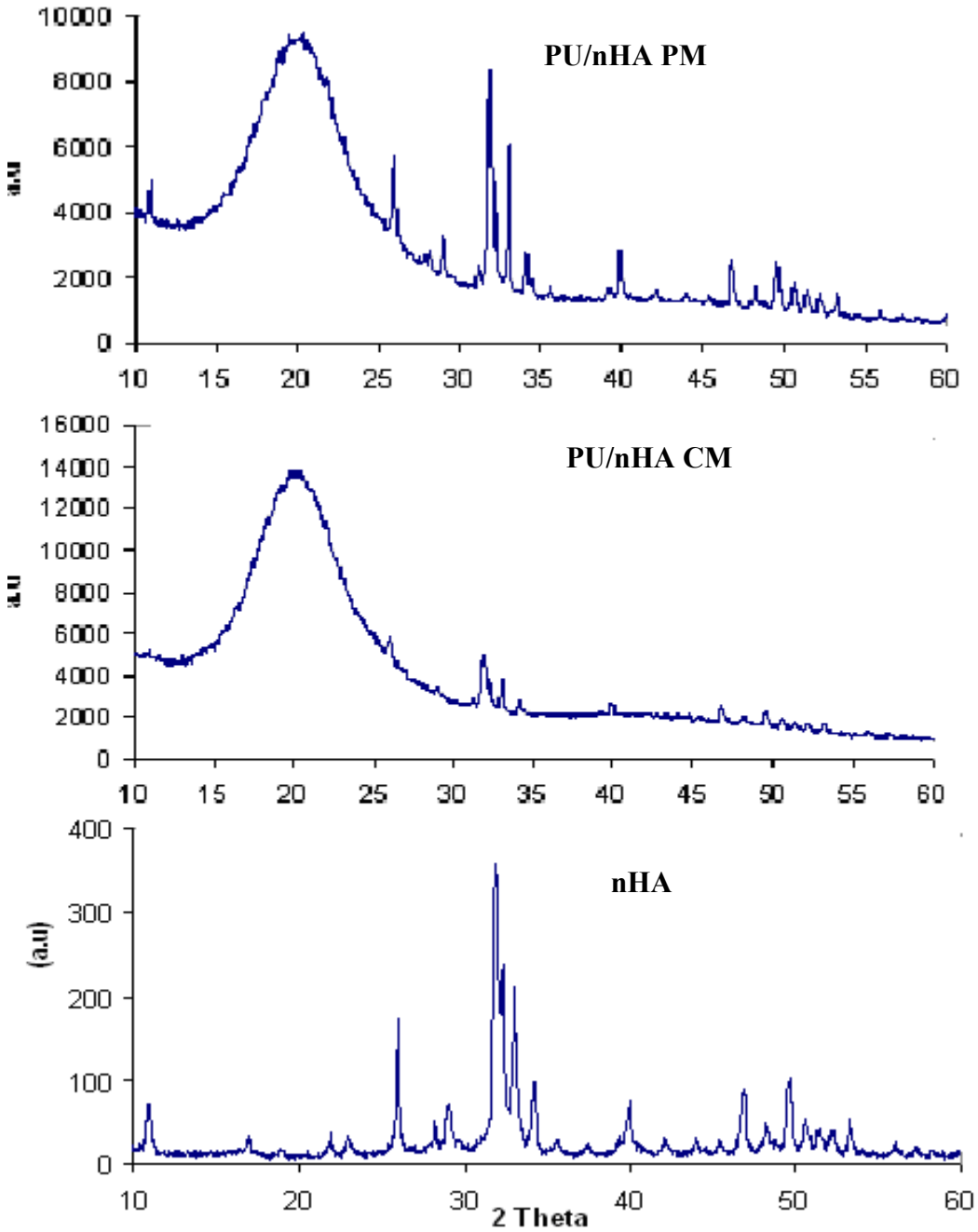

Figure 4.26 Comparative XRD pattern of nano-hydroxyapatite, polyurethane/nano-hydroxyapatite chemically mixed (PU/nHA CM), and polyurethane/nano-hydroxyapatite physically mixed (PU/nHA PM)

4.3.3- Thermal Characterisations

4.3.3.1- Thermogravimetric Analysis (TGA)

The results of thermal characteristics of PU/nHA composites were measured by using TGA and compared with PU and the resulting pattern is given in Figure 4.27.

The initial and second thermal decomposition values of PU/nHA tabulated in Table 4.17. In this study, it was observed that PU/nHA5 and PU/nHA10 composites showed the initial thermal decomposition at 298°C and 299°C and the final temperature at 394°C and 396°C respectively. There was no significant difference on the thermal behaviour of these composite but higher concentrated i.e. PU/nHA15 and PU/nHA20 composites showed significant difference, where the initial temperature is 341°C and 345°C and final temperature was 400°C and 428°C respectively. The secondary decomposition for PU/nHA5 and PU/nHA10 was observed at 503°C and 502°C respectively and for higher concentrated nano-hydroxyapatite composites i.e. PU/nHA15 and PU/nHA20 the decomposition started at 526°C and 525°C respectively.

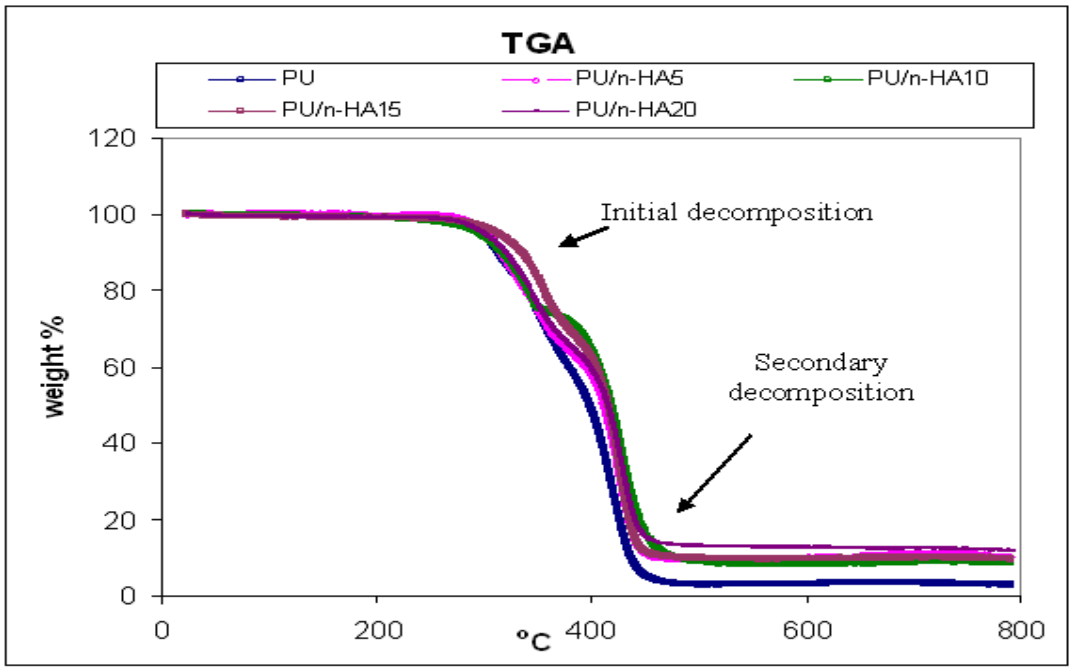

Figure 4.27 Comparative TGA patterns of PU and PU/nHA composites showing initial and secondary thermal decompositions

Table 4.17 Initial and second thermal decomposition of PU/nHA composites

Thermal Decomposition	PU/nHA5	PU/nHA10	PU/nHA15	PU/nHA20
First Stage:				
Initial Temperature (°C)	298	299	341	345
Final Temperature (°C)	394	396	400	428
Second Stage:				
Initial Temperature (°C)	503	502	526	525
Final Temperature (°C)	660	625	661	680

4.3.3.2- Differential Scanning Calorimetry (DSC)

The comparative DSC thermogram is presented in Figure 4.28 and it was observed that PU (control) and PU/nHA5 has almost the same pattern. The endothermic peak of PU (hard segment) was observed at 185°C, whereas for PU/nHA5, the peak appeared with slight increase at 195°C. In comparison, the higher concentrated nano-hydroxyapatite based polyurethane composites i.e. PU/nHA10, PU/nHA15, and PU/nHA20 had higher glass transition (endothermic peak) temperature and peaks observed in between 220-225°C. In addition, an exothermic peak appeared at 18°C in PU/nHA10 composite, which was not present in other samples.

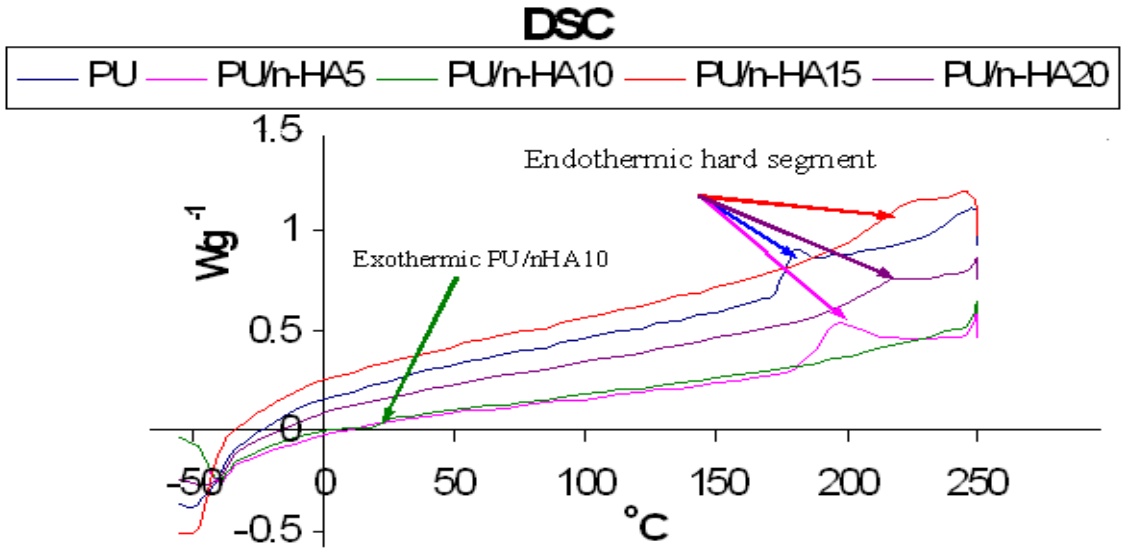

Figure 4.28 Comparative DSC thermogram of PU and PU/nHA composites showing endotherm T_g peaks

4.3.4- Biological Analysis

4.3.4.1- Biostability Analysis

Several studies suggested that chemical and morphological nature of biomaterial surface determined to a large extent how the biomaterial interacts with the host tissue and the physiological fluids after implantation (Hench and Ethridgo, 1982; Davies, 1988; Aoki, 1991). It is significant to evaluate the surface properties, such as wettability, so that future relationship with *in-vivo* behaviour might be established. In order to overcome the disadvantages of physical mixing method, such as fast degradation of nano-composites, the chemically crosslinked composites enhance the mechanical and physical properties (Chang *et al.,* 2003: Xu *et al.,* 2007). It is established that the side groups will play an important role in the hydrolytic degradation of PU. The location of these side groups will result in different rates of hydrolysis. When a hydrocarbon side chain is attached to the soft segment component of the PU it increases the hydrophobicity (Stirna *et al.,* 2002). Hence the structure and functionality of side groups will affect the degradative hydrolysis rate (Furukawa, 1997). The surface grafted PU will play an important role, not only in improving the biocompatibility, but also in biostability in relation to degradative hydrolysis**.**

In this study, the hydrophobicity and biostability of control (PU) and experimental (PU/nHA) composites were analysed by using the contact angle measurement (Section 3.8.6.1.2, Chapter 3), weight loss measurement (Section 3.8.6.1.3, Chapter 3) and were also characterised using FTIR (Section 3.8.3.1, Chapter 3), Raman Spectroscopy (Section 3.8.3.2, Chapter 3), XRD (Section 3.8.4.1, Chapter 3) and SEM (Section 3.8.4.3, Chapter 3) techniques. The FTIR and Raman spectral results for 1 and 7 days and SEM images of day 7 are given in Appendix (Appendix 3).

4.3.4.1.1-Contact Angle Measurements

The contact angle measurement for the control and experimental materials are given in Figure 4.29. The surface contact angle values and standard deviations are tabulated in

Table 4.18. It was observed that the surface contact angle increased with the increase in concentration of nHA. The significant difference ($p \leq 0.05$) was observed for PU/nHA15 and PU/nHA20 composites as compared to other samples.

Table 4.18 Contact Angle Measurement values of PU and PU/nHA composite with standard deviation

Samples	Contact Angle (°) ± SD
PU	73.96 ± 0.32
PU/nHA5	75.82 ±0.08
PU/nHA10	79.18 ± 0.19
PU/nHA15	89.00 ± 0.15
PU/nHA20	93.10 ± 0.11

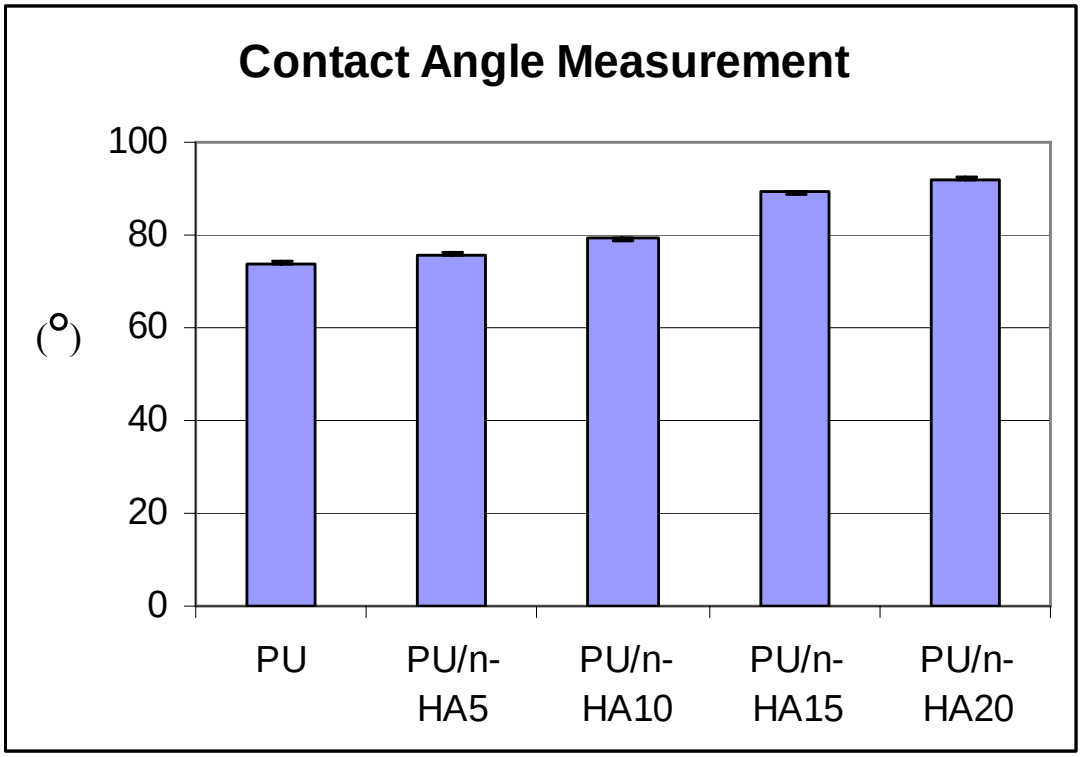

Figure 4.29 Contact angle measurements with standard deviations of PU and PU/nHA composites prior to immersion in media

4.3.4.1.2- Weight Loss Measurement

The change in weight loss for samples immersed in deionised water and PBS is given in Table 4.19 and 4.20 respectively. The graphical pattern of the weight loss for deionised water and PBS is presented in Figure 4.30 (a & b) respectively. It was observed that the samples immersed in deionised water showed more weight loss than PBS samples.

Table 4.19 Weight loss measurement in % ± SD for samples immersed in deionised water

Samples	Day 1	Day 7	Day 14	Day 21	Day 40	Day 90
PU	0 ± 0.0002	-0.22 ± 0.0003	-0.74 ± 0.0001	0.7 ± 0.006	0.95 ± 0.004	1.95 ± 0.004
PU/nHA5	-0.03 ± 0.0004	0 ± 0.0002	0.49 ± 0.003	0.97 ± 0.006	1.08 ± 0.045	2.13 ± 0.063
PU/nHA10	0 ± 0.0002	0.25 ± 0.008	0.38 ± 0.004	0.66 ± 0.004	0.93 ± 0.008	2.06 ± 0.087
PU/nHA15	0 ± 0.0005	0.34 ± 0.004	0.39 ± 0.008	0.54 ± 0.009	0.61 ± 0.005	2.19 ± 0.067
PU/nHA20	0 ± 0.0004	0.22 ± 0.008	0.26 ± 0.004	0.34 ± 0.008	0.82 ± 0.005	1.83 ± 0.089

Table 4.20 Weight loss measurement in % ± SD for samples immersed in PBS

Samples	Day 1	Day 7	Day 14	Day 21	Day 40	Day 90
PU	-0.7 ± 0.006	-0.7 ± 0.006	0 ± 0.0004	0.96 ± 0.007	1.26 ± 0.054	1.84 ± 0.065
PU/nHA5	-0.05 ± 0.001	0.43 ± 0.0037	0.44 ± 0.003	0.89 ± 0.002	1.06 ± 0.008	1.63 ± 0.005
PU/nHA10	0.01 ± 0.002	0.37 ± 0.057	0.39 ± 0.068	0.69 ± 0.043	0.98 ± 0.072	1.15 ± 0.032
PU/nHA15	0.01 ± 0.0006	0.32 ± 0.064	0.32 ± 0.071	0.57 ± 0.035	0.98 ± 0.064	1.05 ± 0.066
PU/nHA20	0 ± 0.0004	0.22 ± 0.005	0.29 ± 0.003	0.37 ± 0.003	0.94 ± 0.008	1.33 ± 0.079

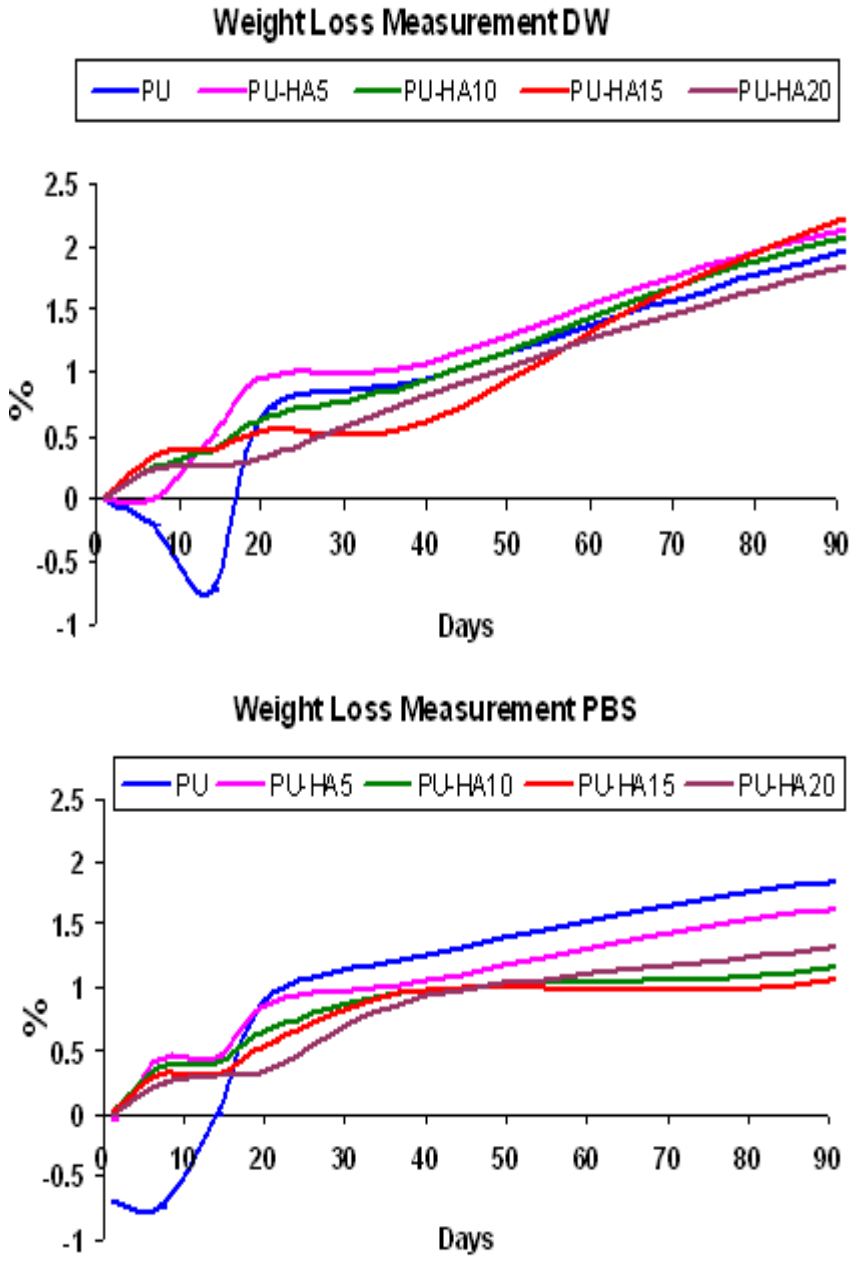

Figure 4.30 Weight loss measurement in deionised water (DW) and PBS

4.3.4.1.3- Fourier Transform Infrared Spectroscopy (FTIR)

The comparative FTIR spectra of PU samples before and after treated with deionised water and PBS are given in Figure 4.31 and 4.32 respectively. The spectral results were based on control group in comparison to 14, 40 and 90 days. After hydrolysis the spectra showed no significant change at N—H (3320 cm^{-1}), C—H (2939-2796 cm^{-1}), C=O (1730-1700 cm^{-1}) and C—O—C (1110-950 cm^{-1}) group. However, the spectra showed the change of peak position at carbonyl region (1675 cm^{-1}). The spectral pattern of PU/nHA5 before and after treatment with deionised water and PBS are given in Figure 4.33 and 4.34 respectively. The intensity of N—H peak was increased with the immersion time. Higher intensity was observed in the samples treated with deionised water than PBS. The slight spectral changes were observed in the carbonyl region, where the intensity of 1650 cm^{-1} peak was increased with immersion time. The peak at 1150 cm^{-1} was observed before immersion in deionised water, which was not visible in treated sample. The amide group (1500-1200 cm^{-1}) showed no change in that region. Figure 4.35 and 4.36 showed the spectral changes for PU/nHA10 composite immersed in deionised water and PBS respectively. With the immersion time, the broadness of N—H peak was observed in both media. FTIR spectrum of the sample immersed for 40 days in deionised water showed slightly different pattern than others. The changes appeared at carbonyl (1650 cm^{-1}) and ether region (1120 cm^{-1}). This peak emerged in both regions, which was expected either due to hydrolysis of chain bond or due to hot pressing technique which was used during the preparation of samples. It is envisaged that this scission was due to oxidation degradation rather hydrolysis. However, the 40 days sample in PBS showed only emergence of peak at ether region and not at carbonyl region. It was interesting to find that the peak observed in FTIR spectrum of 40 days sample, whereas, no such peaks were presented in FTIR spectrum of 90 days sample. FTIR spectrum of PU/nHA15 sample showed no significant shifting and emergence of peaks in deionised water and PBS is given in Figure 4.37 and 4.38 respectively. Same pattern was observed for PU/nHA20 samples. Figure 4.39 showed the samples immersed in deionised water and Figure 4.40 presented the FTIR spectrum for PBS treatment.

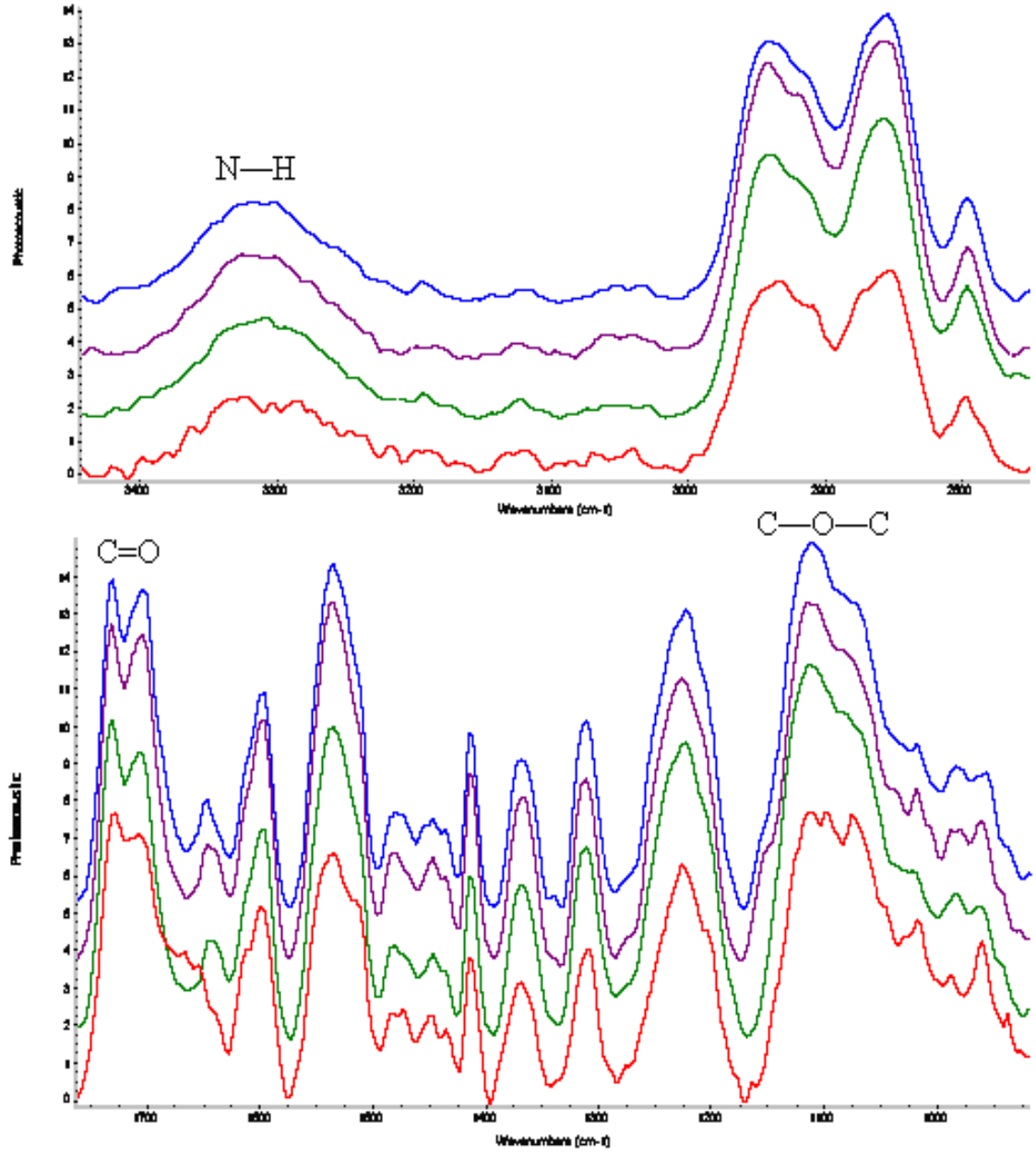

Figure 4.31 Comparative FTIR spectra of PU immersed in deionised water analysed control PU (red) with day 14 (green), day 40 (violet), and day 90 (blue)

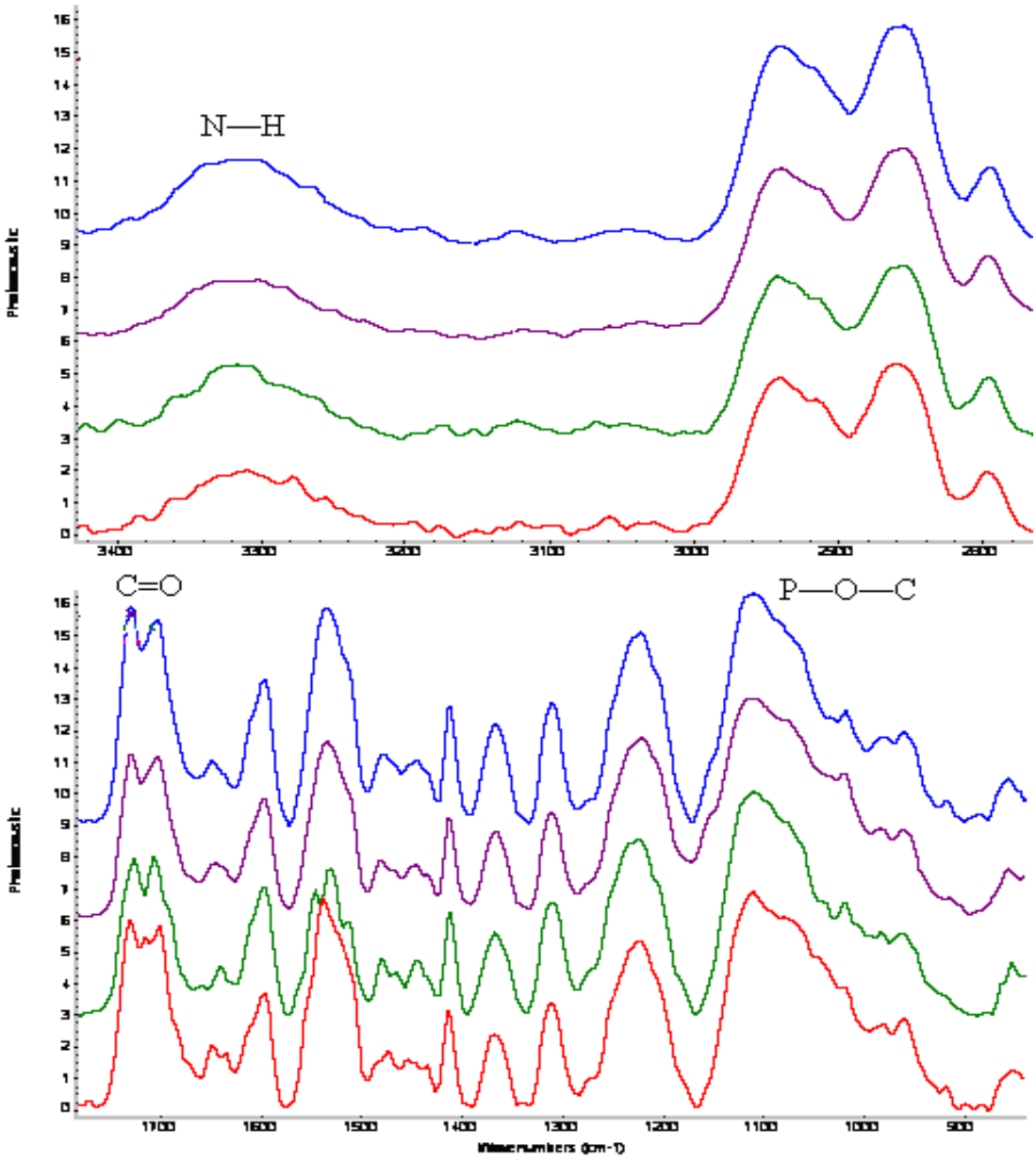

Figure 4.32 Comparative FTIR spectra of PU immersed in PBS analysed control PU (red) with day 14 (green), day 40 (violet), and day 90 (blue)

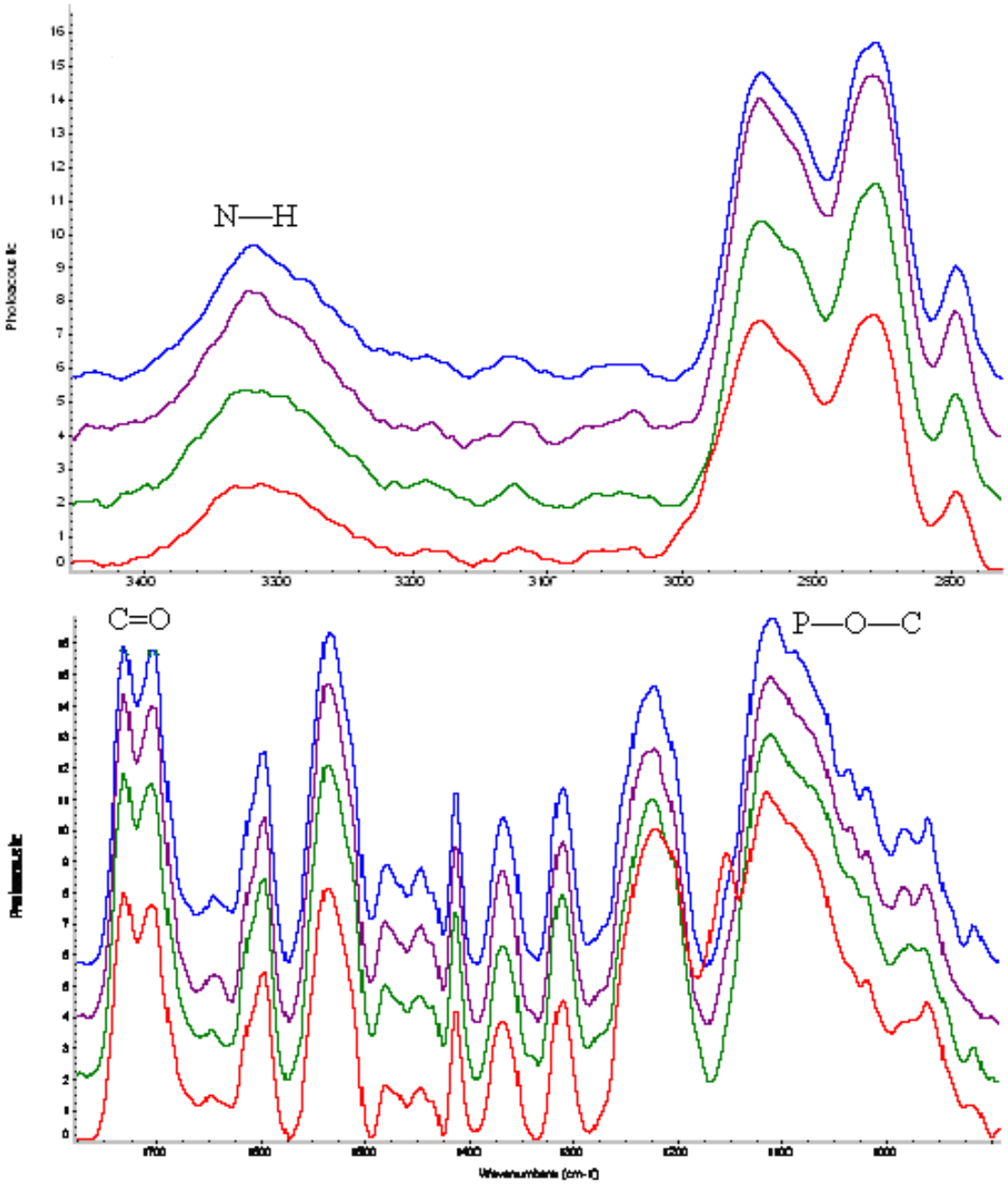

Figure 4.33 Comparative FTIR spectra of PU/nHA5 treated with deionised water analysed control PU/nHA5 (red) with day 14 (green), day 40 (violet), and day 90 (blue)

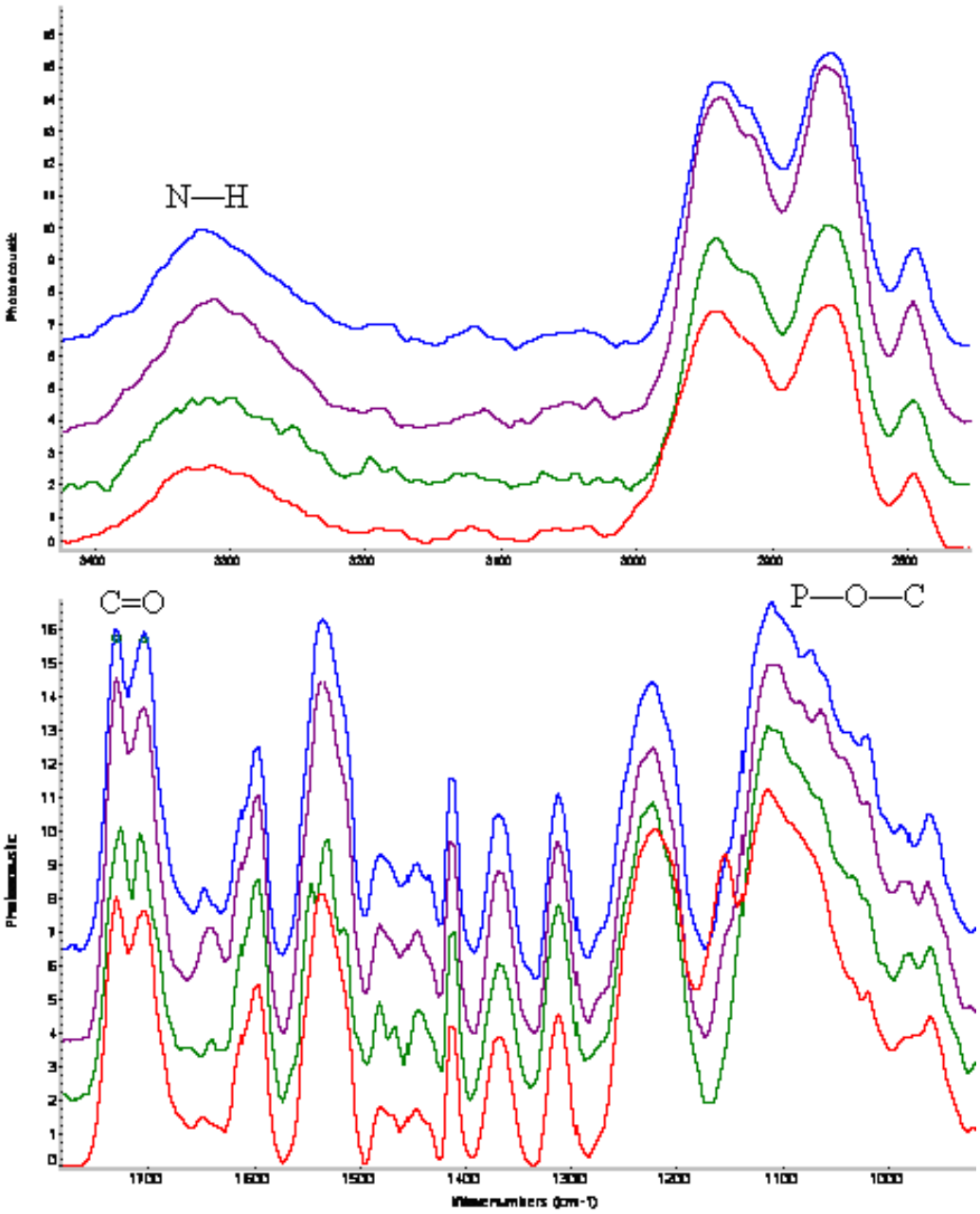

Figure 4.34 Comparative FTIR spectra of PU/nHA5 treated with PBS analysed control PU/nHA5 (red) with day 14 (green), day 40 (violet), and day 90 (blue)

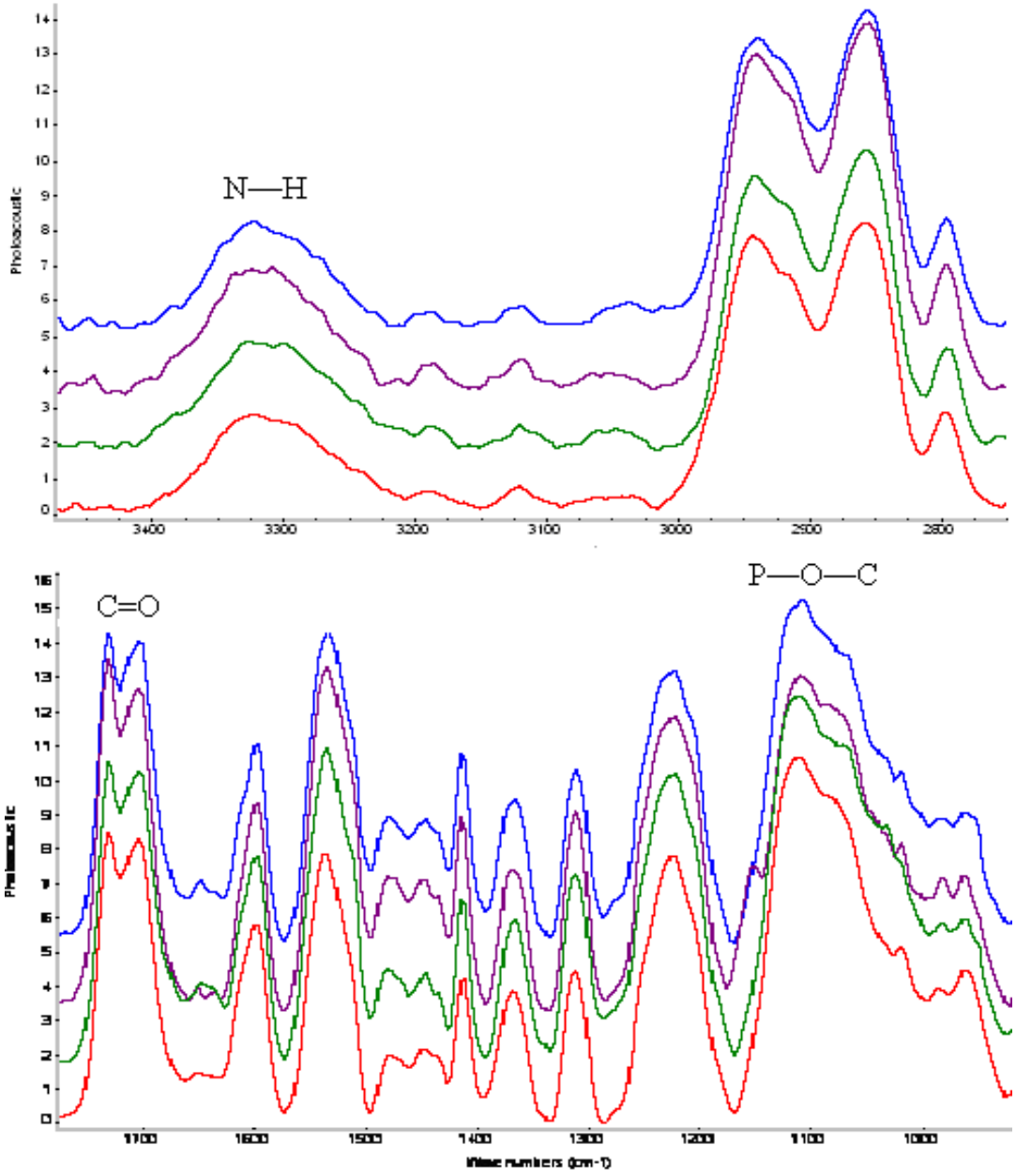

Figure 4.35 Comparative FTIR spectra of PU/nHA10 treated with deionised water analysed control PU/nHA10 (red) with day 14 (green), day 40 (violet), and day 90 (blue)

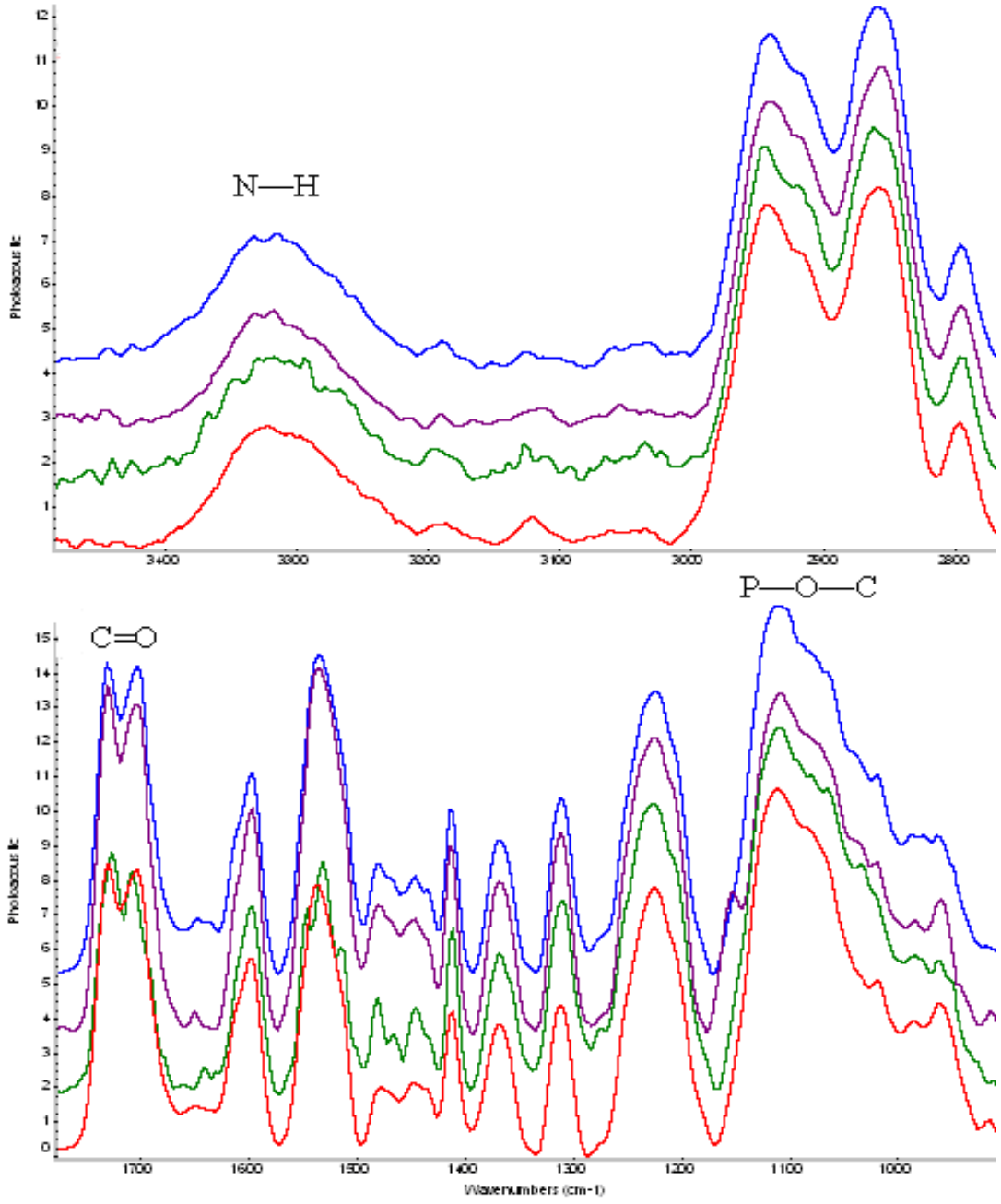

Figure 4.36 Comparative FTIR spectra of PU/nHA10 treated with PBS analysed control PU/nHA10 (red) with day 14 (green), day 40 (violet), and day 90 (blue)

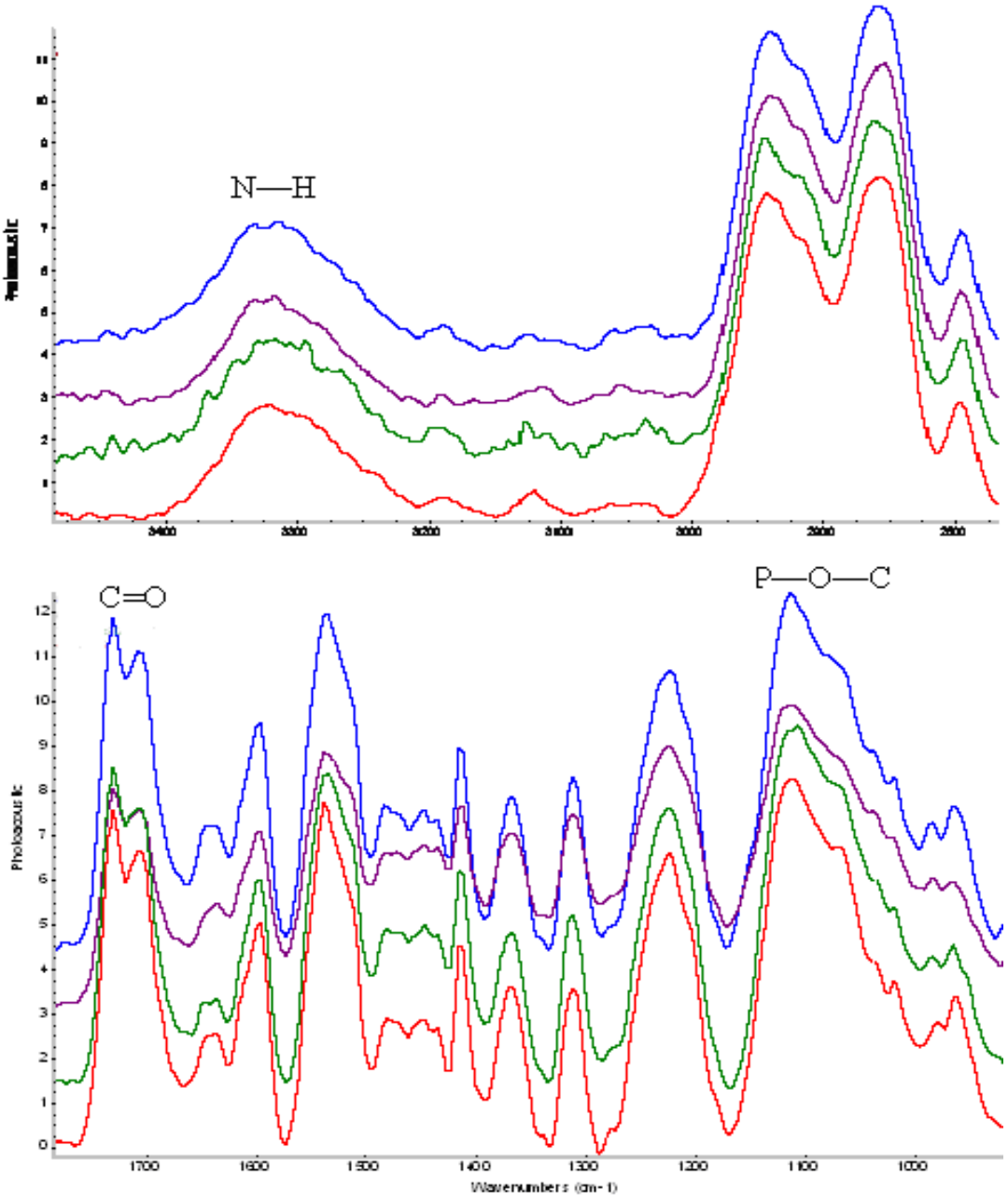

Figure 4.37 Comparative FTIR spectra of PU/nHA15 treated with deionised water analysed control PU/nHA15 (red) with day 14 (green), day 40 (violet), and day 90 (blue)

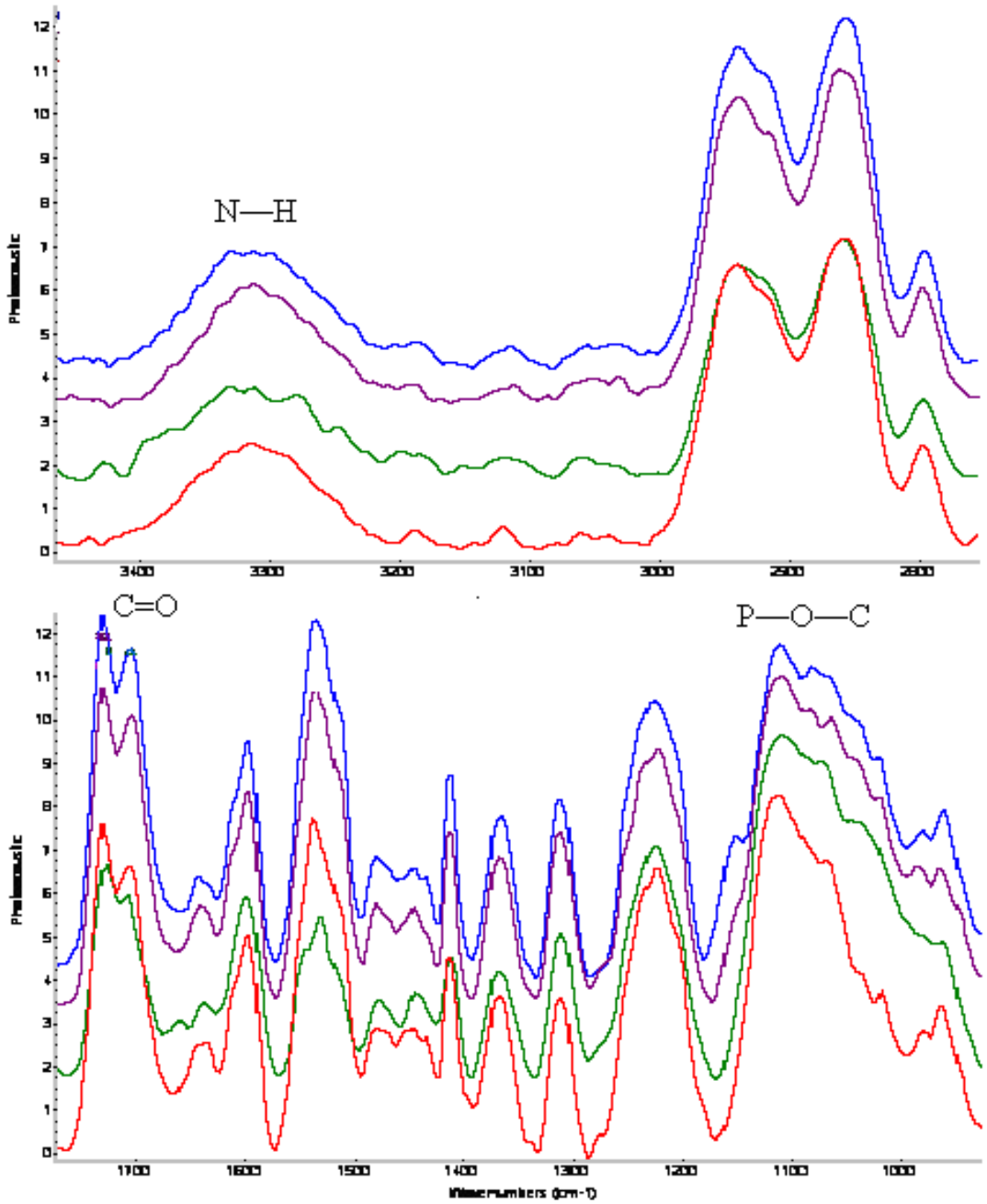

Figure 4.38 Comparative FTIR spectra of PU/nHA15 treated with PBS analysed control PU/nHA15 (red) with day 14 (green), day 40 (violet), and day 90 (blue)

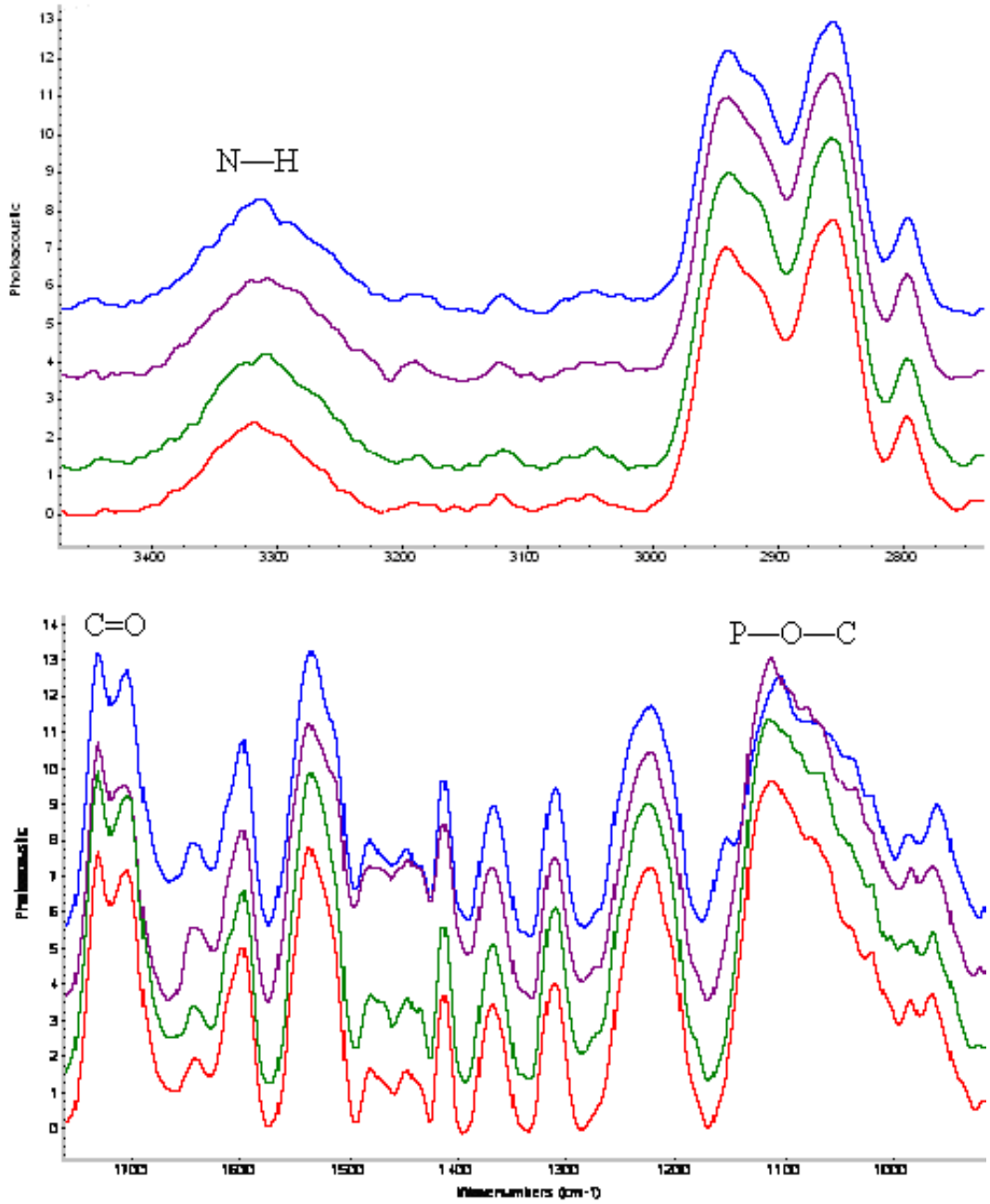

Figure 4.39 Comparative FTIR spectra of PU/nHA20 treated with deionised water analysed control PU/nHA20 (red) with day 14 (green), day 40 (violet), and day 90 (blue)

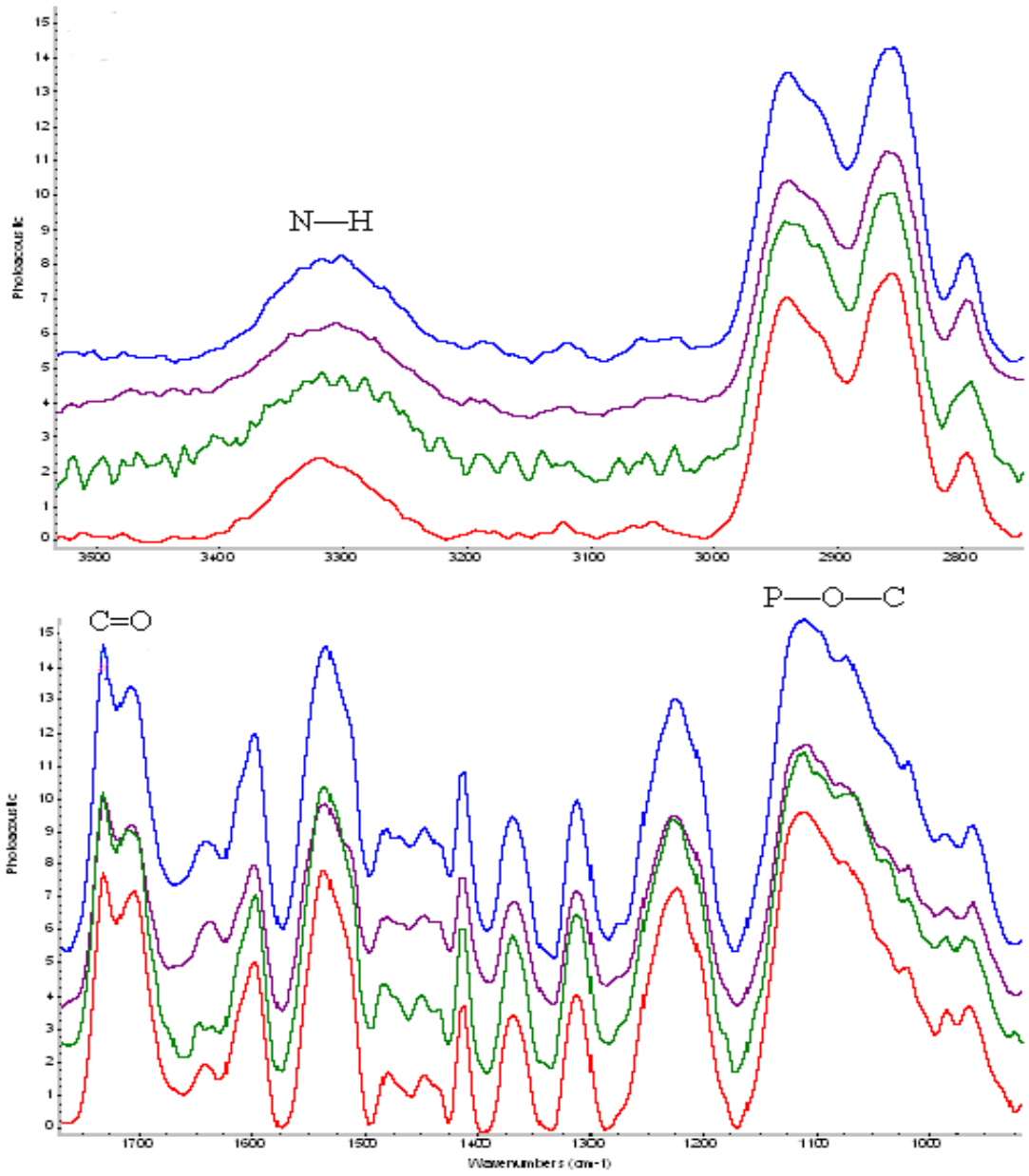

Figure 4.40 Comparative FTIR spectra of PU/nHA20 treated with PBS analysed control PU/nHA20 (red) with day 14 (green), day 40 (violet), and day 90 (blue)

4.3.4.1.4- Raman Spectroscopy

Raman spectra of PU sample are given in Figure 4.41 [(a) deionised water and (b) PBS]. It was observed that there was no shifting of peaks that indicated that there was no chain

scission in polyurethane sample due to well-interlinked hard and soft segments. Raman spectra of PU/nHA5 samples treated with deionised water and PBS are given in Figure 4.42 (a & b). The spectrum showed no changes in the sample treated with deionised water; however, the spectrum of 90 day PBS sample showed emergence of shoulder peaks in carbonyl (1716 cm^{-1}) and amide region (1286 cm^{-1}). Figure 4.43 (a & b) showed no spectral changes for PU/nHA10, however, PU/nHA15 and PU/nHA20 showed significant changes at 90 days as shown in Figure 4.44 (a & b) and Figure 4.45 (a & b) respectively. Raman spectrum of 90 day samples showed peaks emergence in amide (1250 cm^{-1}) and ether region (1105 cm^{-1}), whereas, no changes were observed up to 40 days.

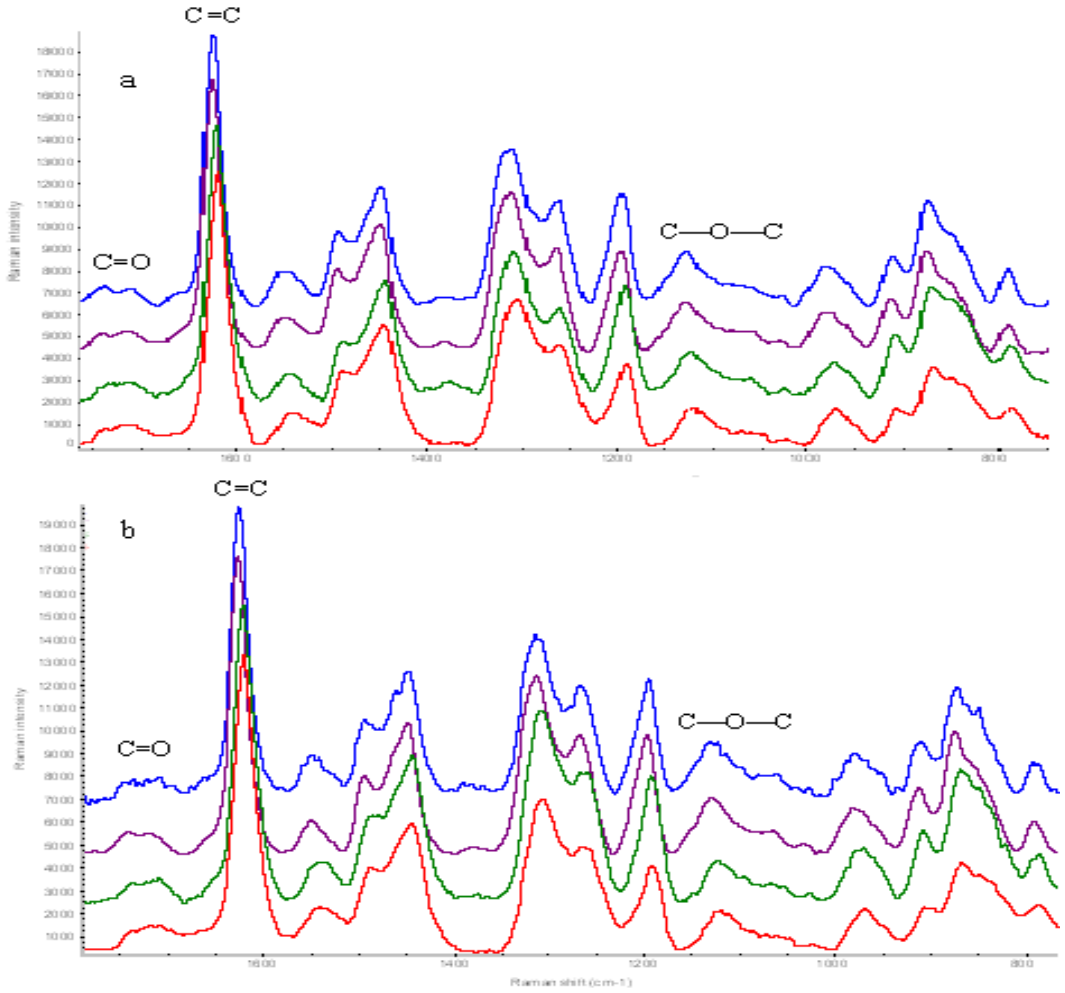

Figure 4.41 Comparative Raman spectra of PU treated with (a) deionised water and (b) PBS analysed control PU (red) with day 14 (green), day 40 (violet), and day 90 (blue)

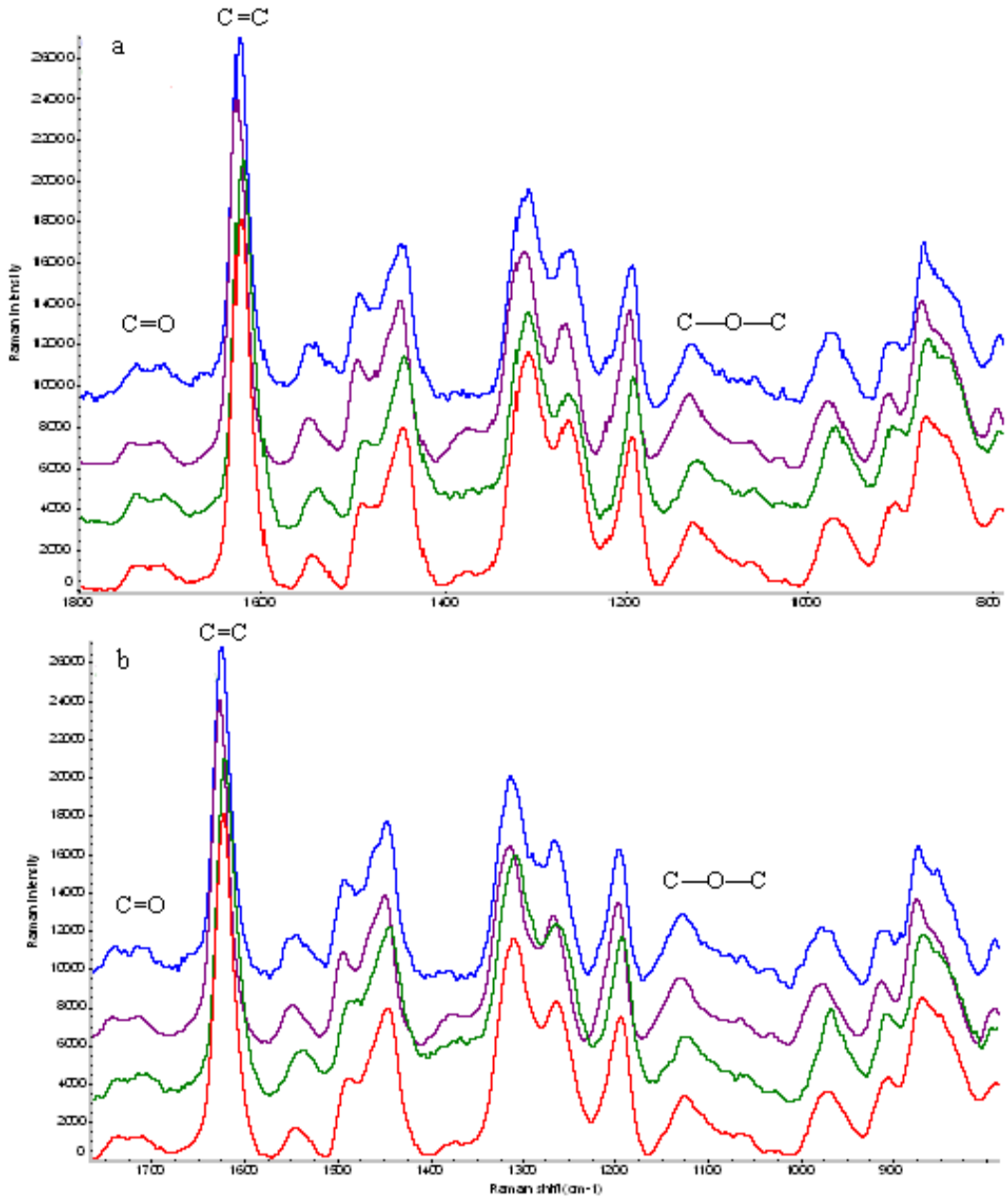

Figure 4.42 Comparative Raman spectra of PU/nHA5 treated with (a) deionised water and (b) PBS analysed control PU/nHA5 (red) with day 14 (green), day 40 (violet), and day 90 (blue)

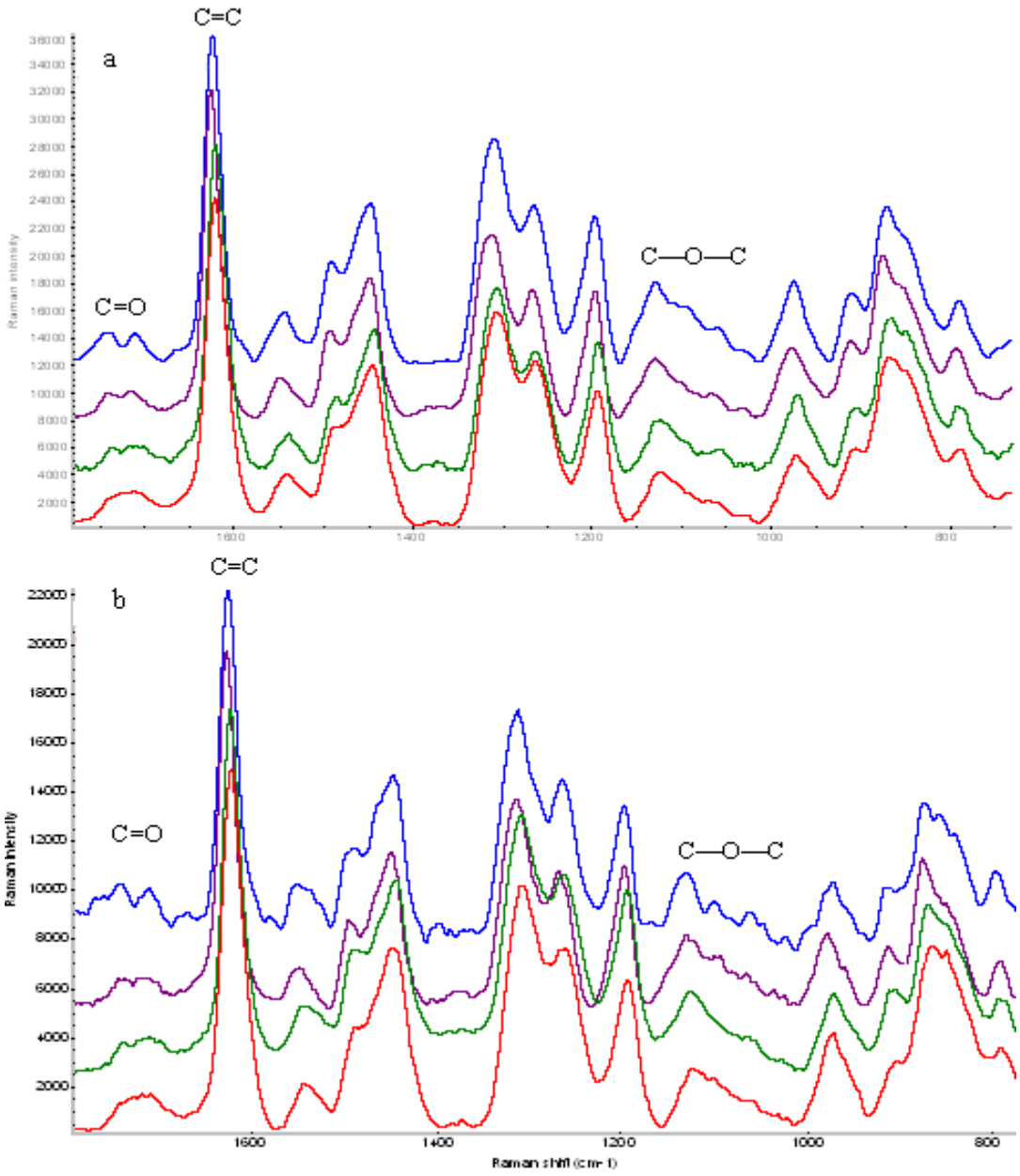

Figure 4.43 Comparative Raman spectra of PU/nHA10 treated with (a) deionised water and (b) PBS analysed control PU/nHA10 (red) with day 14 (green), day 40 (violet), and day 90 (blue)

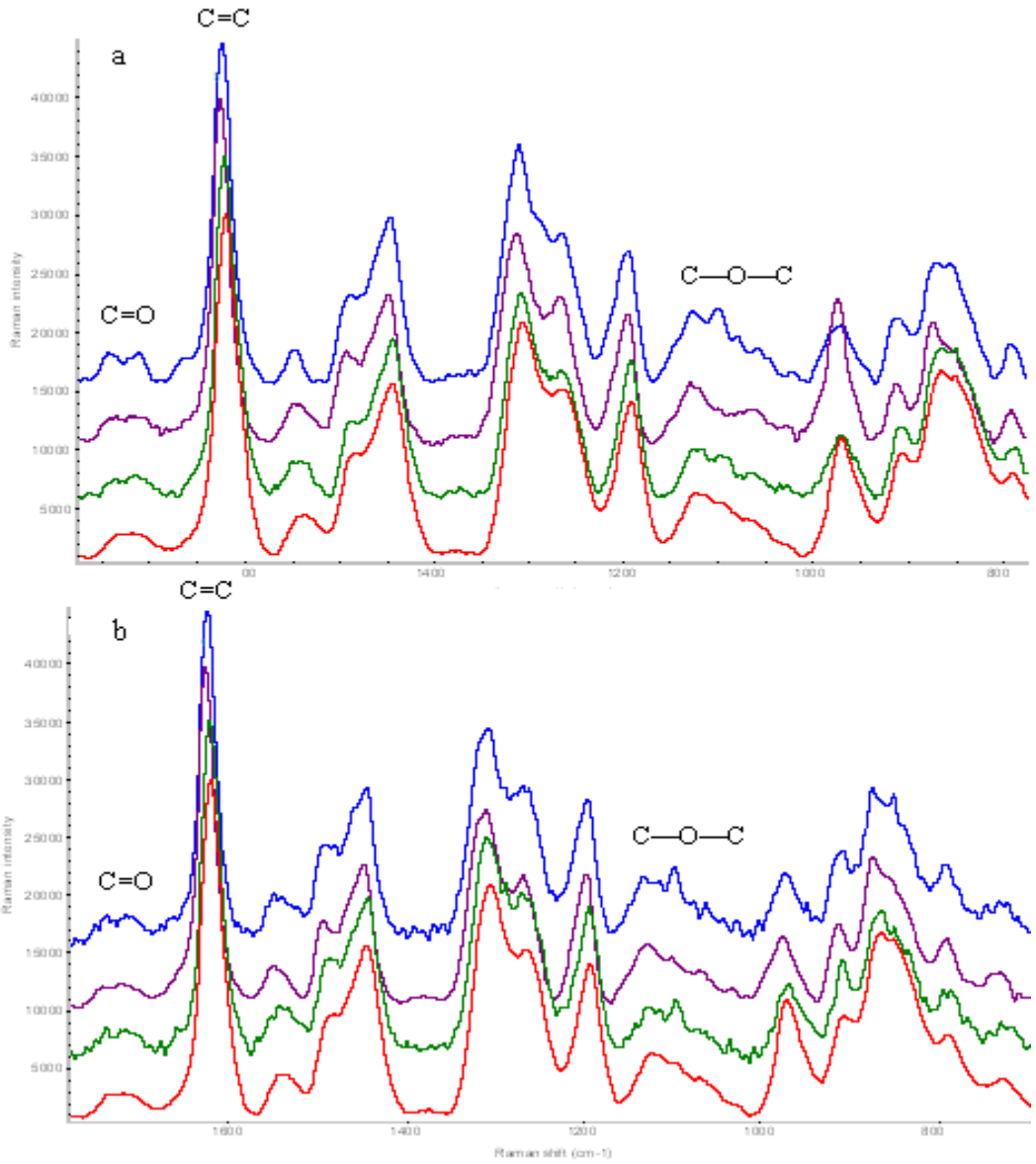

Figure 4.44 Comparative Raman spectra of PU/nHA15 treated with (a) deionised water and (b) PBS analysed control PU/nHA15 (red) with day 14 (green), day 40 (violet), and day 90 (blue)

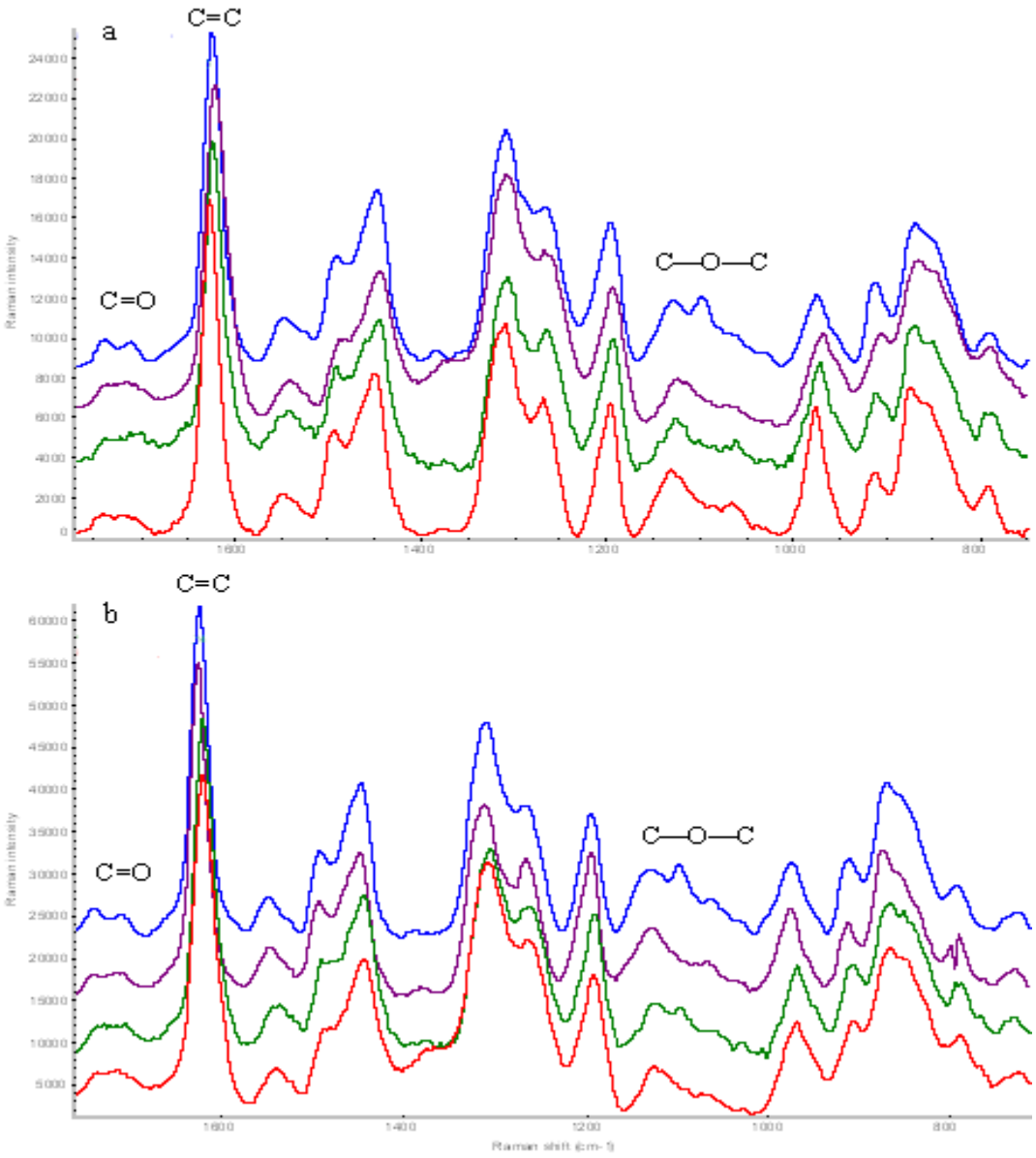

Figure 4.45 Comparative Raman spectra of PU/nHA20 treated with (a) deionised water and (b) PBS analysed control PU/nHA20 (red) with day 14 (green), day 40 (violet), and day 90 (blue)

4.3.4.1.5- X-ray Diffraction (XRD)

The XRD pattern of PU samples is given in Figure 4.46 and showed almost same pattern after treated with deionised water and PBS. The specimens immersed in PBS had low crystallinity as compared to deionised water. XRD patterns of PU/nHA5 (Figure 4.47) and PU/nHA10 (Figure 4.48) showed sudden decrease in crystallinity after 1 day immersion; however, from day 1 to 90, the crystallinity remained same in both solutions. XRD pattern of PU/nHA15 (Figure 4.49) in deionised water presented gradual decrease in crystallinity, whereas, samples in PBS showed no change in the pattern. The crystallinity of PU/nHA20 (Figure 4.50) remained same up to 40 days; however, XRD pattern of 90 day sample showed decrease in crystallinity.

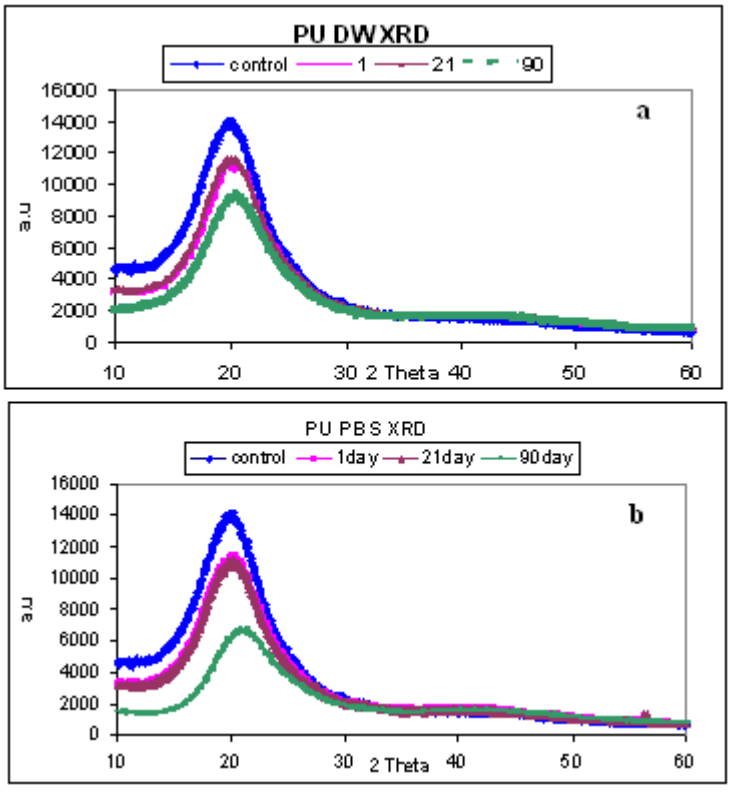

Figure 4.46 Comparative XRD pattern of PU samples treated with (a) deionised water (b) PBS

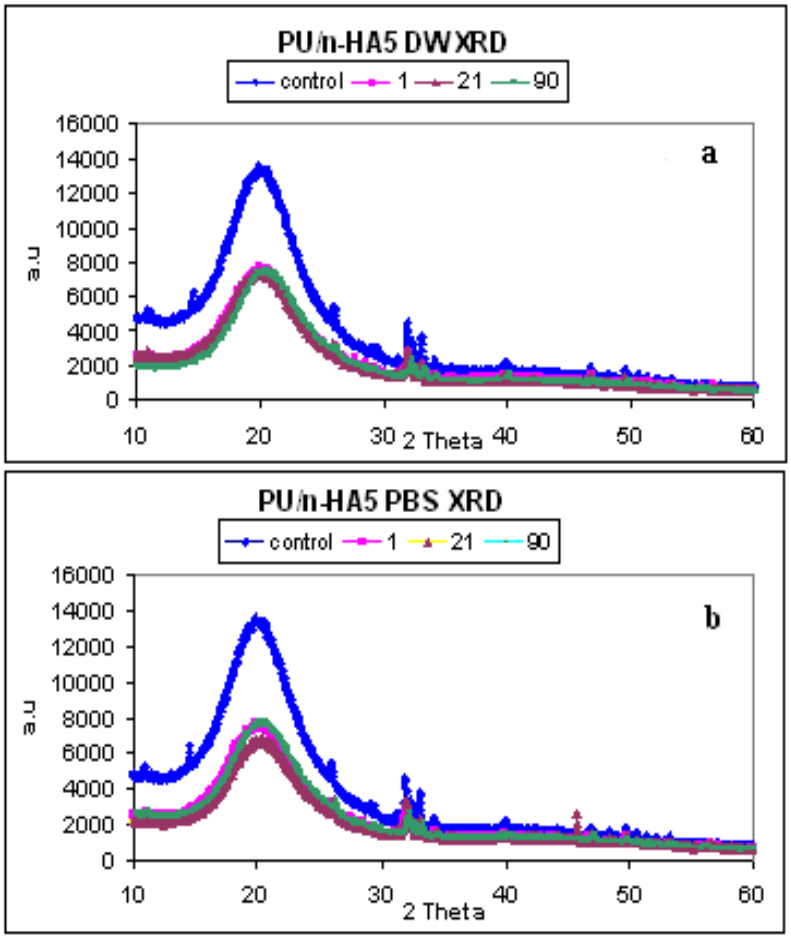

Figure 4.47 Comparative XRD pattern of PU/nHA5 samples treated with (a) deionised water (b) PBS

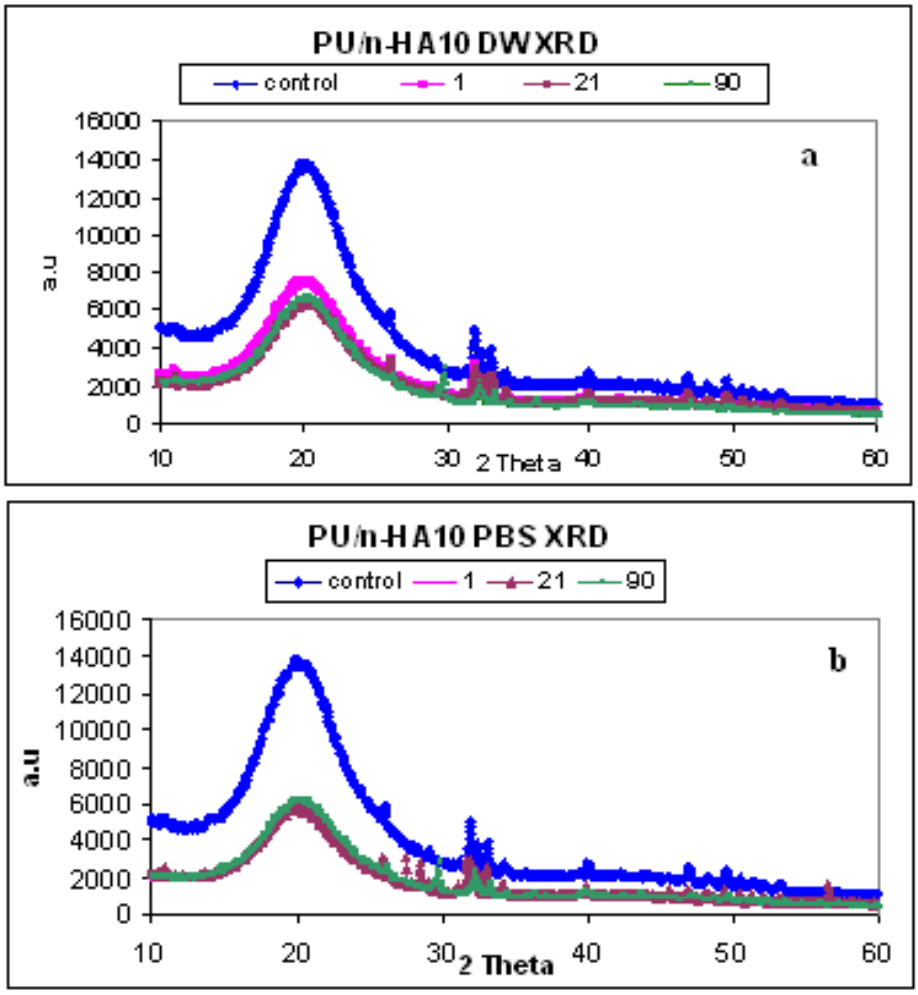

Figure 4.48 Comparative XRD pattern of PU/nHA10 samples treated with (a) deionised water (b) PBS

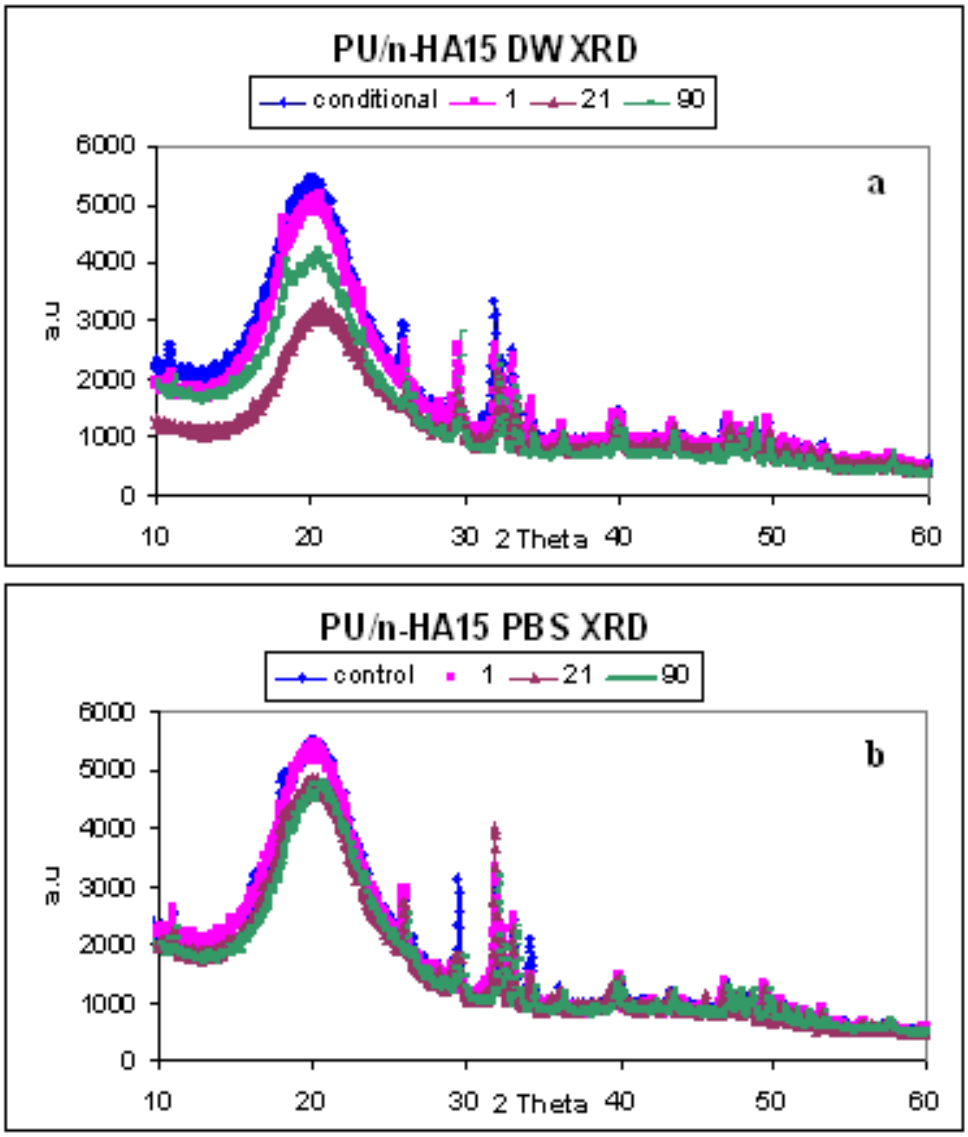

Figure 4.49 Comparative XRD pattern of PU/nHA15 samples treated with (a) deionised water (b) PBS

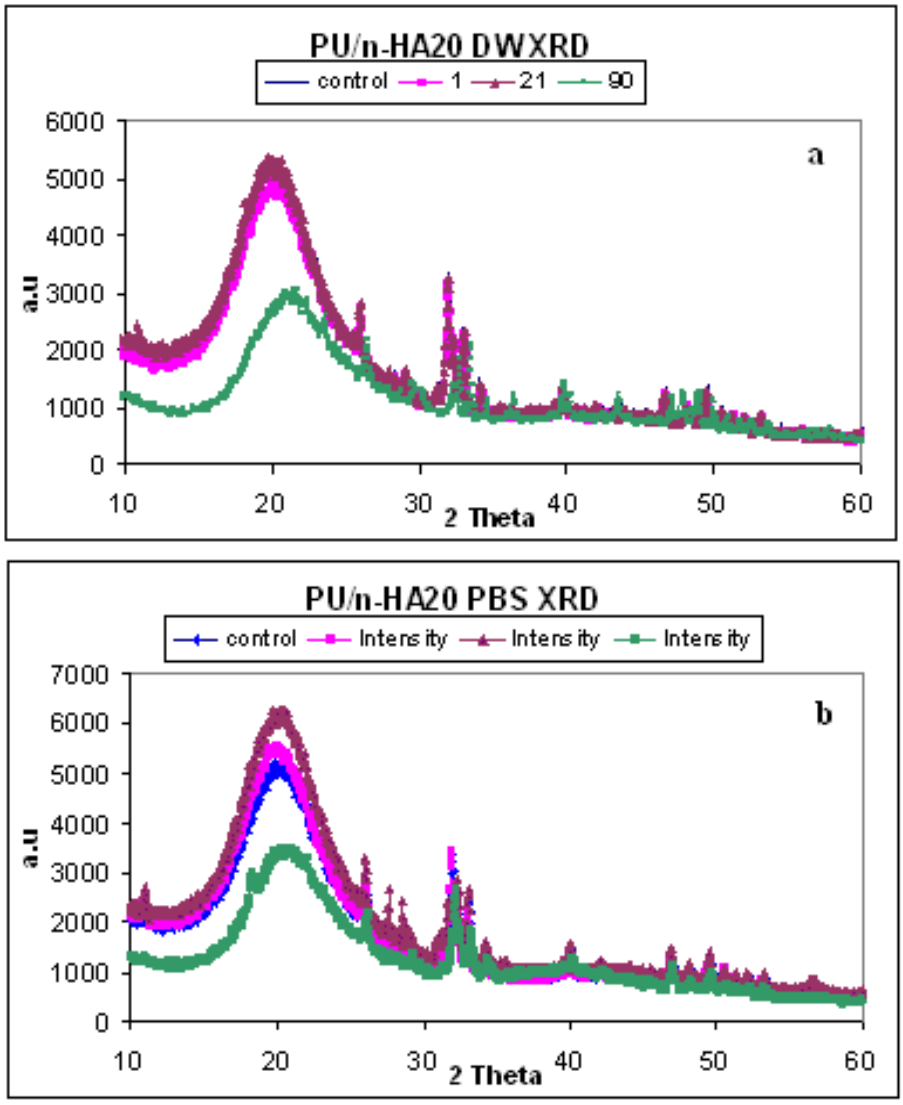

Figure 4.50 Comparative XRD pattern of PU/nHA20 samples treated with (a) deionised water (b) PBS

4.3.4.1.6- Scanning Electron Microscopy (SEM)

The comparative SEM images of PU samples in deionised water (DW) and PBS at 1, 14 and 90 days are given in Figure 4.51. These images showed that PU film surfaces were relatively smooth and free of significant surface defects. SEM image of 90 day sample showed few pits with the nominal size of 2-3 μm on the surface. Figure 4.52 and 4.53 presented the comparison of PU/nHA5, PU/nHA10 and PU/nHA15, PU/nHA20 respectively. The surface of samples did not present any pits; however, cracks appeared on the surface.

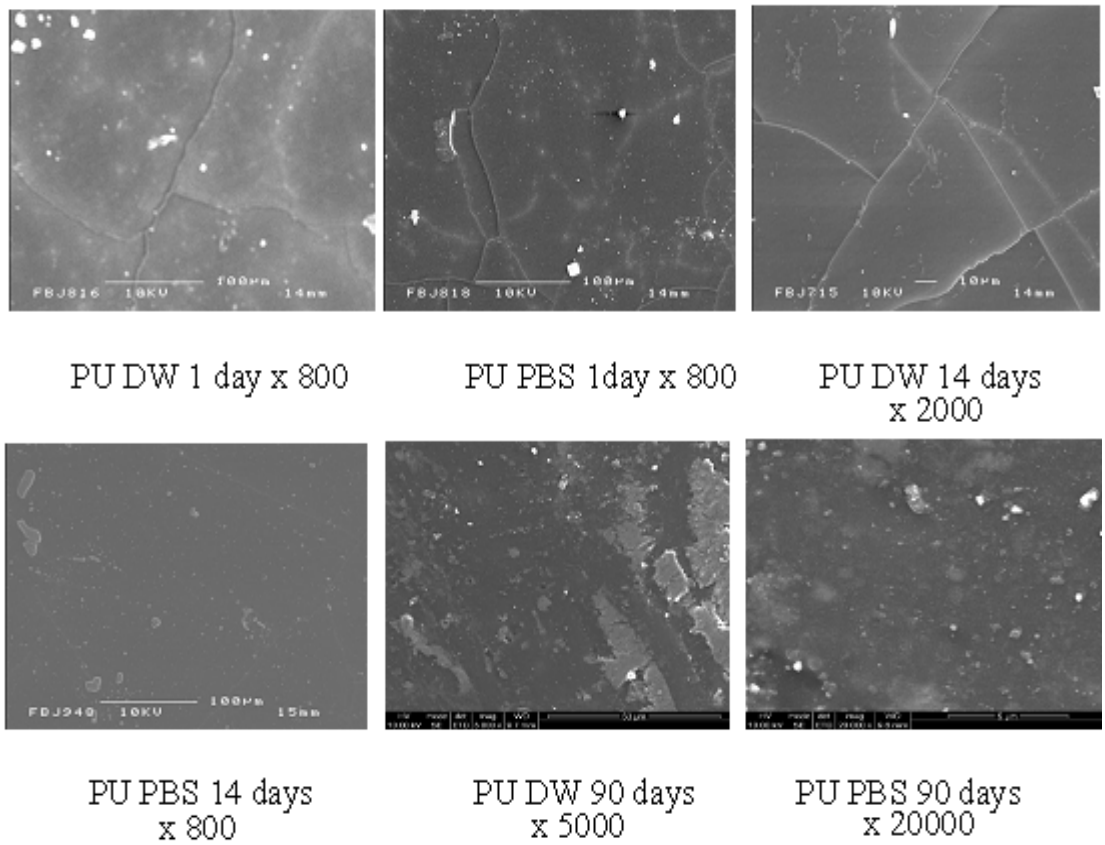

Figure 4.51 SEM images of PU samples treated with deionised water (DW) and PBS at predetermined time intervals

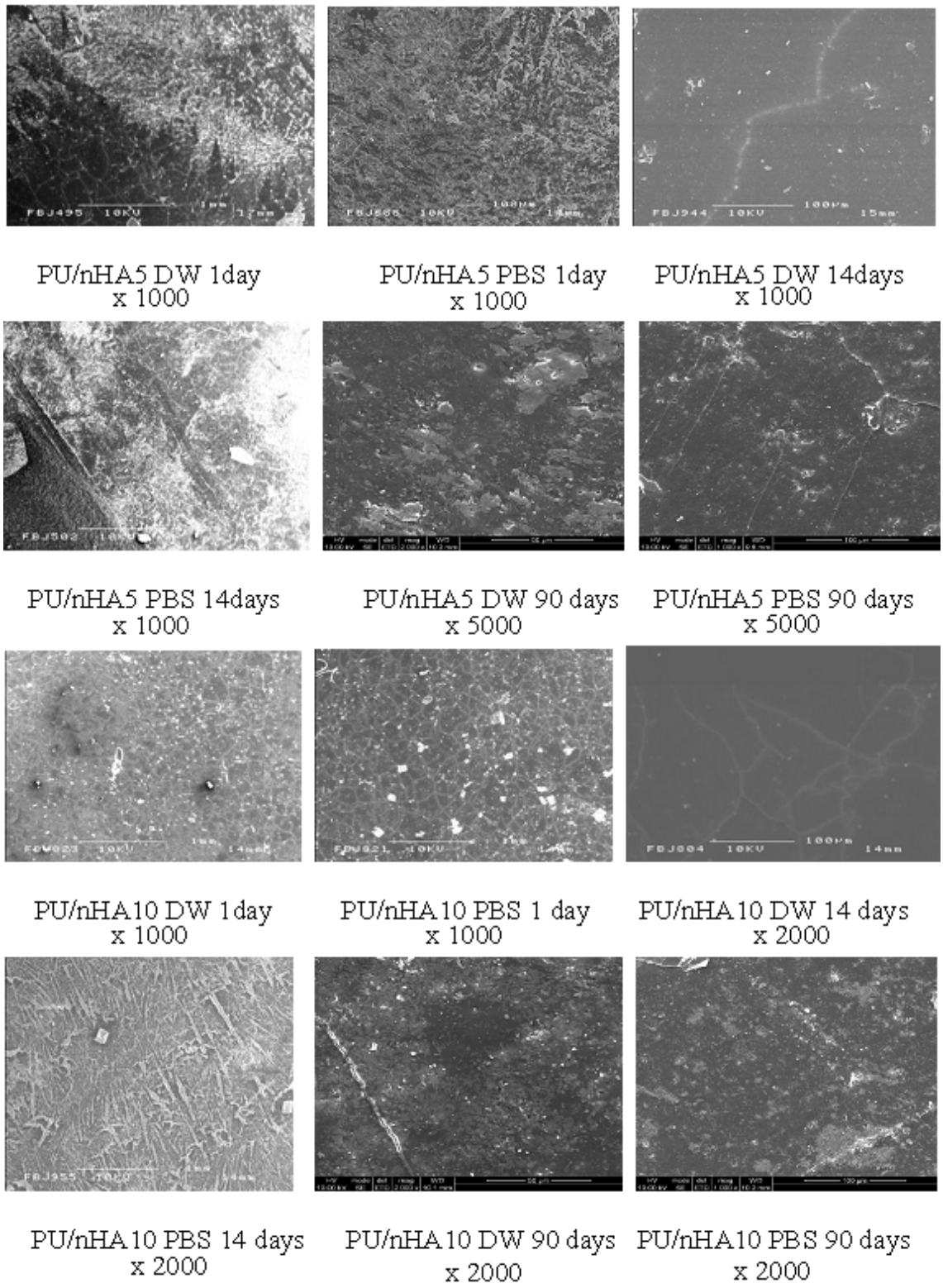

Figure 4.52 SEM images of PU/nHA5 and PU/nHA10 samples treated with deionised water (DW) and PBS at predetermined time intervals

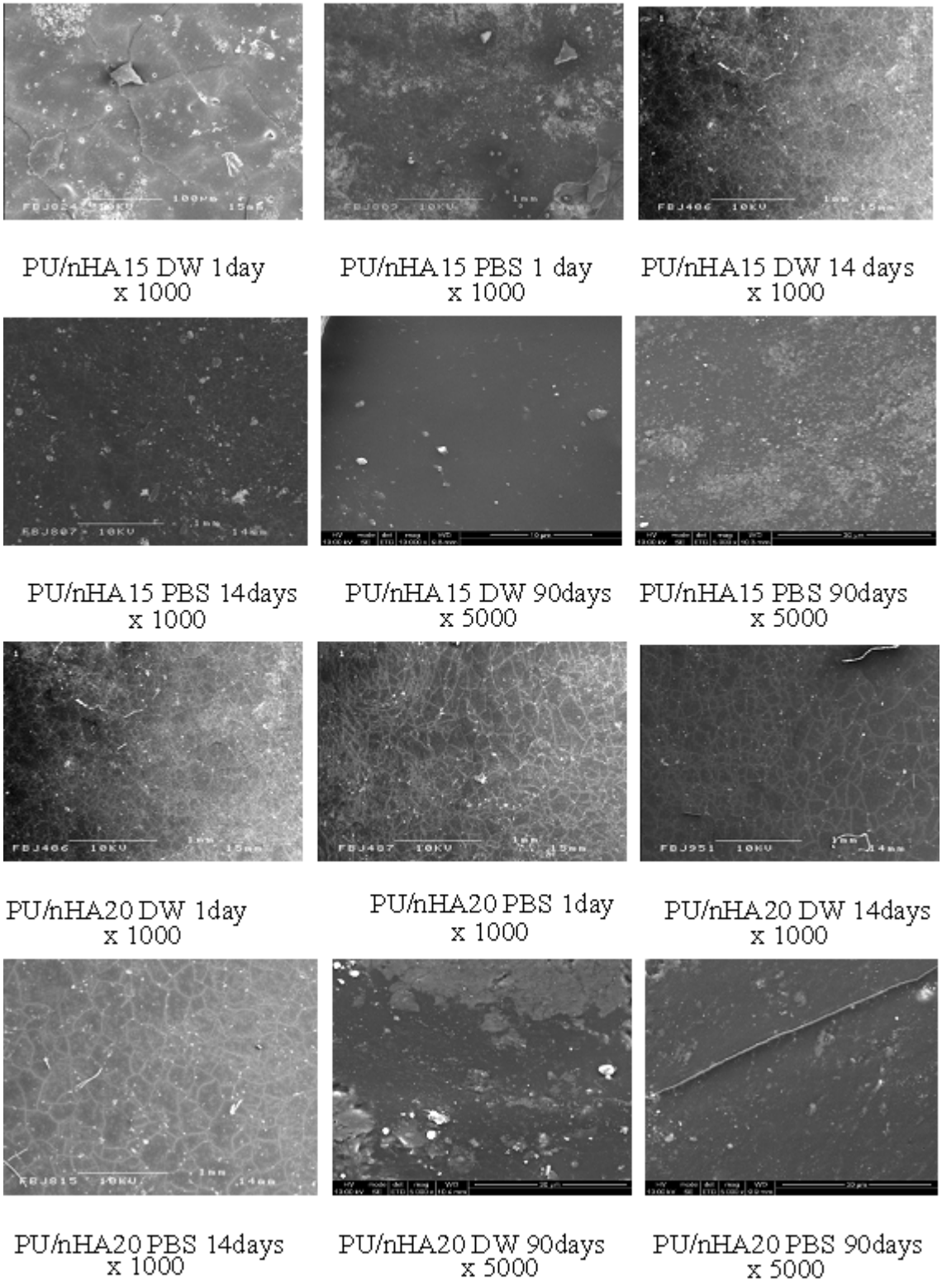

Figure 4.53 SEM images of PU/nHA15 and PU/nHA20 samples treated with deionised water (DW) and PBS at predetermined time intervals

4.3.4.1.7- Conclusion

The hydrophobicity of the samples increased with the increase in the concentration of nHA. FTIR and Raman spectroscopies confirmed the hydrolytic stability of PU/nHA composites. In addition, SEM images provided the result with little degradation on the surface. Hence, the incorporation of nHA in polyurethane increased the resistance to hydrolytic degradation.

4.3.4.2- Bioactivity Analysis

It is well established that HA forms bonelike apatite layer on its surface when treated with SBF (Kim *et al.,* 2005; Chetty *et al.,* 2008). Several methods to improve the bioactivity of the materials have been investigated including incorporation of bioceramic fillers or coating into PU (Ignatius *et al.,* 1997; Causa *et al.,* 2006; Qu *et al.,* 2007). In this study, the *in-vitro* bioactivity results are based on morphological, structural and physical analysis; however, the FTIR (Section 3.8.3.1, Chapter 3) and Raman spectra (Section 3.8.3.2, Chapter 3) of apatite formation for all days and samples are not shown here; remaining figures are in appendix (Appendix 4).

4.3.4.2.1-Scanning Electron Microscopy (SEM)

The SEM images of PU and PU/nHA composite samples after immersion in m-SBF at 1, 7, 14, 21, and 40 days are given in Figure 4.54 - 4.58. It was observed that in PU samples (Figure 4.54) there was no visible apatite formation on the surface of immersed samples up to 14 days. The EDS analysis also confirmed that only C and O peaks were presented, which were expected to be from PU or from carbon coating. However, the 21 and 40 day samples showed apatite formation on the surface. SEM image of 21 days showed an apatite layer which did not cover the entire surface of the specimens. This aggregated apatite consisted of small irregular shaped particles with a size of about 0.5-1 μm. The elemental analysis showed Ca-rich apatite with a molar Ca/P ratio of 2.1. SEM image of 40 day sample showed thicker apatite layer. The apatite layer was dense, continuous and covered almost the whole surface of the specimen. Morphological

studies of the PU/nHA composite surfaces immersed for 40 days in m-SBF presented an apatite (calcium phosphate) layer on the surface of the composites. PU/nHA5 (Figure 4.55), PU/nHA10 (Figure 4.56), PU/nHA15 (Figure 4.57), and PU/nHA20 (Figure 4.58) composite samples showed that the apatite layer was not prominent at 1 day; however, it was observed that with the increase in immersion time the apatite globules packed tightly with each other. Initially the apatite particles were scattered on the surface, but at 14 days' incubation, the sample surface developed a dune-like apatite layer and this structure changed the original morphology of the samples completely. SEM images of 21 days immersion showed the dune-like layer evolved into more smooth hillocks, with a subtle net-like texture consisting of short micro-rods. The layer growing on the surface coating was quite dense and homogeneous. These newly developed calcium phosphate layer showed the same morphology as the amorphous coatings, in addition EDS analysis showed the presence of Na, Mg with Ca and P ions.

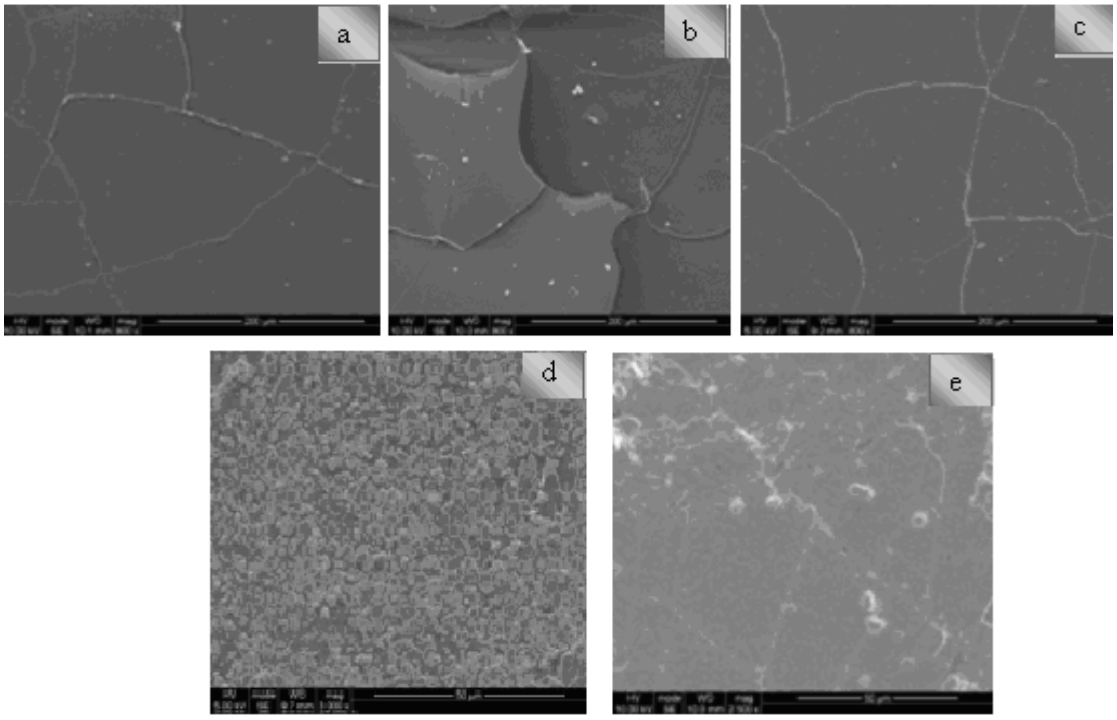

Figure 4.54 SEM images of PU with magnification values at (a) 1 x800, (b) 7 x800, (c) 14 x800, (d) 21 x1500, and (e) 40 days x2000

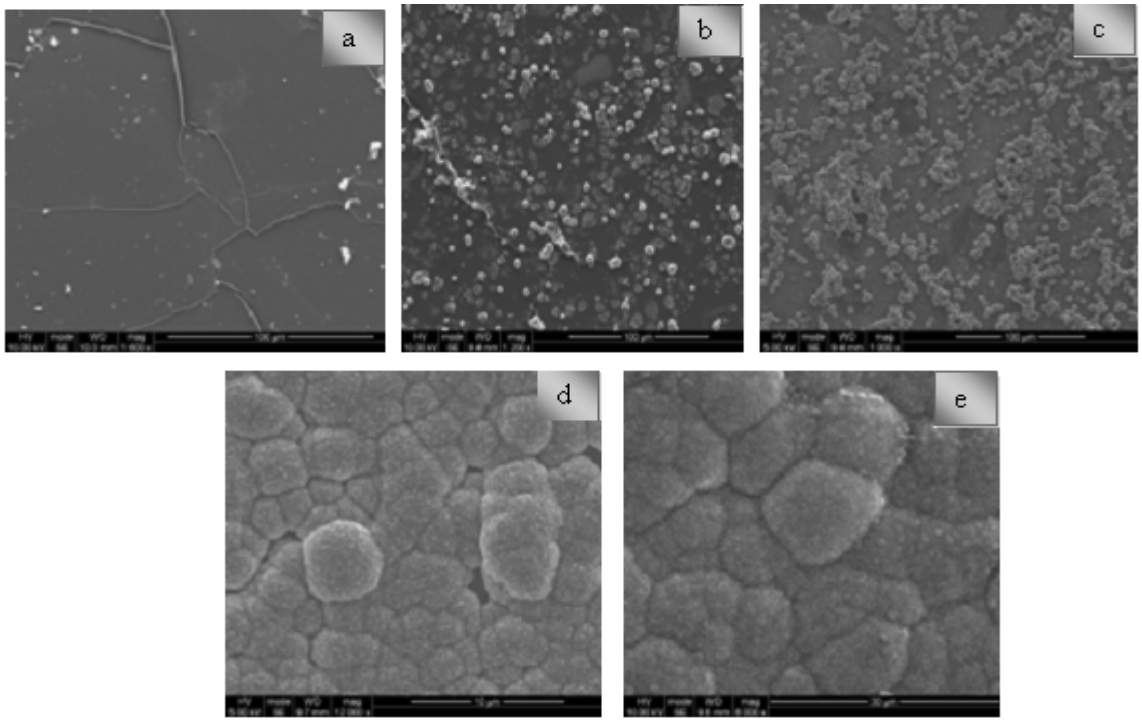

Figure 4.55 SEM images of PU/nHA5 with magnification values at (a) 1 x800, (b) 7 x800, (c) 14 x800, (d) 21 x2000, and (e) 40 days x3000

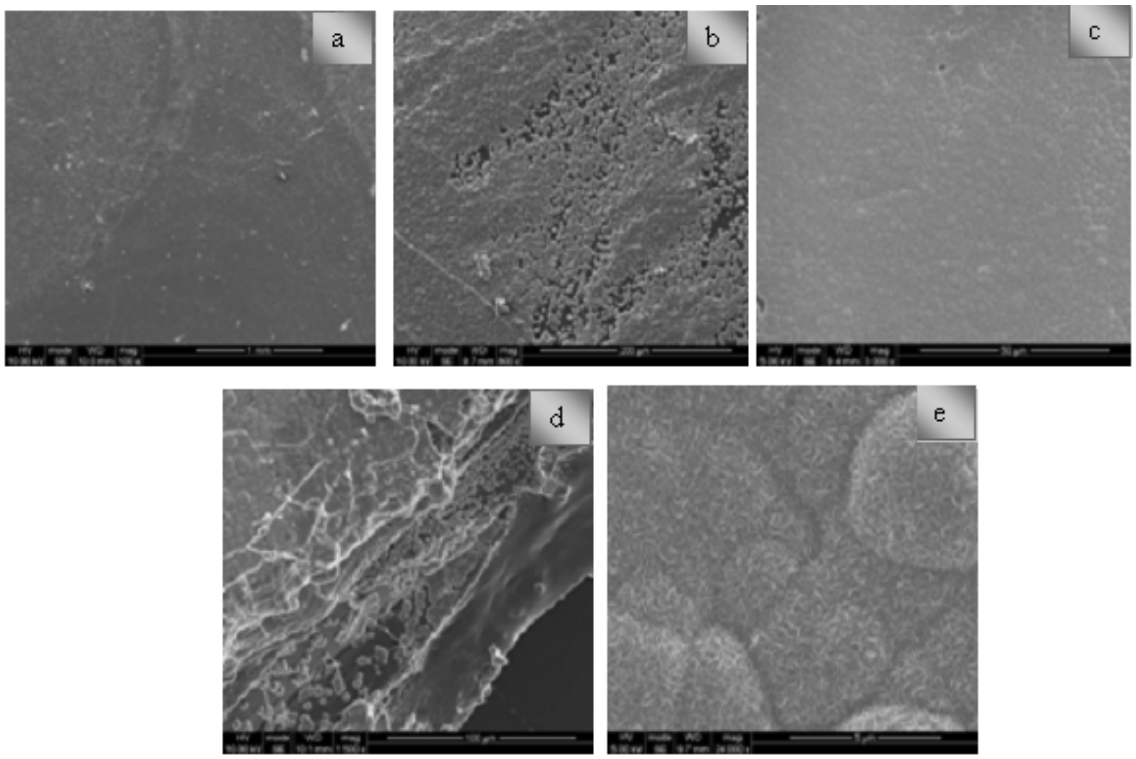

Figure 4.56 SEM images of PU/nHA10 with magnification values at (a) 1 x800, (b) 7 x800, (c) 14 x800, (d) 21 x1500, and (e) 40 days x3000

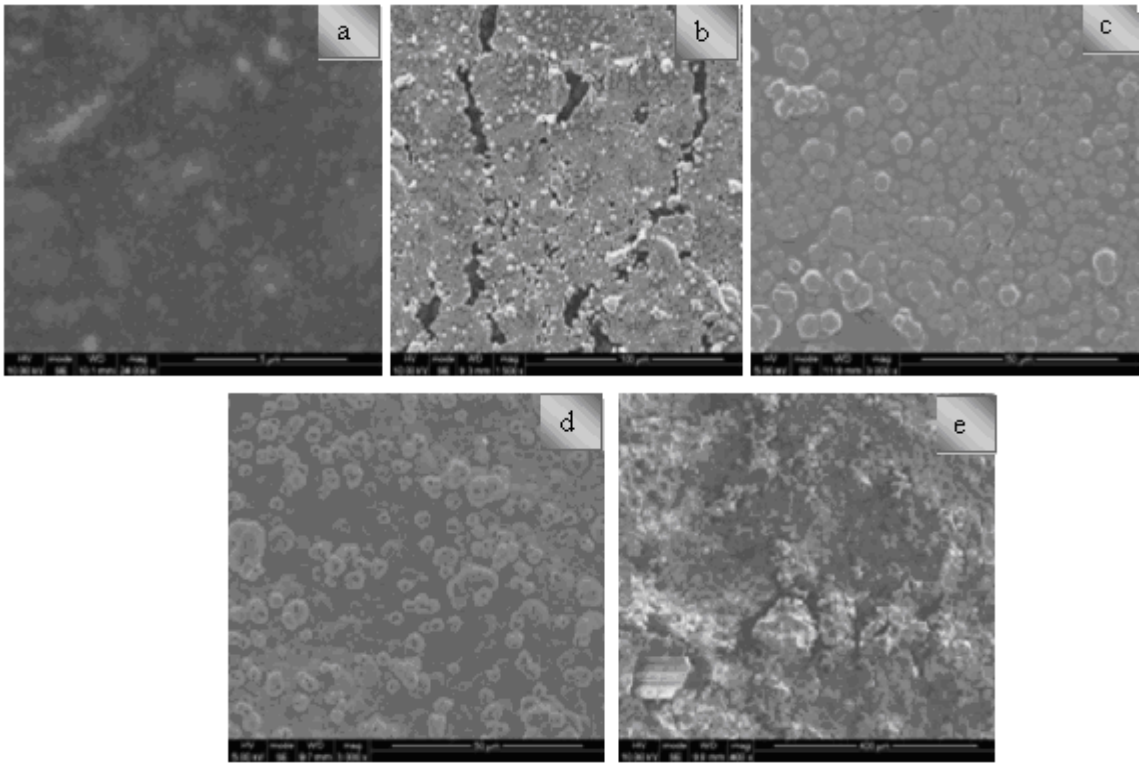

Figure 4.57 SEM images of PU/nHA15 with magnification values at (a) 1 x800, (b) 7 x800, (c) 14 x800, (d) 21 x1500, and (e) 40 days x2000

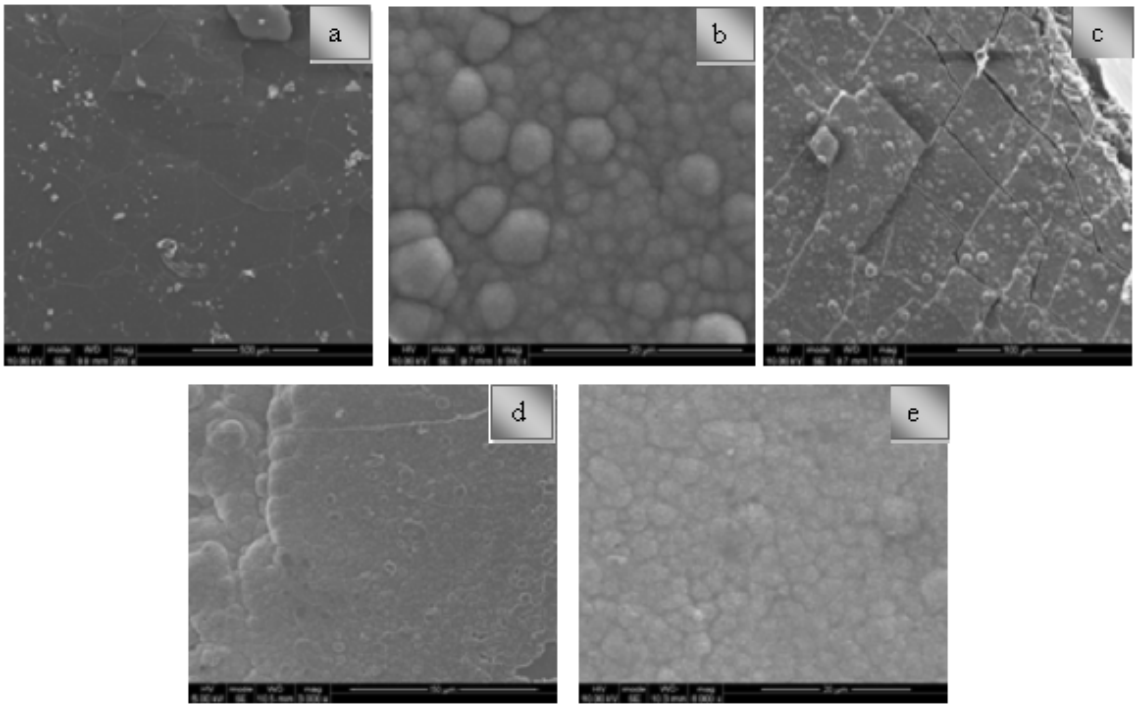

Figure 4.58 SEM images of PU/nHA20 with magnification values at (a) 1 x800, (b) 7 x800, (c) 14 x800, (d) 21 x1500, and (e) 40 days x2000

4.3.4.2.2- Fourier Transform Infrared Spectroscopy (FTIR)

The comparative FTIR spectra of PU at 1, 7, 21, and 40 days immersion are given in Figure 4.59 (a-d). In PU spectra the significant shifting and emerging of new peaks were not observed up to 21 days; however, at 40 days broadness and emergence of peaks were observed at 3320 cm^{-1} (N—H) and 1010 cm^{-1} (C—O—C) respectively. PU/nHA5 composite (Figure 4.60) showed the same pattern that with the increase in immersion time, there was an emergence and shifting of peaks. The shifting of peaks were also observed at 603 and 562 cm^{-1} due to presence of bending peaks of phosphate. However, PU/nHA10 (Figure 4.61) showed that with the increase in concentration of nHA in PU the emergence of peaks became more significant. The shoulder peaks appeared at 1030 and 532 cm^{-1}. These peaks showed the presence of apatite on the surface and attributed to stretch and bending peaks of phosphate (Rehman and Bonfield, 1997). PU/nHA15 and PU/nHA20 composites (Figure 4.62-4.63) spectra showed different pattern and changes appeared at 7 days spectrum. The presence of apatite layer changed the characteristic pattern of peaks at 1400-1200 cm^{-1}, 1100-900 cm^{-1} and 600-500 cm^{-1} suggested the apatite layer presented on the surface of samples and changed the structural properties of the material.

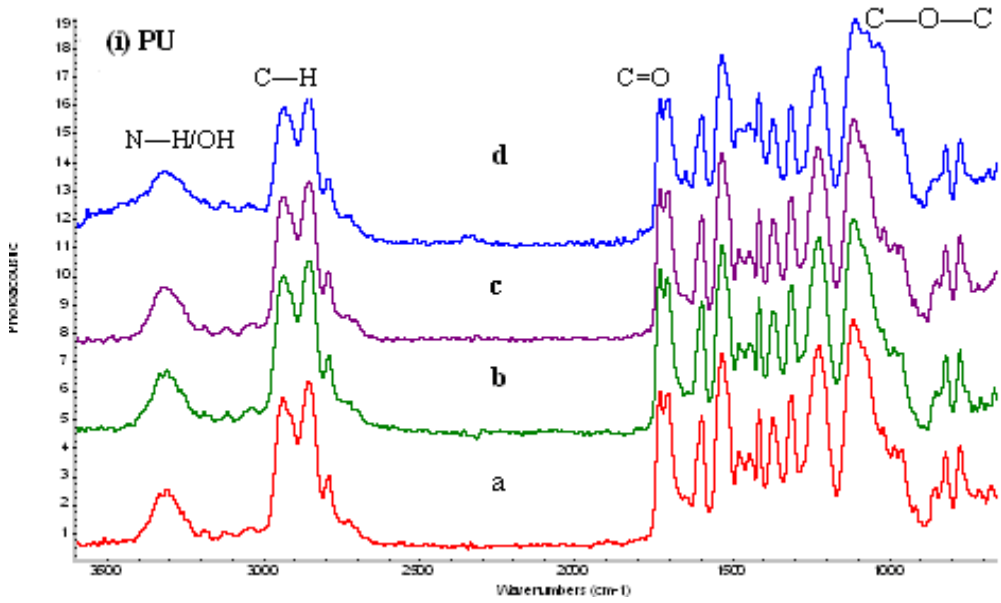

Figure 4.59 FTIR spectrum of PU after immersion in m-SBF at (a) 1, (b) 7, (c) 21, (d) 40 days

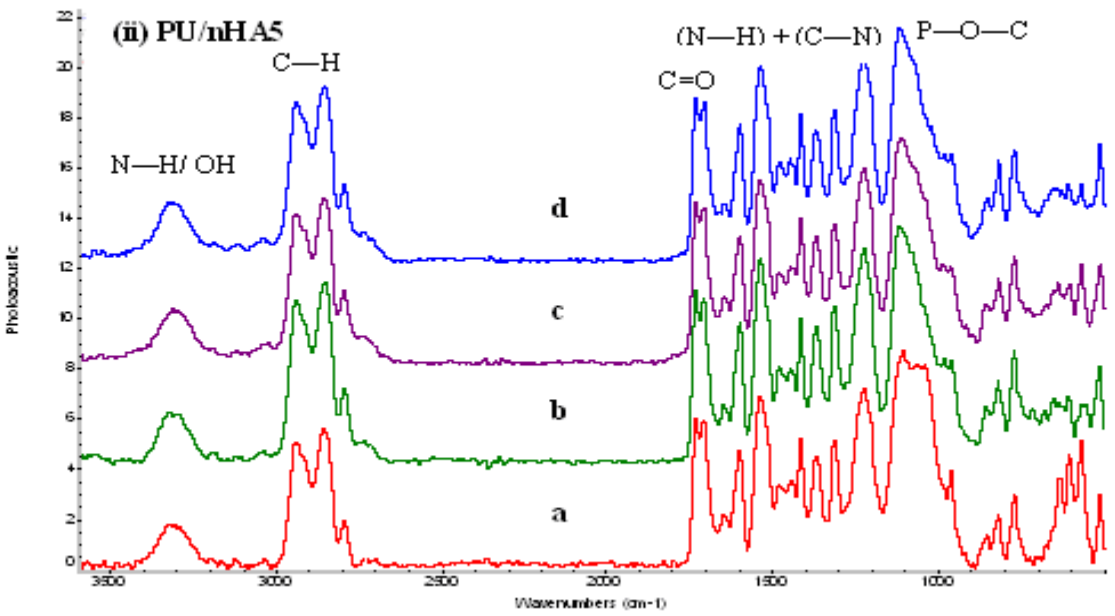

Figure 4.60 FTIR spectrum of PU/nHA5 after immersion in m-SBF at (a) 1, (b) 7, (c) 21, (d) 40 days

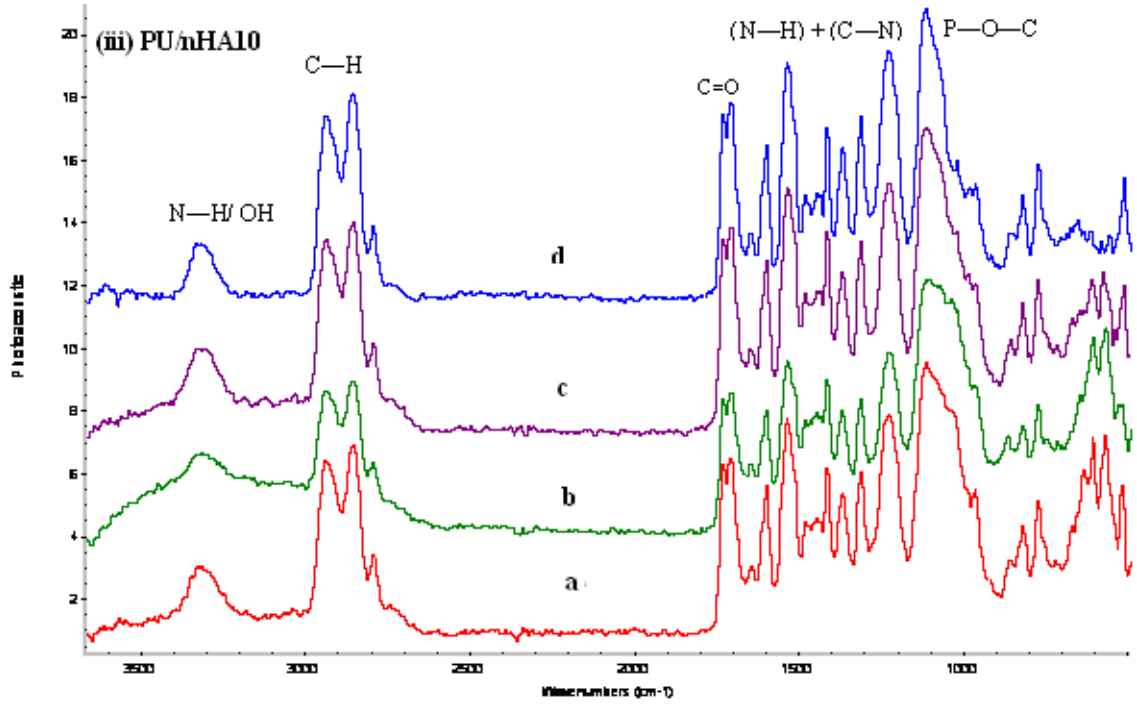

Figure 4.61 FTIR spectrum of PU/nHA10 after immersion in m-SBF at (a) 1, (b) 7, (c) 21, (d) 40 days

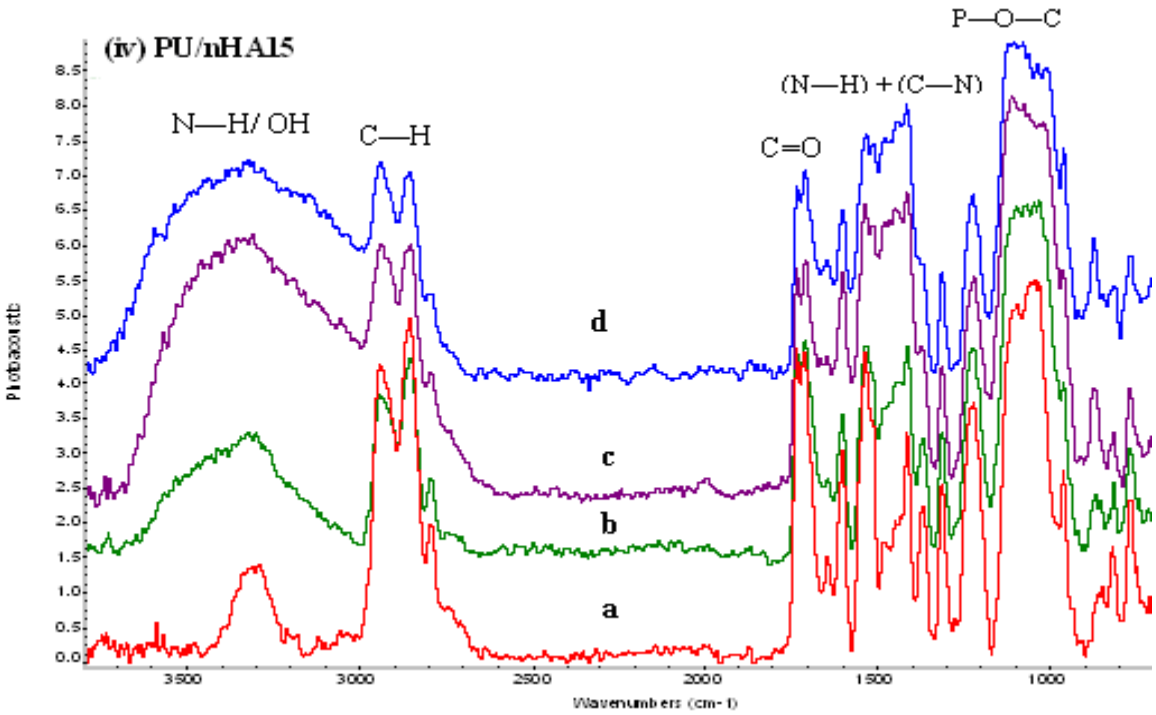

Figure 4.62 FTIR spectrum of PU/nHA15 after immersion in m-SBF at (a) 1, (b) 7, (c) 21, (d) 40 days

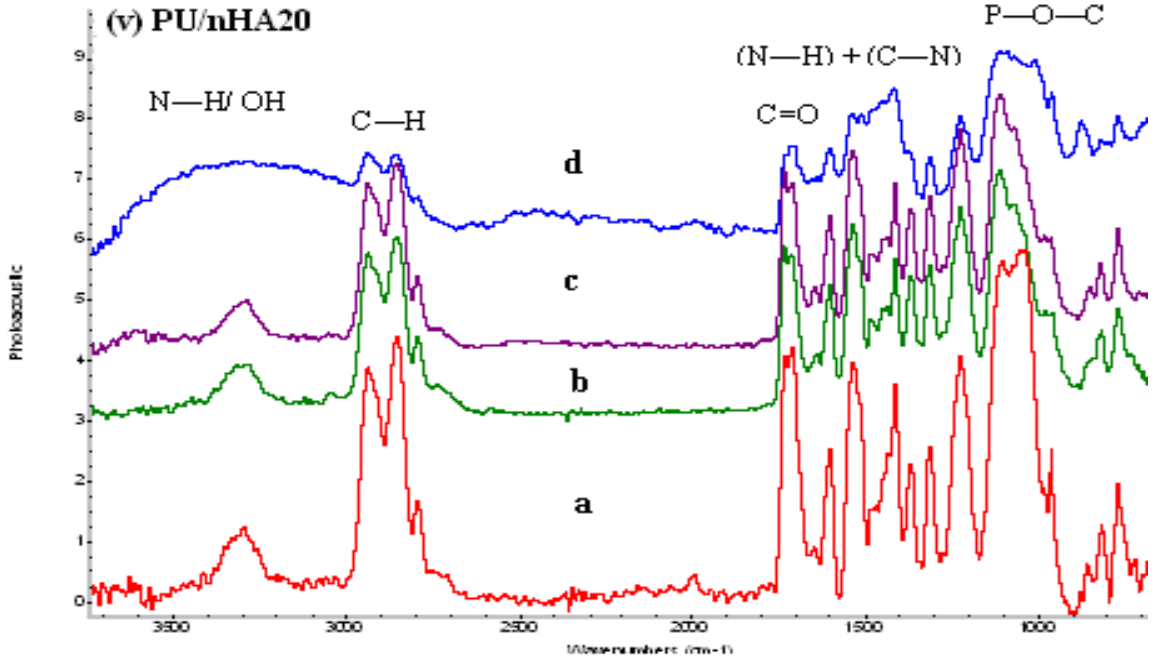

Figure 4.63 FTIR spectrum of PU/nHA20 after immersion in m-SBF at (a) 1, (b) 7, (c) 21, (d) 40 days

4.3.4.2.3- Raman Spectroscopy

The comparative Raman spectra of PU (Figure 4.64) and PU/nHA composites (Figure 4.65-4.68) presented the precise picture and the characteristic peaks after immersion. In PU samples the samples at 1 and 7 days showed almost the same pattern, whereas, at 21 days slight emergence of shoulders were observed at 960 cm^{-1} which was attributed the presence of v_1 phosphate on the surface of sample. Whereas, Raman spectrum of 40 days showed that the peak at 960 cm^{-1} became prominent and a new peak emerged at 1000 cm^{-1} attributed to v_3 of phosphate (Koutsopoulos, 2002). The peak at 1500 cm^{-1} attributed to carbonate was also appeared at 21 days and became more significant at 40 days. Raman spectra of PU/nHA composites presented the changes in the characteristic peaks with time. The intensity of peak at 960 cm^{-1} increased with the increase in time and it was attributed to phosphate. The spectrum of 40 days showed the significant changes not only in phosphate region (960 cm^{-1}) but also in amide region (1500-1200 cm^{-1}). The presence of carbonate in the apatite layer changed the structure of the spectrum and shifting of peaks and emergence of shoulders confirmed that the apatite layer formed on the surface of samples. The spectrum of PU/nHA15 and PU/nHA20 showed significant change and the peak at 960 cm^{-1} appeared with high intensity. The 40 day spectrum of PU/nHA20 presented the high intense peak of phosphate and the shifting of adjacent amide and ether peaks.

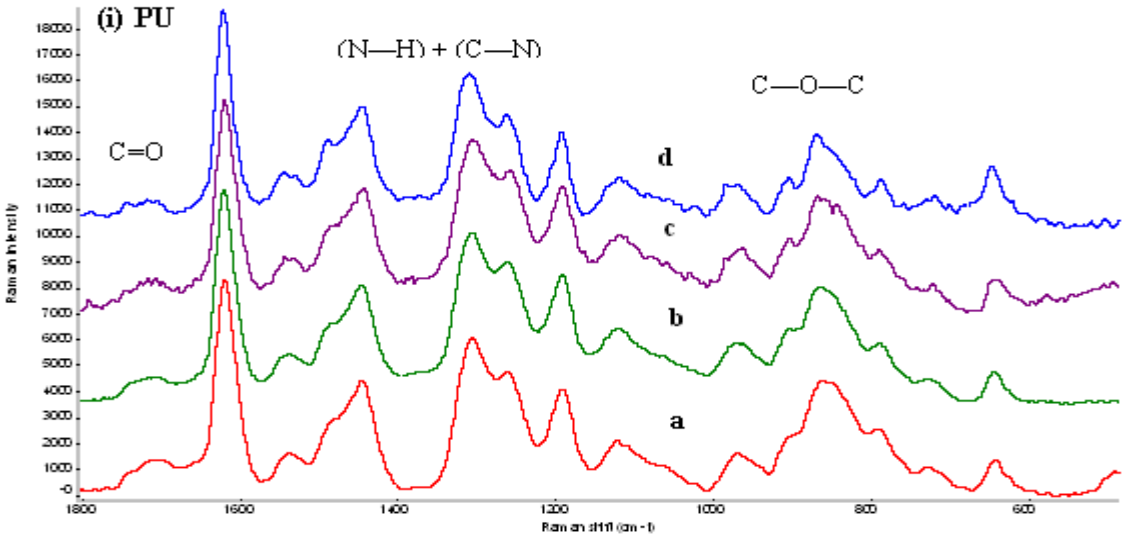

Figure 4.64 Raman spectrum of PU after immersion in m-SBF at (a) 1, (b) 7, (c) 21, (d) 40 days

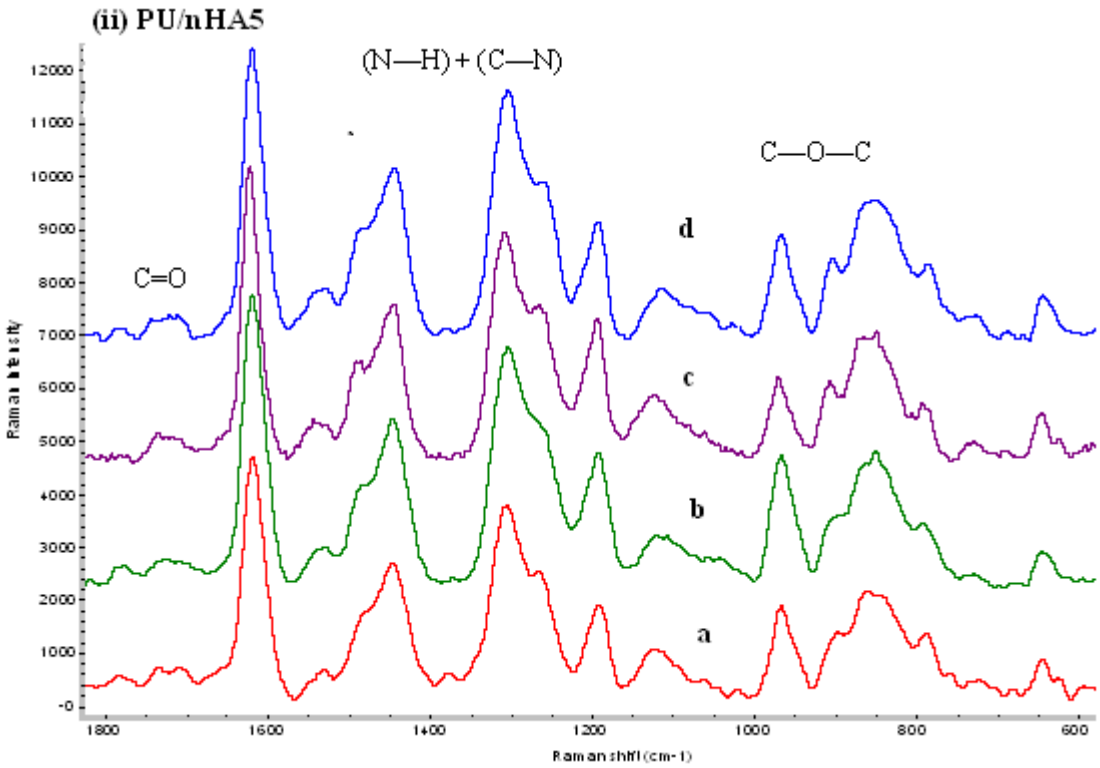

Figure 4.65 Raman spectrum of PU/nHA5 after immersion in m-SBF at (a) 1, (b) 7, (c) 21, (d) 40 days

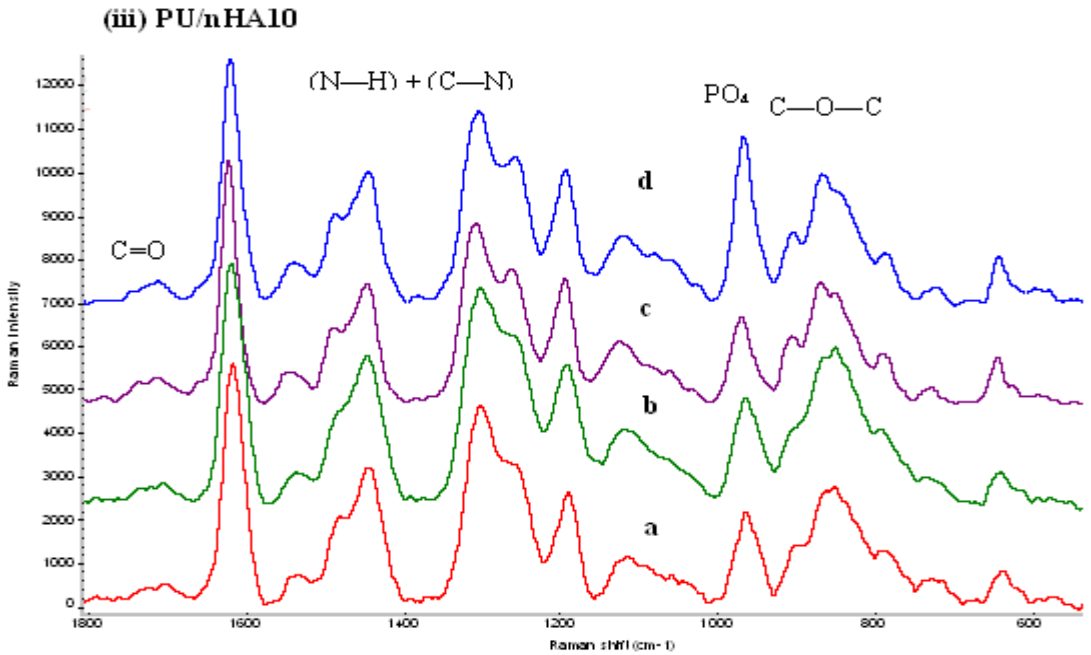

Figure 4.66 Raman spectrum of PU/nHA10 after immersion in m-SBF at (a) 1, (b) 7, (c) 21, (d) 40 days

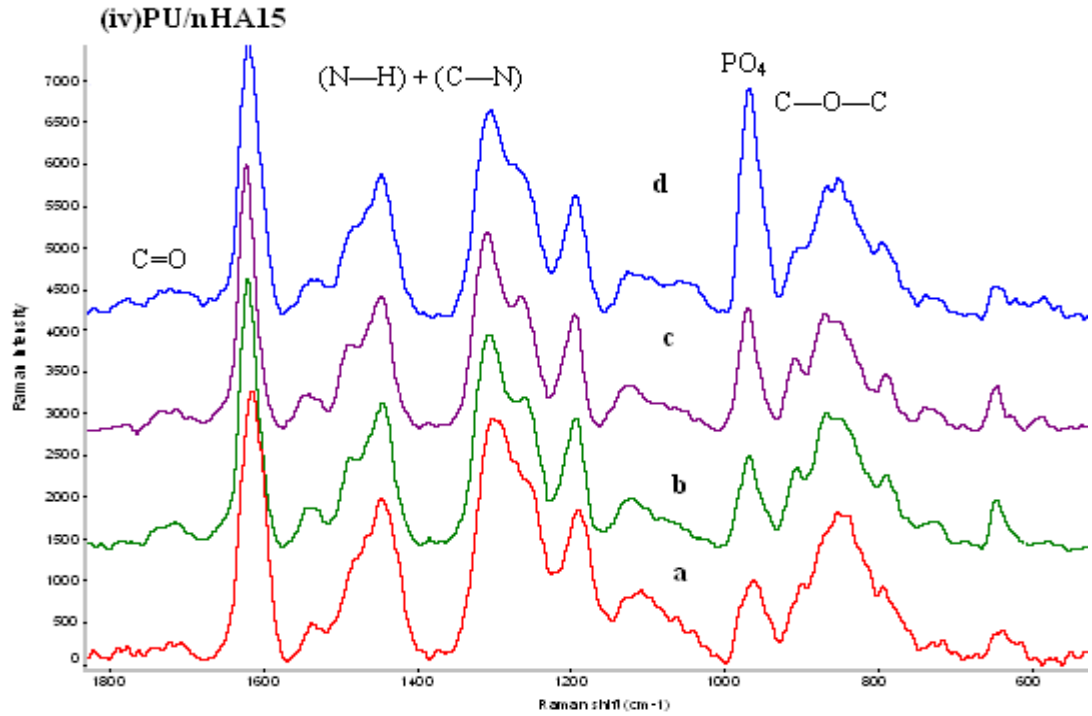

Figure 4.67 Raman spectrum of PU/nHA15 after immersion in m-SBF at (a) 1, (b) 7, (c) 21, (d) 40 days

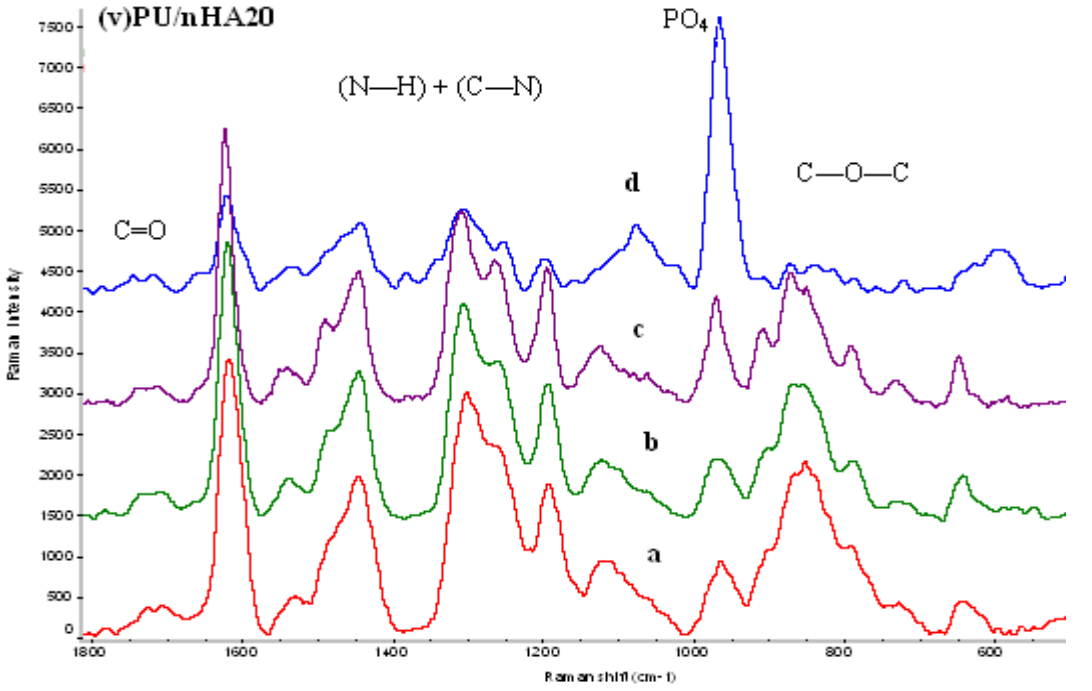

Figure 4.68 Raman spectrum of PU/nHA20 after immersion in m-SBF at (a) 1, (b) 7, (c) 21, (d) 40 days

4.3.4.2.4- X-ray Diffraction (XRD)

The XRD pattern of the PU is given in Figure 4.69. The comparative XRD pattern of 1 and 40 days showed a broad band at 10-25º and a sharp peak at 29º. It was observed that XRD pattern of PU did not show presence of any band assigned to apatite. The comparative XRD patterns of the PU/nHA5 – PU/nHA20 are given in Figure 4.70 - 4.73. In all cases, a broadening and intensity decreased with the immersion time; however, the higher concentration of nHA showed variation in the sharpness of the peaks at 40 days. The XRD patterns showed the diffraction peaks (210, 112, and 300) that confirmed the presence of apatite on the surface of samples. It was observed that samples with higher concentration of nHA showed more apatite peaks at 39.89º (310) and 47º (222). However, it was difficult to estimate the exact presence of apatite or phase composition of the calcium phosphates from this technique.

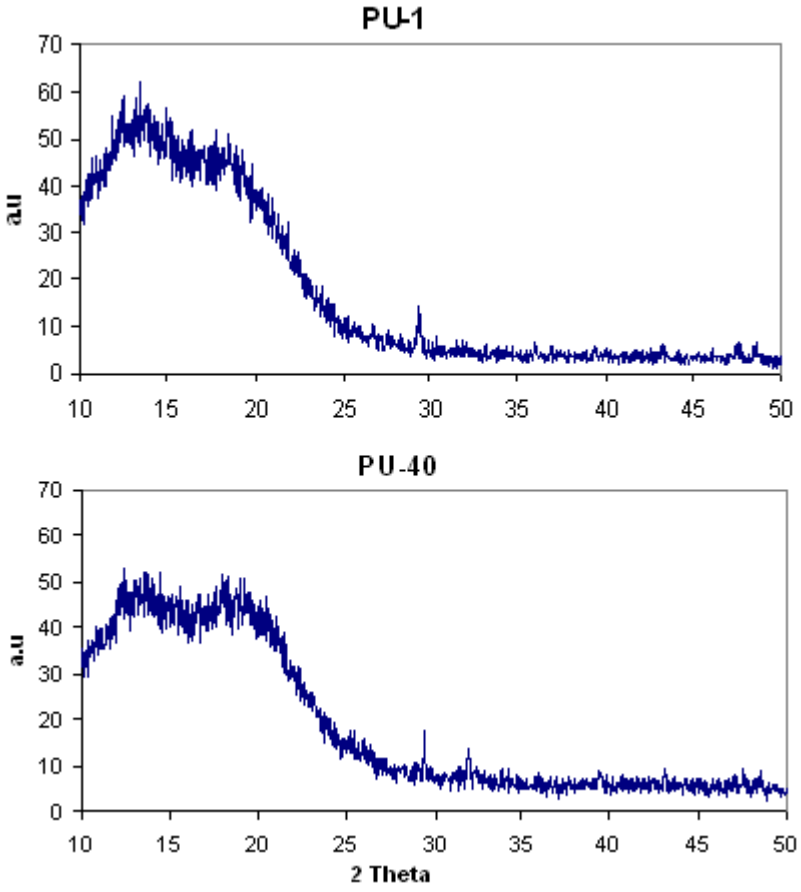

Figure 4.69 Comparative XRD pattern of PU at 1 and 40 days

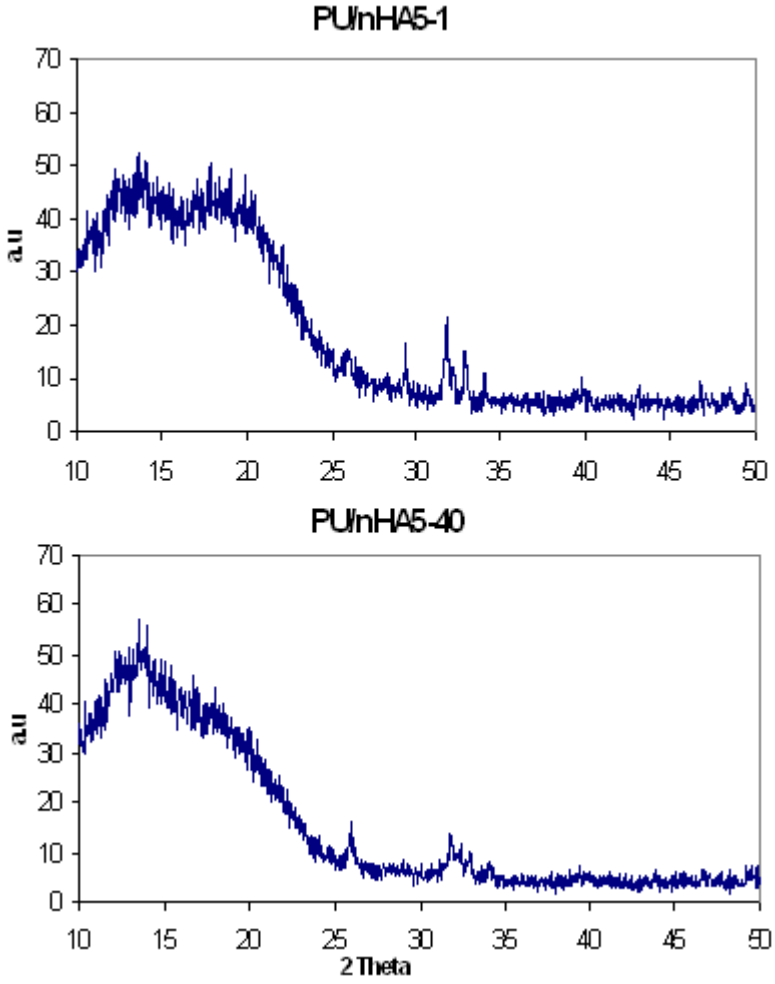

Figure 4.70 Comparative XRD pattern of PU/nHA5 at 1 and 40 days

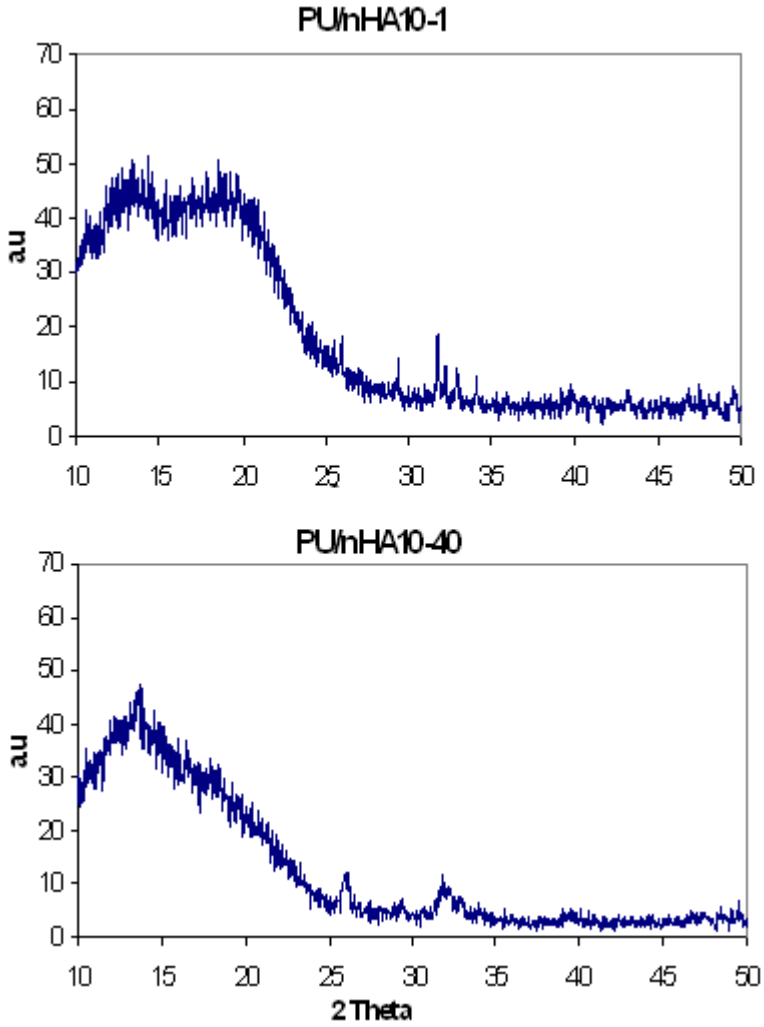

Figure 4.71 Comparative XRD pattern of PU/nHA10 at 1 and 40 days

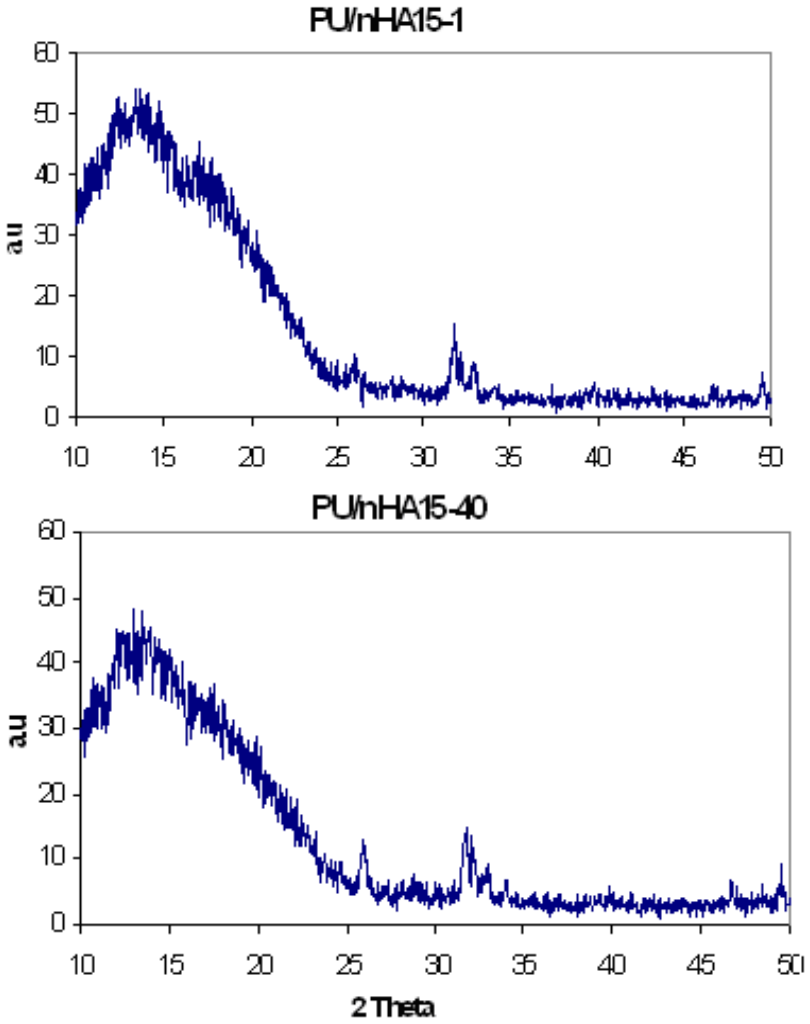

Figure 4.72 Comparative XRD pattern of PU/nHA15 at 1 and 40 days

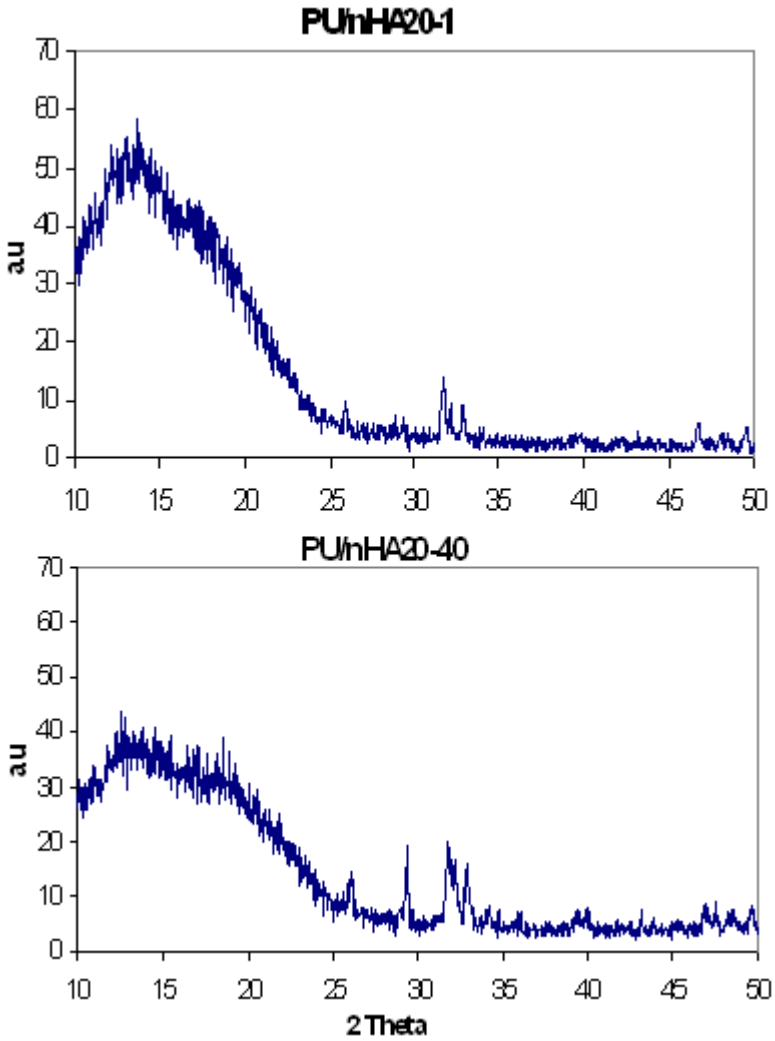

Figure 4.73 Comparative XRD pattern of PU/nHA20 at 1 and 40 days

4.3.4.3- Bioadhesion Analysis

The adequate adhesion at interface is crucial to the success of restorative materials to reinforce tooth structure and provide a marginal seal that prevents leakage (Guzman-Ruiz *et al.,* 2001). Poor marginal adaptation and subsequent loss of retention of restoration are frequent clinical findings throughout the dentine bonded interface that occurs rapidly (Breschi *et al.,* 2008).

The current *in-vitro* bioadhesion study provides the results obtained using push-out test (Section 3.8.6.3.3, Chapter 3) and the surface analysis was done using SEM with EDS (Section 3.8.6.3.4, Chapter 3).

4.3.4.3.1- Push-Out Test

The mean push-out bond strength values for both groups i.e. deionised water and artificial saliva are given in Figure 4.74. The each value with standard deviations of the samples immersed in deionised water and artificial saliva are tabulated in Table 4.21 and 4.22 respectively. The following features were observed:

1. The bond strength for GC Fuji IX and Filtek Supreme was remained constant and the difference was not significant ($p = 0.52$) with immersion time
2. The bond strength for PU/nHA composites showed little increase from 7 to 21 days but there was an observable increase in 40 and 90 days. Comparing the values between 7 and 90 days, all samples showed significant increase ($p \leq 0.05$) for all concentrations of nHA in both media
3. There was a trend for higher concentration of nano-hydroxyapatite to have higher bond strength e.g. in deionised water the bond strength for PU/nHA10 (0.72 ± 0.15 MPa) was lower than that for PU/nHA20 (0.8 ± 0.25 MPa), however the difference was not significant ($p = 0.46$), whereas, in artificial saliva PU/nHA10 (0.80 ± 0.15 MPa) was slightly lower than PU/nHA20 (0.89 ± 0.22 MPa) with no significant difference ($p = 0.49$)

Table 4.21 Push-out bond strength values (MPa) and standard deviations for deionised water where n = 5

Samples	Day 7	Day 21	Day 40	Day 90
GC Fuji IX	7.0 ± 2.1	7.1±1.6	6.8 ± 2.0	6.6 ±1.7
Filtek Supreme	28.0 ± 1.9	28.0 ± 2.4	28.3 ± 1.7	28.7 ±2.2
PU/nHA10	0.45 ± 0.09	0.49 ± 0.09	0.56 ± 0.11	0.72 ± 0.15
PU/nHA15	0.47 ± 0.11	0.49 ± 0.16	0.56 ± 0.18	0.76 ± 0.14
PU/nHA20	0.48 ± 0.15	0.51 ± 0.18	0.59 ± 0.2	0.8 ± 0.25

Table 4.22 Push-out bond strength values (MPa) and standard deviations for artificial saliva where n = 5

Samples	Day 7	Day 21	Day 40	Day 90
GC Fuji IX	7.2 ± 1.6	7.4 ± 1.4	6.9 ± 1.3	6.8±1.8
Filtek Supreme	28.1 ± 2.4	28.2 ± 2.8	29.4 ± 2.2	29.6 ± 3.2`
PU/nHA10	0.46 ± 0.085	0.51 ± 0.095	0.66 ± 0.1	0.8 ± 0.15
PU/nHA15	0.48 ± 0.11	0.52 ± 0. 16	0.69 ± 0.18	0.86 ± 0.14
PU/nHA20	0.49 ± 0.12	0.54 ± 0.15	0.77 ± 0.18	0.89 ± 0.22

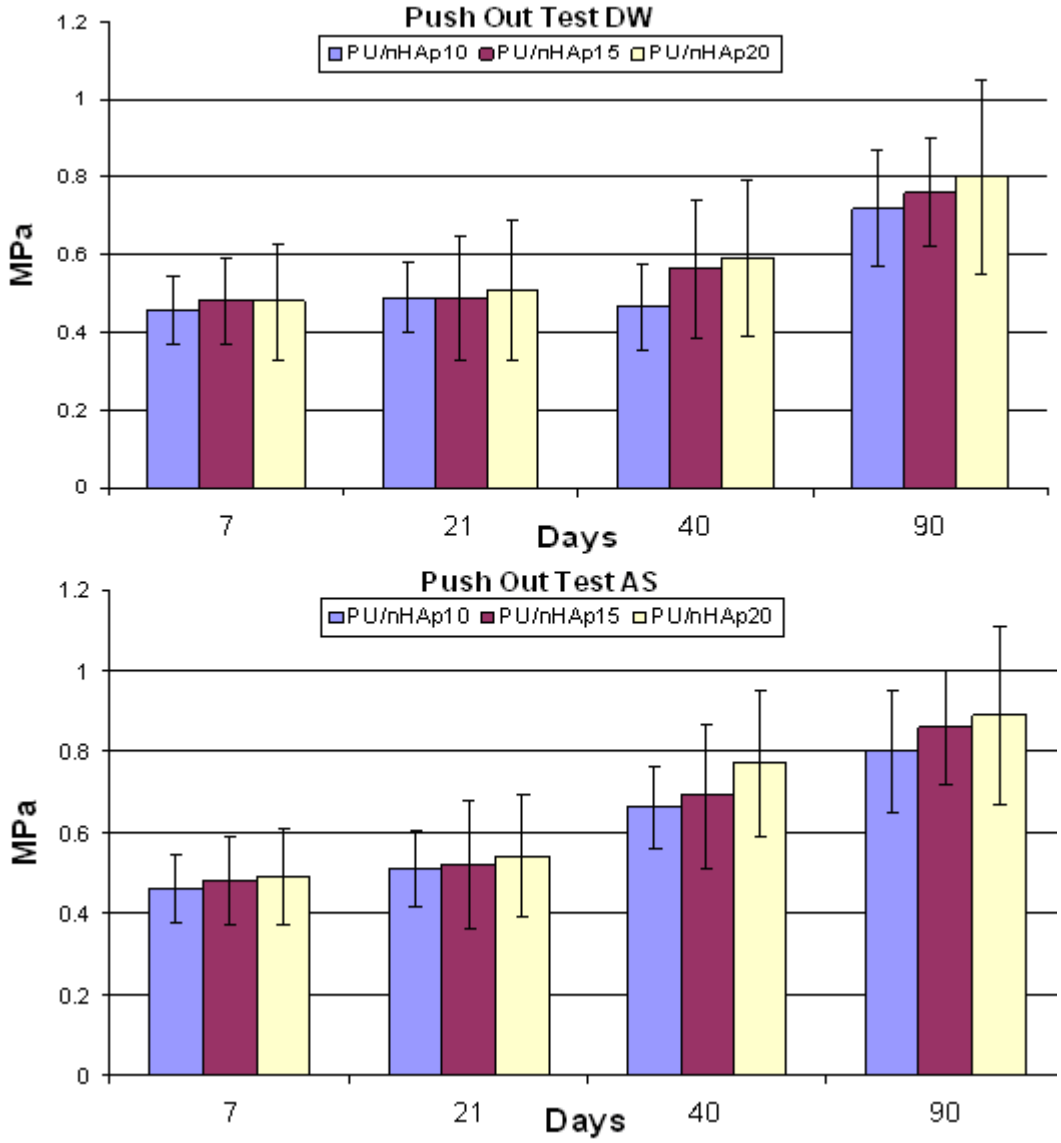

Figure 4.74 Push-out test of the samples immersed in deionised water (DW) and artificial saliva (AS)

4.3.4.3.2- Scanning Electron Microscopy (SEM) / EDS

SEM images of GC Fuji IX after 40 and 90 days' immersion in deionised water and artificial saliva are shown in Figure 4.75 (a & b) respectively. It was observed that with the increase in immersion time the adhesion of the material to tooth structure increased. The EDS analysis showed the presence of Ca and P peaks at 90 day sample in artificial saliva.

The adhesion pattern for Filtek Supreme is presented in Figure 4.76 and it was observed that there was a very minimal attachment of the composite to tooth structure in both media at 90 days. However, the tooth structure was slightly ruptured from the surface suggesting the micro-mechanical attachment of the composite to the tooth. The morphological image of PU and dentine at 40 days immersion in deionised water and artificial saliva is given in Figure 4.77. The PU samples immersed in deionised water did not show adherence to the tooth structure, whereas, a little adherence was observed with the samples immersed in artificial saliva. SEM image of 90 days' immersion showed more adherence as compare to 40 day samples.

SEM images of PU/nHA composite adhesion to tooth structure are given in Figure 4.78 – 4.80. It was observed that with the increase in concentration of nHA in PU there was more adherences. In addition to SEM, EDS analysis confirmed the presence of Ca and P on the surface layer of composite materials indicating the formation of apatite layer on the surface of composite. The cross section of PU/nHA20 and its attachment with dentine is given in Figure 4.85.

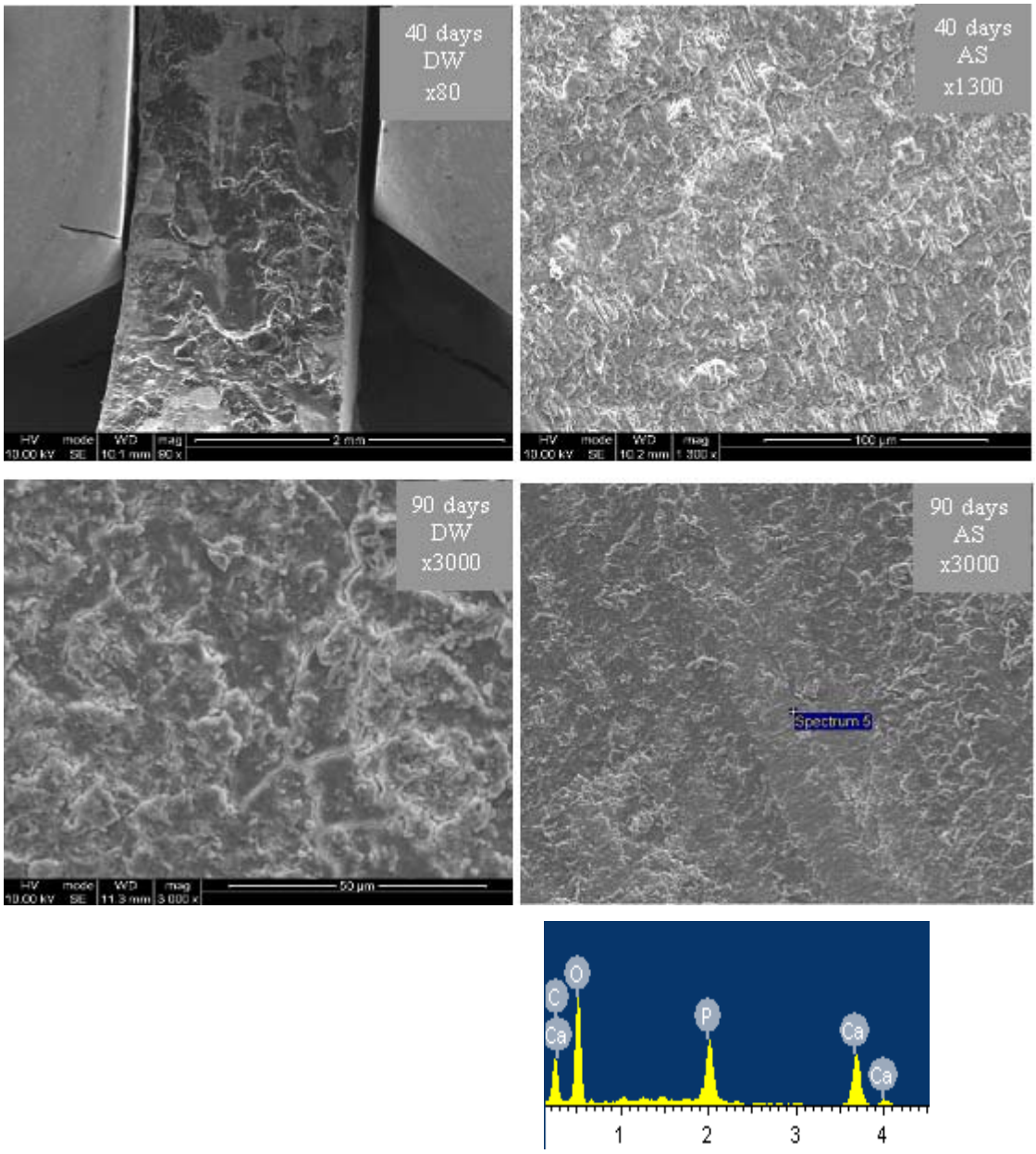

Figure 4.75 SEM image with EDS analysis of GC Fuji IX adhesion with dentine with magnification values at 40 and 90 days in deionised water and artificial saliva

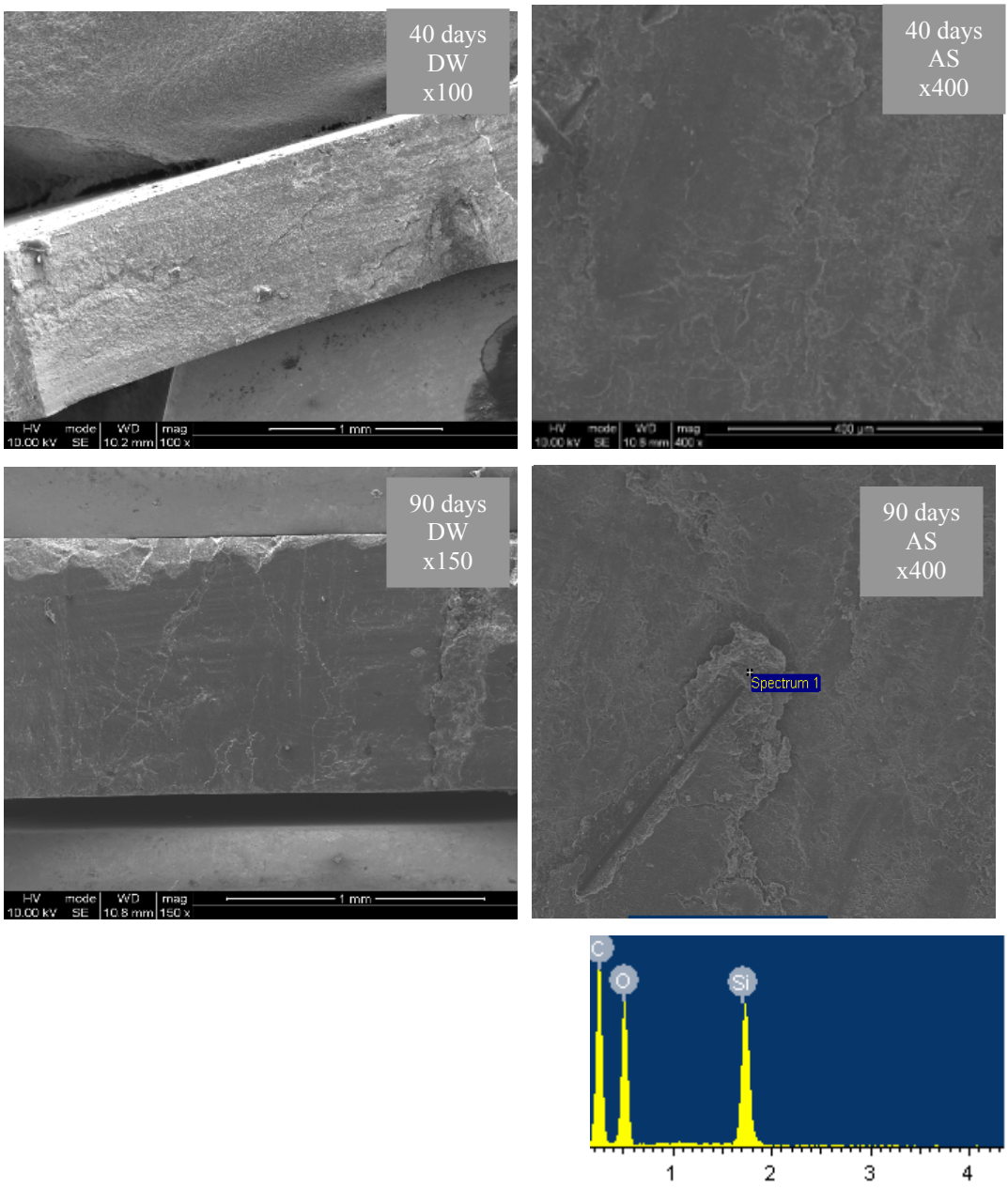

Figure 4.76 SEM image with EDS analysis of Filtek Supreme adhesion with dentine with magnification values at 40 and 90 days in deionised water (DW) and artificial saliva (AS)

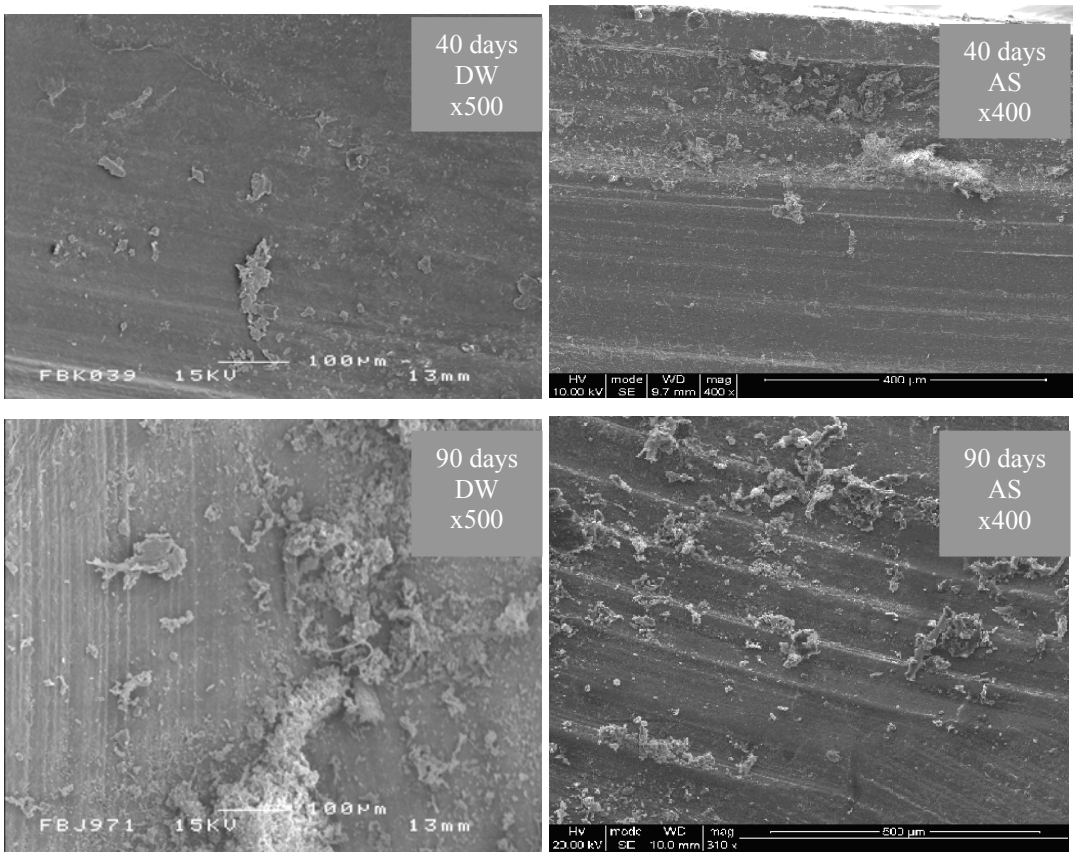

Figure 4.77 SEM images of PU adhesion with dentine with magnification values at 40 and 90 days in media: deionised water (DW) and artificial saliva (AS)

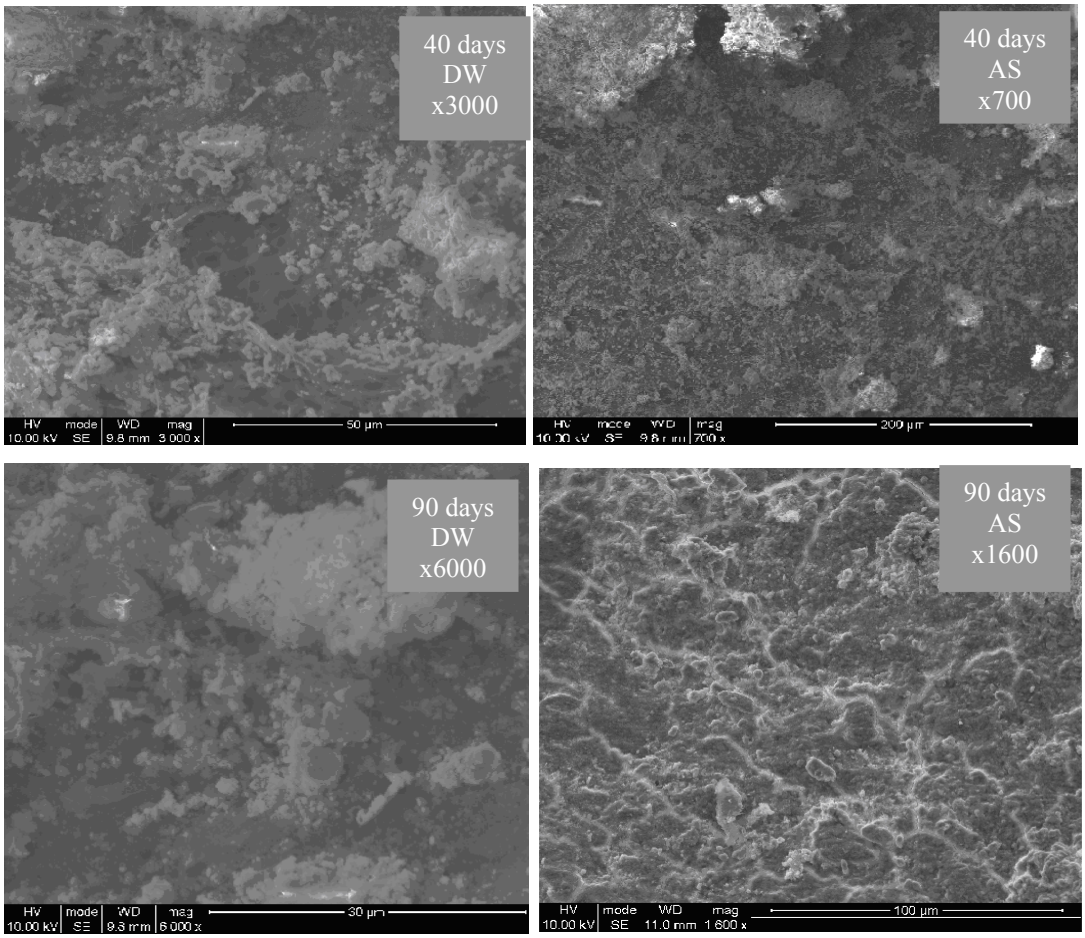

Figure 4.78 SEM images of PU/nHA10 adhesion with dentine with magnification values at 40 and 90 days in media: deionised water (DW) and artificial saliva (AS)

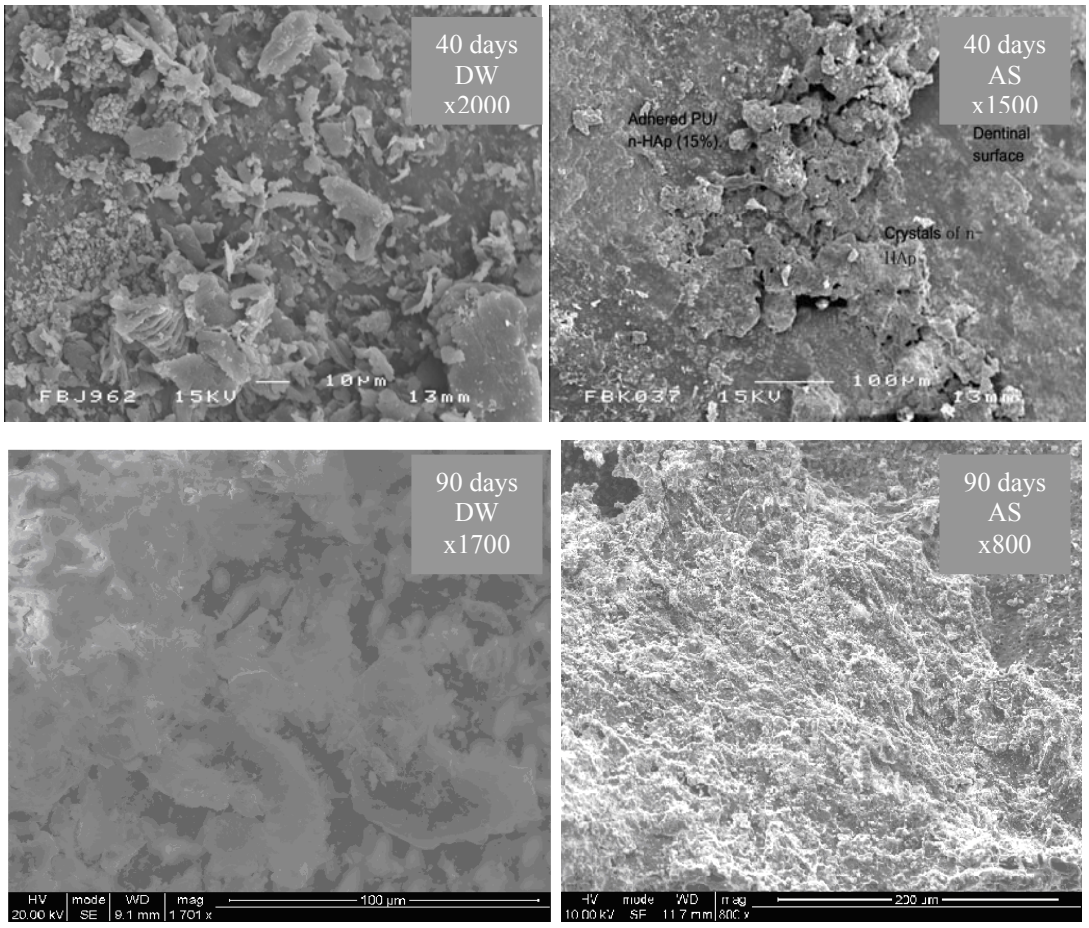

Figure 4.79 SEM images of PU/nHA15 adhesion with dentine with magnification values at 40 and 90 days in media: deionised water (DW) and artificial saliva (AS)

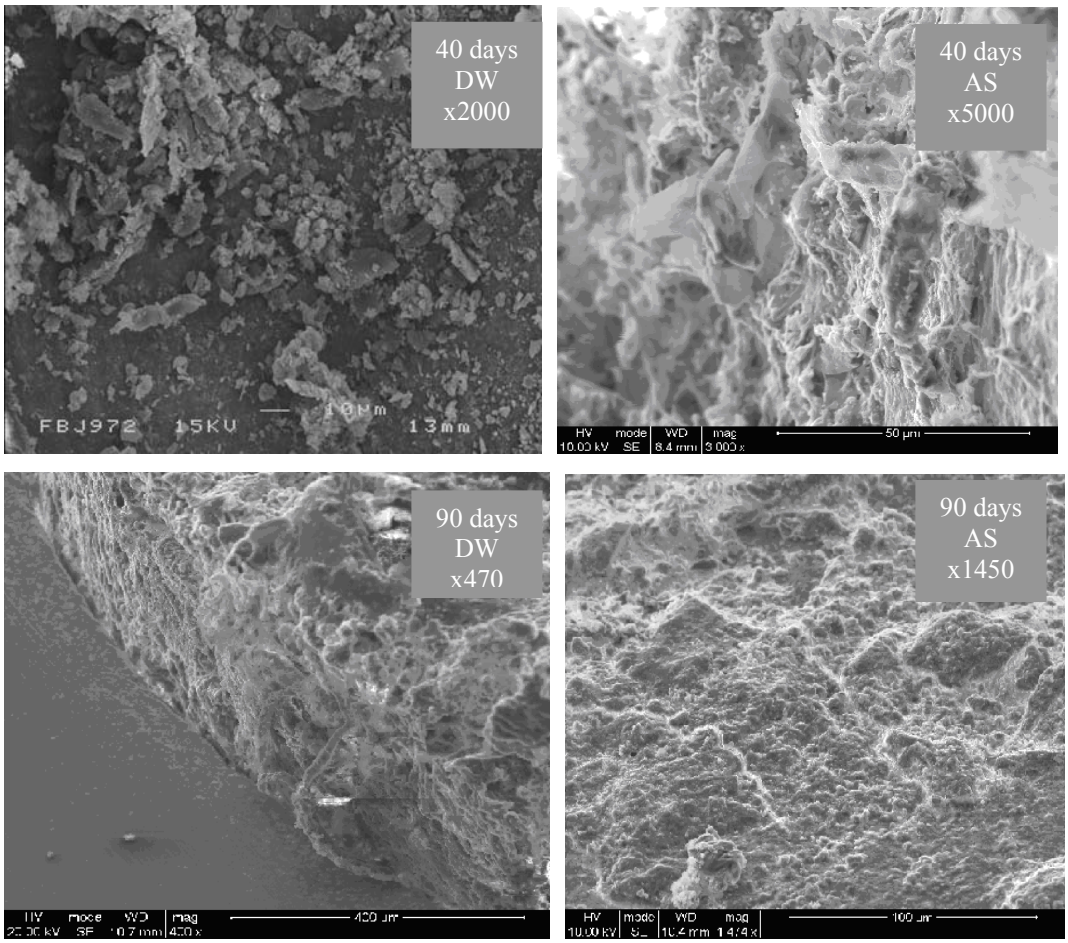

Figure 4.80 SEM images of PU/nHA20 adhesion with dentine with magnification values at 40 and 90 days in media: deionised water (DW) and artificial saliva (AS)

4.3.4.4- Biocompatibility

4.3.4.4.1- Cell Culturing

In-vitro studies showed that both materials i.e. PU and PU/nHA20 were non-cytotoxic to osteoblast-like cells in culture. Figure 4.81 presents cell attachment and proliferation and values are tabulated in Table 4.23. The experimental materials showed continuous proliferation of the cells and the viable cells presented in the culture medium increased with time of incubation and higher for the PU than PU/nHA20, whereas, control group (plastic plate) showed continuous growth up to 5 days and then the values decreased.

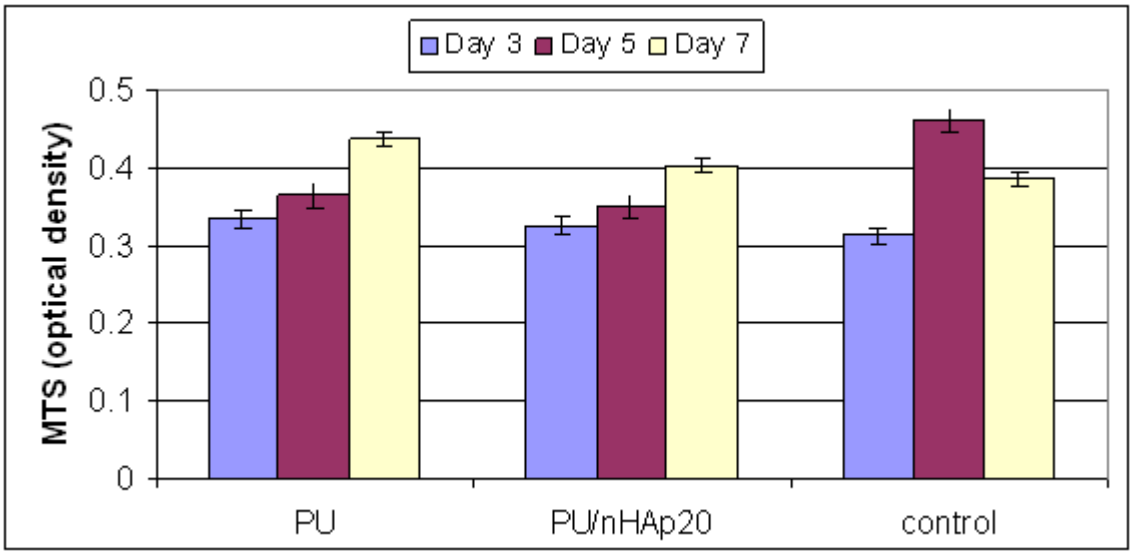

Figure 4.81 Cell culturing values of PU, PU/nHA20 and control group

Table 4.23 Cell culturing values for experimental materials and control group

Days	PU	PU/nHA20	Control
Day 3	0.33 ±0.01	0.32 ±0.01	0.31 ±0.00
Day 5	0.36 ±0.01	0.3 ±0.01	0.45 ±0.03
Day 7	0.43 ±0.01	0.40 ±0.01	0.38 ±0.02

4.3.4.4.2- Bacterial Adhesion

In this preliminary study the adhesion of the *Streptococcus sanguinis* (*S. sanguinis*) is given in Figure 4.82. It was observed that more bacteria were adherent to PU than PU/nHA20 composite. The values for PU and PU/nHA20 composite were 33.90 ±16.15 and 0.99 ±0.83 cfu/disc respectively.

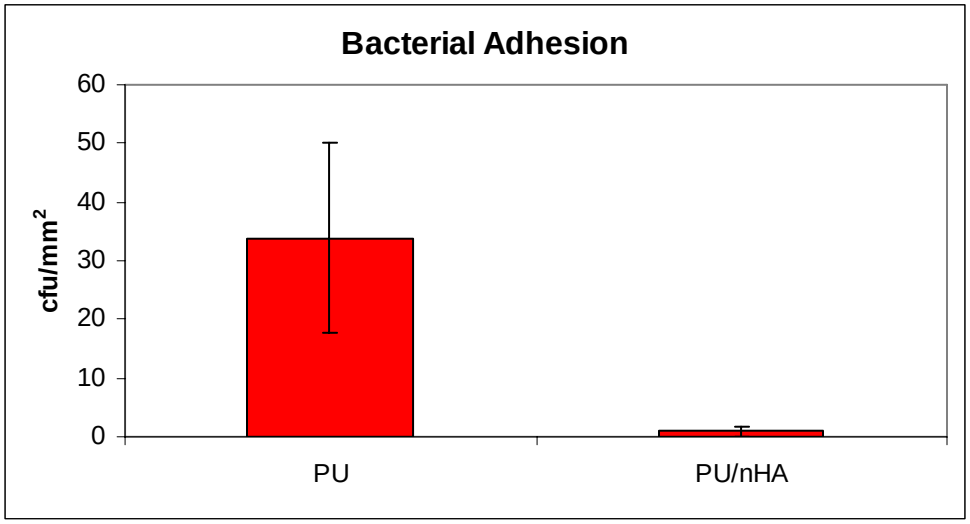

Figure 4.82 Bacterial adhesion values for PU and PU/nHA20

4.4- Synthesis of Electrospun Nano-fibres

SEM images of electrospun mats of PU, physically mixed PU/nHA and chemically mixed PU/nHA is given in Figure 4.83 – 4.86. Unlike conventional fibres the morphological appearance of fibres showed quite uniform size. The deviation in size was from nano to sub-micron. SEM images of PU fibres showed the beaded structure, whereas chemically mixed PU/nHA composite were smooth and no beaded nano-fibres. However, the images of physically mixed PU/nHA showed some loose nHA particles on the surface of fibres.

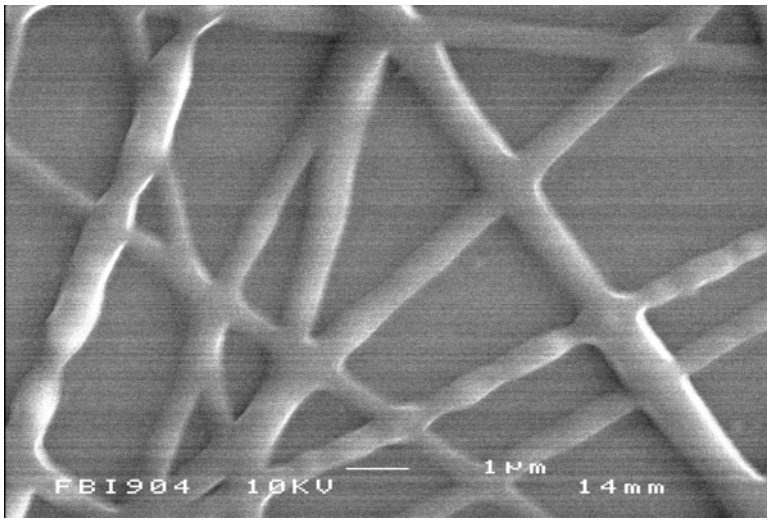

x 25000

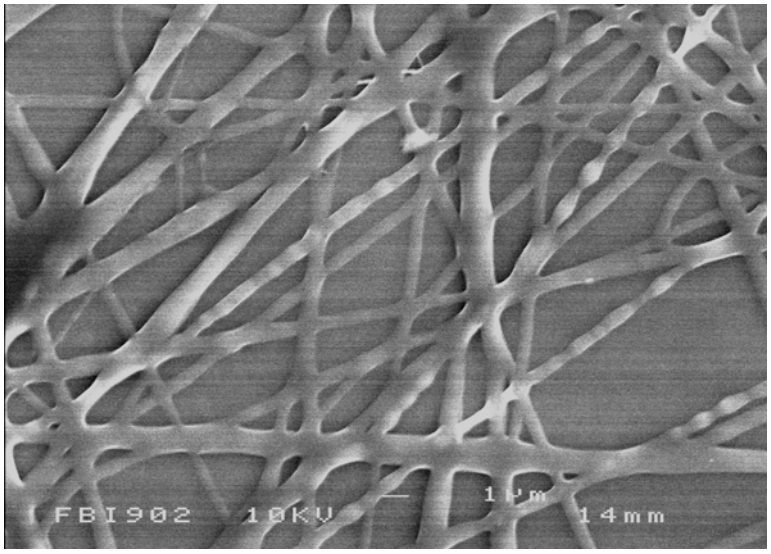

x 20000

Figure 4.83 SEM images of electrospun polyurethane nano-fibres

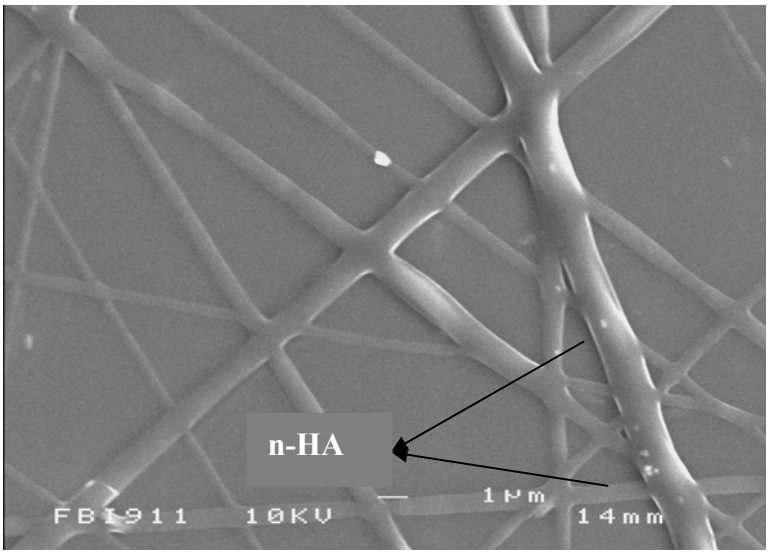

x 30000

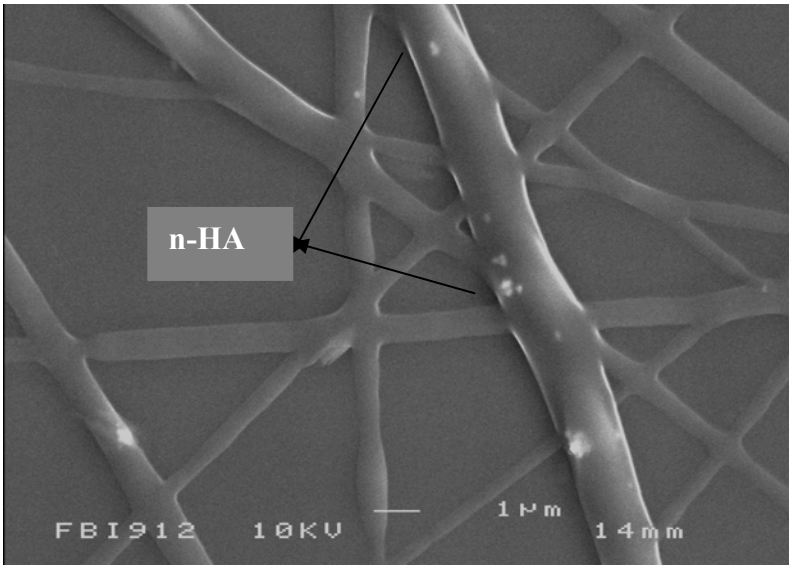

x 32000

Figure 4.84 SEM images of electrospun PU/nHA PM composite nano-fibres

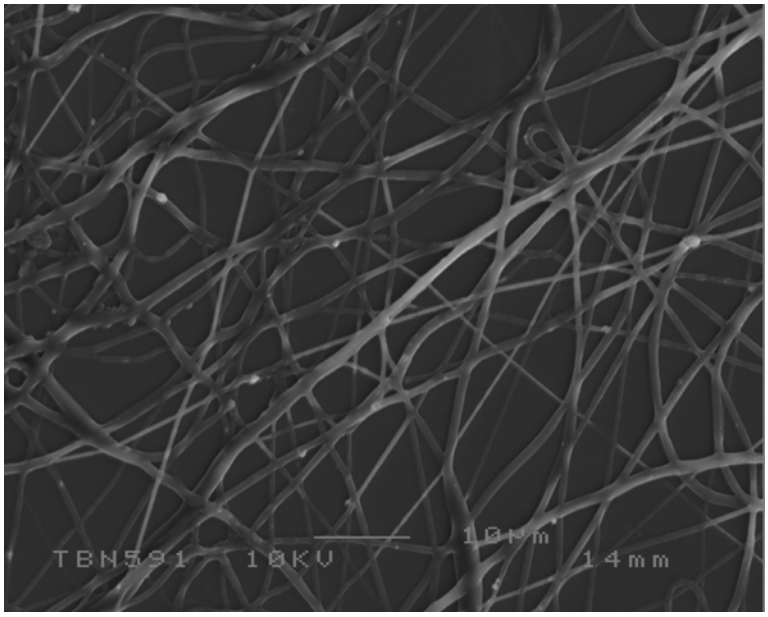

x 10000

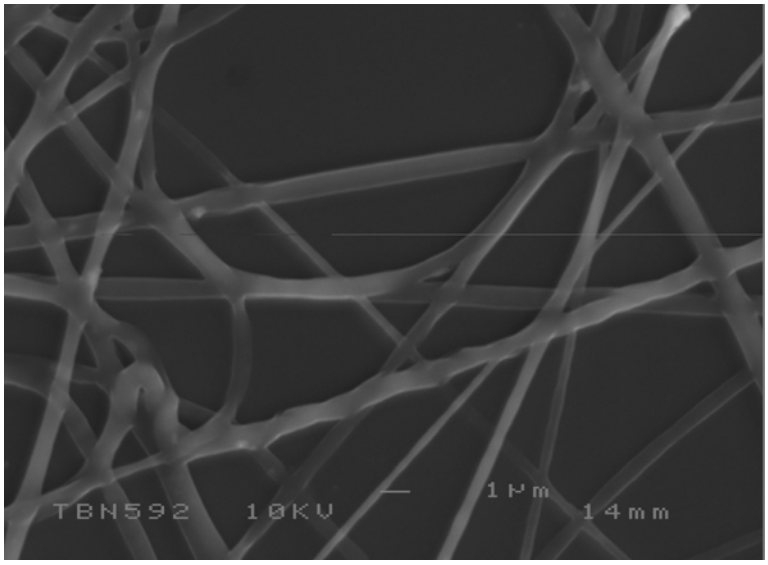

x 20000

Figure 4.85 SEM images of electrospun PU/nHA CM composite nano-fibres

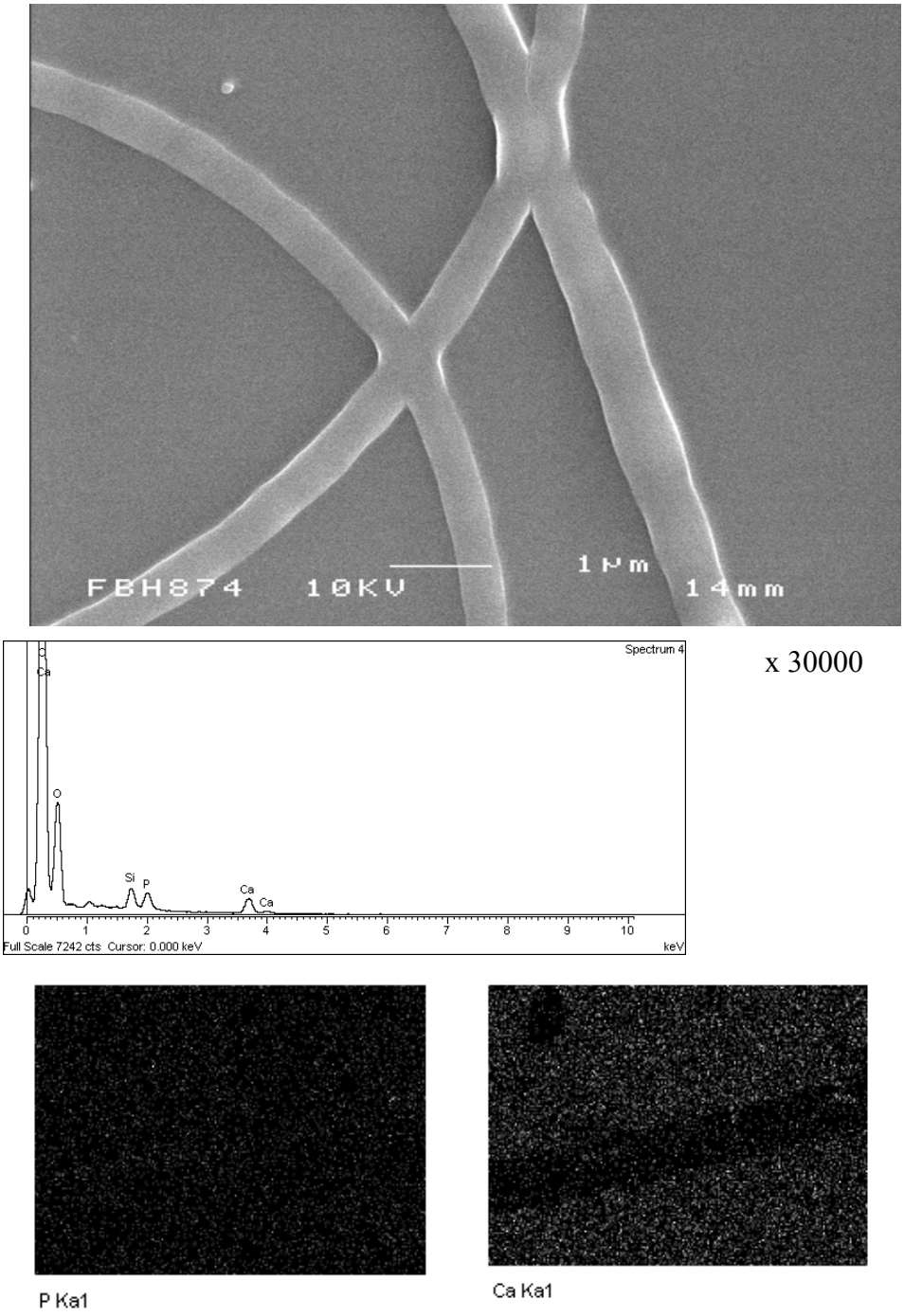

Figure 4.86 SEM images and EDS spectrum and map of electrospun PU/nHA CM composite nano-fibres

Chapter 5 Discussion

Introduction

This chapter explains the detailed description of results described in Chapter 4. All the synthesised materials processed in this study, including nano-hydroxyapatite, polyurethane, and polyurethane/nano-hydroxyapatite composites, were fully characterised by using Fourier Transform Infrared (FTIR) and Raman Spectroscopies. However, one of the problems associated with Infrared and Raman methods is the identification of bands, especially in complex and synthetic apatites. The vibrational activity is different in Raman and Infrared, some modes are active for both, but others are active either for Raman or Infrared. The band positions for these characterisations are influenced by both composition and structure (Penel *et al.,* 1998). Therefore, it is advantageous to analyse materials, both with the Raman and FTIR spectroscopic techniques, to achieve a complete finger printing of the chemical structural properties. NMR spectra provide useful information for the identification of their chemical composition and help in the conformational analysis of the chemical structure.

Physical characterisation provides surface and morphological properties of the sample. In this study, surface properties were analysed by using XRD with low analytical limits; however it analysed the purity (single or multiphasic) and crystallinity of required samples (Hench and Wilson, 1999). Nano-hydroxyapatite phase, ratios of other phases, and the lattice parameters were analysed with this technique. In order to clarify the morphology and structure, the present study emphasised the electron microscopic analyses i.e. transmission electron microscope (TEM) and scanning electron microscopy (SEM). In particular, bright field images and selected area electron diffraction patterns revealed the nano-structure of hydroxyapatite, surface roughness, changes and adhesion with adjacent structures.

The thermal analysis (TGA and DSC) techniques provide information about the structural transformation in polyurethane and polyurethane/nano-hydroxyapatite

composites. This transformation included glass transitions, melting, and crystallisation processes.

5.1- Synthesis of Nano-Hydroxyapatite

The sol-gel technique provides a homogenous system at a molecular level and helps in obtaining a good initial stage for synthesis of different materials. The method of synthesis used in this study has produced nano-apatite particles. The resulting amount of gel was attributed to the fact that the high alkalinity of the systems favoured the formation of calcium phosphates through reactions between the Ca and P precursors. The experimental powders contained non-stoichiometric apatite phase although the ratio (1.66) was close to stoichiometric ratio (1.67) (Elliott, 1994).

During the synthesis of nHA, control over the nano-structure was a big challenge. The biological process gave some clues to achieve controlled nucleation and crystal growth process mediated by macromolecule control and cell organisation. In this study, the pH value was maintained at 10.5 because the pH has influence on the dissociation of H_3PO_4 reagents and subsequent properties. At low pH values, the phosphate ions i.e. H_2PO_4 and HPO_4 are present in large number and are incorporated into lattice that results in HA crystals with calcium vacancies and which are unstable during the heat treatment. High pH is preferable for the stoichiometric structure and produce thermally stable HA. The heat treatment (sintered) process is an essential step in the apatite production; results in obtaining material with different phase composition and properties. The calcium deficient and non-sintered HA materials are less thermally stable than sintered HA and start to decompose at 650°C (Slosarczyk *et al.,* 1996).

The chemical composition and physical characteristics of the apatite powder with particle size and surface area were analysed. The synthesis of Ca-deficient nHA by using sol-gel was a challenging experiment. In all preparations nHA was identified as the only crystalline phase in the precipitated powders by the analytical techniques. The resulting nano-apatites were characterised using FTIR, Raman spectroscopy, XRD, electron microscopy (SEM, TEM) and BET.

5.1.1- Fourier Transform Infrared Spectroscopy (FTIR)

FTIR spectral data obtained in this study, as described in Section 4.1.1, Chapter 4, are in agreement with the findings of the previous researchers (Rehman and Bonfield, 1997; Koutsopoulos, 2002). It has been reported that hydroxyl (OH) stretch and bending peaks were present at 3569 and 624 cm^{-1}, whereas Koutsopoulos (2002) reported at 3572 and 631 cm^{-1} respectively. The weak hydroxyl (OH) stretches were observed in the FTIR spectra for as-prepared powder at 3571 cm^{-1}. In contrast, the hydroxyl peaks in the FTIR of heat treated powders were considerably stronger and sharper. The reduced intensity of the hydroxyl peaks for the fresh powders could be due to water in the hydroxyapatite particles (Isobe *et al.,* 2002). In this study, hydroxyl (OH) stretch was stronger and sharper and observed at 3571 cm^{-1} (Figure 5.1). Generally, the peak possesses low intensity and a broad band of water in freshly prepared powder is well developed but after heat treatment, the peak becomes relatively more defined and water band diminishes.

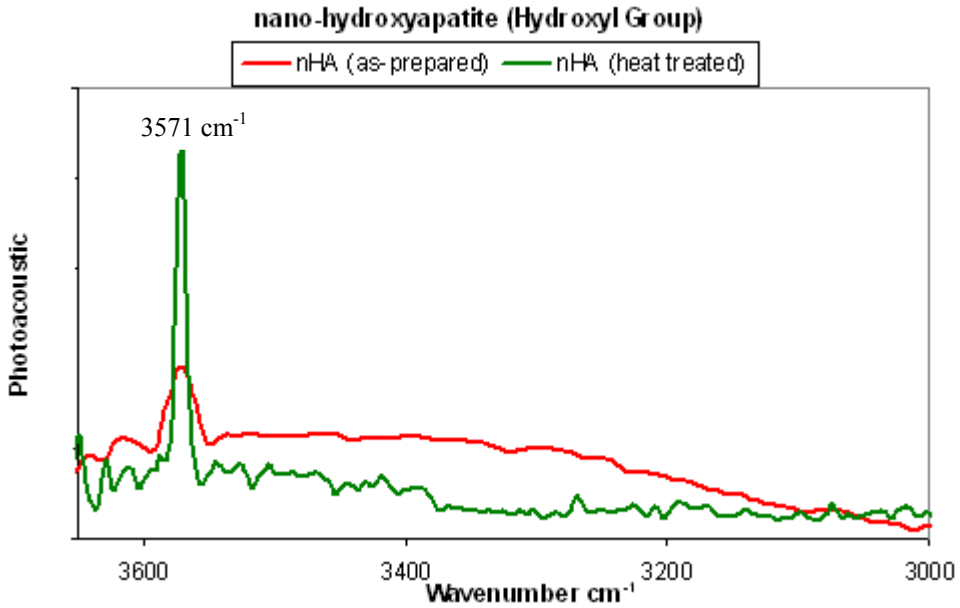

Figure 5.1 Comparative FTIR spectra of as-prepared (red) and heat treated (green) nano-hydroxyapatite in the range 3600 – 3000 cm^{-1} showing hydroxyl peak

Isobe et al. (2002) stated that "the band that disappeared after heating is assigned to the stretching mode of the hydrogen bonded OH and/or water, and the remaining band, after

heating, is assigned to that of the structural OH of hydroxyapatite". It has been suggested that upon heating, the crystals became more closely packed and aligned resulting in a more even distribution of hydroxyl groups on the surface of HA (Phillips, 2004).

FTIR spectrum of carbonate peaks (Figure 5.2) showed the carbonate ions occupying two different sites in apatites. However, the heat treated powders had weak carbonate bands. The peaks at 1650-1300 cm^{-1} were due to v_3 vibrational mode and the peak at 873 cm^{-1} was due to v_2 vibrational mode carbonate ion. Peaks at 1650-1300 cm^{-1} were assigned the surface carbonate ions rather than the ions in the lattice of phosphate. The maturation and formation of apatite crystals caused the split of peaks at 1650 and 1470 cm^{-1} (Elliot *et al.,* 1985; Rehman and Bonfield, 1997).

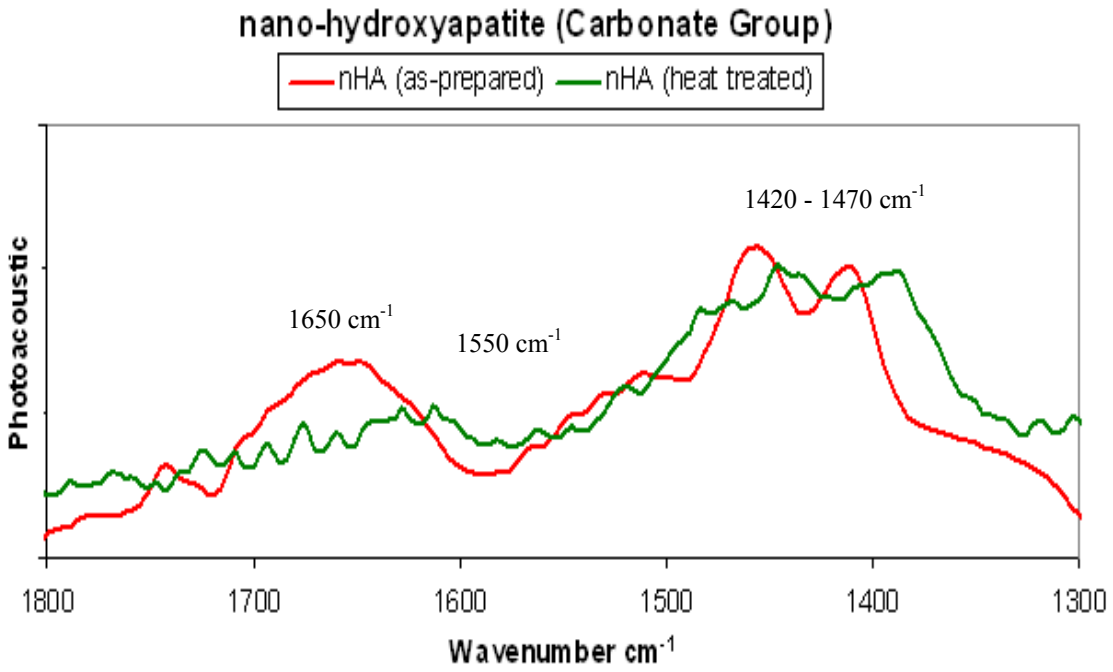

Figure 5.2 Comparative FTIR spectra of as-prepared (red) and heat treated (green) nano-hydroxyapatite in the range 1800 – 1300 cm^{-1} showing carbonate peaks

It has been established that hydroxyapatite structure could substitute carbonate ions at two different sites: A, where they substituted for OH^- ions and B, where they replaced PO_4^{3-} ions. The bands at 1470-1420 cm^{-1} (v_3 CO_3) and at 873 cm^{-1} (v_2 CO_3) were the

characteristic bands of carbonate ion in B-site. In addition, the peak at 1550 cm^{-1} attributed to the carbonate ion in A-site (Krajewski *et al.,* 2005). In FTIR for the as-prepared powders, a weak band due to phosphate stretching vibration (ν_3) was in the range 1100-1030 and 946 cm^{-1}. The phosphate peaks (Figure 5.3) in heat treated nano-hydroxyapatite were observed at 1040, 946, 603 and 569 cm^{-1}. The peak at 1040 cm^{-1} was triply degenerated vibration v_3, and 946 cm^{-1} was the non-degenerated symmetric stretching mode v_1, of P—O bond of the phosphate group and the peak at 603 and 569 cm^{-1} assigned to a triply degenerated bending mode v_4, of the O—P—O bond. Arends et al. (1987) reported phosphate v_4 bending peak at 633 cm^{-1}; however, Rahman and Bonfield (1997) described this peak as liberation mode of hydroxyl group. The phosphate v_2 band was observed in 470-490 cm^{-1} range. These were very weak bands in as-prepared, which were more intense in the heat treated powders. An increase in the number and intensity of observed phosphate peaks suggested an alignment of the nano-hydroxyapatite structure due to an increased crystallinity.

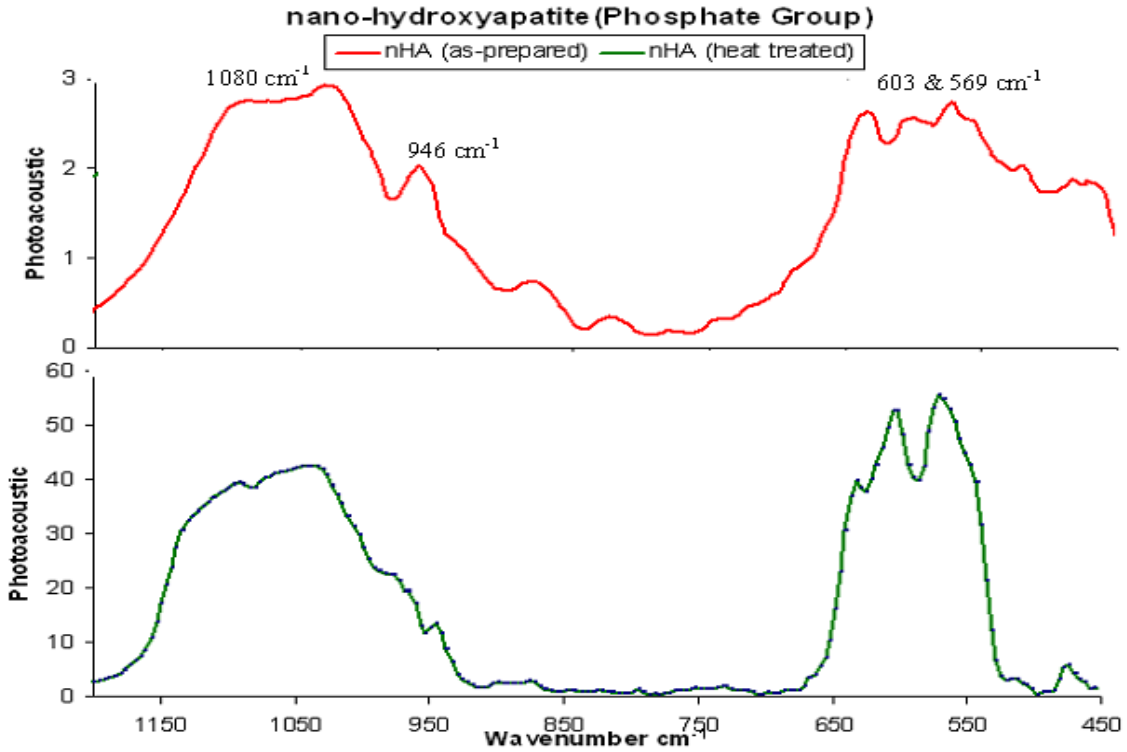

Figure 5.3 Comparative FTIR spectra of as-prepared (red) and heat treated (green) nano-hydroxyapatite in the range 1200 – 450 cm^{-1} showing phosphate peaks

It has been reported that band in the region 2280-1900 cm^{-1} and at 2380-1800 cm^{-1} were assigned to tribasic orthophosphate (PO_4^{3-}) and dibasic orthophosphate (PO_4^{-2}) respectively (Chapman and Thirlwell, 1964; Arends *et al.,* 1987; Gibson and Bonfield, 2002). However, the peaks (Figure 5.4) at 2000 and 2070 cm^{-1} were considered to be the v_3 cyananmide and cyanate (Dowker and Elliot, 1983). These peaks attributed to the addition of the ammonia during the synthesis process. Ammonia was used to increase the pH of the reaction mixture to raise the mixture to the desired pH 10.5.

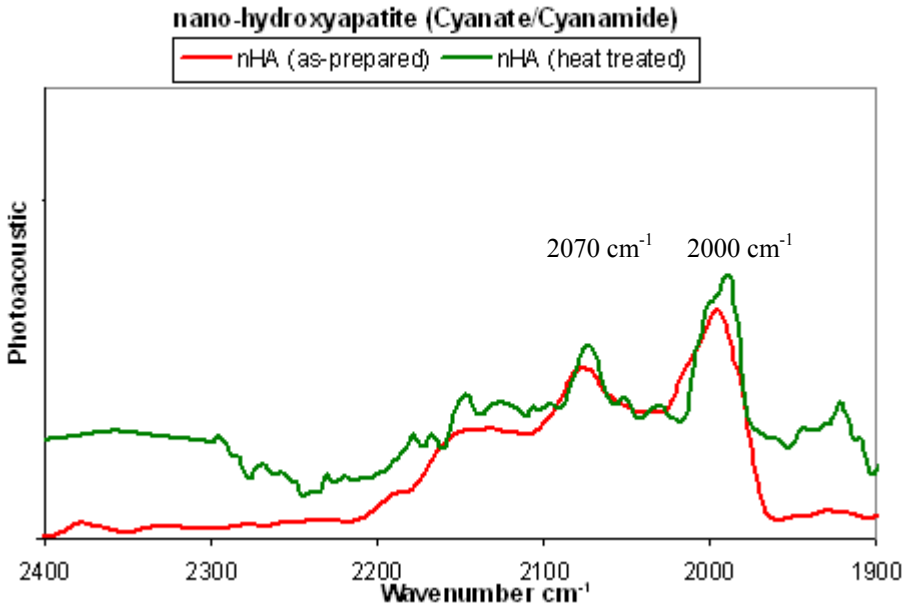

Figure 5.4 Comparative FTIR spectra of as-prepared (red) and heat treated (green) nano-hydroxyapatite in the range 2400 – 190 cm^{-1} showing cyanate/cyanamide peaks

5.1.2- Raman Spectroscopy

The results of Raman spectroscopy of nano-hydroxyapatite are described in Section 4.1.2, Chapter 4. The Raman peaks observed in this study were almost similar to the results reported by different researchers previously (Koutsopoulos, 2002; Antonakos *et al.,* 2007). The v_3 and v_1 stretching phosphate peaks (Figure 5.5) appeared at 1077, 1047 cm^{-1} and 961 cm^{-1} respectively. The v_4 and v_2 phosphate bending peaks were observed at 586 and 432 cm^{-1}. All bands have been assigned to internal vibrational modes of the phosphate groups (Koutsopoulos, 2002; Rapacz-Kmita *et al.,* 2005). After

heat treatment the peaks became intense. This splitting of the v_4 vibrational band indicated the low site symmetry of molecules, as two and three observed bands confirmed the presence of more than one distinction site for the phosphate group (Rehman and Bonfield, 1997).

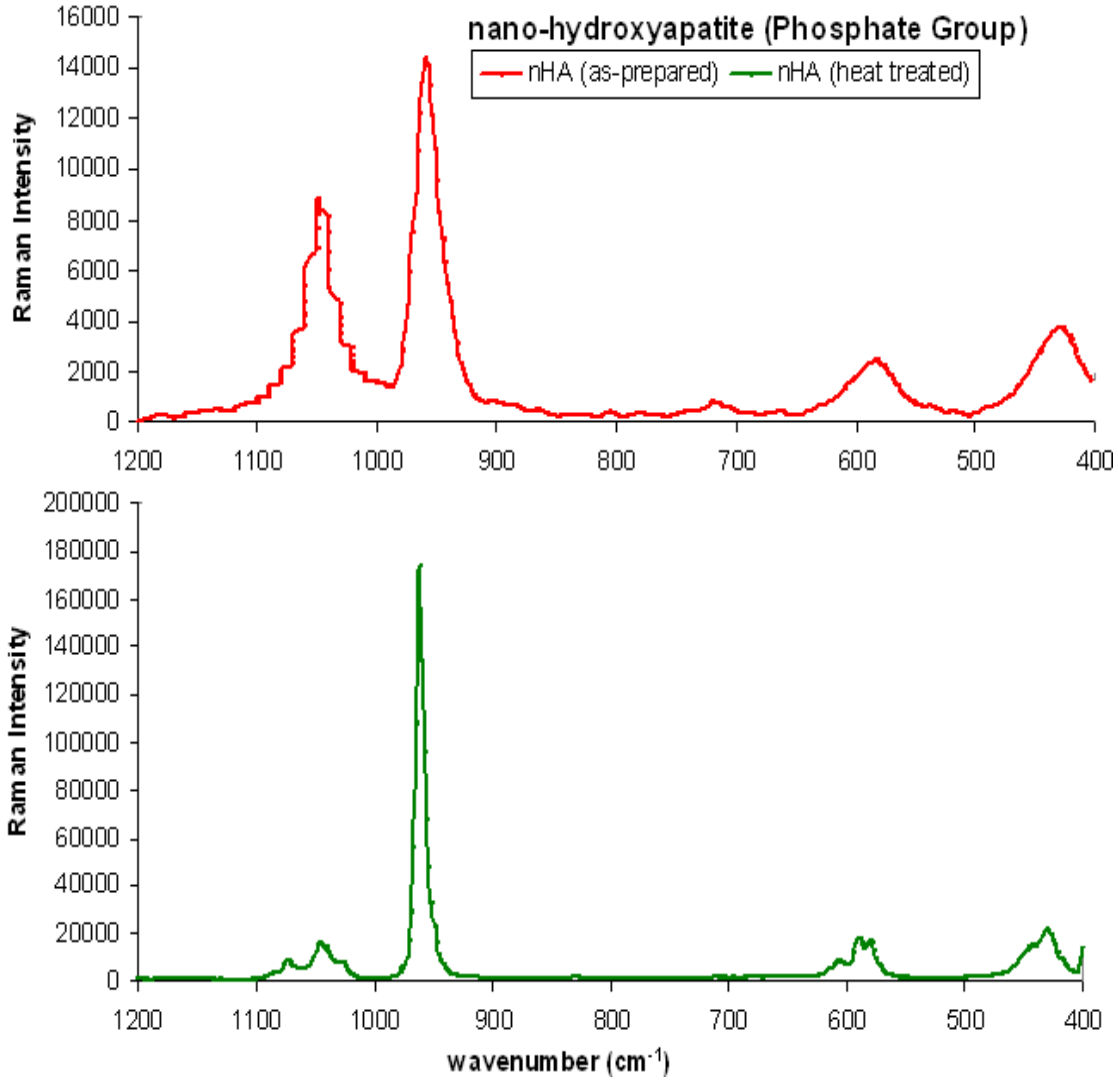

Figure 5.5 Comparative Raman spectra of as-prepared (red) and heat treated (green) nano-hydroxyapatite in the range 1200 – 400 cm^{-1} showing phosphate peaks

In comparison to the synthetic HA, the dentine or enamel was also characterised by Raman spectroscopy. Raman spectra of the enamel showed same characteristic peaks as observed in this study for synthetic nHA. The sharp and intense band, v_1, related to the

symmetrical stretching of tetrahedron of oxygen atoms surrounding the phosphorous atom (Pezzotti, 2005).

5.1.3- X-ray Diffraction (XRD)

The comparative XRD patterns are given in Section 4.1.3, Chapter 4 that showed significant difference in the crystallinity of powder before and after heat treatment. Before heat treatment the powder showed amorphous structure, whereas the heated sample showed characteristic crystalline HA peak. The peaks became intense and narrower, although the increase in intensity was not linear. The diffraction patterns showed sharp clear reflections corresponded to HA, which confirmed the phase purity and high crystallinity degree of the materials produced.

XRD pattern of nHA heat treated at 700°C (various experiments were conducted in this study and little variations were expected due to characterisation techniques of XRD machines) indicated an increase in crystalline size of the heat treated HA. The heat treatment played an important role in formation of pure crystalline HA. In this study, the powder sample was heat treated at 700°C and nHA lines became distinct and the width of lines became narrower, which suggested an increase in the crystalline degree. XRD patterns clearly showed the amorphous to crystalline HA without the formation of major secondary phases. XRD peak broadening with the heat treatment could measure crystal size in a direction perpendicular to the crystallographic plane. With the increase in temperature main difference was observed with the presence of tricalcium phosphate (β-TCP) and calcium oxide (CaO).

In the preliminary study resulting powders were heat treated from 40 – 900°C and clear phase changes of apatite powder observed from amorphous to crystalline structure. The XRD pattern of samples aged at 40°C showed NH_4NO_3 phases, which were expected due to use of NH_4OH to control pH throughout the experiment, however; it was found that with the increase in temperature during heat treatment, NH_4NO_3 peaks disappeared and were not observed in XRD pattern of samples heat treated at 400°C, 700°C and 900°C. The heat treatment was conducted at high temperature, which led to

decomposition and eventually formed β-TCP and CaO. At 900°C, the peaks at 31.13° and 37.92° attributed to β-TCP and CaO respectively. These peaks were in relation with previous study by Feng et al. (2005).

5.1.4- Morphology

SEM and TEM images are described in section 4.1.4, Chapter 4. The typical microscopic view of nHA structures showed fine distributed nHA crystalline material. The variation in size of the particles was due to high temperature during synthesis, low temperature during ageing time and then increase in temperature during heat treatment. The parameters that influence the morphology, stoichiometry, and level of crystallinity are temperatures, concentrations of the reagents, addition rate, stirring, maturation, and the presence of environmental impurities (Siddharthan *et al.,* 2006). The effect of these parameters forms needle-like crystallite hydroxyapatite (Kumar *et al.,* 2001); however, these variations in shape have been reported in conventional synthesis with an increase in temperature during heat treatment (Liu et al, 2001; Siddharthan *et al.,* 2006). The size, morphology and ordering of nHA powders have been affected by temperature and maturation conditions. These factors subsequently increase the particle size and crystallinity (Meyer and Fowler, 1982; Lazic *et al.,* 2001). Macromolecules such as stearic acid, monosaccharide and related molecules can also exert significant control on the morphology (Yan *et al.,* 2001). However, these macromolecules are all liner structure molecules, but the disadvantage is that liner molecules are not suitable for constructing ordered structures of the nano-particles, which is due to the distribution of molecular weight (number of repeating units) (Zhang *et al.,* 2005).

5.1.5- BET Analysis

BET surface area results are described in Section 4.1.5, Chapter 4 that supported the SEM and TEM data, suggesting that the as-prepared nano-hydroxyapatite sol-gel method produced a fine powder with a surface area 110 m^2/g. Heat treatment at 700^oC has the effect of reducing surface area of particles to 37 m^2/g. Patel et al. (2001) reports

that heat treatment has the effect of reducing surface area of HA particles as the temperature increases, where a surface area of 70-80 m^2/g at 400°C reduce to 5-7 m^2/g at 1000°C. Surface area can be used to calculate the average grain size of a powder as described by Kong *et al.* (2002). An empirical equation using the surface area and density, and assuming spherical particles, is shown below:

$$t = 6 \diagup \rho.SA \qquad \textbf{(eq. 5.1)}$$

Where t is the average grain size in micro metres (μm), ρ is the density (g/m^3) and SA is the surface area (m^2/g).

Using the surface area results obtained for nano-hydroxyapatite as described in Section 4.1.5, Chapter 4, and assuming the theoretical density of hydroxyapatite (3.16 g/cm^3 ICDD 9-432), values could be calculated for the average grain size of the powders produced in this study and are given in Table 5.1. The calculated particle sizes of as-prepared (fresh) and heat treated nano-hydroxyapatite were in line with the experimental data. The obtained average size of particles was 20-150 nm in length and 15 nm in width. From this calculation it is suggested that the maximum number of heat treated particles was of approximately 51 nm in size and proved that heat treatment had the effect of increasing the particle size of particles by nearly three times.

Table 5.1 Table showing calculated particle sizes for nano-hydroxyapatite

Surface Area, m^2/g		**Particle Size, nm**	
As-prepared	Heat Treated	As-prepared	Heat Treated
110	37	17.2	51

5.1.6- Significance

The structural characteristics of nHA were affected by the synthetic precursors, pH values, reaction temperature, and post-treatment processes including ageing and heat treatment (Lacefield, 1998). The ageing and maturation phase affects the crystal size and the crystals becomes thicker and aggregation more distinct (Lazic *et al.,* 2001). The

molar ratio of Ca/P (1.66) reflected the presence of phosphate group and a presence of carbonate were observed at a low level. The higher surface area of nano-particles has significant number of OH groups on the surface of hydroxyapatite particles (Yesinovski and Eckert, 1987; Liu *et al.,* 1998). The presence of OH group on the surface has a distinct feature that it shows reactivity towards the other group such as isocyanate to create the urethane linkage.

In this study, carbonate group was present in the resulting hydroxyapatite powder. Bone, enamel and dentine contain carbonated hydroxyapatite of different compositions with a few percentages of carbonate ions i.e. 2 to 8%. The synthetic hydroxyapatite has the ability of bond to bone, whereas, with the low content of carbonate the rate of osseointegration is relatively slow. It has been reported that the carbonate content can create an effect on phosphate bands. With increase in carbonate content, the v_3 PO_4 mode becomes progressively less resolved and at the same time the v_1 PO_4 mode broadens (Leeuwenburgh *et al.,* 2004). However, the FTIR spectrum in this study, showed intense PO_4 peak, which attributed the presence of low number of carbonate present in the nano-hydroxyapatite.

The nHA would be more interesting from a biological viewpoint because of its similarity to tooth structure. It offers possibility to enhance the rate of bonding formation and to have better mechanical properties due to its high surface area to volume ratio, superior chemical homogeneity and micro-structural uniformity (Zhu *et al.,* 2006). It is suggested that the synthesis of nano-scale hydroxyapatite improved the clinical application (Cao *et al.,* 2004).

5.1.7- Conclusion

The recent trend focused on overcoming the limitations of calcium phosphate group precisely hydroxyapatite, and improving their mechanical and biological properties by using nanotechnology. Nano-hydroxyapatite has significant properties due to its grain size, large surface area to volume ratio and fine structure almost similar to biological

apatite. These properties have large impact on interaction of nano-hydroxyapatite with polymer matrix and their monomers. In addition, it is able to bond with the living tissue by stimulating a specific biological response. This study showed that with sol-gel technique pure apatite could be produced. The presence of component groups were identified by using FTIR and Raman Spectroscopy and XRD proved the crystallinity of the powder. FTIR and Raman showed quail-quantitative results about the type of compounds, their structure and crystallinity. The identifications of groups such as OH, PO_4 and CO_3 are possible with these techniques. XRD gave information on the types of compounds and the possible presence of impurities at high temperature. By using SEM, TEM and BET, it was observed that the resulting powder was nano-size with high surface area. Hence, it is expected that the nano-hydroxyapatite powder were proved to be a potential osteoconductive material and show its tendency toward the monomer matrix. Recently much attention has been focused on composites based on nano-hydroxyapatite and polymers.

5.2- Synthesis of Polyurethane

Several classes of reactions involving isocyanate groups are possible due to multiple structures. Reaction can occur across C=N bond in a variety of ways, including adduct formation, cyclo-addition, oligomerisation and insertion reaction. A primary reaction in the polymerisation of isocyanates is insertion reaction. In isocyanate group the reaction mechanism proceeds with a nucleophilic attack at carbon atom. The end product of this reaction is a urethane linkage (Rehman, 1996).

The reaction of isocyanates with compounds containing –OH groups are capable of much wider application in polymer formation. The –NCO group can react generally with compounds containing active hydrogen atom. When isocyanate group reacts with alcohol, a urethane is formed,

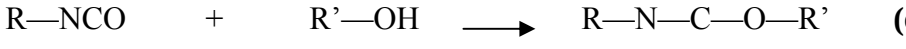

(eq. 5.2)

The position and intensity of these vibrations are extremely sensitive to the strength and specificity of the hydrogen bonds formed.

5.2.1- Fourier Transform Infrared Spectroscopy (FTIR)

FTIR spectrum of polyether based polyurethane is given in (Figure 4.6), and described in Section 4.2.1.1, Chapter 4. FTIR spectroscopy was used to analyse the degree of hard and soft segment interaction in polyurethane samples. These two incompatible structures helped in the formation of phase-separated systems. This phase separation system of well-defined polyurethane consisted of the reaction product of hard and soft segments. In urethane hard domains, hydrogen bonding results from hydrogen atoms of N—H groups (proton donor) and C==O groups (proton acceptors). When hard and soft segments were mixed at the molecular level, the oxygen in soft segment backbone also acted as a proton acceptor in forming hydrogen bonds with N—H groups of hard segment urethane groups (Miller *et al.,* 1985). The phase separation in polyurethanes can be analysed by measuring the intensity and position of hydrogen bonded N—H stretching vibration. The N—H absorption region (between 3500 and 3200 cm^{-1}) indicated hydrogen bonding. The quantitative analysis of hydrogen bonds formed by using N—H stretching band was complex due to the significant band overlap which might have resulted from large differences in the inherent extinction coefficient as a function of hydrogen bond strength (Lee *et al.,* 1988). In this study, free N—H stretching band near 3420 cm^{-1} was not observed. The bands at 3320 and 3295 cm^{-1} (Figure 5.6) were assigned to N—H groups, hydrogen bonded to C==O groups and the ether oxygen (C—O—C) respectively. With the increase in number of N—H**….**C==O bonds the number of N—H**….**C—O—C (ether) hydrogen bonds should diminish. The increase of 3320 cm^{-1} peak was obvious, as phase separation proceeded; it grew from a weak shoulder into dominant peak that clearly indicated the formation of hydrogen bond (Lee and Hsu, 1989). The exact position of the N—H depends on the strength of hydrogen bond; however, the bond strength depends on local geometry, such as linearity of the involved bonds and the distance between groups (Lee *et al.,* 1987).

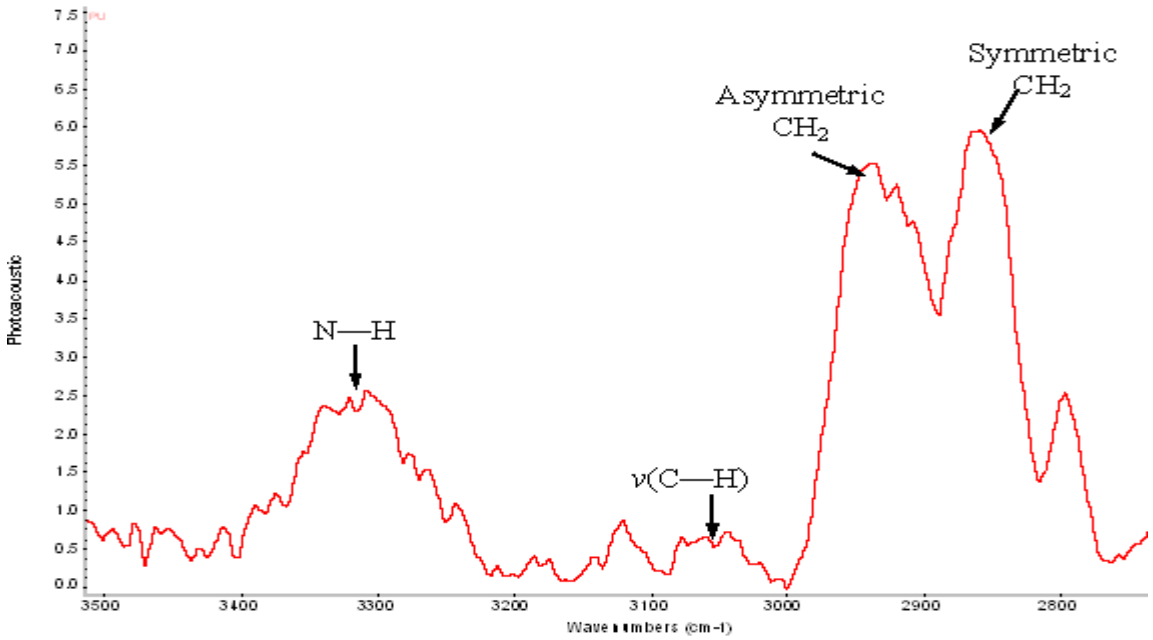

Figure 5.6 FTIR spectrum of polyurethane showing N—H and C—H groups

The C—H bands appeared at various positions due to presence of different CH_2 groups in the polymer chain which were expected to come from chain extender (butane diol) and polyols. Peaks at 2941 and 2920 cm^{-1} were CH_2 peaks of polyols and assigned as asymmetric and symmetric stretching respectively. The peak at 817 cm^{-1} was attributed to γ(C-H) from butane diol (West and Cooper, 1977; Grobe *et al.,* 1987).

The carbonyl absorption region was observed at 1780-1660 cm^{-1}. Peaks due to bonded C==O stretching appeared at 1705 cm^{-1} and the free C==O stretching observed at 1730 cm^{-1}. Hydrogen bonding in the carbonyl stretching region was less complex than that in N—H stretching region due to the fact that carbonyl groups remained in a hard segment chain and bond to N—H group in the hard block (Rehman, 1992). In the carbonyl region, the peak due to hydrogen bonded C=O stretching appeared at 1705 cm^{-1} was more prominent than the free C=O stretching. The dominance of the bonded C=O peak indicated that a large fraction of the hard domains were hydrogen bonded. The bonded C=O peaks are generally broader for the low hard segment content polyurethane and this broadening was observed in all spectra and in representing spectrum (Figure 5.7).

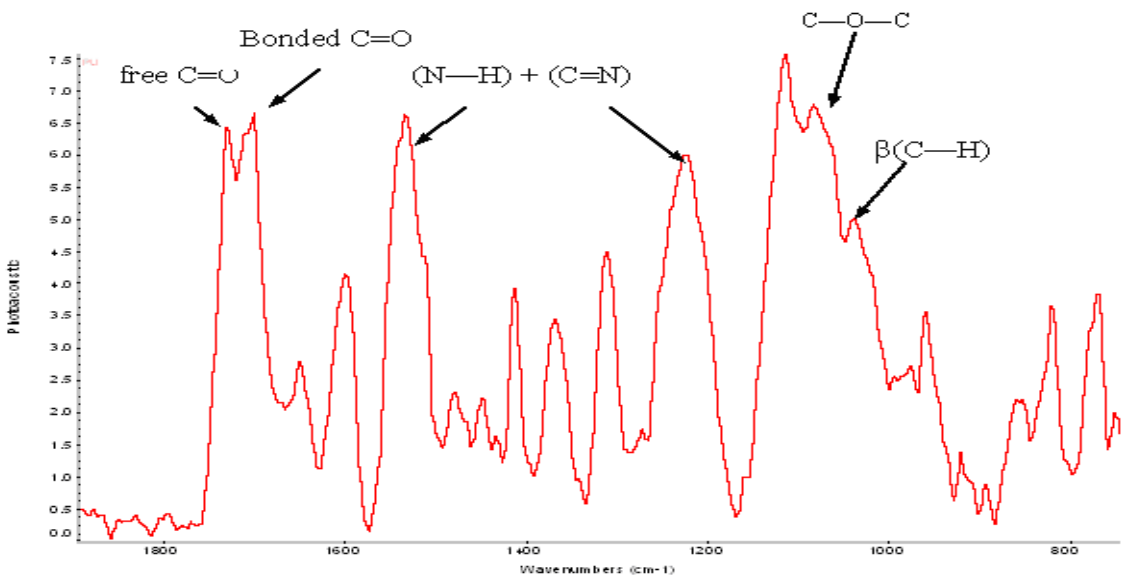

Figure 5.7 FTIR spectrum of polyurethane showing mainly carbonyl, amide and ether groups

The peak at 1599 cm^{-1} was assigned to ν(C=C) in benzene ring and 1535 cm^{-1} was amide II δ(N-H) + ν(C==N). A weak CH_2 peak appeared at 1481 cm^{-1} and 1413 cm^{-1} was attributed to strong ν(C-C) in benzene ring. Peak at 1311 cm^{-1} was assigned to amide III δ(N-H) + ν(C==N), β(C-H) peak and δ(N-H) + ν(C==N) appeared at 1222 cm^{-1}. The region at 1111 cm^{-1} was $\nu(CH_2—O—CH_2)$ of ether peak and 1017 cm^{-1} was weak β(C—H) in benzene ring.

5.2.2- Raman Spectroscopy

Raman spectrum of polyether based polyurethane is given in (Figure 4.7), and described in Section 4.2.1.2, Chapter 4. The spectrum showed C—H group at 2920 and 2869 cm^{-1} assigned to asymmetric and symmetric stretching peaks respectively. Peaks at 1443 and 1305 cm^{-1} were assigned δ(CH_2) bending vibration and δ(CH) respectively. The spectroscopic region at 1800-1570 cm^{-1} (Figure 5.8) was assigned to carbonyl symmetric stretch vibration which consisted of three characteristic bands. Peak at 1700 cm^{-1} was attributed as ordered hydrogen bond in hard phase and a shoulder peak was observed in this region. Peak at 1712 cm^{-1} corresponded to disordered hydrogen-bond and 1730 cm^{-1} attributed to free carbonyl group. The aromatic breathing mode and

symmetric stretched vibration (C==C) was observed at 1619 cm^{-1}. Peak at 1528 cm^{-1} assigned to *v*(aromatic, C==C), urethane amide II: *v*(C—N) + δ(N—H) and similar to isocyanate asymmetric and symmetric stretching vibrations. In literature this band has been attributed to *para* (4.4'-isomer) di-substituted phenylene ring vibration in MDI. However, the other isocyanate peak at 2200 cm^{-1} was not visible suggesting the peak belonged to urethane amide II and unreacted isocyanate monomer was not present in the polymer. The unreacted monomers may cause unintended side effects such as toxic, irritation, or allergic reactions. The in-phase combination of N—H in-plane bending and C—N stretching vibrations were predominantly observed at 1305 cm^{-1} and were assigned to urethane III band. The band corresponding to ether (C—O—C) stretch was observed at 1118 cm^{-1} and a weak peak at 1080 cm^{-1} was attributed to C(O)—O—C stretch of the hard segment (Stephenson *et al.,* 1961; Ferry *et al.,* 1996; Parnell *et al.,* 2003; Cai and Singh, 2004).

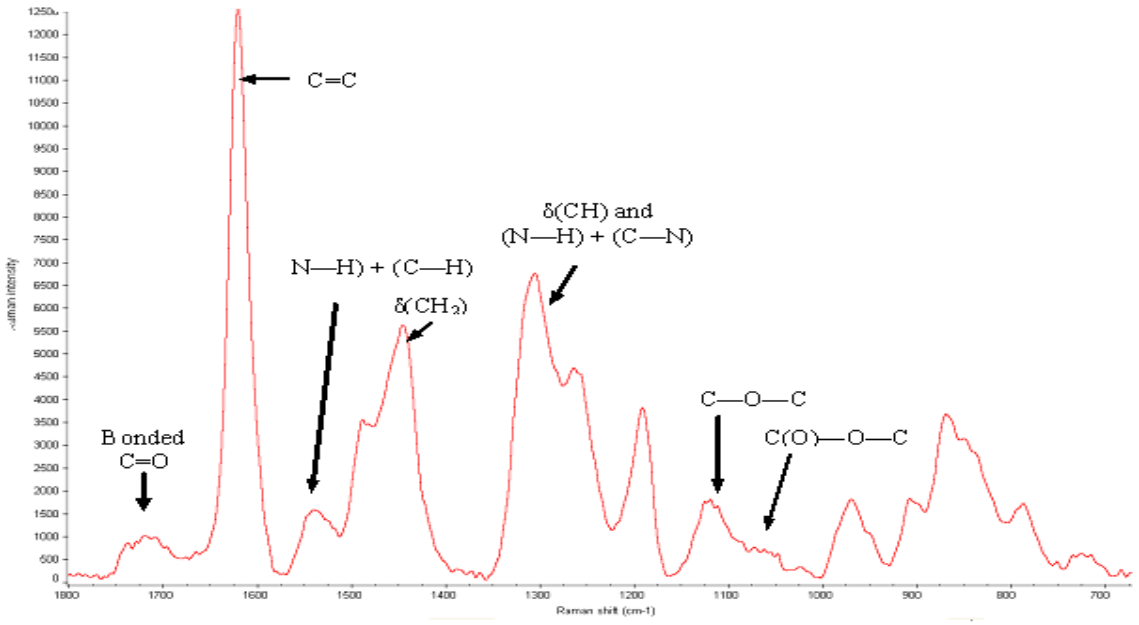

Figure 5.8 Raman spectrum of polyurethane showing mainly bonded carbonyl, benzene, amide and ether groups

5.2.3- ^{13}C Nuclear Magnetic Resonance (^{13}C NMR)

^{13}C Nuclear Magnetic Resonance (NMR) spectrum of polyether based polyurethane is given in (Figure 4.8), and described in Section 4.2.1.3, Chapter 4. High resolution

^{13}C NMR spectra of polyurethane were obtained which provided useful information for the identification of their compositions. The monomeric and polymeric compounds used in this study produced highly characteristic patterns. ^{13}C NMR study was conducted using THF and it has been reported that N—H proton signals were sensitive to the environment such as solvent, water, and temperature. Kricheldorf and Hull (1981) described the chemical shift of polyurethane and related materials in various solvents using ^{13}C NMR. The C==O resonance signals of polyurethane were assigned at 153.12 ppm. The other small peak at 154.39 ppm was assigned to urethane. The signals at 135.92-139.23 ppm were due to ipso carbons (C-1). There were five different primary peaks that could be assigned to aromatic carbons ranging from 118.94 to 139.23 ppm. The intensities of signals at 120-121 ppm were halves of signals at 118-119 ppm.

It is expected that the signals at 120-121 ppm might be para carbons (C4) and the signals at 118-119 ppm were due to ortho carbon (C2) (Kaji *et al.,* 1992). However, peak appeared at 119 ppm might be assigned -CH_2 as compared to data published by Bretimaier and Voelter (1987) and Levy et al. (1980). It should be noted that the peak observed for the –CH_2 was seen as a doublet because the carbon was spin-coupled to another group causing multiplicity (Chamberlain, 1974). The peak at 129 ppm was attributed to C—H (Levy *et al.,* 1980). The aromatic carbons served as characteristic signals of anomalous linkages. The C2 signals were the easiest ones to detect and were isolated from main urethane signals. Their intensities were stronger because of attaching a proton and were duplicated by the symmetry. The methyleneoxy carbon attached to –CONH showed peaks around 65.01 ppm (Prasath *et al.,* 2004), while the peak at 64.76 ppm was assigned to soft-segment carbons adjacent to oxygen. The smaller peak at 41.23 ppm was attributed to the methylene carbon in the MDI hard segment and the methylene group peaks also appeared at 25.27- 28.09 ppm (Wang *et al.,* 2003).

5.2.4- X-ray Diffraction (XRD)

XRD results of polyether based polyurethane is given in (Figure 4.9), and described in Section 4.2.2.1, Chapter 4. The pattern showed a broad band, which was expected due to the amorphous structure or presence of small crystalline structure or diffraction form

large crystal (Takahashi *et al,* 1996; Stanciu *et al.,* 1999; Billmeyer Jr., 2000; Mondal and Hu, 2006a, b; Chun *et al.,* 2006). The crystallinity of peak depends on the preparation of sample. Samples showed sharp peaks if they slowly cooled from the isotropic state. However, when samples were quenched from the mesophase, the exhibiting peaks appeared broad and weak (Jeong *et al.,* 2000). The results in this study suggested appearance of broad band at 20°. The soft segments formed crystalline structure in segmented polyurethane due to their long order structure (Hu and Mondal, 2005). Rahman and Kim (2007) studied XRD pattern of different soft segments (PTMG, PPG, PCL) and it was observed that all polyols have crystalline structure, but none of them showed sharp crystalline peak. All samples showed broad haloes, which could be due to amorphous structure or presence of small amount of crystalline structure. In this study, the presence of high ratio of hard segment showed crystallinity of polyurethane. It has been reported that the molecular distance, bond length and bond angles attributed to lattice space (Ning *et al.,* 1996). The hydrogen bond interaction contributed to higher ordering of polymer segment in hard micro-domains and their aggregation increased the degree of crystallinity (Cooper *et al.,* 1976; Culin *et al.,* 2002). The diffraction peak from partially ordered structure formed at hard segment domain, whereas inter-chain attractions such as dipole-dipole interaction and hydrogen bonding brought the hard segment together. The polymeric chain was dynamic and flexible, but the presence of peak supported hard segment in polyurethane.

5.2.5- Thermogravimetric Analysis (TGA)

Thermogravimetric Analysis (TGA) results of polyether based polyurethane is given in (Figure 4.10), and described in Section 4.2.3.1, Chapter 4. Thermal decomposition process provided specific information regarding internal structures of polymers. In this study, TGA of polyurethane provided a plot of weight change against temperature in a controlled dynamic temperature environment. The obtained data of thermal degradation was almost in agreement with other studies based on pure polyurethane (Desai *et al.,* 2000; Herrera *et al.,* 2002; Yang *et al.,* 2005; Kumar *et al.,* 2006; James *et al,* 2006), whereas, variation was observed by using different methods of

preparation and ratios of hard and soft segments.

The typical weight loss *vs.* temperature curve showed several regions of distinctly different slopes. The first slope of initial decomposition occurred at 295°C (weight loss: 4%) and extended up to 400°C (weight loss: 30%). The second and third decomposition slope was due to soft segment initiated at 410°C and 430°C respectively, with a plateau of almost 75°C length before the complete degradation which finished at almost 680°C. Initial degradation was due to hard segment and secondary degradation was due to decomposition of soft segment. The particular feature might have several interpretations, which depend on the mechanisms of thermal depolymerisation. The different slopes would represent regions in temperature where chain scission occurred. Wang et al. (2000) reports that initial degradation corresponds to hard segment, as diisocyanates have a limited thermal stability and their decomposition starts at around 285°C. It has been established that urethanes have lower thermal resistance (Perez-Liminana *et al.,* 2005). Therefore, by increasing the temperature, additional decomposition process occurred. Thermal stability of polyurethane was dependent on the crystallinity of hard segment and strength of a bond. Higher degree of crystallinity of hard segment leads to higher degradation temperature of soft segment (Song *et al.,* 1996; Gnanarajan *et al.,* 2002). The appearance of hydrogen bonding interaction in polyurethane is due to N—H groups. This bonding and its strength leads to a need for extra energy for the network to degrade. Several studies (Petrovic *et al.,* 1994; Gradwell *et al.,* 1998) reported that amount of weight loss of first region was related to the hard segment concentration, suggesting that the degradation started in hard segment, while the second part related to the degradation of soft segment. However, in contrast, few studies (Herrera *et al.,* 2002; Kumar *et al.,* 2006) have reported that the weight loss in first step was due to soft segment of polyurethane and the main pyrolysis product was carbon dioxide. The second stage degradation and thermal decomposition was of hard segment due to liberation of HCN, nitrites of aromatic carbons and ethers. The degradation and weight loss corresponds mainly to dopant loss and beginning of main chain degradation (Jeevananda *et al.,* 2001: 2003).

In this study, it was maintained that TGA characterisation was conducted under inert

nitrogen because polymer with carbon backbone thermally decomposed with oxidation in air, where carbon could react with oxygen readily. In an inert atmosphere, decomposition of polymers occurred in a way that tend to conserve the structure of matrix, thus bond breaking inside polymer matrix required a large amount of energy (Achilias *et al.,* 2008). The heating rate in this study was maintained at 20°C, although variation in heating rate was not studied. It has been reported that with the increase in heating rate TGA curves and peak temperature shifted to higher values (Achilias *et al.,* 2008).

The degradation process can be characterised by activation energy, using three kinetic analyses using the Ozawa, Flynn, and Salin models (Lage *et al.,* 2001; Lin *et al.,* 2001; Tien and Wei, 2002). The mechanism changes during the degradation of polyurethane; activation energy is not only a function of chemical structure of polymers but also varies with the conversion. It provides parameter for the assessment of the thermal stability of polyurethane.

The first method of calculating the activation energy was proposed by Flynn (Lage *et al.,* 2001). This method was applied to low conversion, between 1 and 5% of non-isothermal differential weight loss method with a constant heating rate β. The conversion, α is defined by:

$$\alpha = 1 - w\,(t) / w_o \qquad \textbf{(eq. 5.3)}$$

where, w_o and $w(t)$ represent initial weight and weight at any time, t, during degradation, respectively.

The second method of calculating activation energy was proposed by Ozawa and Flynn (Lage *et al.,* 2001), which required several TGA curves at different heating rate (β). It consisted of plotting the logarithm of heating rate (log β) versus 1/T for each degree of conversion (α). From these iso-conversion curves, activation energy was calculated from the slope of lines using the expression

$$E_a = -(\text{slope})R/0.457 \qquad \textbf{(eq. 5.4)}$$

where, R is the gas constant.

Third method needs only one non-isothermal TGA measurement; the decomposition rate could be expressed by an equation

$$d\alpha / dt = k(1 - \alpha)^n \quad \textbf{(eq. 5.5)}$$

where, α is defined in eq. 5.1, da/dt is the decomposition rate, n is the empirical order of decomposition, and *k* is the decomposition rate constant.

In this study, the current data was analysed by Ozawa model and plotted by the logarithm of heating rate against the reciprocal absolute temperature (1/T) for each conversion degree (α), defined as the weight loss at a given temperature.

The above theoretical interpretations are based on the assumption that a higher activation energy value results in better thermal stability. TGA technique as applied on polyurethane is an effective technique for deriving basic information about the polymer systems such as depolymerisation mode. The clinical significance such as mixing variables and later the incorporation of filler percentage can also be observed by using this technique. However, the important clinical significance of bio/dental material is the glass transition temperature which was assessed by DSC.

5.2.6-Differential Scanning Calorimetry (DSC)

Differential Scanning Calorimetry (DSC) result of polyurethane is given in (Figure 4.11), and described in Section 4.2.3.2, Chapter 4. The peak at higher temperature was associated with micro-phase separation transition to disordered state i.e. dissolution of micro-phase structure. The melting point (T_m) of endotherm fell into two categories: low-temperature endotherms which were related closely to the crystallisation temperature (T_c) and high temperature endotherm which showed the behaviour of conventional crystallisable homopolymers with folded chain lamellar morphologies, i.e. where T_m increased linearly with T_c. Multiple endotherms in melt-crystallised polyurethanes were the result of melting of distinct crystal population.

During each endothermic process, hard segment crystals not only melt, but also mix with the soft microphase (Koberstein and Galambos, 1992). In accordance with current study, it is established that the glass transition of polyurethane is around -20 to -40°C attributed to soft segment, while endotherm between 150-200°C corresponds to melting temperature of hard segment (Song *et al.,* 1996).

If sample melts and quenches to form a structure at low temperature, and then brought directly up to a higher temperature, it crystallises easily to give structures with significantly higher melting point (George and George, 2001). Same behaviour was observed in this study because the pattern of DSC thermogram was divided into three sections; first, to heat from -60 to 150°C, secondly, to quench back to -60°C and then heated up to high temperature (250°C). The possible explanation of high temperature curve was due to crystal nuclei, which remained after initial partial melting, and seed crystallisation at higher temperature.

It has been identified that three endothermic transitions were associated with ordering of hard segments (MDI/BD). The lowest temperature endotherm (60-80°C) was attributed to disturbance of short-range order of the hard segment micro-domains. Two high temperature endotherms were attributed to disruption of long-range (120-190°C) and microcrystalline order (above 200°C) of hard micro-domains (van Bogart *et al.,* 1981). Blackwell and Lee (1984) reported multiple melting in MDI polyurethane and found that MDI/BD hard segment crystallised initially in contracted conformations. The extended crystalline polymorph has lower melting point that developed upon elongation and annealing. Melting temperature was not observed in this study; it could be due to linear polyurethane elastomers with alternating block copolymers that showed rubber-like elasticity over a wide temperature range but melted at high temperature. It is assumed that micro-phase separation properties occurred due to segmental incompatibility between two blocks. One phase was glassy or crystalline (hard) and other was rubbery (soft). Kornfield et al. (1991) reports the progressive increase in mobility with temperature first near the interface and then interior of hard micro-phase. This information can be used to gain knowledge about the other properties such as

higher glass transition temperature, corresponding to range over which a rigid polymer becomes flexible.

5.2.7- Conclusion

FTIR and Raman spectroscopy confirmed the presence of characteristic peaks of polyurethane. The resulting peaks showed linkage between isocyanate (hard segment) and hydroxyl group (soft segment) and formed N—H group. The bonded and free C=O peak appeared in resulting spectra; however, the intensity of bonded C=O was higher than latter. These both N—H and bonded C=O showed hydrogen bonding in polyurethane. It was further confirmed by using ^{13}C NMR and details of individual carbon presence and linkages among the groups were described. XRD analysis provided information about crystallinity of polyurethane and surface characteristics. The thermal analysis was performed by using TGA and DSC. These techniques confirmed the presence of hydrogen bonding between hard and soft segment and phase mixing. The presence of two degradation steps was attributed to network structure of polymer. The high glass transition was further confirmed from DSC and showed endothermic transition of soft segment and hard segment. Hence, it is confirmed that chemical (structural), physical and thermal characterisations prove the synthesis of polyether based polyurethane with existing hydrogen bonds forming the N—H and N—H**…..**C=O groups.

It is desirable for a dental restorative material to show biostability and have bioactive, biocompatible and bonding properties, which are not found in the current RBC. The bioactive adhesion exhibits a specific biological response at the interface of the material, which results in the formation of bond between the tissue and the material. This study confirmed the synthesis of nano-hydroxyapatite (inorganic fillers: osteoconductive) and polyurethane (organic matrix) successfully. The interfacial linkage between polyurethane and nano-hydroxyapatite is one of the major factors that determine the ultimate physical and mechanical properties of the composite. This study is mainly

focused on the synthesis of a covalently linked polyurethane/nano-hydroxyapatite restorative composite.

5.3- Synthesis of Polyurethane/Nano-hydroxyapatite Composites

5.3.1- Grafted MDI/Nano-hydroxyapatite

The coupling of nHA and MDI is carried out in solvent and their reaction pathway is confirmed by spectroscopic evaluation as described in Section 4.3.1.1.1, Chapter 4. The results confirmed the grafting of nHA and MDI. Its structural analysis indicated that certain functional groups (-OH) on the surface of nano-apatite had reactivity towards isocyanate. This preliminary study provided a baseline and confirmation of linkage between nHA and PU.

It is important to consider the availability of hydroxyl groups on the surface of nHA. The hydroxyapatite (hydroxyl group) has tendency to absorb moisture from environment and it is necessary to remove surface absorbed water. In this study, all the nano-hydroxyapatite samples were completely dried before reactions. The isocyanate group of MDI reacted mainly with hydroxyl (OH) group of nano-hydroxyapatite. The resulting N—H peak appeared at 3330 cm^{-1} and showed urethane linkage formation. Isocyanates are very reactive chemicals and are well known for their role in producing polyurethanes. Dong et al. (2001) reported the reaction of isocyanate (HMDI) with calcium hydrogenphosphate ($CaHPO_4$), rather than hydroxyapatite. They suggested that the linkage between the HMDI and calcium hydrogenphosphate powder is a urethane linkage. However, in present study, isocyanate showed its reactivity towards nano-hydroxyapatite. It was found (Figure 5.9) that after reaction the isocyanate group was completely reacted and the peak at 2200 cm^{-1} (NCO) disappeared. The expected reaction of nano-hydroxyapatite and isocyanate are as follow:

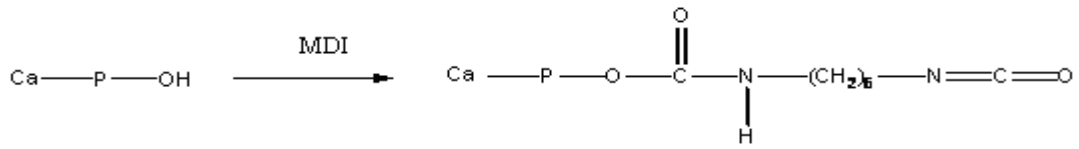

(eq. 5.6)

where, Ca—P—OH (hydroxyapatite)

This grafting could be advantageous for the coupling of osteoconductive fillers in polymer composite with polyurethane.

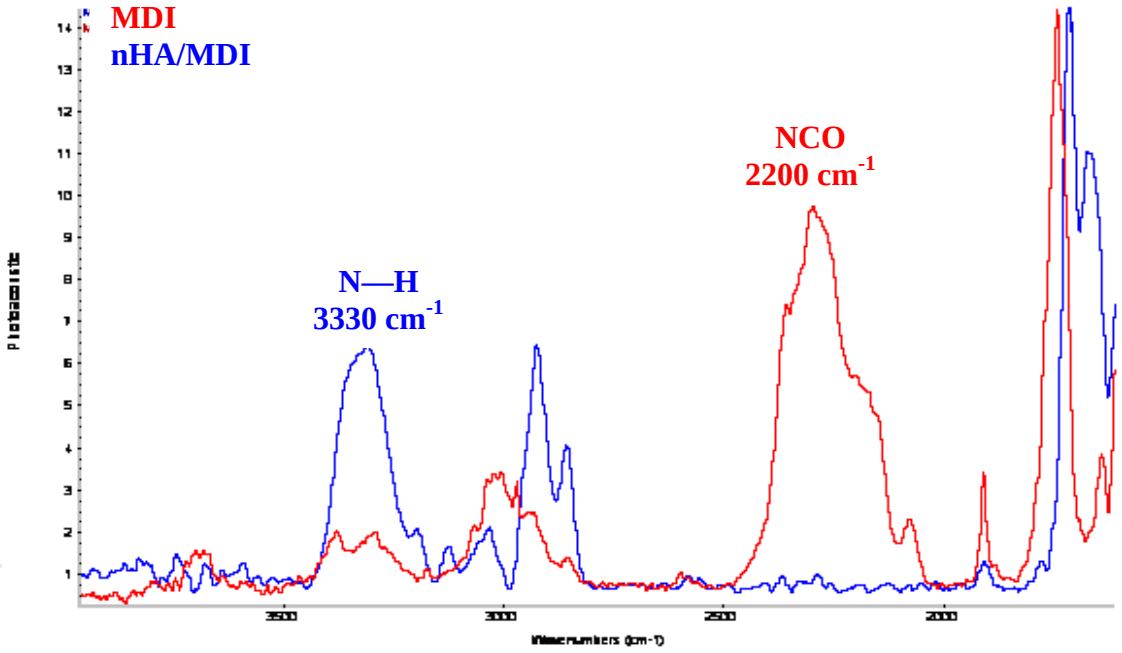

Figure 5.9 Comparative FTIR of MDI and MDI/nHA showing formation of urethane linkage at 3320 cm^{-1} and after reaction isocyanate (NCO) peak (2200 cm^{-1}) completely disappear

5.3.2- Physically Mixed Polyurethane/Nano-hydroxyapatite Composites

FTIR spectrum of physically mixed polyurethane/nano-hydroxyapatite is given in (Figure 4.13) and described in section 4.3.1.1.2, Chapter 4. The hydroxyl stretch at 3571 cm^{-1} were observed and the peaks assigned to asymmetric and symmetric CH_2 stretches were also observed, indicating that the polyurethane was also sharing the surface coating with hydroxyapatite. The spectrum clearly showed presence of intense

PO_4 band at 1017 cm^{-1}, although it was of reduced intensity compared to the nano-hydroxyapatite reference. Combined with the presence of hydroxyl and phosphate peak after mixing with polyurethane, this suggests that a bond between polyurethane and nano-hydroxyapatite has not been formed but merely a physical mixture. Hence, physical mixing only provided the nano-hydroxyapatite as filler particles but did not show any linkage and coating of the polymer on the surface. The physically mixed apatite in composite without linkage could lead to weight loss and abrasion on applying load. The presence of hydroxyapatite on surface could weaken the material due to release of particles and insoluble particles released from polymer and moved into adjacent area. It has been reported that dissolution of high surface area particulate could effectively minimise the fall in pH associated with healing process as hydroxide ions were released from the hydroxyapatite (Gross and Babovic, 2002).

5.3.3- Chemically Mixed Polyurethane/Nano-hydroxyapatite Composites

The representing FTIR spectrum of chemically mixed polyurethane/nano-hydroxyapatite composite is given in (Figure 4.14) and described in Section 4.3.1.1.3, Chapter 4. The *in-situ* polymerisation reaction was found to be more successful than physically mixed reaction. The possible reason could be due to the reactivity of hard segment with OH group of nano-hydroxyapatite at early stage. The reactivity led to grafting and developing of chemically linked composite, whereas, during physical mixing the hard segment has already reacted with soft segment and NCO (hard segment) groups were not available for OH group (nano-hydroxyapatite). Therefore, in physically mixed composites the nano-hydroxyapatite was present as loose particles in polyurethane. In chemically mixed spectrum the hydroxyl stretch was not seen in the spectrum after reaction, which suggested that linkage has occurred via the surface hydroxyl groups of soft segment and/or nHA. It is expected that approximately all OH groups from nHA have reacted with NCO group. The unreacted isocyanate (NCO) peak at 2200 cm^{-1} was not visible after the reaction. The (C—H) CH_2 stretch peaks were assigned at 2935 and 2859 cm^{-1} and attributed to asymmetric and symmetric stretching peaks of CH_2 respectively. The comparative spectra of PU and PU/nHA

composite are given in Figure 5.10. The difference was observed with PU spectrum, the intensity of bonded carbonyl peak was shifted to 1701 cm^{-1}. Peak at 1731 cm^{-1} was assigned to free C=O and peaks at 1716 and 1701 cm^{-1} were attributed to hydrogen bonded carbonyl linkage. Amide absorption bands appeared at 1598 and 1539 cm^{-1}. Peak at 1109 cm^{-1} corresponded to linkage between phosphate group (1040 cm^{-1}) of nHA and ether (1111 cm^{-1}) group of PU and assigned as P—C—O. The existence of amide bands and the disappearance of isocyanate band indicated that surface reactive groups of nHA indeed reacted with isocyanate groups and resulted in the formation of urethane linkage. The polyurethane on the surface of nHA was identified by the urethane linkage, CH_2 vibration, bonded C=O and C-O-C (P—C—O) vibration. The quantities of the C=O groups participating in hydrogen bonding is an assessment of the phase separation in the material (Ning *et al.,* 1996). Due to the relatively complex structure of nHA, it was difficult to propose that polyurethane could bond with apatite structure. It was expected that there was sharing of bond between –C, –O, and apatite structure. The –O and –C have charges before reaction and appeared as N=C=O, but after bonding HN—C—O showed the dipole moment. This study had already proved that nano-hydroxyapatite had large surface area (Section 4.1.5, Chapter 4), and possibly there were relatively large amounts of atoms on the surface and a large fraction of surface OH groups.

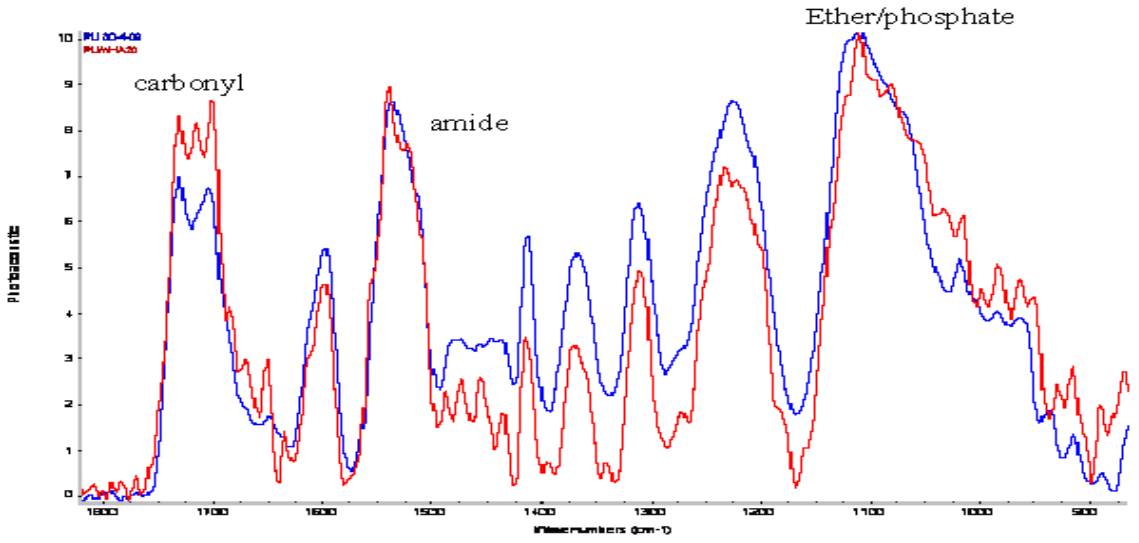

Figure 5.10 Comparative FTIR spectra of PU and PU/nHA composite showing carbonyl (1750-1650 cm^{-1}), amide (1550-1225 cm^{-1}) and ether/phosphate region (1100-900 cm^{-1})

The -OH group presented on the surface of nHA seems to be a reactive group, which could be used to make a covalent linkage with polymer. It was expected that linkage between polyurethane and nano-hydroxyapatite surface was a covalent linkage (urethane linkage: N—H). Covalent bonding of nHA with PU has the potential to improve the interface of composite matrix, therefore leading to significant improvement of the bioactive, bonding and mechanical properties.

5.3.4- Comparative Spectra of Composites with Different Concentrations of Nano-hydroxyapatite

The comparative FTIR spectra of different concentrations of nano-hydroxyapatite in polyurethane are given in (Figure 4.15) and described in Section 4.3.1.1.4, Chapter 4. These spectra exhibited the reactivity of functional groups of nano-particles towards polyurethane, mainly hydroxyl group (-OH) and isocyanate (-NCO) and helped in formation of urethane (N—H) linkage. With the increase in concentration of nano-hydroxyapatite the shifting of peak (Figure 5.11) was expected due to availability of more hydroxyl group and showed affinity toward isocyanate. Therefore, it is suggested that the –OH groups of nHA formed a linkage with the -NCO of isocyanate in addition with the –OH from polyether copolymer.

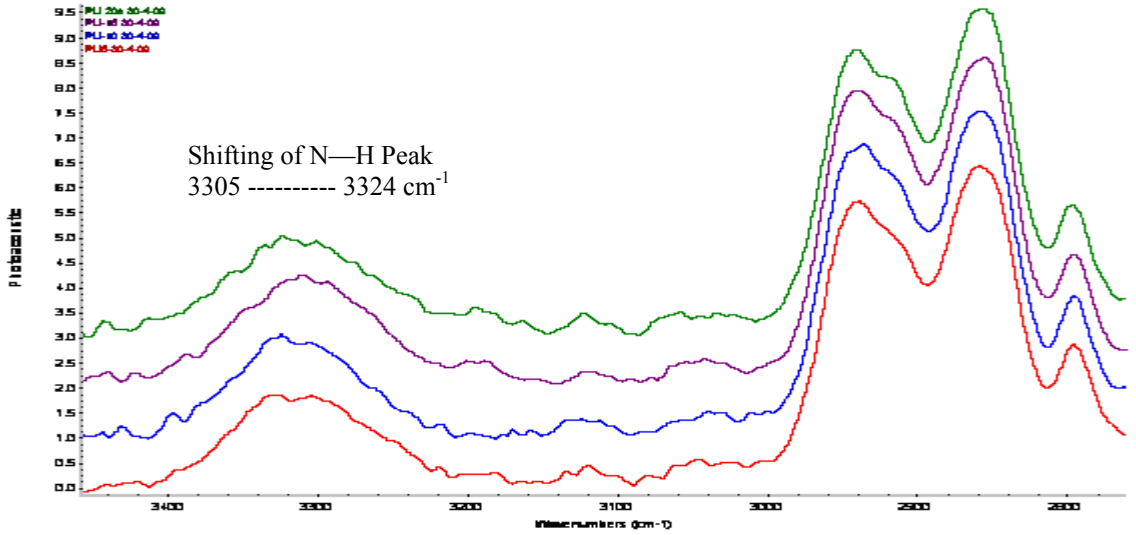

Figure 5.11 Comparative spectra of N—H band region of PU/nHA5 (red), PU/nHA10 (blue), PU/nHA15 (violet), and PU/nHA20 (green)

The FTIR spectra of carbonyl region (Figure 5.12) showed the hydrogen bonded urethane-carbonyl (N—H**….**C=O) and it was observed that urethane—carbonyl hydrogen bonded peak shifted with the increase in concentration of nano-hydroxyapatite and shoulder peaks emerged in this region. The carbonyl peaks were not only limited at 1731-1701 cm^{-1}, but with the increase in concentration of nano-hydroxyapatite (PU/nHA15 and PU/nHA20), new peaks appeared at 1716 and 1650 cm^{-1}, attributing to bonded carbonyl group. The carbonyl absorption peaks at 1695-1615 cm^{-1} were assigned secondary amide absorption bands. The bonded carbonyl peak created urethane-carbonyl (N—H**…..**C=O) hydrogen bond. The higher concentration of nano-hydroxyapatite helped in the formation of strong covalent and hydrogen linkages. It is expected that strong bonding between organic and inorganic components of restorative materials could improve the properties and applicable for clinical application with better results.

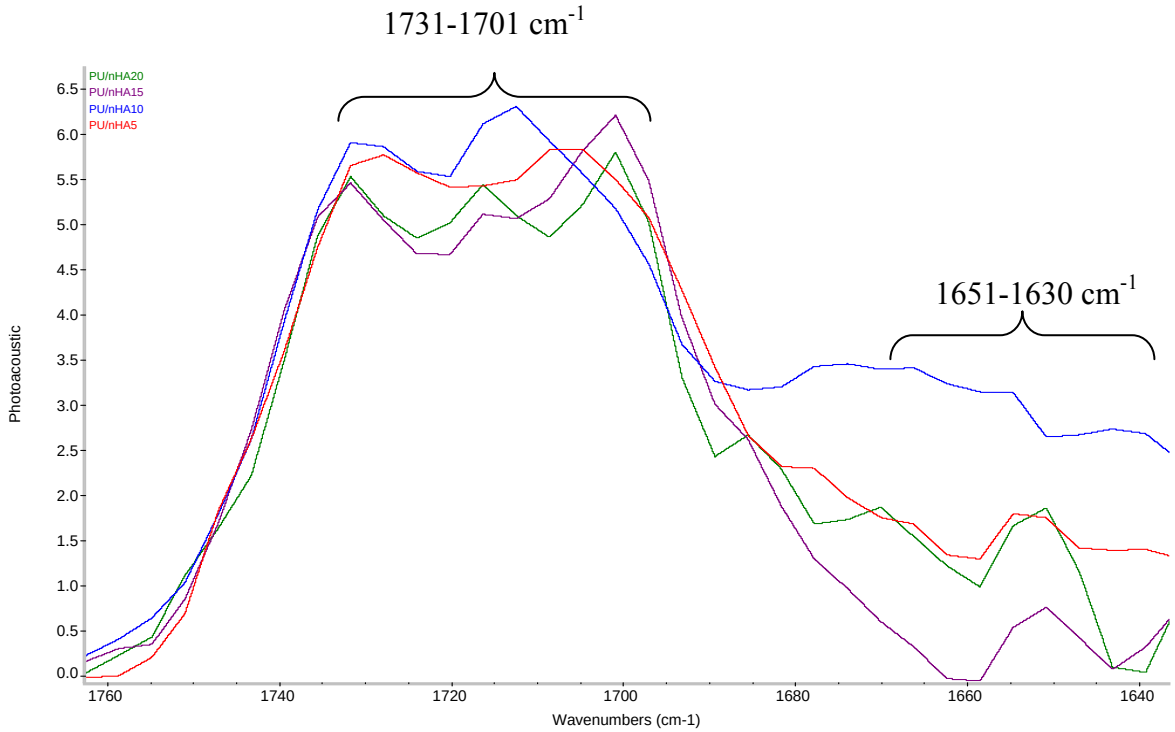

Figure 5.12 Comparative spectra of C=O band region of PU/nHA5 (red), PU/nHA10 (blue), PU/nHA15 (violet), and PU/nHA20 (green)

A limited number of studies (Li *et al.,* 1998; Dong *et al.,* 2001; El Hammari *et al.,* 2007) are reported in the literature investigating the effect of polyurethane on hydroxyapatite. In those studies HMDI and phenylphosponic acids were used to modify the surface of hydroxyapatite particles. It has been found that the surface P-OH groups of the hydroxyapatite could be regulated by modification with alkyl phosphates resulting in a more hydrophobic surface that has a higher affinity to other biomaterials.

Li et al. (1998) studied the grafting of isocyanate with nano-apatites; they compared the IR spectra of nano-apatite before and after grafting reaction, and claimed that there was no change of peak intensity at 875 cm^{-1}, and no new peak from P—O—C. Therefore, their data did not support the reaction mechanism between HPO_4^{-2} and isocyanate. El Hammari et al. (2006) studied the grafting of phenylphosphonic and phenylphosphite acids with porous calcium hydroxyapatite and they reported that there was a new peak which they suggested as P—C or C==C. In comparison to previous studies, current data showed shifting and emergence of peaks in this region and it was expected that phosphate group showed its reactivity towards ether group. The comparative spectra (Figure 5.12) showed change in peak intensity and emergence of new shoulder peaks at 1108-850 cm^{-1}, which was attributed to OP—C—O- [linkage of PO_4^{3-} and vibrational (C—O—C)].

It has been reported that if P—O—CO—NH existed, the carbonyl absorption band should be shifted to higher wave number at 1716 cm^{-1} (Dong *et al.,* 2001). Current data provided the evidence peak at 1716 cm^{-1}, indicating the formation of P—O—CO—NH bond. There are three possible reactive groups, which can react with isocyanate groups. These groups are surface absorbed water, HPO_4^{-3}, and OH^- (Arends *et al.,* 1987; Zhu *et al.,* 2006). It was maintained that before experimental procedure nano-particles were completely dried. Therefore, it was expected that no surface absorbed water involved in reaction with isocyanate (polyurethane). The HPO_4^{-3} on the surface of nano-apatite is due to non-stoichiometric structure or the hydrolysis of PO_4^{-3} ions on the surface (Li *et al.,* 1994; 1994a; Christoffersen and Christoffersen, 1982). Therefore, it is assumed that phosphate group has potential to react with polyurethane and help in linkage formation.

Raman spectroscopy (Figure 4.18) and ^{13}C NMR spectrum (Figure 4.21) compliment the FTIR data, confirming the presence of linkage between polyurethane and nano-hydroxyapatite. Raman spectroscopic studies have been limited to tissues, which contain only a few percentage of organic materials. Hence, the peaks of hydroxyapatite did not make significant effect on the intensity of the polyurethane peaks, but the additional peaks supported the claim that the linkage between the polyurethane and nano-hydroxyapatite existed. The ^{13}C NMR showed urethane and carbonyl peaks and change in peak position was observed after reaction. The successful bonding of nano-hydroxyapatite to polymer provided to make a chemically linked composite which was expected to show better properties. In this study, the data was based on ^{13}C NMR only, it is recommended to perform ^{1}H NMR and ^{31}P NMR to evaluate the linkage of phosphate with polyurethane.

5.3.5- X-ray Diffraction (XRD)

XRD patterns are given in (Figure 4.22-4.25) and described in Section 4.3.2.1, Chapter 4. These patterns showed that linkage of nano-hydroxyapatite was mainly with hard segment of the polyurethane and it was expected that there was no or very minimal linkage with the soft segment. Therefore, when the X-ray beams came on the hard segment section, the peaks of nano-hydroxyapatite also appeared on the pattern. The low intensity of peak as compared to polyurethane was due to presence of polyurethane on outer surface and the arrangement of nano-particles. If the dispersed atoms were not arranged periodically or regularly, but in are independent manner, the rays scattered in a random phase and appeared weak. However, if the atoms arranged periodically, then the scattering pattern should be strong because scattered rays cancel each other (Cullity and Stock, 2001).

5.3.6- Thermogravimetric Analysis (TGA)

Comparative TGA pattern is given in (Figure 4.27) and described in Section 4.3.3.1, Chapter 4. TGA was used to determine the temperature at which the complete burnout of polyurethane based composite occurred and showed the weight change of samples

with temperature. It was noticed that the nano-hydroxyapatite could enhance the heat resistance of polyurethane. The polyurethane/nano-hydroxyapatite (PU/nHA5) showed almost the same pattern as pure polyurethane with slight increase in the thermal stability. However, PU/nHA10, PU/nHA15, and PU/nHA20 composites showed enhancement in thermal stability. It was observed that with increase in concentration of nHA there was an increase in high temperature endotherm of samples.

The onset of decomposition temperature was increased slightly and full decomposition was increased to a higher temperature. It has been reported that incorporation of nano-particles could improve the thermal stability of the polymer composites (Gilman *et al.,* 2002; Yang *et al.,* 2005). Higher concentrated inorganic fillers greatly reduced the chemical bond movements of organic component, which led to higher decomposition temperature of the composites. The results in this study also indicated that the interfacial interactions of higher concentrated (nHA) composites such as PU/nHA20 were greater as compared to other samples. The significance of using thermally stable dental material is related to its clinical application in oral cavity, where variation in temperature (5-70°C) can be anticipated. If restorative materials show thermal stability then minimal changes in the matrix can be expected, which helps to keep the rigid structure of the material; however, the glass transition temperature is the key point to consider.

5.3.7- Differential Scanning Calorimetry (DSC)

The glass transition temperature (T_g) is determined with DSC (Figure 4.28) and described in Section 4.3.3.2, Chapter 4. Nano-hydroxyapatite and linkage with hard segment increased the ability of chains to undergo segmental motion which increased the T_g values. Unexpected behaviour was observed with PU/nHA10 composite, where the T_g became lower in this sample. It was assumed that it was due to disordered arrangement of crystals and mixing of hard and soft segment was not complete at higher temperature, therefore the peak at lower temperature was associated with disruption of some new poorly organise structure. The other reason could be due to relaxation of

mixed amorphous intermediate phase (soft and hard segment) and relaxation of enthalpy in crystalline part of these segments. The reason for higher T_g of PU/nHA15 and PU/nHA20 composite was due to high content of intermediate phase that could form additional hydrogen bonding with carbonyl groups. The enhancement of T_g indicated the presence of nano-apatite in hard segment and possible hydrogen bonding between them. It was assumed from this study that with the increase in concentration of nano-hydroxyapatite, the phase transition temperature was increased. Higher concentrations of nano-hydroxyapatite increased the crystallinity of composite which increased phase transition temperature of composite. It has been reported that amorphous material showed low phase transition temperature (Cao and Liu, 2006). Therefore, this study also revealed an increase of the internal order within the hard segment domains coupled with nano-hydroxyapatite. The phase separation observation with the increase in T_g, indicated that incorporation of nano-hydroxyapatite led to bond strength near inter-phase boundary. The presence of high endothermic peak was due to disordering of hard and soft micro-phase to form a homogeneous structure i.e. upon heating at high temperature, hard segment mixed with soft segments. However, in other study, Krol and Pilch-Pitera (2007) reported that T_g usually decreased with increase in length of a urethane segment, but there was increase in melting points with long linear urethane segment.

The other possible reason of higher T_g was increase in NCO/OH ratio, which restricted the mobility of molecular chain. It has been observed that with increase in content of hard segment the T_g of polyurethane increased. The addition of hard segment such as MDI enhanced the crosslinking of structure rather than phase separated structure (Yoon and Ratner, 1988). The crosslinking restricted the mobility of polymer chains; therefore the T_g increased. The T_g of soft segments shifted to some extent with change in concentration; this was an indication of phase mixing. In case of phase separation, the glass transition of soft segment should be relatively insensitive to variation in the ration of soft and hard segment (Desai *et al.,* 2000). This decreased chain mobility in structure proved another evidence of coupling in composite.

5.3.8- Conclusion

These results showed that a covalently linked PU/nHA composite was successfully developed. The chemical linkage of nano-hydroxyapatite with polyurethane was confirmed and comparison of physical and chemical mixing of polyurethane/nano-hydroxyapatite has shown that no linkage was present in physical mixed samples, whereas, chemical mixing showed covalent and hydrogen bonds. The FTIR, Raman and ^{13}C NMR spectroscopies confirmed the bonding of polyurethane with nano-hydroxyapatite. The presence of urethane linkage and bonded carbonyl group were analytically discussed. Different concentrations of nano-hydroxyapatite were used and it was noticed that 20% filler content showed significantly improved linkage compared to others. These improvements were attributed to presence of a great number of hydroxyl groups on surface and are available for bonding with isocyanate group. XRD patterns confirmed the presence of nano-hydroxyapatite in polymer and obvious differences were observed with physically mixed composite. Thermal properties also improved with increase in concentration of nano-hydroxyapatite.

5.4- Biostability Analysis

5.4.1- Introduction

The nHA affects the general properties of polyurethane based composite; however, further characterisations should be evaluated. It is necessary for newly developed bio/dental material for its suitability to be assessed. These newly developed composite networks are considered to be largely insoluble structures with chemically linked and thermally stable organic-inorganic components. These composites may absorb water and chemicals from the environment and may release components and this process may serve as precursor to a variety of physical and chemical reactions that cause a biological concern and deteriorating effects on the structure and function of the composites. These effects may include volumetric changes, physical changes such as plasticisation and softening, and chemical changes such as oxidation and hydrolysis. The presence of polyether in this composite is expected to be hydrolytically stable; however, it is

generally accepted that all polymers degrade to some extent. It is important to consider the hydrolytic stability of dental composite as they are prone to exposed to the environment such as saliva containing water. In this study, these criteria were achieved by taking biostability analysis in deionised water and phosphate buffer solution (PBS).

5.4.2- Contact Angle Measurements

Contact angle measurements are presented in (Figure 4.29) and described in Section 4.3.4.1.1, Chapter 4. The degree of contact angle allowed characterising the surface wettability of a material, and could act as an indicator of hydrophilicity/hydrophobicity of composite. An increasing contact angle means a decrease of surface wettability. In this study, it was expected that nHA incorporated effectively with PU micro-spheres and content of nHA incorporation increased with increase in concentration of nano-particles and resulted in more uniform particle distribution. The encapsulation of nHA particles and modification by grafting with polymer caused better dispersion in organic phase and less aggregate formation. This low aggregation was due to stabilising effect of polymer chain grafting onto nano-particles surface. This grafting process led to modification of inorganic particle surface and the surface became more hydrophobic and compatible with polymer (Qiu *et al.,* 2007). The hydrophobic behaviour of composite suggested a different molecular arrangement within surface. It has been well established that the nHA has high surface-volume area and high surface area has more functional binding sites for polymer. The interaction between PU and nHA indicates that small particles act as nucleating agents more effectively (Chen and Sun, 2005). This strong interaction between polymer and nano-apatite allow more resistance toward media**.** Liu *et al.* (1997) also suggests that water uptake for composite decreases with incorporation of nano-apatite into polymer.

5.4.3- Weight Loss Measurement

Weight loss measurements in deionised water and phosphate buffer saline are described in Section 4.3.4.1.2, Chapter 4 and the values tabulated in Table 4.18 and 4.19

respectively. The composites with higher concentration of nHA showed lower weight loss as compare to PU and composites with lower concentration. The weight loss continued to increase substantially, where weight loss occurred by dissolution of both inorganic particles and organic components in media. At 90 days, variations in results were observed, PU and PU/nHA composites (PU/nHA5, PU/nHA15 and PU/nHA20) showed almost same result whereas, PU/nHA10 showed higher values. It was assumed that there might be some agglomerated free dispersed nHA particles, which did not interact with PU. Nano-hydroxyapatite were expected to be encapsulated by polyurethane; however, there must be some leaching from the interface. The leaching of nano-particles could start later, since water diffused through matrix to reach the particle-matrix interfaces.

5.4.4- Fourier Transform Infrared Spectroscopy (FTIR)

The FTIR spectroscopy of PU and PU/nHA composites is described in Section 4.3.4.1.3, Chapter 4. Biostability was analysed in deionised water and PBS and the structural characterisations showed that there was no significant shifting and emergence of peaks. The interpretation was that there was no or very minimal adsorption of solution content during immersion. It has been reported previously that the polyether based polyurethane films incubated in PBS retained the characteristic infrared peaks (Christenson *et al.,* 2006).

It was evident from this study that during degradation process of PU there was broadness of peak at 3320 cm^{-1} that confirmed the adsorption of water on surface and formation of hydroxyl group. No evidence of hard segment leaching was observed from PU and PU/nHA composites. It is established that the isocyanate peak usually appeared at 2220 cm^{-1}, which was not observed in this study suggesting that there was no unreacted and leaching of unreacted isocyanate. Same behaviour was observed in carbonyl (C==O) and ether (C—O—C) region, where there was no significant shifting and broadness of peak. Therefore, it is claimed that there was no obvious chain scission, which proved that polyether based composite shows resistance toward water and PBS.

5.4.5- Raman Spectroscopy

Raman spectroscopy has been described in Section 4.3.4.1.4, Chapter 4. This spectral data obtained in this study supported the previously conducted studies on polyether based polymers (Loh *et al.,* 2007; Neugebauer, 2007). The intense bands showed absorption of water and it was expected that –OH formed a bond with aromatic and C—H peaks. CH structure behaved as donor whereas, water molecule behaved as acceptor. Hydrogen bonds possess cohesive interactions C—H—O where H and O carrying positive charge and negative charge respectively. Whereas, C is more negative even than on H (CH donors contain partial positive or zero charge on C); however, this shows that reaction is electrostatic predominantly, so it is also believed that these forces can be van der Waal forces, which weaken as the distance between the bonds increase (Steiner and Saenger,1993).

5.4.6- X-ray Diffraction (XRD)

XRD patterns are given in (Figure 4.46-4.50) and described in Section 4.3.4.1.5, Chapter 4. The patterns showed that broadness of peaks were almost same in all samples, which showed that there was no possible alteration in the structure of specimens. The possible explanation for decrease in intensity was due to basic characteristic of PU. Because of mobility of soft segments, the surface composition of segmented PU varied in order to find composition that could reduce the interfacial free energy. It was evident that when environment was polar i.e. water, PU has high proportion of polar hard segment at interface, whereas, more non-polar soft segment appeared at surface when environment was non-polar i.e. air (Wen *et al.,* 1997; Santerre *et al.,* 2005).

5.4.7- Scanning Electron Microscopy (SEM)

SEM results are presented in (Figures 4.51-4.53 and are described in Section 4.3.4.1.6, Chapter 4. The pitting of the surface was attributed to extraction of low-molecular

weight degradation product that resulted from chain scission. It was assumed that the extent of degradation was insufficient to cause noticeable surface damage. The cracks usually appeared in areas of devices where stress levels on polymer were high. However, fissures also appeared when even no additional stress had been placed on polymer. This micro-fissure phenomenon, known as environmental stress cracking, is believed to be a result of residual polymer surface stress (Santerre *et al.,* 2005). It was observed that cracks were present even before media ageing. It was expected that these cracks were generally produced due to hot pressing during sample formation. One of the disadvantages of hot pressing technique was the oxidative and thermal degradation of polyether urethane. It has been suggested that polyether urethane displayed the requisite level of hydrolytic stability, but is susceptible to oxidation, which was confirmed by in-*vivo* and in-*vitro* studies (Smith, 1987; Stokes *et al.,* 1987; Ratner *et al.,* 1988; Gogolewshi *et al.,* 1989). Therefore, it is recommended that for degradation analysis samples should be prepared by solvent casting technique. With solvent technique the resulting cracks can be avoided which appeared after hot pressing technique.

It has been reported that polyurethane composite based on less number of methylene (CH_2) groups exhibited more hydrolysis (Rehman, 1996); such as poly ether glycol (PEG) appeared to be less hydrolytically stable than PTMG. In this study, PU and PU/nHA composites were based on PTMG and observed result also supported the Schollnberger and Stewart's (1971) suggestion that polyurethane based on a higher methylene group concentration has better hydrolytic stability. The structures of PTMG are regular, so easy to form crystal structures and cohesion force of the soft segments is high; therefore water molecules find it hard to penetrate into film membranes. It is established that higher molecular weight polymers show better water resistance. Soft segments of higher molecular weight are easy to crystalline thus water molecules find it hard to penetrate into the membranes; therefore, water resistance increases (Bai *et al,* 2007). The contents of hard segment are other factors that control the amount of water absorption. With the increase in contents of hard segment, hydrophilicity increases due to presence of more urethane groups thus increasing water uptake (Lligadas *et al.,* 2007). In this data, the hydrolytic stability was due to formation of stable hydrogen bond

between hard segment and soft segment and stable hydrogen and covalent bond between nHA and PU components. It has been suggested that stable H-bonded hard segment micro-domains and other H-bond along chains contributed to the formation of protective structure and it is well correlated with *in-vivo* findings from several investigations (Pande, 1983; Pinchuk *et al.,* 1988: Santerre *et al.,* 2005). The process such as applied stress could affect the structure of hard segment and perturbation of this structure should also affect the biostability of PU (Hergenrother *et al.,* 1993). The stress-strain character of PU is highly dependent on nature of hard segment and their association with micro-domains (Smith *et al.,* 1987; Lelah and Cooper, 1987) and PU surfaces are highly correlated with H-bonded state of the PU (Tang *et al.,* 2001a:b).

5.4.8- Conclusion

The low weight loss in higher nHA concentrated composites could be due to strong interaction between nano-particles and polymers and formation of less water soluble compounds. Agrawal and Athanasiou (1997) and Verheyen et al. (1992) reported that blending of hydroxyapatite and polymer slowed the rate of degradation. Ara et al. (2002) also studied the calcium phosphate (CP) based polymer and found that with the inclusion of CP there was delay in rate of degradation. In this study, the control polymer and experimental polymer composites were based on hydrophobic polyols. It is suggested that the segmented polyurethane based on hydrophobic soft segment exhibited distinct micro-phase separation between hard and soft segment (Takahara *et al.,* 1991). Due to large difference in surface free energy between two segments, the polyol soft segment may be enriched at air-solid interface (Jayabalan *et al.,* 2000). The difference in weight loss can be explained by considering the concentration of nano-particles. Based on these results, it was assumed that main degradation was from polymer components. The incorporation of nHA in composites increased the resistance toward hydrolytica degradation. Hence, PU/nHA composites have acceptable biostability with no significant degradative effect and their long term properties were more superior to PU.

5.5- Bioactivity Analysis

5.5.1- Introduction

In the field of biomaterials, bioactivity is a well-known concept; however in dentistry it has received little attention. Attempts have been made to develop materials that possess bioactivity and promote remineralisation of tooth by releasing Ca^{2+} and PO_4^{2-} ions, but so far no truly bioactive dental material has been available commercially. In this study, the *in-vitro* bioactivity of experimental composites was investigated with SEM as described in Section 4.3.4.2.1, Chapter 4.

5.5.2- Scanning Electron Microscopy (SEM)

The apatite layer can reproduce on surfaces of bioactive material in acellular protein-free SBF with ion concentrations nearly equal to those of human blood plasma. It is envisaged from the SEM results that formation of an apatite layer on surface of synthetic material could provide favourable condition for synthetic material to bond to living tissue. The morphological appearance (Figure 4.55-4.58) showed that the surface layer consist of nano-sized apatites similar to bone mineral in its structure and composition. The apatite nucleation ability of each functional group largely varied depending upon the structure of substrate. This confirmed that samples with higher concentration of nHA had more tendencies to develop apatite layer as compared to composites with low concentration. It is reported that not only solid state functional group, but water soluble functional groups are also effective for apatite nucleation. Any organic polymer can exhibit bioactivity, if the surface is modified with a functional group effective for the apatite nucleation (Kokubo, 2005).

5.5.3- Fourier Transform Infrared (FTIR) and Raman Spectroscopy

It was interesting to note that the apatite layer formed on the PU samples after 21 days of immersion in m-SBF, although these samples did not contain any bioactive component. FTIR and Raman spectra of samples are described in Section 4.3.4.2.2,

4.3.4.2.3, Chapter 4 respectively. The PU spectra showed that the level of deposition of apatite layer was small and did not show the peak indicative of phosphate (calcification) deposit. This particular peak might not develop until there was substantial surface calcification. In comparison, PU/nHA composites showed initiation of apatite layer at day 1 and formation was observed at 7 days. However, compared to crystalline hydroxyapatite, the newly developed apatite layer composed of clusters with imperfect structural unit of apatite, which might be an embryonic form of ideal calcium apatite lattice. This was due to incorporation of carbonate and magnesium in the clusters layer, which might be the cause of the poorly crystalline structural arrangement. The coating released both Ca^{2+} and PO_4 ions by dissolution of amorphous phase after contact with m-SBF, resulting in an increase of super-saturation. The FTIR spectra showed that with increase in immersion time the broadness of N—H peak (3320 cm^{-1}) was due to water absorbance. The absorbed water appeared to bond on the structure of layer, i.e. layer was highly hydrated. The significant changes observed in ether/phosphate region were due to presence of phosphate group on the surface of apatite layer. It was expected that this newly developed apatite layer was mainly carbonated; therefore, changes were observed in the amide region of polymer. The presence of carbonate in apatite layer changed the structure and shifting of peaks and emergence of shoulders confirmed that apatite layer formed on the surface of samples.

5.5.4- X-ray Diffraction (XRD)

XRD patterns described in Section 4.3.4.2.4, Chapter 4 and showed that composites before and after immersion indicated the growth of apatite crystals relative to period of immersion. The presence of new peak was attributed to apatite reflections that indicated the differences in composition among the sample. However, the mechanism of apatite formation should be clear for those samples which do not contain any bioactive components.

The theory of apatite formation is based on complex processes that involve growth and control of nucleation from aqueous solution. The growth of apatite nuclei is due to uptake of calcium and phosphate ions from the solution. Generally nucleation in SBF

solution divides into two types: homogeneous nucleation occurs spontaneously in a solution, and heterogeneous nucleation occurs on a foreign substrate. It shows that SBF may induce heterogeneous nucleation and growth of apatite when in contact with foreign surfaces. It is interesting to find that either Ca^{2+} or phosphate can initiate the first step for nucleation. It has been anticipated from ionic nature that electrostatic interaction triggers the initial step of nucleation. Therefore, if Ca^{2+} ion adsorption triggers nucleation, such a surface may be negatively charged, whereas if phosphate ion adsorption initiates then the surface may be positively charged (Dalas *et al.,* 1991). Most of the macromolecules known to promote surface nucleation contain functional groups that are negatively charged at the crystallisation pH. Therefore, more negative charges on the surface may promote apatite formation (Li *et al.,* 2002).

The biological activity of polymer composite is low; the coating of their surface with hydroxyapatite layer can enhance this. It is expected that the layer coating on polymer-based material improves the tissue compatibility. Their surface property may transform to biological type of apatite (carbonate apatite) through a series of surface reactions including dissolution-precipitation and ion exchange. It has been suggested that formation of carbonate apatite on the surface of bioactive materials is thought to be participating to form a strong chemical bond (Stoch et al., 1999). The binding of Ca^{2+} ion is an initial step for calcification in living tissues. The polyurethane contained negatively charged, non-ionic group (CONH and OH) and positively charged group [(NH)-terminated] which are very weak apatite-inducing surfaces. The apatite formation is totally inhibited with the CH group. The apatite formation capability observed for negatively charged group-bearing surfaces apparently proceed by complexation of Ca^{2+} with surface negatively charged group and its subsequent complexation with phosphate ion. The adsorptions of a phosphate group on amino group terminated surface induce little apatite formation. This may be due to lack of complexation of Ca^{2+} ion with the phosphate ion-surface amino group complex. The calcium ion complexation with non-ionic groups such as CONH and OH proceeds via ionic-dipolar interaction. Low apatite formation induction in the case of CH-terminated might indicate that ion-induced dipole interaction between the hydrocarbon and Ca^{2+} ion, which is the weakest of

interaction forces among those of the interactions. The negatively charged surfaces act as a potent substrate for apatite nucleation (Tanahashi *et al.,* 1997).

It has been reported that a tight chemical bond that forms between bone apatite and the surface apatite, tends to reduce the interface energy between them. Alkali ions releasing from materials can be effective for accelerating the apatite nucleation, since increasing the ionic activity product of the apatite in SBF by increasing pH, i.e. concentration of OH ions which is a component of apatite (Kokubo, 1998). The apatite nuclei spontaneously have grown by consuming the calcium and phosphate ions from the surrounding fluid on the surface of the substrate in situ, to form a dense and uniform apatite layer. The growth of the apatite was controlled by adsorption of the ion at the surface or transport of ions between the apatite and solution (Kokubo, 1996).

5.5.5- Conclusion

The incorporation of nHA in these composites increased the bioactivity. The SEM images, XRD, FTIR and Raman Spectroscopy confirmed the presence of apatite layer on the surface of these samples. With the increase in concentration of nHA the thickness of apatite layer was observed. Hence, these PU/nHA composites have acceptable bioactivity and their long term biostablity was more superior to PU as described in Section 5.4. It is suggested that with these bioactive properties PU/nHA composites may interact with dentine and minimise the problems of interfacial linkage in existing composites.

5.6- Bioadhesion Analysis

5.6.1- Introduction

PU/nHA composite results are described in Chapter 4, Section 4.3.4.2, shows bioactive response in m-SBF. This study was conducted to investigate the potential use of nano-composites for dental applications and provided the evidence of enhanced bioactivity; however, it would be interesting to find the adhesion with hard living tissue

i.e. dentine. The adhesion is the prerequisite to subsequent cell functions e.g. proliferation, formation of mineral deposits. Bioadhesion analysis results described in Section 4.3.4.3, Chapter 4, provide the evidence that nano-apatite based polymers could promote adhesion and bond strength which is critical for the clinical success of the dental restorative materials.

The results obtained in this study were mainly based on the analysis of adhesion of the control materials i.e. Fuji IX and Filtek Supreme and experimental samples i.e. PU and PU/n-HA composites, with dentine structure. The bond strength of samples was characterised using Push-out test and the resulting samples were microscopically analysed using SEM (field emission and EDS). These methods are most widely used methods to quantitatively analyse the bonding of different materials with tooth structure while intact and after mechanical testing to observe the failure of adhesion at the interfacial level.

The development of resin bonding to tooth structure progresses through number of distinct stages, commonly known as generations. Due to difference in composition of enamel and dentine, the techniques for preparing the interface for increasingly hydrophobic monomers develop. The success of restorative dentistry concept has resulted in the usage of polymer-based sealers for endodontic treatments (Sly *et al.,* 2007). To evaluate bond strength, the push-out test is an efficient and reliable method because it allows assessment of regional difference in bond strength with acceptable variability of the data distribution. It is an appropriate method to analyse the bond strength at the adhesion interface (Nagas *et al.,* 2007).

5.6.2- Push-out Test

It has been reported that the superficial dentine layer of old extracted teeth showed most tubules apertures occluded, whereas, in freshly extracted teeth all tubule apertures were occluded. Therefore, the adhesive strength was always slightly greater with old extracted teeth than freshly extracted teeth. The lower density and much less intertubular dentine surface per unit area caused the decreasing adhesive strength in deep layer. Generally

dentine was believed to be more mature in the superficial layer (Nakamichi *et al.,* 1983). In this study, the non-linear bond strength with deionised water and artificial saliva with high standard deviation values were expected due to extracted human molar teeth which have been randomly selected, and the selection of teeth was anonymous. The cylindrical cavity was prepared and strength was analysed with deeper surface of dentine; therefore, it was assumed that the non-linear bond strength with higher standard deviation was due to interaction of composite with deeper surface of dentine. It is expected that load conditioning factors such as strain rate, machine's rigidity, load cell and speed control could affect the mechanical properties of the samples (Davis, 2004). It is recommended that a load cell that is exceedingly stiff (with very low compliance) or an instrument in which compliance is withdrawn by a feedback mechanism should be used (Lee et al., 2007). The load cell used for Fuji IX and Filtek Supreme are in accordance with the literature (Atai et al., 2004; Boyd and Towler, 2005). Until now, there is a lack of adequate knowledge and use of this variable for polyurethane based composites during push-out test, therefore; test results cannot be directly compared. However, it was claimed from manufacturers that Instron load cells have been tested for accuracy and repeatability on calibration apparatus traceable to international standards, with an uncertainty of measurement not exceeding one third of the permissible error of the load cell. The accuracy has been found to be equal to or better than 0.025 % of the cell rated output or 0.25 % of the indicated load, whichever is the greater.

The bond strength values of current study were low as compared to GC Fuji IX and Filtek Supreme. Previous studies showed that the bond strength of GIC and resin-based composite to tooth structure was 5-6 MPa (Wilson and McLean, 1988; Arora and Deshpande, 1998) and 26 MPa (Cunha *et al.,* 2007) respectively. Lucas et al. (2003) reported that HA-modified Fuji IX exhibited bond strength values of 5.2 MPa. In this study, the high variation in values was due to compositional difference of these restorative materials and the method of application in tooth cavity. Fuji IX derives from the formulation of alumino-silicate glass and carboxylic acids. The matrix of the set cement is a highly cross-linked structure and has tendency to adhere to dentine. In resin-

based composites, the mechanism involves the formation of a hybrid layer and the acidic conditioners dissolve the smear layer and demineralise the HA crystals of dentine surface, followed by infiltration of monomers into exposed collagen fibres (Lee *et al.,* 2008). In contrast to direct filling materials, Fisher et al. (2007) has reported the micro-push-out bond strength value of different obturating materials: zinc oxide-eugenol—based sealer and gutta percha (0.79MPa), epoxy amine resin—based sealer and gutta percha (2.00MPa), Epiphany sealer and Resilon (1.10MPa), Active GP obturation system (1.10MPa), and EndoREZ obturation system (0.09MPa). The current data were in accordance to obturating material and hypothesised the future application for endodontic treatment while providing direct adhesion and avoiding micro-leakages. Hence, these results helped to make the speculation that this novel bioactive material has potential for use as dental restorative material.

5.6.3- Scanning Electron Microscopy (SEM) / EDS

The morphological appearance with EDS analysis of PU/nHA composites showed that adherence could be due to ion-transport mechanism; ion transport is achieved through a coupling between the ions and polymer segmental motion, where the ionic transport takes place in the amorphous phase of a polymer matrix. This indicates that both soft and hard segments have an influence on ion transport (Zhu *et al.,* 2001). Dentine contains mainly Ca^{2+}, PO_4^{3-} and some minor ions such as Na^{+}, Mg^{+}, and F, whereas, the ether (C—O—C) and carbonyl groups (C=O) participate in transport of cations and contribute to ionic conductivity of the material. However, the bond strength of the PU samples was not sufficient enough to withstand the pressure applied during the push-out test.

It was speculated that the presence of Ca^{2+} and P in PU/nHA composites enhanced the pattern of apatite layer and more apatite layer was formed with the samples immersed in artificial saliva compared to deionised water due to the presence of ions in artificial saliva. The dentine proteins might have affinity toward Ca^{2+} ions and these proteins acted as calcium accumulators and reservoirs for apatite crystallisation. Therefore, these proteins played integral role in the laying down and maintenance of the calcified matrix

in dentine (Hoshi *et al.,* 2001). However, the SEM images showed that the attachments of the experimental composites were not sufficient enough as compared to existing resin-based dental composite. The procedure of adhesion of existing resin-based composite with tooth includes usage of adhesives; however, the gaps and porosity at interface is common due to polymerisation shrinkage that may have pulled out the resin tags from dentinal tubules (Griffiths *et al.,* 1999). The adequate adhesion at interface is crucial to the success of these resin-based restorations to reinforce tooth structure and provide a marginal seal that prevents leakage (Guzman-Ruiz *et al.,* 2001). It is expected that experimental time period also influenced the adhesion of composites with dentine as it has been reported that resorption of synthetic HA in 3 months is only 5.4% and it requires many years for complete resorption; however it acts as carriers for osteoinduction growth factors and osteogenic cell populations, which helps in their utility as bioactive delivery vehicles (Helm *et al.,* 2001). The nano-size and even distribution of the nHA is important for mechanical strength and possibly for tissue-bonding ability of the composites (Li *et al.,* 1995). The nHA can enhance the mineralised tissue, bone formation and bone adaption on its surface that provides an environment favourable to osteoblastic differentiation (Itoh *et al.,* 2004). There are certain factors which can affect the osteointegration between bone and an implanted material. These factors include a number of host biological and surrounding tissue responses, properties such as topography and chemistry control the type and magnitude of cellular and molecular events at the tissue implant interfaces, the design of biomaterial with surface properties of hard tissue and characterised by surface grain sizes in the nanometer scale that would lead to the formation of a new surface at the tissue/biomaterial interface and therefore improve the efficacy of biomaterial (Webster *et al.,* 1999).

In current study, the adhesion of the experimental composite with hard tissue was directly related to the tissue response at the material interface. The interfacial bonding mechanism showed that an acid condition might produce at composite and this acid condition was due to cellular activity and enzyme production. The acidic condition initiated partial dissolution of nHA, causing release of Ca^{2+}, HPO_4^{2-}, and PO_4^{3-}, and

enhanced the super-saturation of micro-environment with respect to the calcium-phosphate phase. The surface characteristics of nHA could be changed with this dissolution and a layer of carbonated-apatite could precipitate on the surface through seeded growth on nHA crystals (Cao and Hench, 1996; Seo and Lee, 2008). Furthermore, it is interesting to find out the influence of other matrix phases e.g. polymer on the HA tissue-bonding capacity, where urethane functional group can form a stronger bond to the collagen matrix of dentine. However, the guiding effect and the osteoconductivity of nHA is still a dominating effect in HA-containing composites (Hunter *et al.,* 1996). The crystalline dense nHA was used in this study, which was chemically linked with PU and the crystalline *nHA-coated-PU* have been used to provide an enhanced quality of bone apposition and rate of fixation for long term prosthesis. In comparison to dense HA, porous hydroxyapatite accommodates cells in the structure whereas, dense hydroxyapatite has rough surface which enables the growth and proliferation of cells on its surface (Cerroni *et al.,* 2002; Kumar *et al.,* 2005). The physically mixed polymer/HA shows instability and particulate debris reactions at the interface, whereas, the HA grafted polymer can induce the deposition of Ca^{2+} and PO_4 ions in the form of an hyroxyl-carbonate apatite layer and open the way for developing bioactive tissue-bonding (Cao and Hench, 1996).

5.6.4- Conclusion

This study showed adhesion of PU/nHA composite with dentine, however, the bond strength values were not high as compared to other restorative material. The difference in values was due to difference in the composition of the restorative material. It was interesting to find that apatite layer formed on the surface of material/tissue interface. This apatite layer showed tendency to make bond with tooth structure. Push-out test showed the bond strength values and SEM images with EDS analysis confirmed the adhesion of composite with hard tissue. It was found that with the increase in concentrations of nano-hydroxyapatite, the bond strength and adhesion increased ($p \leq 0.05$). Higher values and adhesion were achieved with the samples immersed in

artificial saliva as compared to deionised water, however the difference was not significant.

5.7- Biocompatibility

5.7.1- Introduction

A successful attempt has been conducted to design and produce bioadhesion, which simulates the surface topography of normal living hard tissue. However, these materials should be harmless to oral tissues. Furthermore, it should contain no toxic, leachable, or diffusible substance that can be absorbed into the circulatory system, causing systemic toxic responses, including teratogenic or carcinogenic effects. It is expected that cells placed in contact with a biomaterial surface may show a range of responses. The biocompatibility of a polymer depends on the specific adsorption of proteins onto the polymer surface and the subsequent cellular interaction (Beloti *et al.,* 2003).

5.7.2- Cell Culturing

The results of cell culturing and proliferation were described in Section 4.3.4.4.1, Chapter 4. In this study, polyether based polyurethane was used, which was hydrolytically resistant and showed prolonged stability. The *in-vitro* cytotoxicity study was performed to evaluate the biocompatibility of material, indicating cellular behaviour consisting of cell adhesion and growth pattern, which resulted from complex processes with biological and non-biological mechanisms. The extract dilution assays and direct contact assay on cell culture were used. In addition, MTS assay was used to determine cell viability in examining cell attachment and proliferation.

The cell seeded on the surface of polymers, while few cells might migrate to polystyrene surface in the plate, since the cells that migrated to the plate from polymer remained healthy. In addition, the direct contact could also provide information for the effects on cell-material interface as well as those samples were not releasing any toxic substances. These results suggested that both samples encouraged the cells to grow with favourable

cellular attachment; however, higher values were observed with PU samples as compared to PU/nHA composite. The possible reason was due to hydrophilic nature of PU and hydrophobic behaviour of PU/nHA. The general concept of cell interaction demonstrates that cells usually attach much more readily to hydrophilic materials than hydrophobic surface. The contact angle results (Figure 4.29) showed that PU/nHA20 were more hydrophobic than PU and the result of this study also exhibited that PU (comparatively less hydrophobic) showed more cell proliferation and differentiation than PU/nHA20 (more hydrophobic). However, it is not that only hydrophilic materials shows cell interaction, but the hydrophobicity also leads to improvement of cell adhesion and spreading (Schiraldi *et al.,* 2004). Cellular adhesion properties are critical for normal cell function as they determine subsequent cellular proliferation, morphology, and structural properties. The engagement of adhesion receptors may trigger second messenger responses within cells (Sank *et al.,* 1993).

Osteogenesis, induced by osteoblastic cells, was characterised by sequence of events, involving cell attachment and cell proliferation and followed by expression of osteoblast phenotype (Deligianni *et al.,* 2001). Clinical success of biomaterial is largely dependent on interaction with surrounding biological medium and success may be achieved when it is able to promote bone growth at its surface and osteoconductivity occurs without leading to an adverse reaction of host tissue (Redey *et al.,* 2000).

Among polymers good cell attachment and spreading are observed with high energy substrate and poor cell attachment and spreading on low-energy substrate, which is due to the minimal energetic state of a system in equilibrium. The affinity of cells towards surface is related to its high surface energy resulting from presence of polar chemical groups on the surface (Redey *et al.,* 2000). The microstructure of the PU and PU/nHA20 led to high elasticity for samples so they could tolerate the force imposed by cells for being stretched. The polyurethane surface supported a significant degree of cell spreading due to presence of hard segments, which were distributed throughout the soft domains (Sheikh, 2003). It is reported that hard segments are a necessary element for cell growth; however, cells can grow perfectly on the disperse phase of hard segments, but not on the continuous hard segment surface, where the other requirement for cell

growth is ratio of hard/soft segment. Lee et al. (1996) also reported that surface tension is not the only factor which affects the cell interaction but, microphase factor also influences cell growth on the surface of a sample. In view of this, some factors are important in determining cell growth on polyurethane and polyurethane based composites. The first factor is surface morphology and the existence of a dispersed phase (hard/soft). The second factor is hydrophilic (less hydrophobic) property and surface energy of materials.

It is possible to assess that cells are viable in the presence of HA and the viability levels are similar among different HA concentrations (Oliveira *et al.,* 2006). In this study only 20% wt/wt of nHA were used with PU. These results showed that samples with nHA also exhibited attachment and proliferation of the cells, suggesting marked biocompatibility of the samples. It is expected that the nanostructures provided the dense surface, which in turn increased the surface energy, while the high surface energy promoted initial attachment and spreading of the cells and improved their attachment (Li *et al.,* 2007). However, the effect of hydroxyapatite properties on tissue response has not yet been fully understood. The cellular responses depend upon physical and chemical characteristics of substrate and particularly relate to the chemical composition, crystallinity, particle size, and surface structure. The chemical and crystallographic characteristics are reported to influence osteoblastic activity. Variation in surface texture or micro-topography may affect the cellular growth and that induces the specific adsorption of proteins, which influence the cell reaction and it is noticed that there is significantly larger level of cell attachment on the rough surfaces (Deligianni *et al.,* 2001).

Cell proliferations are inversely related to the HA particle size. It is suggested that nHA particles could stimulate osteoblastic proliferation more compared with micro-HA. This is due to enhanced interfacial adhesion of nHA to cells and high surface area per HA volume for cell growth, which might result in increased cellular adherence and proliferations (Shi *et al.,* 2009). The morphology of HA was another parameter for estimating the biological effect. The cell experiments showed that nHA with spherical structure showed more favourable properties than rod-like HA for osteoblasts. This

might be due to well organised surface which seems beneficial (Zhao *et al.,* 2007; Shi *et al.,* 2009). This study also supported these concepts because spherical nano sized hydroxyapatite was used with polyurethane that exhibited hydrophobic surface with high surface energy.

5.7.2.1-Conclusion

In conclusion, it was observed that the PU and PU/nHA20 composites were not cytotoxic, biocompatible and cells adhered and proliferated well when compared to control plastic plate. In addition, MTS assays revealed that cells were able to grow and proliferate. During cell culture, extra care should be provided due to sensitivity of cells to some components. Hence, the biocompatibility test showed that the PU/nHA20 showed low rate of cell growth compared to PU; however, the cells were still growing and facilitated both adhesion and proliferation. It is suggested that cell behaviour and interaction with a bioactive material surface were dependent on physical and chemical properties such as topography, hydrophilicity/hydrophobicity, surface charge and composition i.e. micro-phase structure.

5.7.3- Bacterial Adhesion

The *in-vitro* bacterial adhesion analysed in this study were carried out in static and submerged conditions and in non-nutrient media. The results are described in Section 4.3.4.4.2, Chapter 4. The number of attached bacteria (colony forming) per cm^2 of the polymeric surface were determined and observed during first 2 hours. The initial rate of cell adhesion to the surface was described as first order dependency on cell concentrations. The correlation was not found between substrate surface free energy and adhesion of all bacterial strains. In this period of time the adhesion of the bacteria were not related to the surface hydrophobicity/hydrophilicity and it is suggested that the number of bacteria adhering after 1 hour was much more strain dependent than substratum dependent (Gottenbos *et al.,* 2000; Karakecili and Gumusderelioglu, 2002).

S. sanguinis is a member of the viridans group of streptococci. It is the first bacteria to colonise tooth surfaces, where it functions as a 'pioneer' by forming dental plaque, which leads to dental caries, periodontal diseases, and alteration of dental restorations. *S. sanguinis* has been reported to be closely related to infective endocarditis, which is frequently caused by oral bacteria (Yamaguchi *et al.,* 2006). They possess only a single sortase (Srt) gene in its genome. It has been reported that Srt gene might be involved in bacterial adhesion and colonisation because Srt A anchors one or more surface proteins associated with adhesion. Hence, it is assumed that Srt A is one of factor for infection and colonisation (Yamaguchi *et al.,* 2006).

Due to clinical application, the incidence of infections related to biomaterials is increasing (Kiem *et al.,* 2004). To avoid biomaterial related infections, it is important to understand the pathogenesis of infections. Bacterial adhesion to biomaterial surfaces is believed to be an essential step in the pathogenesis of these infections. The mechanism of bacterial adhesion are not defined; however, a variety of factors influence initial bacterial adhesion i.e. presence of adhesive molecules and dissolved proteins and surface properties of both bacteria and biomaterials (Karakecili and Gumusderelioglu, 2002). Therefore, there are two main approaches to prevent bacterial adhesion with the biomaterial surface; i) development of polymers with antiadhesive properties, (ii) development of polymers with antimicrobial properties (Pavithra and Doble, 2008).

The physical and chemical surface properties of biomaterials represent important determinants of adsorption of bacterial adhesion and colonisation. A new biomaterial can be developed by substitution of different chemical groups on polymer chains or by polymerisation of appropriate monomers. These copolymers could induce specific interactions with the components of living systems (Berlot-Moirez *et al.,* 2002). Surface modification of the polymer can achieve (i) reducing adhesion of proteins on the surface, (ii) promoting attachment and adhesion of certain types of cells, (iii) reducing bacterial adhesion, (iv) improving chemical inertness, (v) eliminating segregation of constituents on the surface and (vi) improving the degradation resistance (Pavithra and Doble, 2008).

This study showed less number of bacterial adhesions on PU/nHA20 as compared to PU. Three primary factors that influence bacterial adhesion on a polymeric surface are the (i) nature of the environment i.e. temperature, time of exposure, bacterial concentration, the presence of antibiotics and fluid flow condition near the surface, (ii) type of microorganism i.e. surface properties of the organisms, presence of fimbriae and flagella, and the production of an extracellular polysaccharide coat and (iii) the properties of the materials; surface chemistry and charge, microarchitecture, degree of hydrophobicity/hydrophilicity and hydrodynamic forces acting on the material (Pavithra and Doble, 2008). In comparison with other restorative materials it was reported that unpolished glass ionomer showed more bacterial adhesion as compared to unpolished resin-based composite, whereas, after polishing resin-based composite showed more surface roughness and bacterial adhesion increased. The binding of bacteria on glass ionomer was due to more inorganic particles i.e. roughness on the surface (Carlen *et al.,* 2001). In infected root canals, surface attachment capacity may be of significance in the pathogenesis since bacteria are found to invade dentinal tubules and morphological observations have indicated that organisms attach to the inner dentinal walls of infected root canals (de Paz *et al.,* 2005).

The surface free energy of solid surfaces gives a direct measure of intermolecular or interfacial attractive forces. The microbial adhesion to surfaces with different surface energies was analysed. It is suggested that microbial adhesion is less to low-energy surfaces (Hamza *et al.,* 1997); however, there are some contrary findings that high-energy surfaces have less adhesion than low surface energy (Brink *et al.,* 1993). Baier and Meyer (1992) recommended 20-30 mJ/m^2 as the optimum range of the surface energy of a surface to inhibit adhesion and suggest that the efforts to reduce surface energy below this range are counterproductive (Zhao *et al.,* 2007). However, in this current study, the surface energy was not measured but it was expected that PU/nHA20 has higher surface energy than PU, so this study was in support of Brink et al. (1993) suggestions or it could be assumed that surface energy was in the range of mentioned value.

Surface properties such as hydrophobicity, hydrophilicity, steric hindrance, surface roughness and surface topography all affect attachment of bacteria. Pasmore et al. (2002) observed that bacterial cells were readily removed from the smooth surface, with removal becoming more difficult after long attachment time (Webster *et al.,* 2005). The quality and crystallinity of the HA is also another factor to affect the results. The dense HA used in this study was purely crystalline and with expected smooth surface; however, it was reported that after implantation the surface became rougher due to absorption and the roughness of HA surface was prone to microbial attachment (Ichikawa *et al.,* 1998). The origin of adhesion in HA-base was mainly ascribed to wettability of the substrates. However, different methods applied to modify surface energy and wettability properties mainly allow on/off switching of the wettability (Aronov *et al.,* 2007).

5.7.3.1- Conclusion

It is summarised that the surface of materials need to be modified to prevent the bacterial adhesion. The promising trend in the development of biomaterial is based on development of advanced materials with biomimetic features on surface. The modification of surface properties enhances the surface affinity to selective adhesion and proliferation of biological cells and tissue compatibility.

5.8- Synthesis of Electrospun Nano-fibres

The above results based on biostability, bioactivity, bioadhesion and biocompatibility confirmed the successful development of a novel composite. The difference of physical and chemical synthesis of composite was further assessed by fabricating the nano-fibres. These fibres resulted in polymeric sheets or fibre mats. In this study, the resulting electrospun fibres (Section 4.4, Chapter 4) were of three different types: linked meshwork, meshwork with loose nano-particles and beaded fibres. It is expected that these fibres will provide useful information about the confirmation of chemically linked

polymer composite and it was hypothesised that these fibres will be later used to reinforce the nano-composites to increase the mechanical and physical properties.

The electrospinning process depend on the condition applied (voltage and flow rate) and the solution, and these are varied to form fibres or drops. The selected polymer composites were dissolved in DMF to prepare 10% wt solution. The resulting fibres and drops were characterised with SEM. The parameters which influenced the results were applied voltage, solvent type, polymer solution flow rate, and polymer concentration (Cai and Singh, 2004). The thick coating of the nano-fibres was not achieved in this study due to short period of time. This study mainly focused on the electrospinning process for the production of nano-fibres and assessed the morphological behaviour. The reduction in diameter from a millimetre scale to nano-scale was due to instability, where the jet was stretched by whipping and bending. Electrospinning was driven by electrostatic forces and required only small amount of polymer solution (Berkland *et al.,* 2004). It was reported that the electrospun beaded nano-fibres of the polymers were related to the instability of the jet of polymer solution (Lee *et al.,* 2003; Berkland *et al.,* 2004). The smoothness and splaying of nano-fibres was attributed to the increasing DMF volume fraction, surface tension and viscosity decreased, while conductivity and dielectric constant increased. The solvent composition and various solution properties conducted an important role in determining the fibre formation (Lee *et al.,* 2003). The size of nano-fibres depends on the incorporation of nHA that could cause the increased viscosity of the solution. The increase in viscosity of the solution was due to the increased molecular entanglement or linkage between polyurethane and nano particles. In order to confirm the presence of nHA in fibres, EDS was performed with SEM. The elements of calcium and phosphate were not present in polyurethane fibres, however presence of these elements was observed from nHA in PU/nHA composite. Hence it was confirmed that particles existed in fibres. In PM fibres the nano-particles were present mainly on the surface and were not completely incorporated within the fibres. In comparison, there were no visible nano-particles on CM fibres. The bonding between the polyurethane and nHA has been proven in this study and no nHA particles were observed in SEM images, it showed that the interface

between polyurethane and nHA has been linked. It is established that the presence of Ca^{2+} stimulates osteoblastic proliferation and depress osteoclast-mediated bone resorption through negative feedback loops (Yoshimoto *et al.,* 2003) and high concentration of P induces osteoblasts apoptosis (Zaidi *et al.,* 1991). Higher concentration of Ca^{2+} promotes osteoblastic differentiation, leading to bone mineralization. This response contributes to maintenance of bone homeostasis, and the differential reactivity (Maeno *et al.,* 2005). Through the electrospinning process, nano-fibres results in high specific area that is advantageous for its biomedical and dental application. The nano-fibres were randomly distributed with no clear alignment. Electrospun nano-fibre orientation can be explained using a fibre orientation angle. Fibre orientation angle in nonwoven mats can be described as the angle formed between the fibre axis and a line parallel to the web centerline (Meleti *et al.,* 2000). Charged forces on the fibres, with the help of accelerating and deflecting electric fields, leads the fibres to form three dimensional structures (Doshi and Reneker, 1995). The random distribution of nano-fibres in all directions could be due to the spiral shape of electrified jet with increasing radial dimension. HA is known to enhance cell adhesion through an inherently high capacity of adsorbing proteins. With in the scope of this SEM images, it was observed that there were no holes and pores in nano-fibres, this would enhance the reinforcement of composite and the mechanical properties.

Chapter 6 Conclusions and Future Works

6.1- Conclusions

- A novel bioactive composite based on nano-hydroxyapatite with chemically linked polyurethane has been synthesised using chemical mixing with *in-situ* polymerisation process.
- FTIR, Raman and ^{13}C NMR spectra confirmed the urethane linkage. FTIR spectra indicated the presence of a new peak at 3324 cm^{-1}. The appearance of bonded C=O peaks in between 1716-1700 cm^{-1} also confirmed the urethane**….**carbonyl hydrogen bond and it was observed that with the increase in concentration of nano-particles, the urethane-hydrogen bond peak became more intense. Coupling is believed to occur between the phosphate and ether group and formed P—C—O.
- The thermal properties of polyurethane and polyurethane/nano-hydroxyapatite composites were analysed using TGA and DSC. The TGA curve showed that thermal decomposition of composites was increased with higher concentrations of nano-apatites indicated strong molecular interaction of organic-inorganic components. DSC thermograms showed endothermic peaks at higher temperature attributed to increase crystallinity and molecular arrangement.
- The novel composites were assessed for hydrolytic stability and were characterised with FTIR, Raman, XRD, and SEM. Contact angle measurement was analysed and it was found that composites with higher concentration of nano-hydroxyapatite were more hydrophobic and showed long-term stability.
- The *in-vitro* bioactivity analysis showed that the presence of nano-hydroxyapatite accelerated the precipitation of apatite layer on the surface and it showed that with the increase in concentration of nano-hydroxyapatite the thickness of calcium phosphate (apatite) layer increased. The formation of layer on polyurethane was observed at 21 days due to nucleation process, however, polyurethane/nano-hydroxyapatite composites showed the pattern of apatite layer at 7 days and with the

increase in immersion time the globules of apatite layer were tightly packed with each other.

- The bioadhesion with dentine showed the adherences were achieved at the interface between the composite and tooth. The samples immersed in artificial saliva showed more adherence and bond strength values than deionised water, however the difference was not significant. The presence of calcium-phosphate component in composite enhanced the adhesion compared to polyurethane. The bond strength values of the novel composite was not higher compared to existing direct restorative materials, however, the values were in accordance with existing obturating materials e.g. gutta percha and Resilon.
- The biocompatibility was achieved performing cell culturing and bacterial adhesion. It was interesting to find that both samples i.e. polyurethane and polyurethane/nano-hydroxyapatite showed cell proliferation on the surface; however more growth were observed with polyurethane due to hydrophilic nature of polyurethane samples. In comparison there was 97.09% reduction in bacteria adhering to the grafted composite compared to polyurethane.
- The nano-fibres of composite were successfully collected by electrospinning process. The morphological appearance of the chemically mixed nano-fibres was smooth and uniformed size with no visible nano-hydroxyapatite particles on the surface. These high surface area nano-fibres would have potential to reinforce the composites in biomedical and dental applications because of their bioactivities and capability to have tailor-made mechanical properties.
- It is proposed that this bioactive composite could be use as dental materials, especially for endodontic obturations. The direct bonding was achieved and it is expected that this bonding will provide a mean of improving the interfacial linkages not only between the two phases but also with the living tissues. Excessive characterisations confirmed its suitability to use dental restorative materials, however further characterisations specifically *in-vivo* studies should be performed.

6.2- Future Works

The data showed the covalent linkage between the polymer and nano-particles and the physical and thermal and biostability results proved that this material could be used for dental and biomedical applications. By achieving the resulting data presented in this study, there is a scope for further work and potential for advance studies based on these findings.

It would be interesting if the further studies would be conducted on mechanical and biological bases.

1- Mechanical Testing

The viscoelastic properties should be assessed using Dynamic Mechanical Analysis. It is important to find out the strength and the elongation behaviour along with elastic modulus of the samples.

2- Bioadhesion

As it is hypothesised that this novel composite is to be used in root canal obturations, its bioadhesion properties should be investigated with root dentine using push out test and SEM. The adhesion should be compared in deionised water and artificial saliva with existing obturating materials i.e. Gutta Percha and Resilon.

3- Biocompatibility

a- Cell Culturing

Osteoblasts like cells are to used in prolonged studies (at least 14-21 days) with alkaline phosphatase (ALP) enzyme activity to assess cell differentiation.

b- Bacterial Adhesion

The bacterial adhesion of the novel composite with other bacteria such as *Streptococcus mutans*, E. coli, and anaerobes are to be assessed with extended time period e.g. 24-48 hours and varying time intervals. The experimental samples should be divided into two segments; (i) dry samples, (ii) pre-soaked with artificial saliva.

4- Clinical Assessment

The clinical practicality of obturating the root canals with the novel composite is to be explored *in-vivo*.

References

Abu Bakar MS, Cheang P, Khor KA., 2003, Mechanical properties of injection molded hydroxyapatite-polyetheretherketone biocomposites. Composites Science and Technology, 63, 421-425.

Achilias DS, Karabela MM, Sideridou ID., 2008, Thermal degradation of light-cured dimethacrylate resins Part I. Isoconversional kinetic analysis. Thermochimica Acta, 472, 74-83.

Adabo GL, dos Santos Cruz CA, Fonseca RG, Vaz LG., 2003, The volumetric fraction of inorganic particles and the flexural strength of composites for posterior teeth. Journal of Dentistry, 31, 353-359.

Adhikari R, Gunatillake PA, McCarthy SJ, Meijs GF., 2000, Mixed macrodiol-based siloxane polyurethanes: Effect of the comacrodiol structure on properties and morphology. Journal of Applied Polymer Science, 78, 1071-1082.

Adhikari R, Guntilake PA, McCarthy SI, Meijs GF., 1999, Effect of chain extender structure on the properties and morphology of polyurethanes based on H_{12}MDI and mixed macrodiols (PDMS-PHMO). Journal of Applied Polymer Science, 74, 2979-2989.

Agrawal CM and Athanasiou KA., 1997, Technique to control pH in vicinity of biodegrading PLA-PGA implants. Journal of Biomedical Materials Research (Applied Biomaterials), 38, 105-114.

Ahmad Z,. 2007, Synthesis and novel processing of polyurethanes. PhD Thesis, University of London.

Ajayan PM and Tour JM., 2007, Materials Science: Nanotube composites. Nature, 447, 1066-1068.

Alberola ND, Merle G, Benzarti K., 1999, Unidirectional fibre-reinforced polymers, analytical morphology approach and mechanical modelling based on the percolation concept. Polymer, 40, 315-328.

Ambard JA and Mueninghoff L., 2006, Calcium phosphate cement: Review of mechanical and biological properties. Journal of Prosthodontics, 15, 321-328.

Angker L, Swain MV, Kilpatrick N., 2003, Micro-mechanical characterisation of the properties of primary tooth dentine. Journal of Dentistry, 31, 261-267.

Antonakos A, Liarokapis E, Leventouri T., 2007, Micro-Raman and FTIR studies of synthetic and natural apatites. Biomaterials, 28, 3043-3054.

Antonio N., 2003, Ten Cate's Oral Histology, development, structure, and function, 6th edition, Mosby, USA.

Anusavice JK., 2003, Phillip's Science of Dental Materials, 11th edition, Elsevier Science, USA.

Aoki H., 1991, Medical application of hydroxyapatite. In: Aoki H, Sawai K., Science and medical applications of hydroxyapatite. pp.1-214, Takyama Pres System Centre, Tokoyo.

Ara M, Watanabe M, Imai Y., 2002, Effect of blending calcium compounds on hydrolytic degradation of poly (DL-lactic acid-co-glycolic acid). Biomaterials, 23, 2479-2483.

Arcis RW, Macipe AM, Toledano M, Osorio E, Clemente RR, Murtra J, Fanovich MA, Pascual CD., 2002, Mechanical properties of visible light-cured resins reinforced with hydroxyapatite for dental restoration. Dental Materials, 18, 49-57.

Arends J, Christoffersen J, Christofferson MR, Eckert H, Fowler BO, Heughbaert JC, Nancollas GH, Yesinowski JP, Zawacki SJ., 1987, A calcium hydroxyapatite precipitated from an aqueous solution. Journal of Crystal Growth, 84, 515-532.

Aronov D, Karlov A, Roseman G., 2007, Hydroxyapatite nanoceramics: Basic physical properties and biointerface modification. Journal of the European Ceramic Scociety, 27, 4181-4186.

Asaoka K and Hirano S., 2003, Diffusion coefficient of water through dental composite resin. Biomaterials, 24, 975-979.

ASM-International, 1996, Metals Handbook Ninth Edition, volume 10, Materials Characterization, ASM Handbook Committee. Metals Park, Ohio.

Atai M, Nekoomanesh M, Hashemi SA, Amani S., 2004, Physical and mechanical properties of an experimental dental composite based on a new monomer. Dental Materials, 20, 663-668.

Aurobind SV, Amirthalingam KP, Gomathi H., 2006, Sol-gel based surface modification of electrodes for electro analysis. Advances in Colloid and Interface Science, 121, 1-7.

Babu EJP, Savithri S, Pillai STU, Pai CB., 2005, Micromechanical modelling of hybrid composites. Polymer, 46, 7478-7484.

Bai CY, Zhang XY, Dai JB, Zhang CY., 2007, Water resistance of the membranes for UV curable waterborne polyurethane dispersions. Progress in Organic Coatings, 59, 331-336.

Baier RE and Meyer AE., 1992, Surface analysis of fouling-resistant marine coatings. Biofouling, 6, 165-180.

Balamurugan A, Kannan S, Rajeswari S., 2003, Synthesis of hydroxyapatite on silica gel surface by using glycerine as a drying control chemical additive. Materials Letters, 57, 1244-1250.

Banwell CN., 1994, Fundamentals of molecular spectroscopy. 4th edition, McGraw-Hill.

Beech DR., 1972, A spectroscopic study of the interaction between human tooth enamel and polyacrylic acid (polycarboxylate cement). Archives of Oral Biology, 17, 907-911.

Beloti MM, Hiraki KRN, Barros VMR, Rosa AL., 2003, Effect of chemical composition of Ricinus communis polyurethane on rat bone marrow cell attachment, proliferation, and differentiation. Journal of Biomedical Materials Research, 64A, 171-176.

Berkland C, Pack DW, Kim K., 2004, Controlling surface nano-structure using flow-limited field-injection electrostatic spraying (FFESS) of poly ($_{D,L}$-lactide-co-glycolide). Biomaterials, 25, 5649-5658.

Berlot-Moirez S, Djavid GP, Montdargent B, Jozefowicz M, Migonney V., 2002, Modulation of Staphylococcus aureus adhesion by biofunctional copolymers derived from polystyrene. ITBM-RBM, 23, 102-108.

Best SM., 1990, Characterisation, sintering and mechanical behaviour of hydroxyapatite ceramics. PhD Thesis, University of London.

Bigi A, Boanini E, Rubini K., 2004, hydroxyapatite gels and nanocrystals prepared through a sol-gel process. Journal of Solid State Chemistry, 177, 3092-3098.

Bilginer S, Esener T, Soylemezoglu F, Tiftik AM., 1997, The investigation of biocompatibility and apical microleakage of tricalcium phosphate based root canal sealers. Journal of Endodontics, 23, 105-109.

Billmeyer Jr. WF., 2000, Textbook of polymer science. pp. 238-290, John Wiley & Sons, Singapore.

Blackwell J, Lee CD., 1984, Hard-segment polymorphism in MDI/diol-based polyurethane elastomers. Journal of Polymer Science: Polymer Physics Edition, 22, 759-772.

Bonfield W, Grynpas MD, Tully AE, Bowman J, Abram J., 1981, Hydroxyapatite reinforced polyethylene —a mechanically compatible implant for bone replacement. Biomaterials, 2, 185-186.

Bonzani IC, Adhikari R, Houshyan S, Mayadunne R, Gunatillake P, Stevens MM., 2007, Synthesis of two-component injectable polyurethanes for bone tissue engineering. Biomaterials, 28, 423–433.

Bose S, Saha SK., 2003, Synthesis of hydroxyapatite nanopowders via sucrose-templated sol-gel method. Journal of American Ceramic Society, 86, 1055-1057.

Bouchemal K, Briancon S, Perrier E, Fessi H, Bonnet I, Zydowicz N., 2004, Synthesis and characterization of polyurethane and poly(ether urethane) nanocapsules using a new technique of interfacial polycondensation combined to spontaneous emulsification. International Journal of Pharmaceutics, 9, 89-100.

Bouyer E, Gitzhofer F, Boulos IM., 2000, Morphological study of hydroxyapatite nanocrystal suspension. Journal of Materials Science: Materials in Medicine, 11, 523-531.

Bowen RL and Marjenhoff WA., 1992, Dental composites/glass ionomers: the materials. Advances in Dental Research, 6, 44-49.

Boyd D and Towler MR., 2005, The processing, mechanical properties and bioactivity of zinc based glass ionomer cements. Journal of Materials Science: Materials in Medicine, 16, 843-850.

Braga RR and Ferracane LJ., 2004, Alternatives in polymerization contraction stress management. Critical Reviews in Oral Biology and Medicine, 1, 176-184.

Braga RR, Ballester RY, Ferracane JL., 2005, Factors involved in the development of polymerization shrinkage stress in resin composites, a systematic review. Dental Materials, 21, 962-970.

Breitmaier E and Voelter W., 1987, Carbon-13 NMR Spectroscopy. 3rd Edition, VCH.

Brenda KE., 1992, Synthesis and characterisation of strain-sensitive polyurethane-diacetylene copolymer coatings. PhD Thesis, University of London.

Breschi L, Mazzoni A, Ruggeri A, Cadenaro M, Di Lenarda R, Dorigo EDS., 2008, Dental adhesion review: Aging and stability of the bonded interface. Dental Materials, 24, 90-101.

Bretcanu O, Samaille C, Boccaccini AR., 2008, Simple methods to fabricate Bioglass-derived glass–ceramic scaffolds exhibiting porosity gradient. Journal of Materials Science, 43, 4127-4134.

Brink LES, Elbers SJG, Robbertsen T, Both P., 1993, The anti-fouling action of polymers preadsorbed on ultrafiltration and microfiltration membranes. Journal of Membrane Science, 76, 281-291.

Brosco HV, Bernardineli N, Moraes GI., 2003, "In vitro" evaluation of the apical sealing of root canal obturated with different techniques. Journal of Applied Oral Science, 11, 181-185.

Brown WP, Fulmer M., 1991, Kinetics of hydroxyapatite formation at low temperature. Journal of American Ceramic Society, 74, 934-940.

Buchanan LS., 1996, The art of endodontics: files of greater taper. Dentistry Today, 15, 42-49.

Buchko CJ, Chen LC, Shen Y, Martin DC., 1999, Processing and microstructural characterization of porous biocompatible protein polymer thin films. Polymer, 40, 7397-7402.

Burel F, Feldman A, Bunel C., 2005, Hydrogenated hydroxyl-functionalized polyisoprene (H-HTPI) and isocyanurate of isophorone diisocyanate (I-IPDI): Reaction kinectics study using FTIR spectroscopy. Polymer, 46, 15-25.

Cai S and Singh BR., 2004, A distinct utility of the amide III infrared band for secondary structure estimation of aqueous protein solution using partial least squares method. Biochemistry, 43, 2541-2549.

Calais JG, Soderholm KJM., 1998, Influence of filler type and water exposure on flexural strength of experimental composite resin. Journal of Dental Research, 67, 836-840.

Calandrelli L, Immirzi B, Malinconico M, Volpe MG, Oliva A, Ragione DF., 2000, Preparation and characterisation of composites based on biodegradable polymers for "in vivo" application. Polymer, 41, 8027–8033.

Cao A, Okamura T, Ishiguro C, Nakayama K, Inoue Y, Masuda T., 2002, Studies on syntheses and physical characterization of biodegradable aliphatic poly(butylene succinate-*co*--caprolactone)s. Polymer, 43, 671-679.

Cao M, Hu C, Wang E., 2003, The first fluoride one-dimensional nanostructures: micremulsion-mediated hydrothermal synthesis of BaF2 whiskers. Journal of American Chemical Society, 125, 11196-11197.

Cao M, Wang Y, Guo C, Qi Y, Hu C., 2004, Preparation of ultrahigh-aspect-ratio hydroxyapatite nanofibers in reverse micelles under hydrothermal conditions. Langmuir, 20, 4784-4786.

Cao Q and Liu P., 2006, Hyperbranched polyurethane as novel solid-solid phase change material for thermal energy storage. European Polymer Journal, 42, 2931-2939.

Cao W and Hench LL., 1996, Bioactive Materials. Ceramics International, 22, 493-507.

Carlen A, Nikdel K, Wennerberg A, Holmberg K, Olsson J., 2001, Surface characteristics and in vitro biofilm formation on glass ionomer and composite resin. Biomaterials, 22, 481-487.

Causa F, Netti PA, Ambrosio L, Ciapetti G, Baldini N, Pagani S, Martini D, Giunti A., 2006, Poly-ε-caprolactone/hydroxyapatite composites for bone regeneration: *in vitro* characterization and human osteoblast response. Journal of Biomedical Materials Research, 76A, 151-162.

Cerroni L, Filocamo R, Fabbri M, Piconi C, Caropreso S, Condo SG., 2002, Growth of osteoblast-like cells on porous hydroxyapatite ceramics: an in vitro study. Biomolecule Engineering, 19, 119–124.

Chamberlain NF., 1974, The Practice of NMR Spectroscopy. Plenum Press, New York & London.

Chan KLA and Kazarian SG., 2006, Macro FTIR imaging in transmission under a controlled environment. Vibrational Spectroscopy, 42, 130-134.

Chang MC, Ko CC, Douglas WH., 2003, Conformational change of hydroxyapatite/gelatin nanocomposite by glutaraldehyde. Biomaterials, 24, 3087-3094.

Chapman AC and Thirlwell LE., 1964, Spectra of phosphorus compounds—I. The infra-red spectra of orthophosphates. Spectrochimica Acta, 2**,** 937–947.

Charriere E, Terrazzoni S, Pittet C, Mordasini P, Dutoit M, Lemaitre J, Zysset P., 2001, Mechanical characterization of brushite and hydroxyapatite cements. Biomaterials, 22, 2937-2945.

Chatzistavrou X, Chrissafis K, Polychroniadis E, Kontonasaki E, Koidis P, Paraskevopoulos KM., 2006, Inducing bioactivity in dental porcelain through bioglass® changes in thermal behaviour. Journal of Thermal Analysis and Calorimetry, 86, 255-259.

Chaudhry AA, Haque S, Kellici S, Boldrin P, Rehman I, Khalid AF, Darr A.J., 2006, Instant nano-hydroxyapatite: a continuous and rapid hydrothermal synthesis. Chemistry Communication, 21, 2286-2288.

Chen B and Sun K., 2005, Poly (ε-caprolactone)/hydroxyapatite composites, effects of particle size, molecular weight distribution and irradiation on interfacial interaction and properties. Polymer Testing, 24, 64-70.

Chen ZQ and Boccanccini RA., 2006, Poly (D,L-lactic acid) coated 45S5 Bioglass® –based scaffolds: Processing and characterization. Journal of Biomedical Materials Research, 77A, 445-457.

Chetty A, Steynberg T, Moolman S, Nilen R, Joubert A, Richter1 W., 2008, Hydroxyapatite-coated polyurethane for auricular cartilage replacement: An in vitro study. Journal of Biomedical Materials Research, 84A, 475–482.

Chiou BS and Schoen PE., 2002, Effects of crosslinking on thermal and mechanical properties of polyurethanes. Journal of Applied Polymer Science, 83, 212-223.

Choi D, Marra KG, Kumta PN., 2004, Chemical synthesis of hydroxyapatite/Poly (ε-caprolactone) composites. Materials Research Bulletin, 39**,** 417–432.

Christenson EM, Patel S, Anderson JM, Hiltner A., 2006, Enzymatic degradation of poly(ether urethane) and poly(carbonate urethane) by cholesterol esterase. Biomaterials, 27, 3920-3926.

Christenson EM, Wiggins MJ, Anderson JM, Hiltner A., 2005, Surface modification of poly(ether urethane urea) with modified dehydroepiandrosterone for improved in *vivo* biostability. Journal of Biomedical Materials Research, 73A, 108-115.

Christoffersen J and Christoffersen MR., 1982, Kinetics of dissolution of calcium hydroxyapatite. V. The acidity constant for the hydrogen phosphate surface complex. Journal of Crystal Growth, 57, 21-26.

Chun BC, Cho TK, Chung YC., 2006, Enhanced mechanical and shape memory properties of polyurethane block copolymers chain-extended by ethylene diamine. European Polymer Journal, 42, 3367-3373.

Coates J., 2000, Encyclopedia of analytical chemistry. John Wiley and Sons Ltd, Chichester.

Coombes AGA, Rizzi CS, Williamson M, Barralet EJ, Downes S, Wallace AW., 2004, Precipitation casting of polycaprolactone for applications in tissue engineering and drug delivery. Biomaterials, 25, 315-325.

Cooper SL, West JC, Seymour RW., 1976, In: Mark HF, Bikales NM, editors, Encyclopedia of polymer science and technology. vol. 1, pp. 521-543, suppl. Wiley-Interscience, New York.

Coreno JA, Coreno OA, Cruz JJR, Rodriguez CC., 2005, Mechanochemical synthesis of nanocrystalline carbonate-substituted hydroxyapatite. Optical Materials, 27, 1281-1285.

Craig RG and Power JM., 2002, Restorative Dental Materials, 11th edition, Mosby

Crisp S, Lewis BG, Wilson AD., 1976, Characterization of glass-ionomer cements: 1. Long term hardness and compressive strength. Journal of Dentistry, 4, 162-166.

Croll TP and Killian CM., 1992, Visible light-hardened glass ionomer-resin cement restorations for primary teeth: new development. Quintessence International, 23, 679-682.

Culin J, Frka S, Andreis M, Smit I, Veksli Z, Anzlovar A, Zigon M., 2002, Motional heterogeneity of segmented polyurethane-polymethyacryalte mixtures: an influence of functional groups concentration. Polymer, 43, 3891-3899.

Cullity BD and Stock SR., 2001, Elements of X-ray Diffraction. 3rd Edition, Practice Hall.

Cuy JL, Mann AB, Livi KJ, Teaford MF, Weihs TP., 2002, Nanoindentation mapping of the mechanical properties of human molar tooth enamel. Archives of Oral Biology, 47, 281-291.

Dalas E, Kallitsis JK, Koutsoukos PG., 1991, Crystallization of hydroxyapatite on polymers. Langmuir, 7, 1822-1826.

Davalou S, Gutmann JL, Nunn MH., 1999, Assessment of apical and coronal root canal seals using contemporary endodontic obturation and restorative materials and techniques. International Endodontic Journal, 32, 388-396.

Davies JE., 1988, The importance and measurement of surface charge species in cell behaviour at the biomaterial interface. In: Ratner BD., Surface characterization of biomaterials, pp. 219-234, Elsevier, New York.

Davis RJ, Tensile Testing, 2004, pp 74-76 ASM International, The Materials information society, OH

de Paz LC, Svensater G, Dahlen G, Begenholtz G., 2005, Streptococci from root canals in teeth with apical peridontitis receiving endodontic treatment. Oral Surgery, Oral Medicine, Oral Pathology, Oral Radiology and Endodontology, 100, 232-241.

de With G and Gorbijn AJ., 1989, Metal fibre reinforced hydroxyapatite ceramics. Journal of Materials Science, 98, 1348-1353.

Deb S, Wang M, Tanner KE, Bonfield W., 1996, Hydroxyapatite-polyethylene composites: effect of grafting and surface treatment of hydroxyapatite. Journal of Materials Science: Materials in Medicine, 7, 191-193.

Deitzel JM, Kleinmeyer J, Harris D, Tan NCB., 2001, The effect of processing variables on the morphology of electrospun nanofibers and textiles. Polymer, 42, 261-272.

Deligianni DD, Katsala ND, Koutsoukos PG, Missirlis YF., 2001, Effect of surface roughness of hydroxyapatite on human bone marrow. Biomaterials, 22, 87-96.

Desai S., Thakore IM, Sarawade BD, Devi S., 2000, Effect of polyols and diisocyanates on thermo-mechanical and morphological properties of polyurethane. European Polymer Journal, 36, 711-725.

Donadel K, Laranjeira MCM, Gonclaves VL, Favere VT, de Lima JC, Prates LHM., 2005, Hydroxyapatite produced by wet-chemical method. Journal of American Ceramic Society, 88, 2230-2235.

Dong GC, Sun JS, Yao CH, Jiang GJ, Huang CW, Lin FH., 2001, A study on grafting and characterization of HMDI-modified calcium hydrogenphosphate. Biomaterials, 22, 3179-3189.

Donovan TE and Chee WWL., 2004, A review of contemporary impression materials and techniques. Dental Clinics of North America, 48, 445- 470.

Doshi J and Reneker DH., 1995, Electrospinning process and applications of electrospun fibres. Journal of Electrostatics, 35, 151-160.

Dowker SEP and Elliott JC., 1983, Infrared study of the formation, loss and location of cyanate and cyanamide in thermally treated apatites. Journal of Solid State Chemistry, 49, 334-340.

Drummond JL, Sakaguchi RL, Racean DC, Wozny J, Steinberg AD., 1996, Testing mode and surface treatment effects on dentin bonding. Journal of Biomedical Materials Research Part A, 32, 533-541l.

Ducheyne P and Qui Q., 1999, Bioactive ceramics: the effect of surface reactivity on bone formation and bone cell formation. Biomaterials, 20, 2287-2303.

Dusek K., 1987, Theory of network formation by additional crosslinking of polyurethanes due to biuret and allophanate formation. Polymer, 17, 481-488.

El Hammari L, Laghzizil A, Saoiabi A, Barboux P, Meyer M., 2006, Chemical modification of porous calcium hydroxyapatite surfaces by grafting phenylphosphonic and phenylphosphite acids. Colloids and Surfaces A: Physicochemical Engineering Aspects, 289, 84-88.

Elliott JC, Holcomb DW, Young RA., 1985, Infrared determination of the degree of substitution of hydroxyl by carbonate ions in human dental enamel. Calcified Tissue International, 37, 372-375.

Elliott JC., 1994, Structure and chemistry of the apatites and other calcium orthophosphates. Elsevier, Amsterdam

Elliott JE, Lovell LG, Bowman CN., 2001, Primary cyclization in the polymerization of Bis-GMA and TEGDMA: A modelling approach to understanding the cure of dental resins. Dental Materials, 17, 221-229.

El-Shafei AA and Moussa MNH., 2001, The corrosion inhibition character of thiosemicarbazide and its derivatives for C-steel in hydrochloric acid solution. Materials Chemistry and Physics, 70, 175-180.

Engqvist H, Shultz-Walz JE, Loof J, Botton GA, Mayer D, Phaneuf MW, Ahnfelt NO, Hermansson L., 2004, Chemical and biological integration of a mouldable bioactive ceramic material capable of forming apatite in vivo in teeth. Biomaterials, 25, 2781-2787.

Fanovich MA, Castro MS, Lopez JMP., 2001, Structural analysis of modified hydroxyapatite powders. Materials Research Bulletin, 36, 487-496.

Feilzer JA and Dauvillier SB., 2003, Effect of TEGDMA/ BisGMA ratio of stress development and viscoelastic properties of experimental two-paste composite. Journal of Dental Research, 82, 824-828.

Feng W, Mu-sen L, Yu-peng L, Yong-xin Q., 2005, A simple sol-gel technique for preparing hydroxyapatite nanopowders. Materials Letters, 59, 916-919.

Ferry A, Jacobsson P, van Heumen JD, Stevens JR., 1996, Raman, infra-red and d.s.c studies of lithium coordination in a thermoplastic polyurethane. Polymer, 37, 737-744.

Fisher MA, Berzins DW, Bahcall JK., 2007, An in vitro comparison of bond strength of various obturation materials to root canal dentin using a push-out test design. Journal of Endodontics, 33, 856-858.

Fong H., 2004, Electrospun nylon 6 nanofiber reinforced BIS-GMA/TEGDMA dental restorative composite resins. Polymer, 45, 2427-2432.

Food and Drug Administration (FDA)., 1998, Dental Composites-Premarket Notification. US Department of Health and Human Services.

Formhals., 1934, US Patent. 1, 975, 504.

Forsten L., 1998, Fluoride release and uptake by glass-ionomers and related materials and its clinical effect. Biomaterials, 19, 503-508.

Fridrikh SV, Yu JH, Brenner MP, Rutledge GC., 2006, Nonlinear whipping behaviour of electrified fluid jets. Polymeric Nanofibers ACS Symposium Series, 918, 36-55.

Friedman CE, Sandrick JL, Heuer MA, Rapp GW., 1977, Composition and physical properties of gutta-percha endodontic filling materials. Journal of Endodontics, 3, 304-308.

Friedrich K and Karsch UA., 1981, Failure processes in particulate filled polypropylene, Journal of Materials Science, 16, 2167-2175.

Frisch KC., 1981, History of Science and Technology of Polymeric Foams. Journal of Macromolecular Science Part A, 15, 1089-1112.

Fu YP, Palo DR, Erkey C, Weiss RA., 1997, Synthesis of conductive polypyrrole/polyurethane foams via a supercritical fluid process. Macromolecules, 30, 7611-7613.

Fujihara K, Kotaki M, Ramakrishna S., 2005, Guided bone regeneration membrane made of polycaprolactone/calcium carbonate composite nano-fibers. Biomaterials, 26, 4139-4147.

Fulmer MT, Martin RI, Brown PW., 1992, Formation of calcium deficient hydroxyapatite at near-physiological temperature. Journal of Materials Science: Materials in Medicine, 3, 299-305.

Furukawa M., 1997, Hydrolytic and thermal stability of novel polyurethane elastomers. Angewandte Makromolekulare Chemie, 252, 33-43.

George ZP and George PK., 2001, Observations during crystallisation of poly(ethylene-*co*-butylene naphthalene-2,6-dicarboxylate)s. Polymer, 42, 8197-8205.

Gesi A, Raffaelli O, Goracci C, Pashley DH, Tay FR, Ferrari M., 2005, Interfacial strength of Resilon and gutta percha to intraradicular dentin. Journal of Endodontics, 31, 809-813.

Gibson IR and Bonfield W., 2002, Novel synthesis and characterization of an AB-type carbonate-substituted hydroxyapatite. Journal of Biomedical Materials Research, 59, 697-708.

Gilman JW, Awad WH, Davis RD, Sheilds J, Harris Jr. RH, Davis C, Morgan AB, Sutto TE, Callahan J, Trulove PC, DeLong HC., 2002, Polymer/layered silicate nanocomposites from thermally stable trialkylimidazolium-treated montmorillonite. Chemistry of Materials, 14, 3776-3785.

Ginebra MP, Driessens FCM, Planell JA., 2004, Effect of the particle size on the micro and nanostructural features of a calcium phosphate cement: a kinetic analysis. Biomaterials, 25, 3453-3462.

Gladys S, Meerbeek BV, Braem M, Lambrechts P, Vanherle G., 1997, Comparative physio-mechanical characterization of new hybrid restorative materials with conventional glass-ionomer and resin composite restorative materials. Journal of Dental Research, 76, 883-894.

Gnanarajan TP, Iyer NP, Nasar AS, Radhakrishnan G., 2002, Preparation and properties of poly (urethane-imide)s derived from amine-blocked-polyurethane prepolymer and pyromellitic dianhydride. European Polymer Journal, 38, 487-495.

Gogolewshi S., 1989, Selected topic in biomedical polyurethane: a review. Colloidal Polymer Science, 267, 757-785.

Gohring TN, Gallo L, Luthy H., 2005, Effect of water storage, thermocycling, the incorporation and site of placement of glass-fibers on the flexural strength of veneering composite. Dental Materials, 21, 761-772.

Goldberg AJ, Craig RG, Filisko FE., 1978, Polyurethane elastomers as maxillofacial prosthetic materials. Journal of Dental Research, 57, 563-569.

Gonon L, Mallegol J, Commereuc S, Verney V., 2001, Step-scan FTIR and photoacoustic detection to assess depth profile of photooxidized polymer. Vibrational Spectroscopy, 26, 43-49.

Gottenbos B, van der Mei HC, Busscher HJ., 2000, Initial adhesion and surface growth of *Staphylococcus epidermidis* and *Pseudomonas aeruginosa* on biomedical polymers. Journal of Biomedical Materials Research, 50, 208-214.

Grad S, Kupcsik L, Gorna K, Gogolewski S, Alini M., 2003, The use of biodegradable polyurethane scaffolds for cartilage tissue engineering: potential and limitations. Biomaterials, 24, 5163-5171.

Gradwell MHS, Hourston DJ, Pabunruang T, Schafer FU, Reading M., 1998, High-resolution Thermogravimetric analysis of polyurethane/poly(ethyl Methacrylate) interpenetrating polymer networks. Journal of Applied Polymer Science, 70, 287-295.

Griffiths MB, Watson TF, Sherriff M., 1999, The influence of dentine bonding system and their handling characteristics on the morphology and micropermeability of the dentine adhesive interface. Journal of Dentistry, 27, 63-71.

Griger A., 1987, Correction of Compositional Variability in the X-ray Diffraction Phase Analysis: X-ray and neutron structure analysis in material science, Edited by Hasek J, Plenum Press.

Grobe GL, Gardella JA, Hopson WL, McKenna WP, Erying EM., 1987, Angular Dependent ESCA and IR studies of segmented polyurethane. Journal of Biomedical Material Research, 21, 211-229.

Gross KA and Babovic M., 2002, Influence of abrasion on the surface characteristics of thermally sprayed hydroxyapatite coatings. Biomaterials, 23, 4731-4737.

Guan J, Fujimoto KL, Sacks MS, Wagner WR., 2005, Preparation and characterization of highly porous, biodegradable polyurethane scaffolds for soft tissue applications. Biomaterials, 26, 3961-3971.

Guggenbichler J-P, Boswald M, Lugauer S, Krall T., 1999, A new technology of microdispersed silver in polyurethane induces antimicrobial activity in central venous catheters. Infection, 27, 16-23.

Guo KT, Scharnweber D, Schwenzer B, Ziemer G, Wendel HP., 2007, The effect of electrochemical functionalization of Ti-alloy surfaces by aptamer-based capture molecules on cell adhesion. Biomaterials, 28, 468-474.

Guo X and Xiao P., 2005, Effects of solvents on properties of nanocrystalline hydroxyapatite produced from hydrothermal process. Journal of the European Ceramic Society, 25, 1359-1364.

Gurgel-Filho ED, Feitosa AJP, Teixeira FB, de Paula MRC, Silva AJB, Souza-Filho FJ., 2003, Chemical and X-ray analyses of five brands of dental gutta-percha cone. International Endodontic Journal, 36, 302-307.

Gutmann JL., 2006, Problem Solving in Endodontics: prevention, identification, and management, 4th edition, Elsevier Mosby, USA.

Guzman-Ruiz S, Armstrong SR, Cobb DS, Vargas MA., 2001, Association between microtensile bond strength and leakage in the indirect resin composite/dentin adhesively bonded joint. Journal of Dentistry, 29, 145-153.

Hakuta Y, Ura H, Hayashi H, Arai K., 2005, Effect of hydrothermal synthetic conditions on the particle size of γ-AlO(OH) in sub and supercritical water using a flow reaction system. Materials Chemistry and Physics, 93, 466-472.

Halvorson RH, Erickson RL, Davidson CL., 2003, The effect of filler and silane content on conversion of resin-based composite. Dental Materials, 19, 327-333.

Hamza A, Pham VA, Matsuura T, Santerre JP., 1997, Development of membranes with low surface energy to reduce the fouling in ultrafiltration applications. Journal of Membrane Science, 131, 217-227.

Han Y, Li S, Wang X, Chen X., 2004, Synthesis and sintering of nanocrystalline hydroxyapatite powders by citric acid sol-gel combustion method. Materials Research Bulletin, 39, 25-32.

Hansel C, Leyhausen G, Mai UEH, Geurtsen W., 1998, Effects of various resin composite (co) monomers and extracts on two caries-associated micro-organisms in vitro. Dental Materials, 77, 60-67.

Heijkants RGJC, van Calck RV, van Tienen TG, de Groot JH, Buma P, Pennings AJ, Veth RPH, Schouten AJ., 2005, Uncatalyzed synthesis, thermal and mechanical properties of polyurethanes based on poly(ε-caprolactone) and 1,4-butane diisocyanate with uniform hard segment. Biomaterials, 26, 4219-4228.

Helm GA, Dayoub H, Jane Jr. JA., 2001, Bone graft substitutes for the promotion of spinal arthrodesis. Journal of Neurosurgery, 10, Art 4.

Hench LL and Ethridgo EC., 1982, Biomaterials: An interfacial approach, Academic Press, New York.

Hench LL and Wilson J., 1999, An Introduction to Bioceramics. World Scientific Publishing, Singapore.

Hench LL, Wheeler LD, Greenspan CD., 1998, Molecular control of bioactivity in sol-gel glasses. Journal of Sol-Gel Science and Technology, 13, 245-250.

Hench LL., 1991, Bioceramics: from concept to clinic. Journal of American Ceramic Society, 74, 1487-1510.

Hench LL., 1997, Sol-gel materials for bioceramic applications. Current Opinion in Solid State & Materials Science, 2, 604-610.

Hench LL., 1998, Bioceramics. Journal of American Ceramic Society, 81, 1705-28.

Hepburn C., 1992, Trends in polyurethane elastomer technology. Iranian Journal of Polymer Science and Technology, 1, 84-110.

Hergenrother RW, Wabers HD, Cooper SL., 1993, Effect of hard segment chemistry and strain on the stability of polyurethanes: in-vivo stability. Biomaterials, 14, 449-453.

Herrera M, Matuschek G, Kettrup A., 2002, Thermal degradation of thermoplastic polyurethane elastomers (TPU) based on MDI. Polymer Degradation and Stability, 78, 323-331.

Hing KA, Best SM, Bonfield W., 1999, Characterization of porous hydroxyapatite. Journal of Materials Science Letters, 10, 135-145.

Ho KS, Hsieh HK, Huang SK, Hsieh TH., 1999, Polyurethane-based conducting polymer blends-1. Effect of chain extender. Synthetic Metals, 107, 65-73.

Hong Z, Peibiao Z, Chaoliang H, Xueyu Q, Aixue L, Li C, Xuesi C, Xiabin J., 2005, Nano-composite of poly(l-lactide) and surface grafted hydroxyapatite: Mechanical properties and biocompatibility. Biomaterials, 26, 6296-6304.

Hoshi K, Ejiri S, Probst W, Seybold V, Kamino T, Yaguchi T, Yamahira N, Ozawa H., 2001, Observation of human dentine by focused ion beam and energy-filtering transmission electron microscopy. Journal of Microscopy, 201, 44-49.

Howard GT., 2002, Biodegradation of polyurethane: a review. International Biodeterioration & Biodegradation, 49, 245-252.

Hrkach JS, Peracchia MT, Domb A, Lotan N, Langer R., 1997, Nanotechnology for biomaterials engineering, structural characterization of amphilic polymeric nanoparticles by ^{1}H NMR spectroscopy. Biomaterials, 18, 27-30.

Hsieh K-H, Liao K-H, Lai E. H-H, Lee B-S, Lee C-Y, Lin C-P., 2008, A novel polyurethane-based root canal—obturation material and urethane acrylate—based root canal sealer—Part 1: Synthesis and evaluation of mechanical and thermal properties. Journal of Endodontics, 34, 303-305.

Hsieh KH, Tseng SM, Chern YC., 1999, Damping properties of interpenetrating polymer networks of polyurethane-modified epoxy and polyurethanes. Journal of Applied Polymer Science, 74, 328-335.

Hu JL and Mondal S., 2005, Structural characterization and mass transfer properties of segmented polyurethane: influence of block length of hydrophilic segments. Polymer International, 54, 764-771.

Huang ZM and Yang AH., 2006, Encapsulation of pure drugs into the central part of polycaprolactone ultrafene fibres. Acta Polymerica Sinica, 1, 48-52.

Hunter GK, Hauschka PV, Poole AR, Rosenberg LC, Goldberg HA., 1996, Nucleation and inhibition of hydroxyapatite formation by mineralized tissue proteins. Biochemical Journal, 317, 59-64.

Ichikawa T, Hirota K, Kanitani H, Miyake Y, Matsumoto N., 1998, In vitro adherence of Streptococcus constellatus to dense hydroxyapatite and titanium. Journal of Oral Rehabilitation, 25, 125-127.

Ignatius A, Unterricker K, Wenger K, Richter M, Claes L, Lohse P, Hirst H., 1997, A new composite made of polyurethane and glass ceramic in a loaded implant model: a biomechanical and histological analysis. Journal of Materials Science: Materials in Medicine, 8, 753-756.

Ingle JI., 2002, Endodontics. 5th edition, Decker.

Isobe T, Nakamura S, Nemoto R, Senna M., 2002, Solid-State double Nuclear Magnetic Resonance study of the local structure of calcium phosphate nanoparticles synthesized by a wet-mechanochemical reaction. Journal of Physics and Chemistry Part B, 106, 5169-5176.

Ito A, Nakamura S, Aoki H, Akao M, Teraoka K, Tsutsumi S, Onuma K, Tateishi T., 1996, Hydrothermal growth of carbonate-containing hydroxyapatite single crystals. Journal of Crystal Growth, 163, 311-317.

Ito Y, Hasuda H, Kamitakahara M, Ohtsuki C, Tanihara M, Kang I-K, Kwon OH., 2005, A composite of hydroxyapatite with electrospun biodegradable nanofibers as a tissue engineering material. Journal of Bioscience and Bioengineering, 100, 43-49.

Itoh M, Shimazu A, Hirata I, Yoshida Y, Shintani H, Okazaki M., 2004, Characterization of CO3Ap-collagen sponges using X-ray high-resolution microtomography. Biomaterials, 25, 2577-2583.

James NR, Philip J, Jayakrishnan A., 2006, Polyurethanes with radiopaque properties. Biomaterials, 27, 160-166.

Jaworek A and Krupa A., 1999, Classification of the modes of EHD spraying. Journal of Aerosol Science, 30, 873-893.

Jayabalan M, Lizymol PP, Thomas V., 2000, Synthesis of hydrolytically stable low elastic modulus polyurethane-urea for biomedical applications. Polymer International, 49, 88-92.

Jeevaananda T and Siddaramaiah S., 2003, Synthesis and characterization of polyaniline filled PU/PMMA interpenetrating polymer networks. European Polymer Journal, 39, 569-578.

Jeevananda T, Begum M, Siddaramaiah S., 2001, Studies on polyaniline filled PU/PMA interpenetrating polymer networks. European Polymer Journal, 37, 1213-1218.

Jeong HM, Kim BK, Choi YJ., 2000, Synthesis and properties of thermotropic liquid crystalline polyurethane elastomers. Polymer, 41, 1849-1855.

Jhon Y-K, Cheong I-W, Kim J-H., 2001, Chain extension study of aqueous polyurethane dispersions. Colloids and Surfaces A: Physicochemical and Engineering Aspects, 179, 71–78.

Jillavenkatesa A, Condrate Sr. RA., 1998, Sol-gel processing of hydroxyapatite. Journal of Materials Science, 33, 4111-4119.

Jinawath S, Polchai D, Yoshimura M., 2002, Low-temperature, hydrothermal transformation of aragonite to hydroxyapatite. Materials Science and Engineering C, 22, 35-39.

Jung HC, Kang SJ, Kim WN, Lee YB, Choe KH, Hong SH, Kim SB., 2000, Properties of crosslinked polyurethanes synthesized from 4, 4'-diphenylmethane diisocyanate and polyester polyol. Polymer Science, 78, 624-630.

Kaji A, Arimatsu Y, Murano M., 1992, 13C NMR study of anomalous linkages in polyurethane. Journal of Polymer Science, Part A: Polymer Chemistry, 30, 287-297.

Karakeccilci AS and Gumusderelcioaglu M., 2002, Comparison of bacterial and tissue cell initial adhesion on hydrophilic/hydrophobic biomaterials. Journal of Biomaterials Science: Polymer Edition, 13, 185-196.

Katz JL, Spencer P, Nomura T, Wagh A, Wang Y., 2003, Micromechanical properties of demineralized dentin collagen with and without adhesive infiltration. Journal of Biomedical Materials Research, 66A, 120-128.

Katz JL., 1971, Hard tissue as a composite material. I. Bounds on the elastic behavior. Journal of Biomechanics, 4, 455-473.

Katz JL., 1980, Anisotropy of Young's modulus of bone. Nature, 283, 106–107.

Kazarian SG, Andrew CKL, Maquet V, Boccaccini AR., 2004, Characterisation of bioactive and resorbable polylactide/Bioglass® composites by FTIR spectroscopic imaging. Biomaterials, 25, 3931-3938.

Keattch CJ and Dollimore D., 1975, An Introduction to Thermogravimetry. 2nd Edition, Heyden & Son Ltd, London.

Kenway R, Layman JM, Watkins JR, Bowlin GL, Matthews JA, Simpson DG, Wnek GE., 2003, Electrospinning of poly(ethylene-co-vinyl alcohol) fibers. Biomaterials, 24, 907-913.

Kerby RE, Tiba A, Knobloch LA, Schricker SR, Tiba O., 2003, Fracture toughness of modified dental resin systems. Journal of Oral Rehabilitation, 30, 780-784.

Kidoaki S, Kwon IK, Matsuda T., 2005, Mesoscopic spatial designs of nano- and microfiber meshes for tissue engineering matrix and scaffold based on newly devised multilayering and mixing electrospinning techniques. Biomaterials, 26, 37-46.

Kiem S, Oh WS, Peck KR, Lee NY, Lee YJ, Song HJ, Hwang SE, Kim CE, Cha YC, Choe WK., 2004, Phase variation of biofilm formation in Staphylococcus aureus by IS256 insertion and its impact on the capacity adhering to polyurethane surface. Journal of Korean Medical Science, 19, 779-782.

Kim BS, Jeong HY, Kim BK., 2005, Surface characterizations of polyurethanes having different types of soft segment. Colloids and Surfaces A: Physicochemical Engineering Aspects, 268, 60-67.

Kim HD, Lee TJ, Huh JH, Lee DJ., 1999, Preparation and properties of segmented thermoplastic polyurethane elastomers with two different soft segments. Journal of Applied Polymer Science, 73, 345-352.

Kim HM, Himeno T, Kokubo T, Nakamura T., 2005, Process and kinetics of bonelike apatite formation on sintered hydroxyapatite in a simulated body fluid. Biomaterials, 26, 4366-4373.

Kim I-S and Kumta NP., 2004, Sol-gel synthesis and characterization of nanostructured hydroxyapatite powder. Materials Science and Engineering B, 111, 232-236.

Koberstein JT and Galambos AF., 1992, Multiple melting in segmented polyurethane block copolymers. Macromolecules, 25, 5618-5624.

Kohler B, Rasmusson CG, Odman P., 2000, A five-year clinical evaluation of class II composite resin restorations. Journal of Dentistry, 28, 111-116.

Kokubo T., 1996, Formation of biologically active bone-like apatite on metals and polymers by a biomimetic process. Themrochimica Acta, 280-281, 479-490.

Kokubo T., 1998, Apatite formation on surfaces of ceramics, metals and polymers in body environment. Acta Materialia, 46, 2519-2527.

Kokubo T., 2005, Design of bioactive bone substitutes based on biomineralization process. Materials Science and Engineering, 25C, 97-104.

Kong LB, Ma J, Boey F., 2002, Nanosized hydroxyapatite powders derived from coprecipitation process. Journal of Materials Science, 37, 1131-1134.

Kornfield JA, Spiess HW, Nefzger H, Hayen H, Eisenbach CD., 1991, Deutron NMR measurement of order and mobility in the hard segment of a model polyurethane. Macromolecules, 24, 4787-4795.

Kothapalli CR, Wei M, Legeros RZ, Shaw MT., 2005, Influence of temperature and aging time on HA synthesized by the hydrothermal method. Journal of Materials Science: Materials in Medicine, 16, 441-446.

Koustsopoulos S., 2002, Synthesis and characterization of hydroxyapatite crystals: A review study on the analytical methods. Journal of Biomedical Materials Research, 62, 600-612.

Krajewski A, Mazzocchi M, Buldini PL, Ravaglioli A, Tinti A, Taddei P, Fagnano C., 2005, Synthesis of carbonated hydroxyapatites: efficiency of the substitution and critical evaluation of analytical methods. Journal of Molecular Structure, 744-747, 221-228.

Kricheldrof HR and Hull WE., 1981, ^{15}N NMR spectroscopy, 27 Spectroscopic characterization of polyurethanes and related compounds. Macromolecular Chemistry, 182-1177-1196.

Kricka LJ and Fortina P., 2002, Nanotechnology and Applications: An All-Language Literature Survey Including Books and Patents. Clinical Chemistry, 48, 662-665.

Krol P and Pilch-Pitera B., 2007, Phase structure and thermal stability of crosslinked polyurethane elastomers based on well-defined prepolymers. Journal of Applied Polymer Science, 104, 1464-1474.

Kuan HC, Chuang WP, Ma CCM, Chiang CL, Wu HL., 2005, Synthesis and characterization of a clay/waterborne polyurethane nanocomposite. Journal of Materials Science, 40, 179-185.

Kulild J, Lee C, Dryden J, Collins J, Feil P., 2007, A comparison of 5 gutta-percha obturation techniques to replicate canal defects. Oral Surgery, Oral Medicine, Oral Pathology, Oral Radiology, and Endodontology, 103, e28-e32.

Kultys A., 2001, Sulfur-containing polyesters. The synthesis and characterization of new diphenylmethane-derivative thiopolyester diols and their use for the preparation of thermoplastic polyurethanes. Macromolecular Chemistry and Physics, 202, 3523-3529.

Kumar H, Kumar AA, Siddaramaiah., 2006, Physico-mechanical, thermal and morphological behaviour of polyurethane/poly (methyl methacrylate) semi-interpenetrating polymer networks. Polymer Degradation and Stability, 91, 1097-1104.

Kumar PRA, Varma HK, Kumary TV., 2005, Rapid and complete cellularization of hydroxyapatite for bone tissue engineering. Acta Biomaterialia, 1, 545-552.

Kumar R, Cheang P, Khor KA., 2001, RF plasma processing of the ultra-fine hydroxyapatite powder. Journal of Materials Processing Technology, 113, 456-462.

Kuriakose TA, Kalkura SN, Palanichamy M, Arivuoli D, Dierks K, Bocelli G, Betzel C., 2004, Synthesis of stoichiometric nano crystalline hydroxyapatite by ethanol-based sol-gel technique at low temperature. Journal of Crystal Growth, 263, 517-523.

Labella R, Braden M, Deb S., 1994, Novel hydroxyapatite-based dental composite. Biomaterials, 15, 1197-2000.

Labella R, Lambrechts P, van Meerbeek B, Vanherle G., 1999, Polymerization shrinkage and elasticity of flowable composites and filled adhesives. Dental Materials, 15, 128-137.

Lacefield WR., 1998, Current status of ceramic coatings for dental implants. Implant Dentistry, 7, 315-22.

Lage LG and Kawano Y., 2001, Thermal degradation of biomedical polyurethanes - A kinetic study using high-resolution thermogravimetry. Journal of Applied Polymer Science, 79, 910-919.

Lamba MKN, Woodhouse KA, Cooper SL., 1998, Polyurethanes in Biomedical Applications, CRC Press.

Lazic S, Zec S, Miljevic N, Milonjic S., 2001, The effect of temperature on the properties of hydroxyapatite precipitated from calcium hydroxide and phosphoric acid. Thermochimica Acta, 374, 13-22.

Lee B-S, Lai H-H, Liao K-H, Lee C-Y, Hsieh K-H, Lin C-P., 2008, A novel polyurethane—based root canal—obturation material and urethane—acrylate—based root canal sealer—Part 2, Evaluation of push-out bond strength. Journal of Endodontics, 34, 594-598.

Lee HK, Kim YH, Khil SM, Ra MY, Lee RD., 2003, Characterization of nano-structured poly (ε-caprolactone) nonwoven mat via electrospinning. Polymer, 44, 1287-1294.

Lee HS and Hsu SL., 1989, An analysis of phase separation kinetics of model polyurethanes. Macromolecules, 22, 1100-1105.

Lee HS, Wang YK, Hsu SL., 1987, Spectroscopic analysis of phase separation behaviour of model polyurethanes. Macromolecules, 20, 2089-2095.

Lee HS, Wang YK, MacKnight WJ, Hsu SL., 1988, Spectroscopic analysis of phase-separation kinetics in model polyurethane. Macromolecule, 21, 270-273.

Lee PC, Chen LW, Lin JR, Hsieh KH, Huang LLH., 1996, Influence of hand segments of polyurethane on cell growth. Polymer International, 41, 419-425.

Lee SH, Chang J, Ferracane J, Lee IB., 2007, Influence of instrument compliance and specimen thickness on the polymerization shrinkage stress measurement of light-cured composites. Dental Materials, 23, 1093-1100.

Leeuwenburgh SCG, Wolke JGC, Schoonman J, Jansen JA., 2004, Influence of precursor solution parameters on chemical properties of calcium phosphate coating prepared using Electrostatic Spray Deposition (ESD). Biomaterials, 25, 641-649.

LeGeros RZ, LeGeros JP, Kim Y, Kijkowska R, Zheng R, Bautista C, Wong JL., 1995, Calcium phosphate in plasma sprayed HA coatings. Ceramic Transmissions, 48, 173-189.

Lelah MD and Cooper SL., 1987, Polyurethane in Medicine. CRC Press, USA.

Levallois B, Fovet Y, Lapeyre L, Gal JY., 1998, In vitro fluoride release from restorative materials in water versus artificial saliva medium (SAGF). Dental Materials, 14, 441-447.

Levy GC, Lichter RL, Nelson GL., 1980, Carbon-13 Nuclear Magnetic Resonance Spectroscopy, 2nd Edition, pp 78, John Wiley & Sons, New York.

Li F, Feng QL, Cui FZ, Li HD., 2002, A simple biomimetic method for calcium phosphate coating. Surface and Coating Technology, 154, 88-93.

Li F, Zuo J, Dong L, Wang H, Luo J, Han W, Huo Y., 1998, Study on the synthesis of high elongation polyurethane. European Polymer Journal, 34, 59-66.

Li H, Khor KA, Chow V, Cheang P., 2007, Nanostructural characteristics, mechanical properties, and osteoblast response of spark plasma sintered hydroxyapatite. Journal of Biomedical Materials Research, 82A, 296-303.

Li J, Faratash B, Hermansson L., 1995, Hydroxyapatite—alumina composites and bone-bonding. Biomaterials, 16, 417-422.

Li J, Fartash B, Hermansson L., 1990, High-strength ceramics with potential bioactivity. Interceramic, 36, 20-23.

Li Y, de Groot K, de Wijn J, Klein COAT, van der Meer S., 1994, Morphology and composition of nanograde calcium phosphate needle-like crystals formed by simple hydrothermal treatment. Journal of Materials Science: Materials in Medicine, 5, 326-331.

Li Y, de Wijn JR, Klein CPAT, van de Meer S, de Groot K., 1994, Preparation and characterization of nanograde osteoapatite-like rod crystals. Journal of Materials Science: Materials in Medicine, 5, 252-255.

Li Y, Klein CPAT, de Wijn J, van de Meer S, Groot K., 1994, Shape change and phase transition of needle like non-stochiometric apatite crystals. Journal of Materials Science: Materials in Medicine, 5, 263-268.

Liaw DJ., 1997, The relative physical and thermal properties of polyurethane elastomers, effect of chain extenders of bisphenols, diisocyanate, and polyol structures. Journal of Applied Polymer Science, 66, 1251-1265.

Lin MF, Tsen WC, Shu YC, Chuang FS., 2001, Effect of silicon and phosphorus on the degradation of polyurethanes. Journal of Applied Polymer Science, 79, 881-899.

Linde A., 1984, Dentin and Dentinogenesis. CRC Press.

Liu C, Huang Y, Shen W, Cui J., 2001, Kinetics of hydroxyapatite precipitation at pH 10 to 11. Biomaterials, 22, 301-306.

Liu CJ, Hsieh KH, Ho KS, Hsieh TT., 1997, 2-Hydroxyethyl Methacrylate-terminated polyurethane/polyurethane interpenetrating polymer networks. Journal of Biomedical Materials Research, 34, 261-268.

Liu D-M, Troczynski T, Tseng JW., 2001, Water-based sol-gel synthesis of hydroxyapatite: process development. Biomaterials, 22, 1721-1730.

Liu D-M, Yang Q, Troczynski T, Tseng JW., 2002, Structural evolution of sol-gel-derived hydroxyapatite. Biomaterials, 23, 1679-1687.

Liu H and Webster TJ., 2007, Nanomedicine for implants: A review of studies and necessary experimental tools. Biomaterials, 28, 354-369.

Liu J, Ye X, Wang H, Zhu M, Wang B, Yan H., 2003, The influence of pH and temperature on the morphology of hydroxyapatite synthesized by hydrothermal method. Ceramic International, 29, 629-633.

Liu Q, de Wijn RJ, de Groot K, van Blitterswijk AC., 1998, Surface modification of nano-apatite by grafting organic polymer. Biomaterials, 19, 1067-1072.

Liu Q, de Wijn RJ, van Blitterswijk AC., 1997, Nano-apatite/polymer composites: mechanical and physiochemical characteristics. Biomaterials, 18, 1263-1270.

Liu Q, de Wijn JR, Bakker D, van Blitterswijk CA., 1996, Surface modification of hydroxyapatite to introduce interfacial bonding with polyactive™ 70/30 in a biodegradable composite. Journal of Materials Science: Materials in Medicine, 7, 551-557.

Liu W and Reneker HD., 2002, Poly(meta-phenylene isophatalamide) nanofibers: Coating and post processing. Journal of Materials Research, 17, 3206-3212.

Liu Z, Liu XH, Zhao Y, Sun XY, Weng SF, Xu DF, Wu JG., 2006, FTIR spectroscopic studies of hydration effect on the molecular structure of polyether urethane. Spectroscopy and Spectral Analysis, 26, 33-36.

Lligadas G, Ronda JC, Marina G, Cadiz V., 2007, Poly (ether urethane) networks form renewable resources as candidate biomaterials: synthesis and characterization. Biomacromolecules, 8, 686-692.

Logothetidis S., 2006, Nanotechnology in medicine: The medicine of tomorrow and nanomedicine. Hippokratia, 10, 7-21.

Loh XJ, Goh SH, Li J., 2007,Hydrolytic degradation and protein release studies of thermogelling polyurethane copolymers consisting of poly[®-3-hydoxybutyrate], poly(ethylene glycol), and poly(propylene glycol). Biomaterials, 28, 4113-4123.

Lopatin CM, Pizziconi VB, Alford TL., 2001, Crystallization kinetics of sol-gel derived hydroxyapatite thin films. Journal of Materials Science: Materials in Medicine, 12, 767-773.

Lourenco N and Santos H., 2005, Using Differential Scanning Calorimetry to characterize the precipitation hardening phenomena in a Cu-9Ni-6Sn Alloy. Journal of Materials Engineering and Performances, 14, 480-486.

Lucas M.E, Arita K, Nishino M., 2003, Toughness, bonding and fluoride release properties of hydroxyapatite-added glass ionomer cement. Biomaterials, 24, 3787-3794.

Maeno S, Niki Y, Matsumoto H, Morioka H, Yatabe T, Funayama A, Toyama Y, Taguchi T, Tanaka J., 2005, The effect of calcium ion concentration on osteoblast viability, proliferation and differentiation in monolayer and 3D culture. Biomaterials, 26, 4847-4855.

Mammone JF and Hudson SM., 1993, Micromechanics of bone strength and fracture. Journal of Biomechanics, 26, 439-46.

Maniglia-Ferreira C, Silva Jr. JBA, de Paula RCM, Feitosa JPA, Cortez DGN, Zaia AA, de Souza-Filho FJ., 2005, Brazilian gutta-percha points. Part I: chemical composition and X-ray diffraction analysis. Brazilian Oral Research, 19, 193-197.

Manogue M., 2005, The Principles of Endodontics. Oxford University Press.

Marsh PD., 1995, The role of microbiology in models of dental caries. Advances in Dental Research, 9, 244-254

Marshall Jr. GW, Marshall SJ, Kinney JH, Balooch M., 1997, The dentin substrate, structure and properties related to bonding. Journal of Dentistry, 25, 441-458.

Martin M and Jedynakiewicz MN., 1998, Measurement of water sorption in dental composites. Biomaterials, 19, 77-83.

Martin M, Jedynakiewicz MN, Fisher CA., 2003, Hygroscopic expansion and solubility of composite restorative. Dental Materials, 19, 77-86.

Mathur AB, Collier TO, Kao WJ, Wiggins M, Schubert MA, Hiltner A, Anderson JM., 1997, In *vivo* biocompatibility and biostability of modified polyurethanes. Journal of Biomedical Materials Research, 36, 246-257.

McCabe FJ and Walls WGA., 1998, Applied Dental Materials. 8th edition, Blackwell Science, Oxford.

McCabe JF and Rusby S., 2004, Water absorption, dimensional change and radial pressure in resin matrix dental restorative materials. Biomaterials, 25, 4001-4007.

McCormick PG and Froes FH., 1998, The fundamentals of mechanochemical processing. Journal of the Minerals, Metals and Materials Society, 50, 61-65.

McLean JW and Gasser O., 1985, Glass-cermet cements. Quintessence International, 16, 333-343.

McSpadden J., 1993, Multiphase gutta-percha obturation technique. Dental Economics, 83, 95-97.

Meleti Z, Shapiro IM, Adams CS., 2000, Inorganic phosphate induces apoptosis of osteoblasts-like cells in culture. Bone, 27, 359-366.

Meng J, Kong H, Xu HY, Song L, Wang CY, Xie SS., 2005, Improving the blood compatibility of polyurethane using carbon nanotubes as fillers and its implications to cardiovascular surgery. Journal of Biomedical Materials Research, 74A, 208–214.

Meyer JL and Fowler BO., 1982, Lattice defects in nonstoichiometric calcium hydroxylapatites. A chemical approach. Inorganic Chemistry, 21, 3029-3035.

Miller JA, Lin SB, Hwang KK, Wu KS, Gibson PE, Cooper SL., 1985, Properties and Polyether-polyurethane block copolymers: Effects of hard segment length distribution. Macromolecules, 18, 32-44.

Mitra SB, Wu D, Holmes BN., 2003, An application of nanotechnology in advanced dental materials. The Journal of American Dental Association, 134, 1382-1390.

Mjor IA and Moorhead JE., 2000, Reasons for replacement of restoration in permanent teeth in general dental practice. International Dental Journal, 50, 361-366.

Mondal S and Hu JL., 2006, Structural characterization and mass transfer properties of nonporous-segmented polyurethane membrane: Influence of the hydrophilic segment content and soft segment melting temperature. Journal of Membrane Science, 276, 16-22.

Mondal S and Hu JL., 2006, Structural characterization and mass transfer properties of polyurethane block copolymer: influence of mixed soft segment block and crystal melting temperature. Polymer International, 55, 1013-1020.

Morgan H, Wilson RM, Elliott JC, Dowker SEP, Anderson P., 2000, Preparation and characterisation of monoclinic hydroxyapatite and its precipitated carbonate apatite intermediate. Biomaterials, 21, 617-627.

Mortazavi V, Fathi MH, Vafaie P., 2004, Effect of the type of restorative material on bonding efficiency and microleakage of a self-etching adhesive system. Journal of Materials Research Science, 4,152-157.

Mostafa YN., 2005, Characterization, thermal stability and sintering of hydroxyapatite powders prepared by different routes. Materials Chemistry and Physics, 94, 333-341.

Moszner N and Klapdohr S., 2004, Nanotechnology for dental composites. International Journal of Nanotechnology, 1, 130-156.

Moszner N, Fischer UK, Angermann J, Rheinberger V., 2008, A partially aromatic urethane dimethacrylate as a new substitute for Bis-GMA in restorative composites. Dental Materials, 24, 694-699.

Mount GJ and Hume WR., 1998, Preservation and Restoration of Tooth Structure. Mosby, London.

Mount GJ and Makinson OF., 1982, Glass-ionomer restorative cements: clinical implications of the setting reaction. Operative Dentistry. 7,134-141.

Mount GJ., 1998, Clinical performance of glass-ionomers. Biomaterials, 19, 573-579. Review.

Murray CB and Kagan CR., 2003, Synthesis and characterization of monodisperse nanocrystals and close-packed nanocrystal assemblies. Annual Review of Materials Science, 30, 545-610.

Nagas E, Cehreli ZC, Durmaz V, Vallittu PK, Lassila LVJ., 2007, Regional push-out bond strength and coronal microleakage of Resilon after different light-curing methods. Journal of Endodontics, 33, 1464-1468.

Nakamichi I, Iwaku M, Fusayama T., 1983, Bovine teeth as possible substitute in the adhesion test. Journal of Dental Research, 62, 1076-1081.

Neugebauer D., 2007, Graft copolymers and hydrophilic and hydrophobic polyether side chains. Polymer, 48, 4966-4973.

Ng YL, Mann V, Rahbaran S, Lewsey J, Gulabivala K., 2007, Outcome of primary root canal treatment, systematic review of the literature - Part 1. Effects of study characteristics on probability of success. International Endodontic Journal, 40, 921-939.

Nicholas LB and Wilson OC., 2003, Surface modification of hydroxyapatite. Part 1. Dodecyl alcohol. Biomaterials, 24, 3671-3679.

Nicholson JW., 1998, Chemistry of glass-ionomer cements: a review. Biomaterials, 19,485-494.

Ning L, De-Ning W, Kang YS., 1996, Crystallinity and hydrogen bonding of hard segment in segmented poly (urethane urea) copolymers. Polymer, 37, 3577-3583.

Ning L, De-Ning W, Kang YS., 1996, Hydrogen bonding between urethane and urea: band assignment for the carbonyl region of *FT* i.r. spectrum. Polymer, 37, 3045-3047.

Niwa J., 1983, Acceleration of bone-repair using hydroxyapatite. Bone Fracture, 5, 124–128.

Njuguna J and Pielichowski K., 2004, Recent developments in polyurethane-based conducting composites. Journal of Materials Science, 39, 4081-4094.

Norton J, Malik KR, Darr JA, Rehman IU., 2006, Recent developments in processing and surface modification of hydroxyapatite. Advances in Applied Ceramics, 105, 113-139.

Oliveira JM, Rodrigues MT, Silva SS, Malafaya PB, Gomes ME, Viegas CA, Dias IR, Azevedo JT, Mano JF, Reis RL., 2006, Novel hydroxyapatite/chitosan bilayered scaffold for osteochondral tissue-engineering applications, scaffold design and its performace when seeded with goat bone marrow stromal cells. Biomaterials, 27, 6123-6137.

Oprea S and Oprea V., 2002, Mechanical behavior during different weathering tests of the polyurethane elastomers films. European Polymer Journal, 38, 1205-1210.

Orlovskii VP, Komlev VS, Barinov SM., 2002, Hydroxyapatite and hydroxyapatite-based ceramics. Inorganic Materials, 38, 973-984.

Ou-Yang H, Paschalis EP, Boskey AL, Mendelsohn R., 2000, Two-dimensional vibrational correlation spectroscopy of *in vitro* hydroxyapatite maturation. Biopolymers, 57, 129-139.

Oyane A, Kawashita M, Nakanishi K, Kokubo T, Minoda M, Miyamoto T, Nakamura T., 2003, Bonelike apatite formation on ethylene-vinyl alcohol copolymer modified with silane coupling agent and calcium silicate solutions. Biomaterials, 24, 1729-1735.

Palin WM, Fleming GJP, Burke FJT, Marquis PM, Randall RC., 2003, The reliability in flexural strength testing of a novel dental composite. Journal of Dentistry, 31, 549-557.

Palin WM, Fleming GJP, Burke FJT, Marquis PM, Randall RC., 2005, The influence of short and medium-term water immersion on the hydrolytic stability of novel low-shrink dental composites. Dental Materials, 21, 852-863.

Pande GS., 1983, Thermoplastic polyurethanes as insulating materials for long-life cardiac pacing leads. Pace, 6, 858-867.

Park C and Robertson RE., 1998, Mechanical properties of resin composites with filler particles aligned by an electric field. Dental Materials, 14, 385-393.

Park JH, Cho YW, Kwon IC, Jeong SY, Bae YH., 2002, Assessment of PEO/PTMO multiblock copolymer/segmented polyurethane blends as coating materials for urinary catheters: in vitro bacterial adhesion and encrustation behaviour. Biomaterials, 23, 3991-4000.

Park MS, Eanes ED, Antonucci MJ, Skrtic D., 1998, Mechanical properties of bioactive amorphous calcium phosphate/methacrylate composites. Dental Materials, 14, 137-141.

Parker S and Braden M., 1989, Water adsorption of methacrylate soft lining materials. Biomaterials, 10, 91-95.

Parnell S, Min K, Cakmak M., 2003, Kinetic studies of polyurethane polymerization with Raman spectroscopy. Polymer, 44, 5137-5144.

Pasmore M, Todd P, Pfiefer B, Rhodes M, Bowman CN., 2002, Effect of polymer surface properties on the reversibility of attachment of Pseudomonas aeruginosa in the early stages of biofilm development. Biofouling, 18**,** 65-71.

Pattanayak A and Jana SC., 2005, Properties of bulk-polymerized thermoplastic polyurethane nanocomposites. Polymer, 46, 3394-3406.

Pavithra D and Doble M., 2008, Biofilm formation, bacterial adhesion and host response on polymeric implants—issues and prevention. Biomedical Materials, 3, 1-13.

Pedicini A and Farris RJ., 2003, Mechanical behaviour of electrospun polyurethane. Polymer, 44, 6857-6862.

Penel G, Leroy G, Rey C, Bres E., 1998, MicroRaman spectral studies of PO4 and CO3 vibrational modes in synthetic and biological apatites. Calcified Tissue International, 63, 475-481.

Perez-Liminana MA, Aran-Ais F, Torro-Palau AM, Orgiles-Barcelo AC, Martin-Martinez JM., 2005, Characterization of waterborne polyurethane adhesives containing different amounts of ionic groups. International Journal of Adhesion & Adhesives, 25, 507-517.

Petrovic ZS, Zavargo Z, Flynn JH, Macknight WJ., 1994, Thermal-Degradation of Segmented Polyurethanes. Journal of Applied Polymer Science, 51, 1087-1095.

Pezzotti G., 2005, Raman piezo-spectroscopic analysis of natural and synthetic biomaterials. Analytical and Bioanalytical Chemistry, 381, 577-590.

Phillips M.J, Darr JA, Luklinska ZB, Rehman I., 2003, Synthesis and characterization of nano-biomaterials with potential osteological applications. Journal of Materials Science: Materials in Medicine, 14, 875-882.

Phillips MJ., 2004, Chemical coupling in biocomposites: surface modification of bioceramics creating chemically bound polymer composites with potential osteological applications. PhD Thesis, University of London.

Pielichowski K, Leszczynska A., 2004, TG-FTIR study of the thermal degradation of polyoxymethylene (POM)/thermoplastic polyurethane (TPU) blends. Journal of Thermal Analysis and Calorimetry, 78, 631-637.

Pinchuk L, Martin JB, Esquivel MC, MacGregor DC., 1988, The use of silicone/polyurethane graft polymers as a mean of eliminating surface stress cracking of polyurethane prosthesis. Journal of Biomaterial Applied, 3, 260-296.

Polizu S, Savadogo O, Poulin P, Yahia L., 2006, Applications of carbon nanotubes-based biomaterials in biomedical nanotechnology. Journal of Nanoscience and Nanotechnology, 6, 1883–1904.

Prasath RA, Nanjundan S, Pakula T, Klapper M., 2004, Synthesis and characterization of calcium containing poly (urethane-ether)s. European Polymer Journal, 40, 1767-1778.

Prosser HJ, Powis DR, Brant P, Wilson AD., 1984, Characterization of glass-ionomer cements. 7. The physical properties of current materials. Journal of Dentistry, 12, 231-240.

Qiu X, Han Y, Zhuang X, Chen X, Li Y, Jing X., 2007, Preparation of nano-hydroxyapatite/poly (L-lactide) biocomposite microspheres. Journal of Nanoparticles Research, 9, 901-908.

Qu X, Cui W, Yang F, Min C, Shen H, Bei J, Wang S., 2007, The effect of oxygen plasma pretreatment and incubation in modified simulated body fluids on the formation of bone-like apatite on poly (lactide-co-glycolide) (70/30). Biomaterials, 28, 9-18.

Qualtrough AJE., 2005, Principles of Operative Dentistry. Blackwell.

Rahman MM and Kim HD., 2007, Charactrerization of waterborn polyurethane adhesives containing different soft segments. Adhesion Science Technology, 21, 81-96.

Rapacz-Kmita A, Paluszkiewicz C, Slosarczyk A, Paszkiewicz Z., 2005, FTIR and XRD investigations on the thermal stability of hydroxyapatite during hot pressing and pressureless sintering process. Journal of Molecular Structure, 744-747, 653-656.

Ratner BD and Castner DG., 1997, Surface Modification of Polymeric Biomaterials. New York, Plenum Press.

Ratner BD, Gladhill KW, Horbett TA., 1988, Analysis of in vivo enzymatic and oxidative degradation of polyurethane. Journal of Biomedical Materials Research, 22, 509-527.

Ratner BD, Hoffman AS, Schoen FJ, Lemons JE., 2004, Biomaterials Science: An Introduction to Materials in Medicine. Ed, Degradation of Material in Biological Environment. pp 411, Academic Press, USA.

Ravey M and Pearce EM., 1997, Flexible polyurethane foam. I. Thermal decomposition of a polyether-based, water-blown commercial type of flexible polyurethane foam. Journal of Applied Polymer Science, 63, 47-74.

Redey SA, Nardin M, Bernache-Assolant D, Rey C, Delannoy P, Sedel L, Marie PJ., 2000, Behavior of human osteoblastic cells on stoichiometric hydroxpayatite and type A carbonate apatite: Role of surface energy. Journal of Biomedical Materials Research, 50, 353-364.

Rehman I. and Bonfield W., 1997, Characterization of hydroxyapatite and carbonated apatite by photo acoustic FTIR spectroscopy. Journal of Materials Science: Materials in Medicine, 8, 1-4.

Rehman IU., 1992, Synthesis of polyurethanes for biomedical use. PhD Thesis, University of London.

Rehman IU., 1996, Biodegradable polyurethane, Biodegradable low adherence film for the prevention of adhesions after surgery. Journal of Biomaterials Applications, 11, 182-257.

Ren Z, Ma D, Yang X., 2003, H-bond and conformations of donors and acceptors in model polyether based polyurethanes. Polymer, 44, 6419-6425.

Ren ZY, Wu HP, Ma JM, Ma DZ., 2004, FTIR studies on the model polyurethane hard segments based on a new waterborne chain extender dimethylol butanoic acid (DMBA). Chinese Journal of Polymer Science, 22, 225-230.

Reneker HD and Chun I., 1996, Nanometer diameter fibers of polymer, produced by electrospinning. Nanotechnology, 7, 216-222.

Rhee S-H, Suetsugu Y, Tanaka J., 2001, Biomimetic configurational arrays of hydroxyapatite nanocrystals on bio-organics. Biomaterials, 22, 2843-2847.

Ritter AV, Swift Jr. EJ., 2000, Medium-viscosity polyether impression material: a case report. Compendium Continuous Education of Dentistry, 21, 993-996.

Roberson TM, Heymann H, Swift EJ., 2002, Sturdevant's Art and Science of Operative Dentistry. 4th edition, Mosby.

Roberts HW, Toth JM, Berzins DW, Charlton DG., 2008, Mineral trioxide aggregate material use in endodontic treatment: A review of the literature. Dental Materials, 24, 149-164.

Rodriguez-Lorenzo LM, Vallet-Regi M, Ferreira JMF., 2001, Fabrication of hydroxyapatite bodies by uniaxial pressing from a precipitated powder. Biomaterials, 22, 583-588.

Rosthauser JW, Haider KW, Steinlein CE., 1997, Mechanical and dynamic mechanical properties of polyurethane and polyurethane/polyurea elastomers based on 4, 4'-diisocyanatodicyclohexyl methane. Journal of Applied Polymer Science, 64, 957-970.

Rozenberg BA, Tenne R., 2008, Polymer-assisted fabrication of nanoparticles and nanocomposites. Progress in Polymer Science, 33, 40-112.

Rutnakornpituk M and Ngamdee P., 2006, Surface and mechanical properties of microporous membranes of poly(ethylene glycol)–polydimethylsiloxane copolymer/chitosan. Polymer, 47, 7909-7917.

Ruys AJ, Wei M, Sorrell CC, Dickson MR, Brandwood A, Milthorpe BK., 1995, Sintering effects on the strength of hydroxyapatite. Biomaterials, 16, 409-415.

Saleh IM, Ruyter IE, Haapasalo M, Orstavik D., 2002,The effects of dentine pretreatment on the adhesion of root-canal sealers. International Endodontic Journal, 35, 859-866.

Sank A, Chalabian-Baliozian J, Ertt D, Sherman R, Nimni M, Tuan TL., 1993, Cellular responses to silicone and polyurethane prosthetic surfaces. Journal of Surgical Research, 54, 12-20.

Sano H, Ciucchi B, Matthews WG, Pashley DH., 1994, Tensile properties of mineralized and demineralized human and bovine dentin. Journal of Dental Research, 73, 1205-1211.

Santerre JP, Woodhouse K, Laroche G, Labow RS., 2005, Understanding the biodegradation of polyurethane, from classical implants to tissue engineering materials. Biomaterials, 26, 7457-7470.

Santos C, Clarke RL, Braden M, Guitian F, Davy KWM., 2002, Water absorption characteristics of dental composites incorporating hydroxyapatite fillers. Biomaterials, 23, 1897-1904.

Sarig S and Kahana F., 2002, Rapid formation of nanocrystalline apatite. Journal of Crystal Growth, 237-239, 55-59.

Sarig S., 2004, Aspartic acid nucleates the apatite crystallites of bone: a hypothesis. Bone, 35, 108-113.

Schilder H., 1967, Filling root canals in three dimensions. Dental Clinics of North America, 11, 723-744.

Schilder H., 2006, Filling root canals in three dimensions. Journal of Endodontics, 32, 281-290.

Schiraldi C, D'Agostino A, Oliva A, Flamma F, De Rosa A, Apicella A, Aversa R, De Rosa M., 2004, Development of hybrid materials based on

hydroxyethylmethacrylate as support for improving cell adhesion and proliferation. Biomaterials, 25, 3645-3653.

Schmitt J and Flemming H-C., 1998, FTIR--spectroscopy in microbial and material analysis. International Biodeterioration & Biodegradation, 41, 1-11.

Schollengerger CS and Stewart FD., 1971, Thermoplastic polyurethane hydrolysis stability. Journal of Elastoplasticity, 3, 28-56.

Schulz W., 2000, Crafting a national nanotechnology effort. Chemical Engineering News, 78, 39-42.

Sebenik U, Golob J, Krajnc M., 2003, Comparison of properties of acrylic-polyurethane hybrid emulsions prepared by batch and semibatch processes with monomer emulsion feed. Polymer International, 52, 740-748.

Seo DS and Lee JK., 2008, AFM analysis of anisotropic dissolution in dense hydroxyapatites. Ultramicroscopy, 108, 1157-1162.

Sheikh N., 2003, The effect of radiosterilization on cytotoxicity of polyurethane film. Nuclear Instruments and Methods in Physics Research B, 208, 215-219.

Shi Z, Huang X, Cai Y, Tang R, Yang D., 2009, Size effect of hydroxyapatite nanoparticles on proliferation and apoptosis of osteoblast-like cells. Acta Biomaterialia, 5, 338-345.

Shih W-J, Chen Y-F, Wang M-C, Hon M-H., 2004, Crystal growth and morphology of the nano-sized hydroxyapatite powders synthesized from $CaHPO_4.2H_2O$ and $CaCO_3$ by hydrolysis method. Journal of Crystal Growth, 270, 211-218.

Shin M, Ishii O, Sueda T, Vacanti PJ., 2004, Contractile cardiac grafts using a novel nanofibrous mesh. Biomaterials, 25, 3717-3723.

Shuk P, Suchanek LW, Hao T, Gulliver E, Riman ER, Senna M, TenHuisen SK, Janas FV., 2001, Mechanochemical-hydrothermal preparation of crystalline hydroxyapatite powders at room temperature. Journal of Material Research, 16, 1231-1234.

Siddharthan A, Seshadri SK, Kumar TSS., 2006, Influence of microwave power on nanosized hydroxyapatite particles. Scripta Materialia, 55, 175-178.

Sideridou I, Tserki V, Papanastasiou G., 2003, Study of water sorption, solubility and modulus of elasticity of light-cured dimethacrylate-based dental resins. Biomaterials, 24, 655-665.

Silikas N, Masouras K, Satterthwaite J, Watts DC., 2007, Effect of nanofillers in adhesive and aesthetic properties of dental resin-composite. International Journal of Nano and Biomaterials, 1, 116-127.

Simmons A, Hyvarinen J, Odell RA, Martin DJ, Gunatillake PA, Noble KR, Poole-Warren LA., 2004, Long-term in vivo biostability of poly(dimethylsiloxane)/poly(hexamethylene oxide) mixed macrodiol-based polyurethane elastomers. Biomaterials, 25, 4887-4900.

Simmons JJ., 1983, The miracle mixture. Glass ionomer and alloy powder. Texas Dental Journal. 100, 6-12.

Sinha A, Nayar S, Agrawal A., 2003, Synthesis of nanosized and microporous precipitated hydroxyapatite in synthetic polymers and biopolymers. Journal of American Ceramic Society, 86, 357-359.

Slosarczyk A, Stobierska E, Paszkiewicz Z, Gawlicki M., 1996, Calcium Phosphate materials prepared from precipitate with various calcium,phosphorous molar ratio. Journal of American Ceramic Society, 79, 2539-2544.

Slosarzyk A, Stobierska E, Paszkiewwicz Z., 1999, Porous hydroxyapatite ceramics. Journal of Materials Science Letters, 19, 1163-1165.

Sly MM, Morre K, Platt JA, Brown CE., 2007, Push-out bond strength of a new endodontic obturating system (Rsilon/Epiphany). Journal of Endodontics, 33, 160-162.

Smith DC., 1998, Development of glass-ionomer cement systems. Biomaterials, 19, 467-478.

Smith R, Williams DF, Oliver C., 1987, The biodegradation of poly (ether urethanes). Journal of Biomedical Materials Research, 21, 1149-1165.

Soderholm K-J, Mariotti A., 1999, Bis-GMA-based resins in dentistry, are they safe? Journal of Australian Dental Association, 130, 201-209.

Song YM, Chen WC, Linliu K, Tseng YH., 1996, Effect of isocyanates on the crystallinity and thermal stability of polyurethanes. Journal of Applied Polymer Science, 62, 827-834.

Speckhard TA and Cooper SL., 1986, Ultimate Tensile Properties of Segmented Polyurethane Elastomers. Factors Leading to Reduced Properties for Polyurethanes Based on Non-Polar Soft Segments. Rubber Chemistry and Technology, 59, 405-431.

Stachelek SJ, Alferiev I, Choi H, Chan CW, Zubiate B, Sacks M, Composto R, Chen IW, Levy RJ., 2006, Prevention of oxidative degradation of polyurethane by covalent attachment of di-tert-butylphenol residues. Journal of Biomedical Materials Research Part A, 78A, 653-661.

Stanciu A, Airinei A, Timpu D, Ioanid A, Ioan C, Bulacovschi V., 1999, Polyurethane/ polydimethylsiloxane segmented copolymers. European Polymer Journal, 35, 1959-1965.

Stansbury JW, Lemon MT, Lu H, Ding X, Lin Y, Ge J., 2005, Conversion-dependent shrinkage stress and strain in dental resins and composites. Dental Materials, 21, 56-67.

Steiner T and Saenger W., 1993, Role of C—H…O hydrogen bonds in the coordination of water molecules. Analysis of neutron diffraction data. Journal of American Chemical Society, 115, 4540-4547.

Stephenson CV, Coburn Jr WC, Wilcox WS., 1961, The vibrational spectra and assignments of nitrobenzene, phenyl isocyanate, phenyl isothiocyanate, thionylaniline and anisole. Spectrochimica Acta, 17, 933-946.

Stirna UK, Tupureina VV, Misane MM, Dzene AV, Sevast'yanova IV., 2002, The effect of location of side chains in segmented poly(ester urethanes) on their hydrolytic and enzymatic degradation. Polymer Science Series, 44A, 510-517.

Stoch A, Jastrzebski W, Brozek A, Trybalska B, Cichocinska M, Szarawara E., 1999, FTIR monitoring of the growth of the carbonate containing apatite layers from simulated and natural body fluids. Journal of Molecular Structure, 511-512, 287-294.
Stock CJR., 2004, Endodontics. 3rd edition, Elsevier, Mosby.

Stokes K, Coury A, Urbanski P., 1987, Auto oxidative degradation of implanted polyether polyurethane devices. Journal of Biomaterials Applied, 1, 411-446.

Storm AJ, Chen JH, Ling XS, Zandbergen W, Dekker C., 2005, Electron-beam-induced deformations of SiO_2 nanostructures. Journal of Applied Physics, 98, 014307.

Suchanek W and Yoshimura M., 1998, Processing and properties of hydroxyaptite-based biomaterials for use as hard tissue replacement implants. Journal of Materials Research, 13, 94-117.

Suchanek W, Yashima M, Kakihana M, Yoshimura M., 1996, Processing and mechanical properties of hydroxyapatite reinforced with hydroxyapatite whiskers. Biomaterials, 17, 1715-1723.

Sue K, Kimura K, Arai K., 2004, Hydrothermal synthesis of ZnO nanocrystals using microreactor. Materials Letters, 58, 3229-3231.

Suzuki O, Kamakura S, Katagiri T, Nakamura M, Zhao B, Honda Y, Kamijo R., 2006, Bone formation enhanced by implanted ocatcalcium phosphate involving conversion into Ca-deficient hydroxyapatite. Biomaterial, 27, 2671-268.

Tadic C, Peters F, Epple M., 2002, Continuous synthesis of amorphous carbonated apatite. Biomaterials, 23, 2553-2559.

Takahara A, Zokkema A, Cooper CL, Coury AJ., 1991, Effect of surface hydrophilicity on ex vivo blood compatibility of segmented polyurethanes. Biomaterials, 12, 324-334.

Takahashi T, Hayashi N, Hayashi S., 1996, Structure and properties of shape-memory polyurethane block copolymers. Journal of Applied Polymer Science, 60, 1061-1069.

Tan S-H, Inai R, Kotaki M, Ramakrishna S., 2005, Systematic parameter study for ultra-fine fiber fabrication via electrospinning process. Polymer, 46, 6128-6134.

Tanahashi M and Matsuda T., 1997, Surface functional group dependence on apatite formation on self-assembled monolayers in a simulated body fluid. Journal of Biomedical Materials Research, 34, 305-315.

Tang RYW, Gonzalez JB, Roberts GD., 1975, Polyurethane elastomer as a possible resilient material for denture prostheses: A microbiological evaluation. Journal of Dental Research, 54, 1039-1045.

Tang YW, Labow RS, Santerre JP., 2001, Enzyme induced biodegradation of polycarbonate-polyurethanes: dependence on hard-segment chemistry. Journal of Biomedical Materials Research, 57, 597-611.

Tang YW, Labow RS, Santerre JP., 2001, Enzyme induced biodegradation of polycarbonate-polyurethanes: dependence on hard-segment chemistry. Journal of Biomedical Materials Research, 56, 516-528.

Tanzi MC, Mantovani D, Petrini P, Guidoin R, Laroche G., 1997, Chemical stability of polyether urehtanes versus polycarbonate urethanes. Journal of Biomedical Materials Research, 36, 550-559.

Ten Cate AR., 1998, Oral Histology, development, structure and function. 5th edition, Mosby.

Teng S, Shi J, Chen L., 2006, A novel method to synthesize large-sized hydroxyapatite rods. Journal of Crystal Growth, 290, 683-688.

Teo WE and Ramakrishna S., 2006, A review on electrospinning design an nanofibre assemblies. Nanotechnology, 17, 89-106.

Theron SA, Zussman E, Yarin AL., 2002, Electrostatic field-assisted alignment of electrospun nanofibers. Nanotechnology, 12, 384-390.

Theron SA, Zussman E, Yarin AL., 2004, Experimental investigation of the governing parameters in the electrospinning of polymer solution. Polymer, 45, 2017-2030.

Thompson JI and Gregson PJ., 1999, Analysis of push out test data based on interfacial fracture energy. Journal of Materials Science: Materials in Medicine, 10, 863-868.

Thylstrup A, Brunn C, Holemen L., 1994, In vivo caries models—mechanisms for caries initiation and arrestment. Advances in Dental Research, 8, 144-157.

Tian J, Yi SZ, Shao Y, Shah H., 1995, SiC nanoparticle-reinforced Hap composites. In: Abstract of the 97th Annual Meeting of the ACerS, Cincinnati, Ohio.

Tien Y.I and Wei KH., 2002, The effect of nano-sized silicate layers from monmorillonite on glass transition, dynamic mechanical and thermal degradation properties of segmented polyurethane. Journal of Applied Polymer Science, 86, 1741–1748.

Trigwell S, De S, Sharma R, Mazumder MK, Mehta JL,. 2005, Structural evaluation of radially expandable cardiovascular stents encased in a polyurethane film. Journal of Biomedical Materials Research Part B: Applied Biomaterials, 76B, 241-250.

Tsuda H and Arends J., 1997, Raman spectroscopy in dental research: A short review of recent studies. Advance Dental Researches, 11, 539-547.

Turssi CP, Ferracane JL, Vogel K., 2005, Filler features and their effects on wear and degree of conversion of particulate dental resin composites. Biomaterials, 26, 4932-4937.

Umare SS and Chandure AS., 2008, Synthesis, characterization and biodegradation studies of poly(ester urethane)s. Chemical Engineering Journal, 142, 65-77.

Vaidya A and Chaudhury MK., 2002, Synthesis and surface properties of environmentally responsive segmented polyurethane. Journal of Colloid and Interface Sciences, 249, 235-245.

Vallet-Regi M and Gonzalez-Calbet JM., 2004, Calcium phosphates as substitution of bone tissues. Progress in Solid State Chemistry, 32, 1-31.

van Bogart JWC, Bluemke DA, Cooper SL., 1981, Annealing-induced morphological changes in segmented elastomers. Polymer, 22, 1428-1438.

Verheyen CCPM, De Wijn JR, Van Blitterswijk CA, De Groot K., 1992, Evaluation of hydroxyapatite/poly(L-lactide) composites: mechanical behavior. Journal of Biomedical Materials Research, 26, 1277-1296.

Viitala R, Jokinen M, Peltola T, Gunnelius K, Rosenholm JB., 2002, Surface properties of in vitro bioactive and non-bioactive sol-gel derived materials. Biomaterials, 23, 3073-3086.

Vijayalakshmi U and Rajeshwari S., 2006, Preparation and characterization of microcrystalline hydroxyapatite using sol gel method. Trends of Biomaterial Artificial Organs, 19, 57-62.

Wakasa K, Yoshida Y, Ikeda A, Natsir N, Satou N, Shintani H, Yamaki M., 1997, Dental application of polyfunctional urethane comonomers to composite resin veneering materials. Journal of Materials Science: Materials in Medicine, 8, 57-60.

Wang C, Hsu C, Lin JH., 2006, Scaling Laws in electrospinning of polystyrene solutions. Macromolecules, 39, 7662-7672.

Wang LF, Ji Q, Glass TE, Ward TC, McGrath JE, Muggli M, Burns G, Sorathia U., 2000, Synthesis and characterization of organosiloxane modified segmented polyether polyurethanes. Polymer, 41, 5083-5093.

Wang LF., 2005, Effect of soft segment length on the thermal behaviors of fluorinated polyurethanes. European Polymer Journal, 41, 293-301.

Wang M and Bonfield W., 2001, Chemically coupled hydroxyapatite-polyethylene composite, structure and properties. Biomaterials, 22**,** 1311–1320.

Wang Q, Xian W, Li S, Liu C, Padua G.W., 2008, Topography and biocompatibility of patterned hydrophobic/hydrophilic zein layers. Acta Biomaterialia, 4, 844-851.

Wang YZ, Hsu YC, Wu RR, Kao HM., 2003, Synthesis and structure properties of polyurethane based conducting copolymer I. ^{13}C NMR analysis. Synthetic Metals, 132, 151-160.

Wataha JC., 2001, Principles of biocompatibility for dental practitioners. The Journal of Prosthetic Dentistry, 86, 203-209.

Webster TJ, Siegel RW, Bizios R., 1999, Osteoblast adhesion on nanophase ceramics. Biomaterials, 20, 1221-1227.

Webster TJ, Tong Z, Liu J, Banks MK., 2005, Adhesion of Pseudomonas fluorescens onto nanophase materials. Nanotechnology, 16, 449-457.

Wei K, Wang Y, Lai C, Ning C, Wu D, Wu G, Zhao N, Chen X, Ye J., 2005, Synthesis and characterization of hydroxyapatite nanobelts and nanoparticles. Materials Letters, 59, 220-225.

Wen J, Somorjai G, Lim F, Ward R., 1997, XPS study of surface composition of a segmented polyurethane block copolymer modified by PDMS end groups and its blend with phenoxy. Macromolecules, 30, 7206-7213.

West JC and Cooper SL., 1977, Infrared Studies of Block Copolymers. Journal of Polymer Science, 60, 127-131.

Whitworth JM, Makhani SH, McCabe JF., 1999, Cure behaviour of visible light-activated pattern materials. International Endodontic Journal, 32, 191-196.

Williams DF., 1982, Biodegradation of surgical polymers. Journal of Materials Science, 17, 1233-1246.

Williams DF., 1994, Science and applications of biomaterials. Advance Materials Technology and Monitoring, 2, 1-38

Williams DF., 1999, The Williams Dictionary of Biomaterials. Liverpool University Press, UK

Williams DF., 2008, On the mechanisms of biocompatibility. Biomaterials, 29, 2941-2953.

Williams JA, Billington RW, Pearson GJ., 1992, The comparative strengths of commercial glass-ionomer cements with and without metal additions. British Dental Journal, 172, 279-282.

Wilson AD and Kent BE., 1972, A new translucent cement for dentistry. The glass ionomer cement. British Dental Journal, 132,133-135.

Wilson AD and McLean JW., 1988, Glass-ionomer cement. 2nd Edition, Chicago IL, Quintessence.

Wilson AD., 1989, Developments in glass-ionomer cements. International Journal of Prosthodontics. 2, 438-446.

Wilson AD., 1990, Resin-modified glass-ionomer cements. International Journal of Prosthodontics, 3, 425-429.

Wischnitzer S., 1980, Introduction to Electron Microscopy. 3rd Edition, Pergamon Press Inc.

Wu C and Chang J., 2006, A novel akermanite bioceramic: preparation and characteristics. Journal of Biomaterials Application, 21, 119-129.

Wu Y, Hench LL, Du J, Choy KL, Guo J., 2004, Preparation of hydroxyapatite fibers by electrospinning technique. Journal of American Ceramic Society, 87, 1988-1991.

Wunderlich B., 1990, Thermal Analysis. Academic Press, Inc, San Diego, CA.

Wutticharoenmongkol P, Sanchavanakit N, Pavasant P, Supaphol P., 2006, Preparation and characterization of novel bone scaffolds based on electrospun

polycaprolactone fibers filled with nanoparticles. Macromolecular Bioscience, 6, 70-77.

Xin Y, Huang ZH, Yan EY, Zhang W, Zhao Q., 2006, Controlling poly (p-phenylene vinylene)/poly (vinyl pyrrolidone) composite nanofibers in different morphologies by electrospinning. Applied Physics Letters, 89, Art. No. 053101.

Xio H and Song M., 2006, Preparation and characterisation of polyurethane grafted single-walled carbon nanotubes and derived polyurethane nanocomposites. Journal of Materials Chemistry, 16, 1843-1851.

Xu HHK, Schumacher GE, Eichmiller FC, Peterson RC, Antonucci JM, Mueller HJ., 2003, Continuous-fiber perform reinforcement of dental resin composite restorations. Dental Materials, 19, 523-530.

Xu T, Zhang N, Nichols HL, Shi D, Wen X., 2007, Modification of nanostructured materials for biomedical applications. Materials Science and Engineering, 27, 579-594.

Xu Y, Wang D, Yang L, Tang H., 2001, Hydrothermal conversion of coral into hydroxyapatite. Materials Characterization, 47, 83-87.

Yamaguchi M, Terao Y, Ogawa T, Takahashi T, Hamada S, Kawabata S., 2006, Role of streptococcus sanguinis sortase A in bacterial colonization. Microbes and Infection, 8, 2791-2796.

Yamashita K, Oikawa N, Umegaki T., 1996, Acceleration and deceleration of bone-like crystal growth on ceramic hydroxyapatite by electric poling. Chemistry of Materials, 8, 2697–2700.

Yan L, Li Y, Deng Z-X, Zhuang J, Sun X., 2001, Surfactant-assisted hydrothermal synthesis of hydroxyapatite nanorods. International Journal of Inorganic Materials, 3, 633-637.

Yan X, Huang X, Yu C, Deng H, Wang Y, Zhang Z, Qiao S, Lu G, Zhao D., 2006, The in-vitro bioactivity of mesoporous bioactive glasses. Biomaterials, 27, 3396-3403.

Yang B, Huang WM, Li C, Chor JH., 2005, Effects of moisture on the glass transition temperature of polyurethane shape memory polymer filled with nano-carbon powder. European Polymer Journal, 41, 1123-1128.

Yesinowski JP and Eckert H., 1987, Hydrogen environments in calcium phosphates: 1H MAS NMR at high spinning speeds. Journal of American Chemical Society, 109, 6274-1682.

Yilgor E, Burgaz E, Yurtsever E, Yilgor I., 2000, Comparison of hydrogen bonding in polydimethylsiloxane and polyether based urethane and urea copolymers. Polymer, 41, 849-857.

Yin G, Liu Z, Zhan J, Ding F, Yuan N., 2002, Impacts of the surface charge property on protein adsorption on hydroxyapatite. Chemical Engineering Journal, 87, 181-186.

Yoon SC and Ratner BD., 1988, Surface and bulk structure of segmented poly (ether urethanes) with perfluoro chain extenders. 2. FTIR, DSC, and X-ray Photoelectron Spectroscopic studies. Macromolecules, 21, 2392-2400.

Yoshida Y, Shirai K, Nakayama Y, Itoh M, Okazaki M, Shintani H, Inoue S, Lambrechts P, Vanherle G, Meerbeek VB., 2002, Improved filler-matrix coupling in resin composites. Journal of Dental Research, 81, 270-273.

Yoshimin Y and Maeda K., 1995, Histologic evaluation of tetracalcium phosphate-based cement as a direct pulp-capping agent. Oral Surgery, Oral Medicine, Oral Pathology, Oral Radiology and Endodontics, 79, 351-358.

Yoshimoto H, Shin MY, Terai H, Vacanti PJ., 2003, A biodegradable nanofibre scaffold by electrospinning and its potential for bone tissue engineering. Biomaterials, 24, 2077-2082.

Yoshimura M, Sujaridworakun P, Koh F, Fujiwara T, Pongkao D, Ahniyaz A., 2004, Hydrothermal conversion of calcite crystals to hydroxyapatite. Materials Science and Engineering C, 24, 521-525.

Yu C and Abbott PV., 2007, An overview of the dental pulp, its functions and responses to injury. Australian Dental Journal Supplement, 52, 4-16.

Zaidi M, Kerby J, Huang CL, Alam T, Rathod H, Chambers TJ, Moonga BS., 1991, Divalent cations mimic the inhibitory effect of extracellular ionized calcium on bone resorption by isolated rat osteoclasts, further evidence for a "calcium receptor". Journal of Cell Physics, 149, 422-427.

Zaslansky P, Friesem AA, Weiner S., 2006, Structure and mechanical properties of the soft zone separating bulk dentin and enamel in crowns of human teeth: Insight into tooth function. Journal of Structural Biology, 153, 188-199.

Zhang F, Zhou Z-H, Yang S-P, Mao L-H, Chen H-M, Yu X-B., 2005, Hydrothermal synthesis of hydroxyapatite nanorods in the presence of anionic starburst dendrimers. Materials Letters, 59, 1422-1425.

Zhang H, Wang Y, Yan Y, Li S., 2003, Precipitation of biocompatible hydroxyapatite whiskers from moderately acid solution. Ceramic International, 29, 413-418.

Zhang R and Ma PX., 2000, Synthetic nano-fibrillar extracellular matrices with predesigned macroporous architectures. Journal of Biomedical Materials Research Part B: Applied Biomaterials, 52, 430-438.

Zhao C-X and Zhang W-D., 2008, Preparation of waterborne polyurethane nanocomposites: Polymerization from functionalized hydroxyapatite. European Polymer Journal, 44, 1988-1995.

Zhao Q, Wang C, Liu Y, Wang S., 2007, Bacterial adhesion on the metal-polymer composite coatings. International Journal of Adhesion & Adhesives, 27, 85-91.

Zhi J, Yuan JK, Li SF, Chow CW., 2006, Study of FTIR spectra and thermal analysis of polyurethane. Spectroscopy and Spectral Analysis, 26, 624-628.

Zhu W, Wang X, Yang B, Tang X., 2001, A novel ionic-conduction mechanism based on polyurethane electrolyte. Journal of Polymer Science B: Polymer Physics, 39, 1246-1254.

Zhu X, Fibl O, Scheideler L, Geis-Gerstorfer J., 2006, Characterization of nano hydroxyapatite/collagen surfaces and cellular behaviors. Journal of Biomedical Materials Research A, 79, 114-127.

Zia KM, Barikani M, Zuber M, Bhatti IA, Sheikh MA., 2008, Molecular engineering of chitin based polyurethane elastomers. Carbohydrate Polymers, 74, 149-158.

Appendices

Appendix I

1.1- Tooth Structure (Dentine)

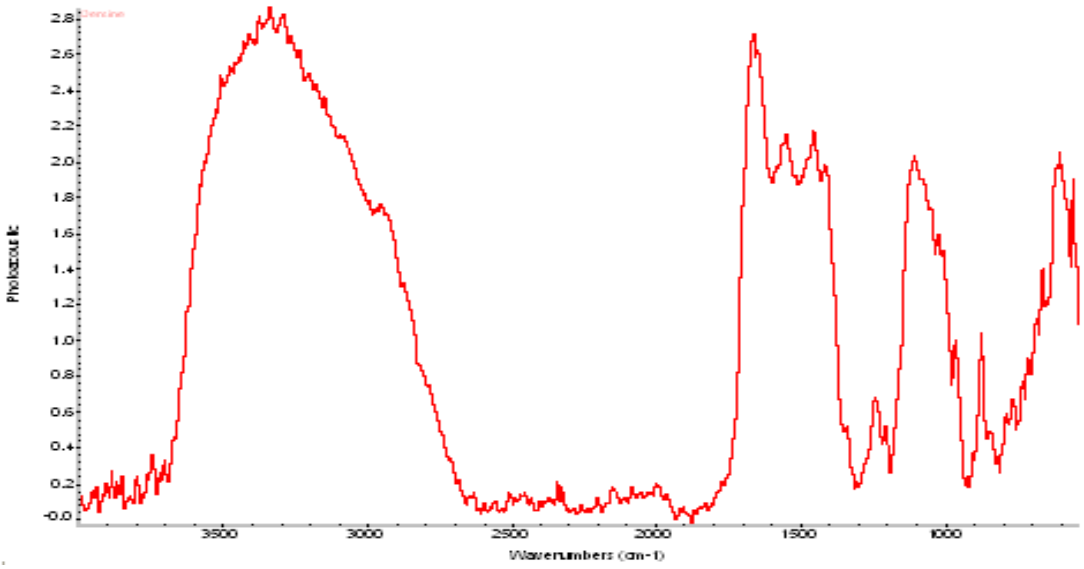

Figure A1.1 FTIR spectrum of dentine showing characteristic peaks of OH (3600-2700 cm^{-1}), amide/CO_3 (1800-1400 cm^{-1}) and PO_4 (1100-950 cm^{-1})

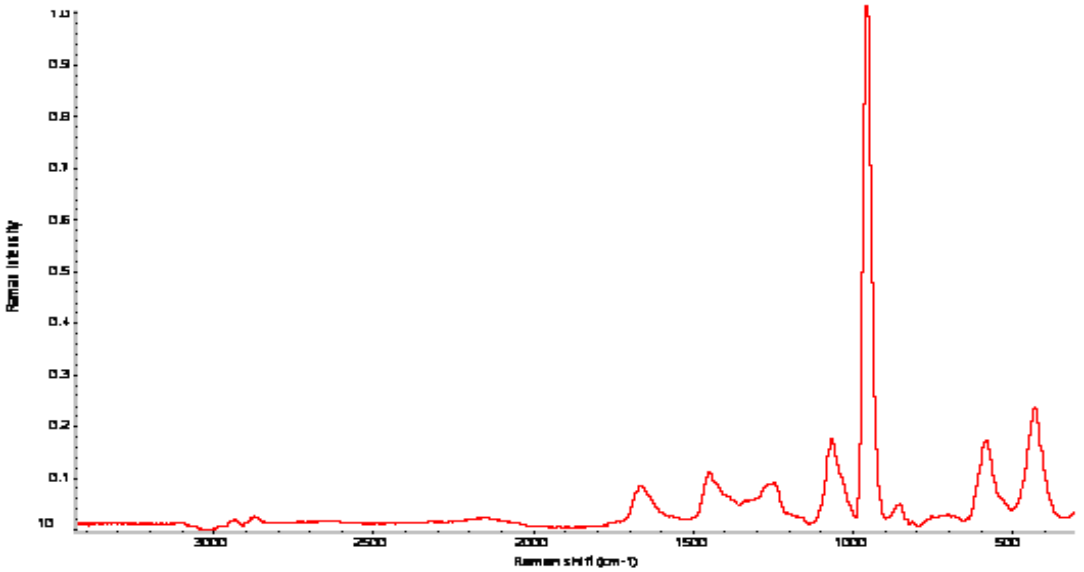

Figure A1.2 Raman spectrum of dentine showing characteristic peaks of amide (1800-1400 cm^{-1}) and PO_4 (960 cm^{-1})

Appendix 2

2.1- Synthesis of Polyurethane

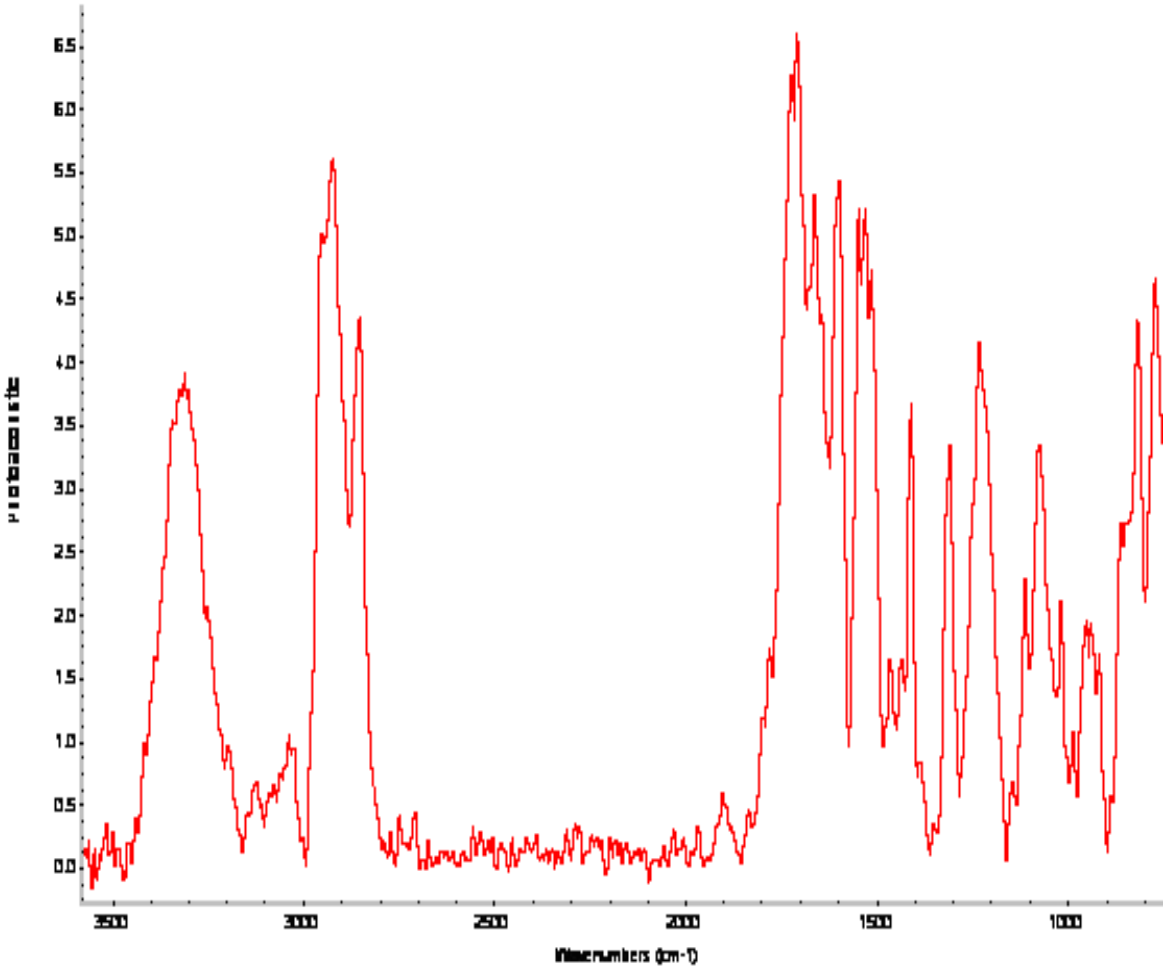

Figure A2.1 FTIR spectrum of polyurethane synthesised by using PEG (soft segment), MDI (hard segment) and BD (chain extender). The spectrum showing characteristic peaks at 3320 cm^{-1} (N—H), 2915 cm^{-1}(asymmetric stretching CH_2), 1690-1685 cm^{-1} (C=O), and 1120-960 cm^{-1} (C—O—C)

2.2- Supercritical Fluid Method

2.2.1- Synthesis of Polyurethane

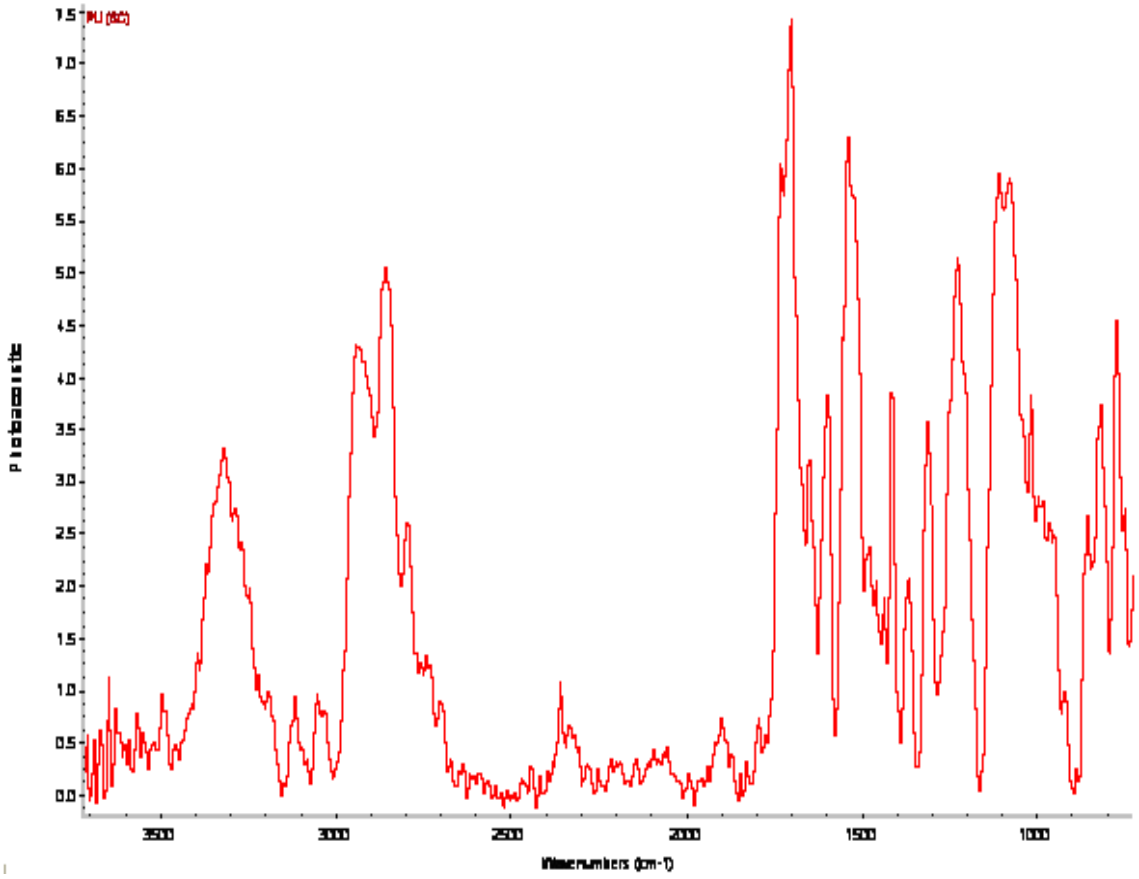

Figure A2.2 FTIR spectrum of polyurethane synthesised using Supercritical Fluid Method. The spectrum showing characteristic peaks at 3320 cm^{-1} (N—H), 2915 cm^{-1}(asymmetric stretching CH_2), 2350 cm^{-1} (CO_2), 1720-1700 cm^{-1} (C=O), and 1150-920 cm^{-1} (C—O—C)

2.2.2- Synthesis of Polyurethane/nano-Hydroxyapatite

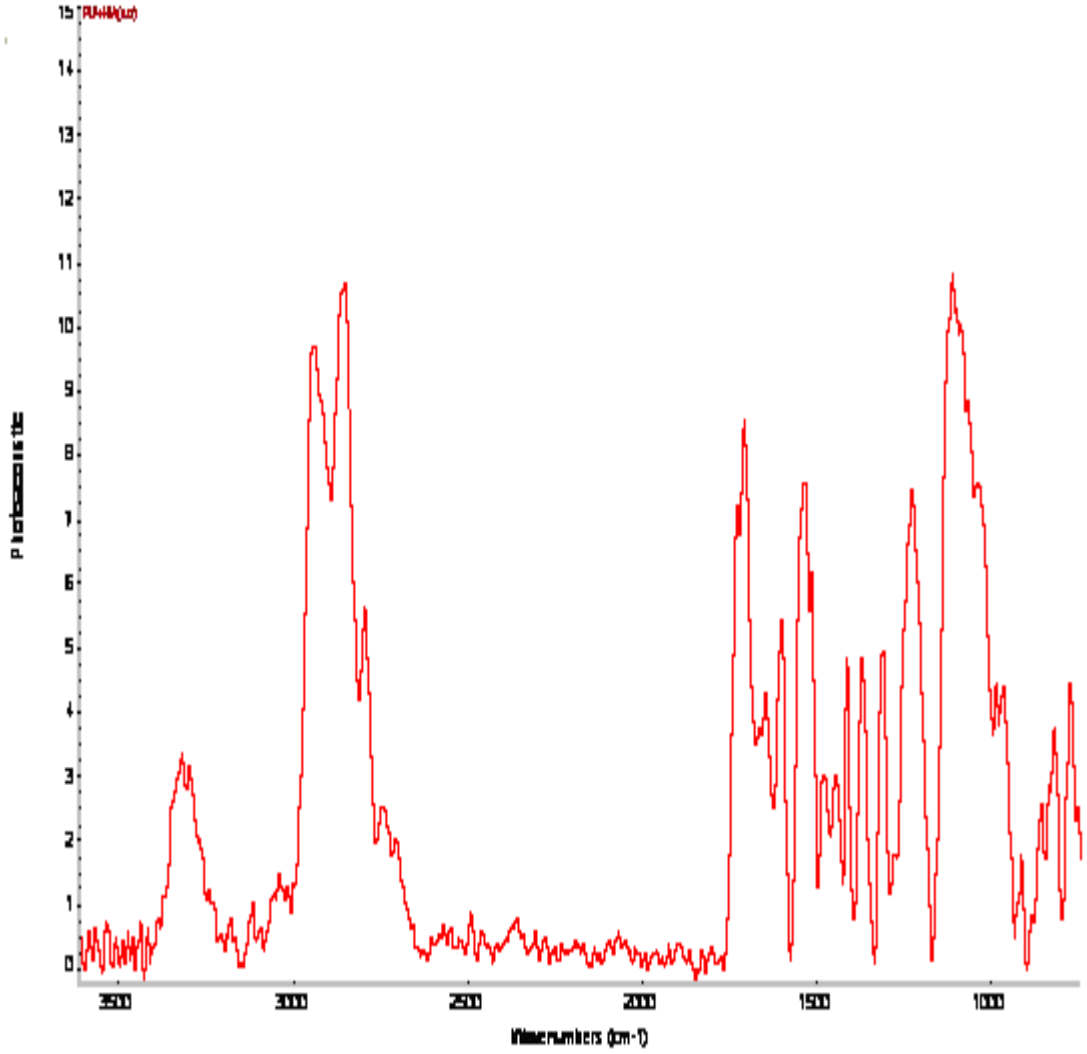

Figure A2.3 FTIR spectrum of polyurethane/nano-hydroxyapatite composite synthesised using Supercritical Fluid Method. The spectrum showing characteristic peaks at 3320 cm^{-1} (N—H), 2915 cm^{-1}(asymmetric stretching CH_2), 1730-1700 cm^{-1} (C=O), and 1150-920 cm^{-1} (C—O—C)

Appendix 3

3.1- Biostability

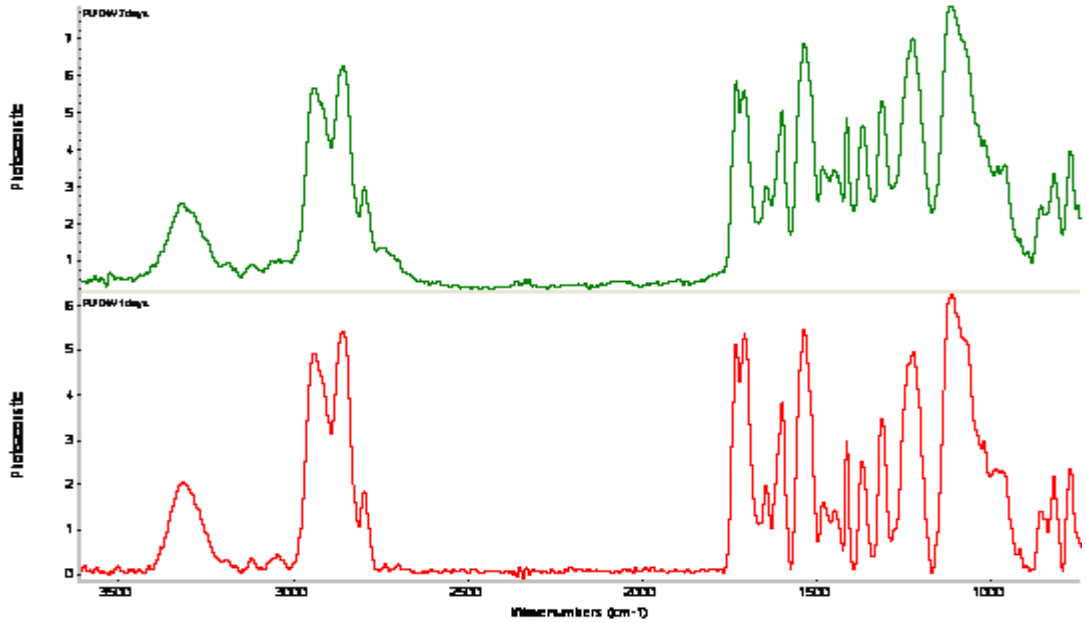

Figure A3.1 Comparative FTIR spectra of PU treated with deionised water at 1 (red), and 7 (green) days

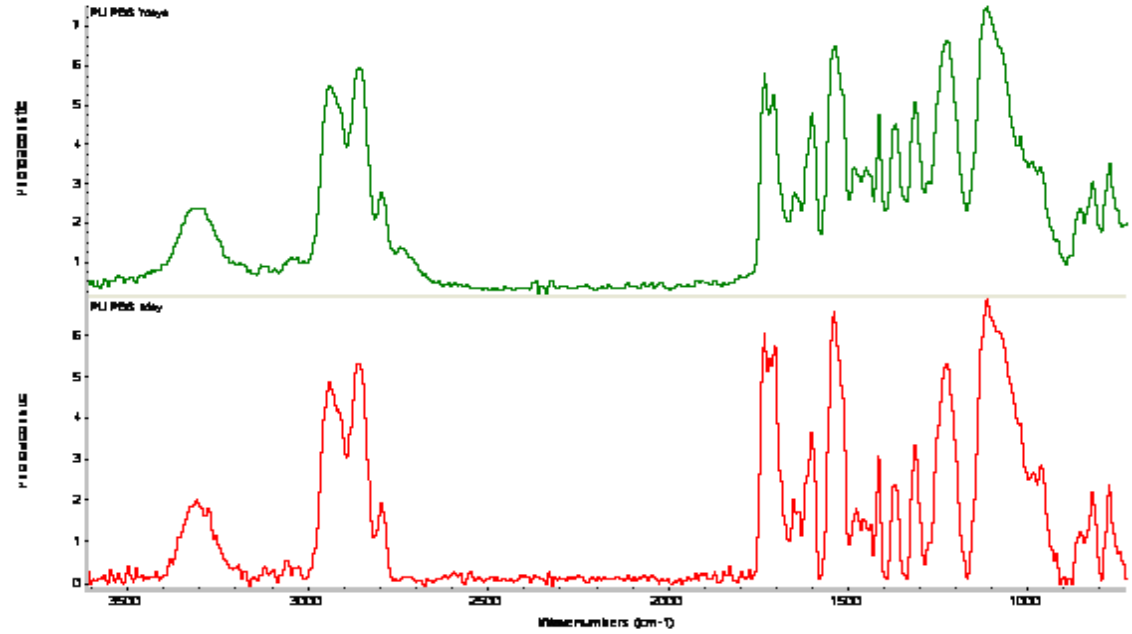

Figure A3.2 Comparative FTIR spectra of PU treated with PBS at 1 (red), and 7 (green) days

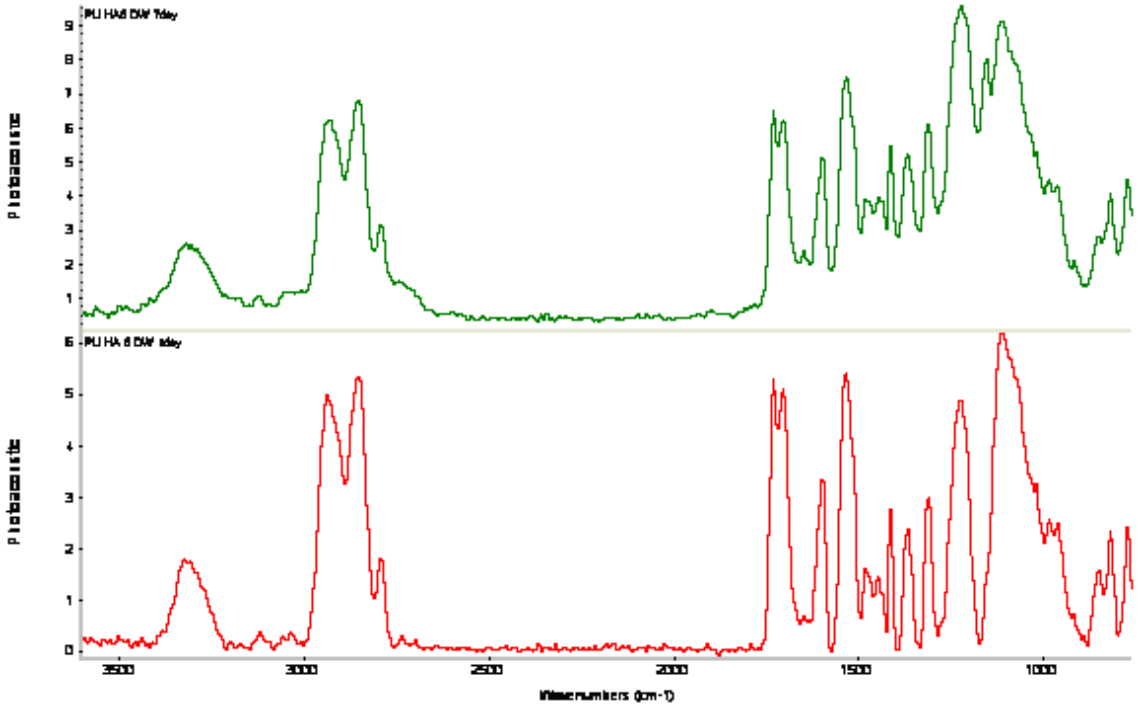

Figure A3.3 Comparative FTIR spectra of PU/nHA5 treated with deionised water at 1 (red), and 7 (green) days

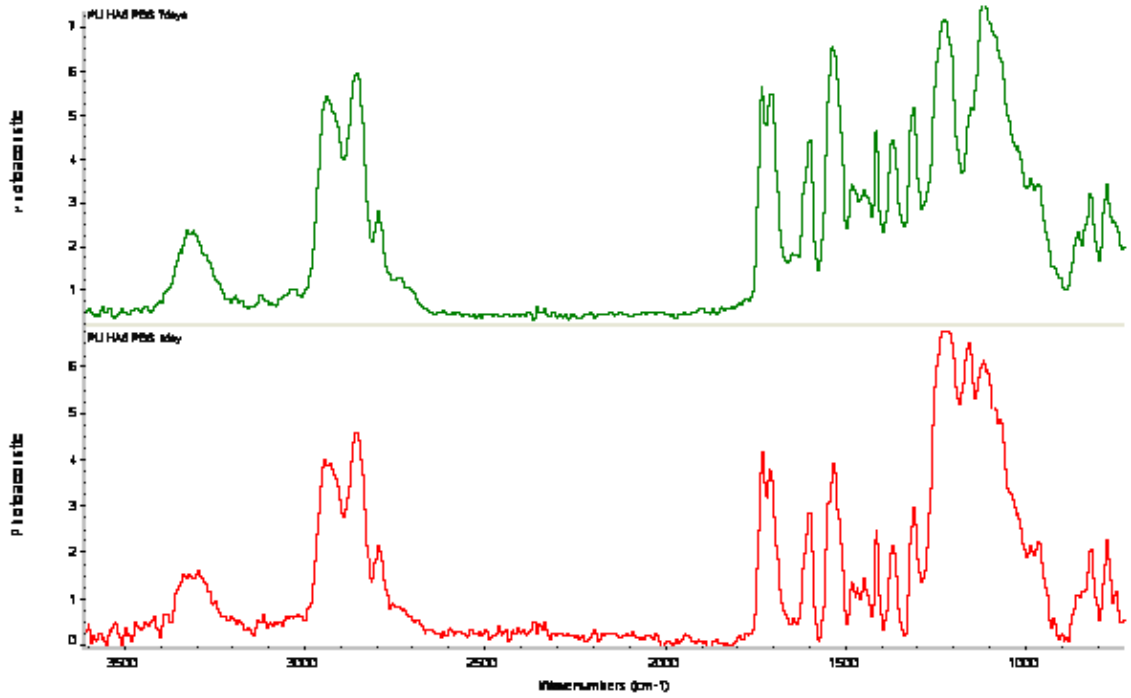

Figure A3.4 Comparative FTIR spectra of PU/nHA5 treated with PBS at 1 (red), and 7 (green) days

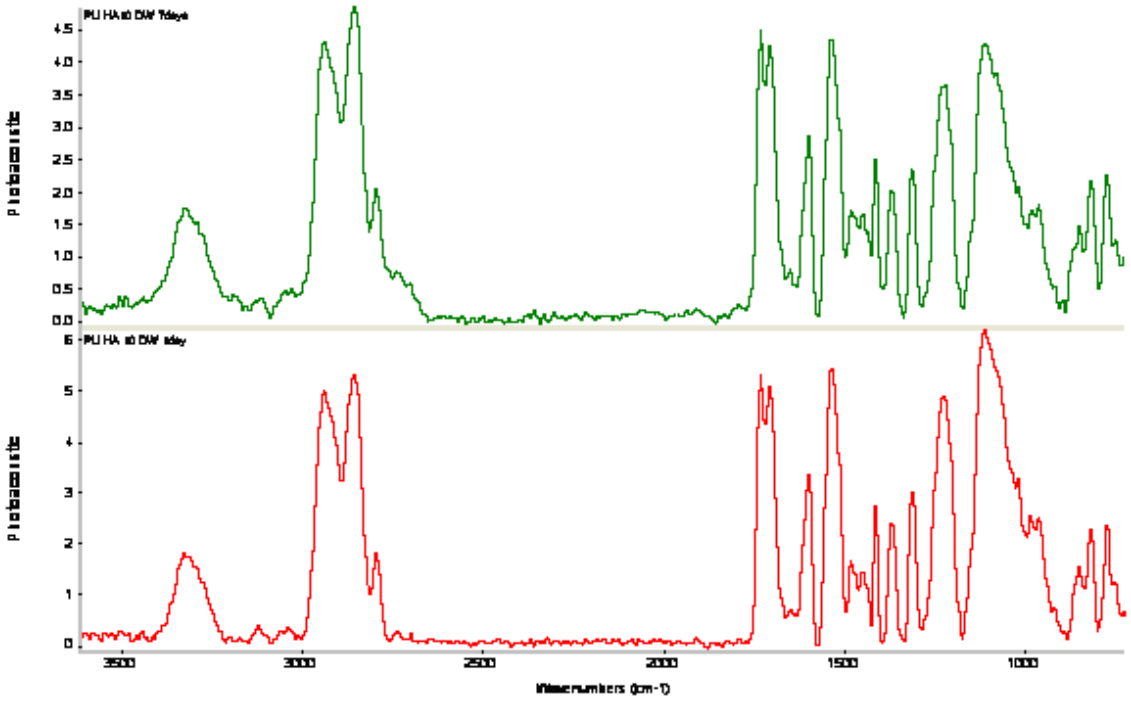

Figure A3.5 Comparative FTIR spectra of PU/nHA10 treated with deionised water at 1 (red), and 7 (green) days

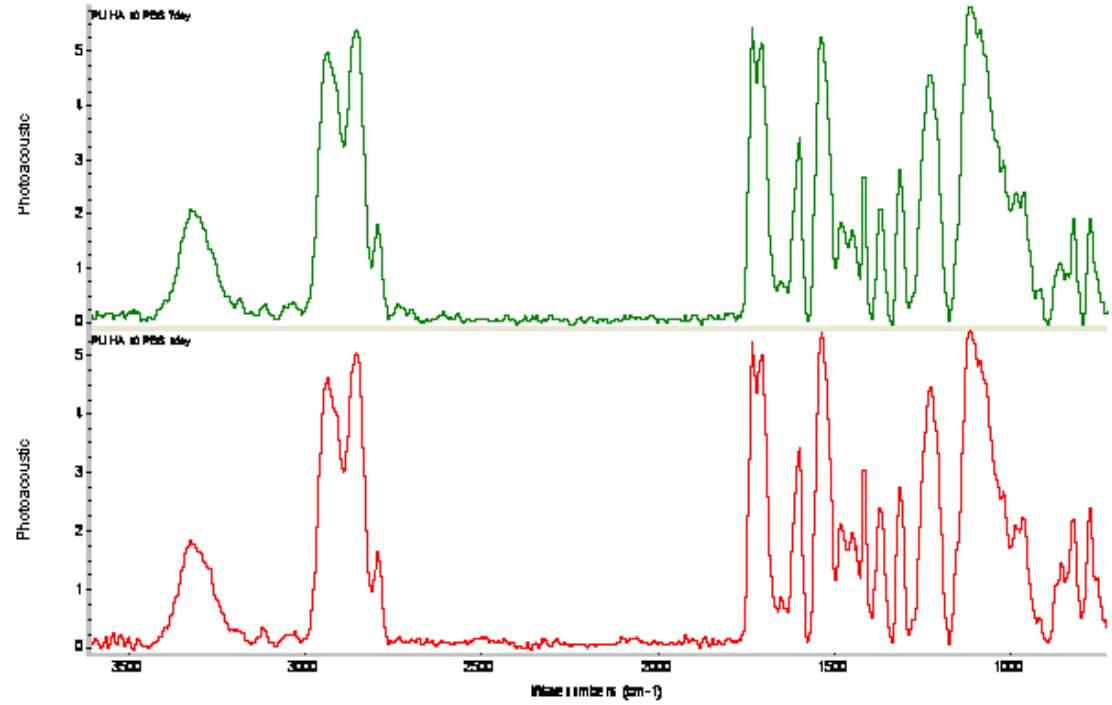

Figure A3.6 Comparative FTIR spectra of PU/nHA10 treated with PBS at 1 (red), and 7 (green) days

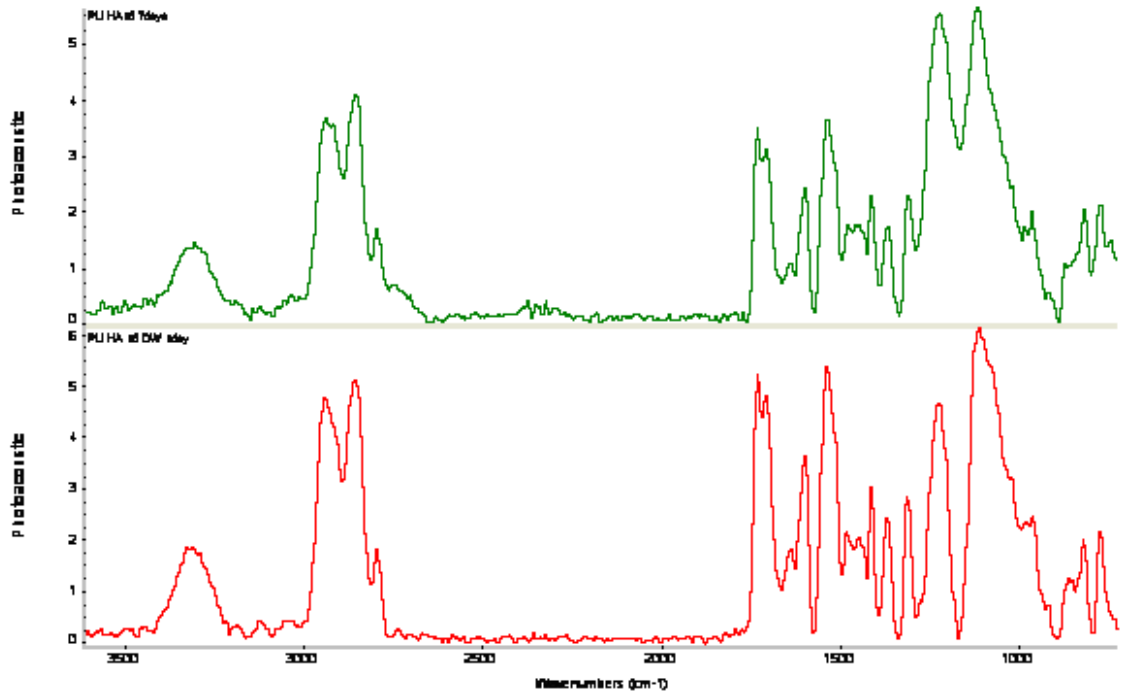

Figure A3.7 Comparative FTIR spectra of PU/nHA15 treated with deionised water at 1 (red), and 7 (green) days

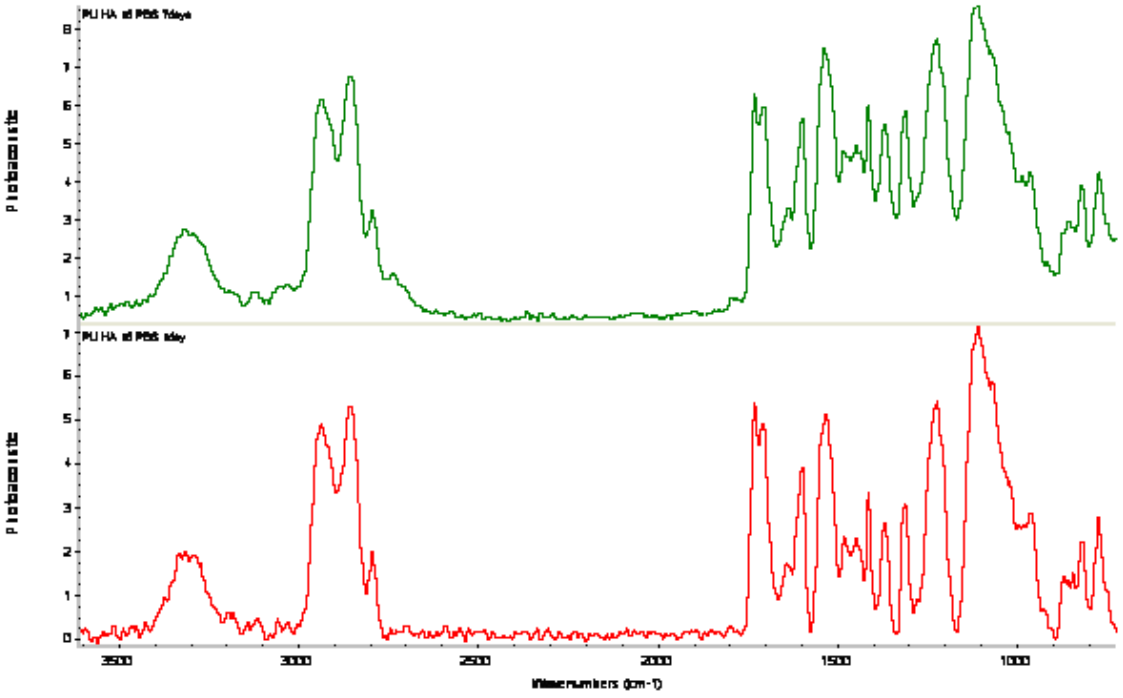

Figure A3.8 Comparative FTIR spectra of PU/nHA15 treated with PBS at 1 (red), and 7 (green) days

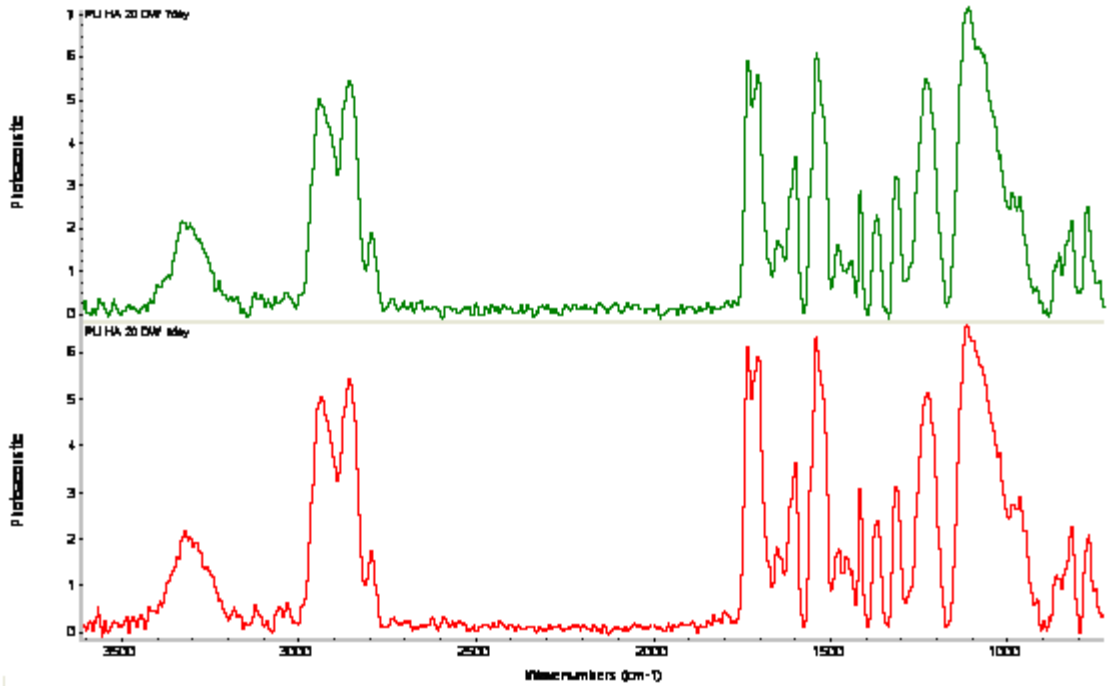

Figure A3.9 Comparative FTIR spectra of PU/nHA20 treated with deionised water at 1 (red), and 7 (green) days

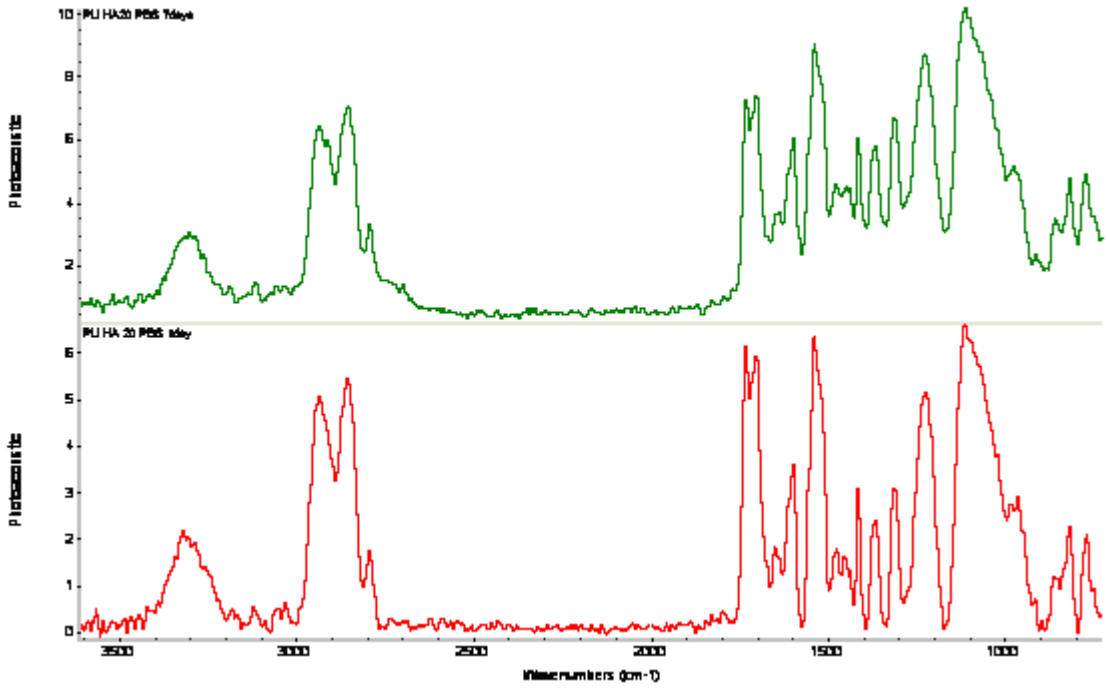

Figure A3.10 Comparative FTIR spectra of PU/nHA20 treated with PBS at 1 (red), and 7 (green) days

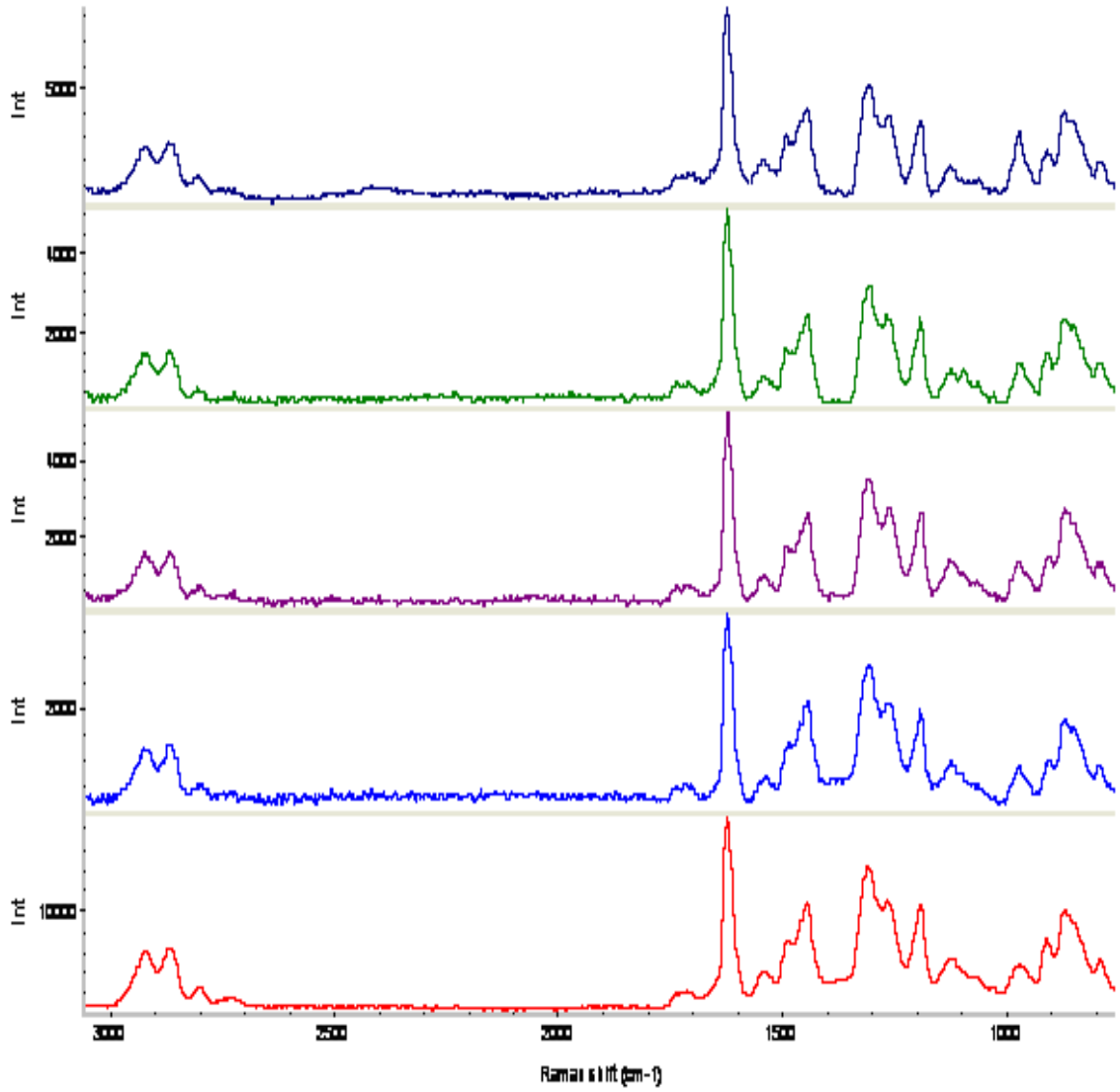

Figure A3.11 Comparative Raman spectra of
PU (red), PU/nHA5 (blue), PU/nHA10 (violet), PU/nHA15 (green) and PU/nHA20 (black) treated with deionised water at 7 days

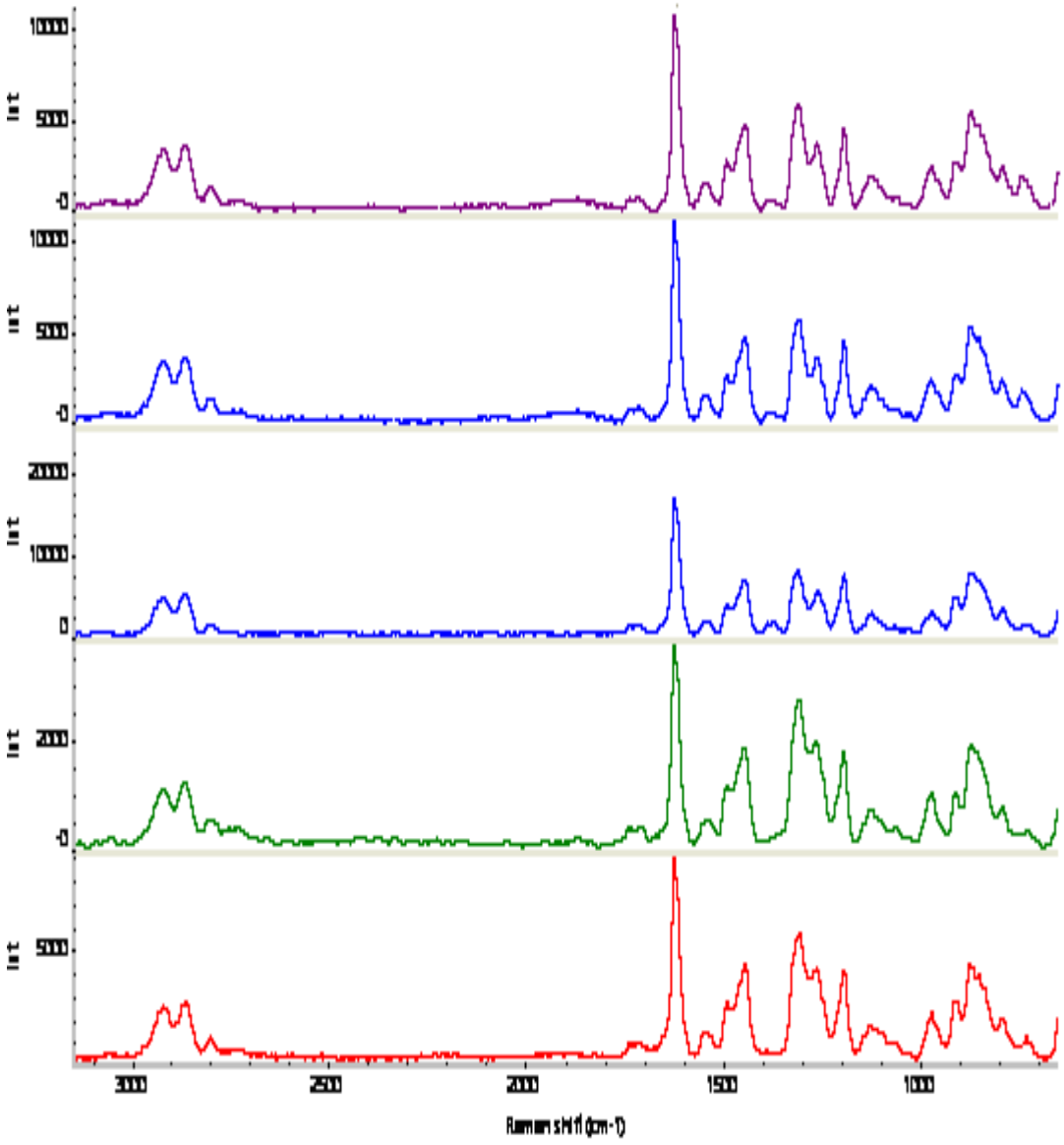

Figure A3.12 Comparative Raman spectra of
PU (red), PU/nHA5 (green), PU/nHA10 (blue), PU/nHA15 (blue) and PU/nHA20 (violet) treated with PBS at 7 days

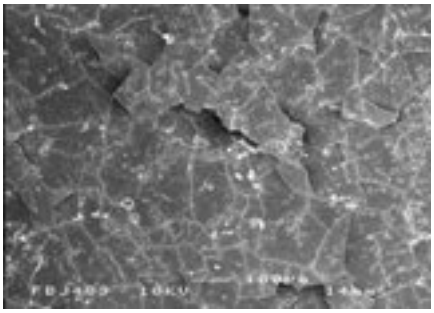

PU DW Day7

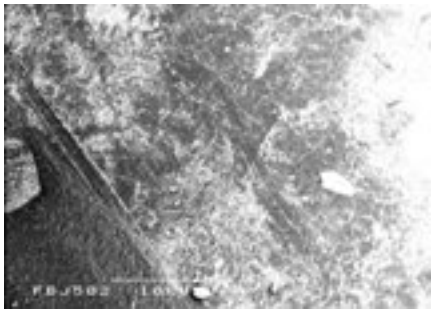

PU PBS Day7

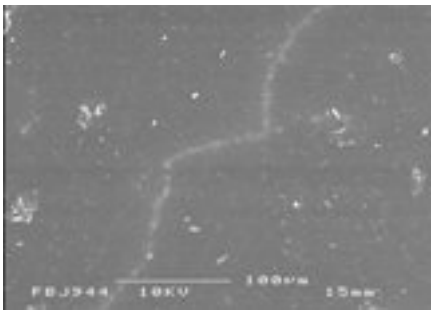

PU/nHA5 DW Day7

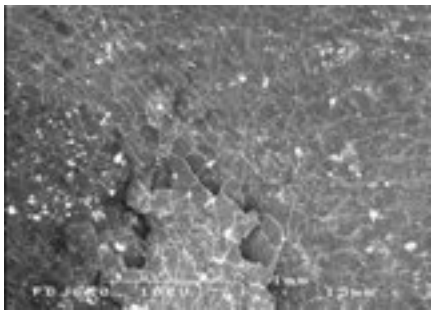

PU/nHA5 PBS Day7

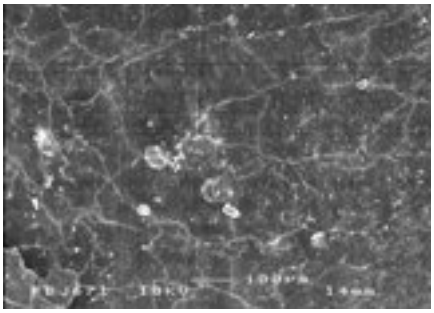

PU/nHA10 DW Day7

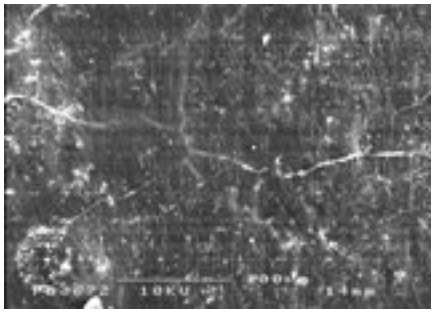

PU/nHA10 PBS Day7

Figure A3.13 SEM images of PU, PU/nHA5 and PU/nHA10 samples treated with deionised water (DW) and PBS at 7 days

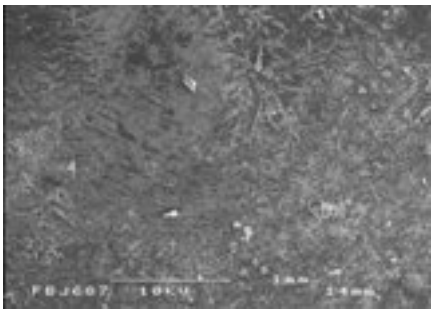

PU/nHA15 DW Day7

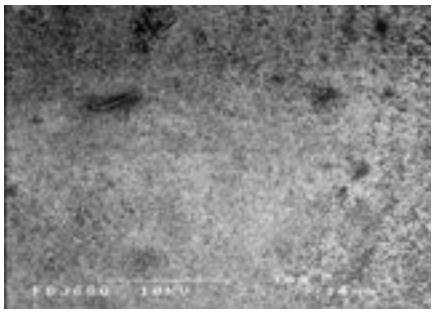

PU/nHA15 PBS Day7

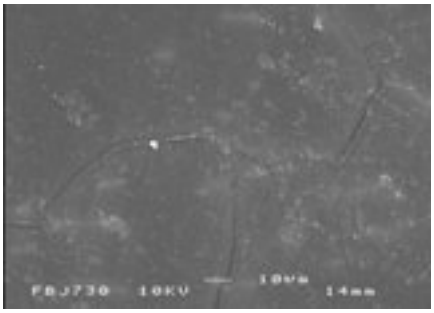

PU/nHa20 DW Day 7

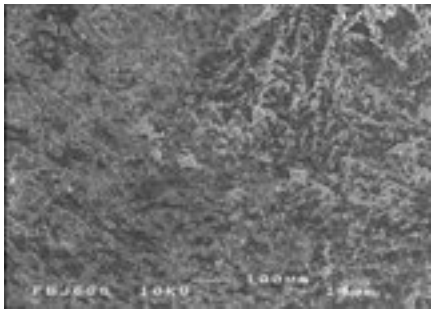

PU/nHA20 PBS Day7

Figure A3.14 SEM images of PU/nHA15 and PU/nHA20 samples treated with deionised water (DW) and PBS at 7 days

Appendix 4

4.1- Bioactivity

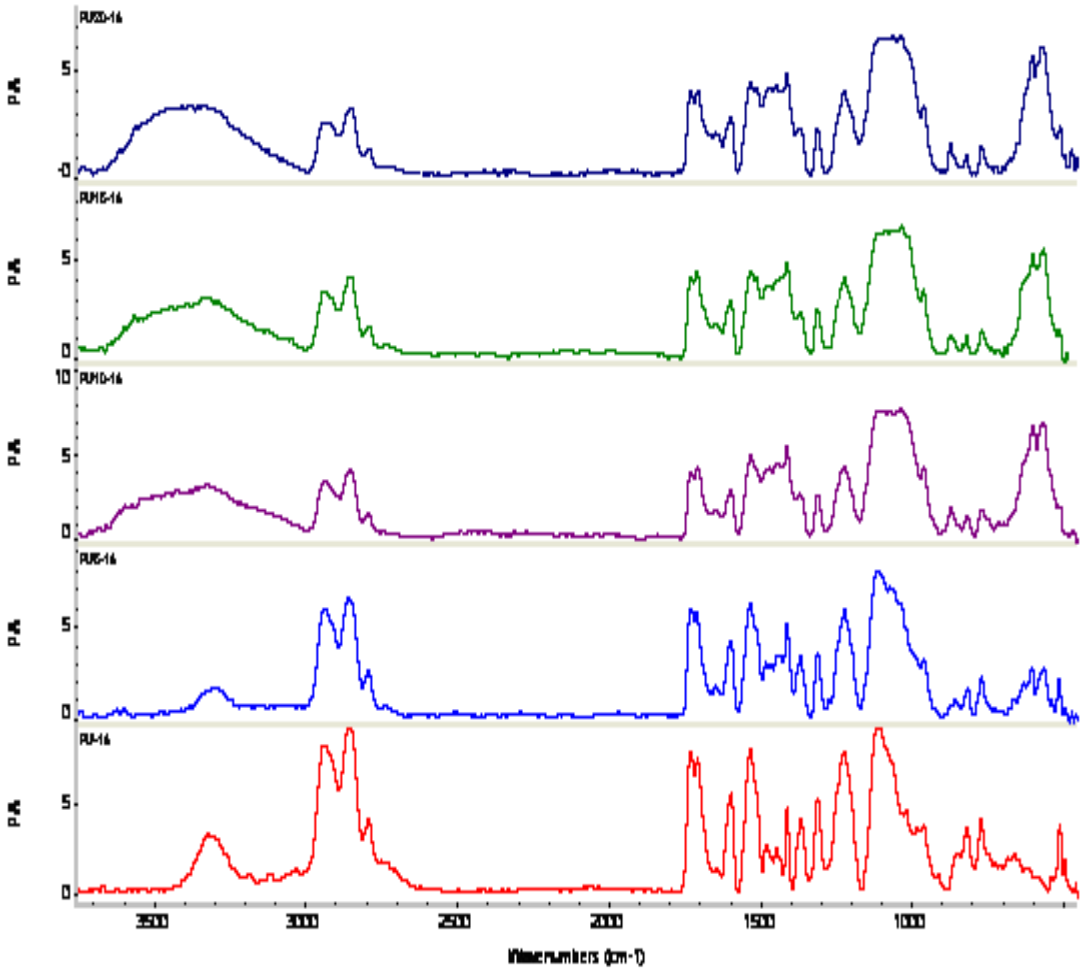

Figure A4.1 Comparative FTIR spectra of
PU (red), PU/nHA5 (blue), PU/nHA10 (violet), PU/nHA15 (green) and PU/nHA20 (black) treated with m-SBF at 14 days

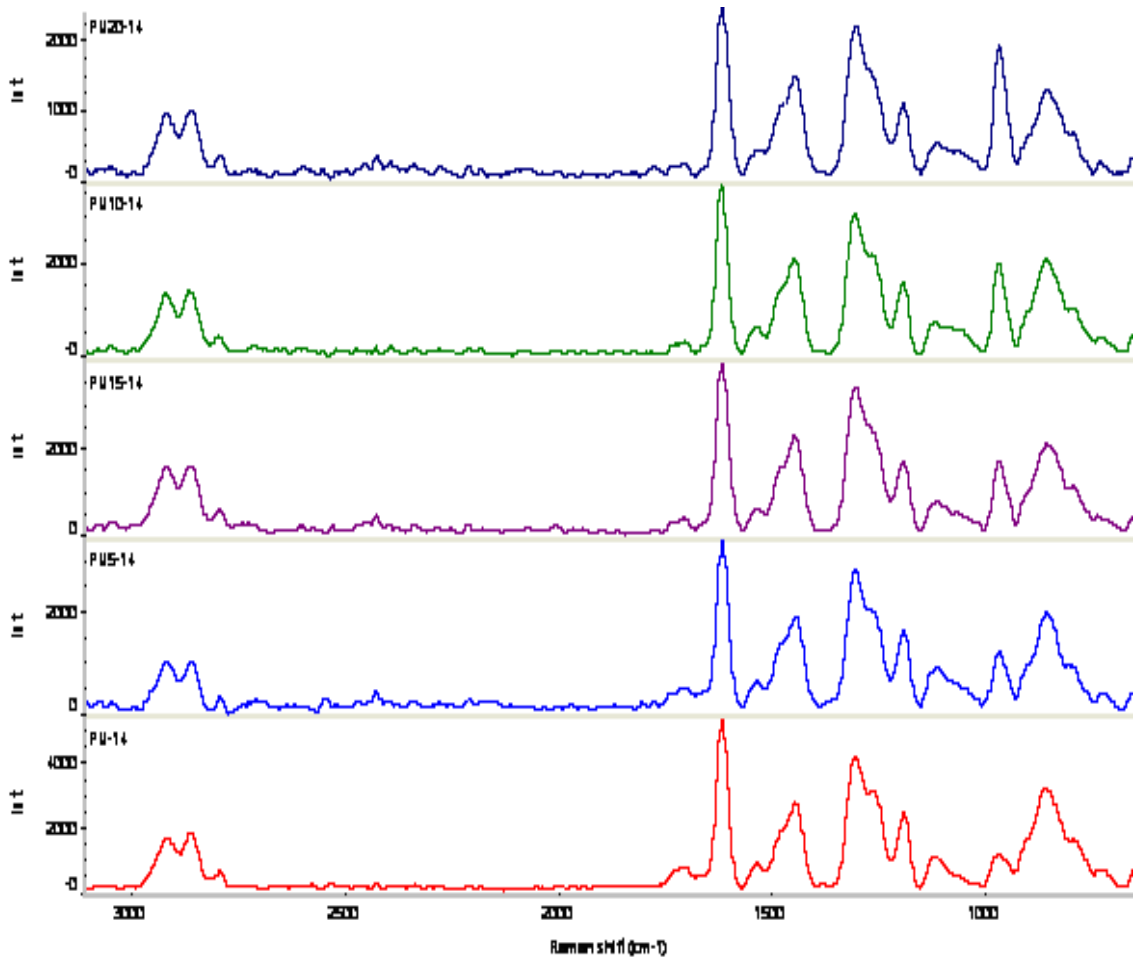

Figure A4.2 Comparative Raman spectra of
PU (red), PU/nHA5 (blue), PU/nHA10 (violet), PU/nHA15 (green) and PU/nHA20 (black) treated with m-SBF at 14 days

Appendix 5

5.1- Bio-adhesion

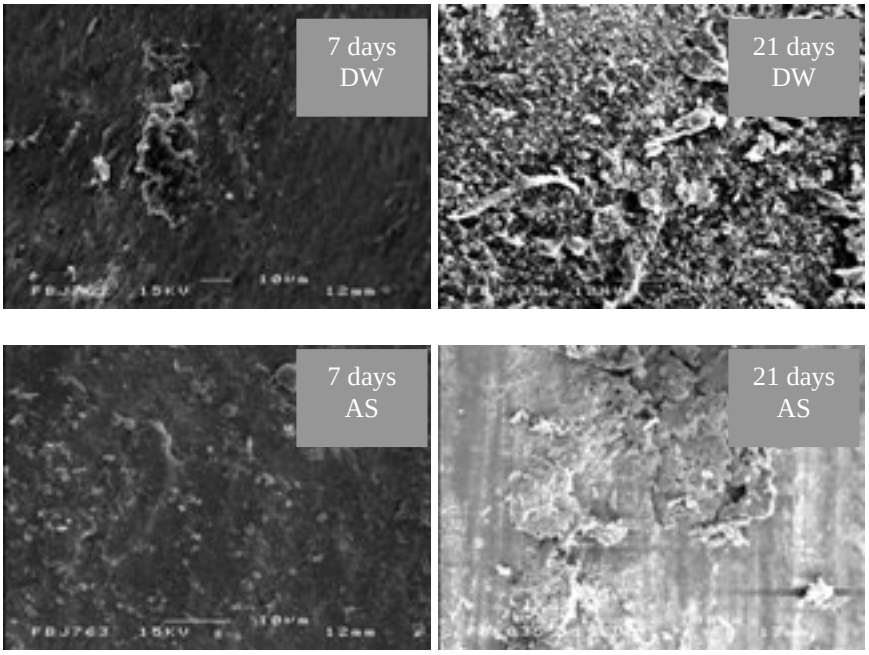

Figure A5.1 SEM images of PU adhesion with dentine at 7 and 21 days in media: deionised water (DW) and artificial saliva (AS)

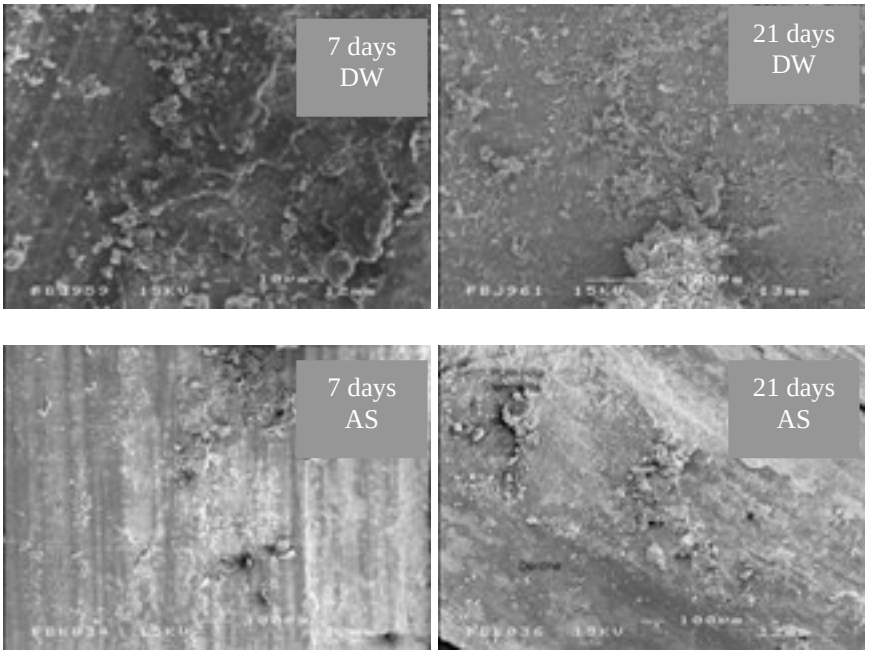

Figure A5.2 SEM images of PU/nHA10 adhesion with dentine at 7 and 21 days in media: deionised water (DW) and artificial saliva (AS)

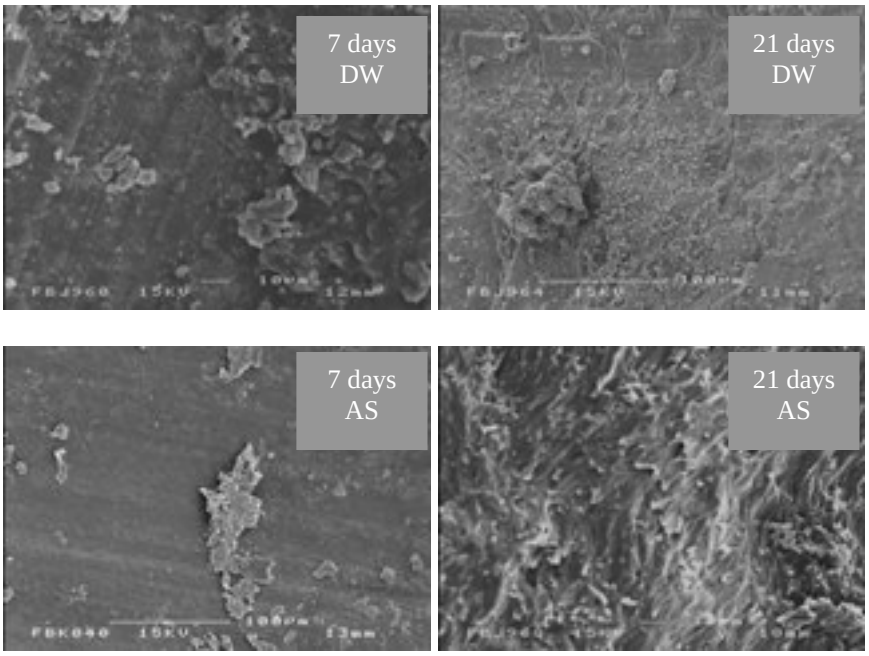

Figure A5.3 SEM images of PU/nHA15 adhesion with dentine at 7 and 21 days in media: deionised water (DW) and artificial saliva (AS)

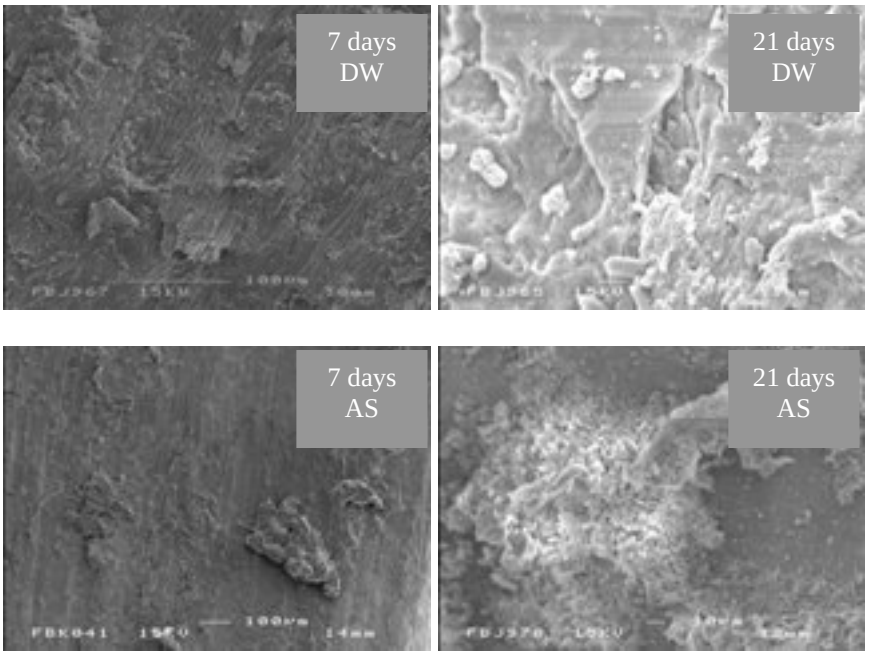

Figure A5.4 SEM images of PU/nHA20 adhesion with dentine at 7 and 21 days in media: deionised water (DW) and artificial saliva (AS)

Appendix 6

6.1- Surface Roughness

6.1.1- Characterisation

Mitutoyo Surftest. 401 Japan was used to analyse the surface roughness. The cut off length was 0.8 mm.

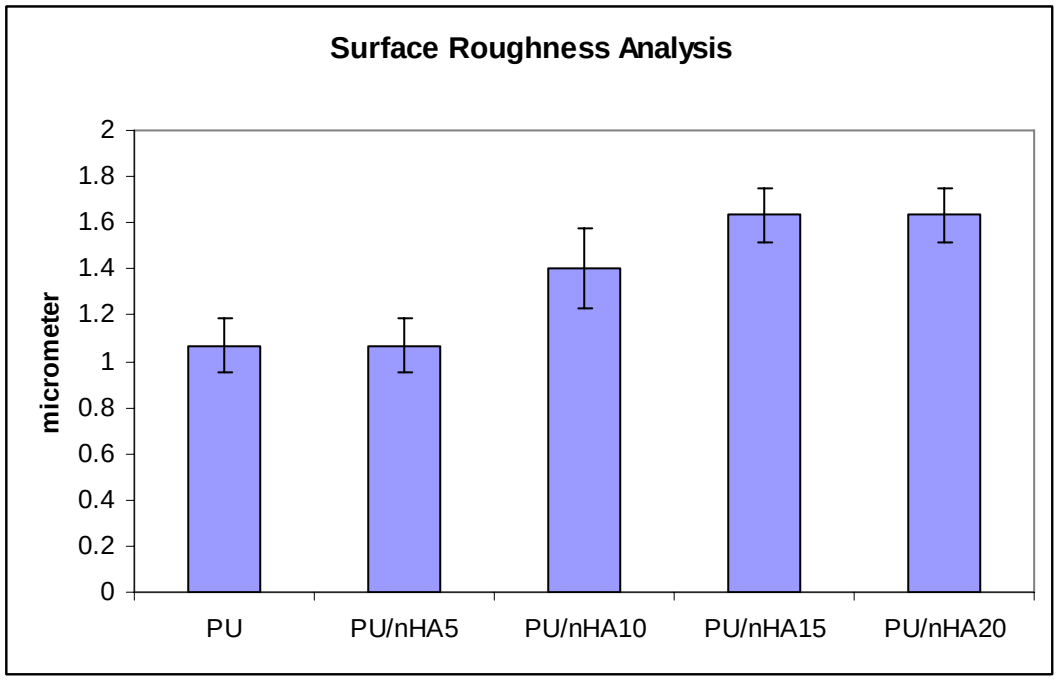

Figure A6.1 Surface roughness analysis of PU and PU/nHA composites

Appendix 7

7.1- Fluoroapatite

7.1.1- Synthesis of Fluoroapatite

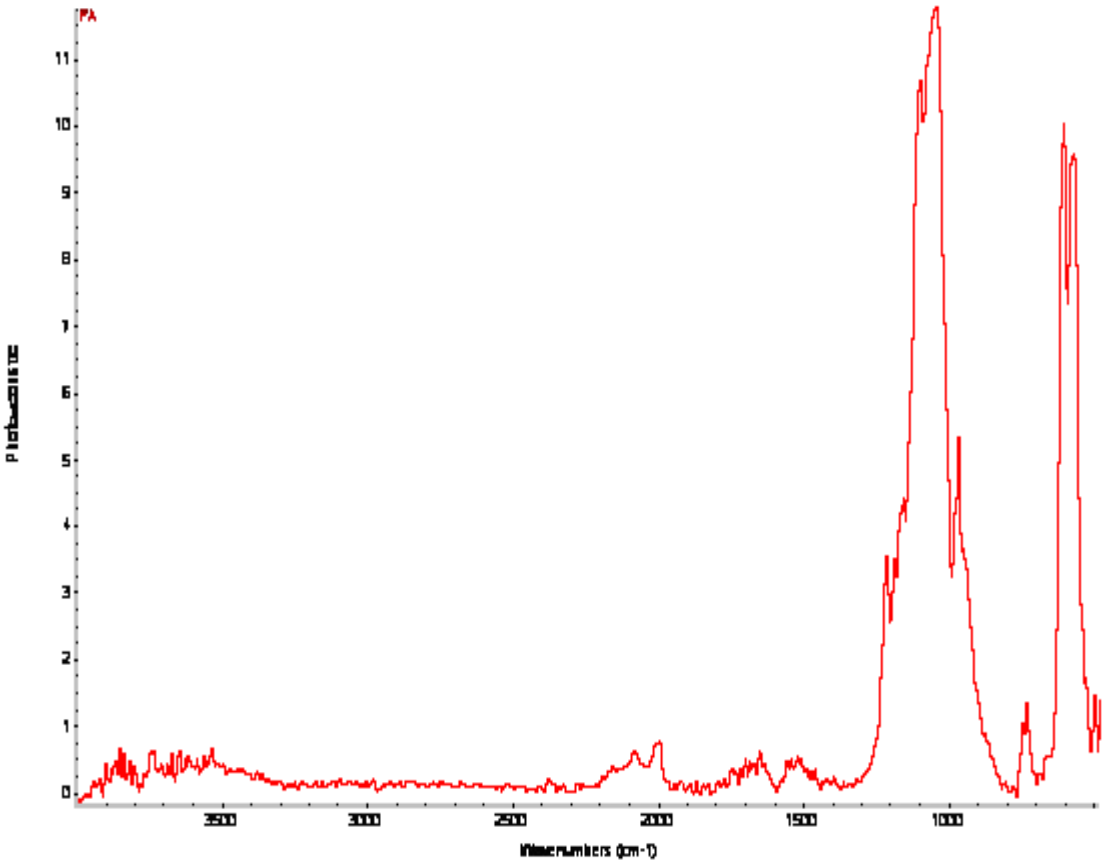

Figure A7.1 FTIR spectrum of Fluoroapatite showing characteristic peaks in between 1200-962 cm^{-1} (stretching PO_4), 1650-1470 cm^{-1} (CO_3), and 579 cm^{-1} (bending PO_4)

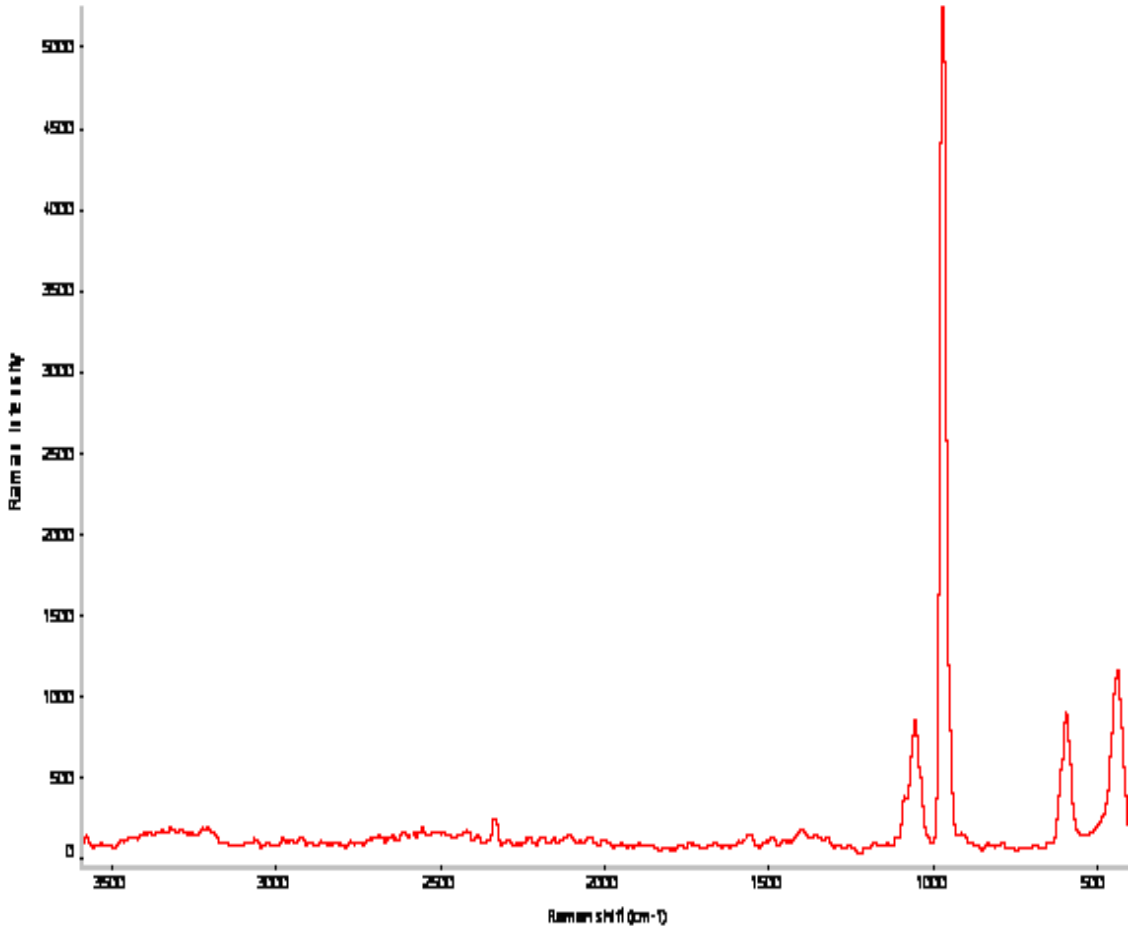

Figure A7.2 Raman spectrum of Fluoroapatite showing characteristic peaks in between 961 cm^{-1} (stretching PO_4), and 579 cm^{-1} (bending PO_4)

7.1.2- Synthesis of Polyurethane/nano-Fluoroapatite composite

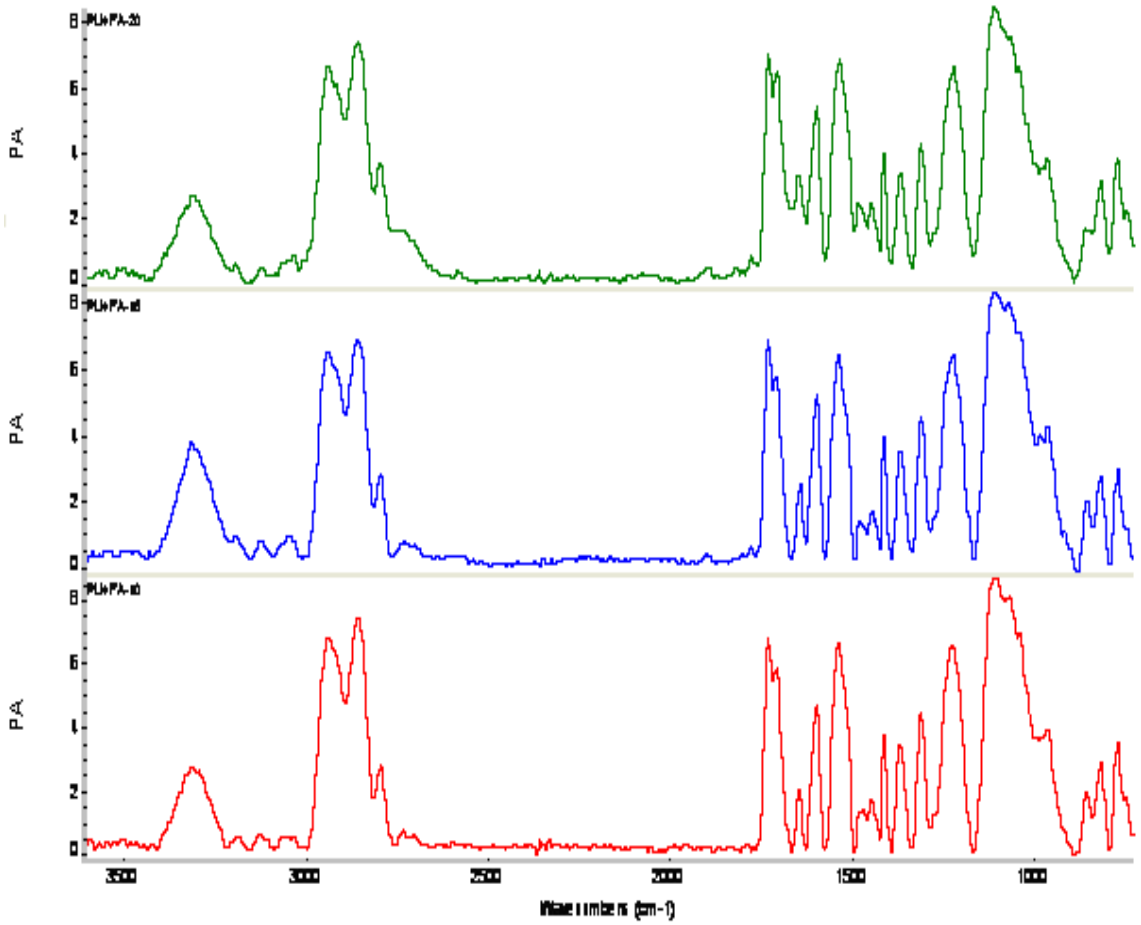

Figure A7.3 Comparative FTIR spectra of PU/nFA10 (red), PU/nFA (blue), and PU/nFA20 (green)

7.1.3- Fluoride Release Analysis

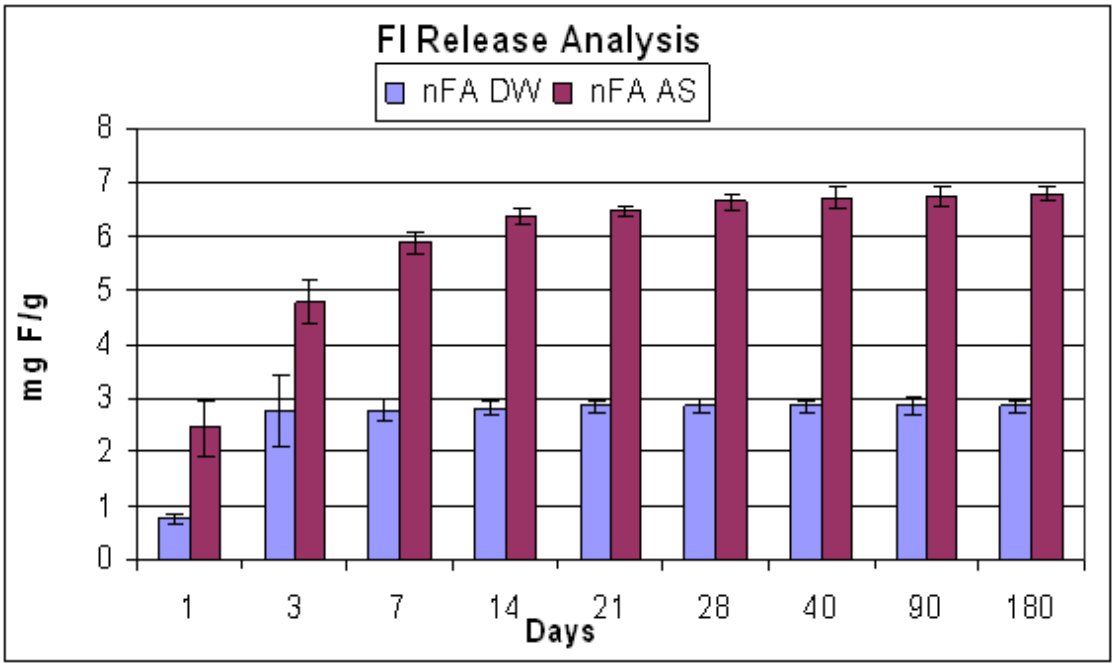

Figure A7.4 Fluoride release analysis of nano-fluoroapatite (nFA) for periodical time interval in deionised water and artificial saliva

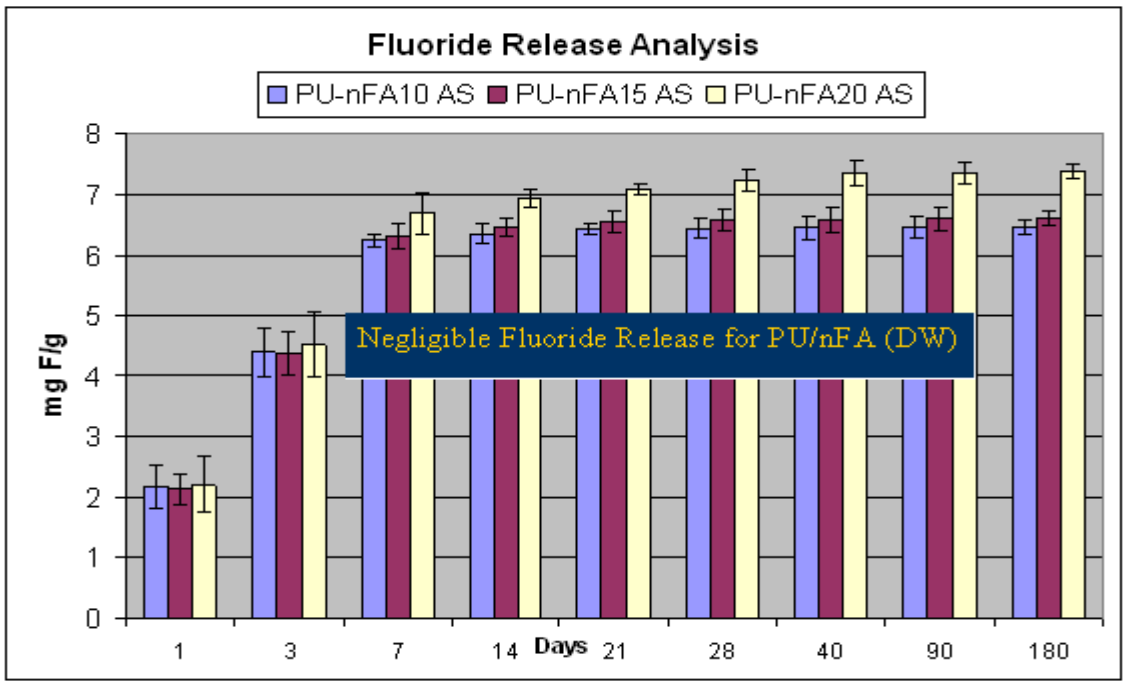

Figure A7.5 Fluoride release analysis of PU/nFA composite treated in artificial saliva. PU/nFA composites immersed in deionised water showed negligible release of fluoride

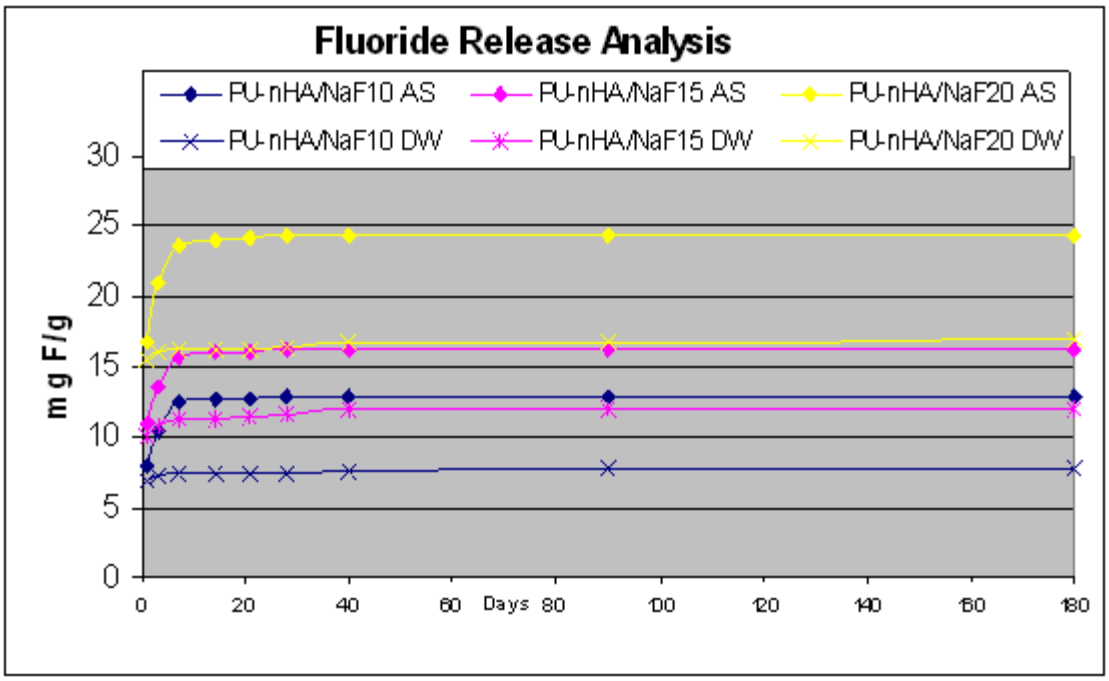

Figure A7.6 General trend of fluoride release analysis PU/nFA composite treated in deionised water and artificial saliva

List of Publications

1- Abdul Samad Khan, Mian Salman Aziz, Deepen Paul, Ferranti Wong, Ihtesham Ur Rehman **(2008)**

"Synthesis and in-vitro analysis of degradative resistance of a novel bioactive composite" Journal of Bionanoscience, 2: 75-88

.

2- A.S. Khan, Z. Ahmed, M.J. Edirisinghe, F.S.L. Wong, I. U. Rehman **(2008)**

Preparation and characterization of a novel bioactive restorative composite based on covalently coupled polyurethane-nanohydroxyapatite fibres, Acta Biomaterialia, 4: 1275-1287.

List of Presentations

Oral Presentations

1- A.S. Khan, R. Whiley, F.S.L. Wong, I.U. Rehman.

British Society for Dental Research Scientific Meeting, Oral Presentation "An *in-vitro* bio-adhesion and biocompatibility analysis of novel bioactive composites" 1st-4th September, 2009, Glasgow, Scotland, Abstract Accepted. Reference Number: 124669

2- A.S. Khan, F.S.L. Wong, I.U. Rehman

22nd European conference on Biomateirals, European Society of Biomaterials, Oral Presentation "Synthesis, in-vitro bio-adhesion and biocompatibility analysis of a novel bioactive composite" 7-11th September, **2009**, Lausanne, Switzerland, Abstract Accepted. Reference Number: 0342_REG20090127010947

3- A.S. Khan, I.J. McKay, F.S.L. Wong, I.U. Rehman, Pan European Federation, International Association for Dental Research, Oral Presentation "Synthesis and *in-vitro* analysis of a novel-bioactive dental restorative composite" 10-12th September, **2008**, London, United Kingdom.
http://iadr.confex.com/iadr/pef08/techprogram/abstract_110560.htm

4- A.S. Khan, S. Aamir, F.S.L. Wong, I.U. Rehman, 86th International Association for Dental Research General Session and Exhibition Meeting, Oral Presentation "Fluoride Release from Novel Bioactive Dental Restorative Composite" 2- 5th July, **2008**, Toronto, Canada.
http://iadr.confex.com/iadr/2008Toronto/techprogram/abstract_109103.htm

Poster Presentations

1- A.S. Khan, F.S.L. Wong, I.U. Rehman
22nd European conference on Biomateirals, European Society of Biomaterials, Poster Presentation "Synthesis and *in-vitro* analysis of a novel bioactive nano-composite" 7-11th September, **2009**, Lausanne, Switzerland, Abstract Accepted, Reference Number: 0652_REG20090316212754

2- Z. Sheikh, N. Roohpour, I.U. Rehman, **A.S. Khan**, International Association for Dental Research General Session and Exhibition Meeting, Poster Presentation "Effect of surface properties on protein adsorption of polyurethane membranes" 2- 5th July, **2008**, Toronto, Canada.
http://iadr.confex.com/iadr/2008Toronto/techprogram/abstract_105029.htm

3- I Rehman **AS Khan**, S Aziz, F Wong, , 8th World Biomaterial Congress, Poster Presentation "Synthesis and in-vitro analysis of degradative resistance of a novel bioactive composite" 28th May-1st June, **2008**, Amsterdam, The Netherlands. Abstract # P-Sat-H-510
http://www.wbc2008.com/wbc2008/Prelim_Announcement/complete_program.pdf

4- A.S. Khan, I.U. Rehman, F.S.L. Wong, 19th European Society for Dental Materials, Poster Presentation "Synthesis and Characterisations of Novel-Bioactive Dental Restorative Composite Based on Polyurethane/nano-Apatites" 30-31st Aug, **2007**, Leeds, United Kingdom.

5- A.S. Khan, N. Roohpour, J.A.Darr, I.U. Rehman, F.S.L. Wong, British Society for Dental Research conference, Poster Presentation "Synthesis and Characterisation of novel-bioactive dental restorative composite" 2-5th April, **2007**, Durham, United Kingdom.
http://iadr.confex.com/iadr/bsdr07/techprogram/abstract_94719.htm

Fluoride Release Analysis from Novel Bioactive Dental Restorative Composite

A.S. Khan, S. Aamir, F.S.L. Wong, I.U. Rehman

"Objective" Fluoride is a well-documented anti caries agent, however the anti-cariogenic effect of the fluoride-releasing material varies and depends upon the amount of fluoride the material releases (Xu et al. 2006, Dental Materials 22:1014). The objective of this study is to evaluate the affect of artificial saliva on the release of fluoride from novel bioactive dental restorative composite.

"Methods" Nano-apatite powder was obtained from the gel form by heat treating. A novel polyurethane composite material was prepared by chemically binding the nano-apatite to the diisocyanate component in the polyurethane backbone by utilising solvent polymerisation. The concentration of nano-apatite was 10, 15 and 20% wt/wt in polyurethane. The procedure involved stepwise addition of monomeric units of the polyurethane, and optimising the reagent concentrations. The samples were based on polyurethane/nano-fluoroapatite (PU/n-FA) and polyurethane/nano-hydroxyapatite/sodium fluoride (PU/n-HA/NaF). Six sample of each material were analysed where polyurethane (PU) was used as control material. The samples were stored in 15ml of deionised water (pH 7.4) and artificial saliva (pH 6.8) at 37ºC and were evaluated after 1, 3, 7, 14, 21, 28, 40, 90 and 180 days by using ion selective electrode. The media solution was replaced after each measurement.

"Result" The fluoride release was linear to square root of time ($R^2 > 0.80$). The fluoride release in artificial saliva was significantly higher ($p \leq 0.05$) than in deionised water. The release of fluoride from PU was significantly lower (0.01 m mole) than experimental samples Composite based on PU/n-HA/NaF showed higher fluoride release values as compare to PU/n-FAp.

"Conclusion" The combined use of polyurethane and fluoride releasing fillers provides sustained release of fluoride over a long period of time. The novel fluoride releasing polyurethane-apatite based composites can provide the anti-cariogenic properties.

Synthesis and *in-vitro* analysis of a novel-bioactive dental restorative composite

A.S. Khan, I.J. McKay, F.S.L. Wong, I.U. Rehman

"Objectives:" It is desirable for a dental restorative material to have bioactive and bonding properties. Hydroxyapatite (HA) has been shown to be osteo-conductive but can only bonds to resin through silane coating. A novel-bioactive composite has been synthesised based on polyurethane (PU) and nano-HA by creating a covalent linkage between them. In this study, its physical and biochemical characteristics were analysed.

"Methods:" Nano-HA powder was produced from the sol-gel. A novel PU-nano-apatite composite material was chemically prepared by utilising solvent polymerisation. The resulting composites were analysed by chemical, thermal, and mechanical characterisations. The resultant composite material was electrospun to form fibre mats. The bio-adhesion with dentine were analysed in distilled water and artificial saliva. Bioactive behaviour was determined in SBF. The composites were hydrolytically degraded in distilled water and PBS and were analysed. Cell growth and proliferation was measured by MTS assay.

"Results:" Spectral analyses showed the grafted isocyanate and ether peaks on HA, indicating that urethane linkage was established. The thermal and mechanical properties were enhanced by nano-HA. The SEM images of electro-spun nano-fibres revealed no loose HA particles. Bio-adhesion and bioactivity analysis showed the composite adhered firmly on the tooth surface (dentine). Higher nano-HA content composite showed thicker layer of adhesion. These composites had high resistance toward hydrolysis and little degradation. Biocompatibility test of the composite showed that the cells were growing although at a lower rate of growth compared to PU.

"Conclusion:" Covalent bond between HA and polymer were found in this novel composite with no silane agent. Bio-adhesion was found between this composite and tooth structure. Hence, it has the potential to be a desirable restorative material.

An *in-vitro* bio-adhesion and biocompatibility analysis of novel bioactive composites

A.S. Khan, R. Whiley, F.S.L. Wong, I.U. Rehman

"Objectives:" A novel polyurethane/nano-hydroxyapatite (PU/nHA).composite with interfacial linkage has been manufactured recently. This study investigated its *in-vitro* bio-adhesion and biocompatibility to human dentine.

"Methods:" A novel PU/nHA composite material was prepared by chemically binding the nHA in PU backbone utilising solvent polymerisation. The concentration of nHA in PU was 10, 15, or 20% wt/wt. Cavities prepared in dentine were filled with GC Fuji IX (GC Corporation, Japan), Filtek Supreme (3M ESPE, UK), and the PU/nHA composites. The samples were stored in deionised water and artificial saliva for a maximum of 90 days and tests were carried out at sequential time intervals. Push-out test was performed using an Instron machine at a cross-head speed of $1mm.min^{-1}$. Afterwards, interfacial adhesion of the composites to dentine was assessed using Scanning Electron Microscopy (SEM). Composite disc samples were incubated with standardised suspensions of *Streptococcus sanguinis* strain NCTC 7863 for 2hrs and washed in PBS. The number of adhering bacteria was determined by vortexing with glass beads and serial dilution followed by plating for colony forming units per disc.

"Results:" For PU/nHA, the mean push-out bond strength in both media increased with increasing immersion time. Samples with higher concentrations of nHA had higher bond strength. Higher bond strength was found in samples immersed in artificial saliva than those in deionised water (Table 1). There was 97.09% reduction in bacteria adhering to the grafted composite compared to PU.

"Conclusion:" Bond strength of PU/nHA composites was similar to existing obturating material. With its low bacterial adhesion it may provide a promising solution to reduce infections. Hence, this novel composite has the potential to be used as a bioactive obturating material.

Table 1 Mean Push-out bond strength values and standard deviations of samples immersed in artificial saliva (AS) and deionised water (DW)

Samples	**Day 7**	**Day 21**	**Day 40**	**Day 90**
PU/nHA10				
AS	0.46 ±0.08	0.51 ±0.09	0.66 ±0.10	0.80 ±0.15
DW	0.45 ±0.09	0.49 ±0.09	0.56 ±0.11	0.72 ±0.15
PU/nHA15				
AS	0.48 ±0.11	0.52 ±0.18	0.69 ±0.18	0.86 ±0.14
DW	0.47 ±0.15	0.49 ±0.16	0.56 ±0.19	0.76 ±0.17
PU/nHA20				
AS	0.49 ±0.12	0.54 ±0.15	0.77 ±0.18	0.89 ±0.22
DW	0.48 ±0.15	0.51 ±0.18	0.59 ±0.20	0.80 ±0.25
GC Fuji IX				
AS	7.2 ±1.6	7.4 ±1.4	6.9 ± 1.3	6.8±1.8
DW	7.0 ±2.1	7.1±1.6	6.8 ± 2.0	6.6 ±1.7
Filtek Supreme				
AS	28.1 ±2.4	28.2 ±2.8	29.4 ±2.2	29.6 ±3.2
DW	28.0 ±1.9	28.0 ±2.4	28.3 ±1.7	28.7 ±2.2

Synthesis, *in-vitro* bio-adhesion and biocompatibility analysis of a novel bioactive composite

A.S. Khan[1], F.S.L. Wong[2], I.U. Rehman[1]

Introduction: It is desirable for a restorative material to have bioactive and bonding properties that exhibit a specific biological response at the interface of the material, which results in the formation of bond between the tissue and the material. Polyurethane (PU) and nano-hydroxyapatite (nHA) have been used in a variety of biomedical and dental applications. The interfacial linkage between PU and nHA is one of the major factors that determine the ultimate properties of the composite. This study focused on the synthesis of a covalently-linked PU/nHA restorative composite and the *in-vitro* bio-adhesion and biocompatibility analysis.

"Methods:" nHA powder was obtained from the gel form by heat treating. A novel PU composite material was prepared by chemically binding the nHA to the diisocyanate component in the PU backbone by utilising solvent polymerisation. The concentration of nHA was 10, 15 and 20% wt/wt in PU. The resulting composites were analysed structurally by using Fourier Transform Infrared (FTIR, Photoacoustic sampling). The *in-vitro* bio-adhesion and bond strength (Push-out test) were analysed with dentine tooth structure. The samples were stored in deionised water and artificial saliva (pH 6.8) for up to 90 days and were analysed with sequential time intervals (7, 21, 40, and 90 days). Push-out test was performed on Instron 6025 with the cross head speed of 1 mm.min^{-1} and a load cell of I KN. The adhesion of the composites with tooth structure was analysed by using Scanning Electron Microscopy (SEM; JEOL 6300 JSM and FEI)) and Energy Dispersive Spectroscopy (EDS). The samples were mounted and were sputter coated under vacuum with carbon. The biocompatibility tests were performed by using cell-culturing and bacterial adhesion. The osteoblast-like cells were supplemented with 10% of fetal calf serum, 0.3µg/ml fungizone (Invitrogen) and 50µg/ml penicillin, 50µg/ml streptomycin (Invitrogen). Cell growth and proliferation was measured by MTS assay. The experimental composite surfaces were investigated for bacterial adhesion using Streptococcus Sanguis in blood plasma.

Results and Discussion: This study successfully achieved the grafted isocyanate and ether peaks on the surface of nano-apatites showing the urethane linkage. The FTIR spectra (Fig. 1) of composites showed that the urethane linkage at 3310 cm^{-1} which was likely to be the grafted peak of HN—CO, showing that covalent bond was formed between nHA and MDI. In Fig. 2 the comparative FTIR spectra showed that the peak at 1702 cm^{-1} attributed to hydrogen bonded (inter urethane bonding) carbonyl band. There was also grafting at OP-HC-O-(linkage of PO_4 and CH_2-O-CH_2) in the range of 1110-900cm^{-1}. The mean push-out bond strength in both media showed that with the increase in immersion time the bond strength of the samples increased, where the samples with higher concentrations of nHA has shown greater values, however, the samples immersed in artificial saliva showed more bond strength than the samples in deionised water. At day 90 PU/nHA20 (0.8 ±0.25 MPa) showed much higher values as compare to PU/nHA10 (0.72±0.15MPa).

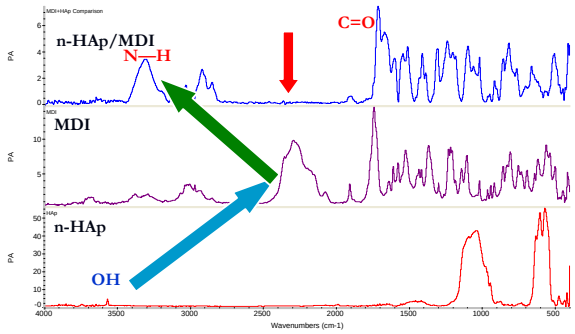

Fig.1 FTIR spectra of grafted MDI and nHA

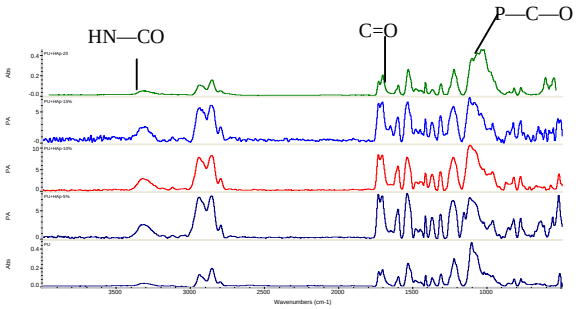

Fig 2 FTIR spectra of PU and PU/n-H composites

SEM analysis showed that at 90 days immersion, samples showed (Figure 3, a, b) more adherence as compare to 40 days immersion.

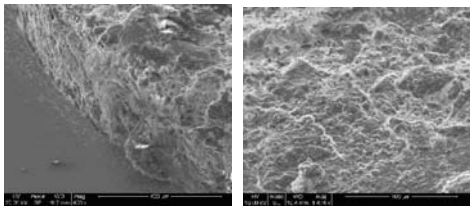

PU/nHA20 90 DW PU/nHA20 90 AS

Fig. 3 SEM images of PU/nHA20 at 90 days

The results of biocompatibility test showed that the nano-apatite based composite showed low rate of cell growth compared to PU, however, the cells were still growing and facilitated both adhesion and proliferation. The resulting grafted composite surfaces reduced bacterial adhesion significantly and the adhesion level differs depending on surface composition and structure.

Conclusion: These composites indicated the formation of covalent bond between nHA and PU and showed higher value of bond strength and adherence with the increase in concentration of nHA. The resulting composites have shown better biocompatibility. It is suggested that these polyurethane composites may be useful for a wide range of biomedical application.

Synthesis and Characterisation of Novel-Bioactive Dental Restorative Composite

A.S. Khan[1], N. Roohpour[1], J.A. Darr[1], F.S.L. Wong[2] and I.U. Rehman[1]

[1]Department of Materials, Queen Mary University of London, E1 4NS

[2]Institute of Dentistry, Queen Mary University of London, E1 4NS

Introduction

It is desirable for a restorative dental material to have bioactive and bonding properties that exhibit a specific biological response at the interface between the tissue and the material. Current resin-base composites, which consist of mainly polymer matrix, filler particles, and coupling agent, do not exhibit these properties. The presence of discrete zones at the interface between these three components could cause water absorption and the osmotic effect would result in swelling and residual pressure on tooth structure[1]. Silane coupling agent contact on the fillers could also cause a decrease in the polymerisation of the resin-based composite[2]. Urethane derivatives have been studied with Bis-GMA, these derivatives have much lower viscosities and water uptake than Bis-GMA and exhibit higher conversion of vinyl group without increasing (and perhaps decreasing) polymerization shrinkage[3]. Urethane based polymers, along with other materials such as acrylic resins or silicone, often used in dentistry for the tissue bearing surface of an extra-oral prosthesis[4]. Nano-particles have tendency to show high surface area to volume, superior chemical homogeneity and micro structural uniformity[5]. Hence, it would be advantageous to combine these two materials to form a new dental material that would possess the above desirable properties..

Aims

- To synthesise a novel bioactive restorative composite by creating a covalent linkage between urethane based polymer and nano-particles.
- To use different (physical and chemical) methods to synthesis this new composite and evaluate the linkage in between them

Methods

Nano-particles were synthesised by the "sol-gel" technique. These nano-particles were incorporated with polymer by using physical (PM) and chemical methods (CM_1 & CM_2). All chemicals were purchased from Sigma Aldrich, USA.

PM: polymer was synthesised by using polyether, 4,4′methylenebis(phenyl isocyanate) (MDI), 1,4-butanediol (BDO). After synthesis polymer was dissolved in solvent and nano-particles were added and stirred it.

CM_1: nano-particles were added to the polyether before the other sgements were added. After mixing it was allowed to polymerise at high temperature to make a composite.

CM_2: nano-particles were added to the unpolymerised polymer and allowed them to polymerise at high temperature .

Characterisation:

SEM (JOEL SEM 6300F, Japan) was used to investigate the morphological pattern of n-HAp and the composite; and UV-spectroscopy (Perkin-Elmer, USA) to show the presence of n-HAp in composite. Spectroscopic analysis were characterised by using Photoacoustic FTIR (Nicolet, UK) with a scan time of 256 and a resolution of 8 cm^{-1}.

Result and Discussion

SEM images of the nano-particles and the composite made using CM methods (Figs 1 & 2 respectively). The measured size of nano-particles were in the range of 100-200nm. These particles are not visible in the polymer apart from a few agglomerated particles on the surface, indicating that nano-particles were dissolved in the polymer matrix. The inclusion of nano-particles offer the possibility to have enhanced bonding properties and improved physical/mechanical properties due to its high surface area to volume[5]. UV-spectroscopy (Fig 3) shows the polymer peak of 300nm and the covalently linked composite characteristic peak of 350nm at 10%T.

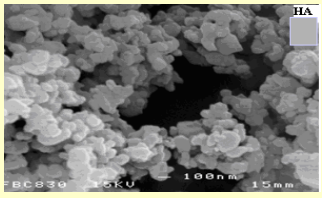

Fig 1 SEM image of nano-particles (40,000x)

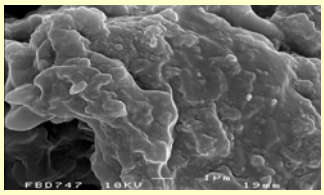

Fig 2 SEM image of the nano-particle/polymer composite (5000x)

The significant shift of peak was clearly observed and it clearly shows the linkage of particles with polymer molecules.

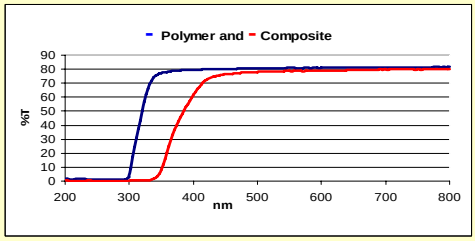

Fig 3 UV spectroscopy of polymer and composite

FTIR spectrum (Fig 4) of polymer/nano-particle composite synthesised by PM, CM_1 and CM_2 shows the broad peak ~3310-3330cm^{-1}, which is due to HN-CO (linkage of OH and NCO). This peak indicates that covalent bond was formed between particles and polymer. CM_1 shows the peak at 1715cm^{-1}, which is the P-O-CO-NH bond formed between MDI and PO_4. The shift of peaks in the range of 1110-900cm^{-1} in CM_1 attributes to the linkage OP-HC-O- and shifting of characteristic peak of HPO_4 (875cm^{-1}) to ~900cm^{-1}. Covalent bonding of particles with polymer has the potential to improve the interface of composite matrix, therefore, leading to significant improvement of the bioactive, bonding and mechanical properties. OH groups present on the surface of nano-particles seem to be a reactive group, due to nano size and large surface area, there are relatively large amounts of atoms on the surface and large fraction of surface OH groups. FTIR spectrum indicates that OH and PO_4 have the reactivity towards isocyanate groups and also forms the urethane linkage. These spectra suggested that more covalent bonds were formed using CM_1 method compared to the other two methods.

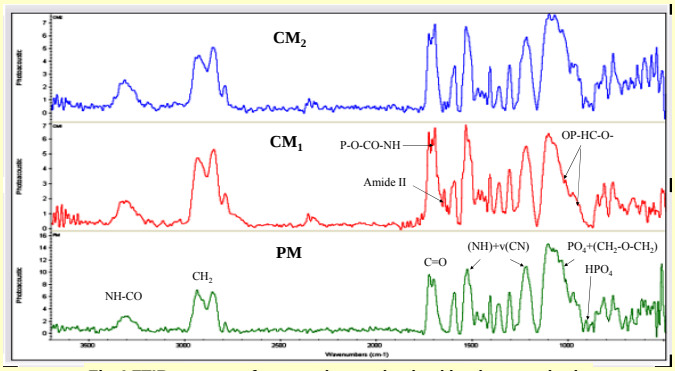

Fig 4 FTIR spectra of composite synthesised by three methods

Conclusion

The new composite synthesised with CM_1 method indicate the formation of covalent bond between nano-particles and polymer through HN-CO and OP-HC-O grafting without intermediate coupling agent. Hence this composite has the potential to be a novel-bioactive dental restorative material that may have the desirable properties of chemical adhesion to enamel and dentine.

References

1. McCabe JF, Rusby S. *Biomaterials*, 2004, p-4001
2. Halvorson RH, Erickson RL, Davidson CL. *Dent Mater*, 2003, p-327
3. Khatri CA, Stansbury JW, Schultheisz CR, Antonucci JM, *Dent Mater*, 2003, p-584
4. Labella R, Braden M, Deb S, *Biomaterials*, 1994, p-1197
5. Zhu X, Eibl O, Berthold C, Scheideler L, Gerstorfer GJ, *Nanotechnology*, 2006, p-2711

Acknowledgment: Principal researcher would like to thank the Department of Materials, QMUL for providing studentship for this project.

Synthesis and in-vitro analysis of degradative resistance of a novel bioactive composite

Abdul Khan[1], Salman Aziz [1], Ferranti Wong [2] & Ihtesham Rehman[1]

[1]School of Engineering and Material Sciences, Queen Mary University of London, London, United Kingdom

[2]Department of Oral Growth and Development, Queen Mary University of London, London, United Kingdom

Email: a.s.khan@qmul.ac.uk

Introduction

The biostability of the polymers and their composites is one of the most critical parameter for their use in biomedical applications[1,2]. A number of bioactive composites have been used in biomedical applications, but their stability has been of concern especially when implanted *in-vivo*.

A novel Polyurethane – Hydroxyapatite composite in which HA nano-particles are covalently bonded to the polymer backbone has been created and the hydrolytic degradation of a series of newly synthesised polyurethane (PU) and polyurethane/nano-hydroxyapatite (PU/n-H) composites have been evaluated in detail

Experimental Methods

Nano-apatite powder was obtained via sol-gel route followed by heat treating. A novel polyurethane composite material was prepared by chemically binding the nano-apatite to the diisocyanate component in the polyurethane backbone by utilising solvent polymerisation. The concentration of nano-apatite was 5, 10, 15 and 20% wt/wt in polyurethane. The PU and PU/n-H composites were hydrolytically degraded in deionised water (pH 7) and in phosphate buffer solution (pH 7.4) at 37°C for a period of up to 6 months and were analysed with sequential time intervals (1, 7, 14, 21, 40, 90, and 180 days). Six samples of each material with the nominal dimensions of 20x10x1 mm^3 were immersed in each media. The specimen films were removed from the solution and vacuum dried at 60°C for 24 hour prior to analysis.

The PU and PU/n-H composites were physically and chemically characterised, by evaluating their surface properties by contact angle measurements, weight loss profile, Fourier Transform Infra Red Spectroscopy couples with Photoacoustic Sampling Cell (FTIR-PAS), Raman Spectroscopy, X-ray Diffraction (XRD), Thermo-gravimetric analysis (TGA) and Scanning electron microscopy (SEM). In addition, the resulting media (solutions) were also analysed by UV spectroscopy to find out any degradative constituents from the samples.

Results and Discussion

Several studies suggest that chemical and morphological nature of biomaterial surface determine to a large extent how the biomaterial interacts with the host tissue and the physiological fluids after implantation[3]. It is significant to evaluate the surface properties, such as wettability, so that future relationship with in-vivo behaviour might be established. An increasing contact angle means a decrease of surface wettability, i.e., more hydrophobic. It is observed that the surface contact angle increased with the increase in n-HA content (Fig. 1). The increase of contact angle of PU/n-HA20 was ~20% than that of PU (90° ±0.35 and 73.96° ±0.32 respectively).

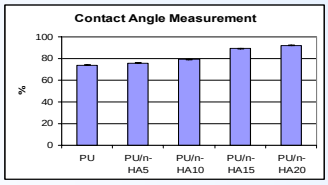

Figure 1 Contact angle measurement with standard deviations of PU and PU/n-HA composites prior to immersion in media

Weight loss of the PU and PU/n-HA composite specimens in DW and PBS increased substantially with time [Fig.2 (a & b)]. The rate of weight loss was significantly low in first 40 days but higher values were observed after 90 days. The composite with higher concentration of n-HA (e.g. PU/n-HA20) had lower weight loss comparing to the PU and the composites with lower concentration of n-HA (PU/n-HA5) - However, PU-n-HA10 shows significantly higher weight loss. The weight loss in the composite specimens occurred by dissolution of both inorganic particles and organic components into the buffer solution. The rate of low weight loss in higher n-HA concentrated composites could be due to the strong interaction between the nano-particles and polymers and formation of less water soluble compounds.

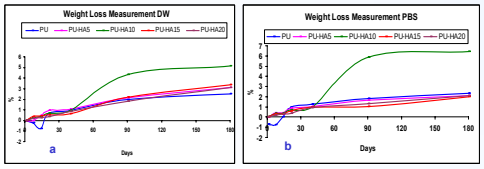

Figure 2 Comparison of weight loss measurement of PU and PU/n-HA composites treated with deionised water (DW) and phosphate buffer solution (PBS)

Figure 3 (a & b) shows the comparative spectra of PU and PU/n-HA20 composite after immersion. The films incubated in DW and PBS retained all the characteristic peaks of the PU and PU/n-HA composites. The spectra of composites showed that the urethane linkage at 3310 cm^{-1} which was likely to be the grafted peak of HN—CO, showing that covalent bond was formed between nano-apatite and PU. The peak at 1702 cm^{-1} attributes to hydrogen bonded (inter-urethane bonding) carbonyl band. There was also grafting at OP-HC-O-(linkage of PO_4 and CH_2-O-CH_2) in the range of 1110-900cm^{-1}. There is no shift of peak and significant emergence of peaks which attribute that there is no adsorption of solution content during immersion, which proves that the polyether based composite shows resistance toward DW and PBS and does not allow interacting with urethane linkage. In this study PU and PU/n-HA composites are based on PTMG and result obtained in this study supported that the that polyurethane based on higher methylene group concentration has better hydrolytic stability. The structures of PTMG are regular, so easy to form the crystal structures and the cohesion force of the soft segments are high, therefore the water molecules are hard to penetrate into the membranes. This hydrolytic stability is also due to formation of stable hydrogen bond between hard and soft segment among PU samples and stable hydrogen and covalent bond between n-HA and PU components. The stable H-bonded hard segment micro-domains and other H-bonded along the chains contributed the formation of protective structure.

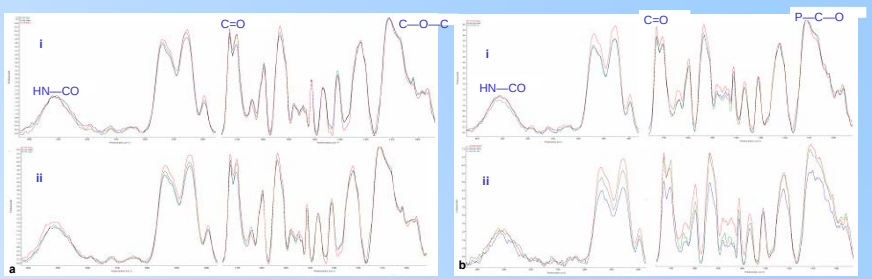

Figure 3 (a & b) FTIR spectra of PU and PU/n-HA composite (i) DW (ii) PBS respectively

As observed in FTIR, no significant changes were observed with the Raman spectra (Fig. 4 a & b) of PU and composite specimens immersed in (i) DW and (ii) PBS. It was observed that there was no shifting of peak that indicates that there was no chain scission in the PU due to well interlinked hard and soft segments. After 90 days, slight increase in intensity of peaks was observed in PU and PU/n-HA composites. The intense bands shows the absorption of water and it is expected that –OH forms a bond with aromatic and C—H peaks. CH structure behaves as a donor whereas, water molecule as an acceptor. In these spectra it is suggested that there is an interaction between C—H and –OH and resulting hydrogen bond establish.

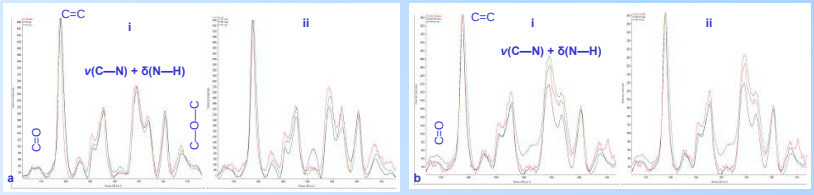

Figure 4 (a & b) FTIR spectra of PU and PU/n-HA composite (i) DW (ii) PBS respectively

The XRD pattern (Fig. 5) of PU samples are similar after treated with deionised water and PBS. Specimen immersed in PBS show low crystallinity as compare to deionised water. After 90 days of immersion in PBS and deionised water, crystallinity decreased by almost 50 and 35% respectively. Similar pattern was observed with PU/n-HA composites. For PU/n-HA20 composites, the sudden decrease in crystallinity was only observed at 90 days in DW and PBS. The broadness of peaks was almost the same for all samples, which shows that there is no possible alteration in the structure of the composites irrespective to n -HA content and the duration of immersion. Fig. 6 shows the TGA pattern of PU and PU/n-HA20 composites and it shows that after immersion there was slight decrease in thermal decomposition but it was not significant.

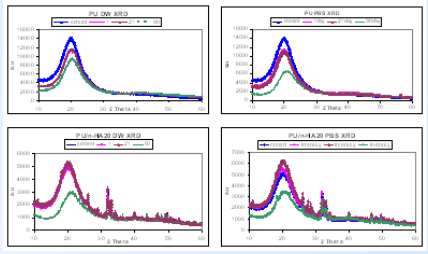

Figure 5 XRD pattern of PU and PU/n-HA after immersion

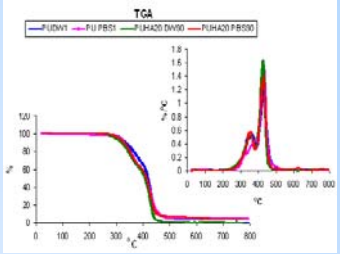

Figure 6 TGA of PU and PU/n-HA after immersion

SEM images (Fig.7) of PU (a & b) and PU/n-HA20 (c & d) were obtained with predetermined time intervals after incubation in DW and PBS. After 90 days, few pits were observed with the nominal size of 2-3 µm. The pitting of the surface was attributed to extraction of low-molecular weight degradation product that resulted from chain scission. It was interesting to find from UV spectroscopy that there was no released or disintegrated components in the media from the samples (PU and PU/n-H composites), which shows the long term stability of the polymer and polymer composite.

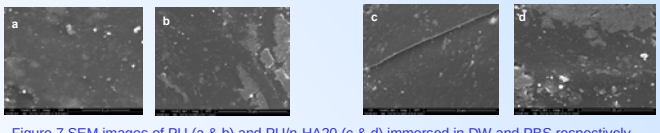

Figure 7 SEM images of PU (a & b) and PU/n-HA20 (c & d) immersed in DW and PBS respectively

Conclusion

Novel composites materials, which are covalently bonded were formed between n-HA and PU through HN-CO and P-C-O grafting without intermediate coupling agent. The incorporation of n-HA in these composites increases the resistance toward hydrolytic degradation. Hence, these PU/n-HA composites have acceptable biostability with no significant degradative effect and their long term properties are more superior to PU. It is suggested that these PU/n-HA composites may be useful for a wide range of biomedical application, i.e., dental and orthopaedic applications.

Acknowledgments: The authors would like to thank Armourers' and Brasiers' Company and School of Engineering and Material Sciences to award the grant.

References:

1. Rehman I.U., *Journal of Biomaterials Applications, 1996:11:182-257*
2. Rehman I.U., Andrews E.H., Smith R., *Journal of Material Science; Materials in Medicine, 1996: 7:17-20*
3. Hench L.L. and Ethridge E.C., Biomaterials: An interfacial approach, Academic Press, New York (1982)

Effect of surface properties on protein adsorption of polyurethane membranes

Zeeshan Sheikh[1], Nima Roohpour[2], Abdul Khan[2] and Ihtesham Rehman[2]

1.IRC in Biomedical Materials, COMSATS Institute of Information Technology, Lahore and Department of Dental Materials, Altamash Institute of Dental Medicine, Karachi,75600, Pakistan.

2. IRC in Biomedical Materials, School of Engineering and Material Sciences, Queen Mary University of London, (UK).

Introduction

The initial rapid adsorption of proteins onto the biomaterial surface is of paramount importance for the success of guided tissue regeneration (GTR) therapy. Protein adsorption is the first event, which occurs in a milieu of a second as a biomaterial comes in contact with blood in vivo. It is in response to the chemo attractant nature of these adsorbed proteins that any biological response is elicited. In contrast surface energy will affect adhesion between biomaterial and surrounded tissue which is a challenge in GTR treatment

Aims & Objectives

The aims & objectives of this study were to study the effects of the surface properties of polyurethane membranes on protein absorption. Investigation using contact angle measurement, ATR-FTIR (Attenuated Total Reflectance-Fourier Transform Infra Red) and Raman spectroscopy.

Experimental Methods

Polymer synthesis & BSA treatment

Polyether polyurethane and PDMS containing modified polyurethanes were synthesized via two step, solution polymerization. Synthesized polymers were cast as membranes and characterized using FTIR and Raman spectroscopy. Surface energy and wettability of polymeric membranes were determined by contact angle measurement. Membranes were soaked in Bovine Serum Albumin (BSA) solutions, (0.3mg/ml) in non-ionized water at 37^{0}C. Protein absorption of membranes was investigated using Raman and ATR-FTIR spectroscopy.

[OCN-R-NCO + *n* HO-R'-OH ------ [O-CONH-R-NHCO-O-R']]*n*

Figure 1. Polyurethane synthesis.

Contact angle & Surface energy analyses

Contact angles and surface energy of Polyether-urethane and PDMS modified polyether-urethane membranes were measured according to the procedure reported by Kwok and Neumann, 1999. The measurements were conducted at room temperature using liquid drops (deionized water and α-bromonaphthalene) of 5 µl in size using a micro-litre syringe. The contact angles of both side of drop were measured. Separate frames were collected every 2 seconds for 20 seconds and mean contact angle was calculated.

Characterization with ATR-FTIR and Raman Spectroscopy

Surface characterizations of the membranes were carried out by using Nicolet 8700 FTIR spectroscope with ATR accessory using Germanium crystal. The resolution range was 8 and spectra obtained over 64 exposures per sample. Raman spectroscopic analyses were carried out by using Nicolet Almega XR Dispersive Raman with 100µm pinhole. A 785 nm laser was used with objective 10X. The exposure time for samples was 1 sec over 128 exposures each.

Results

Contact angle measurement & surface energy values of membrane samples are shown in **table 1**

Table 1. Contact angle measurements & Surface energies of membrane samples.

Polymer Sample	θ with water (^{0})	Surface energy (mNm^{-1})
1.Polyetherurethane unmodified	89.86 ± 1.62°	35.608 mN^{-1}m
2.Polyetherurethane PDMS modified	105.79 ± 2.30°	28.047 mN^{-1}m

Selected ATR-FTIR and Raman spectra shown in **Figures 3 & 4**

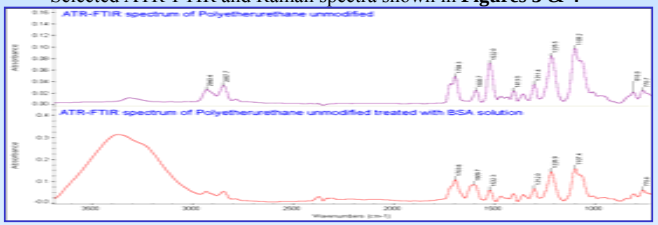

Figure 2. ATR-FTIR Spectra of Polyetherurethane membranes with and without BSA treatment

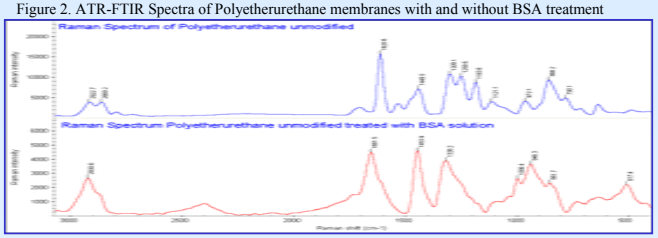

Figure 3. Raman Spectra of Polyetherurethane membranes with and without BSA treatment

Discussion

An increasing contact angle means a decrease of surface wettability, i.e., more hydrophobic.PDMS containing polyurethane showed lower surface energy (28.047mN/m) in comparison with unmodified polyether urethane (35.608mN/m) (**Table 1)**

IR and Raman spectra are significantly informative, as changes observed in Amide I and II bands **(Figures 4 & 5)** of proteins indicated that more proteins adsorb onto surface of the unmodified polyetherurethane membranes in comparison to PDMS containing polyurethane **(Figure 6)**

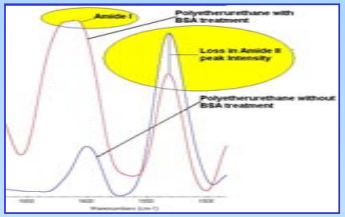

Figure 4. Focus on Amide I & II regions in FTIR spectra of BSA untreated and treated Polyurethane membranes.

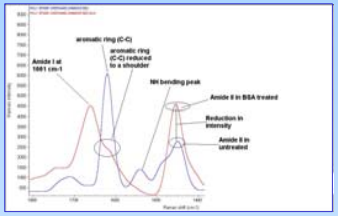

Figure 5. Overlap of Raman spectra of BSA untreated and treated Polyether urethane membranes.

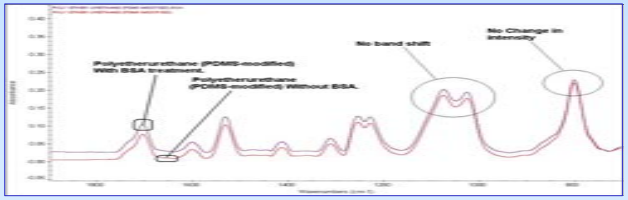

Figure 6. Overlapped ATR-FTIR spectra of Polyetherurethane (PDMS-modified), with & without BSA treatment.

Conclusions

- Unmodified Polyether-urethane shows protein adsorptive ability and thus can be investigated further for GTR therapy.
- PDMS containing polyurethane showed lower surface energy in comparison with unmodified polyether urethane so it could be considered as a hydrophobic surface.
- Incorporation of PDMS in polyurethane will reduce protein absorption as well as reducing adhesion to surrounding tissue.

References:

- Kwok, D. Y. and A. W. Neumann (1999). "Contact angle measurement and contact angle interpretation." Advances in Colloid and Interface Science 81(3): 167-249

Synthesis and *in-vitro* analysis of a novel bioactive nano-composite

A.S. Khan[1], F.S.L. Wong[2], I.U. Rehman[1]

[1]School of Engineering and Material Sciences, Queen Mary University of London, London, United Kingdom

[2]Department of Oral Growth and Development, Queen Mary University of London, London, United Kingdom

Email: a.s.khan@qmul.ac.uk

Introduction

It is desirable for a restorative material to have bioactive and bonding properties that exhibit a specific biological response at the interface of the material, which results in the formation of a bond between the tissue and the material. The bioactivity of the biomaterial is one of the critical parameter to use them for clinical application. Bioactive materials can stimulate a specific response in the surrounding tissues by means of complex mechanism involving three main phases: ion leaching, partial dissolution of the ceramic surface and the precipitation of bonelike apatite layer on the ceramic surface[1]. A novel Polyurethane – Hydroxyapatite composite in which HA nano-particles are covalently bonded to the polymer backbone has been created[2] and the the *in-vitro* analysis was carried out in modified-simulated body fluid (m-SBF) at controlled temperature of 37°C.

Experimental Methods

Nano-apatite powder was obtained via sol-gel route followed by heat treating. A novel polyurethane composite material was prepared by chemically binding the nano-apatite to the diisocyanate component in the polyurethane backbone by utilising solvent polymerisation. The concentration of nano-apatite was 5, 10, 15 and 20% wt/wt in polyurethane. m-SBF was prepared, as described by Oyane et al.[3] by dissolving reagent in deionised water. The films were prepared by solvent casting. The resulting films were cut uniformly into 12 mm diameter. Six samples of each material were used for this study. The samples were sterilised by soaking into 70% ethanol for predetermined time interval and dried before immersion. The sterilised samples were immersed in 15 ml m-SBF containing polystyrene tubes (Fischer Scientific, UK) covered with lids for 1, 7, 14, 21, and 40 days, which were maintained at 37°C. The m-SBF was changed after 14 days to maintain a constant liquid composition. The resulting samples were characterised to evaluate the bioactivity by using Scanning Electron Microscopy (SEM), Energy Dispersive Spectroscopy (EDS), Fourier Transform Infrared (FTIR; Photoacoustic Sampling), Raman Spectroscopy, and X-ray Diffraction (XRD).

Results and Discussion

Several studies suggest that chemical and morphological nature of biomaterial surface determine to a large extent how the biomaterial interacts with the host tissue and the physiological fluids after implantation[4]. This study successfully achieved the grafted isocyanate and ether peaks on the surface of nano-apatites showing the urethane linkage. The comparative FTIR spectra (Fig. 1) of composites showed that the urethane linkage at 3310 cm^{-1} which was likely to be the grafted peak of HN—CO, showing that covalent bond was formed between nHA and MDI. It was observed from FTIR spectra that the peak at 1702 cm^{-1} was attributed to hydrogen bonded (inter urethane bonding) carbonyl band. The grafting was also expected at OP-HC-O- (linkage of PO_4 and CH_2-O-CH_2) in the region of 1110-900 cm^{-1}.

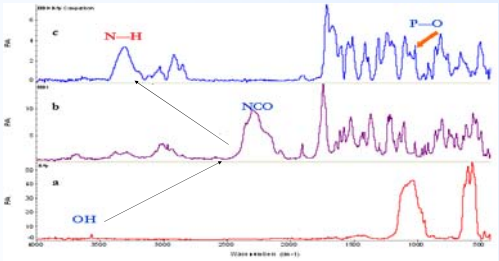

Figure 1 FTIR spectra of grafted nHA/MDI

It was found that the *in-vitro* bioactivity of these PU/nHA composites was dependent on the chemical composition. The introduction of calcium-phosphate into the network facilitated the formation of hydroxylcarbonate-apatite layer on the surfaces of composites. It was observed that with the increase in concentration of nHA, significant amount of calcium-phosphate precipitates were formed on the surface. The thickness of the apatite layers increased with the increase of the immersion time in SBF. It was observed that in PU samples (Fig. 2i) there was no visible apatite formation on the surface of immersed samples up to 14 days. However, 40 day samples showed apatite formation on the surface. Morphological studies of the PU/nHA composite surfaces immersed for 40 days in m-SBF presented an apatite (calcium phosphate) layer on the surface of the composites. PU/nHA5, PU/nHA10 (Fig. 2ii), PU/nHA15, and PU/nHA20 (Fig. 2iii) composite samples showed that the apatite layer was not prominent at 1 day; however, it was observed that with the increase in immersion time the apatite globules packed tightly with each other.

Initially the apatite particles were scattered on the surface, but at 14 days' incubation, the sample surface developed a dune-like apatite layer and this structure changed the original morphology of the samples completely. SEM images of 21 days immersion showed the dune-like layer evolved into more smooth hillocks, with a subtle net-like texture consisting of short micro-rods. The layer growing on the surface coating was quite dense and homogeneous. These newly developed calcium phosphate layer showed the same morphology as the amorphous coatings, in addition EDS analysis showed the presence of Na, Mg with Ca and P ions.

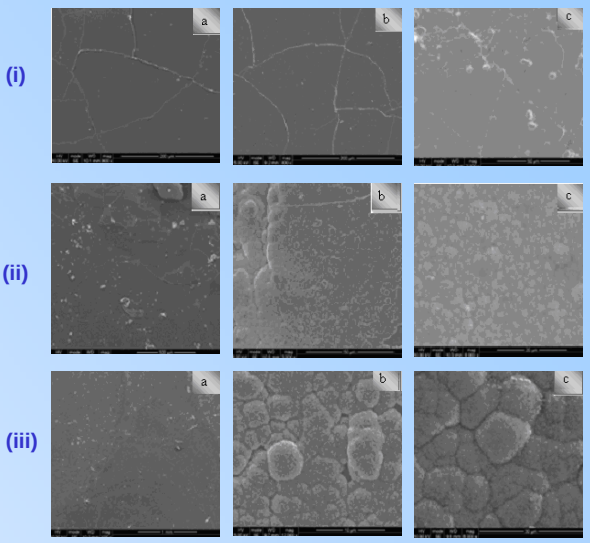

Figure 2 SEM images of (i) PU, (ii) PU/nHA10, and (iii) PU/nHA20 at (a) 1, (b) 14, and (c) 40 days

FTIR (Fig. 3i) and Raman (Fig. 3ii) spectra of PU/nHA20 composites showed different pattern and changes appeared at 7 days spectrum. The presence of apatite layer changed the characteristic pattern of peaks at 1400-1200 cm^{-1}, 1100-900 cm^{-1} and 600-500 cm^{-1} suggested the apatite layer presented on the surface of samples and changed the structural properties of the material. The spectrum of 40 day sample showed broadness and emergence of peaks at 3320 cm^{-1} (N—H) and 1010 cm^{-1} (P—O—C) respectively. The shifting of peaks were also observed at 603 and 562 cm^{-1} due to presence of bending peaks of phosphate. The resulting spectra showed that with the increase in concentration of nHA in PU the emergence of peaks became more significant.

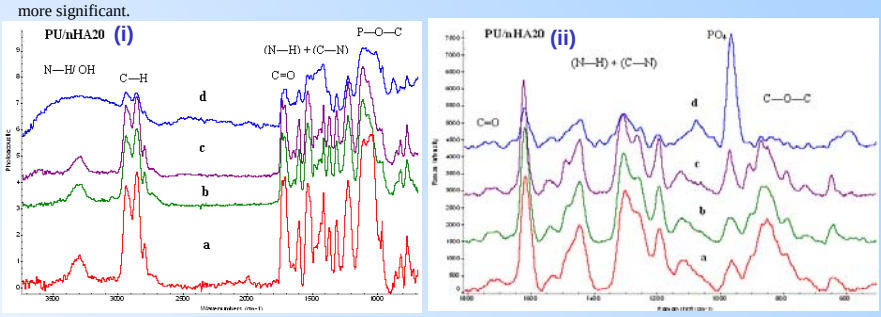

Figure 3 (i) FTIR and (ii) Raman spectra of PU/nHA20 after immersion in m-SBF at (a) 1, (b) 7, (c) 21, (d) 40 days

The comparative XRD pattern of 1 and 40 days showed a broad band at 10-25º and a sharp peak at 29º. It was observed that XRD pattern of PU (Fig. 4a) did not show presence of any band assigned to apatite. In PU/nHA composites, a broadening and intensity decreased with the immersion time; however, the higher concentration of nHA showed variation in the sharpness of the peaks at 40 days. The XRD patterns showed the diffraction peaks (210, 112, and 300) that confirmed the presence of apatite on the surface of samples. It was observed that PU/nHA20 (Fig. 4b) with higher concentration of nHA showed more apatite peaks at 39.89º (310) and 47º (222). However, it was difficult to estimate the exact presence of apatite or phase composition from this technique.

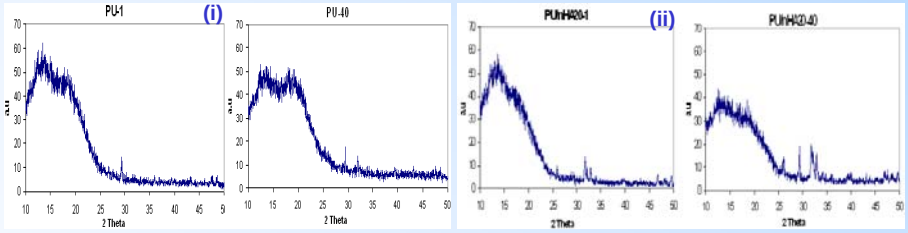

Figure 4 XRD patterns of (i) PU and (ii) PU/nHA20 at 1 and 40 days immersion in m-SBF

Conclusion

These composites indicated the formation of covalent bond between nHA and PU and showed higher tendency of bioactivity with the increase in concentration of nHA. Hence, this newly synthesised bioactive composite has potential to be used as biomaterial.

Acknowledgments: The authors would like to thank Dr. R. Wilson for XRD characterisations and Armourers' and Brasiers' Company, UK to award the travelling grant.

References

1. Chatzistavrou X, Chrissafis K, Polychroniadis E, Kontonasaki E, Koidis P, Paraskevopoulos KM., Journal of Thermal Analysis and Calorimetry, 2006, 86, 255.
2. Khan AS, Ahmed Z, Edirisinghe MJ, Wong FSL, Rehman IU., Acta Biomaterialia, 2008,4, 1275.
3. Oyane A, Kawashita M, Nakanishi K, Kokubo T, Minoda M, Miyamoto T, Nakamura T., Biomaterials 2003, 24, 1729.
4. Hench LL and Ethridge EC., Biomaterials: An interfacial approach, 1982, Academic Press, New York.